Contract No. 027ST-36001-0-3600

October 1991

Optical Intersatellite Link System Study

Volume 1
Final Report

Prepared for the
Department of Communications
by
Spar Aerospace Limited

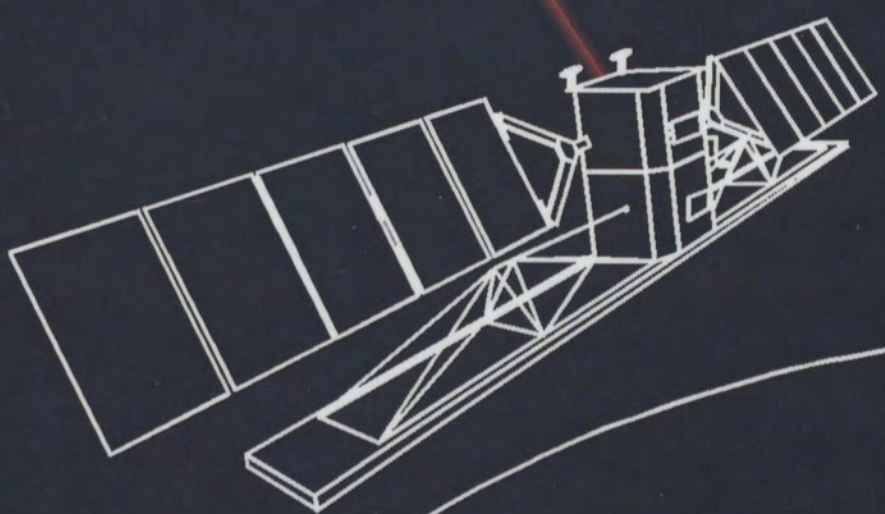

SPAR

COVER: The front cover shows a remote sensing satellite relaying data via an optical crosslink to a geostationary data relay satellite and then to a data acquisition facility on the far side of the earth

Spar Program 3670-F

Optical Intersatellite Link System Study

Volume 1 - Final Report

Prepared for:

Communications Research Centre
3701 Carling Avenue
Materiel Management "Z"
P.O. Box 11490, Station 'H'
Ottawa, Ontario K2H 8S2

Issue A
November 1991

Spar Aerospace Limited

Satellite and Communications Systems Division

21025 TransCanada Highway
Ste-Anne de Bellevue, Quebec
Canada H9X 3R2
Telephone: (514) 457-2150
Fax: (514) 457-2724
Telex: 05-822792

Contents

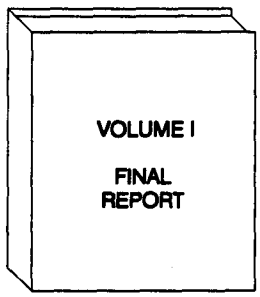

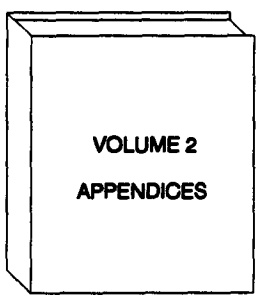

This Page Intentionally Left Blank

Table of Contents

Table of Contents (cont'd)

Table of Contents (cont'd)

Table of Contents (cont'd)

Table of Contents (cont'd)

List of Figures

List of Figures (cont'd)

List of Figures (cont'd)

List of Figures (cont'd)

List of Figures (cont'd)

List of Figures (cont'd)

List of Figures (cont'd)

List of Tables

List of Tables (cont'd)

List of Acronyms

A

ACTS	Advanced Communications Technology Satellite
AFC	Automatic Frequency Control
AGC	Automatic Gain Control
ALC	Automatic Leveling Control
AlGaAs	Aluminum Gallium Arsenide
Al_2O_3	Aluminium Oxide
APD	Avalanche Photodiode
ASIC	Application Specific Integrated Circuit
ASK	Amplitude-Shift Keying
ATS	Applications Technology Satellite
AT&T	Alberta Telephone and Telegraph
Az	Azimuth

B

BAe	British Aerospace
BeO	Beryllium Oxide
BER	Bit Error Rate
BIT	Built-in Test
BPF	Bandpass Filter
bps	bit per second
BW	Bandwidth

C

C	Celsius
CAL	Canadian Astronautics Limited
CFPA	Compound Fine Pointing Assembly
cm	centimeter
CO_2	Carbon Dioxide
CO	Carbon Oxide
Comsat	Communications Satellite
CPA	Course Pointing Assembly
CPM	Course Pointing Mechanism
CRC	Communications Research Centre
CSA	Canadian Space Agency
CTA	Course Tracking Assembly
CTM	Course Tracking Mechanism
CW	Continuous Wave

D

dB	Decibel
dBW	Decibels relative to 1 watt
DC	Direct Current
DDLT	Direct Detection Laser Transceiver
DND	Department of National Defence
DOD	Department of Defense
DRS	Data Relay Satellite
DSS	Department of Supply and Services

E

e.g.	*exampli gratia* (for example)
EHT	Electrically Heated Thrusters
El	Elevation
ESA	European Space Agency
ETS	Engineering Test Satellite

F

FEC	Forward Error Correction
FET	Field-Effect Transistor
FIT	Failures in Time
FM	Frequency Modulation
FOV	Field-of-View
FPA	Fine Pointing Assembly
FPM	Fine Pointing Mechanism
FSDD	Flight System Development and Demonstration
FSK	Frequency-Shift Keying
FTA	Fine Tracking Assembly
FTD	Fine Tracking Detector
FTM	Fine Tracking Mechanism
FY	Fiscal Year

G

GaAs	Gallium Arsenide
Gb	gigabit
Gbps	Gigabit per second
GEO	Geostationary Orbit
GHz	Gigahertz
GSFC	Goddard Space Flight Center

H

HEMT	High Electron Mobility Transistor
HeNe	Helium Neon
H_2O	Water
Hz	Hertz

I

IC	Integrated Circuit
i.e.	*id est* (that is)
IEEE	Institute of Electrical and Electronic Engineers
IF	Intermediate Frequency
InGaAsP	Indiuym Gallium Arsenide Phosphide
Intelsat	International Telecommunications Satellite Organization
IR	Infrared
ISL	Inter-Satellite Link
I&T	Integration and Test

J

J	Joule
JPL	Jet Propulsion Laboratory (NASA)

K

K	Kelvin
kbps	kilobit per second
kg	Kilogram
km	kilometer
Ku-Band	14 GHz Uplink/12 GHz Downlink Fixed Satellite Service

L

LBM	Laboratory Breadboard Model
LCE	Laser Communication Equipment
LCT	Laser Communication Transceiver
LEO	Low Earth Orbit
LITE	Laser Intersatellite Transmitter Experiment
LO	Local Oscillator
LOC	Large Optical Cavity

M

m	meter
M	Millions
Mb	Megabit
MBit	Megabit
Mbps	Megabit per second
MESFET	Metal-Semiconductor Field-Effect Transistor
MgF_2	Magnesium Floride
MHz	Megahertz
MIT	Massachusetts Institute of Technology
MLI	Multilayer Insulation
mm	millimeter
MOPA	Master Oscillator Power Amplifier
mW	Milliwatt

N

N/A	Not Applicable (or Available)
NASA	National Aeronautics and Space Administration
Nd	Neodinium
NEA	Noise Equivalent Angle
NEC	Nippon Electric Corporation
NFD	Narrow-Field Detector
NRZ	Non Return to Zero
ns	nanosecond
nW	Nanowatts
NY	New York

O

O_2	Oxygen
OISL	Optical Inter-Satellite Link
OLL	Optically-Locked-Loop
OLPP	Optical Link Preparatory Program
OOK	On-Off Keying
O/P	Output

P

PAA	Point-Ahead Assembly
PAM	Point-Ahead Mechanism
PAT	Pointing, Acquisition and Tracking
PEEK	Poly Ether Ether Ketone
pF	picofarad
PIN	Positive-Intrinsic-Negative
PM	Phase Modulation
PPM	Pulse Position Modulation
Ps	Probability of Survival
PSK	Phase-Shift Keying

Q

QA	Quality Assurance
QD	Quadrant Detector

QPPM	Quaternary Pulse Position Modulation

R

RAD	Radiation Absorbed Dose
R&D	Research and Development
RF	Radio Frequency
RFE	Receiver Front End
rms	root mean square
Rx	Receive

S

s	second
SBIR	Small Business Innovative Research
SBR	Space-Based Radar
SDI	Strategic Defence Initiative
SDL	Spectra Diode Labs
SILEX	Semiconductor Intersatellite Link Experiment
SiO_2	Silicon Dioxide
SNR	Signal to Noise Ratio
STS	Space Transportation System

T

TBD	To be determined
TDRSS	Tracking and Data Relay Satellite System
ThF_4	Thorium Floride
Tx	Transmit

U

UK	United Kingdom
U.S.	United States
USA	United States of America
USAF	United States Air Force
UV	Ultravoiolet

V

V	Volt

W

W	Watt
WFD	Wide-Field Detector

Y

YAG	Yttrium Aluminum Garnet

Z

ZnS	Zinc Sulfide
ZrO_2	Zirconium Oxide

This Page Intentionally Left Blank

EXECUTIVE SUMMARY


CAL


EG&G


SPAR

EXECUTIVE SUMMARY

This study, of laser intersatellite links was carried out for the Department of Communications under contract No. 36001-0-3600/01-ST.

The objectives of the nine (9) month study were to:

i) identify and research the technical issues, cost and performance trade-offs of an optical link suitable for typical applications such as RADARSAT and Space Based Radar.

ii) to review Canadian Industries capabilities, and

iii) to develop an approach to establish an optical intersatellite capability in Canada, where feasible.

Spar formed a team to undertake the study comprising CAL Corporation and EG&G with Spar acting as the lead contractor. The total contracted effort was 1,160 man hours, 57% Spar, 34% CAL Corp. and 9% EG&G. Additional effort was provided by each team member.

The technology was reviewed to determine the current state-of-the-art and expected performance improvement for lasers, detectors (both direct detection and heterodyne) and both direct and external modulation. Telescope technology was reviewed and an optimum design selected.

Acquisition and tracking concepts and techniques were reviewed to determine the optimum design and evaluate the expected performance. An optimum acquisition procedure was proposed.

The study looked at link parameters between geostationary satellites and for links to inclined and low earth orbits. Performance comparisons were made between four laser types ranging in wavelength from 0.8 to 10.6 μm and for bit rates up to 1 Gbps.

A comparison between heterodyne and direct detection systems showed that incidental losses associated with heterodyne systems and not with direct detection systems largely counteracted the greater sensitivity of the heterodyne receivers. This is particularly true of the shorter wavelength at which the AlGaAs laser operates. The high sensitivity of modern direct detection receivers is close to that achievable with heterodyne reception and an improved performance was found for the direct detection system compared to the heterodyne receiver.

The direct detection sensitivity degrades at higher bit rates so heterodyne systems are expected to predominate above 1 Gbps. Below 100 Mbps a single laser with direct detection is satisfactory while between 100 Mbps and 1 Gbps wavelength multiplexed AlGaAs lasers are expected to be optimum.

On the basis of the technology study, a preliminary terminal design was carried out. The design included a baseline operating at 100 Mbps and two options to support 1 Gbps.

The baseline used an AlGaAs laser with bias voltage modulation and a direct detection receiver. The first option used for such lasers and receivers with the bit rate of each increased to 250 Mbps to achieve the total of 1 Gbps. The second used a single Nd:Yag laser operating at 1 Gbps combined with a heterodyne receiver. A preliminary layout of the optical path was carried out for each of the three configurations. An electrical block diagram was prepared and discussed.

A comparison of the top level parameters of the three systems is presented in the table below.

	Baseline	Option 1	Option 2
Bit Rate	100 Mbps	1 Gbps	1 Gbps
Laser	one AlGaAs	4 AlGaAs	one Nd:Yag
Detector	direct	direct	heterodyne
Mass (kg)	30	36	39
Power (W)	45	50	72
Dimensions (cm)	36 x 26	38 x 30	45 x 27

A survey of Canadian industry was made to identify those companies with a relevant capability. Detailed discussions were held with those companies identified who also have a space capability. From these it was concluded that the Canadian space industry has the technology base from which to develop a complete optical intersatellite capability. What is lacking is a heritage of space qualifiable products and experimentation from which to proceed.

The study team invited MPB Technologies and SED Systems Inc. to join in preparing an outline program leading to a full OISL capability in Canada.

The group observed that US, Japan and Europe are expending significant efforts in developing data relay satellite systems employing intersatellite links. It was also observed that the market is clearly developing for intersatellite links. Further that an International Working Group on Intersatellite Optical Communications comprising representatives from NASA, NASDA, ESA and CSA had been formed. It will discuss the reasons for taking their particular design approaches and examine the possibility of interoperability and cooperative endeavours.

A major concern of the group was that if Canada does not embark upon a significant development program, then we will have abandoned the market to the industry of other nations. The technology gap is not too wide or impossible to close.

The group developed a possible scenario to address this issue. The objective would be to undertake a domestic optical intersatellite link demonstration program. The program would target cooperative work with international partners but should also address standalone work with international partners. Two possible objectives were identified; to develop either the satellite at the geosynchronous end of the link or a payload terminal at the low earth orbit end.

Two parallel thrusts to meet the objectives are discussed and outlined. They are

(i) to embark upon a mission definition and concept exploration activity for the proposed international initiative and

(ii) to immediately undertake an Optical Link Preparatory Program (OLPP) to provide ongoing technology development, evaluation and demonstration through use of a national test bed.

An overall schedule is presented.

The OLPP would quickly establish industries capabilities and provide the technology development for any international cooperative endeavour. Key areas where useful development could be carried out now are detailed including cost and schedule. Start-up costs are not expected to exceed $2M per year.

In conclusion, the study recommends that Canadian Space Agency give serious consideration to the scenario proposed. Further that it contract with the Spar team to fully define the OLPP and its relationship to a potential international cooperative program anticipated value $250K - $500K. This work would become an input into the Long Term Space Plan.

SECTION 1

INTRODUCTION

1.0 INTRODUCTION

This is the final report on a laser intersatellite link study funded by the Department of Communications under contract 36001-0-3600/01-ST.

The requirements of the study are outlined in Section 1.1 and the potential applications in Section 1.2. Sections 1.3 and 1.4 give an historical perspective and a list of ongoing Optical ISL development programs respectively.

The study of the link parameters is reported in Section 2.0 with detailed graphs of link parameters included in Appendix A.

Section 3.0 discusses the review of optical ISL technology and gives the current or projected performance of ISL components.

The link gains and losses are identified in Section 4.0 for both direct detection and heterodyne receivers and for direct modulation laser diodes and externally modulated gas and solid Nd:Yag lasers. Detailed link budgets are presented in Appendix B for a comparison of heterodyne and direct detection systems and in appendix C for a comparison of laser types and laser wavelengths.

Section 5.0 discusses the acquisition and tracking functions. These important functions are essential before transmission of data can begin. Recent ground tests on the SILEX program have successfully demonstrated adequate performance.

Section 6.0 presents the terminal/conceptual design for the baseline direct detection system operating at 100 mbps and for two options for operation at 1 Gbps. Performance parameters are listed for the baseline system with changes indicated for the two optional systems. A telescope is selected and the optical bench dimensions are established for all three systems. An outline is presented for the electrical system which supports the communications signal and controls the system for acquisition and tracking.

The final sections review Canadian optical capabilities (Section 7.0) and outline a roadmap to achieve a Canadian presence in the optical intersatellite link market.

1.1 Requirements

This section summarizes the requirements of the study listing links, lasers, bit rates and modulation types to be treated. The links considered in the study are:

1) Between Geostationary Satellites

   The maximum separation between satellites has been taken as 120 degrees.

2) Between Geostationary and Inclined Geosynchronous Satellites

   Both 24 hour Tundra type inclined orbits and 12 hour Molnya type inclined orbits have been considered. The intersatellite link is considered operational during the 12 hours for Tundra and 8 hours for Molnya that the inclined orbit satellites are operational.

3) Between Geostationary and Leo Satellites

   Specific low earth orbits are considered and analyzed for a 24 hour period to give the full range of conditions between the two satellites.

Four lasers are considered namely:

1. CO_2 gas laser at 10.6μm
2. InGaAsP laser diode at $\approx$1.55μm

3. Nd:Yag laser at 1.06μm
4. AlGaAs laser diode operating in the range of 0.8 to 0.9μm.

Bit rates ranging up to 1Gbps are considered or specifically:

1. Geostationary to geostationary (1Mbps, 100Mbps, 1Gbps)
2. Geostationary to inclined geostationary (1Mbps, 100Mbps)
3. Inclined geostationary to geostationary (1Mbps, 100Mbps)
4. Geostationary to LEO (19.2Kbps)
5. LEO to geostationary (19.2Kbps, 1Mbps, 100Mbps)

The modulation format is also addressed in the study. Types of modulation considered include:

1. Amplitude shift keying (ASK)
2. Frequency shift keying (FSK)
3. Phase shift keying (PSK)
4. Pulse position modulation (PPM)

In addition to the modulation the type of reception namely direct detection or heterodyne, is considered. A heterodyne receiver has, in general, a higher sensitivity and therefore a greater capability of either a higher bit rate or a greater range for the same laser power and telescope aperture. The penalty for this increased sensitivity is increased complexity due to the requirement of a local oscillator laser at the receiving terminal and much higher requirements for frequency stability and mode purity.

A key element of the laser intersatellite link is the acquisition and tracking system. This is particularly critical since the laser beam widths are very small compared to the pointing uncertainty of the satellite platform supporting the laser terminal.

1.2 Applications

Three intersatellite links are included in the study. This section identifies the possible applications for these intersatellite links.

1.2.1 Geostationary to Geostationary

There are two possible scenarios; the first where the two satellites are close together, such as between Intelsat satellites in the same ocean region and second where the two satellites are in different ocean regions.

When the satellites are in different ocean regions an intersatellite link can be used to establish communications between earth stations on opposite sides of the earth. In this way only one uplink and one downlink are used (in conjunction with the ISL) whereas without an ISL, an intermediate ground station would be required to establish the link.

The use of the intersatellite link therefore requires half the uplink and downlink spectrum and thus conserves this scarce resource. When the satellites are close together, it is not possible to save spectrum in the same way but there may be an advantage because not all satellites in the same region will support links to all ground stations. To communicate between a particular ground station and another ground station may best be done via an intersatellite link. The intersatellite link would make possible more flexible interconnection between ground stations and more efficient use of the spacecraft resources.

1.2.2 Geostationary to Inclined Geosynchronous

A system of inclined orbit satellites is designed to give continuous coverage to a designated region by each of the satellites in sequence. During the operational period of each satellite, that satellite is visible to every part of the designated region. An intersatellite link to a geostationary satellite is not needed to relay data back to a ground station within the designated coverage area.

An intersatellite link might be useful if the geostationary satellite was on the opposite side of the earth from the coverage area for the inclined satellite or if the inclined orbit satellite was used on its pass through perogee in the southern hemisphere when the primary coverage are is in the northern hemisphere.

1.2.3 Geostationary to Low Earth Orbit

This is a very likely application of intersatellite links with a high bit rate data link from the low orbit back through the geostationary satellite to the ground and a low rate command capability from ground to the low orbit satellite. Coverage can be provided for more than half the time using only one geostationary satellite and near continuous coverage from only two. Present low earth orbit satellites such as Radarsat, rely on a single hop downlink to a very few ground stations. Data taken when the satellite is not in contact with one of these stations is stored on a tape recorder for later transmission to the ground. An intersatellite link would provide much more coverage capability and a higher transmission reliability.

Low earth orbit satellites that could benefit from an optical intersatellite to a geostationary satellite are:

1. Radarsat
2. Space Based Radar (SBR)
3. EHF Satcom
4. Space Station Freedom

Radarsat and Space Station Freedom have been analyzed in some detail in this study mainly because Radarsat has a near polar orbit and Space Station Freedom has a low inclination orbit, thus they very nearly span the LEO inclination limits of 0 to 90 degrees. Any other low earth orbit satellite should be encompassed within the range of parameters established for these two satellites.

1.3 Background

1.3.1 Gas Laser Communications Systems

1.3.1.1 Historical Perspective

The Helium Neon laser was the first candidate laser selected for free space laser communication applications. In the mid 1960's the NASA Marshall Flight Centre began designing diffraction limited telescopes and low power HeNe lasers for Optical ISL applications. Meanwhile at NASA Goddard, the CO_2 laser was suggested as a potential source for a deep space mission.

In the late 1960's NASA Goddard was working on the development of a CO_2 laser communication system which was schedule to be launched on the ATS-F and ATS-G Advanced Technology Satellites. Due to technical and funding problems this program was cancelled a year after contract award [1].

In the early seventies Hughes began working on 300 Mbps CO_2 system which was also cancelled when NASA abandoned all advanced communications per direction from the US Congress.

More recently the European Space Agency (ESA) has been funding the development of CO_2 lasers for space communications applications. Recent reports however, indicate that this development has been curtailed, having been superseded due to the success of parallel laser diode and diode pumped Nd:Yag laser development programs [2].

For more exotic applications such as satellite to submarine communication, DARPA and the US Navy have funded several development programs. Due to the limited transmission spectral bandpass, unconventional laser sources have been considered. In particular raman shifted Xeon Chloride gas lasers are a primary candidate. Recent reports indicate that advanced engineering for space qualified transmitters will begin sometime in the early 1990's [86]

1.3.1.2 The Fundamentals of CO_2 Laser Communications Systems

Most CO_2 Laser communication systems employ heterodyne or homodyne detection to achieve the required quantum limited sensitivity. The lack of low noise, high frequency detectors along with the high background photon flux in the 10μm region has prevented the use of CO_2 lasers in a direct detection configuration. Heterodyne receivers include the mixing of the optical signal with an optical local oscillator (LO) to downconvert the mixed output to an intermediate signal (LO frequency different than transmitting laser frequency). Homodyne receivers are similar except the mixed output is converted at the baseband frequency (LO frequency same as transmitting laser frequency). A schematic block diagram for a CO_2 based communication system, designed by ESA researchers, is illustrated in Figure 1-1. The more complex homodyne system was selected over the heterodyne system because of the limited available bandwidth of today's HgCdTe detectors [42]. For a given baseband bandwidth Bb, the required detector bandwidth B equals Bb for homodyne systems and 4 to 5 Bb for heterodyne systems. Since IR detector technology is typically limited to 1-2 GHz bandwidths, only Homodyne techniques can be employed for extremely wideband systems (1 GBit/s).

Table 1-1 summarizes the advantages and disadvantages associated with CO_2 based communication system. The relatively high output power of the laser and the high sensitivity and maturity of 10μm heterodyne receiver technology are definite advantages. Furthermore, the longer operating wavelength generates a relatively large beamwidth substantially reducing the pointing and tracking requirements. Wavelength multiplexing is also possible due to the spectral line tunability of the optical source [3].

To support the development of CO_2 laser communication systems ESA has funded the fabrications of a laboratory breadboard system. Figure 1-2 illustrates the configuration employed [2]. An examination of this figure and Figure 1-1 reveals that many of the components which constitute a CO_2 laser communication system are also common to most laser communication systems. Unique components include:

1. the transmitter laser,
2. the local oscillator,
3. the external transmitter laser modulator,
4. the acousto-optic frequency modulator frequency compensation
5. the associated RF and DC power supplies,

Table 1-1 Advantages & Disadvantages of CO_2 Laser Based Communications Systems

	ADVANTAGES
1.	High laser output power available.
2.	High sensitivity & maturity of 10μm heterodyne receiver technology.
3.	The longer operating wavelength generates a relatively large beamwidth substantially reducing the pointing & tracking requirement.
4.	Wavelength multiplexing is possible due to the spectral line tunability of the optical source.
5.	Heterodyne detection at 10μm reduces the impact of solar background induced detector noise.
6.	Compared with 0.8 and 1.1μm systems, 10.6μm systems have reduced sensitivity to sun radiation induced noise.
7.	Beacon lasers can be tuned to operate on a different wavelength (9.2 vs 10.6μm) to improve the channel isolation & system noise performance.
	DISADVANTAGES
1.	Long term life & reliability of the laser and modulators are still unproven.
2.	Direct detection laser diode systems are lighter, more compact and require less power than CO_2 laser systems.
3.	Cryogenic cooling of the detectors is required.

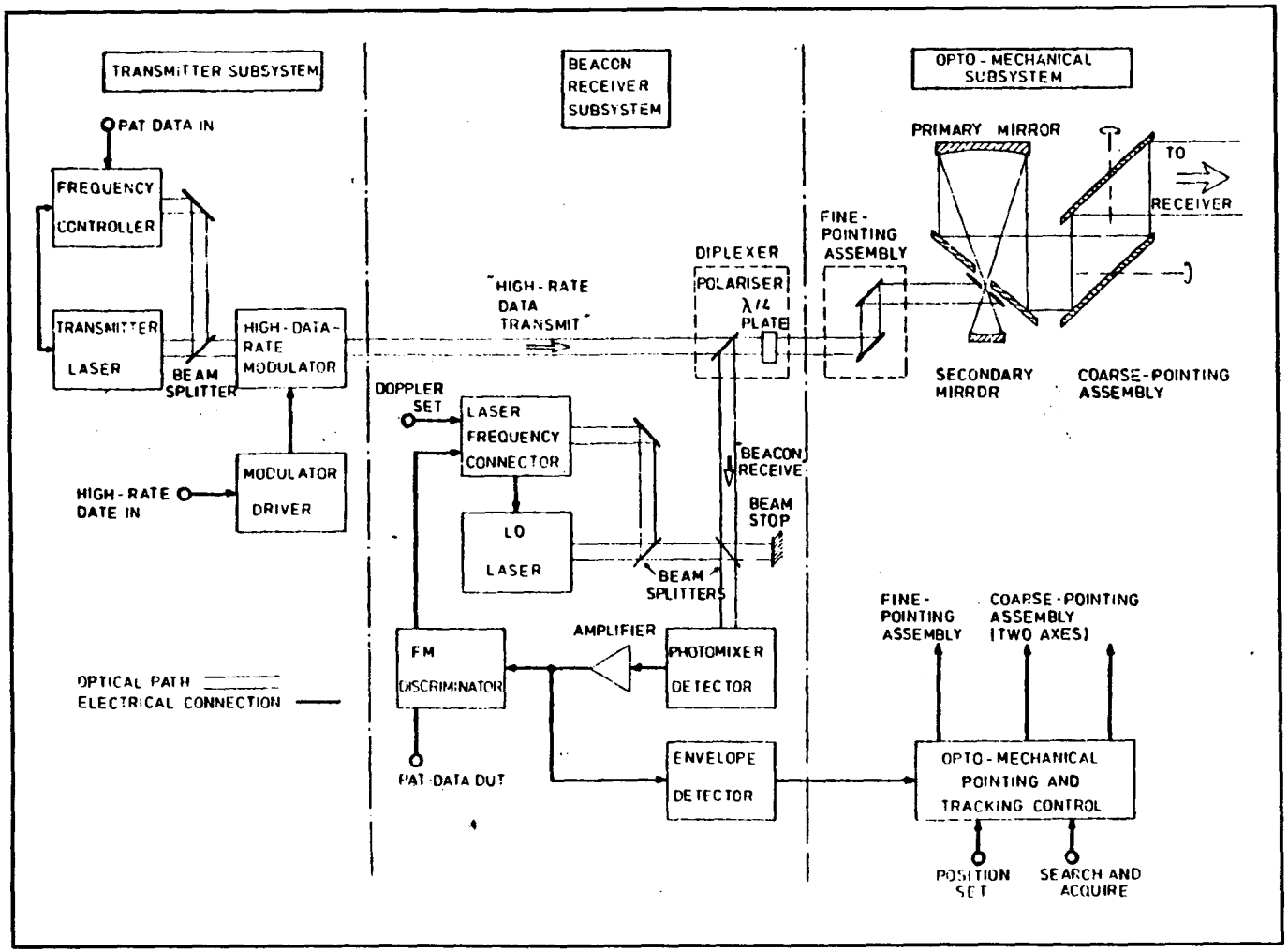

Figure 1-1a Laser Transmit-Terminal Block Diagram

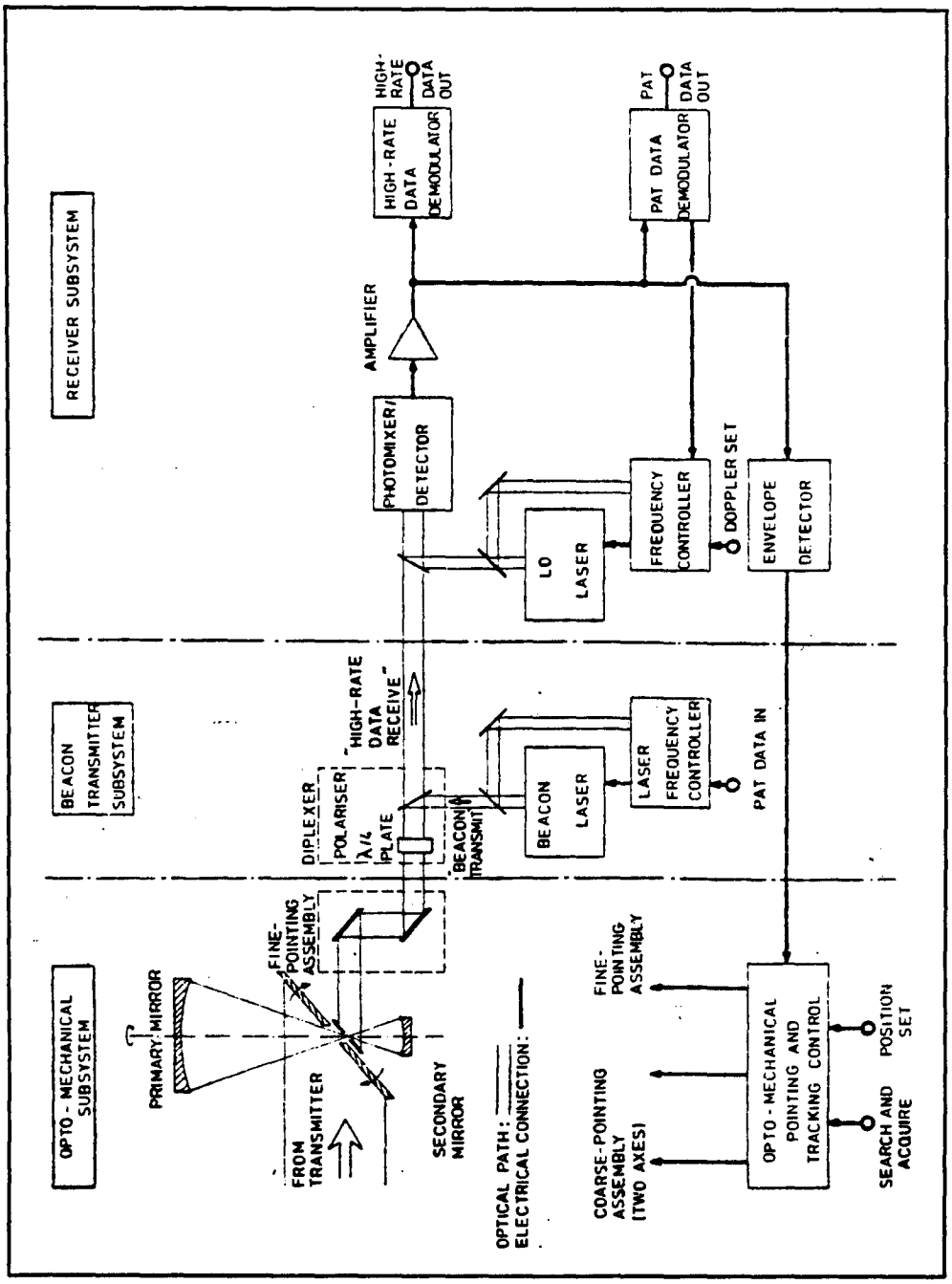

Figure 1-1b Laser Receiver Terminal Block Diagram

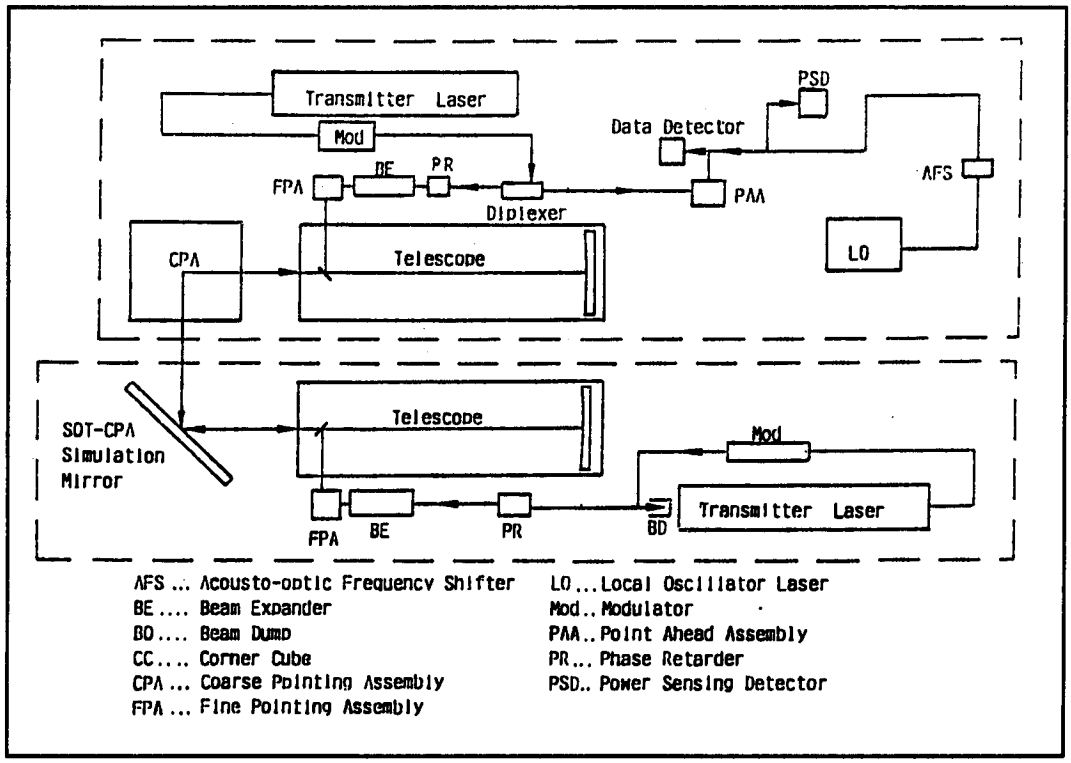

Figure 1-2 Laboratory Breadboard Laser System

6. the infrared detector. Typically, a HgCdTe photovoltaic detector, operating at 10μm and cooled passively to 100K, is employed. Space qualified mechanical cryogenic coolers are also available with a demonstrated five year life.

7. the power sensing diode.

The technology issues associated with each of these devices will be discussed in detail in the following sections.

1.3.2 Solid State Laser Communication System

1.3.2.1 Historical Perspective

In the late 1960's the Air Force Avionics Lab and NASA Goddard began funding the development of direct detection Nd:Yag communication systems.

In the early 1970's the Air Force 405B program developed a communication system concept based upon the mode locked doubled Nd:Yag laser and the CW single frequency doubled Nd:Yag laser system. This program also included component development combined with an engineering model which demonstrated 1 μradian tracking accuracy. A space flight test for this program was contracted in 1975 but it ran into funding problems in 1978. After restructuring, an aircraft to ground test program (AFTS) was defined. This program was funded to completion and very successful tests were run in 1980 demonstrating reliable acquisition and tracking at data rates up to 1 Gbits/sec over 100 Km distances.

The success of the AFTS program in 1980 led to a full scale development program. Although indications are that production is ongoing for an operational DOD system, the classified nature of this work has limited publication in the open literature. McDonnell Douglas has heavily invested in this technology in conjunction with the DSP Crosslink production program

(1984) and the BSTS pre FSD Crosslink program (1989). Both of these projects employ diode pumped Nd:Yag lasers operating at data rates of 1 and 10 Mbits/sec respectively over a 80,000 km distance [91].

However, parallel civilian activities funded by NASA Goddard have led to the development of diode pumped Nd:Yag laser sources [87]. Also JPL is developing a deep space laser communication system using a Q-switched Nd:Yag operating at both 1.06 and .532 μm [89]

1.3.3 Semiconductor Laser Communication Systems

1.3.3.1 Historical Perspective

Semiconductor laser transmitters for space based communication systems are a relatively recent addition to space based communication system design. In the early 1980's development of space qualified laser diodes began. The advantages of A1GaAs/GaAs lasers such as small size and weight, low power consumption, high efficiency and decreased system complexity had long been recognized but poor reliability and low power output limited their usefulness.

One of the earliest programs to develop a space qualified diode laser transmitter was ESA's SILEX project. In this design a .8 μm AlGaAs laser diode will be employed with a peak power of 120 mW.

To address the primary disadvantages of low power and low operating life a variety of NASA, ESA and US Airforce program have been initiated. further discussion of diode laser technology can be found in section 3.1.2 of this report.

1.4 Ongoing Optical ISL Development Programs

Free space communications at optical frequencies is being aggressively developed by many groups around the world. The following lists identifies some of the programs currently under development:

a) SILEX: The Semiconductor Intersatellite Link Experiment Program was established by ESA to permit the demonstration of an interorbital link between SPOT IV and ARTEMIS using a .8μm diode laser.

b) Japans ETS VI Program: The Japanese Engineering Test Satellite-VI will carry an optical payload designed to establish the basic technology for an optical communication system. The communication link will employ a .8μm laser for the downlink and an Argon gas laser for the uplink.

c) The US Advanced Communication Technology Satellite (ACTS) which, until recently, incorporated MIT's Laser Intersatellite Transmission Experiment (LITE) coherent system (NASA and Air Force funded) and GSFC's Direct Detection Laser Transceiver (DDLT) program.

d) To address the different technical and political issues NASA Goddard has divided its overall optical communications program into four different project areas:

   1. Research and Technology
   2. Flight System Development and Demonstration (FSDD)
   3. Laser Communication Transceiver (LCT)
   4. Small Business Innovative Research (SBIR) and small research grants.

e) SDI's Brilliant Pebbles; Brilliant Pebbles is a classified project involving the deployment of a small optical communication terminal on 50 to 100 different satellites.

f) DARPA/US Navy Satellite Submarine Communication System (Submarine Laser Communication Satellite SLCSAT).

g) JPL's Deep Space Communication System

h) BAE's Small Optical user terminal funded in part by ESA.

i) US Laser Crosslink Program (See attached Figure 1-3 illustrating a Telescope design by Kodak for MDAC).

j) Other US programs (Classified/Unclassified) See the attached Figure 1-4 illustrating a 4 channel Cassegrain Telescope with a channel splitter followed by refractive optics for each channel. The four transmitters are refractive lenses mounted in titanium housing for athermalization.

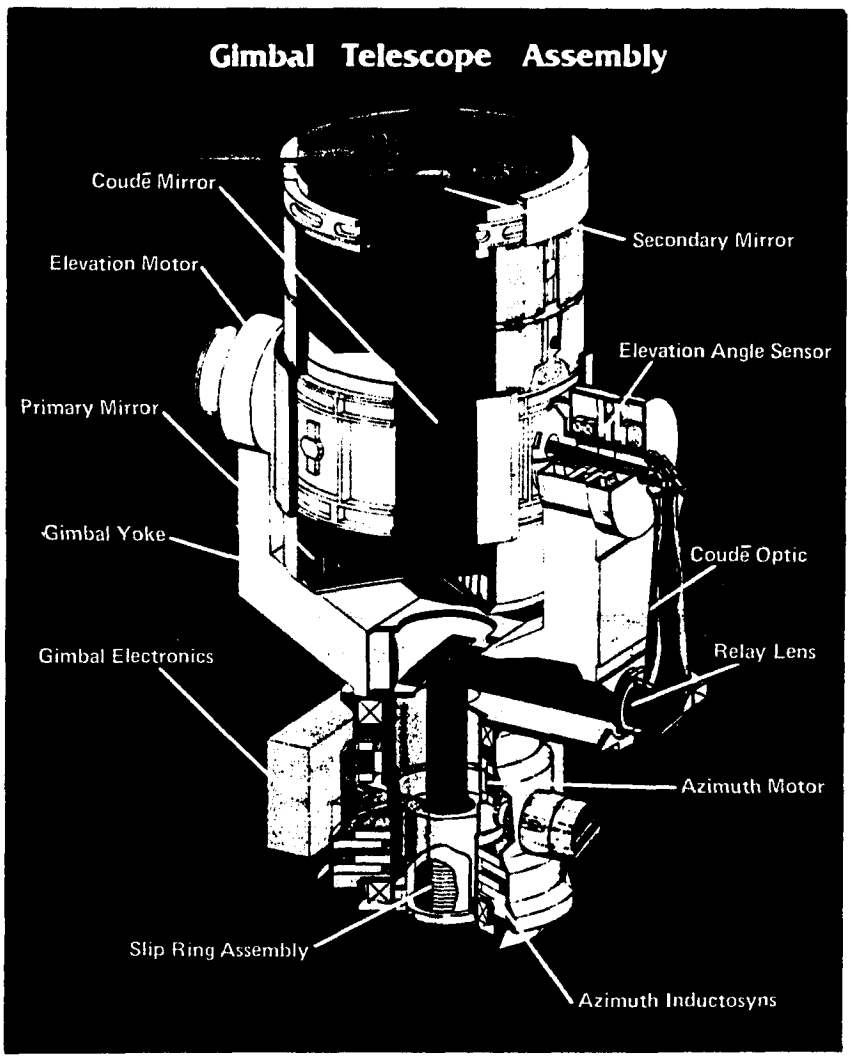

Figure 1-3 Illustration of a Typical Spaceborne Optical Communications Telescope Designed by Eastman Kodak

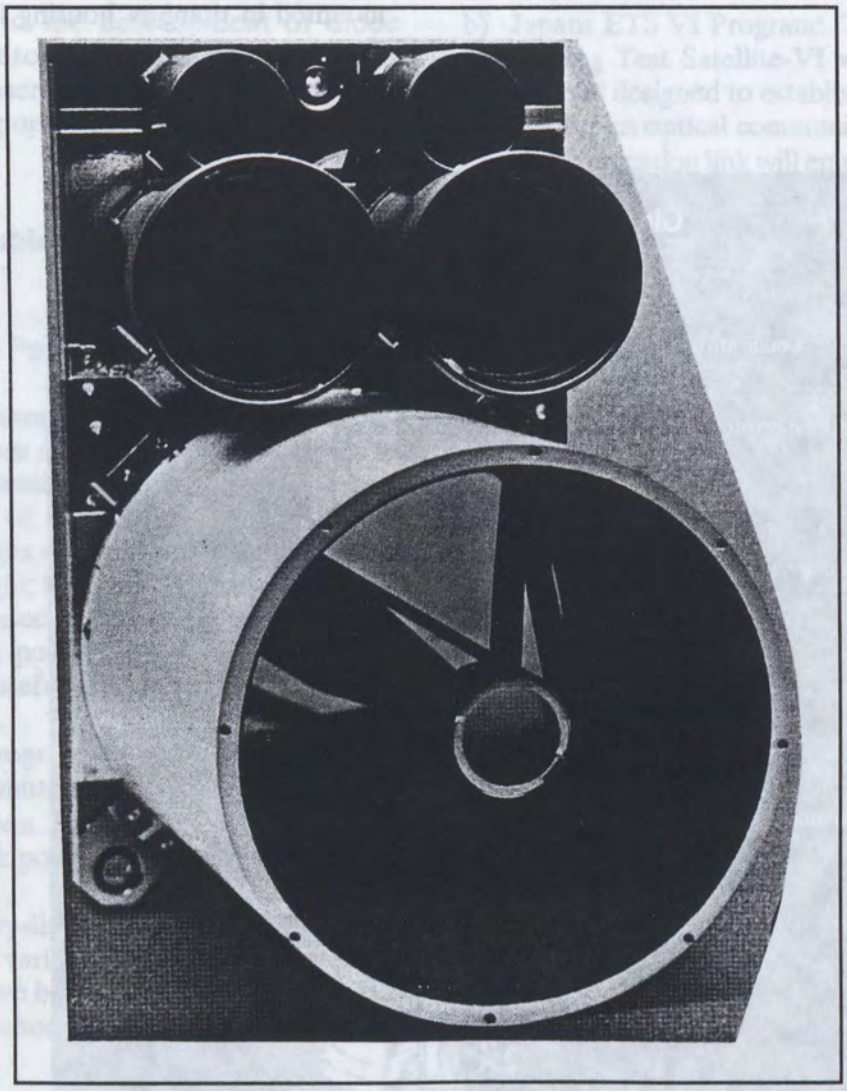

Figure 1-4 A Four Channel Cassegrain Telescope with Refractive Optics

SECTION 2

OPERATIONAL ANALYSIS

2.0 OPERATIONAL ANALYSIS

This section describes the analysis of the three links under study namely;

1) Geostationary to geostationary

2) Geostationary to inclined geosynchronous

3) Geostationary to low earth orbit

There are two inclined geosynchronous orbits, a Molniya type 12 hour orbit and a tundra type 24 hour orbit. There are also two low earth orbits considered namely the Radarsat orbit which is representative of near polar orbits and the Space Station Freedom orbit which is representative of lower inclination orbits. Plots of the link parameters for these links are given in Appendix A.

The orbit parameters used for these orbits are listed in Table 2.0-1.

The link parameters investigated are those which affect the link. These are described below with reference to figures 2.0-1 to 2.0-9 for the link between a geostationary satellite at -90 degrees longitude and Radatsat. The ground trace for Radarsat is shown in Figure 2.0-1.

1) Range

The range (distance between the two cooperating stations) determines the space loss and is a critical parameter in the link design. This is shown for the Radarsat/GEO link in Figure 2.0-2.

Table 2.0-1 Laser ISL Orbital Elements

Geostationary Satellites	EHF Satcom	Tundra	Molniya
a = 42164.54 km e = 0 i = 0 deg raan = 90, 0, +90 deg w = 0 deg v = 0 deg	a = 42164.54 km e = 0 i = 0 raan = TBD w = 0 deg v = 0 deg	a = 42164.17 km e = 0.24917 i = 63.435 deg raan = 0 deg w = 270 deg v = 0 deg	a = 26561.76 e = .722227 i = 63.435 deg raan = 110 deg w = 280.2 deg v = 0 deg
Radarsat (LEO near pole)	Space Station Freedom (LEO near equator)	SBR (tentative)	
a = 7167.055 e = 0.00115 i = 98.556 deg raan = 270 eg w = 90 deg v = 0 deg	a = 6841.14 km e = 0 deg i = 28.5 raan = 0 deg w = 0 deg v = 0 deg	a = 7378. km e = 0 i = 90 raan = arbitrary w = 0 v = 0	

Legend:
a = semi-major axis
e = eccentricity
i = inclination
raan = right ascension of the ascending node
w = argument of perigee
v = true anomaly

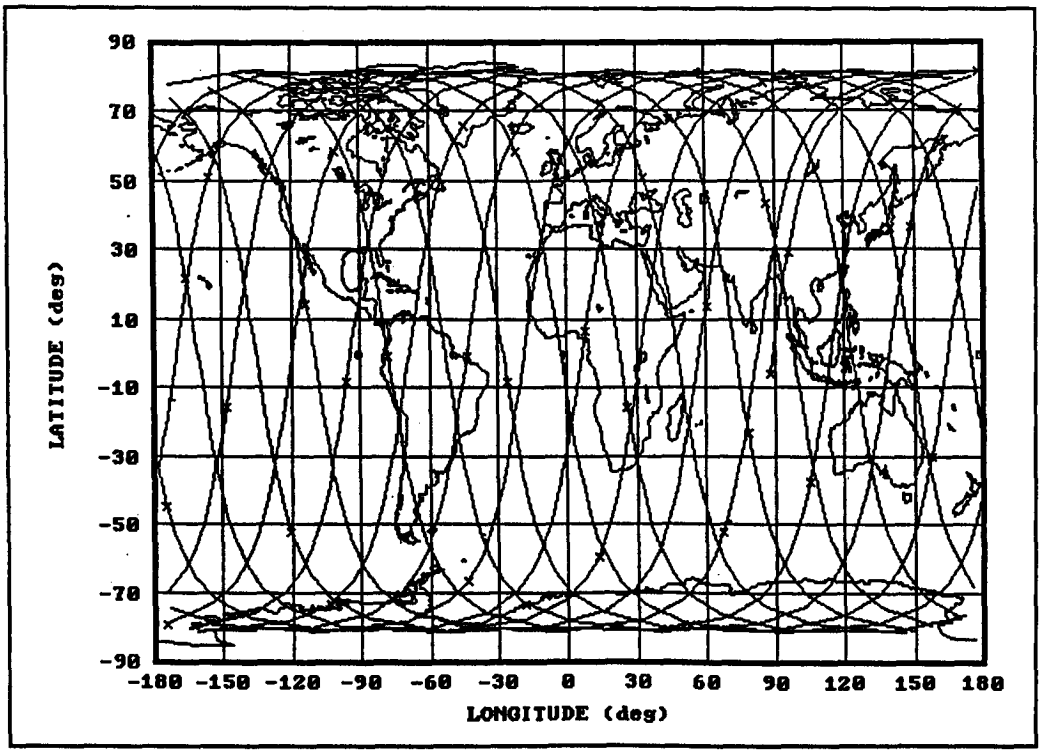

Figure 2.0-1 The Ground Trace of Radarsat over a 24 Hour Period

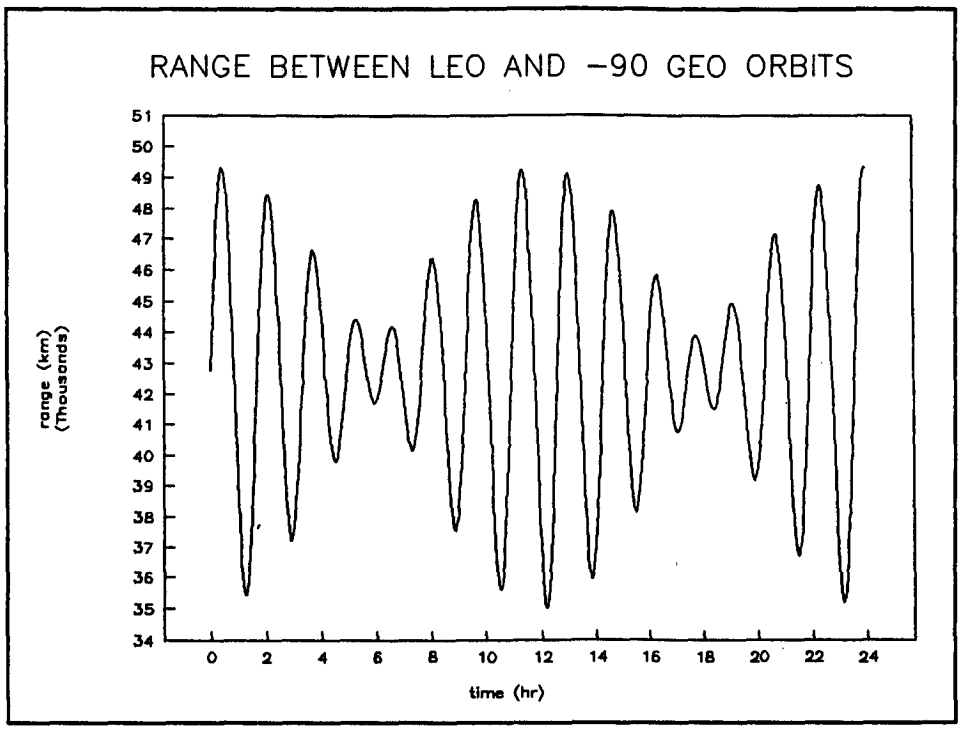

Figure 2.0-2 Range Between Radarsat and a Geostationary Satellite at -90° Longitude

2) Range Rate

The rate at which the range changes in km/sec introduces a doppler shift into the received signal. This is immaterial for a direct detection system but does impact a heterodyne or homodyne system. The range rate for the GEO/Radarsat link is given in Figure 2.0-3.

3) View Angles

Each terminal of the link must have the capability of pointing its telescope at the cooperating terminal. The range of angles encountered is thus an important parameter. The calculated angles depend upon the coordinate system assumed. For the geostationary satellite in the LEO/GEO link, the coordinate system assumed has one axis pointing east, one pointing north and the angles are measured in pitch and roll. For the cooperating low earth orbit satellite it is assumed that the coordinate system has one axis pointing to the zenith and one axis normal to zenith and the angles are measured in azimuth and elevation. Azimuth is measured from the velocity vector.

For the satellite in the inclined molniya or tundra orbit the same coordinate system is assumed as for the low earth orbit satellite with angles measured in azimuth and elevation. However, the inclined orbit satellites are unlikely to be flown in this manner. For example, the configuration chosen for the Archimedes satellites caused it to rotate about an earth-satellite line to enable it to keep the solar panels facing the sun. Molniya, on the other hand is believed to rotate about a satellite - sun line in order to keep the solar array pointing at the sun. The actual angular range required of the ISL telescope will be different for these two cases and in fact both will be different from the selected case. It will be necessary to adjust the computed angles once the satellite configuration has been chosen. For Molinya and Tundra links the angles are measured in azimuth and elevation with the azimuth axis pointing at the center of the earth. Plots of

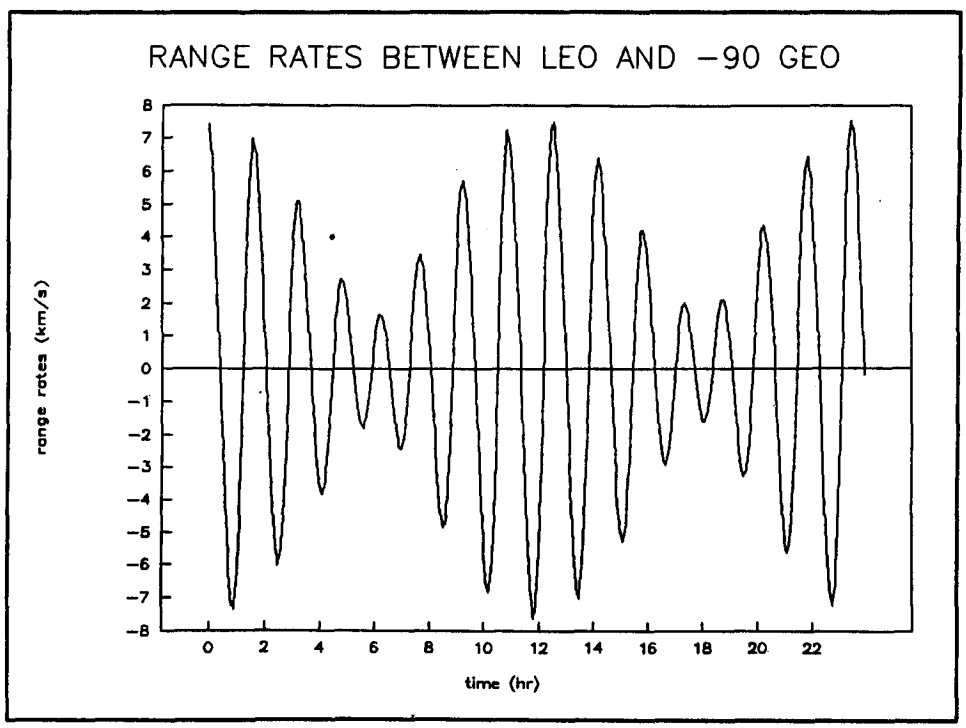

Figure 2.0-3 Range Rate Between Radarsat and a Geostationary Satellite at -90° Longitude

the angles on the geostationary satellite pointing at Radarsat are given in Figures 2.0 - 4a, b and c. The first (a) shows roll as a function of pitch while the other two give pitch and roll as a function of time for a 24 hour period. Figures 2.0-5a, b and c give azimuth and elevation for the Radarsat terminal.

4) Rate of Change of Pointing Angle

The laser terminal has two pointing mechanisms, a course pointing mechanism consisting of the motor driven 2 axis gimbals, and a fine pointing mechanism consisting of electrically driven pointing mirrors. The fine pointing mechanism is used exclusively while it is in range and the course pointing mechanism is only used when the beam is close to the limit of capability of the fine pointing mechanism. The rate of change of angle determines the time interval between motions of the course pointing mechanism. Angular rates for the geostationary terminal are given in Figures 2.0-6a and b and for Radarsat in Figures 2.0-7a and b.

5) Look Ahead Angle

Because the satellites are in motion the direction in which the transmit beam is pointed is different from the direction that the receive beam is pointed. In the case of laser systems the beam width is very narrow, of the same order as the difference between the transmit and receive beam directions, and the beam pointing must be compensated for this effect. The look ahead angle for the geostationary satellite as a function of time is given in Figure 2.0-8 and in Figure 2.0-9 for Radarsat.

2.1 Geostationary to Geostationary Links

This is a fairly simple case in that all link parameters are fixed for any two satellites and depend only upon the angle between the orbital slots.

The range is just the cord across from one satellite to the other given by the equation.

$$R = 2L \sin \theta/2$$

where R is the distance between satellites
L is orbital radius
θ is the angle between the satellites

This is plotted against the angle θ in Figure A.1-1. For geostationary satellites the range is fixed and the range rate is zero.

The pointing requirements are for $\pm$ 90° in pitch and enough in the roll axis to accommodate satellite attitude errors. The rate of change of the pointing angles are nominally zero, except for the need to compensate for the satellite pointing errors. While the range and angles are fixed, the satellites are in constant motion and the transmit beam points in a different direction than the receive beam.

The look ahead angle for Satellite A is calculated by multiplying the component of velocity of the cooperating Satellite B normal to the line of sight by the propagation time for a double pass of the link. This gives the normal component of the distance travelled by the Satellite A in the time it takes a signal to leave the cooperating station and return to that station. To obtain the look ahead angle this distance is divided by the distance between the two terminals. Thus the look ahead angle is given by the equation.

$$A = 2Vn \times T/R$$

where Vn is the component of velocity of the cooperating terminal normal to the line of sight.
T is the propagation delay between the two stations
R is the distance between the two stations.

Since T = R/C where C is the velocity of light

$$A = 2\,Vn/C$$

For the geostationary case

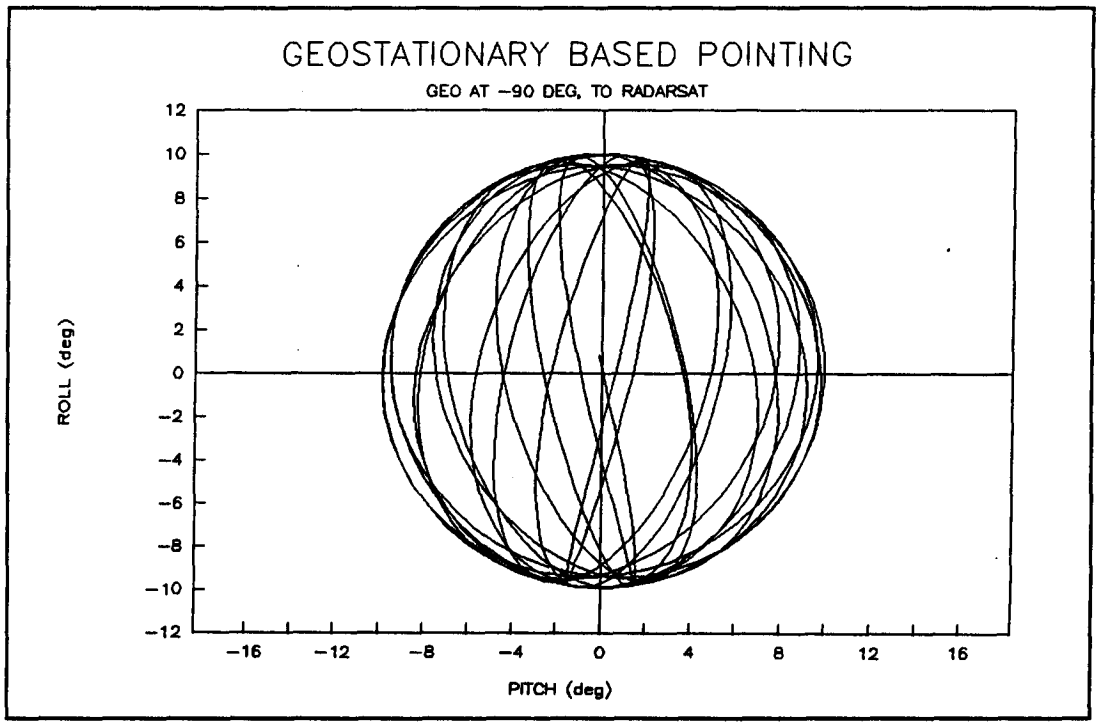

Figure 2.0-4a Pointing Angles over a 24 Hour Period of the Terminal on the Geostationary Satellite at -90° Longitude Required To Point At Radarsat

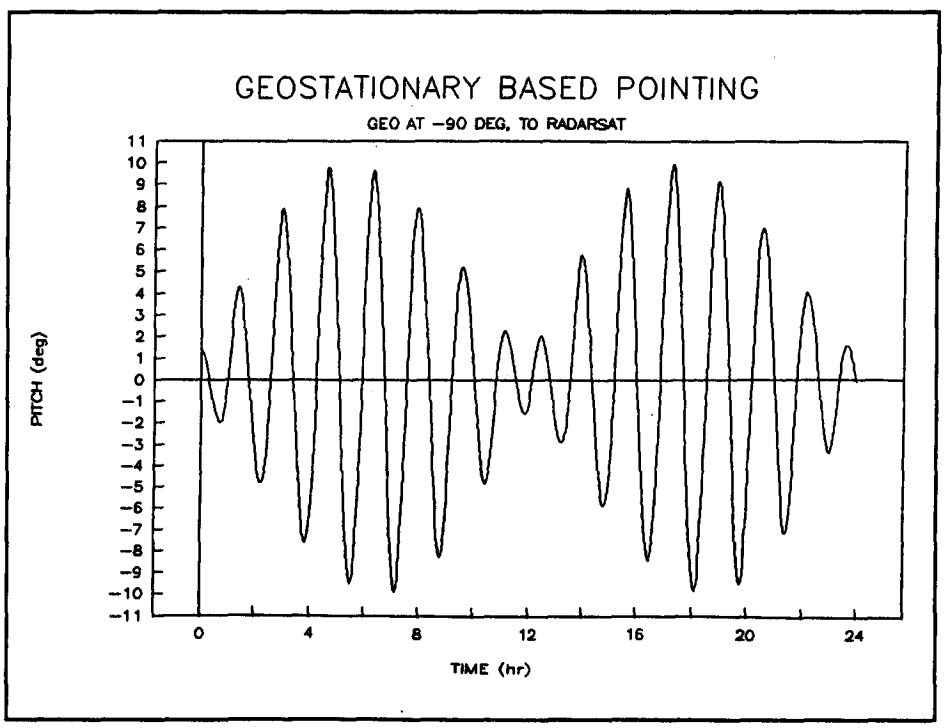

Figure 2.0-4b Time Variation of Pitch Angle on a Geostationary Satellite at -90 Degrees Longitude Required to Point at Radarsat

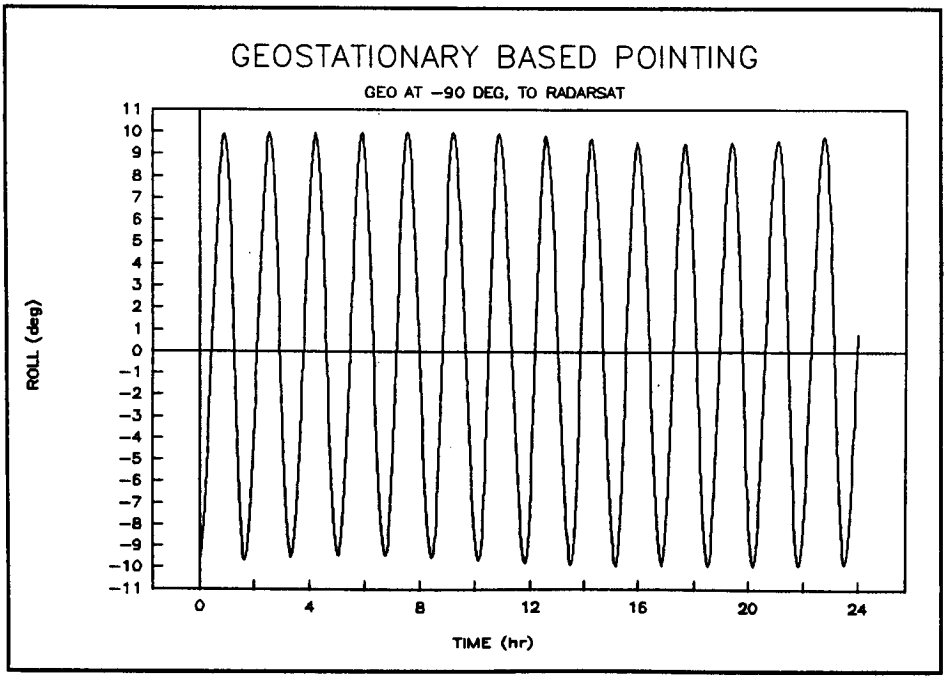

Figure 2.0-4c Time Variation of Roll Angle on a Geostationary Satellite at -90 Degrees Longitude Required to Point at Radarsat

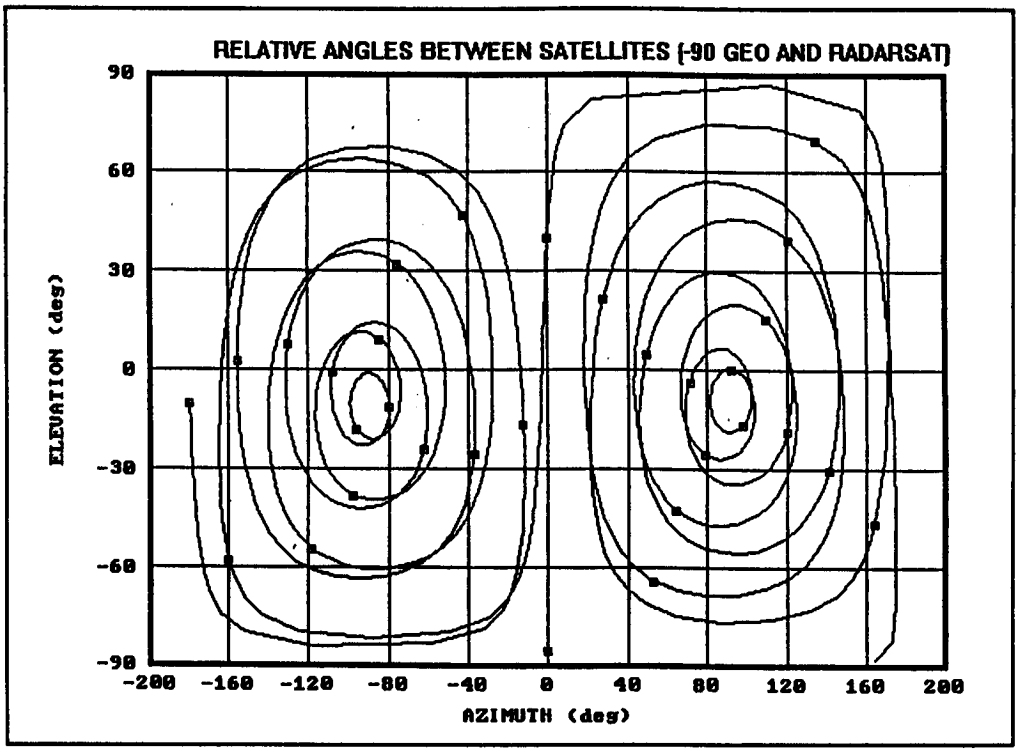

Figure 2.0-5a Pointing Angle over a 24 Hour Period of the Terminal on Radarsat Required to Point at a Geostationary Satellite at -90° Longitude

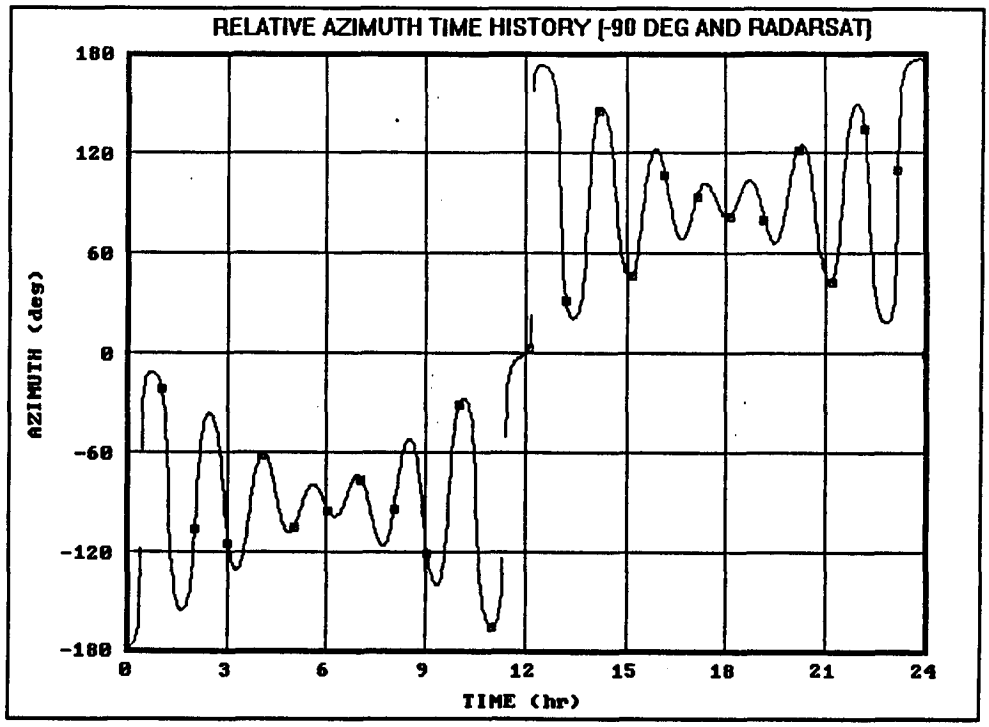

Figure 2.0-5b Azimith Angle on Radarsat, Measured from the Velocity Vector, Required to Point a Geostationary Satellite at -90° Longitude

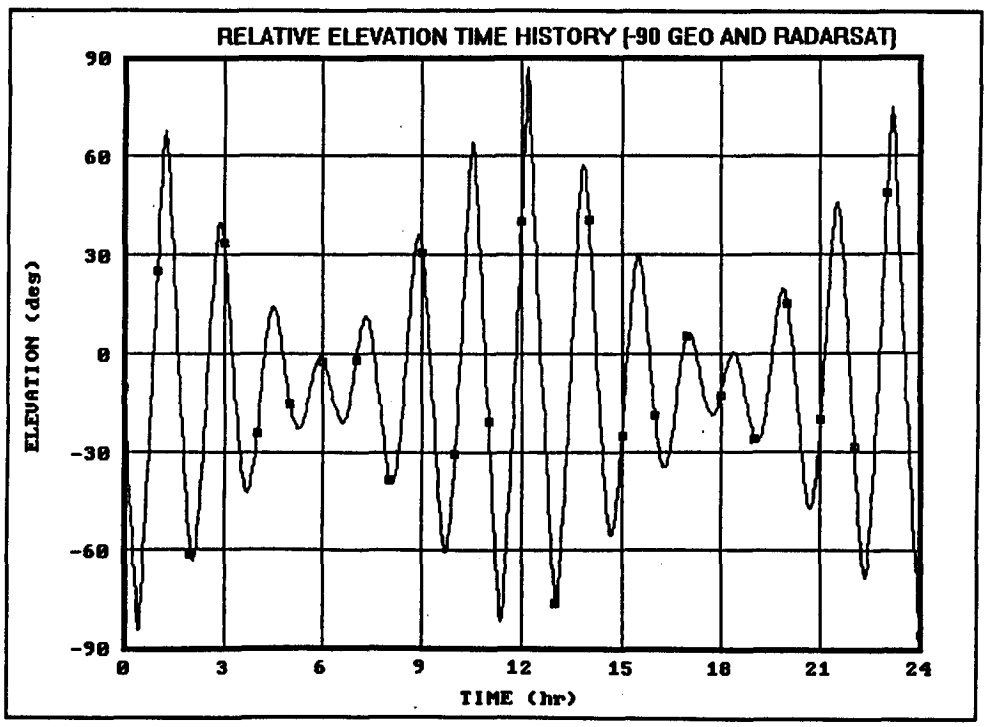

Figure 2.0-5c Elevation Angle on Radarsat Required to Point to a Geostationary Satellite at -90° Longitude

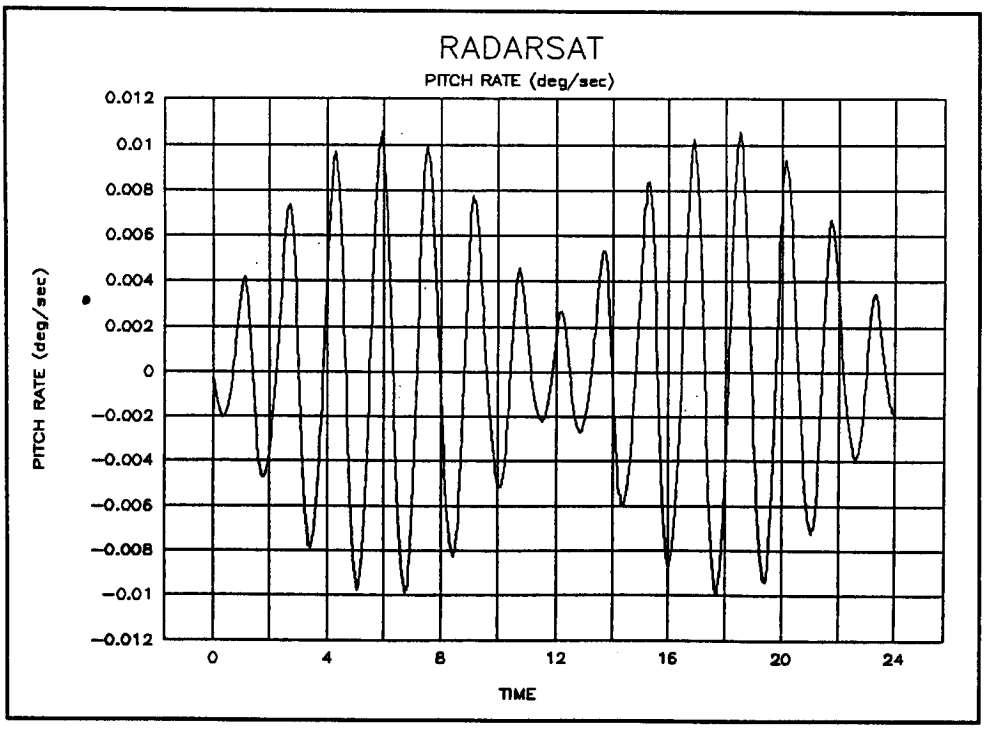

Figure 2.0-6a Rate of Change of Pitch for the Terminal on a Geostationary Satellite at -90° Longitude when Pointing at Radarsat

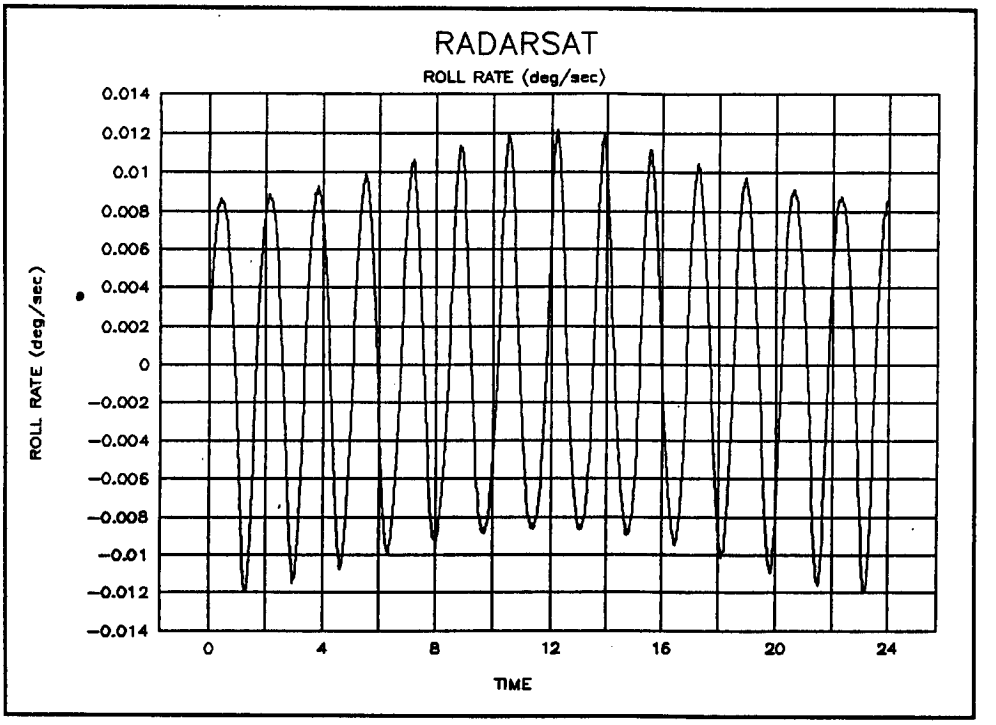

Figure 2.0-6b Roll Rate of Change for the Terminal on a Geostationary Satellite at -90° Longitude when Pointing at Radarsat

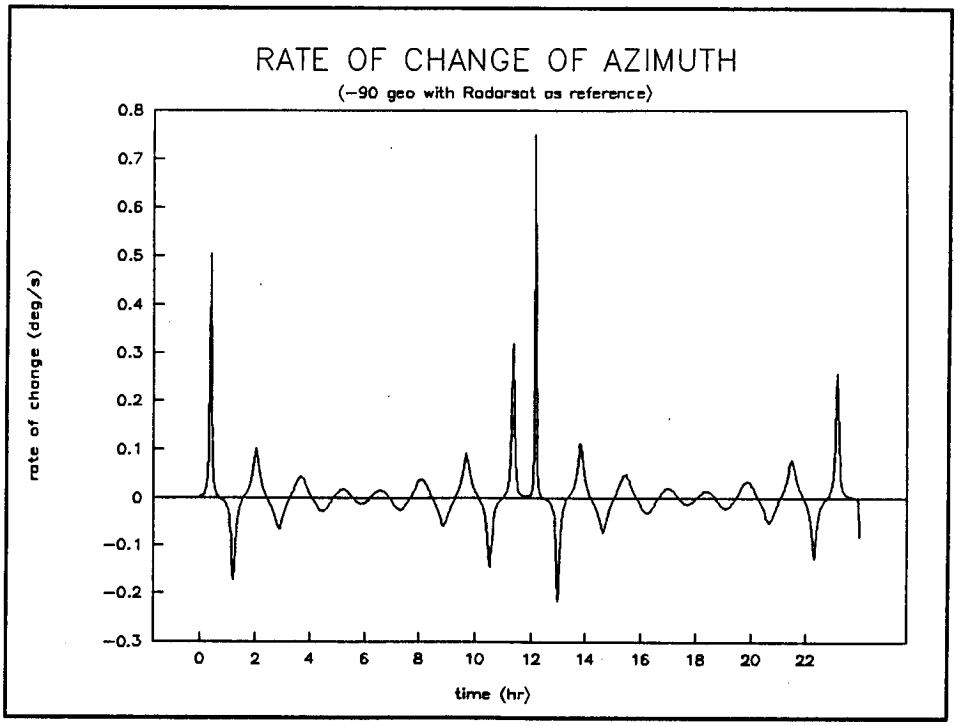

Figure 2.0-7a Rate of Change of Azimuth for the Terminal on Radarsat when Pointing at a Geostationary Satellite at -90° Longitude

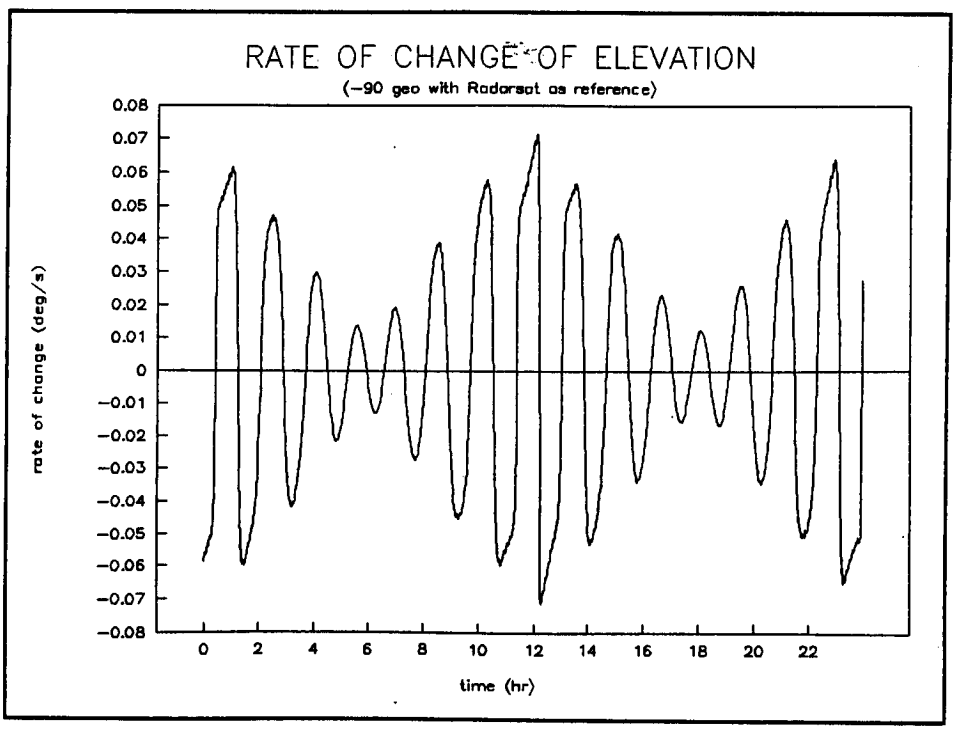

Figure 2.0-7b Rate of Change of Elevation for the Terminal on Radarsat when Pointing at a Geostationary Satellite at -90° Longitude

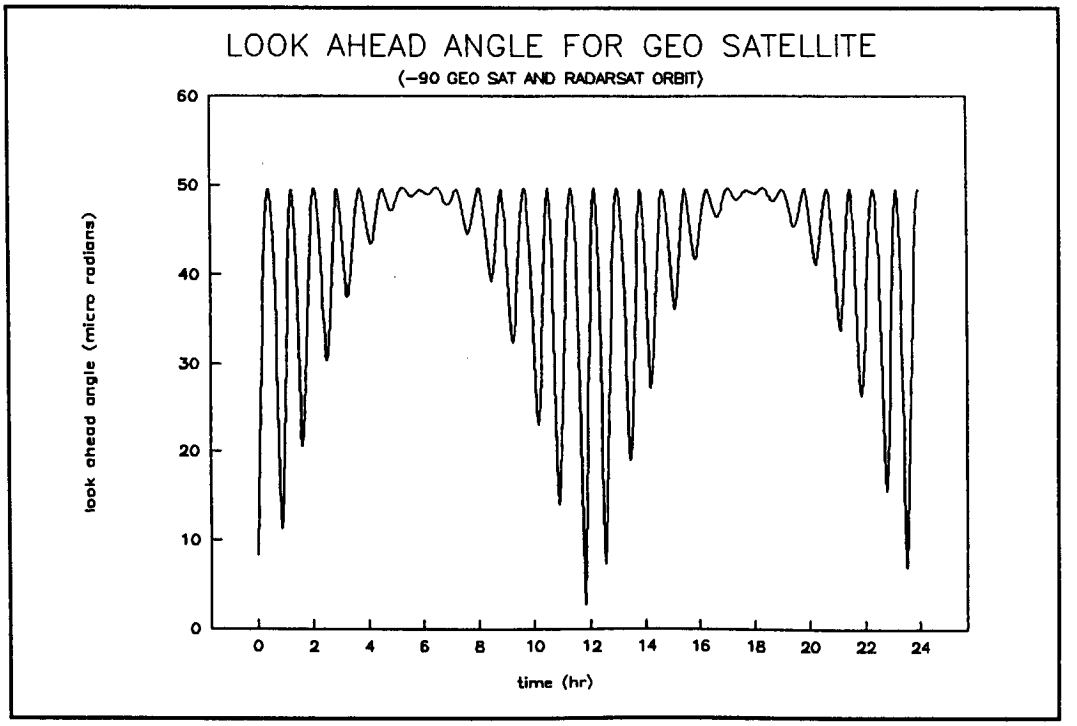

Figure 2.0-8 Look Ahead Angle over a 24 Hour Period for the Terminal on the Geostationary Satellite at -90° Longitude when Pointing at Radarsat

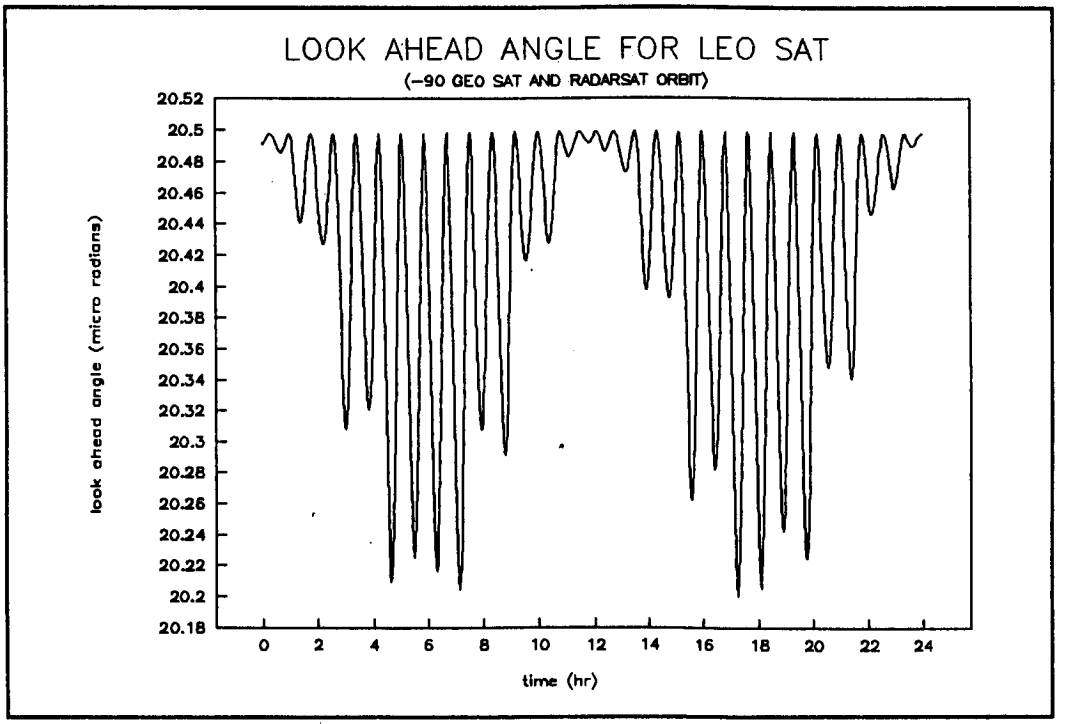

Figure 2.0-9 Look Ahead Angle over a 24 Hour Period for the Terminal on Radarsat when Pointing at the Geostationary Satellite at -90° Longitude

$$Vn = Vo \sin \theta/2$$

where Vo is the velocity of the satellite in the geostationary orbit
θ is the angle between the two satellites

The range between two geostationary satellites is shown in figure A.1-1 as a function of the angle between them. Similarly the look ahead angle is given in figure A.1-2 as a function of the same angle. The maximum values of all parameters are given in table 2.1-1 assuming a maximum separation of 120 degrees and neglecting contributions of satellite positional and attitude errors.

2.2 Geostationary to Inclined Orbit Links

2.2.1 Molniya Type Orbit

Link parameters between the molniya orbit satellite and geostatinary satellites at -90,0 and +90 deg. longitude are presented in Appendix A section A.2.1. The maximum values of the parameters are listed in Table 2.2-1.

2.2.2 Tundra Type Orbit

Link parameters between the Tundra orbit satellite and geostationary satellites at -90,0 and + 90 degrees longitude are presented in Appendix A section A.2.2. The maximum values of the parameters are listed in Table 2.2-2.

2.3 Geostationary to Low Earth Orbit Links

Link parameters between Radarsat and a geostationary orbit at -90 deg longitude are presented in Appendix A, Section A3.1. Those for Space Station Freedom are presented in Section A.3.2.

The maximum values of parameters are listed in Table 2.3-1 for links between a geostationary satellite at -90° longitude and both Radarsat and Space Station Freedom.

Table 2.1-1 Values of Parameters for the Geostationary to Geostationary Link for a Maximum Separation of 120 Degrees Longitude

PARAMETER	VALUE
Maximum avc (deg) between Satellites	120
Maximum Range (1000 km) between Satellites	73
Maximum Range Rate (km/sec) between Satellites	0.0
Pointing limits (degs)on each satellite	pitch ± 30 to ± 90 roll ± 0.0
Maximum rate of change of pointing angle (deg/sec) for each satellite	0.0
Maximum look ahead angle (microradians) on each satellite	17.8

Table 2.2-1 Maximum Values of the Parameters, During the Operational Period, for the Link Between a Geostationary and a Molniya Type Satellite

	First Apogee	Second Apogee
Maximum Range (x1000 km) from Geostationary Satellites at:		
-90° long	45.8	76.1
0° long	62.0	62.5
+90° long	76.1	45.5
Maximum Range rates (km/s) from Geostationary Satellite at:		
-90° long	+1.81, -1.65	+1.25, -1.54
0° long	+1.05, -1.10	+1.78, -1.77
+90° long	+1.25, -1.25	+1.77, -1.67
Pointing limits (degs) on a Geostationary Satellite at:		
-90° long	AZ 88, 106 EL -45, -26	AZ 71, 90 EL -68, -57
0° long	AZ 117, 140 EL -58, -42	AZ 38, 63 EL -53, -42
+90° long	AZ 71, 90 EL -68, -57	AZ 88, 106 EL -45, -26
Pointing limits (degree) on the Molniya Orbit Satellite for Geostationary Satellite at:		
-90° long	AZ -123, -13 EL +45, -34	AZ +60, +167 EL -67, -57
0° long	AZ -37, + 64 EL -47, -39	AZ +144, -116 EL -47, -29
+90° long	AZ +57, + 167 EL -67, -57	AZ -120, -12 EL -35, +3
Maximum rate of change of pointing angle (deg/sec) on a Geostationary Satellite at:		
-90° long	AZ - .0011, + .0035 EL -.0052, + .0034	AZ - .0035, +.0017 EL - .0021, +.0023
0° long	AZ -.0029, + .0037 EL - .0023 + .0024	AZ -.0011, + .0011 EL -.0021 + .0021
+90° long	AZ - .0035, +.0017 EL -.0021, + .0022	AZ -.0017, + .0035 EL -.0053, + .0037

Table 2.2-1 Maximum Values of the Parameters, During the Operational Period, for the Link Between a Geostationary and a Molniya Type Satellite (cont'd)

	First Apogee	Second Apogee
Maximum rate of change of pointing angle (deg/sec) on the Molniya orbit satellite for a geostationary satellite at:		
-90° long	AZ +.0027, +.0052 EL -.0065, + .0082	AZ +.0027, +.0052 EL -.0006, +.0012
0° long	AZ +.002, + .0035 EL -.0013, .001	AZ +.002, + .0035 EL -.0033 + .0033
+90° long	AZ +.0027, +.0053 EL -.0012, + .0006	AZ +.0025, .0052 EL -.0068, +.0082
Maximum look ahead angle (micro radians) on a Geostationary Satellite at:		
-90° long	20	21
0° long	23	23
+90° long	20.5	20.5
Maximum look ahead angle (micro radians) on the Molniya orbit satellite for a geostationary satellite at:		
-90° long	20.5	20.5
0° long	23.5	20.3
+90° long	20.5	20.5

Table 2.2-2 Maximum Values of the Parameters, During the Indicated Period, for the Link Between a Geostationary and a Tundra Type Satellite

	Apogee	Perogee
Maximum Range (x1000 km) from a Geostationary satellite at:		
-90° long	51	40
0° long	68	71
+90° long	85	84
Maximum Range Rates (km/s) from a Geostationary satellite at:		
-90° long	2.07	-1.9
0° long	1.81	-2.36
+90° long	.41	-1.45
Pointing limits (degrees) on a Geostationary satellite at:		
-90° long	AZ +60, +120 EL -22, -6	AZ - 180, +180 EL -45, -6
0° long	AZ 115, 155 EL -42, -37	AZ 155, 245 EL -64, -34
+90° long	AZ +60, +120 EL -76, -54	AZ -180, +180 EL -78, -63
Pointing limits (degrees) on a tundra orbit satellite for a geostationary satellite at:		
-90° long	AZ -180,0 EL -42, -21	AZ 0, +180 EL -21, -6
0° long	AZ -66, +66 EL -54.3, -41-5	AZ -6, +6 EL -59.8, +18.5
+90° long	AZ 0, +180 EL -76.5, -62.5	AZ -180, 0 EL -78, -53.3
Maximum rate of change of pointing angle (deg/sec) on a Geostationary satellite at:		
-90° long	AZ +.0073 EL -.0022	AZ +.0102 EL +.0028
0° long	AZ +.003 EL -.0016	AZ +.006 EL +.0019
+90° long	AZ -.0076 EL +.0014	AZ -.0102 EL +.0013

Table 2.2-2 Maximum Values of the Parameters, During the Indicated Period, for the Link Between a Geostationary and a Tundra Type Satellite (cont'd)

	Apogee	Perogee
Maximum rate of change of pointing angle (deg/sec) on a tundra orbit satellite for a Geostationary satellite at:		
-90° long	AZ +.0082 EL +.0023	AZ +.0102 EL +.0025
0° long	AZ +.0037 EL -.0016	AZ -.0053 EL +.0034
+90° long	AZ +.0082 EL +.001	AZ +.0102 EL +.002
Maximum look ahead angle (micro radians) on a Geostationary satellite at:		
-90° long	15.8	26.5
0° long	19.5	21
+90° long	19.4	26.5
Maximum look ahead angle (micro radians) on a tundra orbit satellite for a Geostationary satellite at:		
-90° long	20.5	20.5
0° long	19.2	19.8
+90° long	20.5	20.5

Table 2.3-1 Maximum Values of Parameters for the Links Between a Geostationary Satellite at -90° Longitude and Low Orbit Satellites

	Radarsat	Space Station Freedom
Maximum Range (x1000 km) from the geostationary Satellite	42.5	42.5
Maximum Range Rate (km/s) from the geostationary Satellite	7.5	7.5
Pointing limits (degrees) on the geostationary Satellites	Pitch -10, +10 Roll -10, +10	Pitch -9.5, +9.5 Roll -5.1, +5.1
Pointing limits (degrees) on the low orbit satellites	AZ -180, +180 EL 0, 90	AZ -180, 180 EL 0, 90
Maximum rate of change of pointing angle (deg/sec) on the geostationary satellite	Pitch .0105 Roll .0105	Pitch .0115 Roll .006
Maximum rate of change of pointing angle (deg/sec) on the low orbit satellite	AZ ** EL .07	AZ ** EL .07
Maximum look ahead angle (micro radians) on the geostationary satellite	50	51
Maximum look ahead angle (micro radians) on the low orbit satellite	20.5	20.5

** The azimuth rate will exceed the maximum slew rate in the vicinity of the keyhold. To minimize this effect place the key hole in an optimum location by choosing a different coordinate system.

SECTION 3

TECHNOLOGY EVALUATION

3.0 TECHNOLOGY EVALUATION

3.1 Lasers

3.1.1 Carbon Dioxide Laser

This section describes the state of the art for Space Based CO_2 Laser Systems.

3.1.1.1 Introduction

For a CO_2 based system, the most critical component is the laser transmitter and the local oscillator. Typically, transmitter output powers of 1 to 10 watts are adequate for most space based laser communication applications. Multipass designs are available to reduce the overall device size and weight. A recent ESA breadboard system employed a 1 Watt laser transmitter [2]. To ensure that the operating life and reliability meet the stringent requirements imposed by the space environment, RF driven waveguide lasers are a leading CO_2 laser technology. To date no CO_2 lasers have been space qualified although several programs will require space qualified units by 1993 as a component in several space based scientific instruments [29, 30].

A local oscillator (LO) power of less than 0.5 Watt is typical. (For optimum performance only 50 mW is desired). Note that a considerable portion of the local oscillator power is lost due to reflections from the beam combining optics. In particular, a 90/10 beam splitter is normally employed to superimpose the 10% of the LO beam onto 90% of the incoming signal beam.

3.1.1.2 Construction

Waveguide lasers are constructed using ceramic capillary tubes or rectangular ceramic channels (typically 2.5 mm square) which are excited externally using capacitively coupled RF power supplies. The ceramic waveguide materials is selected to minimize IR radiation attenuation losses [13], provide high thermal conductivity to cool the gas mixture and to ensure high dielectric insulation and low RF losses. Two of the more commonly employed materials are Berylium oxide (BeO) and aluminium oxide (Al_2O_3). As illustrated in Figure 3.1.1-1 the metal electrodes are often separated from the gas volume by a ceramic layer. In this way the electrodes do not sputter and spread contamination through the gas volume. Overall the laser cross section may be 5 cm square with its length dependent upon the desired output power. Researchers have shown that output power scales more or less directly with an active gain of .5 to .83 W/cm [8, 91]. Therefore a 3 Watt laser will have an active length of only 6 cm.

3.1.1.3 Operating Life

By ensuring the vacuum integrity is preserved and the CO_2 gas component is sustained, extremely long operating lifetimes are possible. Recent reports indicate that continuous operating lifetimes in excess of 30,000 hours have been achieved [7]. This limit represents a laboratory achievement. Commercially available CO_2 lasers however operate for only 8000 to 10,000 hours. Discussions with several vendors indicates that they have demonstrated the ability to mil qualify their products but no military device has yet entered production [32].

Failure mechanisms have not been isolated however, outgassing of water vapour into the gas mixture is the most likely cause. Researchers have demonstrated that by simply replenishing the gas mixture will restore the laser output value. This result confirms that laser failure can not be due to sputtering of the internal laser mirrors. Other experiments have also confirmed the detrimental impact of H_2O on the operation of a waveguide CO_2 laser [33, 34].

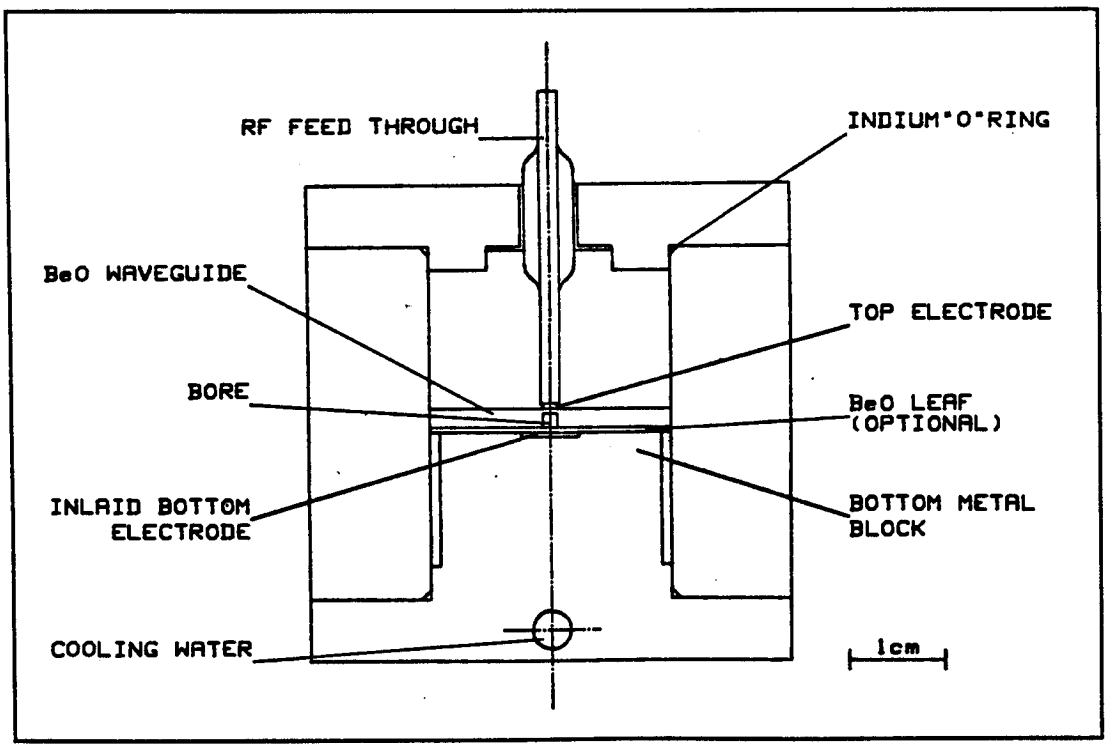

Figure 3.1.1-1 Typical Cross-sectional View of a CO_2 Waveguide Laser

Future improvements to the operating lifetime are likely by increasing bakeout temperature beyond the commonly employed 120°C limit [7]. Such an increase up to 175°C is possible by employing high temperature coatings on the reflective output couplers and moderately high temperature sealing solders. Figure 3.1.1-2 illustrates the outgassing rate of water vapour as a function of the bakeout temperature [35]. This curve illustrates the advantages of maximizing the bakeout temperature and also the benefit of vacuum furnacing all components before assembly. Many researchers are developing elaborate cleaning processes for assembling long life waveguide lasers [34]. To enhance the device operating life a gas reservoir can be positioned together with special catalysts designed to maintain the CO_2, CO and O_2 dissociation products in an equilibrium state.

Waveguide lasers are driven by RF suppliers operating at between 50 to 200 MHz. In turn the RF supply can be driven using a 28 volt DC supply. DC to RF conversion efficiencies as high as 75% have been reported [36]. The RF to laser power conversion is variable depending upon a variety of operating parameters such as RF drive frequency, gas mixture, bore size etc. [12]. Typically a variety of researchers have demonstrated efficiencies which lie within the 8 to 20 percent range [10, 11, 15].

3.1.1.4 Line Tunability

Figure 3.1.1-3 illustrates a typical configuration employed for a sealed line tunable waveguide laser.

The laser transmitter operating frequency is selected using a piezoelectric stabilized optical grating as the rear reflector. Figure 3.1.1-4 illustrates the variety of spectral transitions which are available. Line tunability is a very important feature for two reasons. The transmit and receive beams can be operated at different wavelengths (one direction confined to the 10.4 μm band transitions and the other direction confined tot he 9.4 μm band transitions) such that interference filter/beam splitters can be employed to separate the beams. Furthermore, multiplexed outputs employing two or more wavelengths within a single band can also

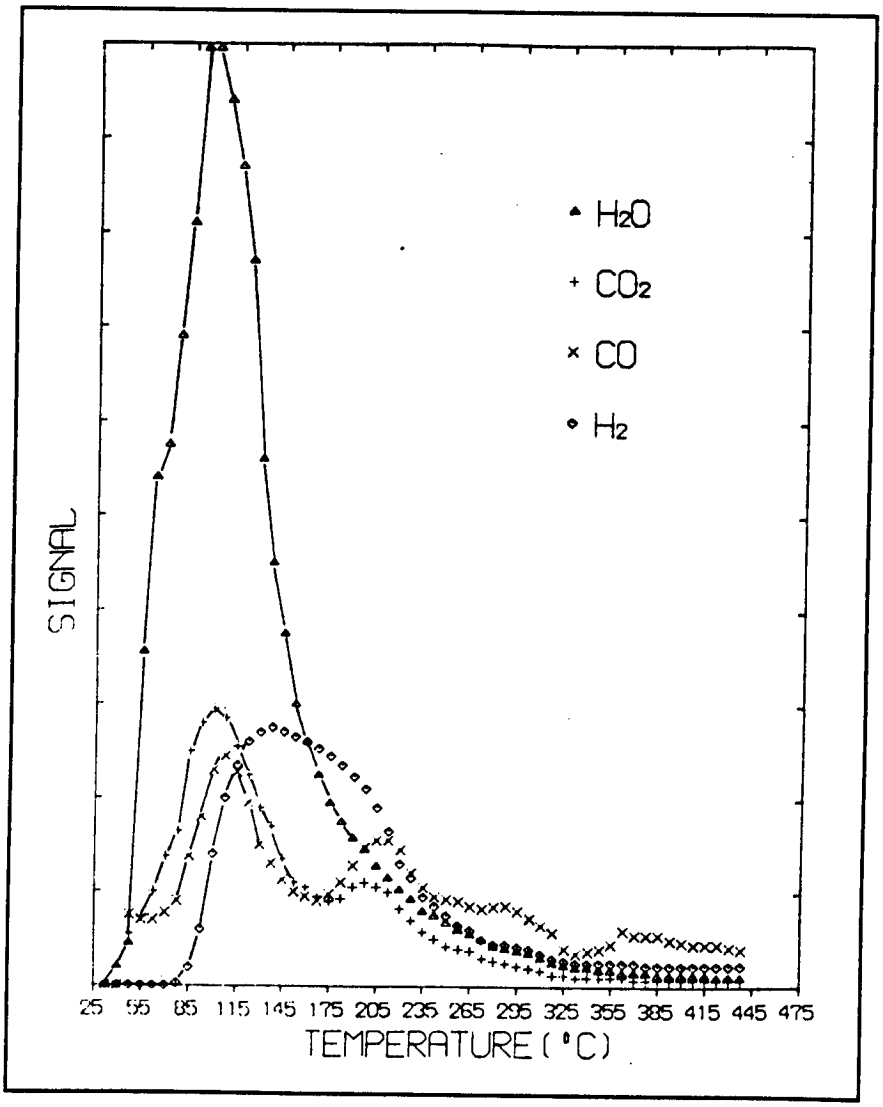

Figure 3.1.1-2 Thermal Desorption Spectra for Stainless Steel Illustrating the Outgassing Rate for Water, Vapour and Other Gases as a Function of Bakeout Temperature

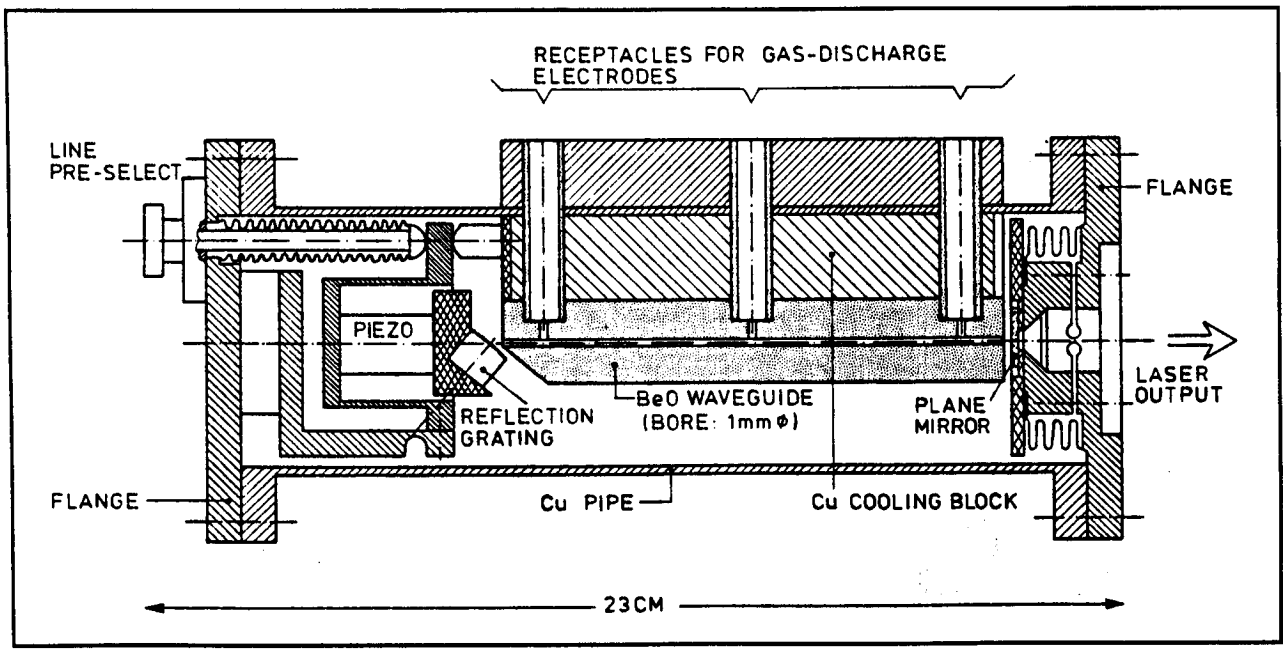

Figure 3.1.1-3 Tunable Local Oscillator CO_2 Waveguide Laser (Free spectral range: 1.2 GHz, Pressure: 200-300 torr, Gas mixture: CO_2N_2:He 1:1:8; Output: 1W on strongest line)

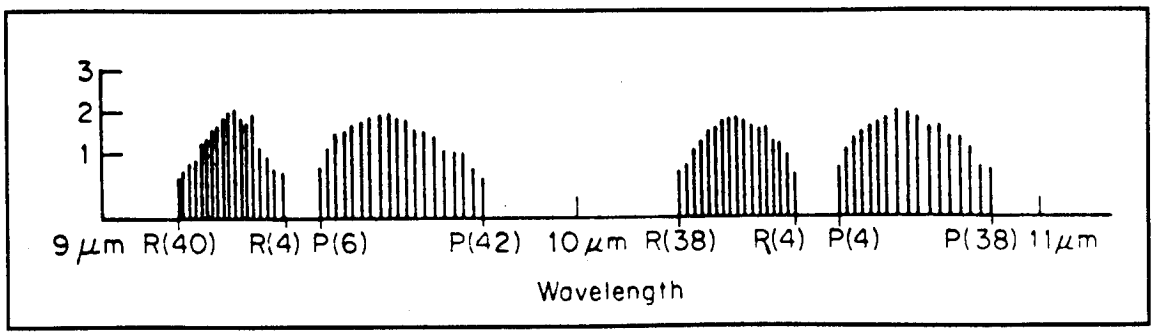

Figure 3.1.1-4 Spectrum of Wavelengths Produced by a Transversely Excited At-line Operation by a cOmmercial Laser. R and P denote rational sublevels for each of the two main vibrational transmitions of the carbon dioxide laser

be employed to increase the quantity of information without having to increase the actual laser modulation rate. Figure 3.1.1-5 illustrates a proposed arrangement. To achieve these results a variety of narrow bandpass optical filters would be required. Figure 3.1.1-6 illustrates the wavelengths available. To reduce the spectral filter manufacturing requirements carbon 12 and carbon 13 isotopes can also be employed to ensure that the wavelengths are adequately separated. Note that in the longwave infrared a transmission rise from 0.1% to 80% within 0.6 μm at an absolute wavelength accuracy of 1% is a very challenging requirement.

The laser gratings can also be adjusted to compensate for doppler induced frequency shifts. Synchronization of the transmitted laser beam frequency and the local oscillator frequency is required to maintain a constant intermediate frequency. Ultra high stability is achieved by modulating the laser cavity length, via the piezoelectrically stabilized grating to maximize the laser output energy for the transition of interest. Further frequency adjustment can be provided by external acousto-optic modulation. The doppler shift varies depending upon the satellite elevation and inclination. An overall 1.4 GHz tuning range illustrated in Figure 3.1.1-7 is consistent with a relative velocity of 7.8 km/s between a GEO and LEO satellite [3].

For the local oscillator source a tuning range of greater than 1.4 GHz has been demonstrated [37]. The tuning range is dependent upon two factors; the laser gain profile width and the free spectral range of the optical cavity. By maintaining the waveguide laser gas pressure greater than 100-200 Torr pressure broadening can be employed to widen the gain bandwidth beyond the width limited by the cavity free spectral range. The free spectral range is defined as the separation between consecutive optical fringes as defined by the laser cavity fabry perot properties. This separation is calculated using the following relationship:

$$\Delta f = \frac{c}{2dn}$$

Where:

n	-	index of refraction
d	m	laser mirror separation (cavity length)
c	ms^{-1}	speed of light

Figure 3.1.1-7 illustrates the typical laser power variation which occurs as the laser frequency is tuned. For a 21 cm long laser cavity a total tuning range of 1.4 GHz is possible. By ensuring that the gas pressure is high enough (100 to 200 Torr) the tuning range is limited only by the laser length. Note that the reduced LO power off line center is not a concern as only very low LO powers (50 mW) are required for optimum heterodyne detector noise performance.

3.1.1.5 Shock and Vibration Sensitivity

Since the laser cavity is simply a Fabry/Perot etalon a small change in the mirror separation (<1 μm) could lead to a laser frequency shift up to 100 MHz. To withstand a space environment the laser optical system must be designed to withstand the shock and vibration forces applied during the launch. To date, no reports have been published detailing the design of a space qualified CO_2 laser, however, several vendors have demonstrated the ability of their devices to withstand standard military shock and vibration requirements [14, 32, 28]. Several CO_2 laser systems will become mil qualified through incorporation into weapon systems such as the ADAD and the M1 Abrams Tank [27].

3.1.1.6 Reliability Predictions

The inaccessibility of satellites and the high cost of repair requires that high reliability standards be maintained for optical ISL's. For example, a reliability of 0.9 per year for an ISL [21] allows a failure rate of approximately 12,000 FIT defined as the number of failures in 10^9 hours). For a CO_2 based ISL system remotely switched redundant units will be required to ensure that the overall system reliability is maintained.

Clearly the CO_2 laser source is the most unreliable and untested component within the optical ISL design. Studies performed to date indicate that CO_2 laser based ISL systems will require three redundant systems

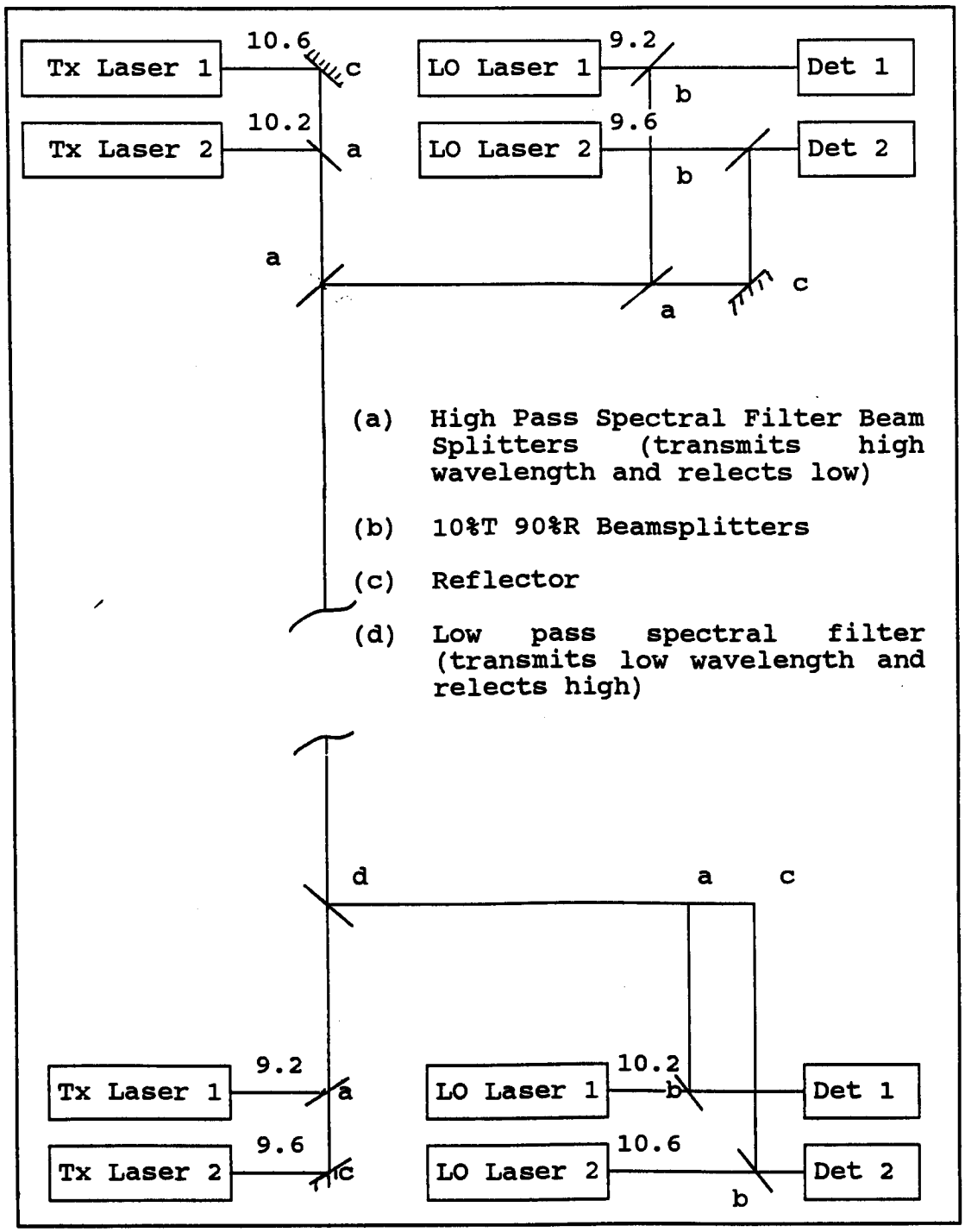

Figure 3.1.1-5 Schematic Diagram of a Wavelength Division Multiple Access Scheme to Increase Transmitter Power Capability

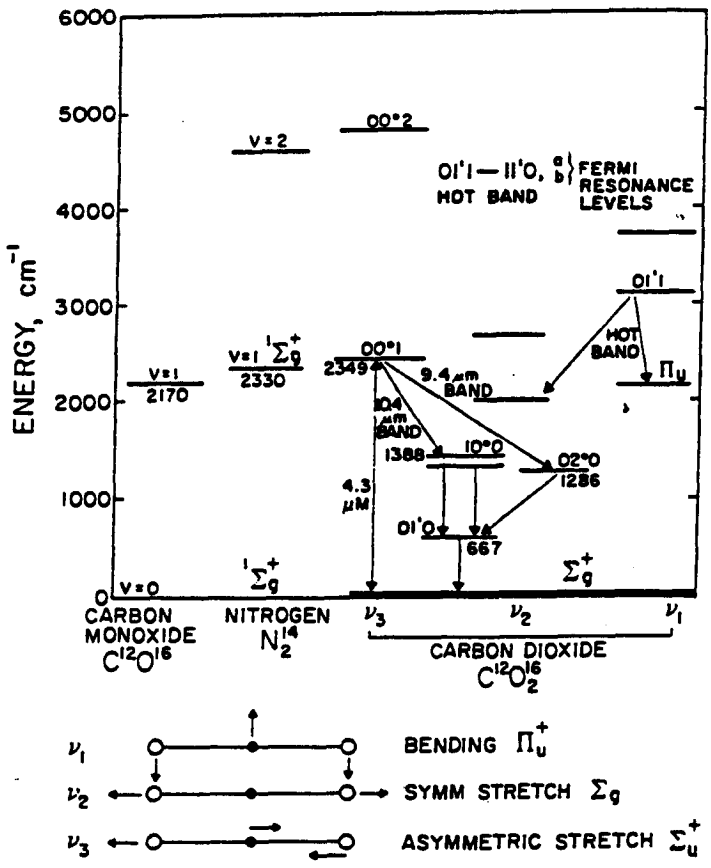

LASING TRANSITIONS

10.4 μ Band: Vibrational Transition (2349cm⁻¹ — 1388cm⁻¹)
00°1 ⟶ [10°0, 02°0]$_I$

often written as 00°1 ⟶ 10°0

9.4 μ Band; Vibrational Transition (2349cm⁻¹ — 1286cm⁻¹)
00°1 ⟶ [10°0, 02°0]$_{II}$
often written as 00°1 ⟶ 02°0
where the bracketed terms I, II above are Fermi Resonance levels

---

Vibrational Rotational Transitions $\nu \longrightarrow \nu'$ (higher to lower vibrational levels)
where $E(\nu, J) - E(\nu', J') = \Delta E \geq 0$
and $\Delta J = \pm 1$
P branch P (J); corresponds to (J-1) ⟶ J
R branch R(J); corresponds to (J + 1) ⟶ J

LASING WAVE LENGTHS OF CO_2 MOLECULE

$^{12}C^{16}O_2$

	00°1 → 10°0		00°1 → 02°0	
J	P Branch	R Branch	P Branch	R Branch
2	10.42	10.38	9.42	9.38
4	10.44	10.37	9.43	9.37
6	10.46	10.35	9.44	9.36
8	10.48	10.33	9.46	9.34
10	10.49	10.32	9.47	9.33
12	10.51	10.30	9.49	9.32
14	10.53	10.29	9.50	9.31
16	10.55	10.28	9.52	9.29
18	10.57	10.26	9.54	9.28
20	10.59 P(20)	10.25 R(20)	9.55	9.27
22	10.61	10.23	9.57	9.26
24	10.63	10.22	9.59	9.25
26	10.65	10.21	9.60	9.24
28	10.68	10.20	9.62	9.23
30	10.70	10.18	9.64	9.22
32	10.72	10.17	9.66	9.21
34	10.74	10.16	9.68	9.20
36	10.77	10.15	9.69	9.19
38	10.79	10.14	9.71	9.18
40	10.81	10.13	9.73	9.17

WAVELENGTH IN μ (MICRONS)

$^{13}C^{16}O_2$

	00°1 → 10°0		00°1 → 02°0	
J	P Branch	R Branch	P Branch	R Branch
2	10.97	10.92	9.84	9.84
4	10.99	10.91	9.86	9.79
6	11.01	10.89	9.87	9.78
8	11.03	10.87	9.89	9.76
10	11.05	10.85	9.90	9.75
12	11.07	10.84	9.92	9.73
14	11.09	10.82	9.94	9.72
16	11.11	10.80	9.96	9.71
18	11.13	10.78	9.97	9.70
20	11.15 P(20)	10.77 R(20)	9.99	9.68
22	11.17	10.76	10.01	9.67
24	11.19	10.74	10.03	9.66
26	11.22	10.73	10.04	9.65
28	11.24	10.71	10.06	9.63
30	11.27	10.70	10.08	9.62
32	11.29	10.68	10.10	9.61
34	11.31	10.67	10.12	9.60
36	11.34	10.66	10.14	9.59
38	11.36	10.64	10.16	9.58
40	11.39	10.63	10.18	9.57

weak transitions

C. Freed, R.G. O'Donnell and A.H.M. Ross — IEEE Transactions on Instrumentation and Measurements. Dec. 1976 Page 431 and references cited.

Molecular Spectra and Molecular Structure Vol. II. Infrared and Roman Spectra of Polyatomic Molecules — G. Herzberg D. Van Nostrand, Co., Inc.

Figure 3.1.1-6 Laser Spectroscope Data

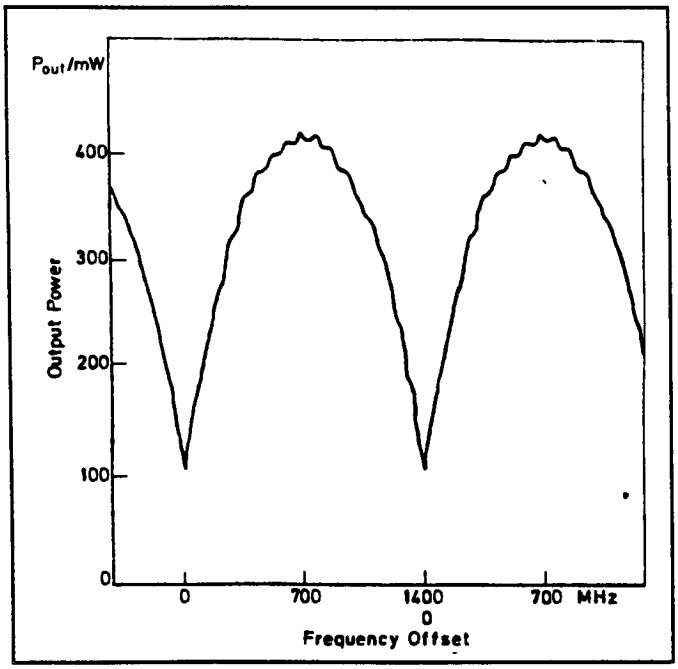

Figure 3.1.1-7 Experimental Verification of 1.4 GHz Tunability of the CO_2 LO Laser

to ensure that the overall system reliability is maintained. This estimate was based upon a 7000 hour CO_2 laser life resulting in a corresponding 100,000 FIT value. Revising the life estimate to a 320,000 hour limit will reduce the laser FIT value to about 50,000. Correspondingly, the system redundancy requirements will also decline depending upon the overall mission life expectancy.

Other critical components for which FIT values are required include the IR detector and optical modulator. Previous estimates for the photovoltaic detector have established the reliability at 1000 FITs. For the modulators life testing is required to establish a reasonable FIT value.

3.1.2 Solid State Laser Technology

3.1.2.1 Semiconductor Lasers

Short wavelength laser technology has a history going back around thirty years, with AlGaAs heterostructures going back fifteen years. Despite this, device improvements continue to occur; all these improvements are aimed at higher power, higher efficiency and higher reliability.

Short wavelength material had a fundamental reliability problem which was not easily sidestepped. At shorter wavelength (say < 850 nm), AlGaAs is slightly absorbing, leading to heating of the laser facets, facet degradation and finally thermal runaway and facet burn-out. The laser designer must avoid these effects as far as possible, using such structures as LOC (Large Optical Cavity) structures in which the active layer can dump photons into a larger cavity, reducing power density at the facet, and/or using disordering of the active layer at the output facet in order to reduce the residual absorption.

In addition, the designer continually strives to improve the efficiency of the electrical to optical conversion process. In the late 80's, this was epitomized by the widespread introduction of quantum well structures grown by MOVPE in which single or multiple quantum wells in the active layer improved both conversion efficiency and temperature stability (Figures 3.1.2-1, 3.1.2-2).

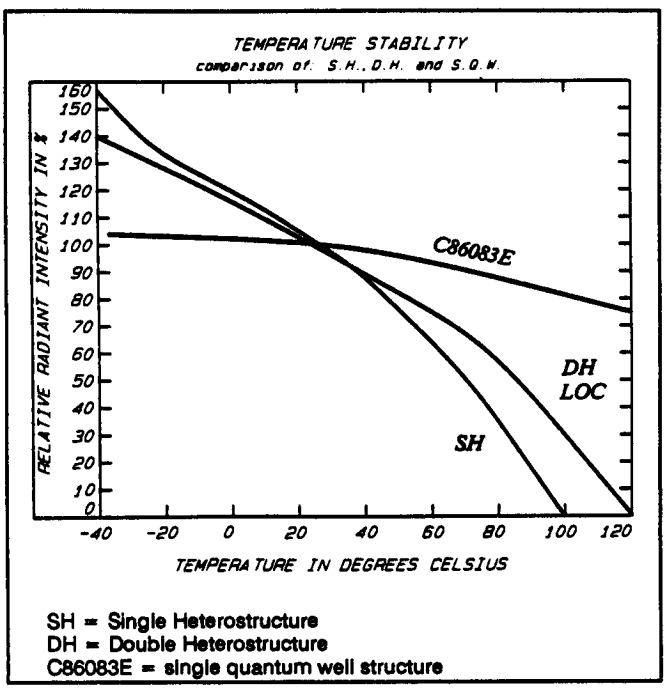

Figure 3.1.2-1 Relative Temperature Stability of Quantum Well Lasers

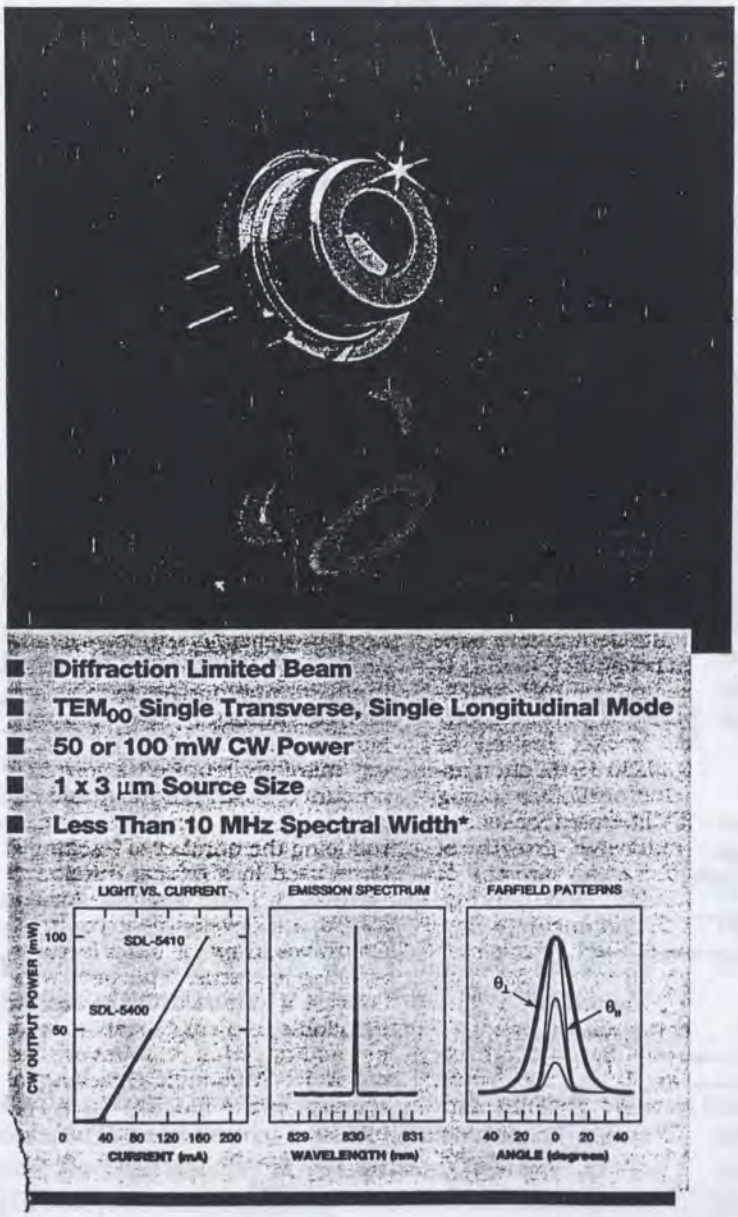

The highest power diffraction limited single mode laser diode is now available from Spectra Diode Labs. The new SDL-5400 Series GaAlAs laser provides up to 100 mW cw power in an optically clean beam.

High resolution applications such as optical data storage, printing, spectral analysis, point-to-point communication and frequency doubling require diffraction limited sources.The SDL-5400 laser diode provides the power and features to dramatically increase the performance of these and many other applications.

- 100 mW of cw power from a 3 µm emitter means small spots and faster writing time for printing and data storage systems.
- Wide dynamic range spectral analysis is achieved by the high power and less than 10 MHz* spectral width.
- Communications systems are enhanced by the 5400's greater than 2 GHz modulation bandwidth.

The SDL-5400 represents a significant breakthrough in GaAlAs technology.

Our years of research in this field has led to new discoveries in laser fabrication techniques. In the 5400 we've combined a single quantum well active region with a real-refractive-index, single-mode waveguide. The result is a diode that exhibits the highest power, greatest efficiency, narrowest linewidth, best spectral stability and highest reliability of any GaAlAs laser.

As with all SDL lasers, options are provided to simplify system integration. Among these are SOT,TO-3 and open heatsink packaging, internal photodiode, thermoelectric cooler and wavelength selection.*

To find out more about the SDL-5400 laser diode call us at (408) 943-9411.

Spectra Diode Labs, 80 Rose Orchard Way, San Jose, CA 95134. Outside the U.S.A., contact the nearest Spectra-Physics sales office.

Figure 3.1.2-2 Quantum Well CW Laser

Structures have evolved towards index-guided structures such as ridge-waveguide, buried heterostructure, and channel substrate in order to give single mode (single wavelength) outputs, as opposed to the simpler and less efficient gain-guided structures.

The most recent development is the addition of "*strained-layer InGaAs*" structures in which the use of Indium in the quantum well leads to a compressive strain which alters the band structure, reduces the density of states, and hence reduces the laser threshold current density and increases the electrical to optical conversion efficiency to values around 50%. Continuing optimization of strained layer InGaAs materials is expected to lead to both improved performance and higher reliability at wavelengths ranging from 650 to 1100 nm.

By comparison, long wavelength semiconductor laser technology seems relatively static. Reliable single-stripe lasers with a few hundred nW of output were available in the mid-80's. Little has changed since. In general, the only potential user of higher power long wavelength diodes is eye-safe free space communications. Higher powers are not useful for fiber optic work, since fiber non-linearity at high launch powers limits the high power requirement.

The limit on higher power long wavelength lasers was due to non-radiative processes particularly Auger recombination, which increased with the power density of the carrier. Recently multiple quantum well and strained layer structures have removed this limit, and higher power lasers may become available [Ref. 52].

3.1.2.2 Semiconductor Laser Amplifiers

A laser is an optical oscillator; this implies gain - from the active layer, and feedback - from the reflective facets. If feedback is suppressed by using antireflection coated or angled facets, then what is left is gain - a semiconductor laser amplifier.

Some applications such as the communications laser, require an output which is single mode, yet is modulated with a high extinction ratio; these requirements conflict with high power output. The solution is the MOPA - "*Master Oscillator Power Amplifier*". The low power, carefully modulated, single mode output from a laser is amplified by a second stage while preserving the quality of the output.

The second stage can even be a quantum well laser array which is in effect injection-locked by an input from the master laser.

The best recent account of such techniques is in the 1990 review by Bernard Seery of the NASA Goddard Optical Communications Program [Ref. 50]. MOPA work aimed at a 1 Watt output is being undertaken by Spectra Diode Laboratories and 240 mW diffraction-limited output at 50 Mb/s has been demonstrated by injection locking at 830 nm (Figure 3.2.2-3).

3.1.2.3 Semiconductor Laser Arrays

While significant amounts of raw power are available from semiconductor laser arrays, there are two issues which must be dealt with. The first is that the physical dimensions of the array, together with the telescope focal length define the minimum illuminated angle and affect the ability to usefully concentrate the power. The second is the tendency of edge-emitting laser arrays to lock into a mode in which adjacent elements have antiphase outputs leading to a far-field, dual-lobe pattern with no on-axis power.

The first issue is not solvable. The second issue is nominally solvable, but to date no space-qualified solution has been published. Ref. 53 is an example of "*Talbot filtering*" which appears to be a trend in current research.

One possible solution is the surface emitting arrays under development in various laboratories. These do not resolve the first issue, that of physical size but some designs, such as that from DSRC in Princeton [Ref. 51] lead to a coherently coupled, diffraction limited, single mode output (Figure 3.1.2-4). Much of this work is classified, therefore, the exact current status is unknown. Ref. 51 reports 300 mW CW and effective phase and frequency modulation at 1.16 GHz.

Injected Power = 6.6 mW
Locking Bandwidth = 0.2 Å or 9 GHz

Optimum effects at 3° to 5° angle of injection

Steering of single lobe with change of injected wavelength

Free-Running Far-field and Spectrum

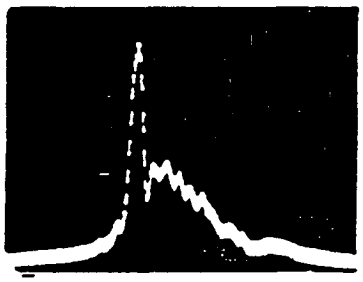

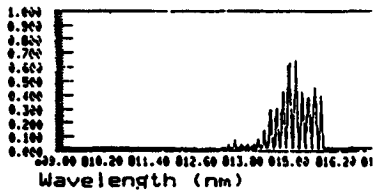

Injection-Locked Far-field and Spectrum

FWHM= 0.5°

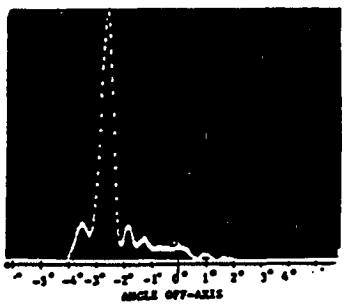

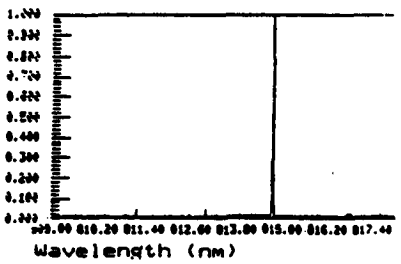

Injection-Locking Configuration

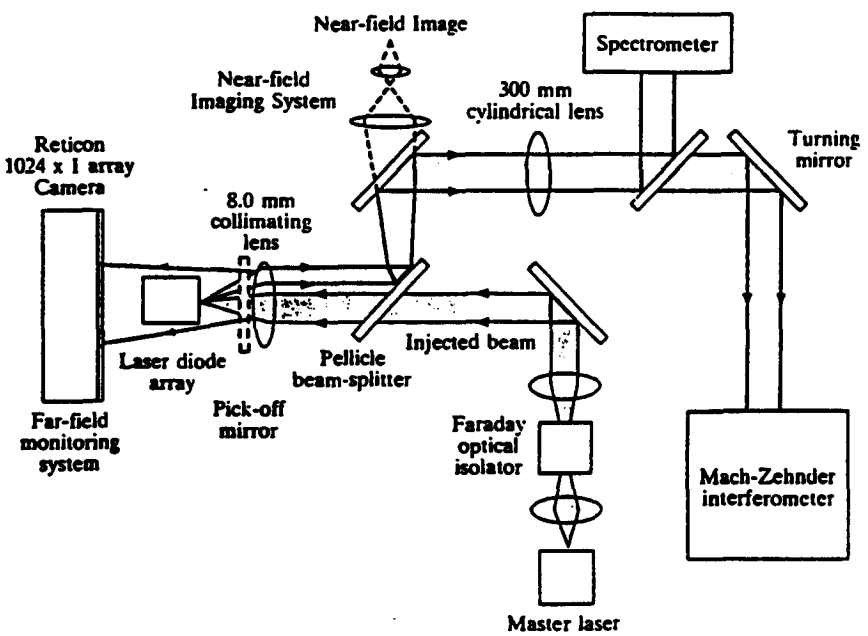

Figure 3.1.2-3 Injection Locked Laser Diode Array

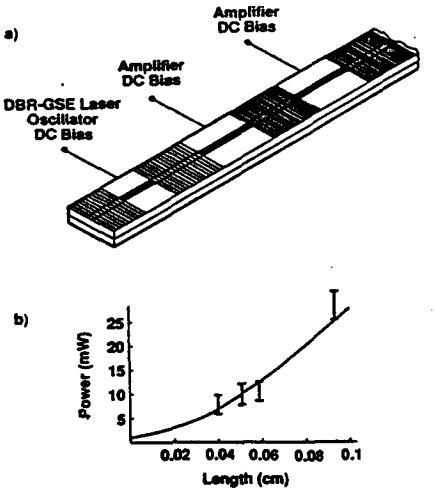

CWF13 Fig. 1. Schematic diagram of a GSE-MOPA array (a), and the calculated GSE power output per amplifier as a function of length (b). The bars indicate measured data points.

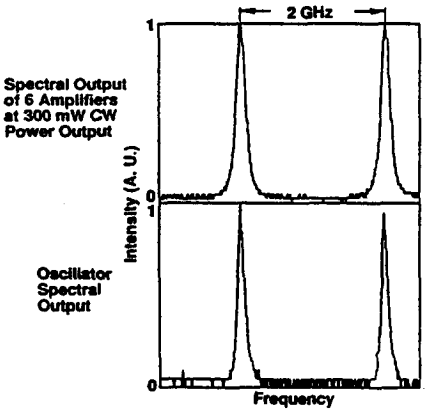

CWF13 Fig. 2. The Fabry–Perot spectrum of 6 amplifiers operating at 300 mW cw along with that of the oscillator used is shown.

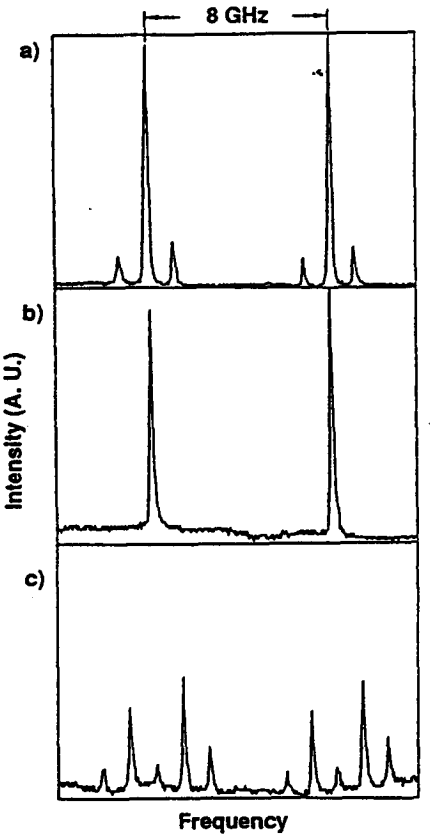

CWF13 Fig. 3. The power spectrum of the amplifiers only, showing phase modulation, with the first amplifier modulated in (a). The power spectrum without modulation in (b). The power spectrum of the amplifiers when only the oscillator was modulated in (c).

Figure 3.1.2-4 Surface Emitting MOPA Array

Semiconductor laser arrays are also used as pump sources for solid-state lasers, particularly Nd:YAG. As such, the only two issues are power output density and reliability; the two are inversely related. Power outputs up to 10W and higher are available from single stripe arrays (Figure 3.1.2-5).

3.1.2.4 Diode Pumped Solid State Lasers

Nd:Yag Lasers at 1064 nm

Solid state lasers, as opposed to many semiconductor lasers, have the advantage of high-quality single frequency, single spatial mode, circular beam profile outputs which are ideally suited to ISL applications, since they obviate the need for beam shaping optics. However, historically the poor reliability of flash lamp excitation sources had been an issue for space programs.

In particular Nd:YAG lasers pumped by 808 nm semiconductor laser pumps are obvious candidates since their 1064 nm output falls (just) within the range of silicon APD operation. Since multi-element arrays are used as pump sources, degradation is "*graceful*" rather than catastrophic.

Nd:YAG technology is a report in its own right. The basic approaches are end-pumped rods, side pumped blocks, and slab pumped configurations (Figure 3.1.2-6, -7, -8). All have their proponents. Probably the most promising current approach is that being pursued by Lightwave Electronics, described as a "*non-planar ring cavity*". This is a chainable MOPA style configuration. A 3-stage version has shown 800 mW output (Figure 3.1.2-9). A particular design feature is the fact that all optical components are metallized, actively aligned and then soldered into place, producing a rugged assembly which is flight qualifiable.

A less well advertised disadvantage of the Lightwave approach is that active piezoelectric and thermoelectric tuning, controlled by a microprocessor, is required to ensure that the cascable stages are aligned in frequency.

A U.S. customer, in private conversation, has claimed access to an alternative to the Lightwave approach. They claim 1W CW from pumped YAG, with an NRZ modulation extinction ratio of $\approx$ 5% at 1 Gb/s, in a technology which is space qualifiable.

Ytterbium: YAG Lasers at 1032 nm

In recent weeks, it has become clear to EG&G that an attractive alternative to Nd:Yag for many applications, including ISL, would be Ytterbium Glass solid-state lasers, emitting at 1032 nm and diode-pumped at 940 nm. A tabular comparison is given in Table 3.1.2-1

In summary, a diode-pumped Yb:YAG laser should be more power efficient, more reliable and more temperature insensitive than its Nd:YAG equivalent. It also has a sensitivity advantage of 1 to 2 dB when used with silicon detectors, and a further 0.25 dB advantage over Nd:Yag in terms of diffractive spreading of the signal power.

Yb:YAG is therefore a highly attractive potential source for ISL's. If an external modulator is required, then Nd:YAG modulators are appropriate with only the minor change of coating wavelength.

3.1.3 Beacon Lasers

3.1.3.1 The Beacon Requirement

For the "Acquisition Phase", one terminal must scan a beacon beam across the uncertainty cone for the other terminal's position. In Ref. 48, equation 5, Witting shows that Acquisition time is inversely proportional to the Beacon Power. For reasonable acquisition times with typical detectors (CCD's with low noise readouts), required beacon powers are a few watts.

A beacon must appear to the searching terminal as the brightest source in its search field-of-view, and must stand out against anything except direct solar background. This leads to a requirement for a source which is:

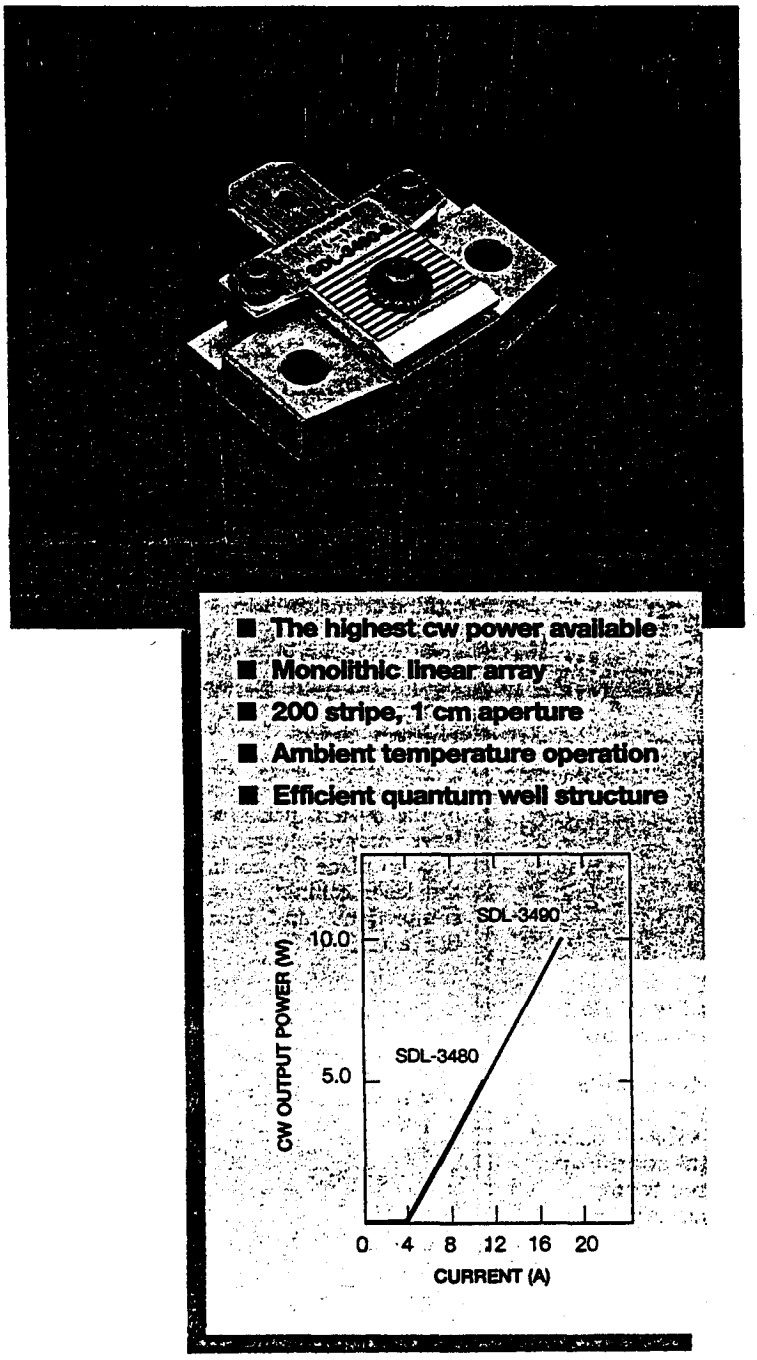

Ten watts of cw power in a linear array format make the SDL-3490 the ideal source for pumping solid state lasers or other applications.

- 10 W cw output increases the performance and efficiency of diode pumped lasers.
- The 1 cm x 1 µm emitting aperture means easy, efficient coupling to side-pumped Nd:YAG or Nd.YLF rods or slabs.
- The output facet is directly available, mounted flush to the front surface of the heatsink allowing close placement to optical elements and laser media.
- The copper heatsink is designed to be readily mounted to an external thermoelectric element or heat removal system.
- Wavelength selection is available as an option for Nd:YAG and Nd:YLF excitation.

SDL's linear array technology means high power and high reliability

The SDL-3490 laser array consists of twenty 10-stripe emitters spaced on a monolithic GaAs bar. A total of 200 emitting stripes sum incoherently to produce up to ten watts output. Reliability is enhanced by the low energy emitted per stripe and heat spreading between groups of arrays. A quantum well active layer structure provides low threshold and excellent electrical-to-optical conversion efficiency.

The very high brightness provided by the SDL-3490 also makes this laser an ideal choice for beacons and high average power illuminators.

To find out more about the SDL-3490 laser diode or the 5 watt SDL-3480 call us at (408) 943-9411.

Spectra Diode Labs, 80 Rose Orchard Way, San Jose, CA 95134. Outside the U.S.A., contact the nearest Spectra-Physics sales office.

Spectra Diode Labs

Figure 3.1.2-5 High Power Multi-Stripe Laser Diode Arrays

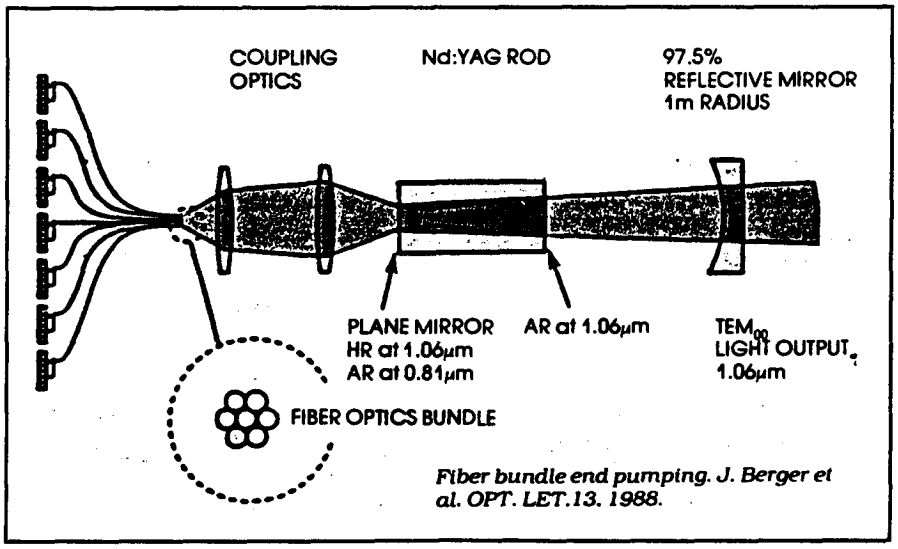

Figure 3.1.2-6 End-Pumped Nd:YAG [ref. 132]

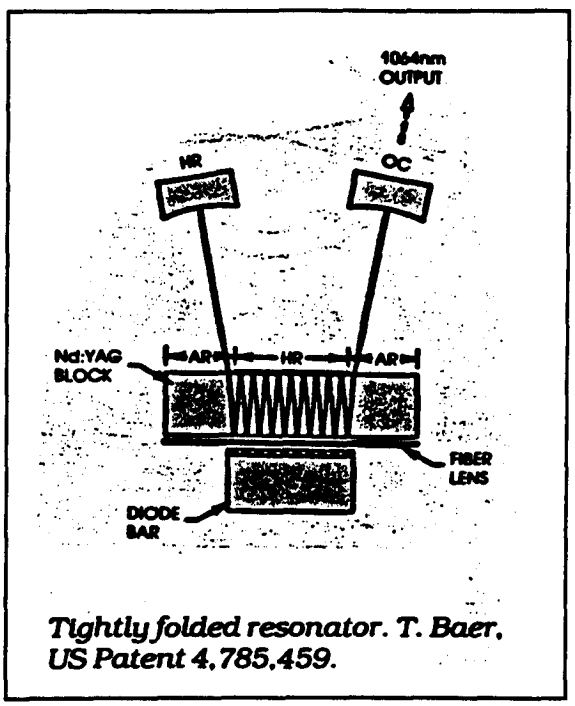

Figure 3.1.2-7 Edge-Pumped Slab Nd:YAG

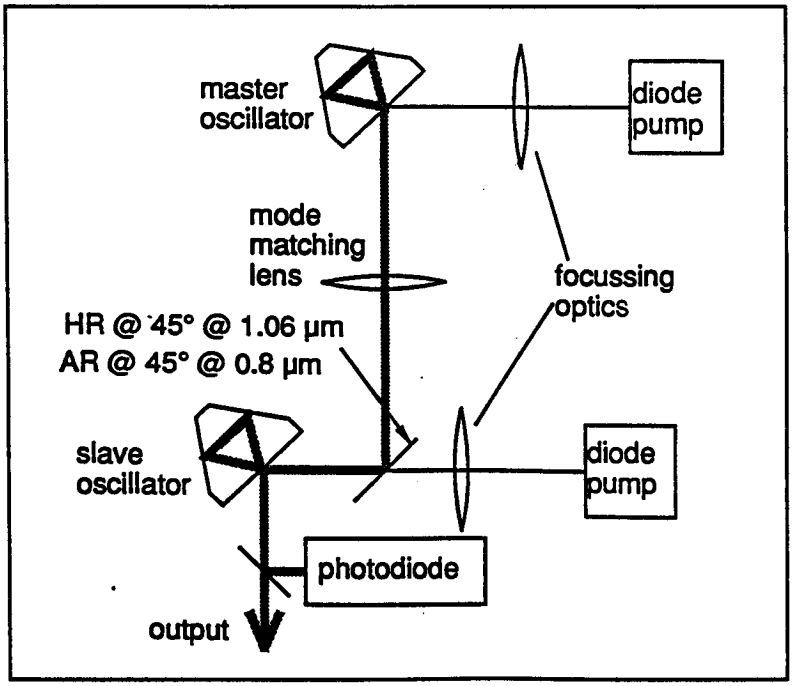

Figure 3.1.2-8 Lightware Pumped MOPA Nd:Yag Schematic

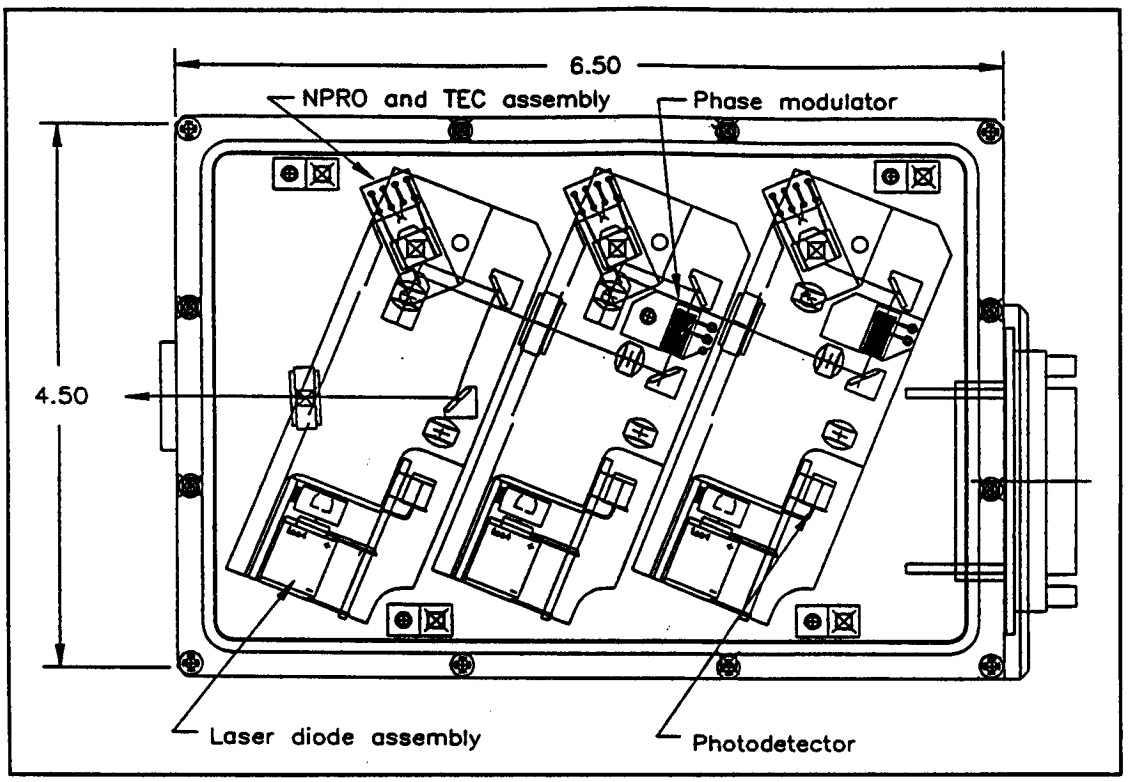

Figure 3.1.2-9 Lightwave 3-Stage NPRO Nd:YAG

Table 3.1.2-1 Comparison Between Nd:Yag and Yb:Yag Lasers

Parameter	Nd:Yag	Ytterbium (Yb):Yag	Comment
Wavelength (nm)	1064 (1047)	1032	The increase in absorption coefficient of silicon as λ decreases gives a 1 to 2 dB increase in sensitivity at the receiver for direct detection. (= 12 cm^{-1} at 1064 nm, 30 cm^{-1} at 1032 nm).
Pump Wavelength (nm)	808	940	Due to AlGaAs self absorption, 808 nm lasers are inherently lower reliability; at 940 nm high reliability strained-layer InGaAs lasers can be built. In addition Nd:Yag has a baseline photon efficiency of 76% (1064/808) whereas Yb:YAG has 91% (940/1032); the residual energy goes to heating the crystal, therefore Yb:YAG has 63% less self-heating per output Watt than Nd:Yag.
Pump Bandwidth(nm)	± 2	± 10	At 808 nm it is: (i) Hard to "hit" the Pump Wavelength, implying low yield and high cost. (ii) Power expensive to thermally control the pump diodes to stay on 808 nm. At 940, with five times greater pump bandwidth (0.3 nm/°C) a ±30°C pump temperature range is acceptable.
Doping Efficiency	Medium	High	Yb:Yag can be doped to higher levels without leading to self-absorption. This increases crystal efficiency per unit volume.

C.W.

To find a flashing source would require synchronization with the flash.

A Laser

To allow the use of narrow-band filters for background reduction. However, a single-mode laser is not required.

Reliable

The source must be good for on-off use over the mission lifetime of up to 10 years. Assuming a 1% duty cycle, this is 1,000 hours. This is short enough to allow some compromise in the lifetime versus output power trade-offs. The use of a multisource beacon ensures reliability via redundancy.

Detector Wavelength

<900 nm for CCD detector compatibility

3.1.3.2 Beacon Options

a) CW Single-Stripe Single Mode Laser Diode

The highest available output power is 100 mW - the SDL-5400 shown in Figure 3.1.3-1. This is not enough. Even combining two using a polarizing beamsplitter does not give adequate output power or redundancy.

b) CW Single-Stripe Multimode Laser Diode

With outputs up to 5 W, at 30% to 50% conversion efficiencies, these give adequate output power but since the stripe is physically long (100 μm), then it can be difficult to collect all the light into the beacon illumination cone in a manner that gives a uniform far field. In addition, proven lifetimes are not adequate.

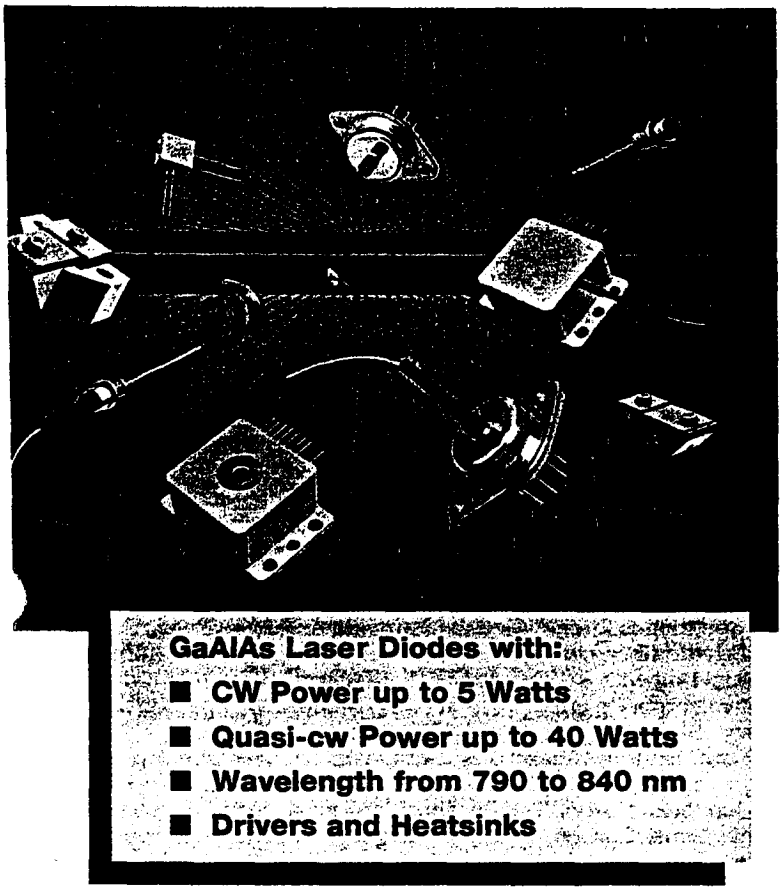

High power in a laser diode is important. Convenient integration into your system is even more important. Spectra Diode Labs laser diodes offer you both.

Our high power, high brightness lasers are available with a variety of options designed to make system integration simple. Among these options are:

- CW, quasi-cw and short pulse operating modes to match a variety of application requirements.
- Open heatsink, submount, sealed device and space-qualified packages to make installation easy.
- Fiber pigtail, fiber stub, and direct-from-the-facet output ports to simplify system design.
- Monitor photodiode and TE cooler options that allow power stabilization and wavelength tuning.
- Wavelength selection which permits matching optical pumping absorption lines or other system requirements.

In addition, we also manufacture special devices to custom requirements. Matching the correct source to your application is easy.

Spectra Diode Labs offers proven technology, high reliability and an unmatched choice of options.

Figure 3.1.3-1 High Power Single Stripe Laser Diodes

c) Optically Combined Single Element AlGaAs Lasers

This solution was selected by MATRA for Silex and was a correct choice for the project being the low risk compromise. As Ref. 49 states, 'it leads to a better overall (optical/electrical) efficiency' than pumped YAG, 'and to a higher reliability due to the use of several distinct optical sources'.

Nineteen 500 mW SDL laser diodes at 850 nm are combined via multimode fiber and a mixing rod to give a 3.8W. collimator output with a far field uniformity better than 1% - Figure 3.1.3-2.

SDL have shown an alternative approach coupling a linear fiber array to a 1cm long bar - Figure 3.1.3-3; 30 watts out at a 75% coupling efficiency was seen.

d) Pumped YAG

The main advantage of YAG as a beacon is that it automatically gives a clean beam profile. A disadvantage is that it is a poor wavelength for CCD's, which have Q.E.'s of below 5% at 1060, as well as suffering from resolution degradation due to the long absorption length for 1060 nm photons in silicon. In addition, as noted above, the pumped YAG has a worse overall efficiency than the optical combiner approach.

e) Long Wavelength Diode Sources

These are available with single element output powers up to a few hundred mW, but both 1300 and 1550 are poor wavelengths for acquisition detectors, since CCD's such as Platinum doped silicide arrays have Q.E.'s of only 5%.

3.1.3.3 Beacon Technology Choice

The logical current choice is either the SDL or the Matra approach which combines the output of many laser elements to give a single bright source with redun-

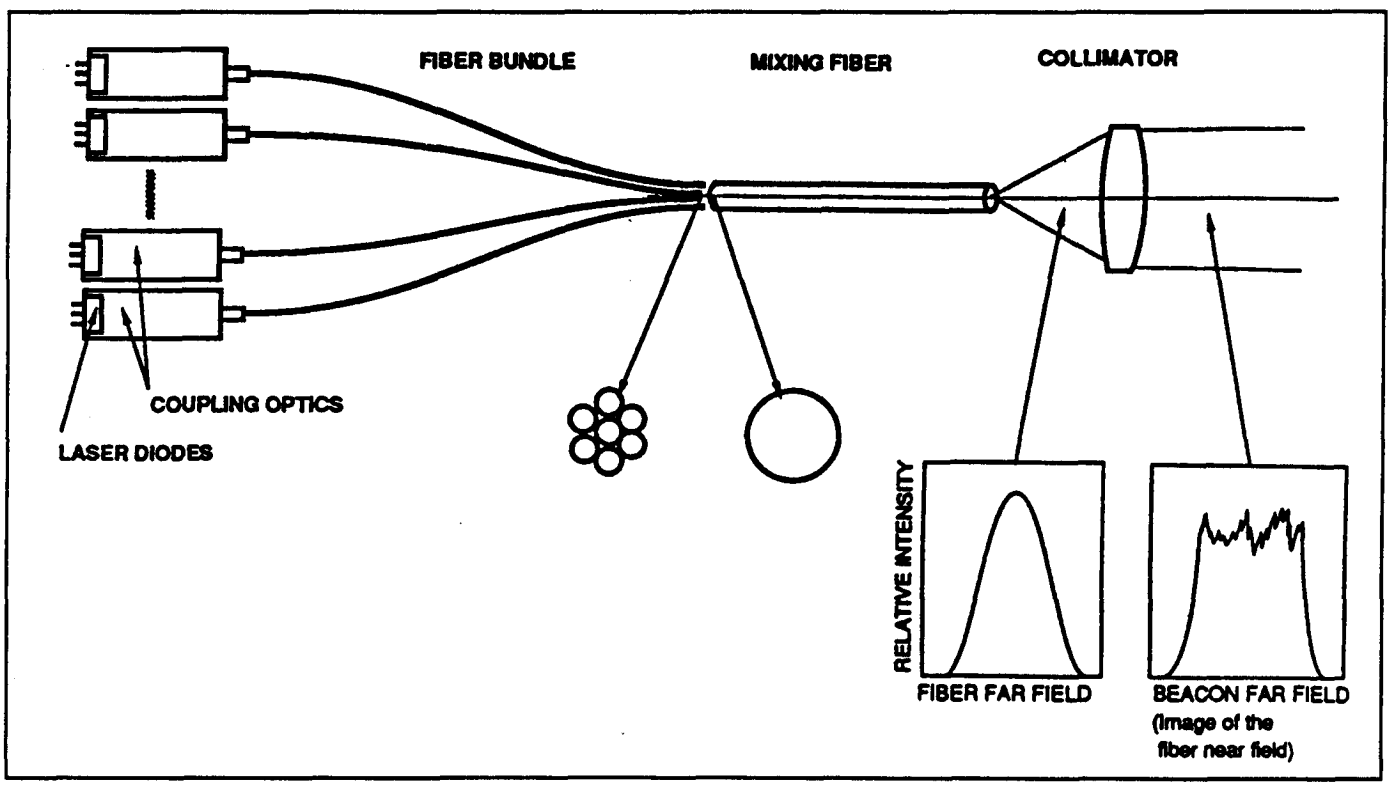

Figure 3.1.3-2 Silex Beacon; Optically Combined (Ref 49)

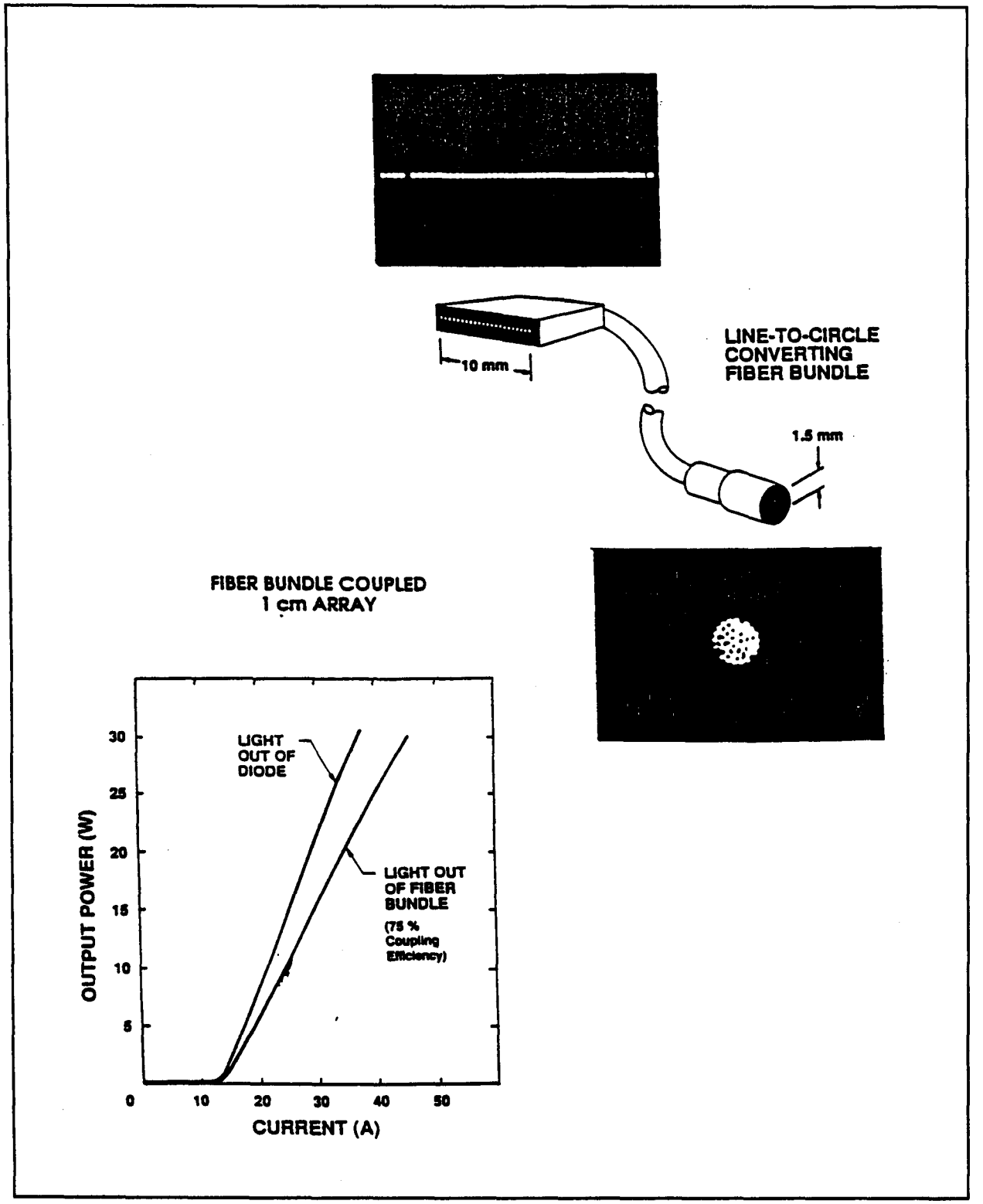

Figure 3.1.3-3 Line Circle Array Output Converter

dant elements. This will remain true until high power highly reliable single element lasers become available.

3.1.4 CW sources for Direct Detection

3.1.4.1 Short Wavelength

Despite the work in progress on injection locked arrays and MODA's, the best current choice is the single element single mode source such as:

SDL-5400	100 mW
Sharp LT025	30 mW
Hitachi HL series	30 mW
Toshiba TOLD series	30 mW
Mitsubishi ML series	30 mW

If higher power is required, then both Silex and NASA Goddard have designs for laser beam combiners which can sum adjacent wavelengths.

Figure 3.1.4-1 shows 70% efficient Goddard diffractive combiner which can handle four laser diodes. Note the complexity of each laser package.

Figure 3.1.4-2 shows a Goddard dichroic beamsplitter combiner which can handle up to seven lasers at 2 nm channel separation.

Figure 3.1.4-3 shows a SILEX design which employs both polarization and wavelength multiplexing (dichroics) to give a four channel mux/demux function with 8nm channel separation. Typical combiner outputs are in the 200 to 300 mW range, obviously depending on the number of channels and the laser source.

A stated advantage of the diffractive combiner is that it is insensitive to laser wavelength drift, whereas the dichroic combiners must use wavelength controlled laser diodes implying power hungry (2W per channel) Peltier heater/coolers.

Semiconductor Laser Drivers

A laser driver must:

(i) Handle the required bit rate in terms of rise/fall times

(ii) Provide low extinction ratio, <5% essential <3% desirable

(iii) Be compact and power efficient

In terms of reported work, that performed by Impellimax Corp (New Hampshire) for NASA Goddard is the most impressive, giving a 15 mm dimension hybrid based on silicon bipolar NPN transistors, with <1ns rise/fall times at 100 mA switching current; Figures 3.1.4-4, -5, -6 (Ref. 55). Typical power requirements of such a driver was 1W at 5V, Ref. 56 is an alternative approach by TRW based on a GaAs FET driver.

3.1.4.2 Nd:Yag

As reported in section 3.1.2.4 a few hundred mW is definitely available, and up to 1W seems attainable with 5% extinction ratios.

3.1.4.3 Long Wavelength Semiconductor Lasers

Similar comments apply as were made with respect to short-wavelength laser diodes. 50 to 100 mW per diode is available, and multiplexers could be made.

3.1.5 Sources for Heterodyne Detection

3.1.5.1 Short and Long Wavelength Laser Diodes

These are grouped together because identical considerations apply.

In principle, sources for heterodyne links can be less powerful than those for direct detection links, since the receivers can be more sensitive. Against this one must set the following additional requirements:

(i) Signal Source

Must be frequency stabilized to better than ± 1 GHz (< 1 part in 10^5)

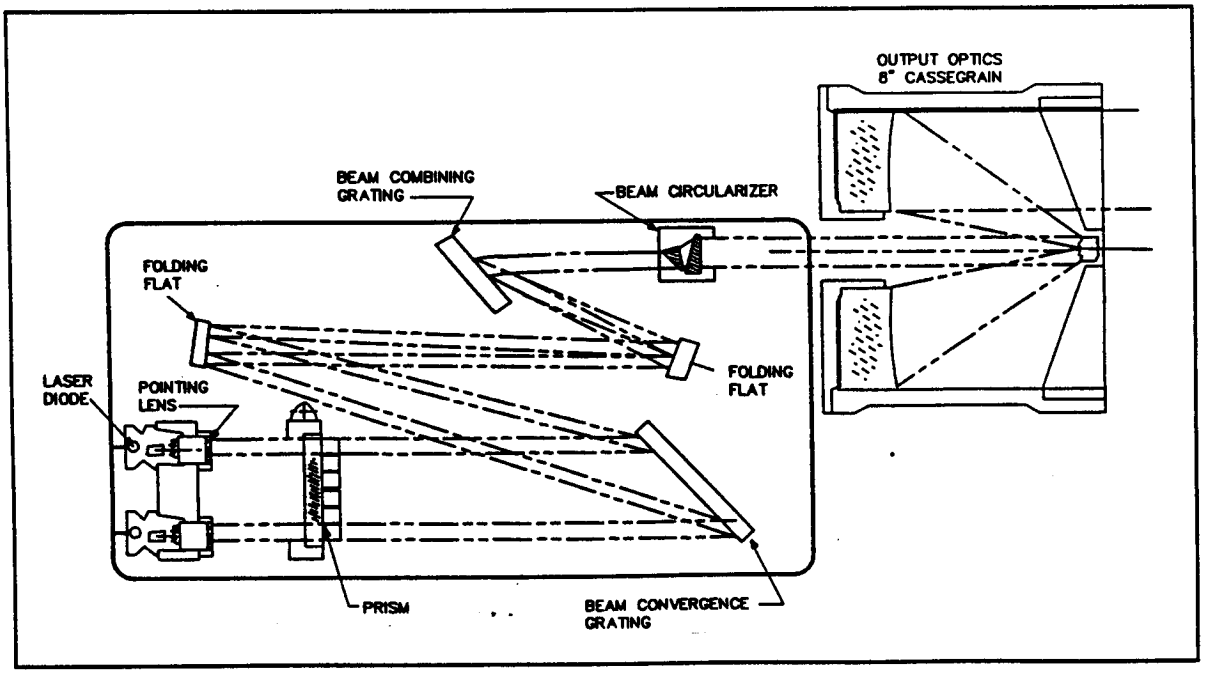

Figure 3.1.4-1a Grating Diffractive Laser Combiner (NASA Goddard)

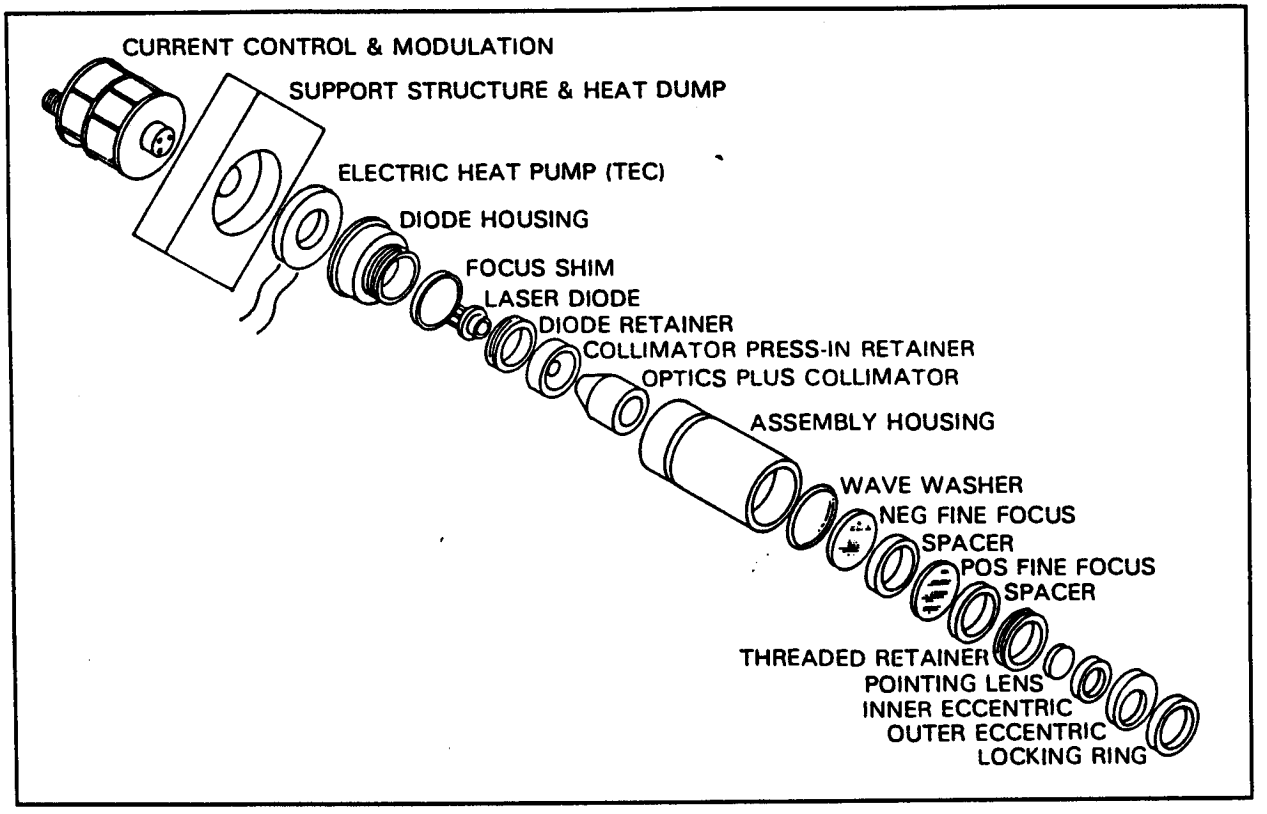

Figure 3.1.4-1b GLBC Laser Diode Header Optomechanical Design

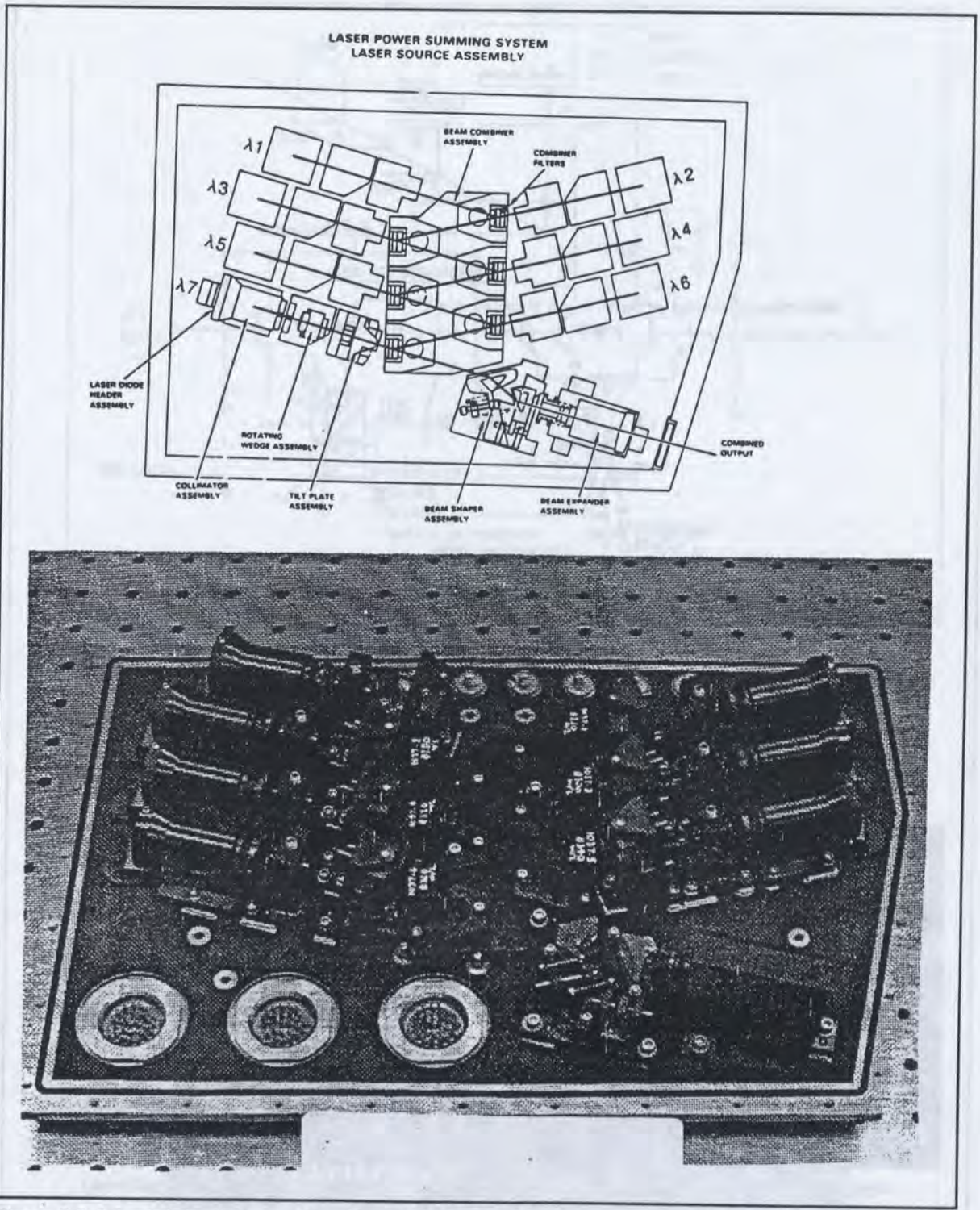

Figure 3.1.4-2 Dichroic Laser Combiner (NASA Goddard)

Fig.1 : Shows the choser polarization lay out

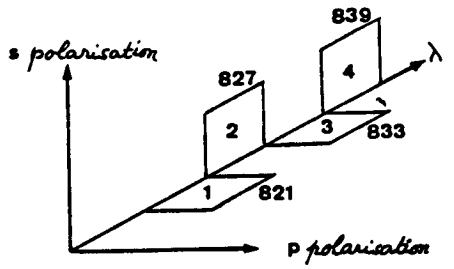

BREADBOARDS LAY OUT

Multi/demultiplexing principles are shown on fig.2 :

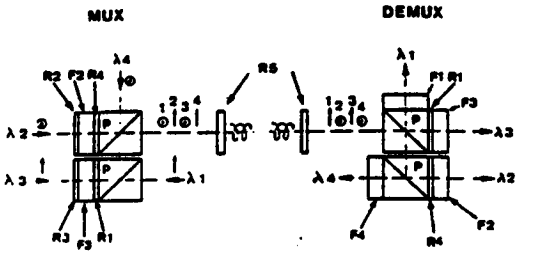

R1 R2 R3 R4 R5 : /4 retarding plates
P : Polarizing cubes.

Optical channels multiplexing :

The optical channels multiplexing technique allows to significantly extend the transmitted data rate.

This requires :
- narrow filters with spectral bandwidth < 8 nm,
- high transmittance ~ 95%,
- background rejection < 10^{-4} (demultiplexer only),
- interchannel crosstalk < 1% (demultiplexer only).

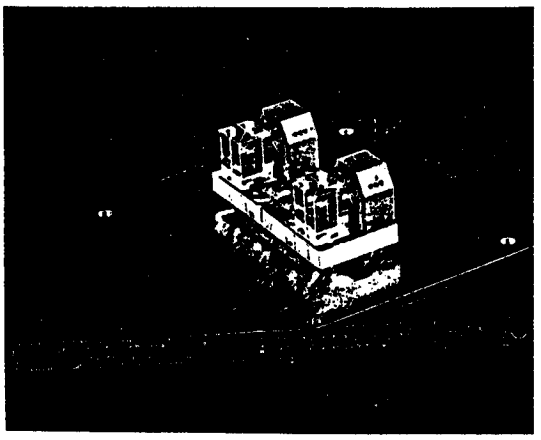

4 channels multiplexer (breadboard)

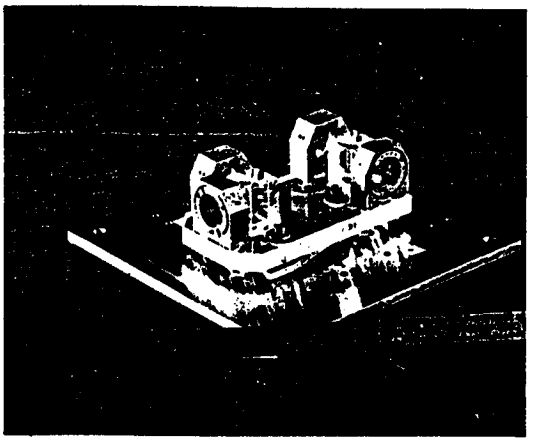

4 channels demultiplexer (breadboard)

Figure 3.1.4-3 Polarization/Dichroic Laser Mux/Demux (Silex)

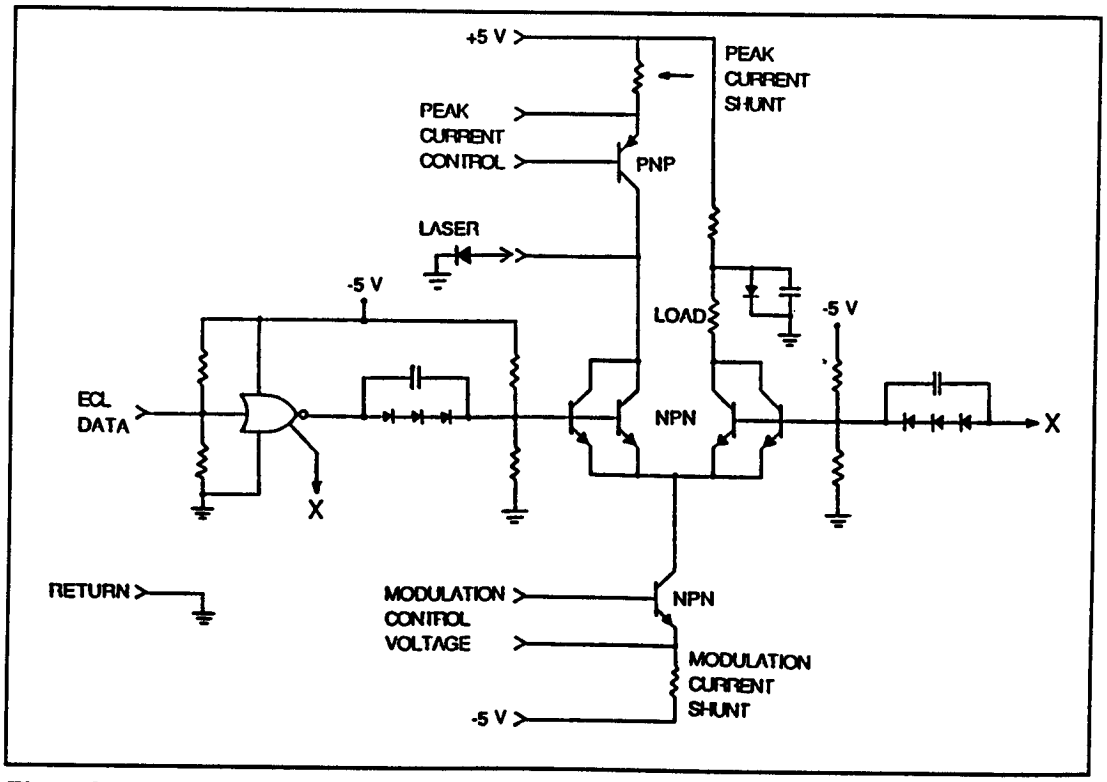

Figure 3.1.4-4 Complete Driver Circuit Sent to Hybrid Manufacturer

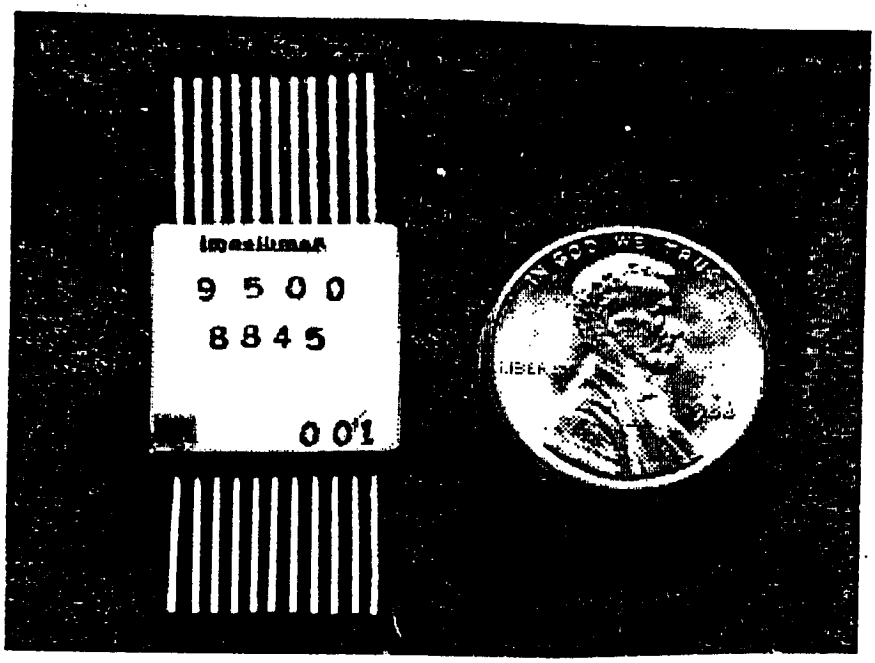

Figure 3.1.4-5 Prototype (#001) Hybrid Curent Driver

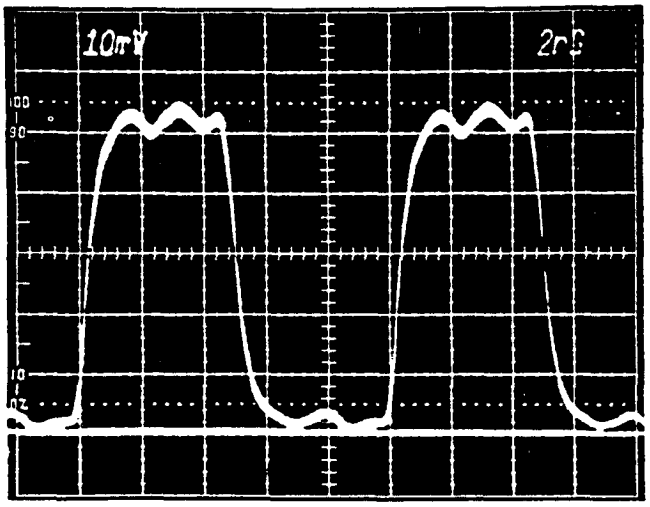

Figure 3.1.4-6 Optical Response of Mitsubishi ML5702A laser diode when driven with 100 mA peak current (40 mA bias). Extinction is essentially complete between optical pulses. Optical output is 30 mW peak. Horizontal scale is 2 ns per major division.

(ii) Local Oscillator

Must be able to lock and track the incoming frequency over a range of ± 10 GHz.

The following section reproduced directly from Ref. 54, is an excellent summary of the issues involved:

The essential features of a space-to-space heterodyne optical communication system using GaA1As lasers are illustrated in the block diagrams of a transmitter and receiver of Figs. 3.1.5-1 and 3.1.5-2. A heterodyne optical communication system operates much like a conventional radio system. The transmitter uses the signal with the information to be transmitted to modulate a transmitter laser; at the receiver, the incoming signal is mixed with a local oscillator. A radio frequency (RF) signal is recovered. Mixing the very weak signal and the strong LO at the receiver raises the signal level well above the noise level of subsequent electronics. The heterodyning can be effective enough that quantum effects are the only limiting factors of the receiver sensitivity. The channel can be modeled as a classical additive white-Gaussian-noise channel, allowing well-known modulation and demodulation techniques to be applied. Near theoretical-optimum receiver sensitivity can be realized with this system, with sufficient frequency selectivity to permit operation even when the sun is directly in the receiver FOV.

As might be expected, a heterodyne optical system imposes demanding technology constraints on system components. Single-frequency laser operation is absolutely essential for the transmitter and LO lasers in a heterodyne system. The transmitter frequency and the receiver LO frequency must be tracked to recover the information in the signal. Single-frequency semiconductor lasers have only been available in quantity for a few years. Until recently semiconductor lasers lased at several frequencies, preventing heterodyne operation.

An example of one of these new lasers is 30 mW Fabry-Perot GaAlAs laser that operates nominally at 830 nm. It is a single spatial-mode laser with electrical-to-optical maximum rated power 30 mW, and biased at twice the threshold current. Figure 3.1.5-3 shows the power spectrum of the laser. This laser operates essentially in a single longitudinal (spectral) mode; the main-to-side mode ratio exceeds 25 dB (typically 27 dB, and a maximum of 35 dB). The mode spacing of 3Å (130 GHz) simply reflects the Fabry-Perot cavity length (300 μm) of the laser. That is, the longitudinal-mode spacing is determined by the cavity length; and integral multiple of half wavelengths must fit within the cavity.

The cavity length also determines the laser's frequency. Modulation of the cavity length is directly reflected in a modulation of the laser frequency, an effect that is used to tune the laser. The tuning is required, among other things, to accommodate the shift in frequency due to the relative motion of the satellites. The maximum Doppler shift encountered in most crosslink applications is about 6Å of tuning range required of the lasers. Most single-frequency GaAl1As lasers today can be tuned far in excess of this amount by temperature-tuning the effective laser-diode-cavity length (Fig. 3.1.5-4). Thermal tuning of the cavity is brought about by expansion and contraction of the temperature dependence of the band-edge absorption within the cavity (-2.7 GHz/K). The total tuning index is 30 GHz/K (or 0.66Å/K).

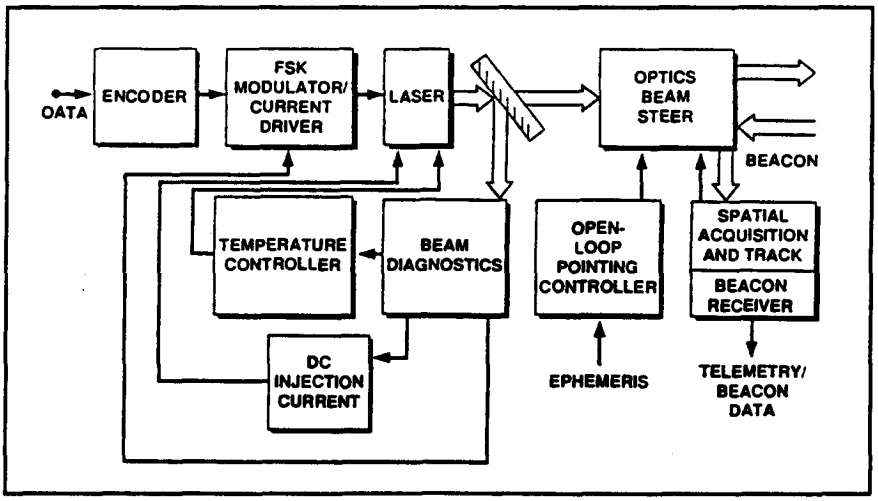

Figure 3.1.5-1 Block Diagram of an Optical Heterodyne Transmitter

Note the feedback from the beam diagnostics package to the FSK modulator, to the dc injection-current source, and then to the temperature controller that stabilizes the laser's cavity length.

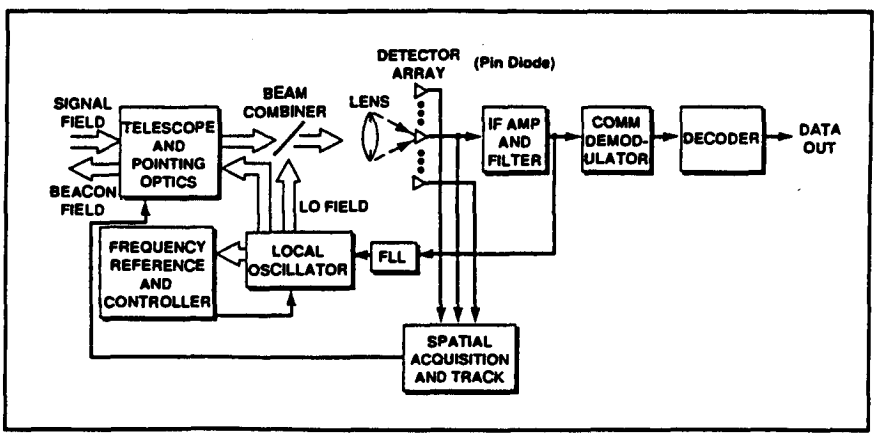

Figure 3.1.5-2 The Optical Receiver

Includes the spatial acquisition and tracking electronics, which provide feedback from the detector array to the telescope and pointing optics.

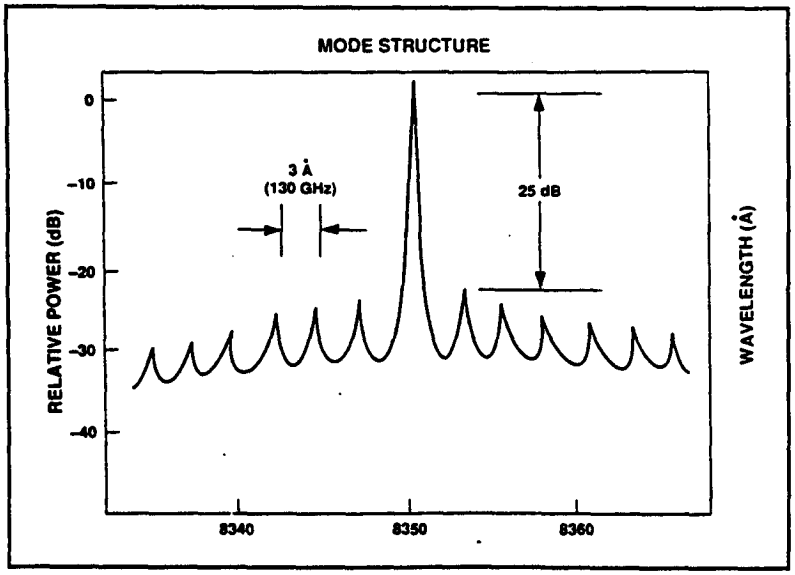

Figure 3.1.5-3 Power Spectrum of a GaAlAs Laser

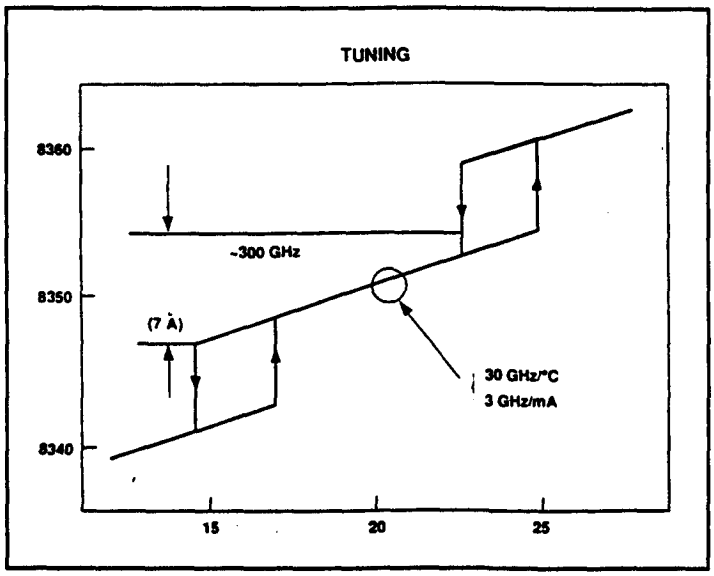

Figure 3.1.5-4 Wavelength vs. Temperature

The laser frequency tunes with bias current in a similar fashion as with temperature. The low-frequency current tuning index is about 3 GHz/mA and is largely due to thermal tuning of the optical length of the Fabry-Perot cavity.

Because of these high tuning sensitivities, the transmitter and LO lasers must be kept at relatively stable temperatures (approximately 0.01K) and bias currents (approximately 10 mA). A frequency-tracking system at the receiver will finish the task of locking the LO laser to the transmitter laser.

In addition to temperature and bias-current effects, the frequency noise characteristics and the line width of the lasers are of concern. Proper design of the frequency-tracking and communication systems requires good characterization of the noise process. The spectrum of the laser frequency noise has a significant 1/f component at low frequencies and it is essentially white between 100 kHz and several GHz. At around 8 GHz a relaxation oscillation resonance takes over and the spectrum decays at 20 dB/decade thereafter (Fig. 3.1.5-5). The white-noise component produces spectral broadening of the laser line and accounts for the predominantly Lorenzian line-shape (Fig. 3.1.5-6). In particular, if the spectrum height of the white frequency noise is S_o (Hz^2/Hz, single-sided), the resultant Lorentzian full-width half-maximum linewidth is: $\Delta\nu = S_o$. The linewidth varies approximately as the reciprocal of the laser output power and, for lasers operating at 30 mW, typical linewidth values are 3 to 8 MHz. The 1/f frequency noise induces random centre-frequency wander of the Lorentzian spectrum, broadening the apparent linewidth by approximately 1 MHz. This part of the noise spectrum is particularly detrimental to a heterodyne system; unattended, the IF signal will eventually stray outside the detector's response-bandwidth. Thus, this component of the frequency noise must be tracked and compensated for by the receiver's frequency-locking system.

Modulation/Demodulation Coherent Source Issues

Development of efficient modulation and demodulation techniques is an important step in realizing the promised performance gains of optical heterodyne communication systems. To a first approximation, the optical heterodyne channel can be modeled as a classical additive white-Gaussian-noise channel. Phase-shift keying (PSK) and frequency-shift keying (FSK) are two modulation schemes commonly used with classical white-Gaussian-noise channels. It would seem that either modulation scheme may be suitable for use with optical heterodyne channels, but the presence of device imperfections, such as nonzero-linewidth lasers at the transmitter and receiver, significantly complicate the analysis and choice of a modulation scheme.

Modulation schemes requiring coherent demodulation, such as PSK, require tracking of the laser phase-noise. For example, for a laser line-width of 5 MHz, 10^{10} to 10^{11} photons/s must be detected at the receiver to phase-lock. Typical optical channels that operate at several hundred Mbps and at a communication efficiency of 10 photons/bit do not offer this required power (10^9 photons versus the required $10^{10\text{-}11}$). This lack of power rules out the possibility of phase locking, unless further laser developments reduce laser linewidths significantly. Laser linewidths can be reduced by using external cavity lasers, which, however, increase the mechanical complexity of the system, thus increasing the cost and decreasing the reliability of the system.

When phase tracking at the receiver is not feasible, one of the most efficient modulation schemes possible is FSK signalling pair with noncoherent demodulation. M-ary FSK signalling (signalling with one of M possible tones) can be conveniently accomplished by direct-current modulation of the semiconductor laser. Noncoherent demodulation of FSK only requires frequency tracking, which has been demonstrated to stabilize center-frequency drift of the laser caused by the 1/f component of the FM noise spectrum to a few MHz rms error. Operational use of such a system has been shown to cause negligible performance degradation.

A GaAlAs laser can be frequency-modulated through direct injection-current modulation, thereby providing both a frequency-modulated transmitter laser and a frequency-agile LO. If an FSK transmitter is to be realized by direct injection-current modulation of a semiconductor diode laser, its modulation characteris-

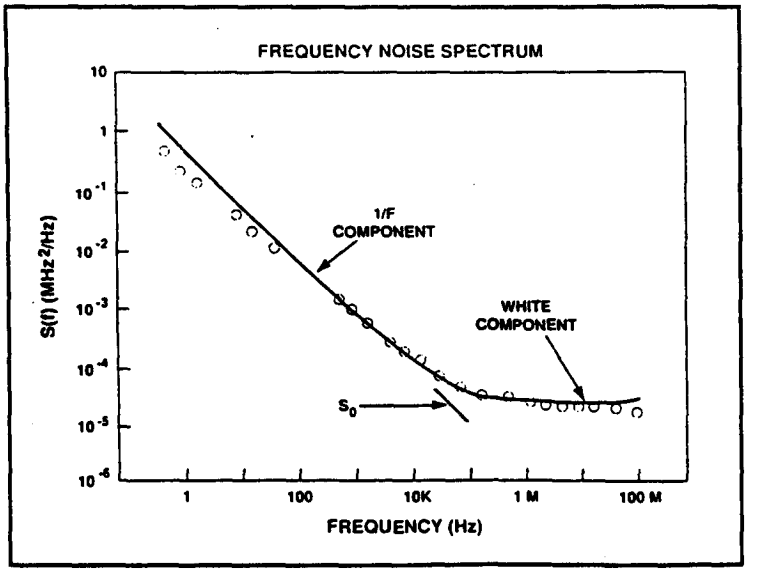

Figure 3.1.5-5 Frequency Noise Spectrum of a Typical Single-Mode Laser Diode

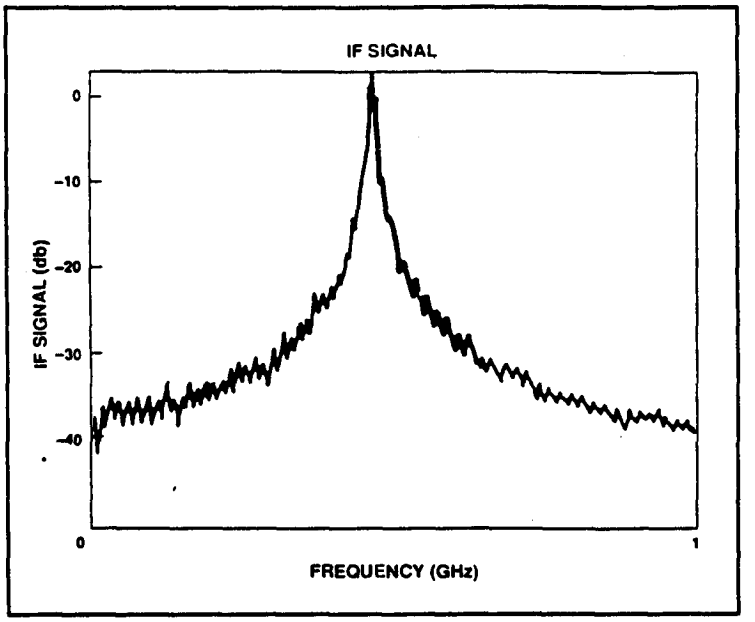

Figure 3.1.5-6 Lineshape of GaAlAs Laser

tics throughout the spectrum of the modulation wavelength must be uniform. In particular, for an FSK injection-current modulator, operating in the 100-Mbps region, the laser must exhibit a flat frequency modulation (FM) transmitter function from DC to a few hundred MHz.

Most GaAlAs lasers do not exhibit flat FM transfer functions; thermally enhanced FM characteristics cause excessive tuning of the diode-laser output frequency at low frequencies. Consequently, the FSK tones often drift - the amount of drift depending upon the bit pattern being transmitted and the duration of a tone. Uncompensated, this thermal frequency drift can severely degrade communication-system performance by spreading tone energy over a wide bandwidth, thus increasing cross talk between frequency slots and creating data-pattern-dependent errors. A passive equalization network, that significantly reduces the effects of low-frequency thermal FM, is simple to implement and requires neither active electronic nor optical components.

Binary and 4-ary FSK modulators have been developed at Lincoln Laboratory. The 4-ary modulator consists of a 0-to-200-mA variable constant-current source used to bias the laser diode. This biasing determines the frequency of tone zero. Incremental injection currents are switched into the bias network via a series of high-speed GaAs field-effect transistors. These currents are summed in the bias network to provide the modulation injection currents that determine the frequencies of tones one, two, and three. Figure 3.1.5-7 shows 4-ary FSK data recovered at the receiver. The modulator can be run at 110-MHz symbol rate with two bits per symbol (4-ary FSK), yielding 220 Mbps. The tone transition time for this system is 1 ns (approximately 10% of symbol duration).

3.1.5-2 Frequency Stabilisation of Semiconductor Lasers

If an optically-locked-loop (OLL) is to be implemented at the receiver, then it is obviously important that the transmitter and receiver L.O. are within the range of the OLL. At the optical frequencies of approximately 3.5×10^{14} involved here, a stability of 1 in 10^5 to 1 in 10^6 is required. The technique employed in to use absorption cells containing (e.g.) rubidium or neon vapour with absorption lines in the wavelength region of interest. A portion of the laser output is split off and the absorption cell throughput is monitored whilst the absorption line position is modulated by the application of a magnetic or electric field. The signal is detected via a lock-in amplifier; the lock-in output drives a

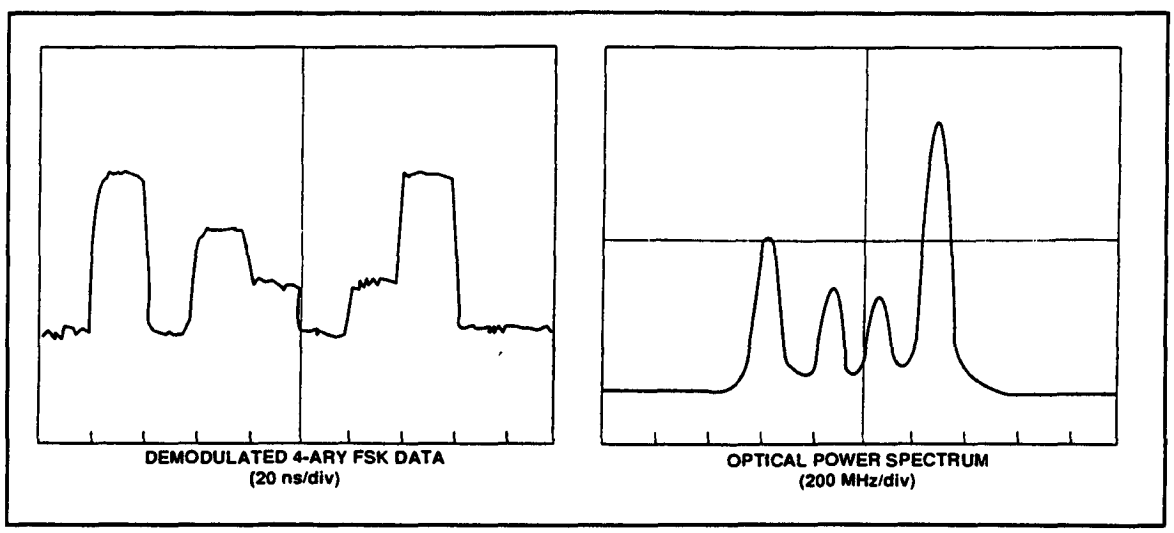

Figure 3.1.5-7 Recovered FSK Laser Output (Left Trace; Time-scale 20 ns/div) and the Time-Averaged Optical Power Spectrum of the FSK Laser Output (Right Trace; 200 MHz/div).

feedback loop which adjusts the laser temperature and drive current to hold it at the absorption line frequency.

Figure 3.1.5-8 (Ref 59) shows an example using tunable DBR (Distributed Bragg Reflector) lasers at 1.5 μm using a C_2H_2 absorption cell. Offset frequency stabilization up to ± 400 MHz is illustrated. The experimental set-up is more complex than would be required for a flight unit, but even so, such a source is non-trivial.

Within Canada, EG&G has previously sponsored such work at Université de Laval.

3.1.5-3 Nd:YAG Lasers for Coherent Links

A huge advantage of Nd:Yag is that the frequency is automatically determined by the nature of the laser material and the output coatings and that a narrow linewidth (10kHz) is simply obtained. The output can be thermally tuned by +/- 100 GHz; conversely, the laser must be thermally stabilized - a non-trivial task for a high power laser.

Frequency or phase modulation must include the use of an additional modulator. Typically an external electro-optic modulator is employed.

3.2 Detectors

3.2.1 Introduction

3.2.1.1 Optical Noise Background

Background Noise at optical wavelengths is characterized by the predominance of shot noise, i.e, the random arrival rate of photons of light.

In this regime, receiver sensitivity is quantified by the number of received photons M required to detect the presence of a bit. As the frequency of the laser increases (wavelength decreases) the energy of a photon increases and the energy represented by M photons increases proportionately. Thus the laser transmitter power increases due to this factor proportional to frequency as the laser wavelength decreases.

The coherent detector diode noise can be predicted using the following relationship [40].

$$P_N = \left[\frac{hf}{exp(hf/kT)-1} + \frac{hf}{\Omega}\right] B$$

Where

P_N - Background Detector noise power
B Hz - Bandwidth
f Hz - Laser frequency
h - Planck's constant
k - Boltzmann's constant
T - Effective background temperature
Ω - Effective quantum efficiency

The first term in the equation represents the thermal noise and the second term represents the quantum noise. Figure 3.2.1-1 illustrates the noise power density versus laser frequency as a function of background scene temperature. If the transmitter signal is represented by Ps, the signal to noise ratio will be adequately described using the following expression:

$$S/N = Ps\Omega/(hfB)$$

The background thermal radiation is broadband since it originates from a thermal source and the received energy depends upon the bandwidth of the receive filters. For direct detection systems, the filtering is done at optical wavelengths and the bandwidth is very large resulting in a large background noise power falling on the detector. For heterodyne systems, the final filtering is done at baseband so that the noise bandwidth is only slightly wider than the signal bandwidth. This makes heterodyne systems much more immune to background thermal radiation such as the sunlight earth.

From Figure 3.2.1-1 it is evident that the short wavelength lasers are much further from the region dominated by thermal background noise and are able to operate more easily in the direct detection mode. In the case of the CO_2 laser, it is much closer to the thermal region and would have difficulty operating with a direct detection receiver.

Figure 3.1.5-8 Principles of Laser Stabilisation

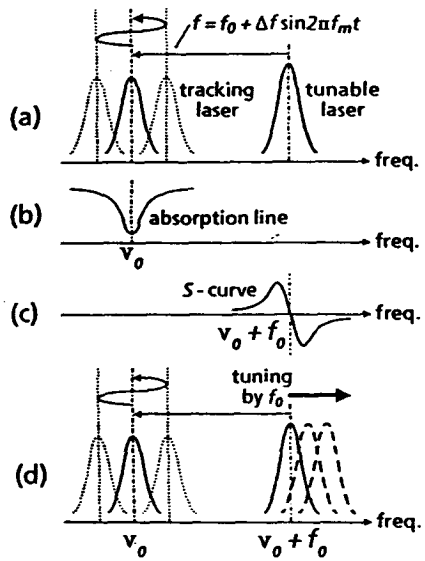

CThB2 Fig. 1. Principle of tunable-laser frequency stabilization: (a) tracking laser locked and modulated to the tunable laser; (b) absorption detected by the tracking laser; (c) lock-in-detected S-curve; and (d) tuning by f_0 with stabilization.

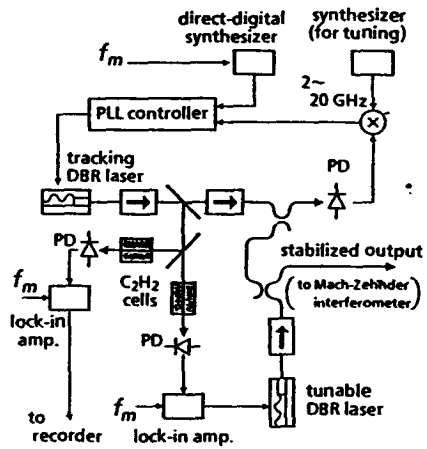

CThB2 Fig. 2. Experimental setup for stabilization of the tunable DBR laser.

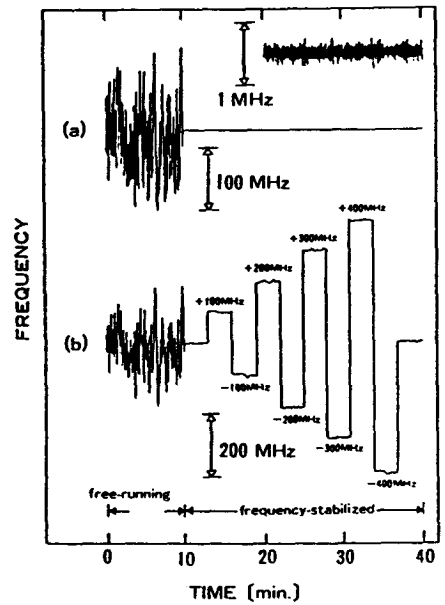

CThB2 Fig. 3. Simultaneous traces of (a) tracking-laser frequency monitored by the independent C_2H_2 cell, and (b) tunable-laser frequency roughly monitored by a waveguide Mach–Zehnder interferometer. Inset on (a) shows the trace magnified 100×.

SPAR

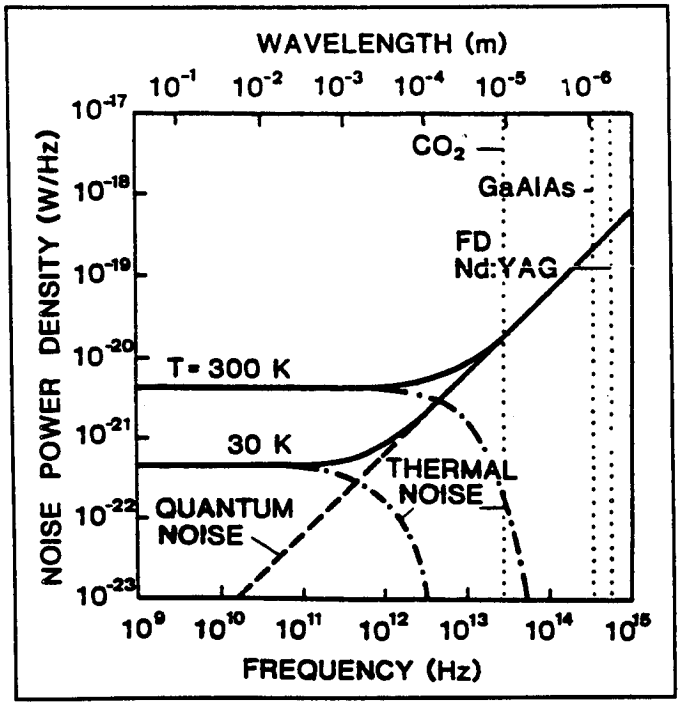

Figure 3.2.1-1 Receiver Noise Power Density Versus Carrier Frequency (Wavelength)

3.2.1.2 Detector Speed

Figure 3.2.1-2 illustrates a typical HgCdTe diode structure for operation at 10.6 μm. To ensure high speed operation three factors must be considered [99]:

a) Diffusion effects: when the depletion region is narrow with respect to the absorption length, only those carriers created within less than one diffusion length will reach the junction and the time required for this action to take place limits the speed.

b) Transit time in the depletion region: the widening of the depletion region causes an increase in the number of carriers generated.

c) Junction capacitance: The photo diode equivalent circuit (Figure 3.2.1-3) shows the presence of a cut off frequency limitation through the $R_L C_D$ time constant.

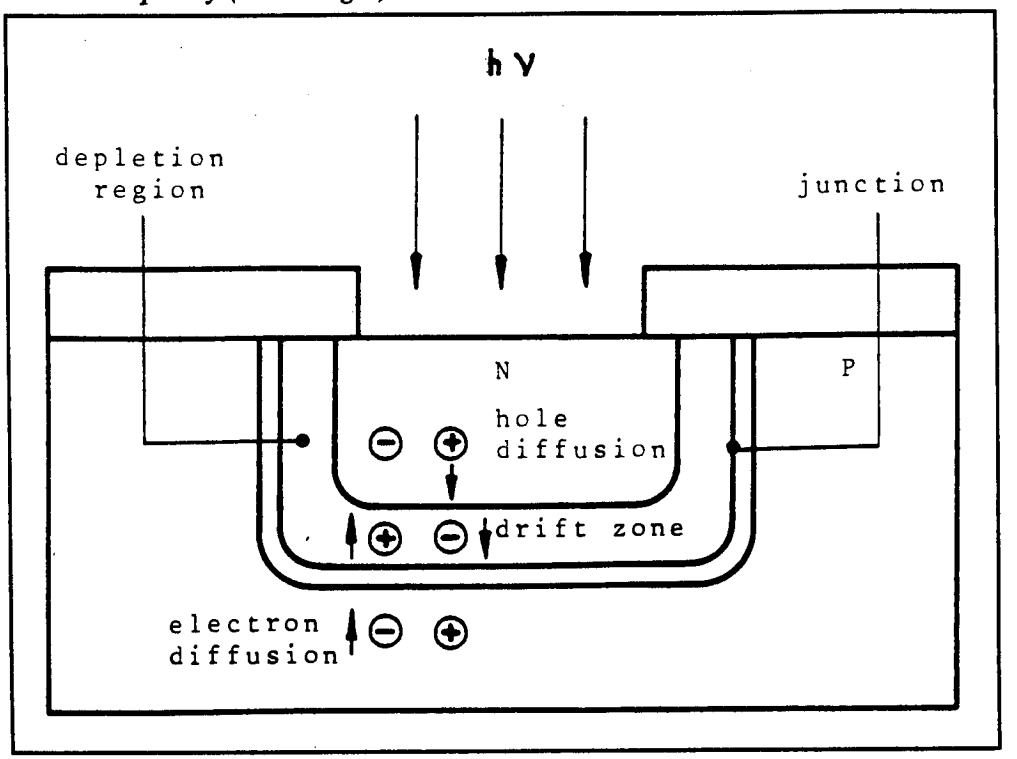

Figure 3.2.1-2 Photon-Induced Current Generation Process in a Photodiode (Junction Depth = Photon Absorption Length)

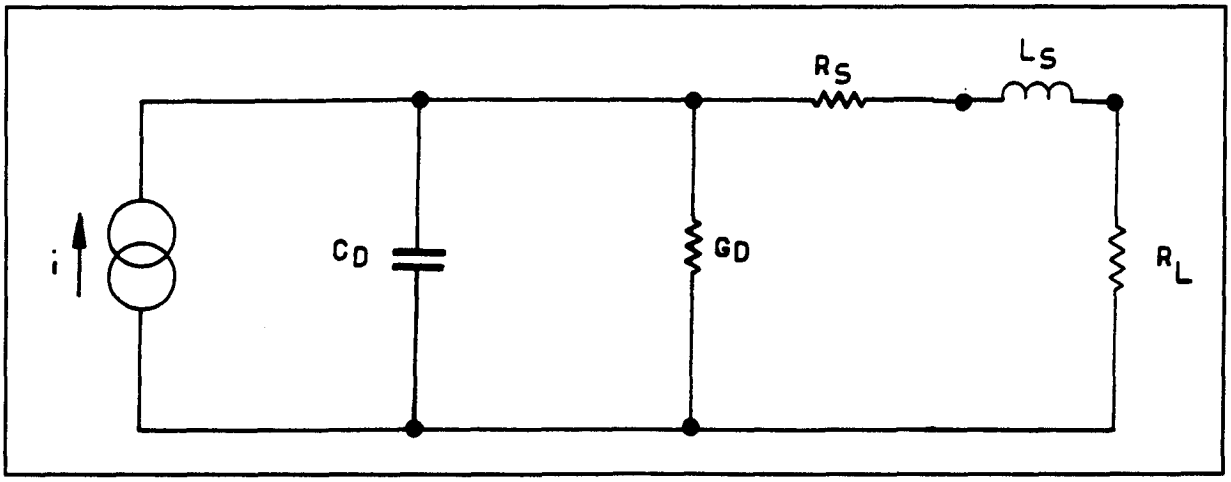

Figure 3.2.1-3 Photodiode Equivalent Circuit

The improvement of the cutoff frequency of a photodiode therefore requires the following efforts:

1. Reduction of the junction capacitance by reducing the surface area and the doping level on either side of the junction.

2. Widening of the depletion region and bringing it closer to the surface. This also requires low doping level, a junction depth adapted to the extension of the depletion region and to the absorption length and elevated breakdown field strength

3.2.2 Communications Receivers

3.2.2.1 Introduction

There are two possible approaches; direct detection or coherent detection. Their relative merits are summarized in Table 3.2.2-1. Essentially, both theoretically and in practice, at bit rates above 1 Gbps, coherent systems give the best sensitivity. Practically, coherent

Table 3.2.2-1 Direct Detection Versus Coherent Detection

	Direct Detection	Coherent
Source Requirement	Simple. Extinction ratio important.	Complex. Thermal Control. Wavelength stabilization.
Receiver	Simple. Requires best APD's.	Complex. Tunable Local Oscillator needed. PIN detectors fine.
Source Extinction Ratio	Important, must be low.	Irrelevant.
Background	Degrades sensitivity.	Almost irrelevant (can look into sun).
Performance at Low Bit Rates	Excellent.	Laser linewidth limited.
Performance at High Bit Rates	Good.	Excellent.
Sensitivity	Good.	Best.
Status	Units in quantity production. Space qualified systems.	Developmental prototypes. Some space qualification done.

receivers will always be more complex, more power hungry, and probably less reliable. For the system designers, the issue is which to choose.

3.2.2.2 Direct Detection Receivers

All direct detection ISL receivers comprise an APD and an optimized hybrid. Figure 3.2.2-1 show a "typical" RFE (Receiver Front End), specifically that designed by EG&G for Matra.

The apertured APD is 100 μm diameter; the estimated capacitance is 0.25 pF, the calculated external quantum efficiency is ≈90% at 820 nm. The excess noise factor F = kM + (1-k)(2-1/M), (≈2 + kM for low k and high M) where the measured k is ≈0.005 at 830 nm. Stable gain (M) at full frequency response is obtained from M ≈1.5 to >1000. The low capacitance and low excess noise are the exceptional and novel features of this APD which contribute to the high receiver sensitivity. The wide gain range allows an AGC function to be performed using APD bias over an optical dynamic range exceeding 20 dB.

The integrating front-end has a transimpedance of ≈400 kΩ and a -3 dB frequency response of 1 MHz. The preamplifier uses a NEC 7200 input MESFET followed by cascode and gain stages around which a 400 kΩ feedback loop is applied. Switchable equalizers give overall -3 dB bandwidths of ≈20, 40, 80 and 160 MHz to match QPPM (Quaternary Pulse Position Modulation) data rates of 15, 30, 60 and 120 Mb/s. Additional stages include ± 4 dB fast (100 μs) elec-

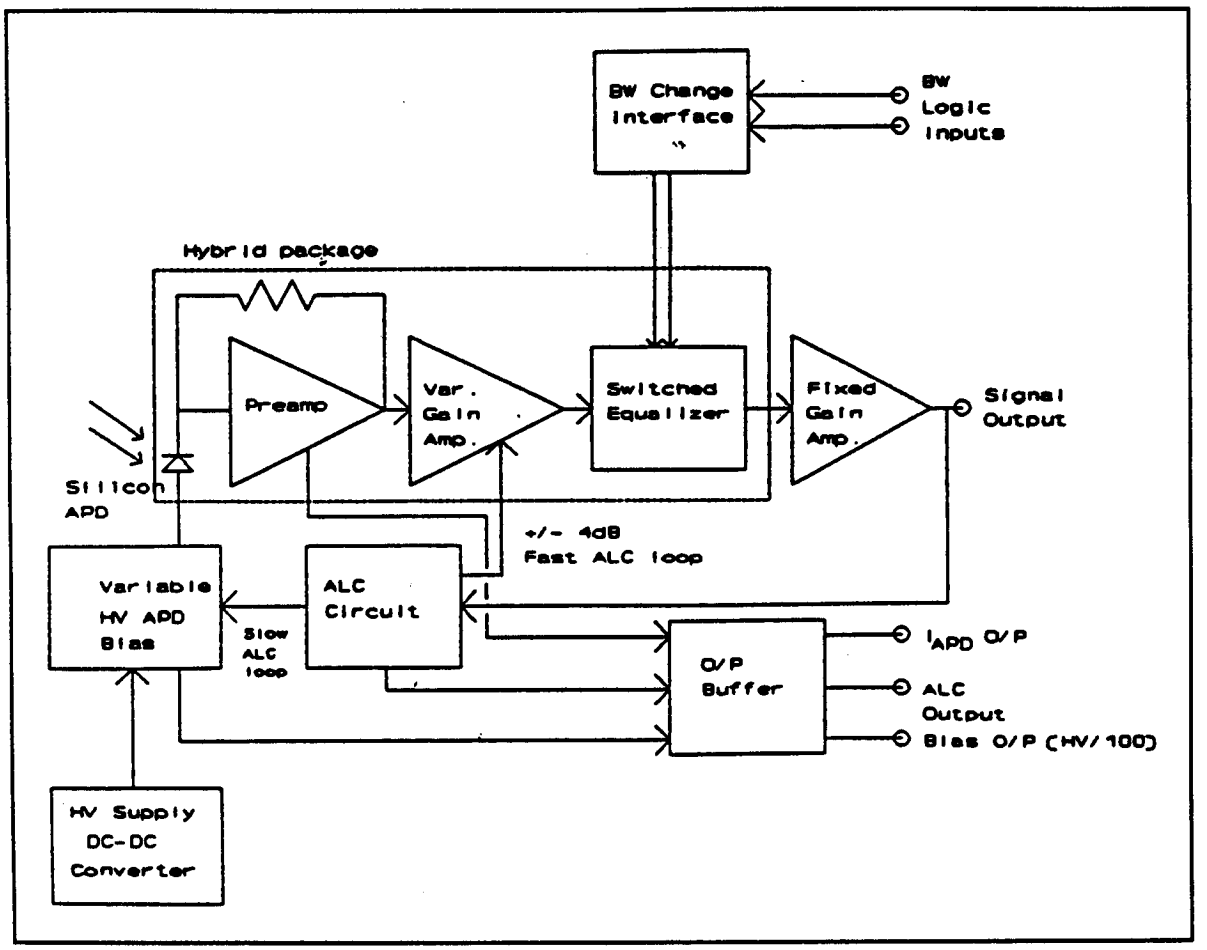

Figure 3.2.2-1 RFE Schematic Circuit Diagram

tronic AGC gain stage and a switched-in gain stage for 120 Mb/s. A space qualified, single bit rate version would consume ≈1 Watt and weigh ≈300 gm. This receiver uses the best available APD. Other work has employed the EG&G C30902E with a 500 μm diameter, 1.2 pf capacitance and a k of 0.02.

The Silex breadboard illustrates an example of the two common modulation schemes, NRZ and PPM (Non Return-to-Zero and Pulse Position Modulation). Figure 3.2.2-2, from Ref. 61, shows bit per word, relative bandwidth and duty cycle for OOK (NRZ) and PPM schemes. (2 PPM is Manchester Biphase Modulation). PPM schemes have three clear advantages over NRZ.

(i) The laser duty cycle is <0.5 for 4 PPM and higher, allowing (as shown by experiment) higher peak powers in inverse proportion to the reduced duty cycle.

(ii) The pulse duty cycle is constant, and the pulse frequency has a lowest harmonic at one fourth the data rate for 4 PPM (known as QPPM for quaternary) and one eighth for 8 PPM. With NRZ, long runs of zeros or ones give a much lower LF cut requirement for the preamp, and a problem with wander on the DC level which complicates the demodulation task - see (iii).

(iii) PPM schemes always have one pulse per word, allowing use of a PPM maximum likelihood demodulator which looks for the largest pulse within the slots in any given word.

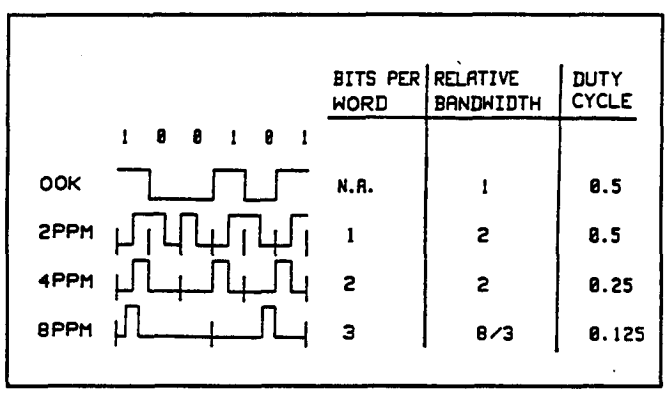

Figure 3.2.2-2 Optical Transmission Schemes for Direct Detection Systems

Experiments show that such a demodulator can give 2 to 3 dB sensitivity improvement over a fixed threshold NRZ demodulator. Davidson and Sun (Ref. 62) have shown a 50 Mb/s demodulator based on standard commercially available ECL chips, with both word clock and slot clock recovery achieved at 20 detected photons/bit, well below the BER = 10^{-6} level of 60 detected photons/bit.

NASA Goddard are committed to QPPM schemes for their direct detection links. Silex was originally committed to QPPM, but shied away from the cost of space qualifying a custom I.C. QPPM demodulator; it is not clear that this was a good decision.

Preamplifiers

Preamplifier design is part science and part art. At low frequencies, dark noise is dominated by the Johnson noise of the feedback resistor. Optimizing the preamplifier design and layout to allow a high value of feedback resistor for any given frequency response is definitely an art. EG&G can now obtain $R_L \times f_{-3dB}$ products of $\approx 10^{13}$ Ω Hz, believed to be close to the best achieved anywhere.

At higher frequencies, (10's of MHz), input capacitance dominates, mitigated by the use of high transconductance FETs. Both GaAs FET's and HEMT's (High Electron Mobility Transistors) have useful properties. As the state of this art improves, so preamps are showing gradual improvements with time. Use of state-of-the-art components implies that these parts are not available from "Space Qualified parts" lists, which leads to increases in cost, risk and development time. Recent development by AT&T of a HEMT with a Gamma/gm 2.4 times better than previously available will lead to improvements in future preamps.

Optical Preamplifiers

As outlined in the laser discussion, a frustrated laser is an optical amplifier. Such an amplifier can be used as a preamplifier for low level signals and a lot of successful work has been done with fibre optic amplifiers operated at 1500 nm. The sensitivity of such a system

is limited by spontaneous emission in the amplifier and theoretical studies (Ref. 63) show a bit rate independent limit of 38 photons/bit. Levels around 150 photons/bit have been achieved at 1500 nm.

Achievement of such an optical preamplifier at ISL wavelengths would be a significant achievement. However, pump powers of a few watts appear to be required to give the necessary gain levels, so there is a clear power dissipation/sensitivity trade-off.

Ytterbium: Yag Optical Preamplifiers at 1032 nm

The same parameters that make Yb:YAG an attractive laser candidate, also make it an attractive optical preamplifier candidate for RFE's operating at 1032 nm. The increased efficiency due to high attainable doping will reduce the required power density for the achievement of amplifier performance. A "perfect" optical preamplifier could have a gain of 30 to 40 dB and a wideband (0 to > 10 GHz) frequency response.

A theoretical frequency independent, sensitivity of 38 photons/bit has been predicted for optical amplifiers, and ≈110 photons/bit has been demonstrated experimentally at 1550 nm with fiber amplifiers at 622 Mb/s and 2.5 Gb/s.

3.2.2.3 Coherent Detection Receivers

For an excellent tutorial review on coherent receivers, see Ref. 64. A brief summary is included here. Details on source, local oscillator and optical locked loop issues were addressed in Section 3.1.5.

A coherent optical receiver is essentially similar in concept to a radio receiver. The received signal is mixed with a local oscillator to give an IF signal. The modulation of this IF is then detected. Such techniques simplify the detector requirements at the expense of complicating the local oscillator requirements.

The incoming signal may be:

ASK (Amplitude Shift Keying)
FSK (Frequency Shift Keying)
PSK (Phase Shift Keying)

The local oscillator must track the incoming optical frequency (≈4.10^{14} Hz) to generate a constant IF; such an OLL (Optically Locked Loop) is equivalent to the "AFC" function on an FM radio. The IF may be zero on a homodyne system which gives the lowest noise, or higher on a heterodyne system, which gives higher noise.

Figure 3.2.2-3, taken from Leeb [64], shows absolute sensitivity limits in photons/bit. Note that the direct

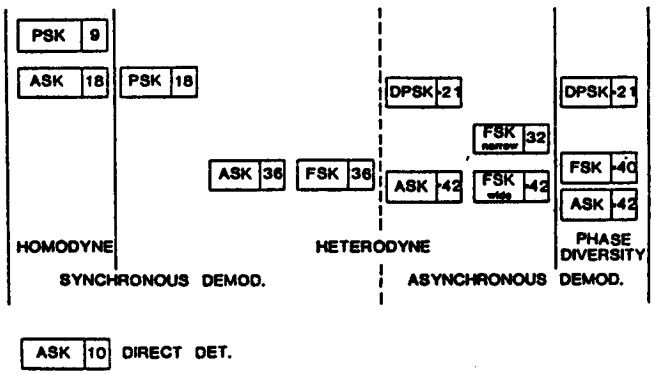

Absolute sensitivity limits, expressed in photons/bit, for various coherent receiver concepts and binary modulation formats, to achieve a bit-error-rate of BER = 10^{-9}. For frequency shift keying (FSK) the amount of frequency deviation (narrow, wide) makes a slight difference. For comparison, the limit for direct detection on-off keying (≡ASK) is given, too.

Figure 3.2.2-3 Coherent Detection Sensitivity Limits

detection limit at BER of 10^{-9} is 10 photons/bit, and is surpassed only by PSK homodyne, but coherent limits are generally more attainable than direct detection limits.

Figure 3.2.2-4 illustrates coherent receiver principles in terms of the receiver schematic and the photocurrent frequency spectrum. A heterodyne receiver is less sensitive than homodyne because it requires twice the electrical bandwidth, allowing more noise through; in addition, the high IF may lead to problems with receiver noise of the local oscillator power is not sufficiently high.

Figure 3.2.2-5 shows homodyne and heterodyne receiver configurations with OLL's included. (These do not in themselves address the problem of polarization alignment between the local oscillator and the incoming signal - a necessary condition for coherent detection). In carefully controlled experiments, such receivers have shown sensitivities within 1 dB of the theoretical limits.

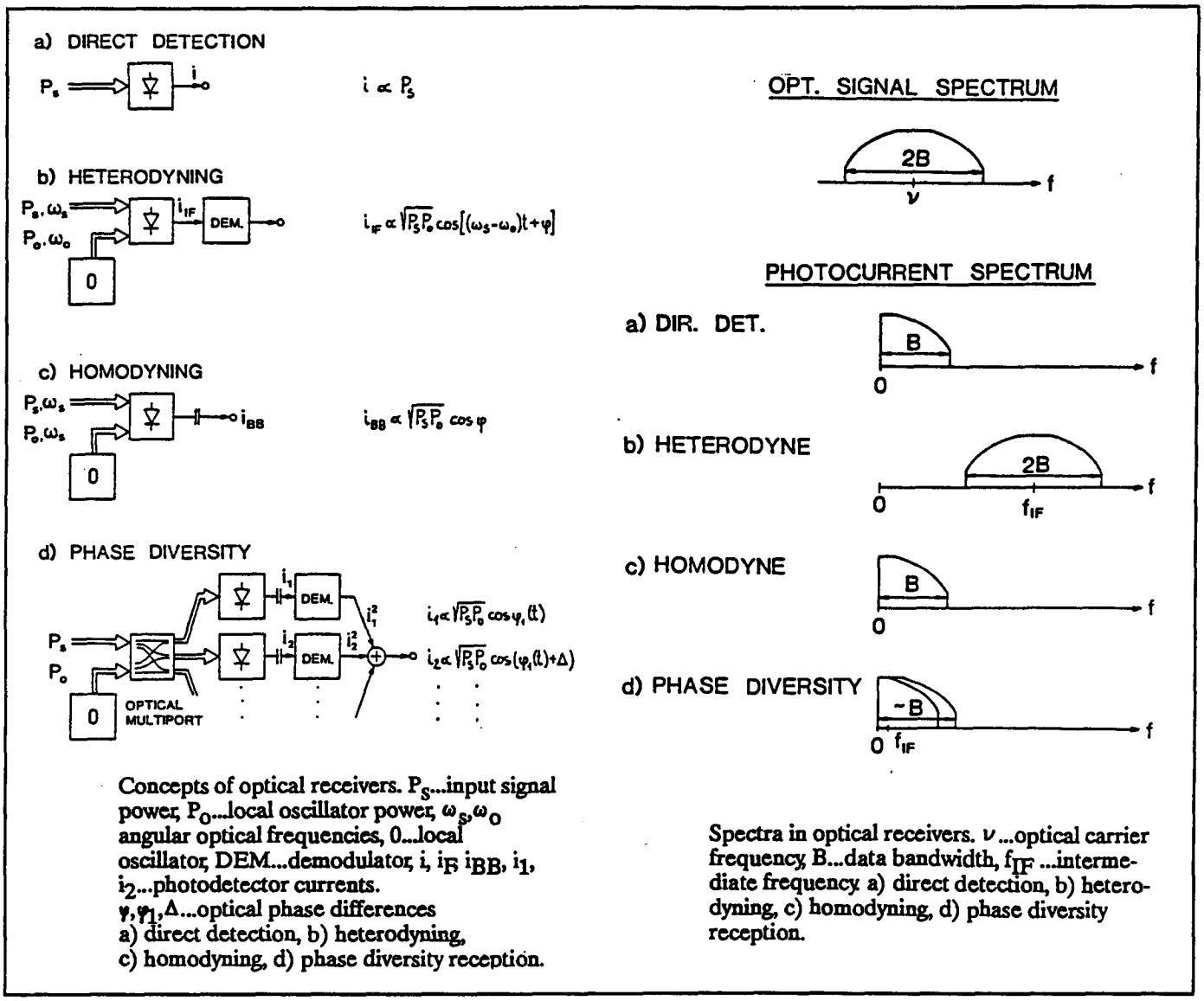

Concepts of optical receivers. P_S...input signal power, P_O...local oscillator power, ω_S, ω_O angular optical frequencies, 0...local oscillator, DEM...demodulator, i, i_F i_{BB}, i_1, i_2...photodetector currents. $\varphi, \varphi_1, \Delta$...optical phase differences a) direct detection, b) heterodyning, c) homodyning, d) phase diversity reception.

Spectra in optical receivers. ν...optical carrier frequency, B...data bandwidth, f_{IF}...intermediate frequency a) direct detection, b) heterodyning, c) homodyning, d) phase diversity reception.

Figure 3.2.2-4 Coherent Receiver Principles

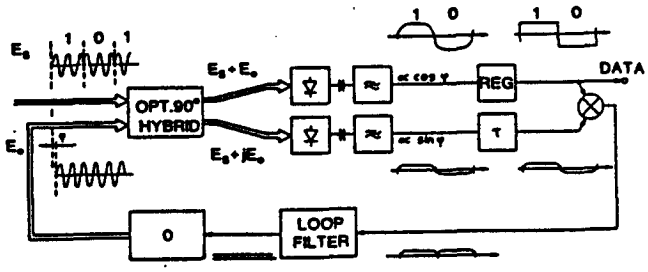

Homodyne receiver for PSK ("decision driven Costas phase-locked loop"). E_S,E_O... input and local oscillator field, φ...phase error, REG...regenerator, τ...one bit delay, 0...local oscillator.

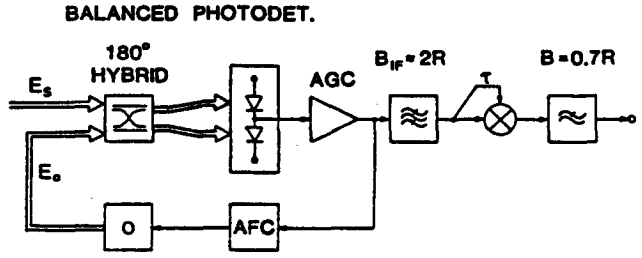

Heterodyne receiver for DPSK, with balanced photodetector. AGC...automatic gain control, AFC...automatic frequency control, B_{IF}, B... filter bandwidth, R...data rate, τ...delay.

Figure 3.2.2-5 Homodyne and Heterodyne Receivers

A further difficulty with coherent system is that laser phase and frequency noise, as represented by laser linewidth, is a severe limitation at low data rates. Figure 3.2.2-6 shows sensitivity limits for various coherent receiver techniques as a function $\Delta v/R$ (laser linewidth/data rate).

Finally, when looking at reported results, a number of factors must be taken into account.

i) All 1300 and 1500 nm results are for fibre optic systems which give perfect mode matching in a single mode fibre. A free space link will show imperfect matching (Airy to Gaussion) leading to a 1 to 2 dB probable power penalty.

ii) Wave front aberrations in the incoming signal and the local oscillator will lead to a further loss; $\lambda/13$ rms gives a 1 dB loss.

iii) Beamsplitters will lead to further losses of a fraction of a dB.

iv) Polarization mismatching may lead to further losses.

It would appear that with free-space, coherent links, performance will always be 1.5 to 3.0 dB worse than the best fibre optic examples. Wavefront alignment problems are discussed in more detail below.

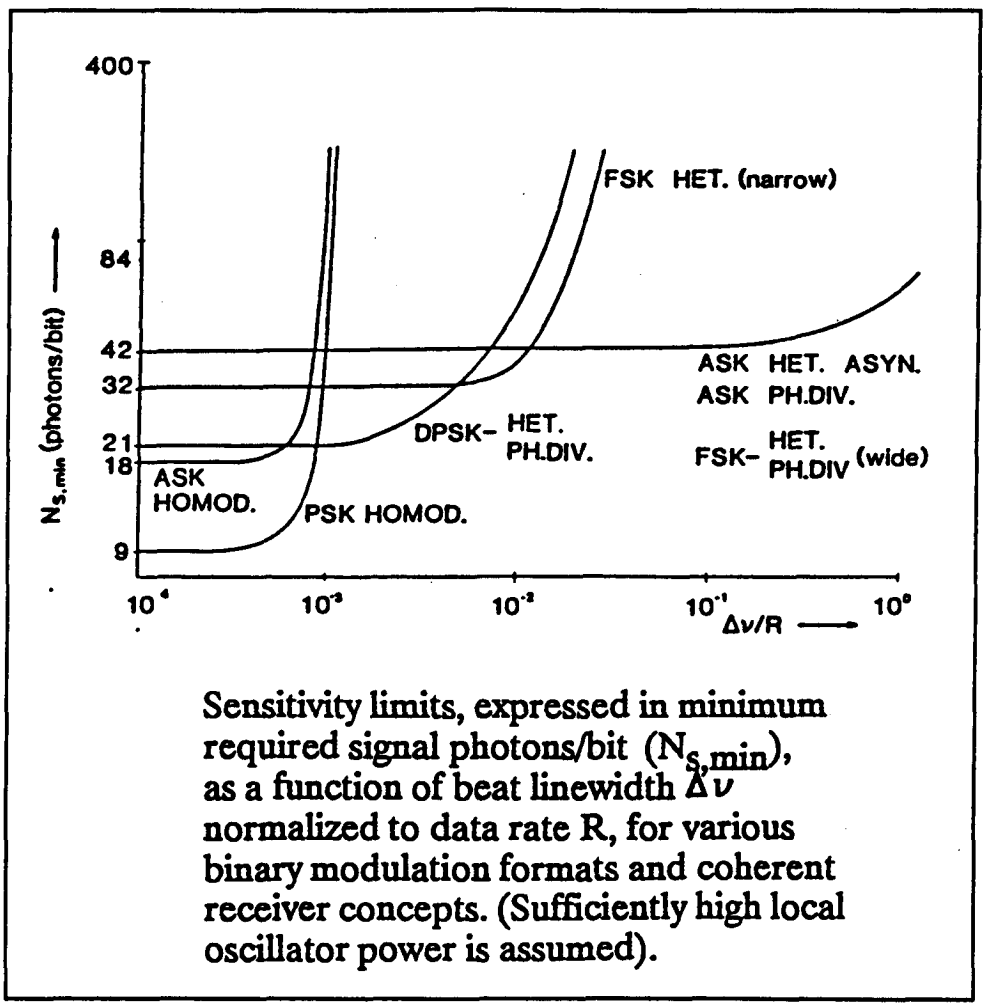

Sensitivity limits, expressed in minimum required signal photons/bit ($N_{s,min}$), as a function of beat linewidth $\Delta\nu$ normalized to data rate R, for various binary modulation formats and coherent receiver concepts. (Sufficiently high local oscillator power is assumed).

Figure 3.2.2-6 Coherent Receiver Laser Linewidth Dependence Limits

Photomixing and Alignment Losses

Alignment of the local oscillator and the received signal beam is essential and is normally achieved using an active control loop in the receiver. Anomalous effects due to local heating may occur if either of these beams is focused too tightly. Theoretical studies have shown that a Gaussian local oscillator beam provides very efficient optical mixing for signal beams with Airy intensity distributions if the diffraction limiting spot matches the detector areas [6]. With this technique a mixing loss of only 1.3 dB has been demonstrated [3]. In the same demonstration additional losses of 0.3 and 1.8 dB arose due to polarization effects and wavefront errors respectively.

The laser local oscillator power output is controlled by stabilizing the laser on a single spectral transition line and further externally modulating the output power. For a 10.6 μm laser system an acousto-optic modulator can be employed to control the output power which is monitored via an optical beam splitter using an external power sensing detector. The acousto optic modulator also allows fast frequency tuning of the LO radiation to compensate for mechanical disturbances.

In the Homodyne detection scheme employed by ESA the photomixer acts as a phase detector for the optical phase lock loop. This loop together with an active loop filter and the associated electronics produces a control voltage which drives the voltage controlled optical local oscillator (via the grating and acousto-optic modulators) so that the LO laser phase is synchronized to the instantaneous phase of the incoming signal wave [41]. Figure 3.2.2-7 illustrates the ESA 10.6 μm receiver concept [42].

ESA has examined a variety of receiver electronics designs for a 10.6 μm band system including a linear phase lock loop, a low intermediate frequency translation loop (LIFTZ) and a costa receiver [96]. As illustrated in Figure 3.2.2-8 experimental work performed at a data rate of 140 MBit/sec successfully demodulated .12 nW sideband powers at bit error rates of 10^{-6} (50 photons/bit).

Detector Efficiency Factors

Studies have shown that the local oscillator power must be selected such that the heterodyne noise equivalent power is minimized. Figure 3.2.2-9 illustrates the noise optimization which may occur as the local oscillator power is increased. Variations between detectors also limit the practical performance of a heterodyne detection system. The ideal heterodyne detector should exhibit the following characteristics:

a. Wide bandwidth with a flat response

b. High quantum efficiency (typical diodes exhibit 50% QE for 10.6 μm operation)

c. Capability to handle high local oscillator powers

d. Be physically robust with a long stable operating life.

e. Have well matched amplifier electronics

For most applications, an effective quantum efficiency is employed which includes the impact of these factors. As reported, typical diodes will exhibit a quantum efficiency of 0.5 - 0.6 at 1 GHz. A further increase in the operating frequency will reduce the efficiency considerably as illustrated in Figure 3.2.2-10 [97]. However, enhanced performance can be obtained by cooling the amplifier electronics as illustrated in Figure 3.2.2-11. [98].

MPB Technologies have been funded by CRC to undertake research in ISL (Ref. 92, 1986 and Refs. 93 and 136, 1990). This work included both direct detection and heterodyne (FSK) detection at 1 Gb/s. The achieved sensitivities of $\approx$ 665 photons/bit (-38 dBm) in heterodyne mode and $\approx$ 730 photons/bit in direct detection (10^{-6} BER, 840 nm, 10101100 data stream) were not particularly impressive, but did serve to explore some of the areas to be worked on. MPB specifically identified:

- APD responsivity; the Antel APD used was fast but had poor responsivity. Better APD's are now available with lower excess noise.

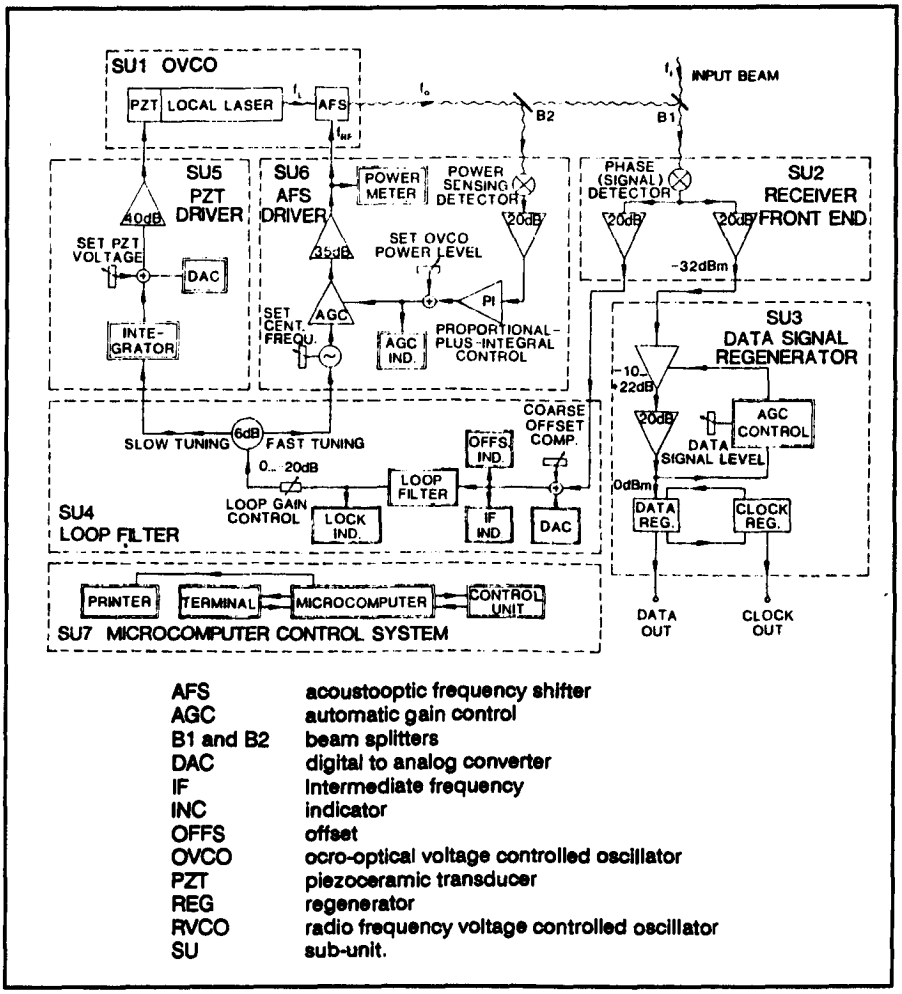

AFS	acoustooptic frequency shifter
AGC	automatic gain control
B1 and B2	beam splitters
DAC	digital to analog converter
IF	intermediate frequency
INC	indicator
OFFS	offset
OVCO	ocro-optical voltage controlled oscillator
PZT	piezoceramic transducer
REG	regenerator
RVCO	radio frequency voltage controlled oscillator
SU	sub-unit.

Figure 3.2.2-7 Block Diagram of a CO_2 Laser Receiver

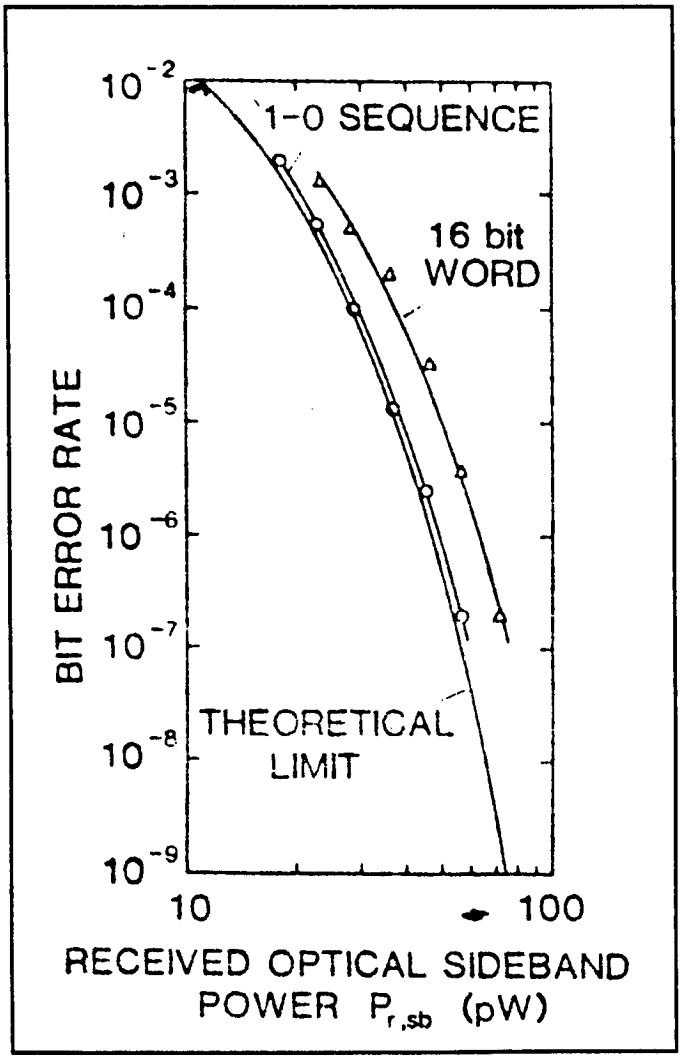

Figure 3.2.2-8 BER of Detector Plus Receiver Front End Versus Optical Input Side Band Power at 140 Mbps

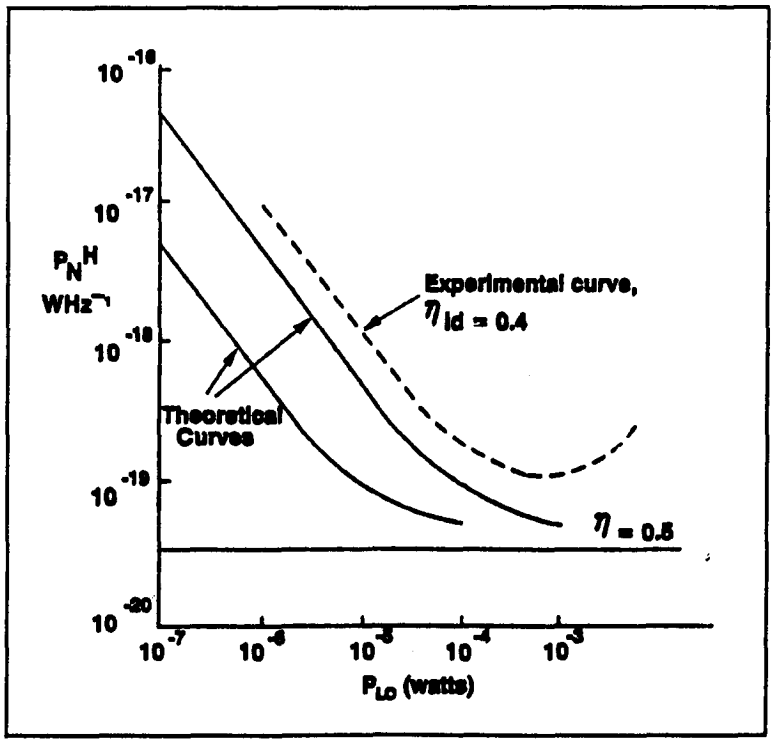

Figure 3.2.2-9 Curves for the Heterodyne Noise Equivalent Power PH/N Plotted Against Applied Local Oscillator Power P_{LO}

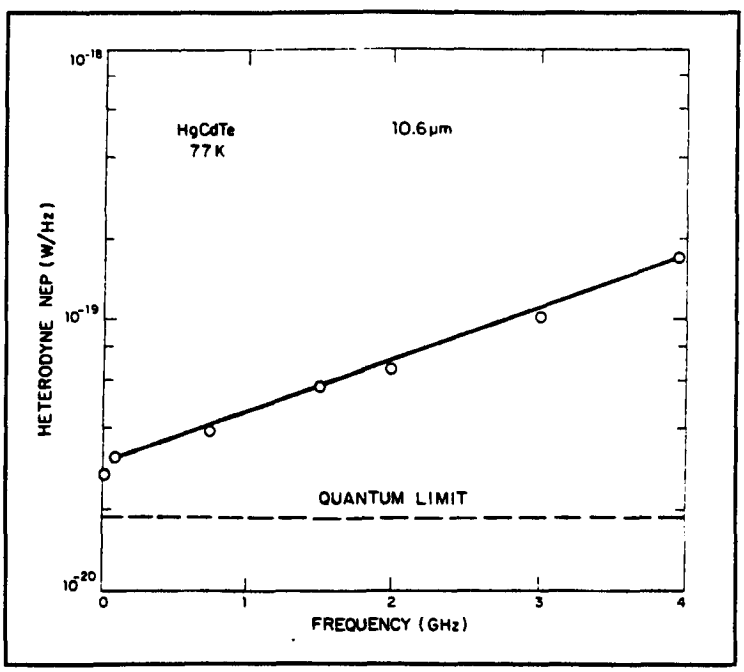

Figure 3.2.2-10 State-of-the Art Heterodyne NEP as a Function of RF Frequency

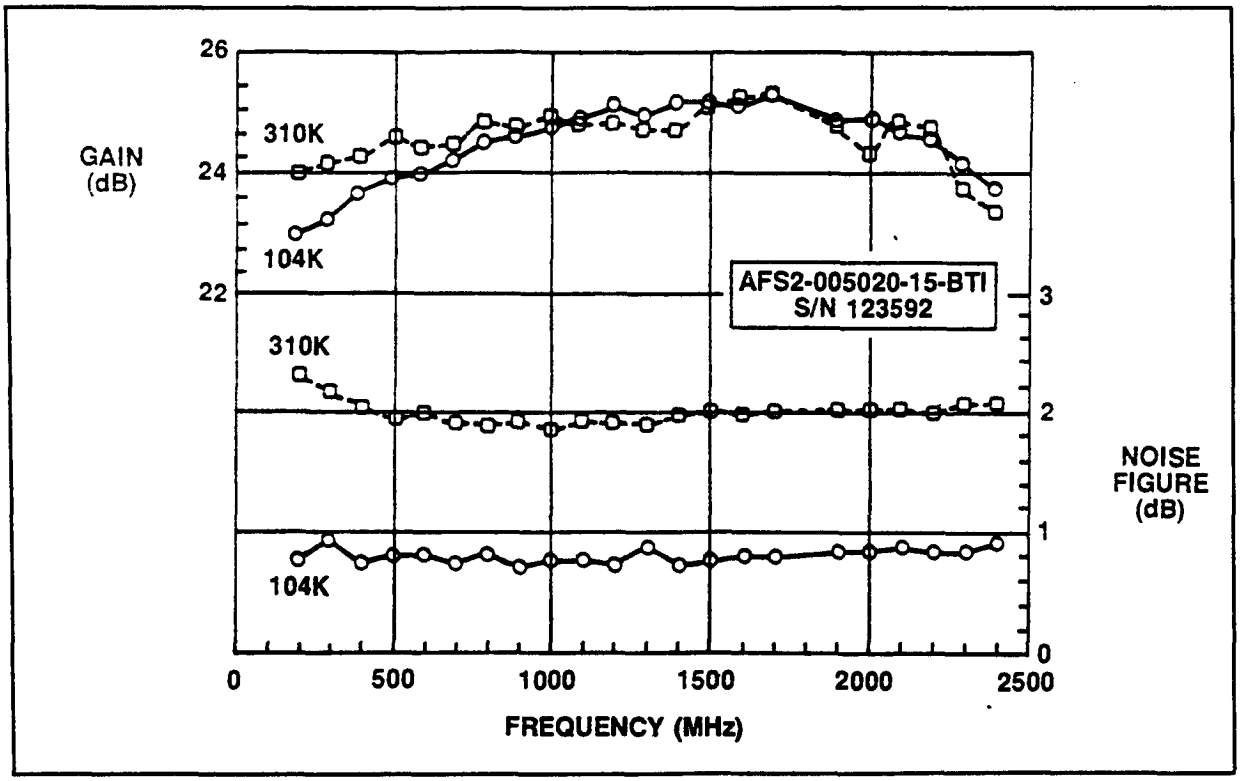

Figure 3.2.2-11 Effect of Temperature on Gain and Noise Figure of Novel Miniature GaAs FET Amplifier

- Preamp responsivity; the APD worked into 50Ω whereas higher transimpedance preamps could be made.
- Limited local oscillator power; there was a system limit and required the use of APD's which have worse excess noise than PIN's.

3.2.2.4 Cryogenic Cooling

One of the major technical disadvantages associated with a CO_2 based laser communication system is the need to cryogenically cool the detector to 80-100K. Such temperatures can be obtained using either a passive radiative cooler or using a long life cryogenic mechanical cooler.

The least expensive option is to passively cool the detector using the low effective heat sink temperature of deep space (4K). The successful implementation of such a cooling technique requires that the cold plate be shielded against direct or reflected sunlight and the thermal emission from the earth's atmosphere and from the spacecraft structure. Traditionally, passive cooling techniques are applied to small thermal loads in which the heat load is less than 100 m Watts and the minimum operating temperature is greater than 80K [16]. The primary advantage of the passive approach is that it requires no moving parts thereby demonstrating an inherently long life with no power requirements.

Should larger cooling capabilities been required a mechanical cryogenic cooler may be used. To meet this requirement a split Stirling cryogenic cooler has been designed for space applications. A single unit currently provides about 800 mW of cooling power at 80K with an overall drive power of 40 Watts. These units have undergone space qualification testing and have demonstrated a potential operating life in excess of 5 to 10 years. Currently operating lifetimes greater than 26,000 hours have been demonstrated (1990) with the tests ongoing [18]. Current plans call for the first space deployment of these devices on the Improved Strato-

spheric Mesospheric Sounder (ISAMS) to occur sometime in 1991 [17].

Further improvements in the cooling power of these devices can be obtained by ganging together two or more expanders at a single location. In addition, mounting the units back to back reduces vibration effects to acceptably low levels (0.5 - 0.05 Kms). Excess cooling capacity could also be employed to temperature stabilized the transmitting or LO lasers as well as the primary laser modulator unit.

3.2.2.5 Summary of Detection Results and Predictions

Figure 3.2.2-12 summarizes reported direct detection and coherent results at frequencies up to 1.2 Gb/s. The individual results are tabulated in Table 3.2.2-1.

Based on these results, Figure 3.2.2-13 shows estimated achievable free space receiver performance versus data rate for direct detection, and for coherent links. The direct detection results assume zero background. With a few hundred pW of background, the performance will be a few dB worse at low data rates and ≈1 dB worse at high data rates.

Table 3.2.2-1 Reported Sensitivity Results

Data Rate	avelengt	Sensitivity, BER=1E-		Technique	Detector	Theoretical?	Group
Mb/s.	nm.	Photons/bi	dBm				
100	830	37	-60.5	DD-NRZ	SIAPD	Yes	EG&G
500	830	54	-51.9	DD-NRZ	SIAPD	Yes	EG&G
2500	1300	36	-48.6	CPFSK			NTT
120	1300	880	-47.9	DD-NRZ	InGaAs APD		DSRC/EG&G
565	1300	400	-44.6	DD-NRZ	InGaAs APD		DSRC/EG&G
1000	1300	470	-41.4	DD-NRZ	InGaAs APD		DSRC/EG&G
2000	1300	990	-35.2	DD-NRZ	InGaAs APD		DSRC/EG&G
565	1300	65	-52.5	DPSK			Siemens
200	1530	46	-59.2	FSK			AT&T
1000	1508	26	-54.7	BPSK			AT&T
140	1320	18	-64.2	PSK			Bellcore
500	800	80	-50.0	CCPPM	SIAPD	Yes	JHU
2000	1320	132	-44.0	PSK			Bellcore
5000	1550	62	-44.0	PSK			NTT
160	1500	57	-59.2	FSK			STC
140	1300	46	-60.1	FSK			STC
565	1060	150	-48.0	DPSK			DLR
140	1542	78	-58.5	FSK			Siemens
110	830	22	-62.4	4-FSK			MIT
1000	1527	86	-49.5	FSK			AT&T
4000	1527	240	-39.0	FSK			AT&T
565	1060	24	-56.0	PSK			Siemens
25	830	72	-57.3	DD-QPPM			JHU
622	1537	110	-50.5	DD-Opt. Amp.			BTRL
2500	1537	110	-44.5	DD-Opt. Amp.			BTRL
1200	1537	130	-47.0	DD-Opt. Amp.			BTRL
All	All	38		DD-Opt. Amp.		Yes	Bellcore
1.5	1300	1470	-64.7	DD-Opt.Fbk.			AT&T

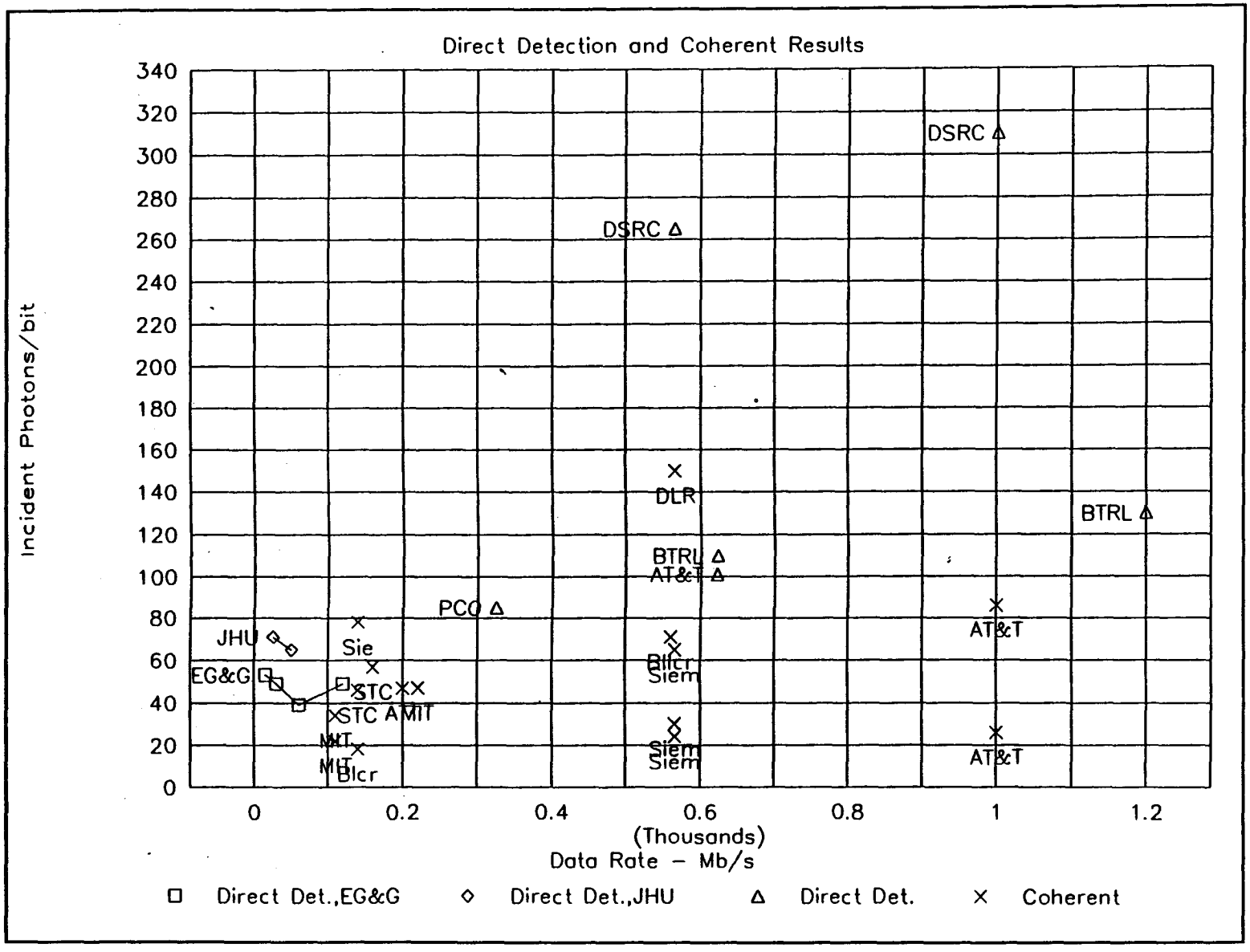

Figure 3.2.2-12 Reported Sensitivities, BER=1E-6

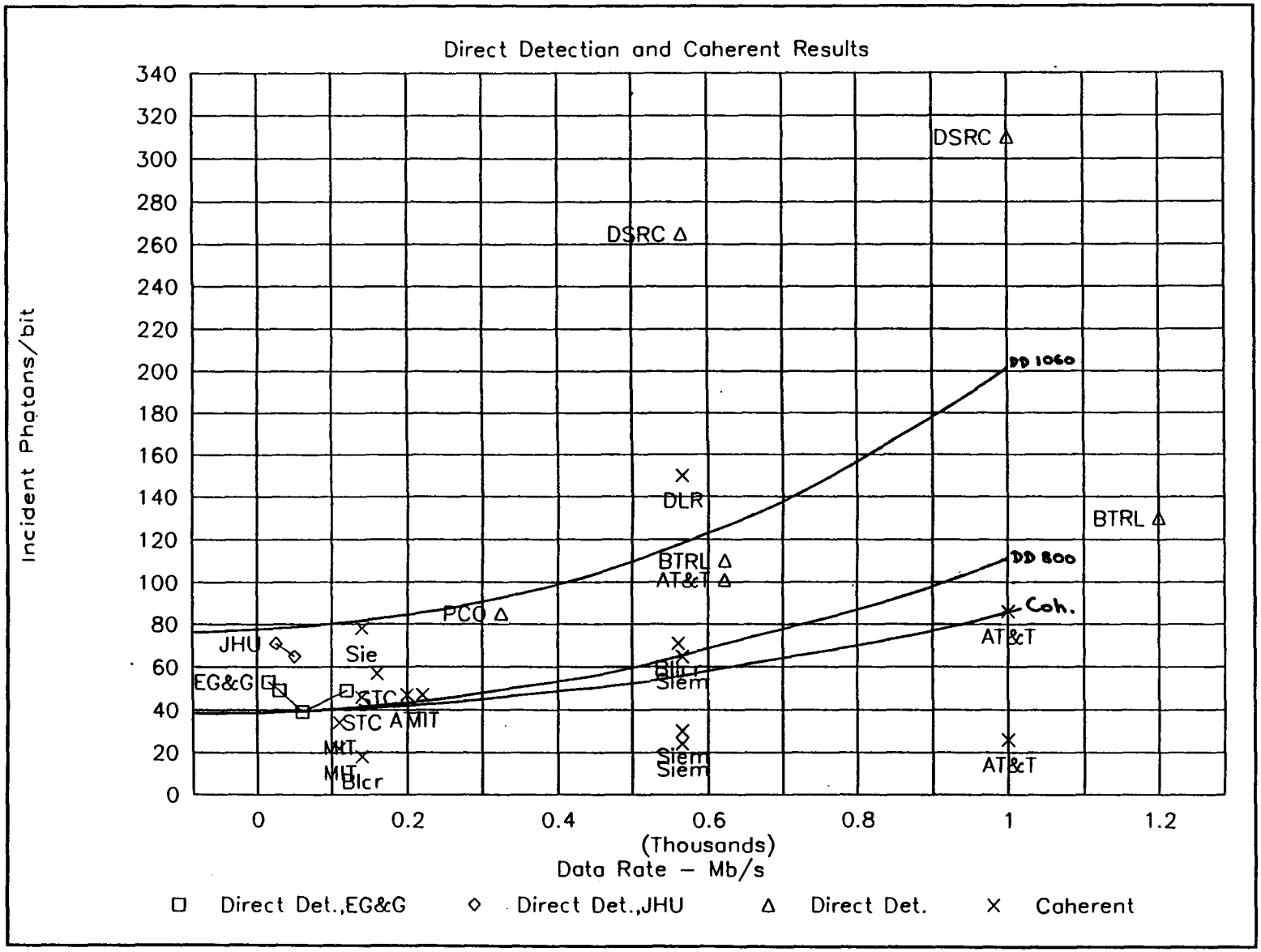

Figure 3.2.2-13 Reported Sensitivities, BER = 1E-6

3.2.3 Receivers for Acquisition, Tracking and Communication

3.2.3.1 CCD (Charge Coupled Device) Technology

A CCD is a multiplexed area array with a serial readout which is an effective acquisition and tracking detector in the 500 to 900 nm regime. A typical CCD has high quantum efficiency in this regime, but at wavelengths 850 nm, the long absorption length in silicon degrades spatial resolution compared with shorter wavelengths, Figure 3.2.3-1.

Critical CCD specifications include:

- Pixel size, typically 10-40 μm square
- Fill factor; the percentage of imaging area/total area. This can be 100% for back-entry and/or frame transfer devices
- Dark noise, in electrons/pixel/second. It may be reduced by cooling.

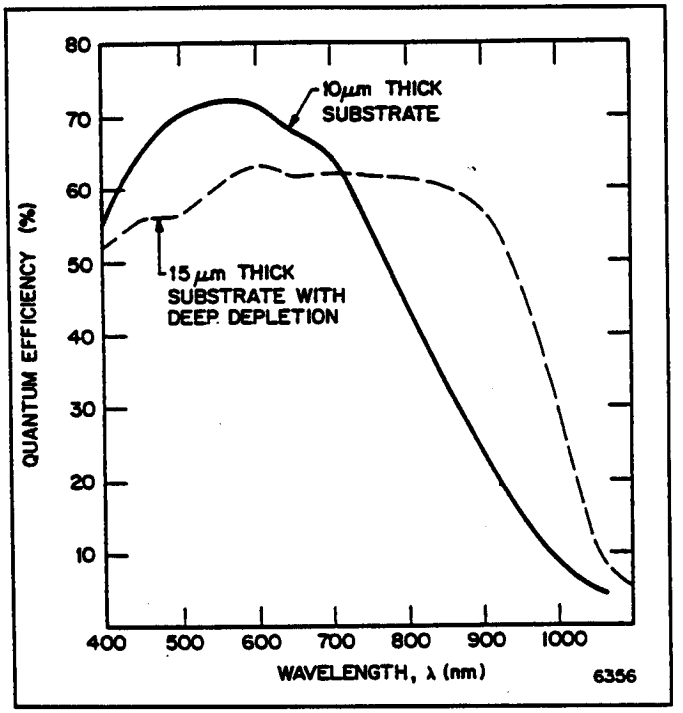

Figure 3.2.3-1 CCD Spectral Response Curves (Ref. 57)

- Readout noise; typically 10 to 30 electrons at a few MHz using correlated double sampling, with levels as low as 5 electrons at a 50 kHz readout rate possibly attainable, Ref. 59.
- Frame rate; >10 kHz desirable for tracking.
- Dynamic range; to avoid saturation and image blooming

Once a source is imaged on the CCD, interpolation algorithms may be used to determine the image position to better than the single pixel resolution. Figure 3.2.3-2 shows a typical curve of rms position error versus SNR, with a "limiting" value of approximately 0.05 pixels at SNR of approximately 30.

In addition to a wide variety of low frame rate commercially available CCD's, both NASA Goddard and ESA (Silex) have sponsored the development of custom CCD's with fast frame rates designed to implement acquisition, rally and tracking functions. A summary of their Technical Specifications is given in Table 3.2.3-1.

The Kodak array is actually an interline transfer CCD closing out data from parallel photodiode arrays.

Both the HS-40 and TH31160 readout electronics have both "rally" and "tracking" modes. The tracking algorithm concentrates on the group of four pixels in which the beacon image is located; a centroiding algorithm then locates the effective image position to a fraction of a pixel. The accuracy depends on the SNR. Figure 3.2.3-3 shows a breadboard TH31160 based unit built by SIRA (UK) for silex.

The solar, terrestrial, lunar, planetary and stellar backgrounds constitute a structured background noise which can bias the centroiding algorithm. The magnitude of these depends upon the spectral filtering which in turn depends upon the beacon or communications source spectral definition/stability.

Typically these sensors require between 0.5 and a few pW to acquire and to track. For tracking, this is typically <10% of the incident communications signal.

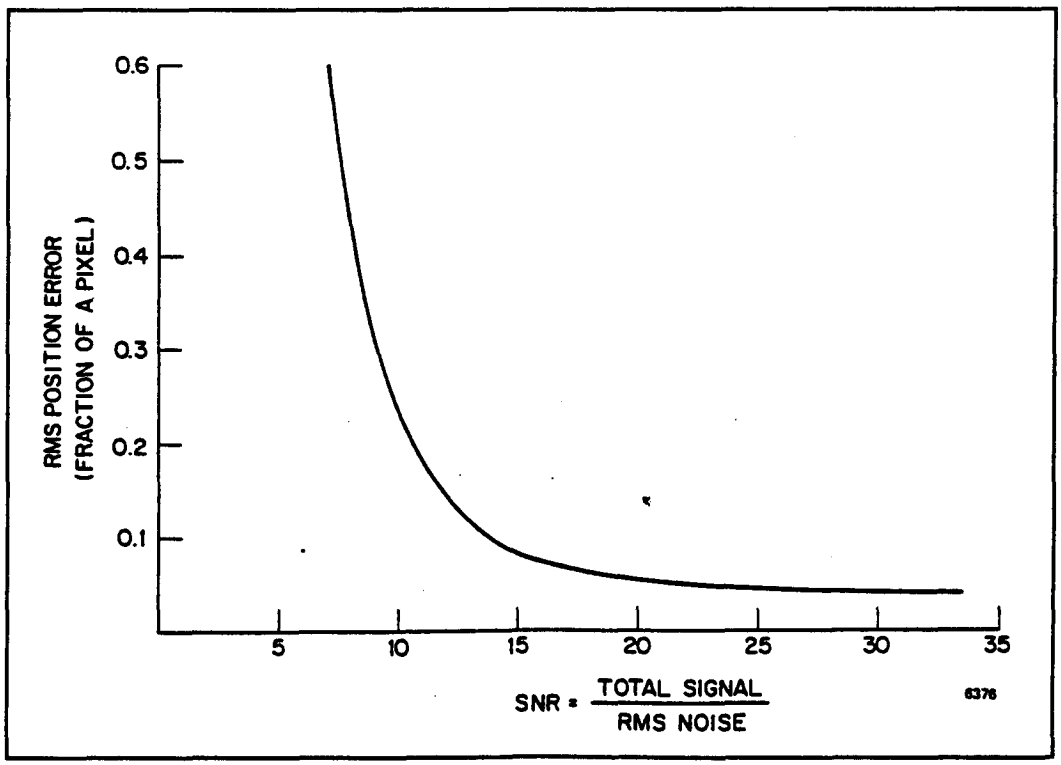

Figure 3.2.3-2 Plot of rms Position Error vs. SNR

Table 3.2.3-1 Technical Specifications

Manufacturer	Kodak	Thomson	Thomson
Sensor Type No.	HS-40	TH 7863	TH 31160
Q.E. @ nm	45% @ 840 nm		
Pixels	128 x 128	288 x 384	14 x 14
Array Size	3.84 x 3.84 nm		0.322 x 0.322 mm
Pixel Size (μm)	32		23 x 23
Array Fill Factor	0.71	1.00	1.00
Frame Rate	40 kHz	33 Hz	8 kHz
Pixel Rate	10 MHz	3 MHz	3 MHz
Readout Noise (rms electrons)	20		22
Min. Signal (pW)	0.13		
Best Resolution (pixels)	0.03		<0.001
Power Consumption	TBA	TBA	TBA
Mass	TBA	TBA	TBA
Dimensions	TBA	TBA	TBA
Ref.	61	62	60

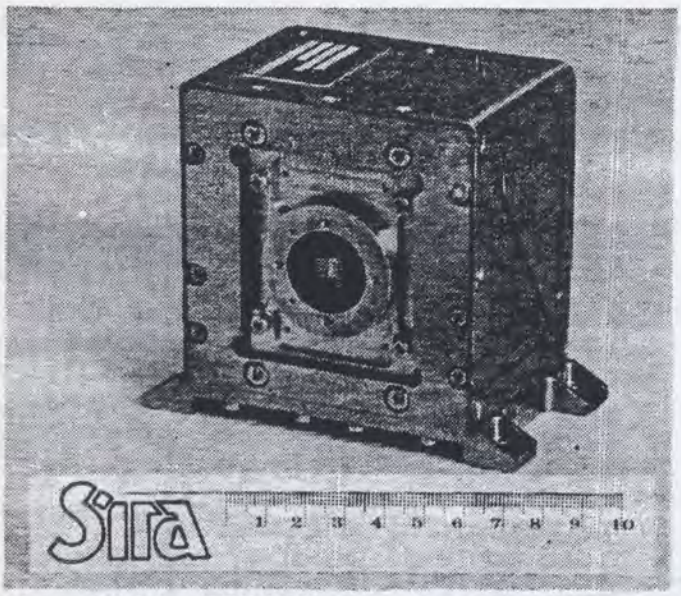

Figure 3.2.3-3 TH31160 CCD - Based Breadboard Tracking Unit (Ref. 60)

CID's have been considered as an alternative, since they have an intrinsic random pixel access, but have readout noise which is almost an order of magnitude higher due to the higher capacitances involved in the charge injection process.

Long-Wavelength CCD's

At longer wavelengths including 1060 nm, the only available CCD's are the platinum-doped and Iridium doped silicide version of the standard silicon CCD array.

PtSi Arrays operate in the 1-5 μm Band with a variable quantum efficiency as illustrated in Figure 3.2.3-4 [82]. For 10.6μm operation, an IrSi CCD would be required, although careful processing is needed to extend its performance out beyond 10.0 μm. Alternatively GaAs CCD structures currently under development at JPL combined with a GaAs quantum well of detector array could be used for 10.6 μm operation [83]. However, the primary disadvantage with any of these technologies is that cryogenic cooling is required. PtSi CCD's must be cooled to 80K and IrSi must be cooled to 40K. Note that both of these temperatures would require mechanical cryogenic cooling since they lie below or

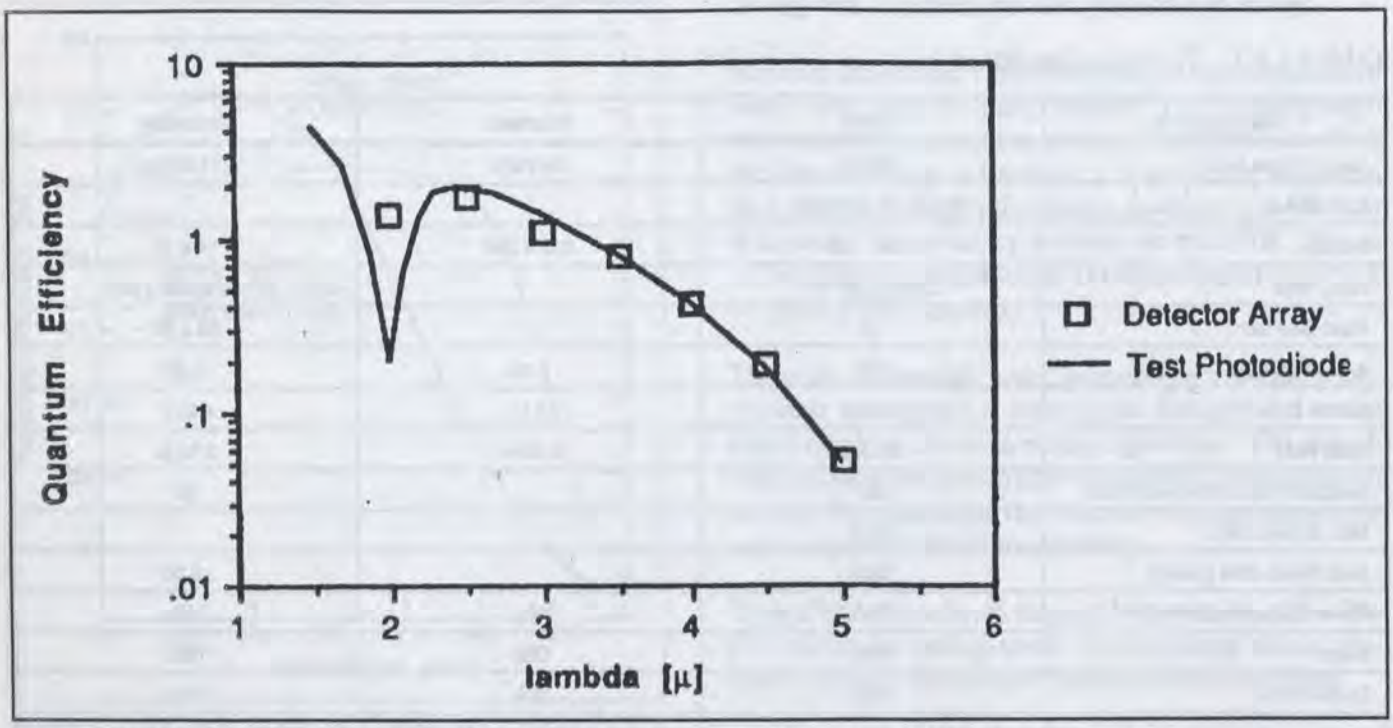

Figure 3.2.3-4 Quantum Efficiency for a PtSi CCD Array as a Function of Wavelength in microns

near the 75 minimum achievable with a passive radiator cooler [84].

3.2.3.2 Quadrant APD Trackers

Early generation of trackers use quadrant silicon APD's with their speed advantage over CCD's. A typical example is the EG&G C30927E, which comes in versions optimized for 800, 900 and 1060 nm. At 800 nm, with a responsibility of 60 Amp/watt and a noise of $\approx 10^{-12}$ $Amp/\sqrt{Hz}$ 1/2, the NEP (Noise equivalent power) is approximately 0.5 pW in a 1 kHz bandwidth. At such wavelengths, a quadrant APD has similar sensitivity to a CCD and has the advantage of readout simplicity. The four quadrant pixels cover a diameter of 1.5 mm.

A disadvantage of such an APD is that the large pixels have proportionally more background per pixel than a CCD pixel, so the sensor is more easily background dominated and limited.

Silicon APD's still retain an advantage at 1060 nm, where the quantum efficiency is 3 to 5 times higher than a comparable CCD.

At 1300 and 1500 nm, a quadrant InGaAs APD could be built but as yet none has been built. Even so, it would have a fairly poor sensitivity, approximately an order of magnitude worse than a silicon APD. A platinum doped silicide CCD with a fast frame rate might be a competitive alternative at 1300 or 1550 nm.

3.3 Modulation

3.3.1 Modulation Techniques

3.3.1.1 Modulators

There are two basic types of modulators used for lasers. These are designated direct modulation and external modulation.

Direct modulation is used with laser diodes by modulating the bias voltage. The time constant of the lasing action is very short so that the emission stops as soon as the bias voltage is removed. Very high bit rates can be achieved in this way. Frequency modulation also occurs if the bias voltage is changed by a small amount while maintaining the voltage well above the threshold voltage for lasing action. Direct modulation of other lasers is also possible but with varying amounts of difficulty.

For lasers which are not easily modulated directly the laser is operated in the CW mode and an external modulator is used to inject information onto the beam.

3.3.1.2 Modulation Types

The types of modulation used for lasers are similar to those used with RF systems. For digital signals the three basic types are phase shift keying (PSK), frequency shift keying (FSK) and amplitude shift keying (ASK) or on-off keying (OOK). Though not apparently proposed for lasers, PSK can be subdivided into BPSK, QPSK, and higher orders. It is also possible to have more than two frequency states and this is easily managed with laser diodes. For amplitude modulation there are several subdivisions in the class of pulse position modulation such as QPPM. QPPM is a different way of modulating the laser which gives a slightly improved performance over straight on-off keying. The time internal occupied by two bits is divided into four time periods and the laser is turned on in only one of these periods. If the two bits are both ZERO then the laser is turned on during the first period. If ZERO and ONE then the laser is on during the second period etc. Thus there is always one pulse for two bits for QPPM whereas the average is one pulse for OOK. However, the single pulse in QPPM is half the duration of a pulse in on-off keying and, since the same number of photons have to be collected in the shorter time period, the laser must operate at twice the peak power level. This concept can be extended to higher orders with 8,16 or more time periods for 3, 4 or more bit intervals.

One method of amplitude modulating the laser, when an external modulator is indicated is to rotate the polarization by 90° for a ZERO and to leave the laser light unchanged for a ONE. The ZERO's are then removed by means of a polarizing plate. This requires

an adequate means of dissipating the energy originally generated during the periods for the zeros and then not radiated. This loss to represents a serious inefficiency factor.

Analog modulation of lasers is also possible but is not being considered in this study.

3.3.1.3 Demodulation Techniques

The demodulation technique is related to the modulation technique. Table 3.3.1-1 shows two detection devices for three basic laser types and the modulators which are possible with each laser. The modulator techniques are on-off keying (OOK) (or amplitude shift keying ASK), frequency shift keying (FSK) and phase shift keying (PSK). These can be accomplished either directly by modulating the laser or externally by modulating the laser beam. The CO_2 and Nd:Yag lasers are not easy to modulate directly so an external modulator is indicated. The laser diode can by amplitude or frequency modulated directly but an external modulator is indicated for phase modulation.

The corresponding demodulation techniques are a basic amplitude detector or a heterodyne or homodyne receiver. The detector comes in three versions, 1) a photo diode followed by a baseband amplifier, 2) an avalanche photo diode (APD) which is a photo diode with internal gain. Either detector may be used for either the direct detection system or the heterodyne system.

The heterodyne system can be either asynchronous or synchronous. The definitions of these two terms in this context are explained by Barry and Lee [43]. The synchronous heterodyne system has a down conversion from optical frequencies to a microwave IF in the gigahertz range followed by a second down conversion where the second local oscillator is phased locked to the IF frequency. The asynchronous heterodyne receiver is a single down conversion to microwave frequencies followed by an envelope detector. Appropriate filters are added to optimize performance. The homodyne receiver with a single local oscillator phase locked to the signal frequency, is classed as a synchronous receiver.

The theoretical minimum number of photons per bit to achieve a BER of 10^{-9} has been derived by Barry and Lee [43] for a number of detection schemes as presented in Figure 3.2.2-3. The theoretical bit error rate versus the number of photons per bit received is presented in Figure 3.3.1-1 [43] for the those detection schemes given in Figure 3.2.2-3. These detector sensitivities are not achieved because of a number of degradations inherent in the detection process. Basically these degradations are caused by imperfections in the detector such as:

1) Detect dark current which raises the noise level of the system and raises the signal power required to achieve the necessary signal to noise ratio.

2) Receiver thermal noise which has the same net effect as detector dark current.

3) Statistical variations in the avalanche gain for an APD increasing the noise content.

4) Less than 100% photo electron efficiency which means that less than 100 detectable electrons are obtained from 100 input photons.

The result of these degradations is that the theoretical minimum sensitivities shown in Figure 3.3.1-1 can never be achieved. Instead, the sensitivities presented in Section 3.2 can be achieved and are considered state-of-the-art performances.

3.3.1.4 Impact of FEC Using Coding

Peile [47] describes the advantages of applying coding to the laser link. He presents the improvement in terms of bit error rate reduction for various Reed Solomon codes. The error rate reduction depends upon the complexity of the code with the longer more complex codes providing a greater reduction in error rate. The longer codes are also more difficult to implement so there is a trade-off between improved performance due to coding versus higher power transmitters, laser telescopes or more sensitive receivers. Figures 3.3.1-2, 3 and 4 are taken from Peile [47].

Table 3.3.1-1 *Possible Combinations of Lasers, Modulators and Detectors*

Detection Process	Lasers	CO_2				Nd:Yag				LaserDiodes			
	Detectors	PINDiode		APD		PINDiode		APD		PINDiode		APD	
	Modulator	Direct	Ext.	Direct	Ext.	Direct	Ext.	Direct	Ext.	Direct	Ext.	Direct	Ext.
OOK													
Direct Detection			X						X			X	
Asynch Heterodyne			X				X		X	X		X	
Synch Heterodyne			X				X		X	X		X	
Homodyne			X				X		X	X		X	
FSK													
Direct Detection												X	
Asynch heterodyne			X				X		X	X		X	
Synch Heterodyne			X				X		X	X		X	
Homodyne			X				X		X	X		X	
PSK													
Direct Detection													
Asynch Heterodyne													
Synch Heterodyne			X				X		X	X		X	
Homodyne			X				X		X	X		X	

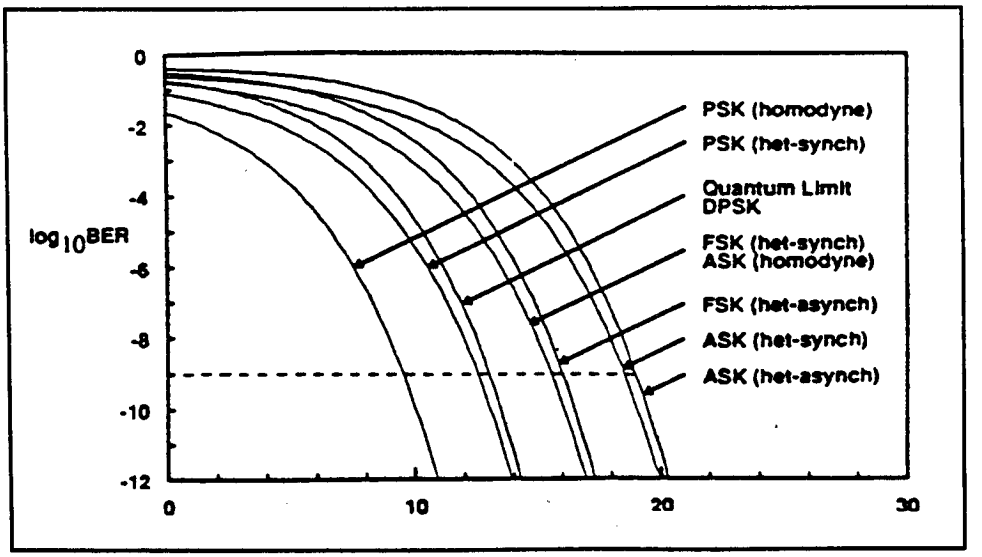

Figure 3.3.1-1 BER Curves for Shot-hoise Limited Operation where M is the Number of Detected Photons per ONE Bit. M is proportional to the received peak power P_S: $M=(^{n}Ps/hv)Tx$ (ref 43).

Figure 3.3.1-2 shows the effect of increasing the block length from 32 bits to 256 bits all with 7/8 coding. With an input error rate of 10^{-2} the output BER is 10^{-5} for a 32 bit code and 10^{-12} for a 256 bit code.

Figure 3.3.1-3 shows the effect of changing the level of redundant bits from 2 bits to 30 bits in a block of 32 bits or the useful bits from 30 bits to 2 bits.

Finally Figure 3.3.1-4 shows the effect of changing the coding rate from 15/16 for K=240 to 1/2 for K=128.

3.3.2 10 Micron Optical Modulator Technology

3.3.2.1 Introduction

There are five basic mechanisms that can be exploited to modulate a CO_2 laser beam; pump power, absorption, spectral, mechano-optic and electro-optic. Some of these mechanisms are inherently connected with the generation of the laser beam or the result of discrete modulator assemblies. The discrete modulators may be further categorized depending upon whether they are placed inside or outside the laser cavity [ref 23].

For CO_2 laser communication systems Electro-optic modulation has gained wide acceptance for the following reasons [ref 3]:

a) All forms of modulation are possible (IM,FM, PM etc)

b) Wide band operation can be achieved.

c) Modulation at different optical wavelengths is possible

d) EO modulators are relatively inexpensive.

The transmitting laser beam can be modulated externally or internally via an EO crystal. Early work on CO_2 based laser systems concentrated on the application of internally mounted modulators [ref 25, 26]. However, to obtain the required high data rates, external modulation has proven to be the most effective technique. Also internal modulators suffer from internal heat dissipation, facet damage and design complexity [ref 21].

The EO modulator consists of a pockets cell (CdTe or Ge) to which a voltage is applied. CdTe is the material of choice at 10.6 μm as it has a low optical absorption

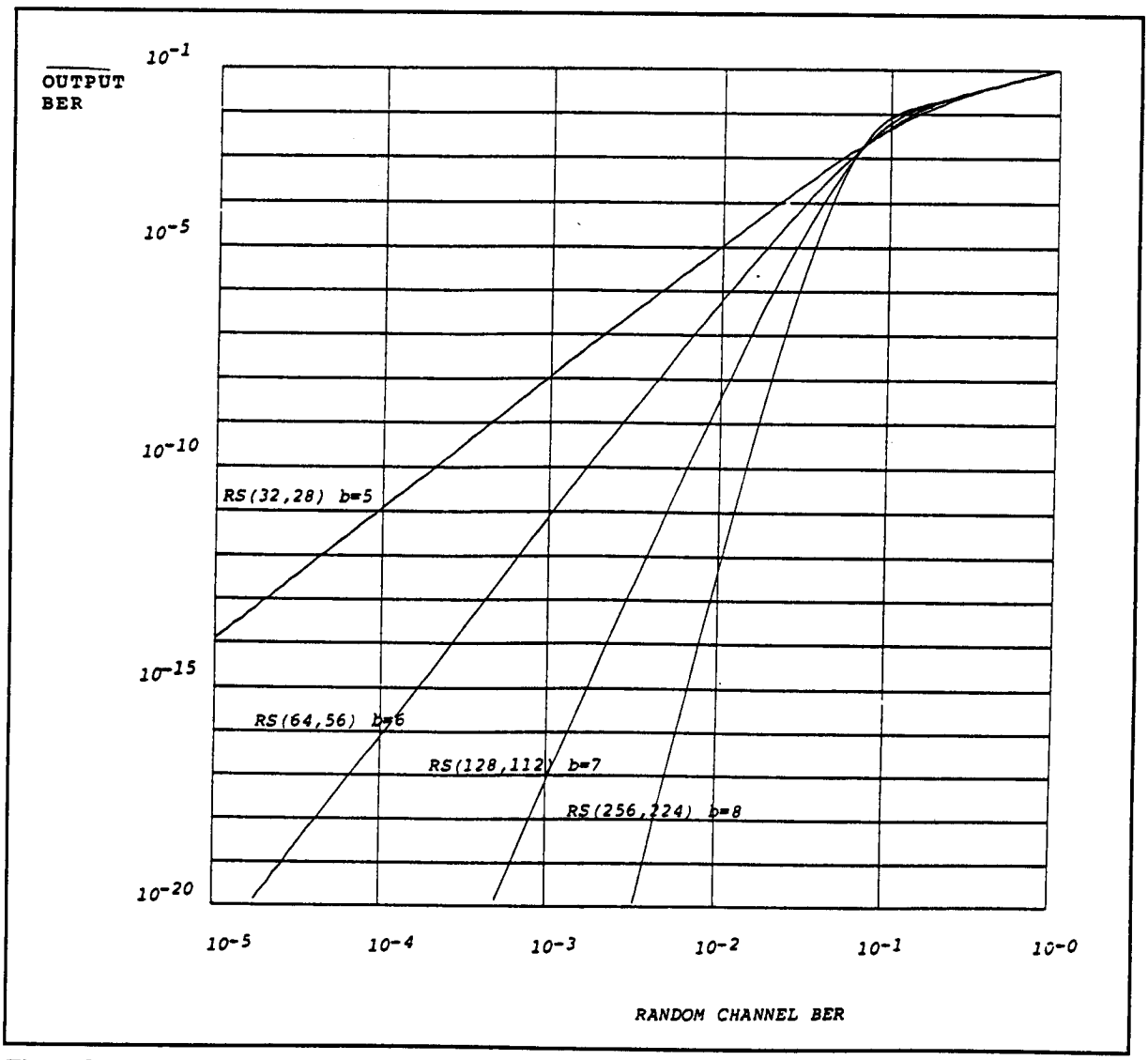

Figure 3.3.1-2 RS Coses of 7/8-th Rate

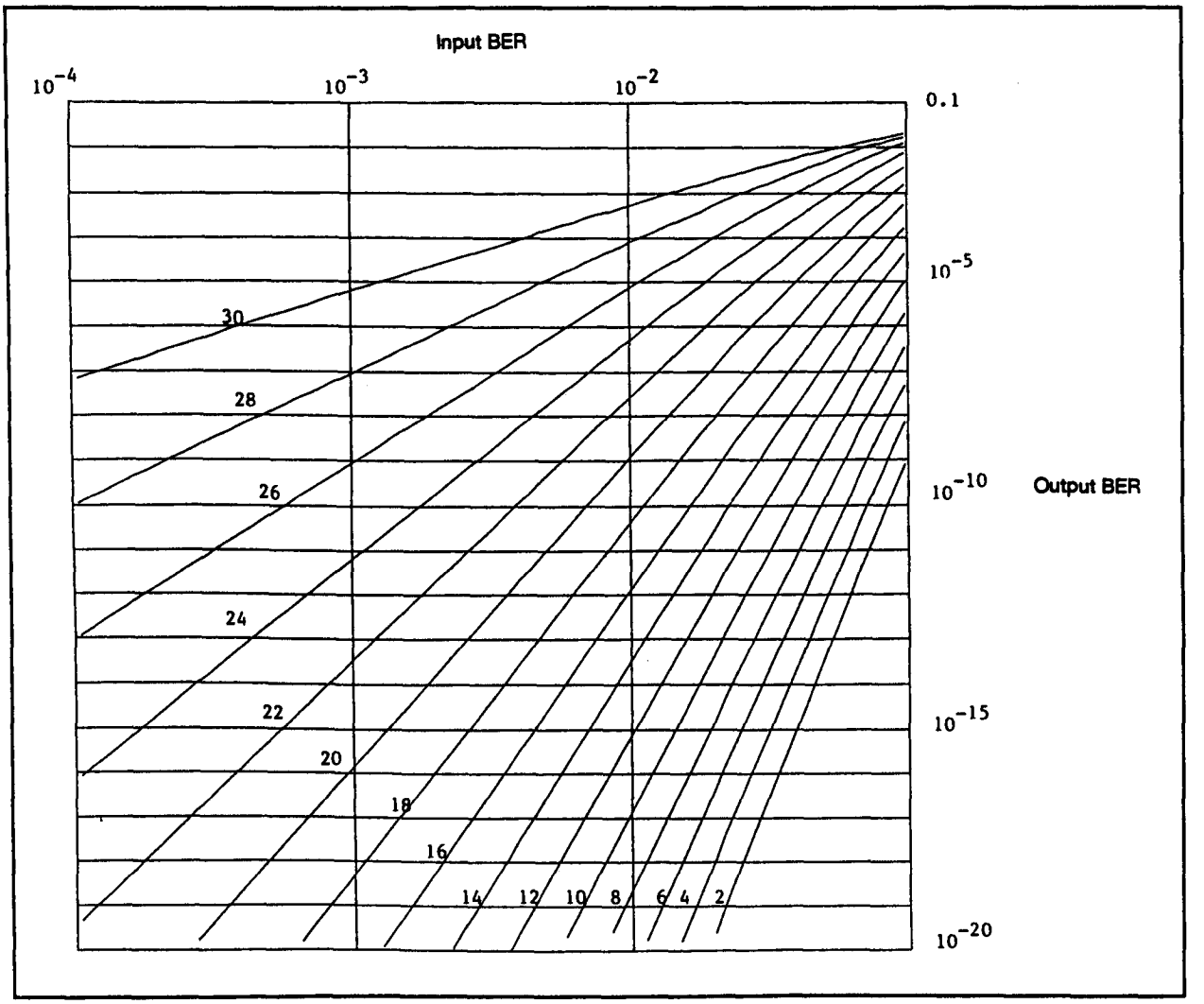

Figure 3.3.1-3 5-Bit RS (32,K) Code Performance

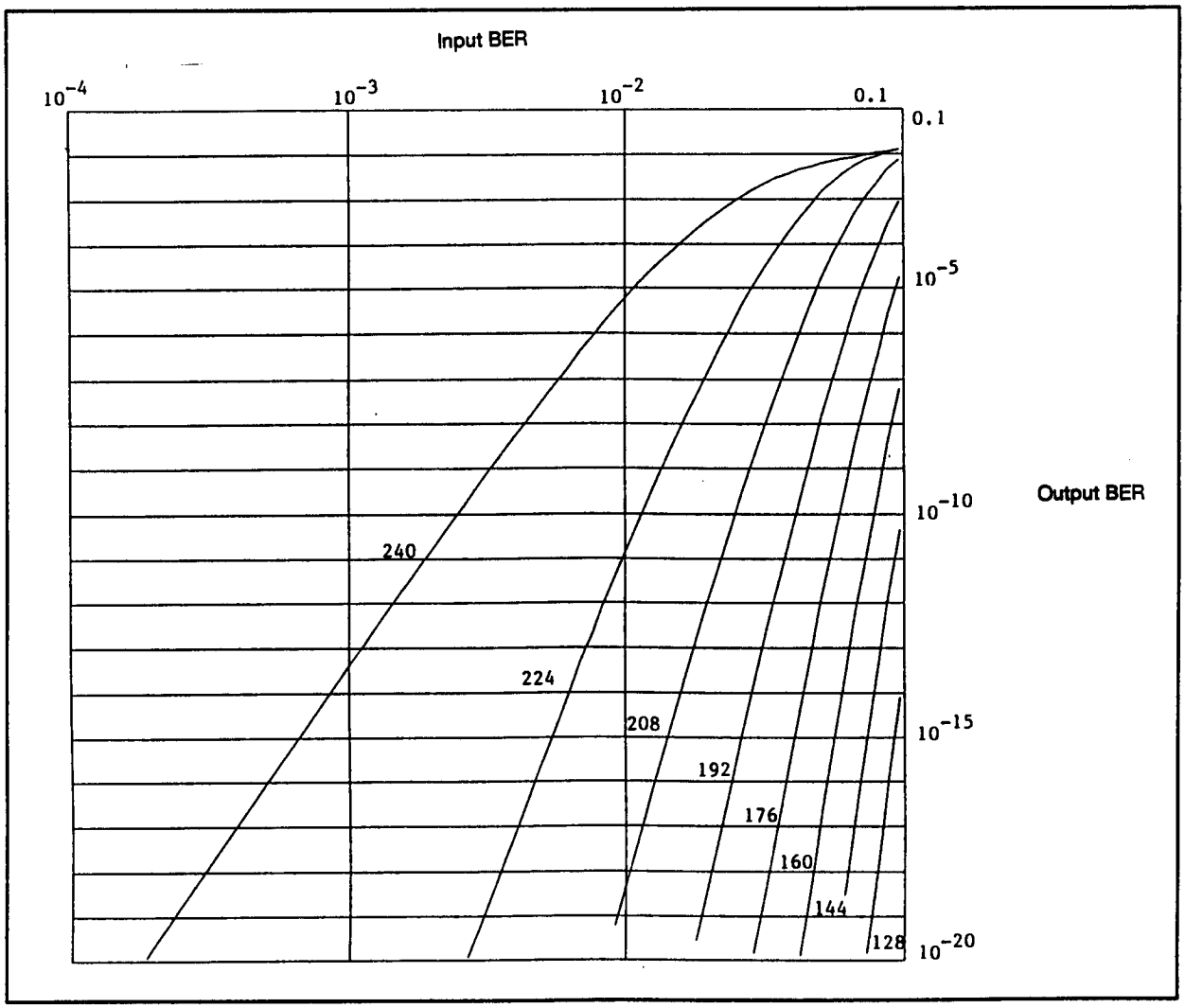

Figure 3.3.1-4 8-Bit RS (256,K) Code Performance

as well as the highest known electro-optic coefficient [30]. Depending upon the nature of the applied field relative to the direction of the laser beam, intensity, phase or frequency modulation can be achieved. For GHz operating frequencies travelling wave techniques are required to correctly apply the modulating voltage.

A number of modulator developments have been ESA [ref 135]. These include two modulators, one for CO_2 and the other for Nd:Yag, for which the development has been completed (refer to Table 3.3.2-1).

Further work include the development of a phase modulator for a Nd:Yag laser.

3.3.2.2 Phase Modulation

ESA has selected phase modulation as the most efficient option. Figure 3.3.2-1 taken from Petch [39] illustrates the principle of the travelling wave modulator employed with the push pull drive circuit. Since the maximum phase shift obtained to date is only 25 degrees, the carrier beam is always stronger than the modulated sideband power. The receiver sensitivity is expressed in terms of modulated power, therefore the efficiency of the modulator (ratio between the modulated sideband power and the carrier power) must be considered as an important loss factor in the transmitter power budget. This loss is not typical for an EO

Figure 3.3.2-1 Modulator Developments Funded by ESA

	Laser	
	CO_2	Nd:Yag
Wavelength	10.6 μm	1.06 μm
Modulation	Phase	Amplitude
Power Handling	6W CW	1W CW
Optical Transmission	80%	86%
Modulation Data Rate	1 Gbps	1 Gbps
Modulating Power	20W	8W
Modulation Depth	33° Phase Shift	100% amplitude
Dimensions (cm)	–	15 x 5 x 5

modulator at shorter wavelengths since EO modulators at 1.06 μm are capable of producing a 180 degree phase shift [ref 2].

Experiments by EX researchers have found that the modulator efficiency at 10.6 μm is typically 1/6. This corresponds to a loss factor of -7.7 dB.

At MIT, Researchers have combined two modulators, as illustrated in Figure 3.3.2-2 to enhance the overall modulation efficiency. For a 1 Ghz bandwidth system the efficiency has been measured between .6 and .8 [38]. For a link budget analysis the worst case loss of 2.2 Db is still a substantial improvement over the ESA work. Furthermore the 180 degree phase shift permits easy separation of the sideband from the carrier using polarizers.

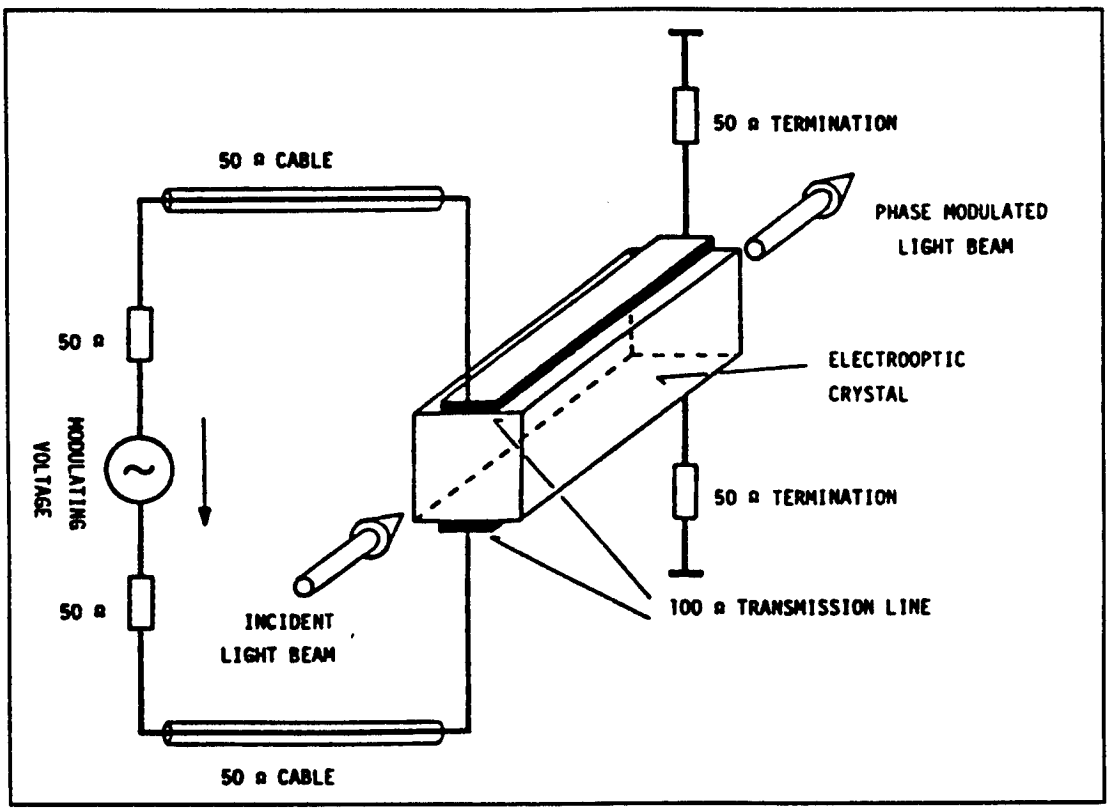

Figure 3.3.2-1 Principle of Travelling Wave Modulator with Push-Pull Drive Circuit

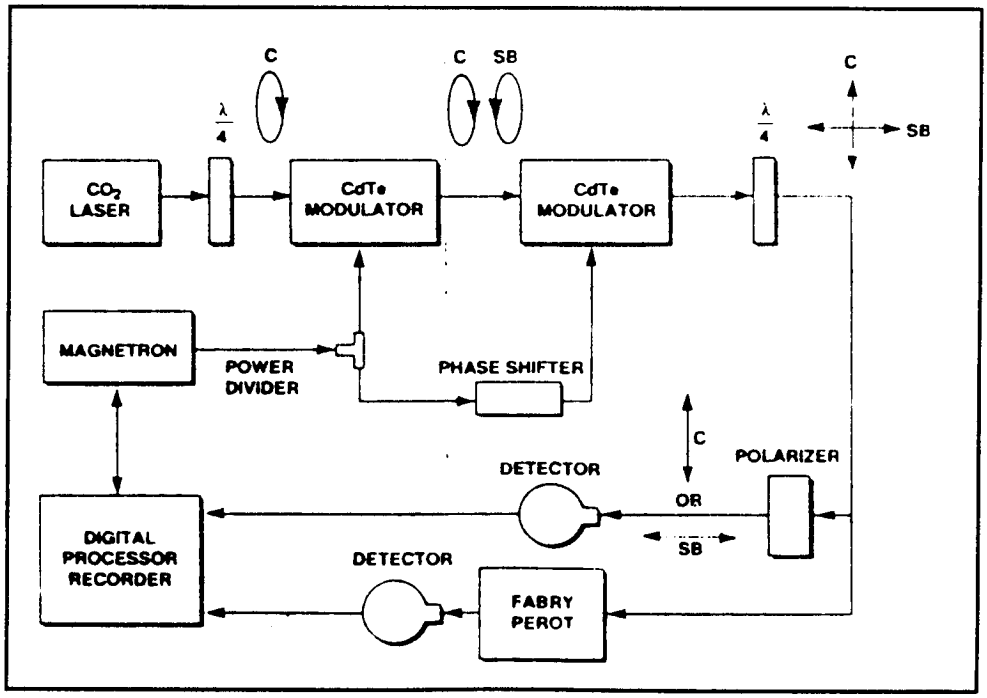

Figure 3.3.2-2 Block Diagram of the Experimental Setup

C and SB refer to the polarization of the optical carrier and the side-band, respectively. Rotation of the polarizer selects the carrier or the sideband of the detector.

A final point worthy of note is that due to the absorption of RF drive power and the laser radiation, precise control of the crystal temperature is essential to obtain a stable modulated beam [ref 6].

3.3.2.3 Modulator Transmission

The ESA modulator design consists of a CdTe crystal which was anti-reflection coated on the input and output faces. Power transmission was predicted to be 75% (-1.2 dB) but experimental measurements have yielded 84% (-.75 dB) transmission. For the link budget analysis a -1.0 dB loss was attributed to transmission through the modulator.

MIT's design also employed a CdTe crystal byte, the optical losses range from 5% (-.22 dB) to 10% (-.46 dB) depending upon the effort expended to accurately align the incoming laser beam. For the link budget analysis a -.5 dB loss attributed to transmission will be assumed.

3.4 Telescope and Optics Evaluation

3.4.1 Telescope Objectives

In an Optical ISL system 4 telescope requirements must be addressed:

- Transmit a communications beam
- Receive a communications beam
- Transmit a wide beacon beam
- Receive a beacon beam

Depending upon the system design, these various telescopes may be combined into a single head which requires the use of numerous optical splitters and combiners linked to the telescope optical path, or they may be left as separate telescopes, allowing them to be individually optimized for their specific purposes. The following subsections state the primary function of the telescope in each of the above cases, and provides an

idea of the types of requirements commonly placed on them in an Optical ISL system.

3.4.1.1 The Telescope as a Communications Transmitter

As a communications transmitter, the telescope's primary function is to improve link gain by focusing the transmitted light into a small enough angular region so that the receiver telescope can collect sufficient light signal with a reasonable aperture size. Although tremendous gains can be achieved with such optics, this must be traded off against the associated pointing requirements which are then needed to point such a tight beam on its target. A typical diffraction limited 200 mm telescope operating at 1000 nm can produce a spot beam with a half amplitude beam radius of 2.5 μrad.

The gain of the transmit telescope depends upon a number of parameters, described in section 3.4.2. The quality of the transmit telescope will generally need to be of significantly better than standard commercial quality to achieve the necessary low wavefront errors, distortions, and transmissivity.

The field of view of the transmit telescope must be capable of keeping the target receiver within the field of view during coarse pointing (a "fine pointing steerable mirror" will generally be used in the optics behind the telescope to keep a pointing lock within this field of view). This range must include jitter from platform vibrations and torques. In addition, if the transmit and receive telescopes are combined, then additional field of view allowance must be made to account for "look-ahead" angles to cover the time lag between the transmit beam and the receive beam.

The magnification of the telescope must be sufficient to reduce the accuracy of the fine pointing mirror pointing requirements while maintaining a "reasonable" mirror steering range that won't shift the output beam by an unnecessarily large amount. The pointing range and accuracy of the fine pointing mirror is discussed in Section 5, "Acquisition and Tracking". A 1:1 telescope with a 1 m focal length will only produce 1 μrad of beam angle shift per 1 μrad of fine steering mirror shift. For a 30:1 telescope, this same angle will require 30 μrad of mirror shift which is much easier to produce and control.

Typical requirements for the transmit telescope will include an aperture diameter of 200-300mm, a field of view of around $\pm$300 μrad from the centre, and a magnification of 30:1.

3.4.1.2 The Telescope as a Communications Receiver

As a receiver, the telescope's primary function is to collect incoming light to be focused onto a communications detector. Equally important however, the receive telescope must be capable of resolving the angular position of the incoming beam onto a fine pointing detector with sufficient accuracy to allow the communications transmit beam to be pointed in return. The most critical parameters here then, are establishing an adequate aperture size (to achieve the necessary collecting capability) and a sufficient image magnification (to amplify the beam position enough for fine pointing position detection). See Section 5, "Acquisition and Tracking" for a discussion of detector position sensitivity.

The telescope aperture size will also play a role in how fine a spot beam can be produced on both the communications and fine pointing detectors. For the fine pointing detector, the spot size depends upon the type of detector used - a quadrant type detector may require a large spot to cover a sufficient area to permit signals from each quadrant to be balanced, while a CCD detector may want the spot resolved to better than an individual CCD pixel. For the communications detector, it is important to keep the central spot (and as many of the sidelobes) within the bounds of the detector to avoid spill-over losses.

The telescope field of view must also be sufficient to keep the receive beam within the fine pointing detector range during coarse pointing.

Typical requirements for the receive telescope will be similar to those for the transmit telescope, and might

include an aperture diameter of 200-300mm, a field of view of around ±300 μrad from the centre, and a magnification of 30:1.

3.4.1.3 The Telescope as a Beacon Transmitter

The beacon beam must be substantially wider than the main communications beam since it is only required to illuminate a large angular region of uncertainty in the target satellite's position. Typically this would be wide enough to include all the initial pointing errors in the acquisition calculations (which includes satellite platform attitude accuracy, coarse pointing gimballing accuracy, and the open-loop target position prediction algorithm accuracy), and might be around ±0.5 degrees. This is tempered however by the fact that available laser power is limited and such a wide beacon beam will therefore require a very large beacon receiver telescope at the receiving end. If the width of the beacon beam cannot practically be made wide enough to cover the entire cone of uncertainty then a "scanning" operation is required to scan a smaller beam across the uncertainty region in an effort to cover the target. Such a scanning operation may be done either by steering the entire beacon telescope, or by using a steering mirror to scan the beam within the beacon telescope's field of view.

In the cases where the output beam covers the full uncertainty region or where a steering mirror will scan the same region, the field of view of the beacon telescope must be at least as large as the uncertainty cone. A typical uncertainty cone is ±0.5 deg (±8700 μrad) for most satellites, although better than ±0.1 deg (±1700 μrad) is achieved on many imaging type missions.

Magnification in the beacon transmit telescope would not be required except to reduce the steering accuracy requirements where a steering mirror is needed. The output beam must be intentionally expanded well beyond the diffraction limit of the optics because of the large beam widths used, since the beacon telescope aperture size does not play a significant role. This allows the beacon optics to be set-up outside the main communications optics, avoiding interference between the two systems and reducing the number of elements required for the communications link path.

3.4.1.4 The Telescope as a Beacon Receiver

The beacon receiver aperture size must be matched to the beacon transmitter (and whether it is scanned) to provide adequate link budget for pointing acquisition.

Unlike the beacon transmit telescope, the beacon receiver telescope is not generally "scanned" during the acquisition process, and its field of view must therefore include the initial pointing accuracy (which includes satellite platform attitude accuracy, coarse pointing gimbal accuracy, and the open-loop target position prediction algorithm accuracy). This will typically be around ±0.5 deg (±8700 μrad).

The beacon beam positional resolution must be better than the resolution of the coarse pointing drive system so that the acquisition process can bring pointing to within the range of the fine tracking process. This would typically require ±100 μrad positional resolution.

3.4.1.5 The Optical Network

The optical network exists behind the main telescope and serves to direct the transmit (or receive) optical beams, split them, and steer them. Although the exact requirements for the optical network depend upon the nature of the telescope concept chosen, the following are some typical requirements:

For the transmit beacon:

- provide a high speed steering mirror or prism, if required, for scanning the transmit beam to cover the initial uncertainty cone.

For the main optical path:

- separate out and divert the received beacon beam to an acquisition detector,

- split portions of the received communications beam to the main communications detector, the fine tracking detector and in some concepts, a look-ahead detector,
- combine the outgoing communications transmit beam into the optics path of the incoming communications receive beam,
- provide a high speed, precision steering mirror or prism for precision tracking of the received communications beam at frequencies beyond the response of the gimbal drive system,
- provide a precision look-ahead steering mirror for steering the transmit beam relative to the receive beam,

To ensure that the incoming and outgoing beams remain tightly aligned and focussed, the optical network will necessarily employ a very stable mechanical platform on which to mount the various elements of the network.

Figure 3.4.1-1 shows a typical optical network from the European SILEX project employing a single telescope for the communications transmitter, communications receiver, and beacon receiver, and beacon transmitter.

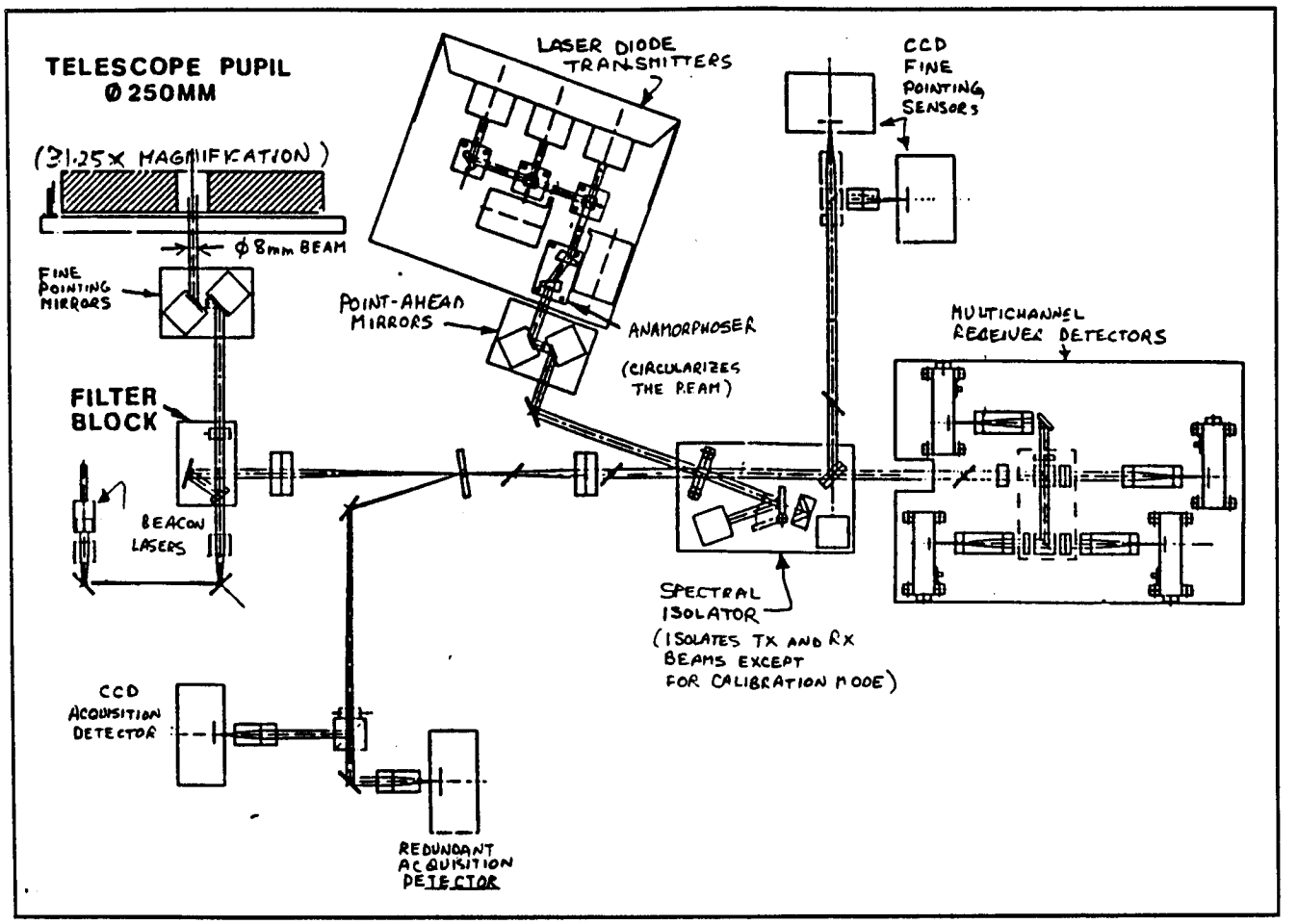

Figure 3.4.1-1 A Typical Optical ISL Terminal Network

3.4.2 Modelling the Optical Link Equation Between Satellites

The optical link between two ISL systems can be represented as shown in Figure 3.4.2-1. The optical path consists of:

- transmitting laser plus local collimating optics and filters,
- transmit optical network (which includes various beam splitters/combiners and steering mirrors),
- transmit eyepiece,
- transmit objective optics
- a free-space link distance R,
- receive objective optics,
- receive eypiece,
- receive optical network (some power will be stripped-off for tracking detectors here),
- receiver detector plus local focusing optics.

The optical link equation between two Optical ISL terminals gives the ratio of the power received at the detector face (P_R) over the output laser power transmitted (P_T) (Ref 1):

$$\frac{P_R}{P_T} = [G(D_T, \lambda, \theta)G(\alpha, \gamma_T)G(\Delta_{RMS})G(N_T, \varepsilon_T)G(TR_{TX})]$$
$$G(R)[G(D_R)G(\gamma_R)G(N_R, \varepsilon_R)G(TR_{RX})G_{Det}] \quad (1)$$

where:

$G(D_T, \lambda, \theta)$	= Gain From Transmit Objective Optics
$G(\alpha, \gamma_T)$	= Loss Due to Transmit Gaussian Beam Profile + Central Obstruction
$G(\Delta_{T\text{-}RMS})$	= Loss Due to Transmit Wavefront Errors
$G(N_T, \varepsilon_T)$	= Loss Due to Secondary Mirror Support Struts on Transmit
$G(TR_T)$	= Loss Due to Transmissivity of Transmit Optics
$G(R)$	= Free Space Loss
$G(D_R)$	= Gain From Receive Objective Optics
$G(\Delta_{R\text{-}RMS})$	= Loss Due to Receive Wavefront Errors
$G(\gamma_R)$	= Loss Due to Central Obstruction on Receive
$G(N_R, \varepsilon_R)$	= Loss Due to Secondary Mirror Support Struts on Receive
$G(TR_R)$	= Loss Due to Transmissivity of Receive Optics
G_{Det}	= Loss Due to Beam Spill-over on the Receive Detector

This equation can be expanded into:

$$\frac{P_R}{P_T} = \left(\frac{\pi D_T}{\lambda}\right)^2 \left(\frac{2J_1(\pi \sin(\theta) D_T/\lambda)}{\pi \sin(\theta) D_T/\lambda}\right)^2 \left(\frac{2}{\alpha^2}\right) e^{-\alpha^2} - e^{-\alpha^2 \gamma_T^2} e^{-\left(2\pi\left(\frac{\Delta_{T\text{-}RMS}}{\lambda}\right)\right)^2} \left(1 - \frac{N_T \varepsilon_T}{2\pi}\right)$$
$$TR_T \left(\frac{\lambda}{4\pi R}\right)^2 \left(\frac{\pi D_R}{\lambda}\right)^2 e^{-\left(2\pi\left(\frac{\Delta_{R\text{-}RMS}}{\lambda}\right)\right)^2} \left(1 - \gamma_R^2\right)\left(1 - \frac{N_R \varepsilon_R}{2\pi}\right) TR_R \quad (2)$$

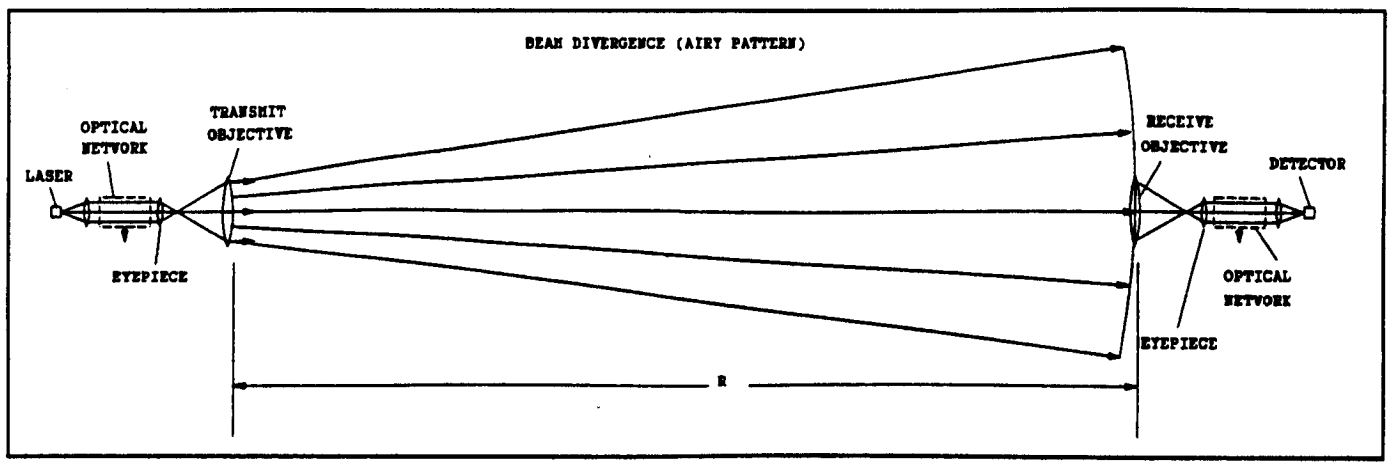

Figure 3.4.2-1 Optical Link Elements

where:

P_R	= Power Received (Watts)
P_T	= Power Received (Watts)
D_T	= Diameter of Transmit Objective (m)
D_R	= Diameter of Receive Objective (m)
R	= Link Distance (m)
α	= a/w
γ_T	= b/a for Transmit Optics
γ_R	= b/a for Receive Optics
a	= $D_T/2$ (m)
b	= Radius of Sec. Mirror Obstr. (m)
w	= Radius of $1/e^2$ Point on Output Gausian Profile (m)
N_T	= Number of Sec. Mirror Struts (Transmit)
N_R	= Number of Sec. Mirror Struts (Receive)
ε_T	= Angle Blocked per Strut (Transmit) (rad)
ε_R	= Angle Blocked per Strut (Receive) (rad)
$\Delta_{T\text{-}RMS}$	= RMS Wavefront Error of Transmit Beam (m)
λ	= Wavelength of Transmit Beam (m)
TR_T	= Transmissivity of Transmit Optics
TR_R	= Transmissivity of Receive Optics
$J_1()$	= Bessel Function of Order 1
θ	= Angle of Receiver from Central Transmit Axis (rad)
$\Delta_{R\text{-}RMS}$	= RMS Wavefront Error in Receive Optics (m)

(Note that this is the link between a single laser and detector pair. TR_T and TR_R transmissivities include the effects of any beam power stripped off for other detectors.)

The constituents of this link equation are described in the following subsections.

3.4.2.1 Ideal Transmit Telescope Gain (Airy Profile)

For communications applications, the telescope gain in a specific direction, $G(D_T, \lambda, \theta)$, is the amplification of the radiated intensity in that direction over the equivalent occurring from an omnidirectional transmitter radiating evenly over the full 4π steradian sphere. For an ideal, uniformly illuminated circular telescope aperture of diameter D_T, the far-field intensity profile is derived from the standard "Airy" interference pattern profile:

$$G(D_T, \lambda, \theta) = \left(\frac{\pi D_T}{\lambda}\right)^2 \left(\frac{2J_1(\pi sin(\theta) D_T/\lambda)}{\pi \sin(\theta) D_T/\lambda}\right)^2 \qquad (3)$$

where:

θ = Angle from central transmit axis
λ = Transmitted Wavelength

Figure 3.4.2-2 shows a logarithmic plot of this ideal antenna gain as a function of angle. Note that $G(D_T, \lambda, \theta)$ is only applicable in the "far-field" range where $R >> D_T$. In the "near-field" range, the intensity profile becomes a more complex function (Ref 65) which is not required for this study.

3.4.2.2 Gaussian Profile Effects on Transmit

Unlike the idealized case above, real lasers do not generally produce a beam of uniform illumination, but produce one which has a profile similar to a "Gaussian" shape as shown in Figure 3.4.2-3. The shape of the Gaussian profile is defined by w, the radius of the point in the beam where the intensity drops to $1/e^2$ of that at the beam centre.

This Gaussian profile has two effects:

a) the edges of the beam are cut-off by the limited diameter of the telescope optics, and

b) the beam is concentrated in the centre of the optical path, and does not make efficient use of the full diameter of the primary optics. The resulting beam has a greater dispersion, similar to that from a uniformly illuminated beam of reduced primary optics diameter.

Equation (3) for $G(D_T,,)$ can be revised as follows:

$$G(D_T,\lambda,\theta,\alpha) = \left(\frac{\pi D_T^2}{\lambda}\right)\left(2\alpha^2\left(\int_0^1 e^{-\alpha^2 v} J_0\left(\frac{\pi D_T}{\lambda}\sin(\theta)\sqrt{v}\right)dv\right)^2\right) \qquad (4)$$

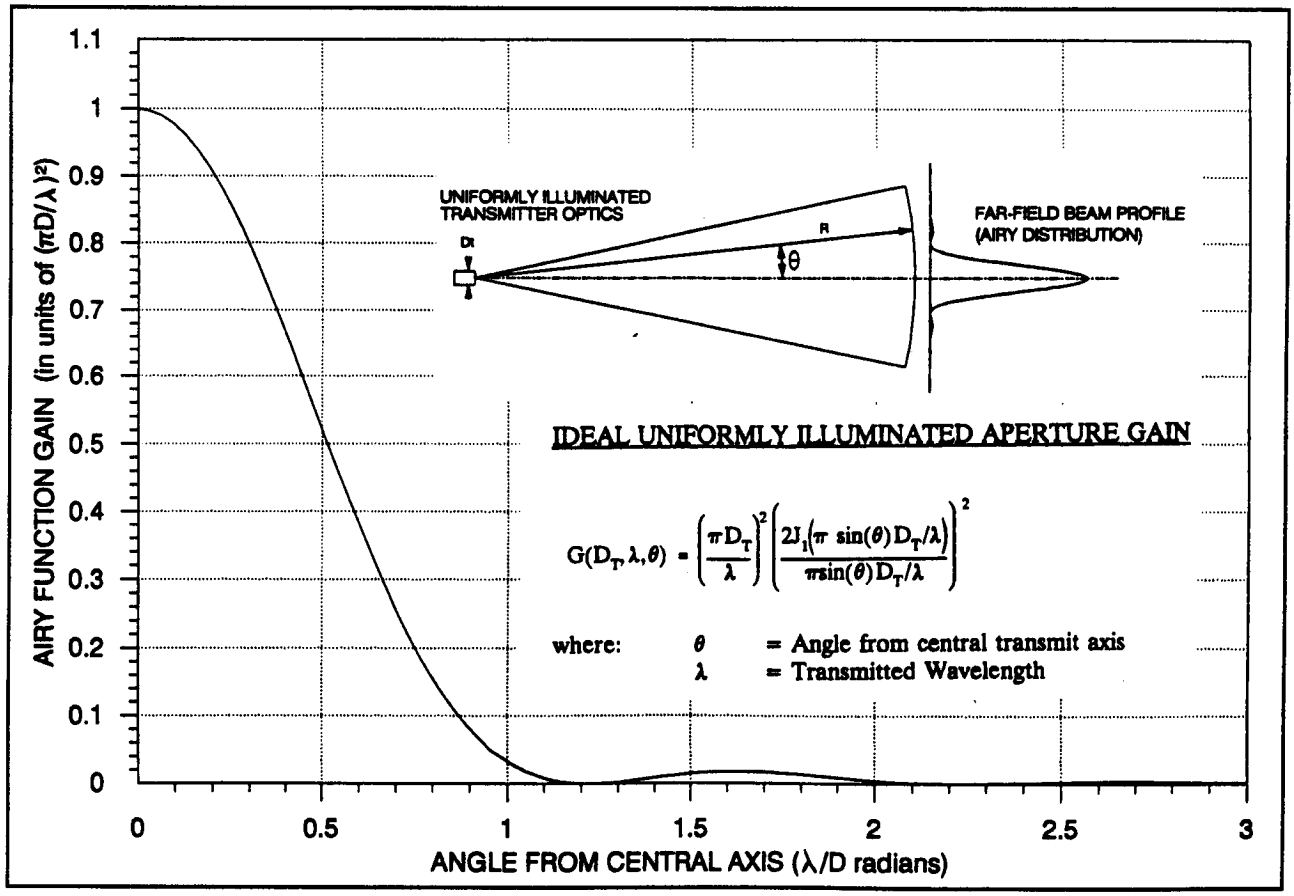

Figure 3.4.2-2 Ideal Telescope Gain Based Upon Airy Distribution Function

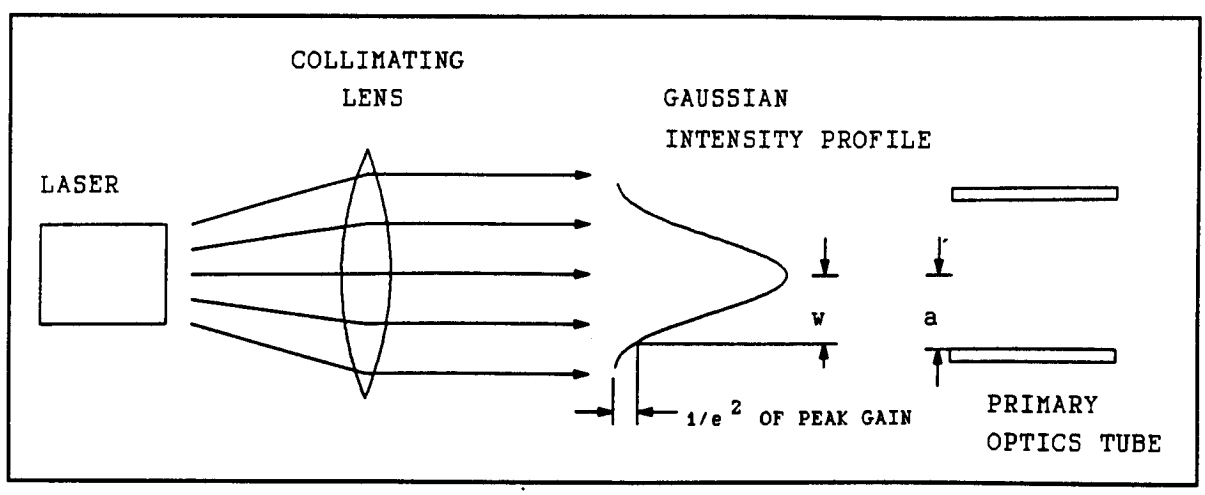

Figure 3.4.2-3 Gaussian Profile of Laser Output Intensity

where

α = a/w
a = radius of primary optics ($=D_T/2$)
w = radius of $1/e^2$ intensity of the Gaussian profile

Although this is a complicated integral, the change in on-axis gain from the ideal case can be computed by the factor $G(\alpha)$, and can be solved relatively easily (References 65, 66):

$$G(\alpha) = \left(\frac{2}{\alpha^2}\right)\left(e^{-\alpha^2} - 1\right)^2 \qquad (5)$$

Note however, that equation (5) ignores the additional beam divergence which accompanies this reduction in on-axis gain. This is addressed in the following section.

3.4.2.3 Central Obstruction Combined with a Gaussian Beam Profile on Transmit

Many telescope types require a secondary mirror placed in front of the objective optical element (the objective), which obstructs a portion of the objective's view. In most cases, the secondary mirror is placed on the optical axis. This affects both the transmit and receive gains by blocking a portion of the beam as shown in Figure 3.4.2-4.

The antenna gain function must now be replaced by:

$$G(D_T,\lambda,\theta,\alpha,\gamma_T) = \left(\frac{\pi D_T^2}{\lambda}\right)\left[2\alpha^2\left(\int_{\gamma_T}^{1} e^{-\alpha^2 v} J_0\left(\frac{\pi D_T}{\lambda}\sin(\theta)\sqrt{v}\right)dv\right)^2\right] \qquad (6)$$

where

γ_T = b/a
b = radius of central obstruction

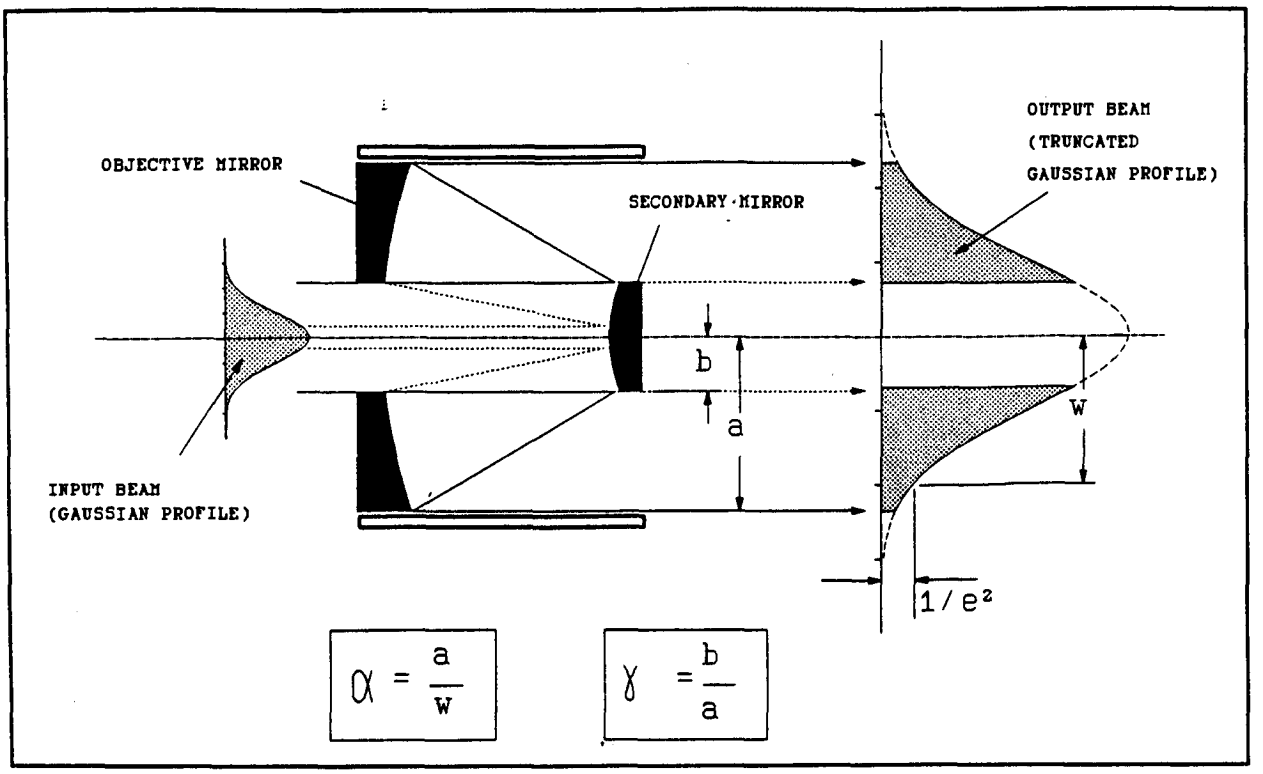

Figure 3.4.2-4 Central Obstruction Effect on a Gaussian Output Beam

Equation (5) showing the change in on-axis gain from the ideal case can now be replaced with:

$$G(\alpha,\gamma_T) = \left(\frac{2}{\alpha^2}\right)\left(e^{-\alpha^2} - e^{-\alpha^2\gamma_T^2}\right)^2 \qquad (7)$$

Because of the complexity of computing $G(D_T, \lambda, \theta, \alpha, \gamma_T)$ in equation (6) however, it is preferrable to use a simplified model of the product $G(\alpha, \gamma_T)G(D_T, \lambda, \theta)$ where $G(D_T, \lambda, \theta)$ from equation (3) provides the "ideal" Airy profile, and $G(,_T)$ from equation (7) provides a simple amplitude scaling factor:

$$G(D_T,\lambda,\theta)G(\alpha,\gamma_T) = \left(\frac{\pi D_T}{\lambda}\right)^2\left(\frac{2J_1(\pi\sin(\theta)D_T/\lambda)}{\pi\sin(\theta)D_T/\lambda}\right)^2 \left(\frac{2}{\alpha^2}\right)\left(e^{-\alpha^2} - e^{-\alpha^2\gamma_T^2}\right)^2 \qquad (8)$$

While this simplified model has the same on-axis gain as the actual case, it provides a slightly pessimistic model of beamwidth as shown in Figure 3.4.2-5.

The central obstruction creates a need to optimize the trade-off between α and γ_T in an effort to maximize the net power being passed through the annular aperture. Although the relationship is a complicated function, Klien & Degnan (Ref 66) show how to derive the following approximation which describes the optimum as a function of γ_T:

$$\alpha_{optimum} = 1.12 + \gamma_T^2(-1.30 + 2.12\gamma_T^2) \qquad (9)$$

This formula is exact at $\gamma_T=0$ and accurate to within $\pm 1\%$ for $\gamma_T \leq 0.4$, and is suitable for conceptual design work in this study. From equation (8), a plot of opti-

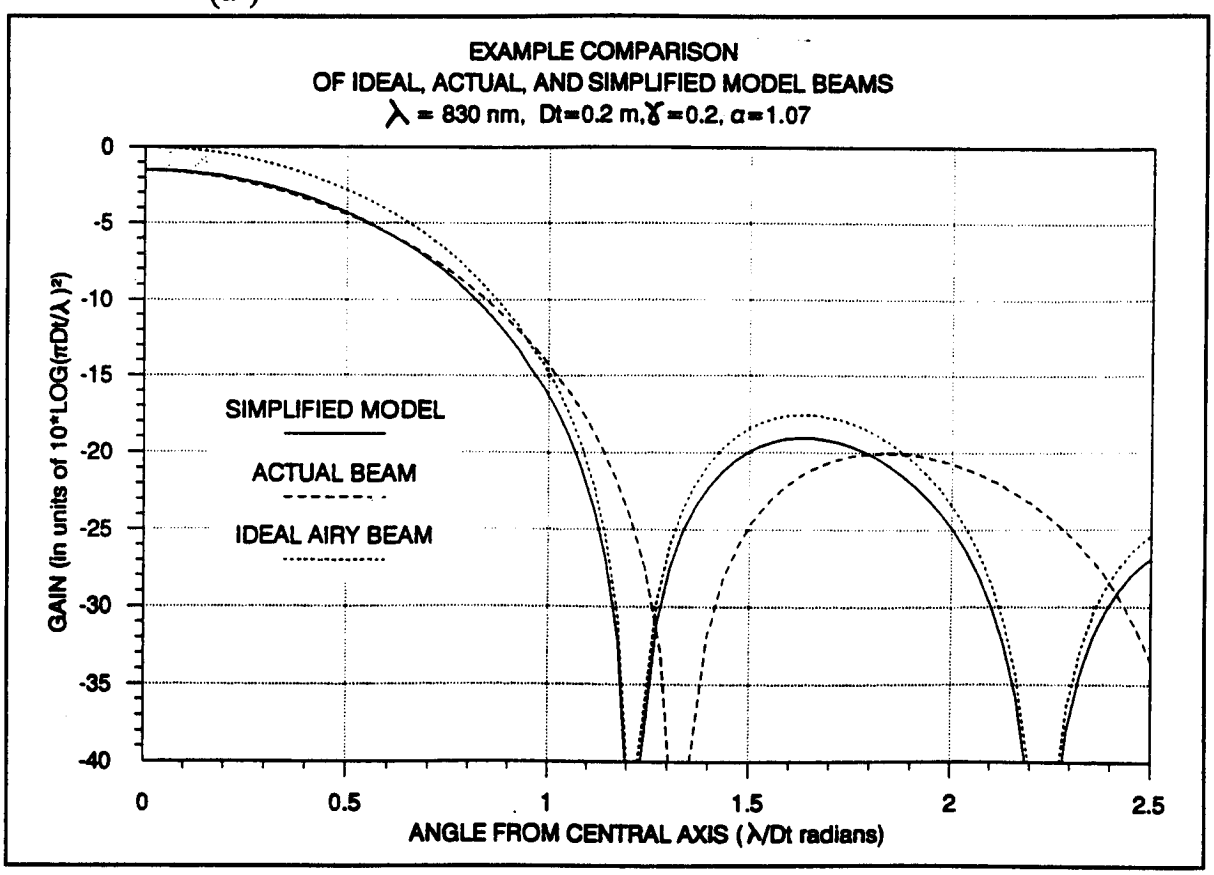

Figure 3.4.2-5 Comparison of Simplified Gain Model With Actual

mized α and $G(\alpha, \gamma_T)$ vs. γ_T can be generated as shown in Figure 3.4.2-6.

A typical value of γ_T would be 0.2, giving an optimum α of 1.07 and a net on-axis gain factor of 0.71.

3.4.2.4 Secondary Mirror Support Struts on Transmit

If struts are used to support a secondary mirror, they are generally arranged symmetrically as radials between the secondary mirror and the outer housing. The blockage of the Gaussian beam obviously depends on their actual cross-sectional area integrated over the Gaussian intensity, and will result in a relatively complex function. For the purposes of this study however, a reasonable approximation is to assume that there are N_T struts, each having an effective angular cross section of ε_T radians as shown in Figure 3.4.2-7.

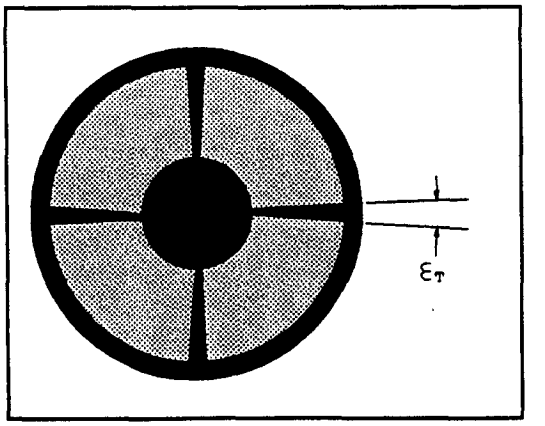

Figure 3.4.2-7 Modelling the Secondary Mirror Support Struts

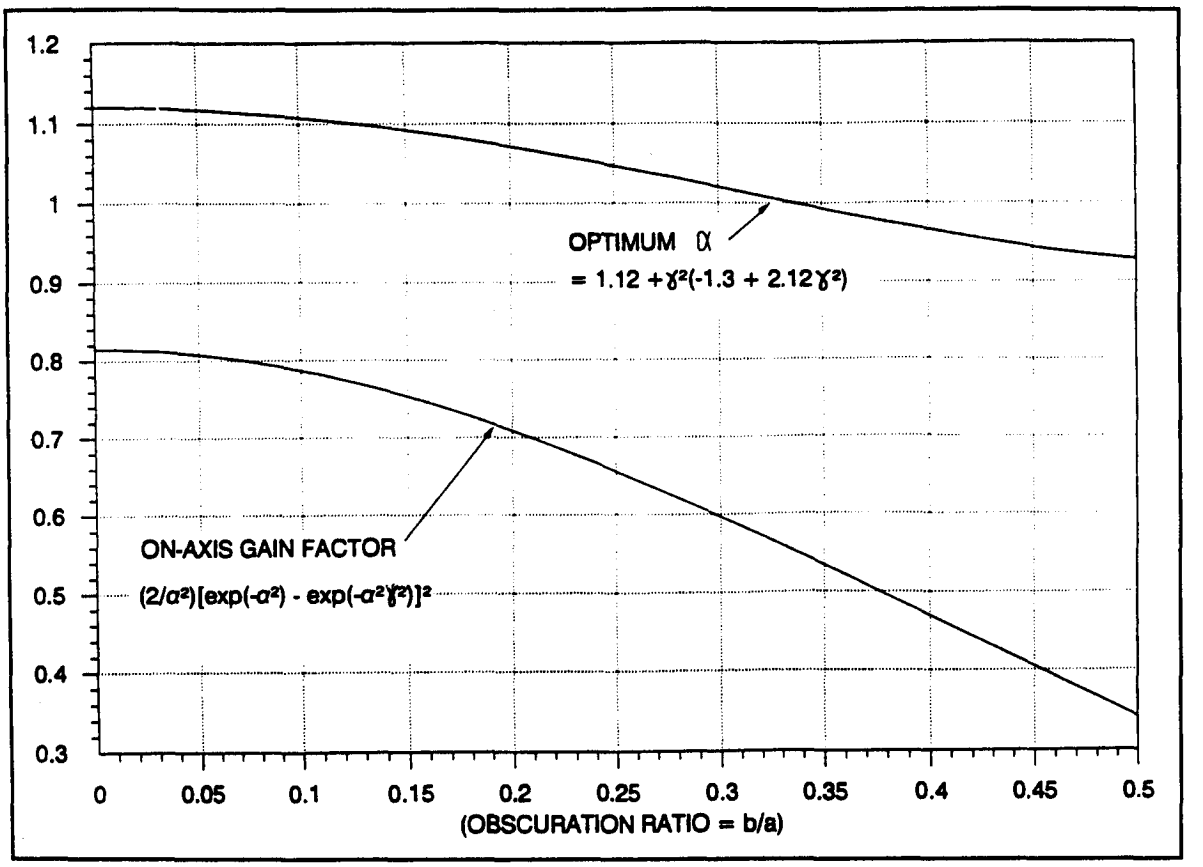

Figure 3.4.2-6 Optimized Gaussian Beam Size vs. Obscuration Ratio

Given these assumptions, the net blockage of the transmit beam is given by:

$$G(N_T, \epsilon_T) = \left(1 - \frac{N_T \epsilon_T}{2\pi}\right) \quad (10)$$

Detailed design work should consider whether it is possible to mount the secondary mirror on the inside of the telescope corrector lens or thermal window, thus eliminating the need for struts.

3.4.2.5 Wavefront Errors

The ability of the transmit telescope to produce an Airy beam pattern as described by $G(D_T, \lambda, \theta)$ depends upon the waves leaving the telescope aperture to be planar, in phase, and travelling 90 degrees to the optical axis. Variations from this case are caused primarily by:

- the emitting laser itself
- surface roughness of mirrors, lenses, and coatings

To handle these parameters, the "RMS wavefront error", Δ_{RMS}, is defined as the mean, localized (ie: variations << beam diameter), random variation of the final wavefront leaving the transmit aperture.

The "Strehl" equation can be used to assess the effects of such wavefront errors by computing mean reduction of the on-axis gain by:

$$G(\Delta_{RMS}) = e^{-\left(\frac{2\pi\Delta_{RMS}}{\lambda}\right)^2} \quad (11)$$

A plot of $G(\Delta_{RMS})$ vs. Δ_{RMS} is given in Figure 3.4.2-8.

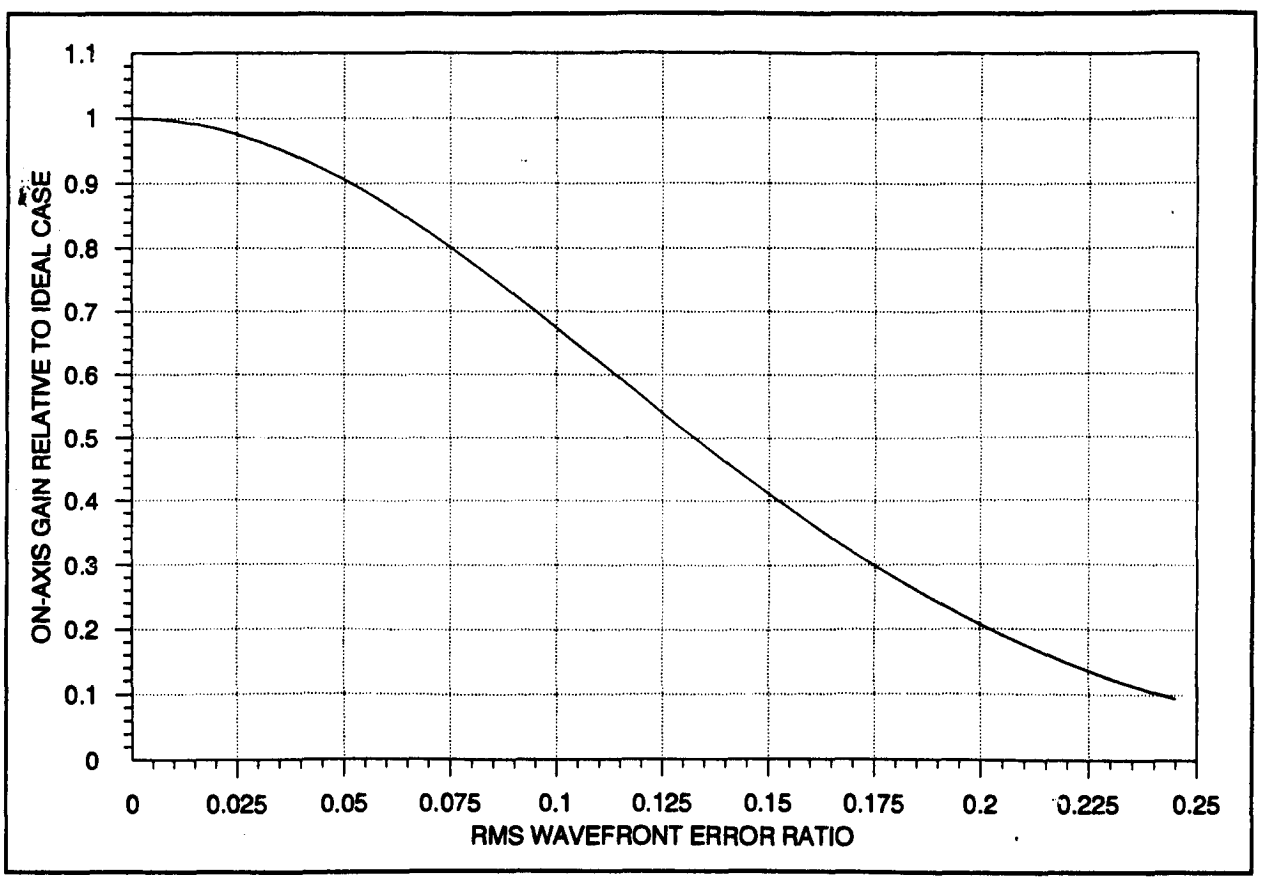

Figure 3.4.2-8 Effects of Random Wavefront Errors (Strehl Equation)

Note that equation (11) is valid only for localized, random surface variations, and cannot be used for large scale optical variations such as overall asphericity or misalignment or defocusing of optical elements since these produce macroscopic, rather than microscopic, variations which are not subject to statistical averaging.

When a number of optical surfaces are involved, the net overall Δ_{RMS} can be determined by:

$$\Delta_{RMS} = \sqrt{\Delta_1^2 + \Delta_2^2 + ... + \Delta_n^2} \qquad (12)$$

For an optical ISL application, it can be seen clearly from Figure 3.4.2-8 that the total random wavefront errors must be kept quite low, typically to $\lambda/10$ if possible.

Table 3.4.2-1 provides examples of surface finishes of typical custom high quality optics elements available commercially. The actual quality depends upon the type of materials chosen and the cost willing to be paid for the finishing.

Additional wavefront aberrations will arise from the laser itself. NASA/Goddard tested an SDL 5410 laser (820-860 nm wavelength) (Reference 67) and achieved wavefront errors less than $\lambda/30$ at output powers up to 200 mW. At lower powers, these wavefront errors dropped to below the accuracy of their experiment ($\lambda/50$).

After computing the RMS wavefront error contributions using equation (12), for a typical optical network of perhaps 20 elements it can be seen that an "average" surface finish of better than $\lambda/40$ might be required for each element in the optical system to achieve a "net" RMS value of $\lambda/10$. Using the Strehl equation (11), this would yield a typical gain reduction factor of around 0.67 (-1.7 dB).

Table 3.4.2-1 Typical Surface Finishes of High Quality Optical Elements

Element Type and Size	Surface Finish (λ = 632.8 nm)
Flat Mirrors & Plates (< 4")	$\lambda/200$
Flat Mirrors & Plates (4-14")	$\lambda/50$
Spherical Mirrors (< 14")	$\lambda/40$
Spherical Lenses (< 14")	$\lambda/40$
Aspherical Mirrors (< 14")	$\lambda/25$
Aspherical Lenses (< 14")	λ/?
Cube Beamsplitters	$\lambda/20$

3.4.2.6 Transmissivity of Transmit and Receive Optics

Transmission loss is also caused by the optical lenses and coatings in the optical network which have finite transmissivities at the desired wavelength. Values for transmissivity vs. wavelength for a number of optical materials can be found in the Schott catalogue and other sources. Typical values, using a 800 nm wavelength, are tabulated in Table 3.4.2-2.

The transmissivities of most optical elements are also subject to a variety of factors such as atmospheric reactions, UV radiation, and proton radiation (see section 3.4.5.2). By carefully designing the telescope to keep radiation sensitive elements protected, the overall loss of transmittance over the life of an optical ISL can be kept below 10%.

Where beam splitters are being utilised, it must be remembered that these elements are designed intentionally to reflect a specific portion of the beam onto an alternate path, and hence will have a much lower through transmissivity than otherwise. "The transmissivity" of the optical network must therefore be assessed for each path independently. Beam combiners on the other hand, are intended to combine more than one beam into a single beam with as little power loss as

Table 3.4.2-2 Transmissivities of Various Optical Elements at 800 nm

Type of Element	Transmissivity
Antireflection Coatings on Lenses	0.9998
Mirror Coatings	0.999
Bulk Fused Silica (Quartz)	0.999 per 25 mm
Bulk SF6 G5	0.964 per 25 mm
Bulk SK4 G13	0.991 per 25 mm
Bulk SF4 G6	0.965 per 25 mm
Bulk SF5 G10	0.991 per 25 mm
Bulk LaF_2	0.993 per 25 mm

possible. At the design wavelength, the net, total transmissivity of a typical high quality narrow band, dichroic beamsplitter (Reference 68), can be made better than 0.95. Polarizing beamsplitters can achieve better than 0.98 transmissivity for each of the polarized components.

For a typical optical ISL system concept, the optical path might consist of the following:

- 1 thermal control window
- 1 primary mirror
- 1 secondary mirror
- ≈10 lenses in the eyepiece
- 1-2 fine pointing mirrors
- 3-4 beamsplitters/combiners
- ≈3-4 lenses at the laser (or detector)

Such a network would yield a typical transmissivity of around 0.80 on each transmit and receive link.

3.4.2.7 Free Space Loss

"Free space loss" accounts for the reduction of effective irradiated power per unit area as a result of distance (R) between an omnidirectional transmitter (transmitting uniformly over the full 4π steradian sphere) and a remote receiver collector. To use normal communications terminology however, the "receive telescope gain" $G(D_R)$ is used instead of collector area. The free space loss is then referenced to an effective collection area of $\lambda^2/(4\pi)$ at a distance R, and is given by the following:

$$G(R) = \left(\frac{\lambda}{4\pi R}\right)^2 \qquad (13)$$

3.4.2.8 Ideal Gain of the Receive Telescope

Unlike a radio receiver antenna, the receive optics will generally focus the incoming signal onto a spot on the detector much smaller than the detector area so that the received signal is essentially constant as long as the incoming spot lies within the detector field of view. The telescope therefore acts like a "photon bucket", channelling the received photons onto the detector surface. Because of this, the calculation for transmit telescope gain (which varies with angle) does not apply to the receive telescope. The efficiency of the receive telescope is essentialy constant within the field of view of the communications detector, and is given by the telescope collection area.

The collection area of the receive telescope is, of course just $\pi D_R^2/4$. To make this compatible with the free space term in section 3.4.2.7 however, the collector area must be referenced to a unit area of $\lambda^2/(4\pi)$ giving the effective receive telescope gain:

$$G(D_R) = \left(\frac{\pi D_R}{\lambda}\right)^2 \qquad (14)$$

3.4.2.9 Central Obstructions and Supports on Receive

At the receive telescope, the incoming beam can effectively be considered to uniformly illuminate the objective optics. The losses due to blockage by any secondary mirror or its supports becomes a simple matter of computing blockage area. The effect of blockage by a circular secondary mirror can be computed from:

$$G(\gamma_R) = (1-\gamma_R^2)$$

where

γ_R = b/a
b = radius of secondary mirror
a = radius of primary mirror

A typical value of γ_R for a Cassegrain style telescope would be 0.2.

Similarly, assuming N_R support struts each with angular blockage ε_R radians, the net reduction in the collector area is given by the factor:

$$G(N_R, \varepsilon_R) = \left(1 - \frac{N_R \varepsilon_R}{2\pi}\right) \quad (15)$$

Again, good design practice should examine whether the secondary mirror can be mounted on the front telescope corrector lens or thermal window, thus avoiding blockage from support struts.

3.4.2.10 Using the Link Equation for System Design

From the discussion in the foregoing sections most of the parameters of the optical link equation in section 3.4.2 can be given preliminary estimates for a standard Cassegrain telescope:

$\gamma_T = \gamma_R = 0.2$

$\alpha = 1.07$

$TR_T = 0.7$
$TR_R = 0.7$

$N_T = N_R = 0$

$\Delta_{T\text{-}RMS} = \lambda/10$
$\Delta_{R\text{-}RMS} = \lambda/10$

The fine pointing system will generally be set to maintain pointing of the transmit beam within the -4 dB (40%) point. From Figure 3.4.2-2 this gives an allowable pointing error of:

$\theta = 0.4\,\lambda/D$ radians

The value of R is determined based upon the maximum link distance for the selected system:

R = 49,000 km (worst case for a LEO-GEO link)
= 104,000 km (worst case for a GEO-TUNDRA link)

The value of λ is determined from the selected laser:

λ = 1060 nm (Nd:YAG Laser)
= 850 nm (AlGaAs Laser)

P_R can be referenced to the number of photons per bit:

$$P_R = h\left(\frac{c}{\lambda}\right)(N)(F) \quad (16)$$

where:

h = Planck's constant (6.63×10^{-34} J-s)
c = speed of light (3.0×10^{8} m/s)
N = required photons per bit based upon the detector sensitivity. This includes ALL detectors in the optical system.
F = bit rate

The detector sensitivity depends on a variety of factors such as the bit rate, detector type, modulation type, bit error rate, etc. For the purposes of this section, a typical value for N might be around 200 photons/bit at 100-1000 Mbps for two redundant communications detectors and two redundant fine pointing detectors.

The optical link equation (2) can now be simplified with these assumptions to give the laser output power required:

$$P_T = 5.1 \times 10^{-24}\left(\frac{NF\lambda R^2}{D_T^2 D_R^2}\right) \quad (17)$$

Using equation (17), Figures 3.4.2-9 and 3.4.2-10 show laser output power required vs. telescope aperture for a number of data bit rates. Figure 3.4.2-9 considers an 830 nm AlGaAs laser while Figure 3.4.2-10 considers a 1060 nm Nd:YAG laser. Both figures assume a combined transmit/receive telescope.

Care must be taken in using the results of Figures 3.4.2-9 and 3.4.2-10 since these are based upon diffraction limited beamwidths. An increasing telescope aperture in these figures therefore implies tighter pointing requirements which reach a practical limit at around 1 μrad (1 sigma). The mass of the telescope also increases roughly with the diameter cubed to account for the increase in volume of the mirrors, lenses, and structural components.

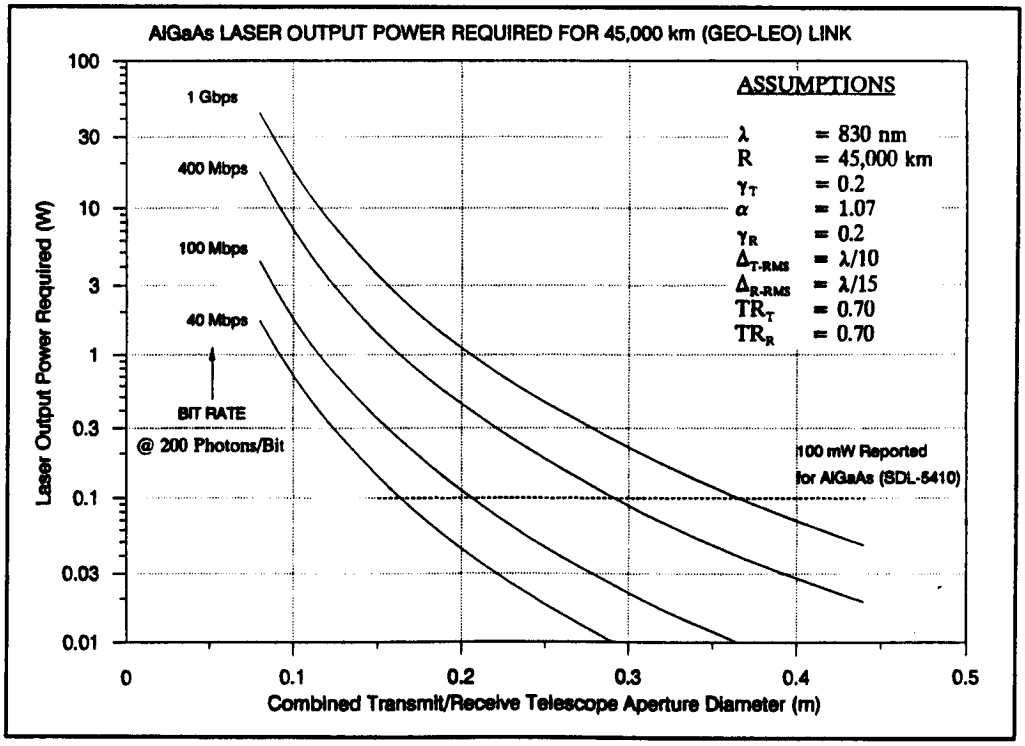

Figure 3.4.2-9 Laser Output Power vs. Telescope Aperture for AlGaAs Laser

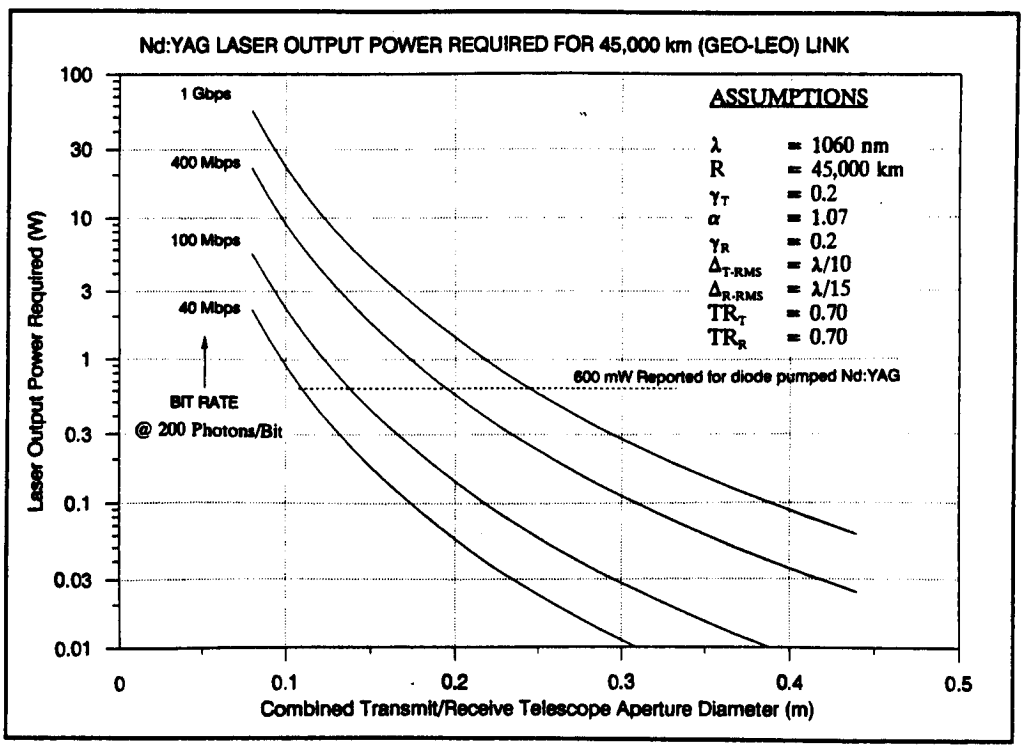

Figure 3.4.2-10 Laser Output Power vs. Telescope Aperture for Nd:YAG Laser

3.4.3 The Primary Telescope

In an optical ISL system the telescope's primary job is to provide a large light collecting aperture and condense it into a much smaller collimated beam diameter (exit pupil diameter) which is fed into the optical network. A collimated beam output from the telescope is preferred because it eliminates many restrictions on the optical network associated with placement of the detectors, angles of incidence at filters, sizes of detector surfaces, etc.

This section examines some of the more common telescope configurations which can be considered for an optical ISL system, and the kinds of advantages and disadvantages each offer.

3.4.3.1 Refractors (Dioptrics)

Refractor telescopes are the original and probably the simplest form of telescopes. They employ aspherical lens for both the objective lens and the eyepiece as shown in Figure 3.4.3-1. Note that the eyepiece is shown as a single element for clarity. The actual eyepiece would generally be a multi-element aplanatic type (see section 3.4.1).

The main attraction of such a telescope is its simple, unobstructed aperture, giving it a good tranmission efficiency, particularly on-axis where the peak intensity of the Gaussian profile exists. Refractor optics are often used for space-based instruments such as boresight horizon limb sensors, sun sensors, star sensors, and some smaller imaging optics where lenses are generally less than a few inches. The focal ratio of the objective lens should not be dropped too low since the high lens curvatures involved lead to image distortions and difficulty with figuring the surface. Typical objective lenses have focal ratios of around 8:1 to 20:1. For apertures over 6 inches the simplicity advantage is often negated by the disadvantages of using the large objective lens which becomes expensive, heavy, and has a long focal length. Table 3.4.3-1 lists these and other trade-offs.

3.4.3.2 Reflectors (Catoptrics)

Pure reflector systems, known as "catoptric" types, use only mirrors to collect and collimate the incoming beam. Using reflecting mirrors has the main advantage of compacting the optical path by reflecting it back-and-forth within a short space. Furthermore, mirrors reflect all wavelengths by the same geometric angle thus avoiding chromatic aberrations which lenses experience because of different refractive indices at different wavelengths. Reflecting mirrors are also less expensive to manufacture in large diameters and can be made lightweight using a number of mass saving technologies (see section 3.4.3.7).

The oldest and simplest form of reflector telescope is the Newtonian, shown in Figure 3.4.3-2. This design uses a parabolic objective mirror which reflects onto a flat secondary mirror. The beam is reflected out of the objective optics path into an eyepiece. This design provides reasonably good performance but requires a relatively long telescope barrel to handle the long focal length of the objective mirror. Since a parabolic mirror

Table 3.4.3-1 Advantages and Disadvantages of Refractor Telescopes

Advantages	Disadvantages
The basic design is very simple.	Aspheric objective lens is expensive in large diameters.
The aperture is clear and unobstructed.	The objective lens is often heavy in large sizes.
	The long focal length of the objective lens requires a long, unwieldly telescope. Alternatively, if the optical length is compacted, the additional multi-element lenses required add significant mass.
	Refractive indices of the lenses varies with wavelength. This requires additional optics (and mass) to correct for this.

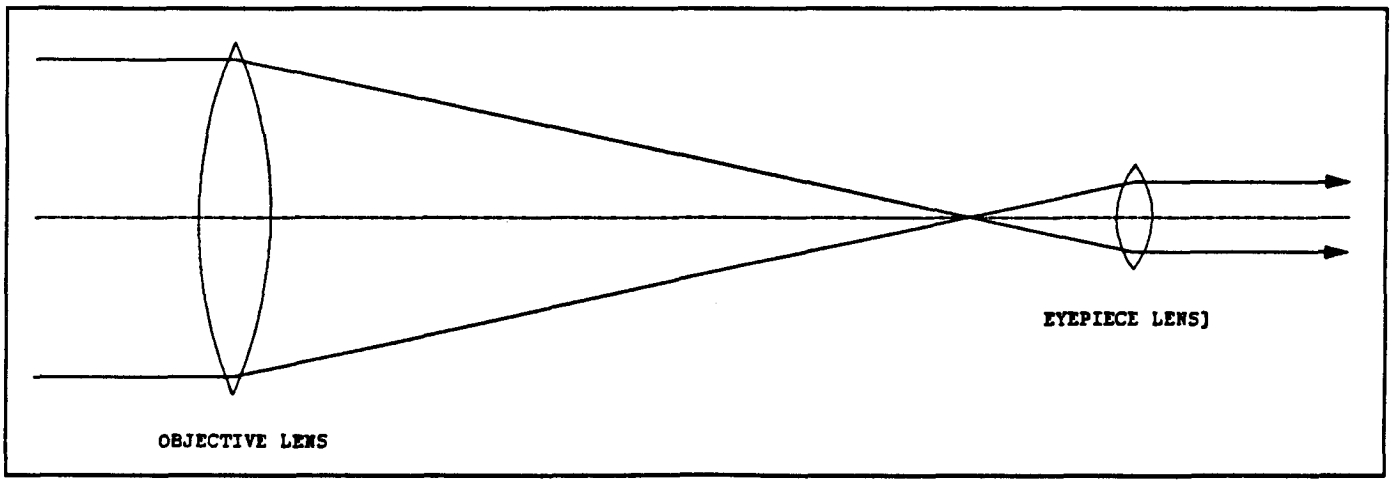

Figure 3.4.3-1 A Refractor Telescope

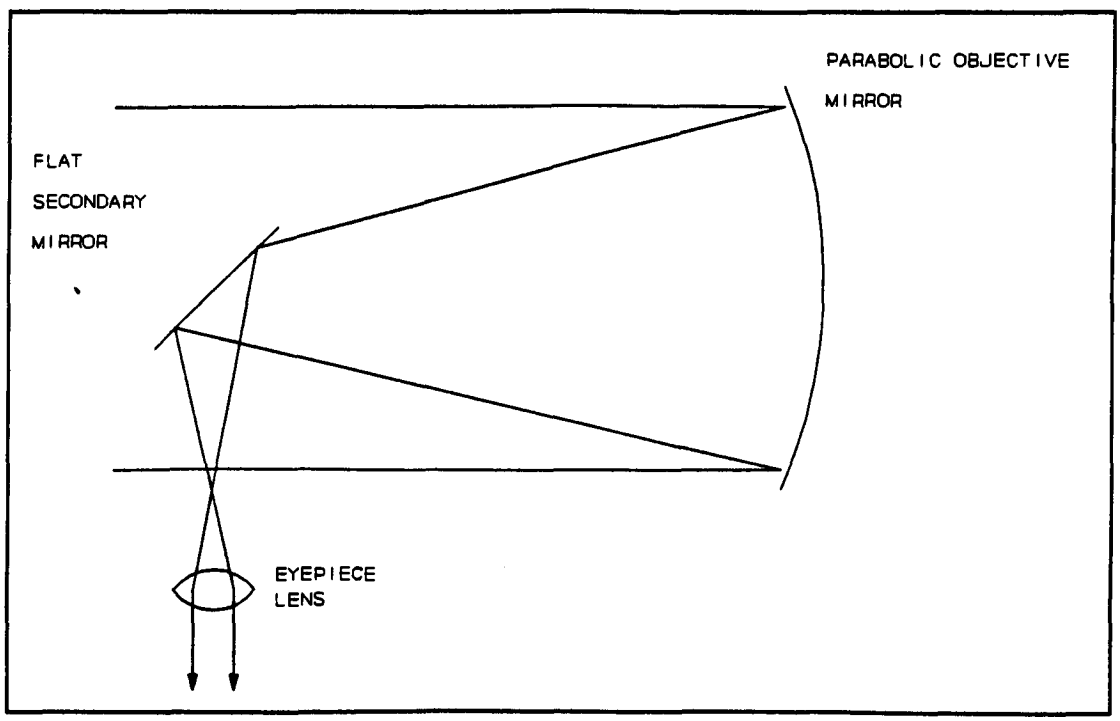

Figure 3.4.3-2 A Newtonian Reflector Telescope

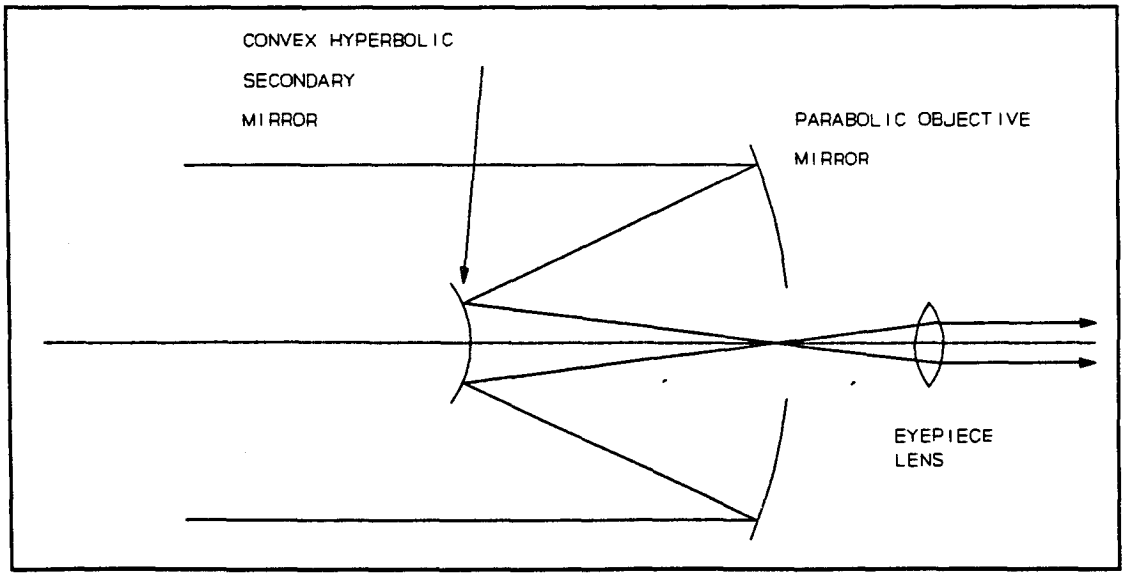

Figure 3.4.3-3 A Cassegrain Reflector Telescope

does not in fact produce an aplanatic image, the quality of the image depends on having a reasonable focal ratio for the objective mirror, typically around 10:1.

To compact the telescope design the secondary mirror can also be made aspheric, changing the effective focal length of the telescope. Figures 3.4.3-3 and 3.4.3-4 show examples of two common such reflector telescope designs, the Cassegrain and Gregorian. The Cassegrain telescope is a combination of a paraboloid objective mirror and hyperboloid secondary mirror. The hyperboloid secondary mirror has the effect of extending the effective focal length of the overall telescope far beyond its physical length. For commerical Cassegrain telescopes a 200 mm objective mirror is often employed in a telescope less than 400 mm long, but the combined objective and secondary mirrors produce an effective focal length of 2000 mm or more. The Gregorian telescope is similar to the Cassegrain except that it is based upon a concave elliptic secondary instead and is therefore placed after the focal point of the primary mirror.

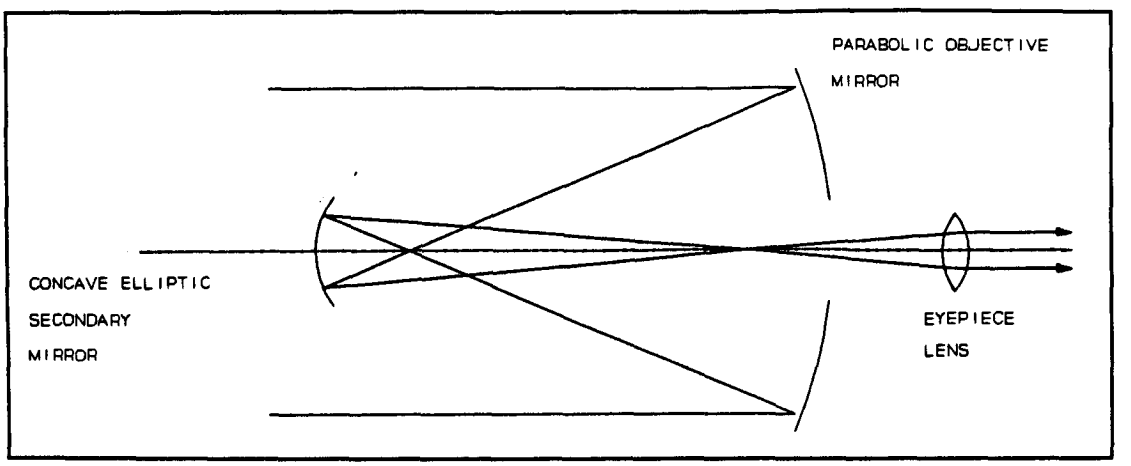

Figure 3.4.3-4 A Gregorian Reflector Telescope

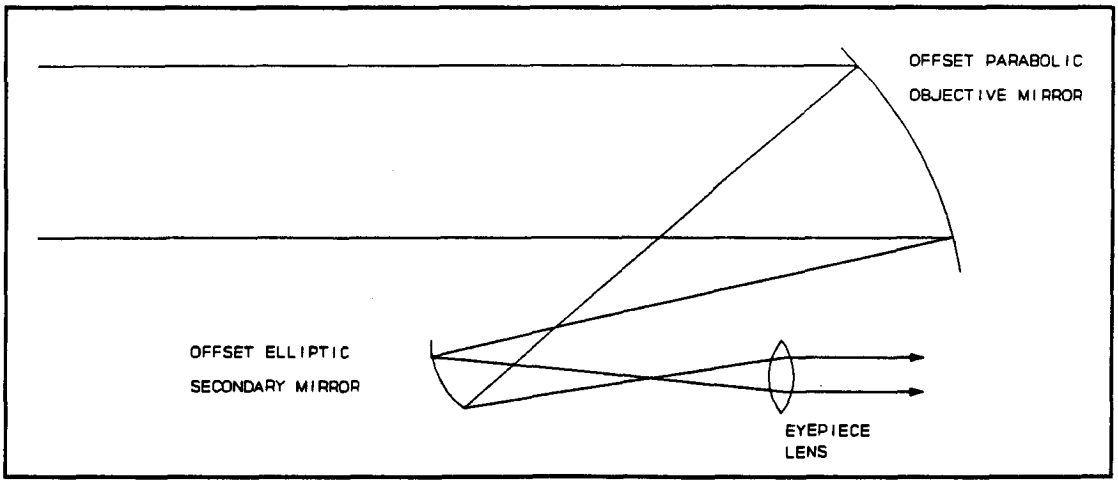

Figure 3.4.3-5 An Offset Gregorian Reflector Telescope

The Cassegrain and Gregorian telescopes are based upon low-order aspheric mirrors which provide good image quality, but still suffer from some degree of off-axis distortions (coma). Variations on the theme are possible which result in nearly perfect image quality, but require the use of higher-order aspherical mirrors which are much more difficult to manufacture. Such combinations are known as Ritchey-Chretien telescopes and are often used in large, earth-based observatories.

To avoid the loss of signal due to the central obstruction, portions of the same mirrors can be employed in off-axis configurations as shown in the example of Figure 3.4.3-5. Such arrangements use small sections of much larger mirrors to avoid the central obstruction. Although in principle this appears attractive, in practice the mirror sections must be manufactured by first forming the full-size mirrors and then cutting the desired sections. This is an expensive process for large mirrors and is therefore only common in smaller instruments.

Table 3.4.3-2 summarizes some of the advantages and disadvantages of reflector telescopes.

Table 3.4.3-2 Advantages and Disadvantages of Reflector Telescopes

Advantages	Disadvantages
Very compact designs produce a long effective focal length in a short distance.	Central obstructions reduce the effective transmission of the telescope, particularly for the Gaussian beam intensity profile.
Large mirrors are less expensive than equivalent sized lenses.	Coatings are necessary to protect metallic mirror surfaces from oxidation and other chemical processes.
Mirrors don't suffer from chromatic aberration.	Large aspheric surfaces are still expensive to fabricate and check-out. High-order aspherics are generally avoided in space-based designs for this reason.
Lightweight mirror manufacturing technologies exist and are continuously improving (eg: foam metal cores, composites, etc...).	
Metal-based mirrors have good conductivity, making thermal control easier.	
Mirrors can be supported by their backs, making structural support and thermal design easier.	

3.4.3.3 Combined Refractors/Reflectors (Catadioptrics)

Adding a front corrector lens to a reflector telescope can allow the objective reflecting mirror to be made spherical while still correcting for off-axis distortions. The large, spherical objective mirror can then be made at a much lower cost. Such combinations of reflecting and refracting elements for the telescope are referred to as "catadioptric" systems. The two most common types of corrector lenses are the Schmidt and the Maksutov, both designed to operate with a spherical objective mirror. The lens in both cases in placed in front of the objective mirror as shown in Figure 3.4.3-6 and 3.4.3-7.

The drawback of the corrector lens is the cost and mass of the lens itself. The Schmidt corrector plate, for example is aspheric, and would cost about the same as any lens of the same diameter and quality. The Maksutov lens is somewhat easier to manufacture since it has a spherical surface, but the thickness and mass of these lenses is usually substantial (eg: 20 mm thick, 3.0 kg for a typical 250 mm aperture).

Despite this, the Schmidt-Casssegrain is among the most popular designs for amateur 8" to 14" telescopes because of their very compact design. The additional cost of the lens for amateur applications is generally modest.

Some of the advantages and disadvantages of catadioptric telescopes are listed in Table 3.4.3-3.

3.4.3.4 Coudé Configurations

A Coudé configuration refers to a telescope which passes its optical beam through the gimbal axes as shown in the example of Figure 3.4.3-8. This arrangement has the advantage of allowing the primary optics to be pointed without having to move the entire optical network. This greatly reduces the mass of the moving portion of the optical ISL, allowing a less massive gimballing system to be employed. A study done by CAL Corp. for the SILEX program showed that mass savings of around 20 kg can be realized by taking the Coudé approach.

Using the Coudé system does incur two complications however:

- It is more difficult to isolate satellite structural noise from the optical path since the optical path passes from the gimballed telescope into the fixed optical network. By contrast, a non-Coudé mount allows noise from the satellite bus to be damped, particularly at higher frequencies, as it passes through the gimbal system before it reaches the optics. The solution to this is to use high speed fine steering mirrors already developed to achieve the necessary

Table 3.4.3-3 Advantages and Disadvantages of Catadioptric Telescopes

Advantages	Disadvantages
Very compact designs produce a long effective focal length in a short distance.	Central obstructions reduce the effective transmission of the telescope, particularly for the Gaussian beam intensity profile.
Large mirrors are less expensive than equivalent sized lenses.	Coatings are necessary to protect metallic mirror surfaces from oxidation and other chemical processes.
The corrector lens seals the telescope, helping protect the mirror finish.	Large aspheric lenses are expensive to fabricate and check. High-order aspherics are generally avoided in space-based designs for this reason.
Lightweight mirror manufacturing technologies exist and are continuously improving (eg: foam metal cores, composites, etc...).	The corrector lens incurs chromatic aberration which must be dealt with in the optical network.
Metal-based mirrors have good conductivity, making thermal control easier.	
Mirrors can be supported by their backs, making structural support and thermal design easier.	

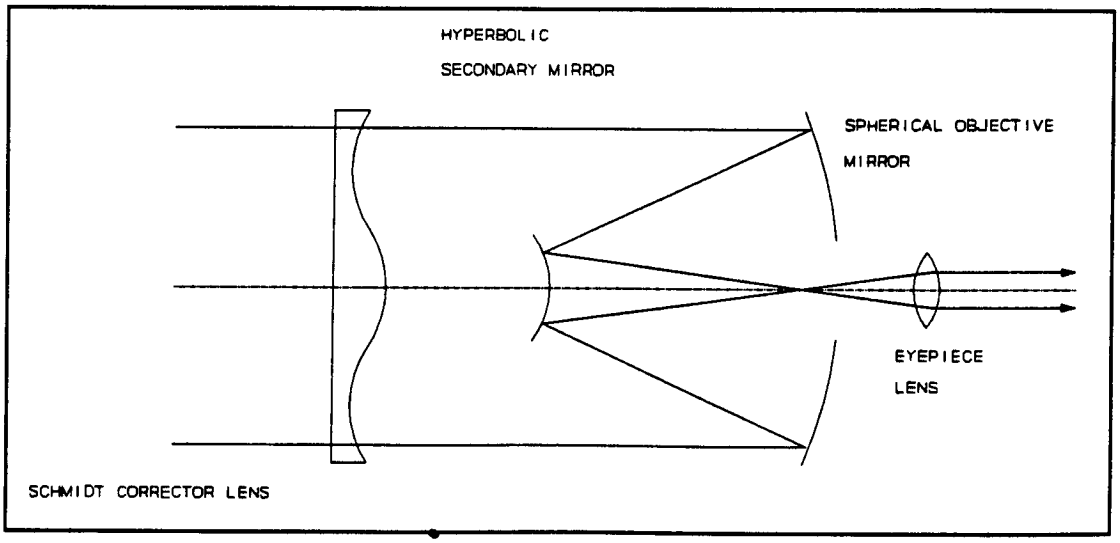

Figure 3.4.3-6 A Schmidt-Cassegrain Telescope

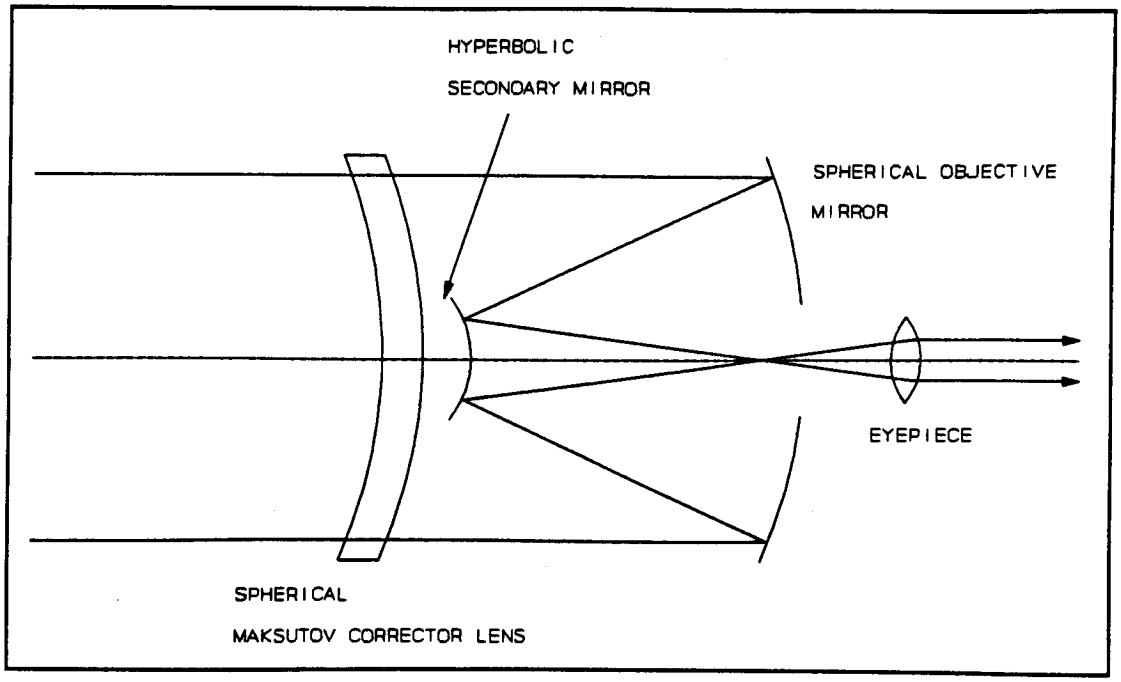

Figure 3.4.3-7 A Maksutov-Cassegrain Telescope

beam pointing stability. These have sufficient response rates to handle over 1 kHz and will handle typical satellite noise arising from motors, sensor movements, etc...

- The output image from a Coudé configuration rotates when either of the gimbal axes is operated. This adds complexity to the coarse pointing system which must de-rotate its output signals to compensate. However, the high processing power of modern space qualified computers should make this an easy function to handle.

Figure 3.4.3-9 shows an example of a Coudé telescope previously designed by CAL Corporation as a lightweight alternative for optical intersatellite link systems. The entire telescope, including coarse pointing drives and the eyepiece has a mass of less than 18 kg.

3.4.3.5 The Periscope Configuration

A modification of the Coudé design, suggested by British Aerospace Ltd. (Ref 101) is to placed the gimbals and flat in front of the objective aperture, thereby allowing the main telescope to remain fixed while only a periscope style pair of flats moves in front of it. This is shown in Figure 3.4.3-10.

This approach has significant merit since the telescope can then be buried behind a spacecraft deck, rather

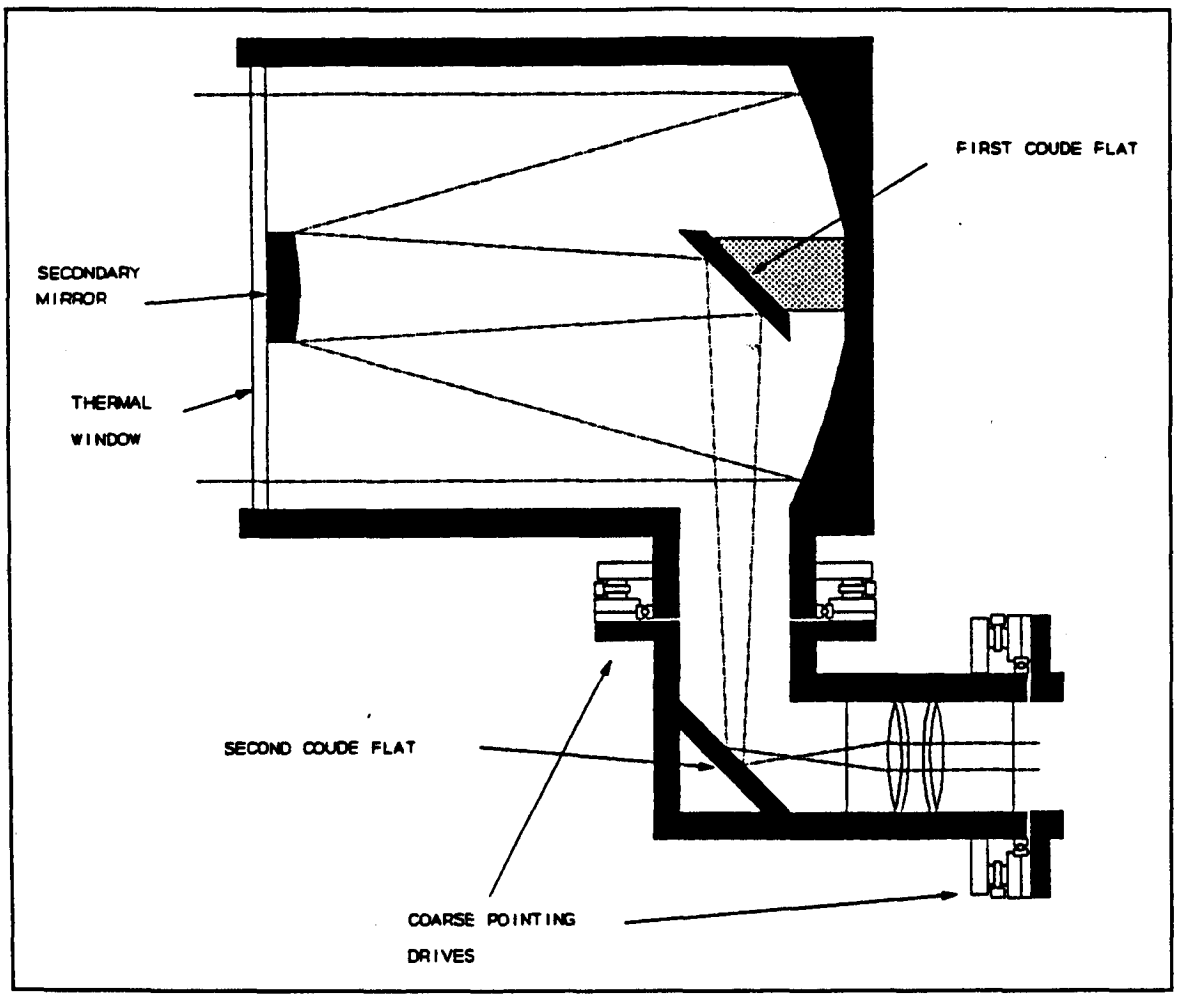

Figure 3.4.3-8 A Coudé Configuration Using a Cassegrain Telescope

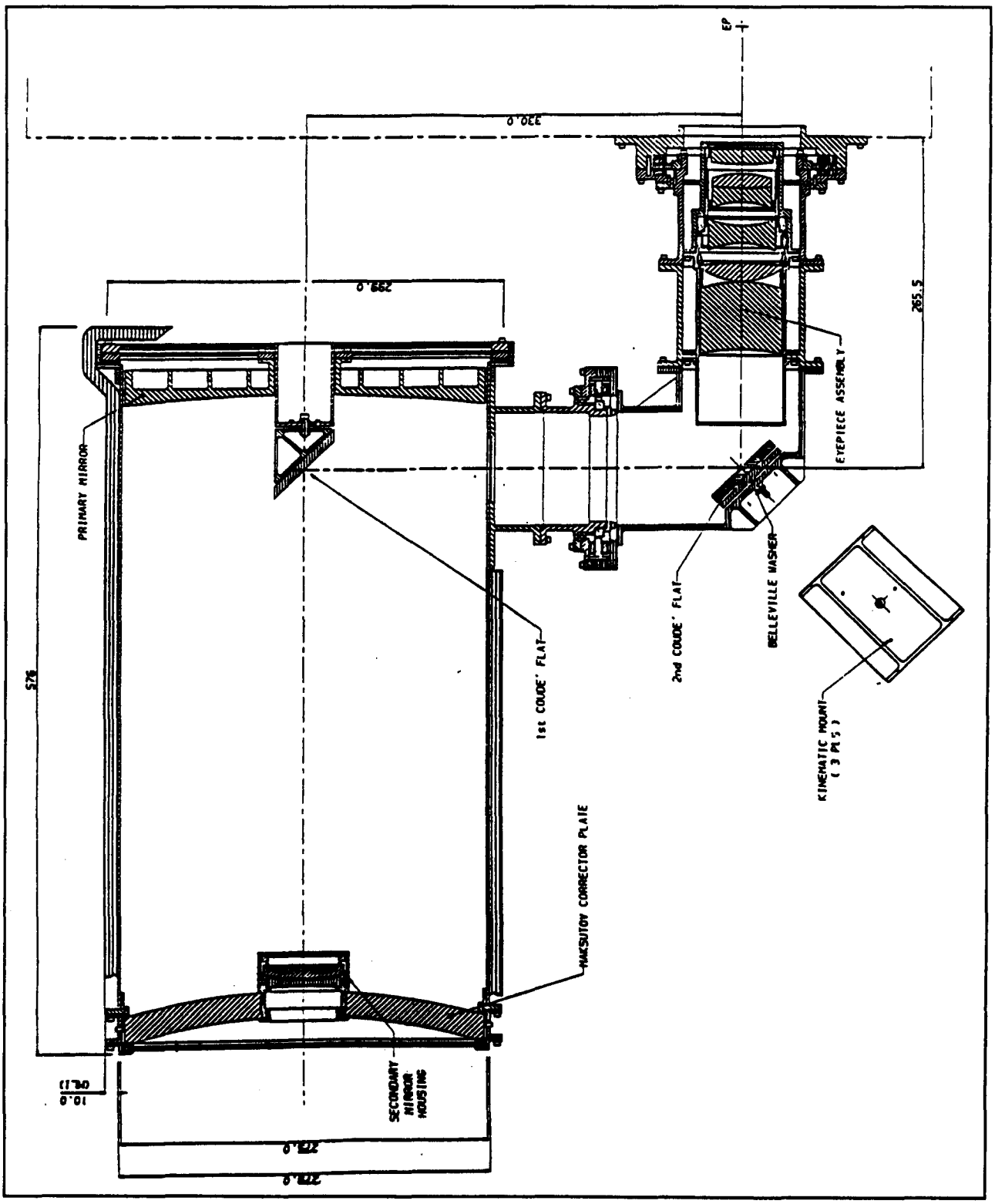

Figure 3.4.3-9 An Existing Space Qualifiable Coudé Telescope Design by CAL Corporation

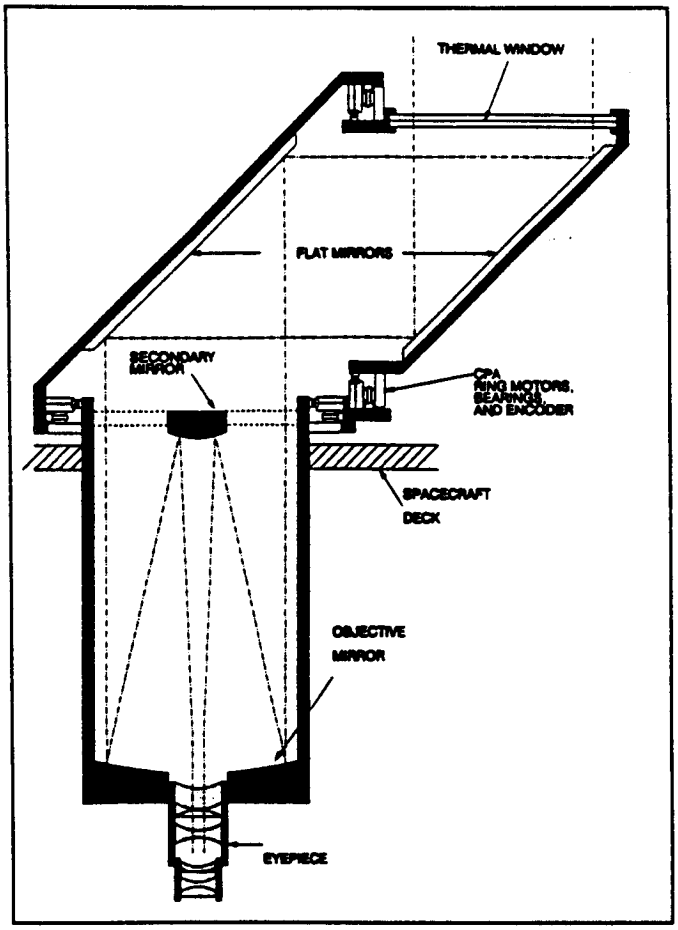

Figure 3.4.3-10 Periscope Configuration (Ref 7)

than exposing it to space. Furthermore, the periscope pointing mechanism uses much less space to move within and, with good design, may not require any special launch tie-downs to support it during launch.

The periscope approach does have limitations when the objective diameter becomes large however, since the mass and cost of the pointing assembly becomes large. Based upon CAL's preliminary design of the standard Coudé design, the mass savings of the periscope design are only realized for aperture diameters of around 150 mm or less. The periscope design also presents the same image rotation complications as the Coudé design.

3.4.3.6 The Meinel Configuration

As an alternative to the standard telescope tube structure for the primary telescope, the Meinel configuration, proposed by the Optical Sciences Center of the University of Arizona (Reference 69) is shown in Figure 3.4.3-11. It consists of an objective mirror with an optics tube installed through its centre. The other end of the tube supports the secondary mirror. Although unusual, the Meinel configuration has considerable merit. Stray light control baffles which are usually required in Cassegrain telescopes, can be included as part of the tube. Because the tube diameter is small, it can be made with a relatively thick wall to provide the necessary structural strength for supporting the secondary mirror. Care must be taken in designing the support vanes connecting the secondary mirror to the tube to ensure sufficient torsional stiffness.

Although this configuration has extremely low mass, it does present disadvantages:

- The optics and the support tube are continually exposed to solar light which may cause thermal problems affecting alignment and optical element characteristics. The design does not permit the use of any thermal protection window (see Section 3.4.5).
- The small diameter of the support tube may lead to low resonance problems during the launch environment.
- Because the primary optics are not sealed, they require more careful environmental control during integration, testing, and launch.
- The design cannot be easily adapted to use a corrector plate.

3.4.3.7 The Dall Configuration

The Optical Sciences Centre of the University of Arizona has also investigated the use of a Dall truss to support the secondary mirror as shown in Figure 3.4.3-12. This approach may improve on the structural integrity of the secondary mirror mount, but still

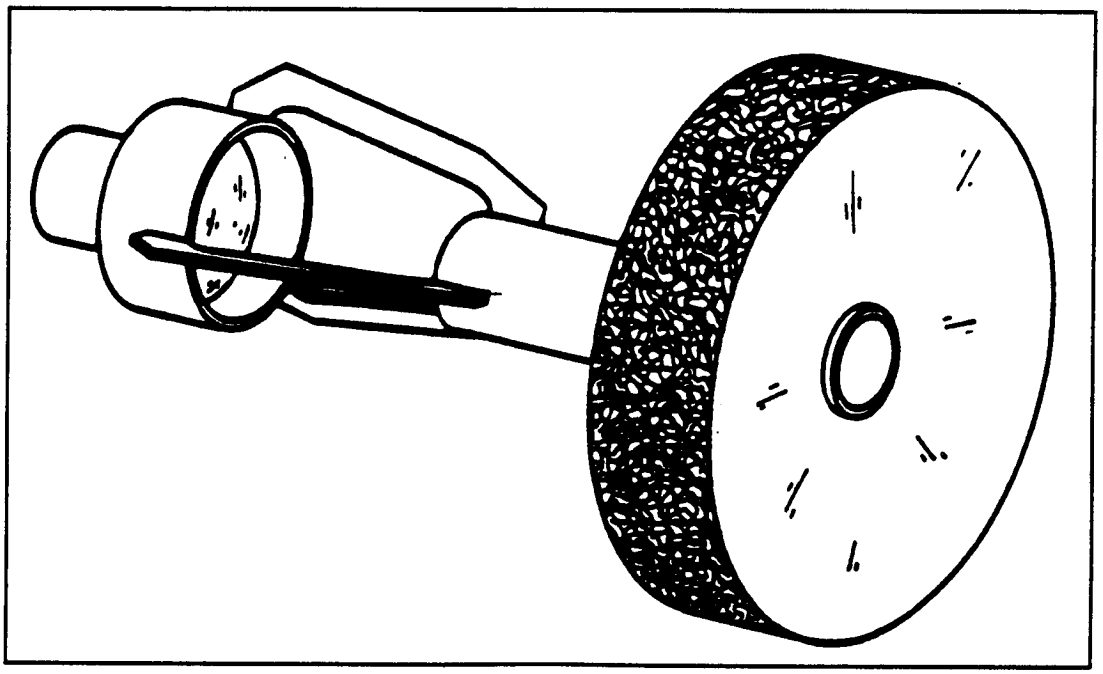

Figure 3.4.3-11 A Meinel Telescope Concept (see Ref 5)

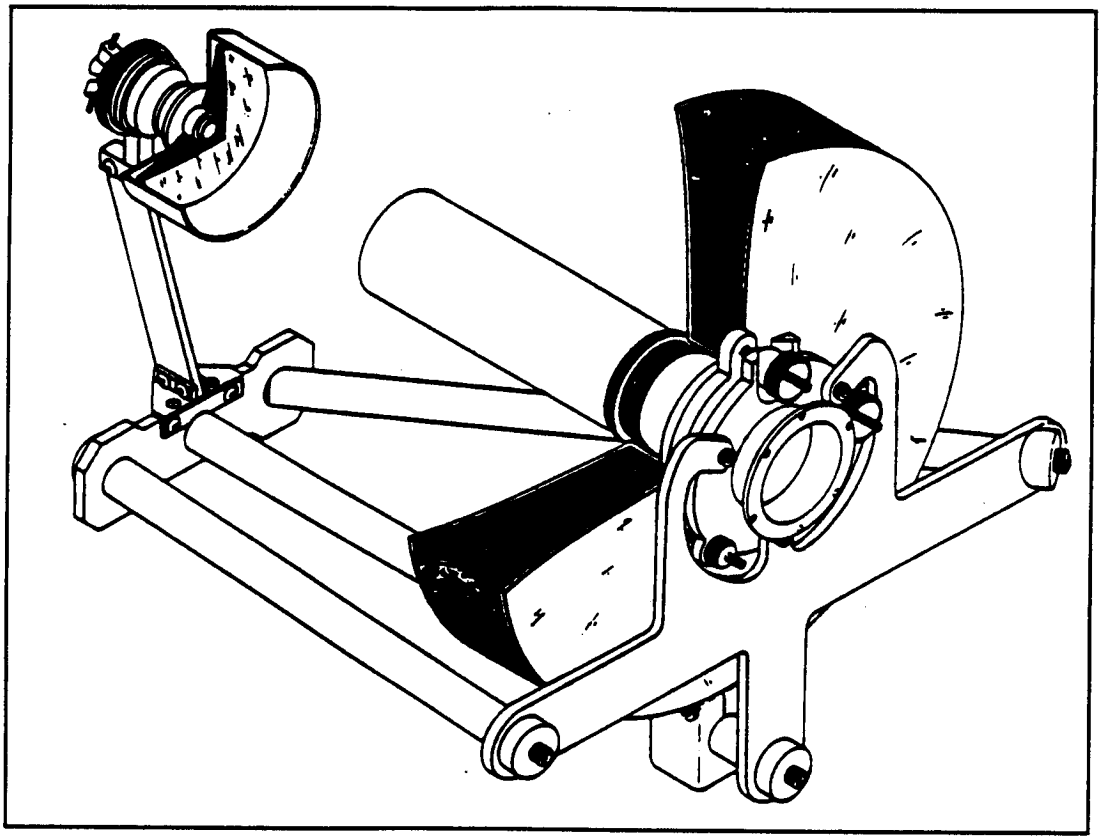

Figure 3.4.3-12 A Dall Configuration

encounters the same disadvantages of the Meinel configuration in section 3.4.3.6.

3.4.3.8 Lightweight Mirrors

The design of a space-qualified mirror must address a number of requirements:

- optical performance:
  - ability to achieve a high performance optical finish on the mirror surface
  - the ability to maintain optical shape under thermal and structural loads
- structural performance:
  - high specific stiffness
  - high natural frequency
  - high dynamic response
  - fracture toughness
- thermal performance:
  - good conductivity to equalize temperatures
  - low distortion from bulk temperature changes
- aging performance:
  - no changes in the above performances with time

To meet these requirements, beryllium is often used for space qualified applications because of its extremely good strength/mass ratio. The mass can be further reduced by around 50% by machining out the back of the mirror. Figure 3.4.3-13 shows an example of such a mirror.

To reduce the mass of very large mirrors (0.25 m and larger), one of the technologies being revisited for space-based telescopes is the use of metal-matrix composites such as SXA (aluminum/silicon carbide). These fabrication techniques allow the mass of the primary mirror to be reduced by nearly 80% of the equivalent solid mirrors.

As described in References 69 and 70, aluminum foam cores, produced by Energy Research and Generation Inc. have been demonstrated in the field. Because of problems associated with machining of aluminum facesheets and nickel plating of the aluminum surface, new development work is looking at the use of nickel foams and hybrid aluminum/silicon carbide compos-

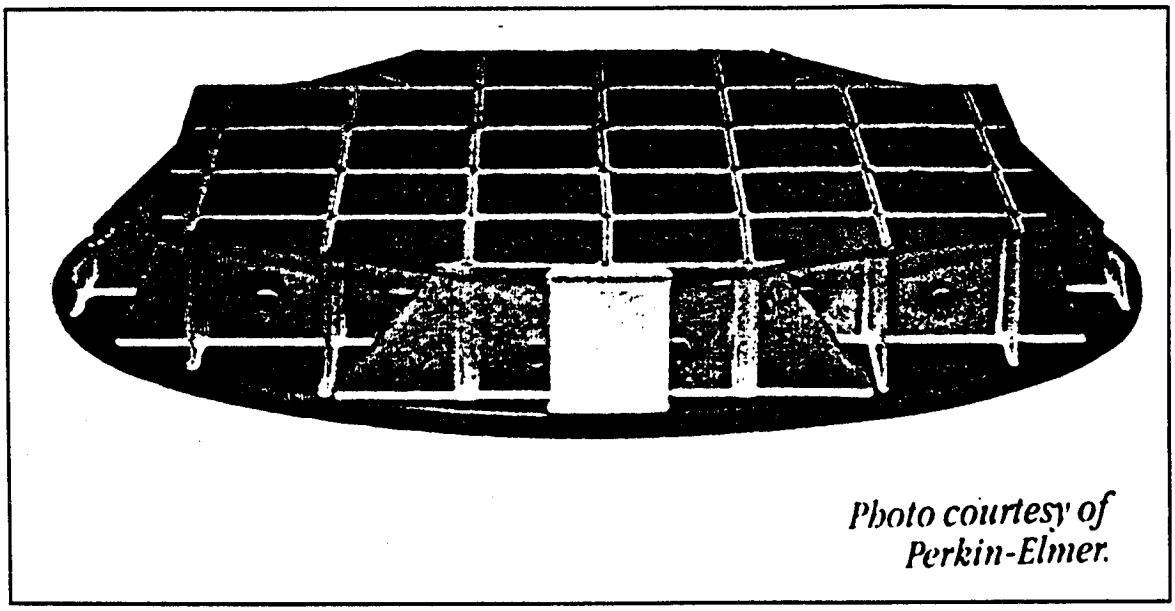

Figure 3.4.3-13 A Mass Reduced Mirror Design

ites. Figure 3.4.3-14 shows an example of a mirror shape fabricated using SXA at the Optical Sciences Center of the University of Arizona.

Using data from Reference 70, Figure 3.4.3-15 shows the expected masses of typical solid berylium, mass reduced berylium, and advanced composite mirrors as a function of diameter. Although the mass savings of the new composite technologies is readily apparent, they do trade-off some structural performance compared to standard berylium. Table 3.4.3-4 shows a comparison of the structural properties of these technologies. Costs were not available for comparison.

3.4.3.9 Combined Optics vs. Separate Receive, Transmit Optics

As discussed in section 3.4.1, an optical ISL system has 4 separate telescope requirements associated with the beacon transmitter, beacon receiver, communications transmitter, and communications receiver. An immediate decision arises as to whether 4 physically separate telescopes are desired or whether some, or all, of these telescope functions should be combined into a single unit. The impact of this trade-off on the design is very significant. To produce, qualify, and integrate 4 physically separate telescopes, for example, incurs a large cost and mass but allows the 4 separate subsystems to be prepared independently making the product development easier. Combining all the requirements into a single telescope means trading-off some design optimization to come up with a common design, but the mass savings of having only one telescope are substantial.

The following are some of the advantages of each approach:

Advantages of Separate Telescopes

- Each optical path can be independently optimized without compromises for other optical paths. Such compromises include fields of view, optical transmission bandpasses, isolation of transmit and receive beams, etc...
- Each telescope function can be handled as a separate development allowing simplified technical and project development interfaces. Separate telescopes can be developed, tested, and qualified independently.

Table 3.4.3-4 Structural Properties of a Number of Mirror Materials (see Ref 69)

Material	Specific Stiffness	Fundamental Frequency	Dynamic Response	Fracture Toughness
	(E/ρ) (m) $\times 10^3$	$(E/\rho^3)^{1/2}$ $(N\text{-}m^{7/2}/_1)^{-1}$ $\times 10^{-3}$	$(\rho/MYS)^2(\rho E)^{1/2}$ (kg/m^7) $\times 10^{-3}$	K_{IC} $(MPa\text{-}m^{1/2})$
AL/SIC 30 v/o SIC -2024 (SXA•)	4.1	70.9	11.4	59 (Wisker Reinforced)
AL 6061-T6	2.6	60.6	23.8	41
Be I-70A	16.8	225	281	9
Sic	10.6	115	1500	(18) Weibull Modulus
Zerodur	3.6	77.2	971	(14) Weibull Modulus

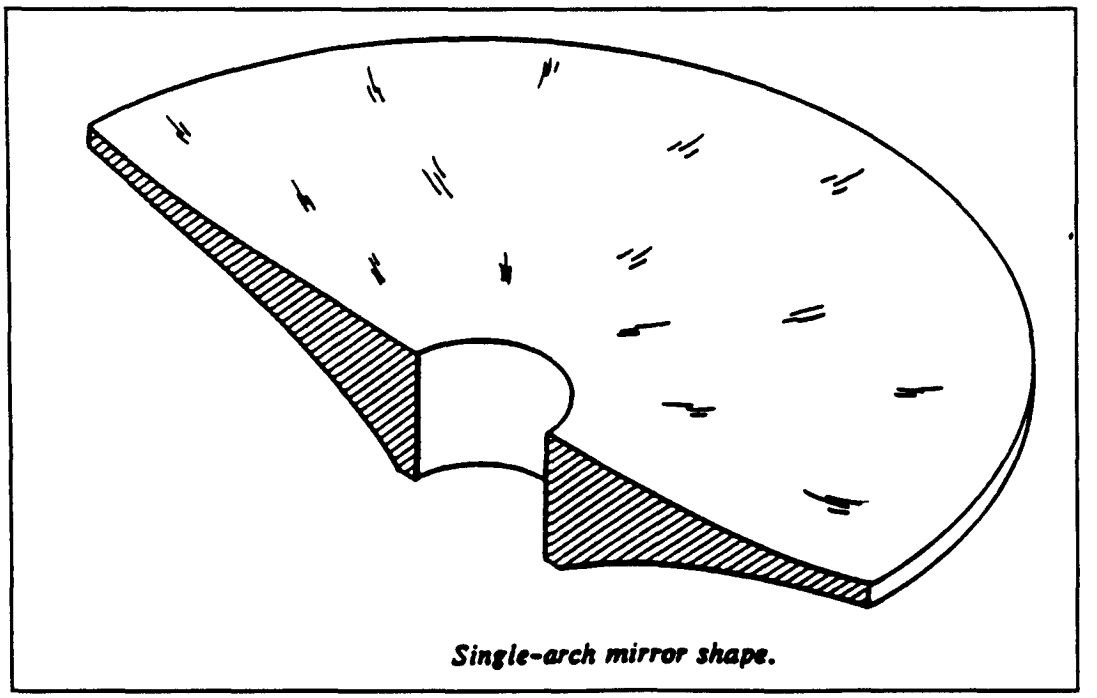

Single-arch mirror shape.

Figure 3.4.3-14 A Successfully Fabricated Mirror Using SXA Metal Composite Foam

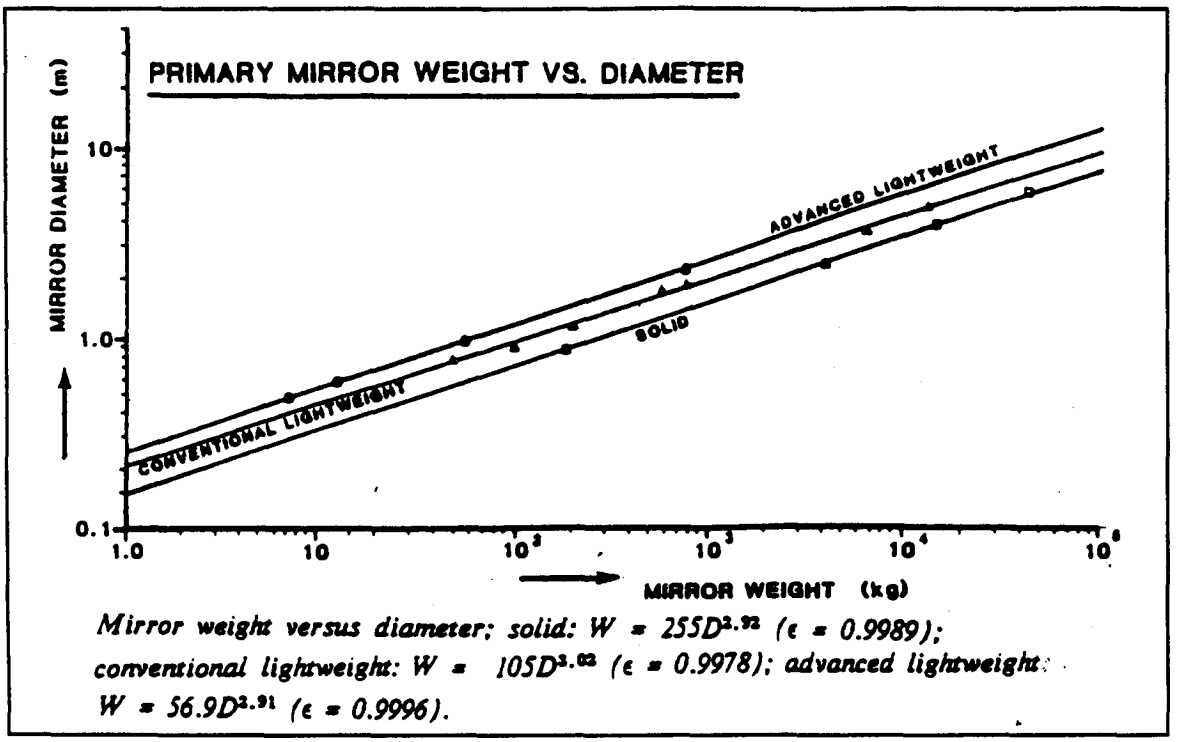

Mirror weight versus diameter; solid: $W = 255D^{2.92}$ ($\epsilon = 0.9989$); conventional lightweight: $W = 105D^{3.03}$ ($\epsilon = 0.9978$); advanced lightweight: $W = 56.9D^{2.91}$ ($\epsilon = 0.9996$).

Figure 3.4.3-15 A Technology Comparison of Primary Mirror Mass vs. Diameter

Advantages of Combined Telescopes

- Large mass savings can be achieved by eliminating additional telescope hardware.
- The reduced number of telescopes will reduce the cost of the system fabrications, testing, and qualification.
- The optical network can be compacted into a much smaller, integrated volume.
- The communications transmit and receive beams are referenced through a single telescope. relative misalignment of the two beams is therefore determined by the integrity of a compact optical network rather than a much larger structure supporting a number of telescopes.
- The Coudé configuration can be employed, reducing the system mass significantly.

First, consider whether the communications transmit and receive beams should be passed through a combined telescope. There are obvious reasons to combine them:

- both generally require a large aperture (typically 250 mm)
- both require identical fields of view (typically 300 μrad)
- because the pointing of the transmit beam is determined from the receive beam, it is safer to use as many common optics as possible so that any change in alignment of one path will also occur to the other. The accuracies required for both beams are extremely tight (typically $\pm 1\,\mu$rad).
- since both beams require fine pointing, a combined telescope allows a single fine pointing assembly to do both functions.

The major drawback of combining the transmit and receive beams is the need to isolate the receiver detectors from any radiation from the transmitter caused by internal reflections or insufficient beam to beam isolation in the common optical components. The power of the transmit beam is sufficient to completely interfere with the incoming signal, and in the worst case might actually destroy the receiver detector. Using different wavelengths or polarizations for the incoming and outgoing beams can allow beamsplitters/combiners to be used to separate or combine them. The additional mass and reduced optical transmissivity of these additional elements is small enough to justify using them, instead of a whole additional separate telescope.

Most current optical ISL concepts employ a combined transmit/receive telescope.

Next, consider whether to include the beacon receiver in the communications optical network. Again, there are some good reasons to consider this:

- the beacon receiver also requires a large aperture to improve its sensitivity.
- keeping the beacon receiver in the communications optical network improves the reliability of maintaining the co-alignment of the incoming beacon and communications beams. The beacon is used to reduce the pointing error to within the range of the fine pointing system, typically within 200 μrad. Any misalignment of the two systems may cause the fine pointing system to fail to acquire the incoming communications beam.

Incorporating the beacon receiver into the communications optics makes the latter more complicated since further isolation is required to keep the communications transmit beam out of the beacon receiver. However, the additional optics hardware and the slight reduction in transmissivity are again justified when compared to the alternative of providing an additional, separate, large aperture telescope.

Lastly, the beacon transmitter can be left separate since it does not have any requirement for the large aperture of the primary telescope. In fact the beacon beamwidth will need to be on the order of 500 μrad or more, and will only require a very small aperture size. Maintaining very tight alignment of the beacon optics with the communications optics is not critital, and if the

beacon requires any wide range (eg: $\pm 8700 \mu$rad) scanning, the additional steering mirror required could compromise the remaining optics network which must then cope with the additional field of view not otherwise needed by the fine pointing system.

Such a beacon unit can be employed as a very small optical unit attached to the side of the main telescope.

3.4.4 COmponents of the Optical Network

3.4.4.1 Eyepiece Optics

The ideal telescope objective (eg: the primary and secondary mirrors) collects incoming light on a flat focal plane at a distance, $f_{objective}$, as shown in Figure 3.4.4-1. The ideal eyepiece then picks-up the light leaving the focal plane and refocuses it into a collimated beam which then enters the rest of the optical network. The focal plane of the objective must therefore be coincident with the focal plane of the eyepiece. The angle at which the collimated beam leaves the eyepiece, $\theta_{eyepiece}$, is related to the angle of the beam incoming to the telescope, $\theta_{objective}$, and the magnification, M, of the combination:

$$\tan(\theta_{eyepiece}) = M tan(\theta_{objective}) \quad (18)$$

where:

$$M = \frac{f_{objective}}{f_{eyepiece}} \quad (19)$$

The magnification required for an optical ISL telescope is typically 20-50, and is driven in large part by the physical range of the fine steering mirrors and the required fields of view of the detectors.

The pupil diameter, p (ie: the diameter of the exit beam) is given by:

$$p = \frac{a}{M} \quad (20)$$

where:

a = diameter of the objective

Therefore, for a typical objective diameter of 300 mm, this produces an eyepiece output pupil diameter of 10 mm.

The aperture of the eyepiece, d, must be sufficient to collect the focal image over the desired telescope field of view, θ_{fov}.

$$d = p + 2(f_{objective} + f_{eyepiece}) tan(\theta_{fov}) \quad (21)$$

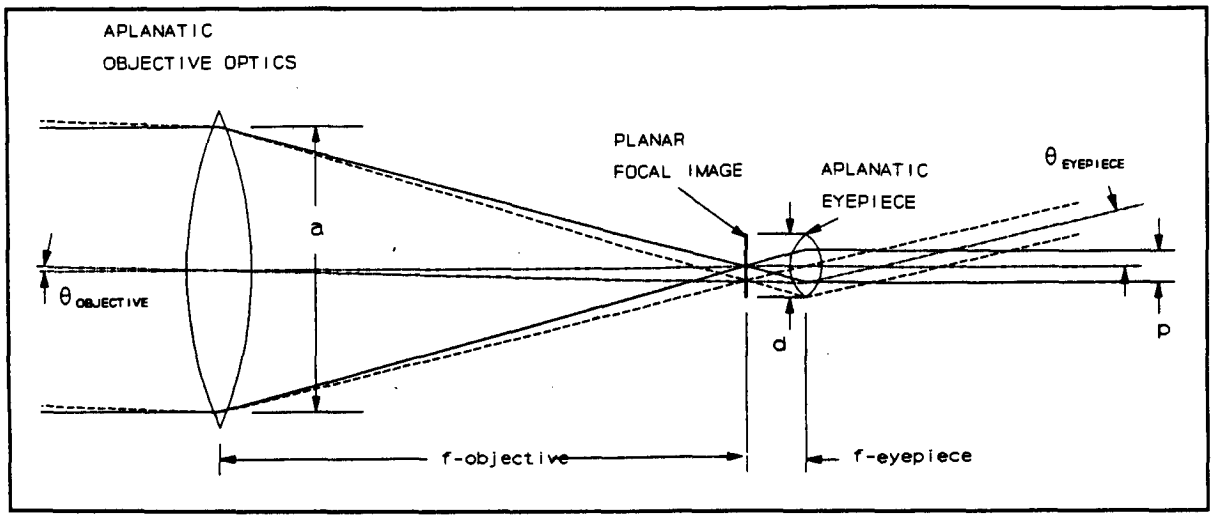

Figure 3.4.4-1 Ideal Focal Plane Between the Objective and Eyepiece

As an example, if $f_{telescope}$ = 1000 mm, $f_{eyepiece}$ = 33 mm, and θ_{fov} = 8700 μrad, this yields a required eyepiece aperture of around 20 mm greater than the pupil diameter.

In practice, a number of factors prevent the design from achieving the ideal image performance:

- non-planar image planes of the objective or eyepiece
- different focal image positions as a function of wavelength
- residual misalignment of the optical elements
- thermal distortions of the optical elements of their support structure
- limitations on the allowable mass (and hence complexity) of the opticaal system

Aplanatic optics produce a focal image which is planar as shown in Figure 3.4.4-1. However, the focal image a more simple objective or a simple eyepiece is usually curved as shown in Figure 3.4.4-2. Such optics only provide reasonable image focusing on-axis, and produce significant coma off-axis.

For the objective optics this situation is acceptable since the effective focal length of the objective is generally long (typically 1000-2000 mm), and its focal image is very nearly planar within the necessary field of view anyway. To improve the image plane, various alternatives for the objective (see section 3.4.3) can be investigated, most noteably the Ritchey-Chretien combination. A refractor-type objective also adds a complication since its focal image position varies with wavelength. If the focal length is long, then very small variations in wavelength can move the image plane well out of the focus for the eyepiece, which has a much smaller focal length.

The eyepiece will generally have a small focal length, $f_{eyepiece}$ of 40-100 mm which creates a non-planar image. Furthermore, since it will generally use lenses, the position of the focal image depends upon the light wavelength. To help correct these problems multi-element "apochromatic" optics can be employed as shown in the examples of Figure 3.4.4-3. Multi-element optics significantly complicate the design however, since they add mass to the system, and they require careful alignment and fixturing of the various elements. Good thermal control of the elements and their mounting structure is also required to prevent spacing or alignment variations and because the performance of the eyepiece may rely on different refractive properties of the elements which change with temperature. The detailed design exercise must trade-off these eyepiece complexities against the additional performance they provide.

A typical solution for an optical ISL system eyepiece might include at least 2 elements, and reach 5 elements or more, depending upon the detailed design exercise. Figure 3.4.4-4 shows an example of an optical ISL

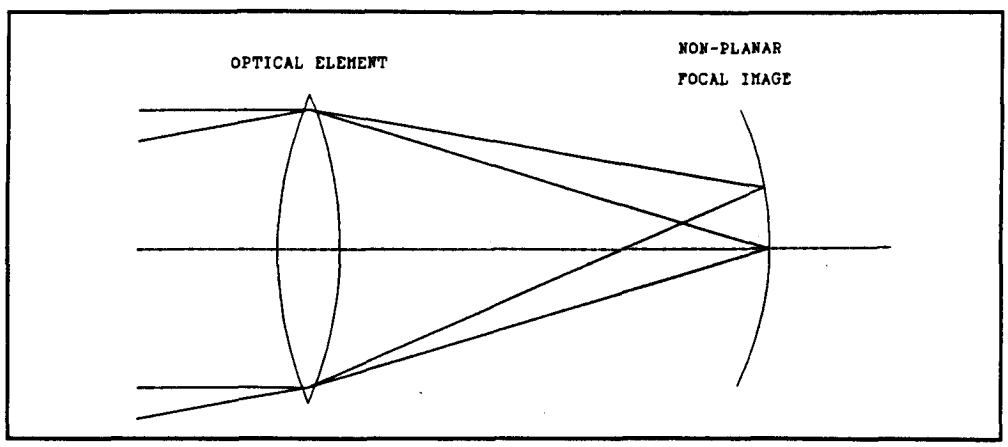

Figure 3.4.4-2 Non-Planar Focal Image of a Typical, Simple Optical Element

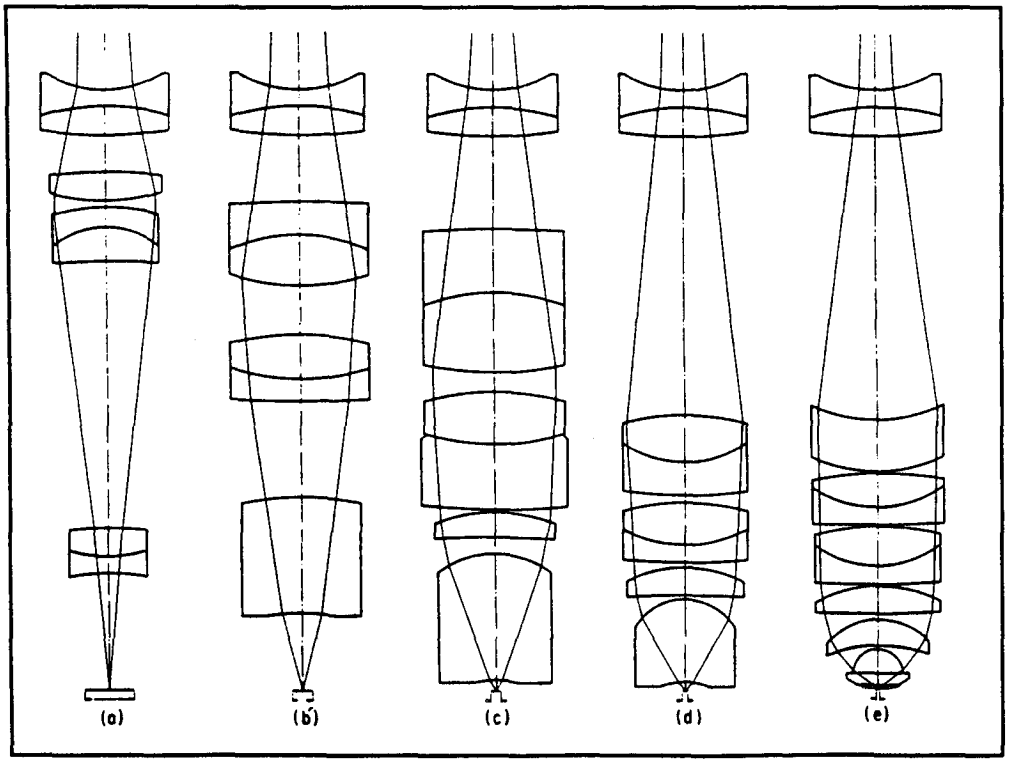

Figure 3.4.4-3 Examples of Apochromatic Multi-Element Eyepieces

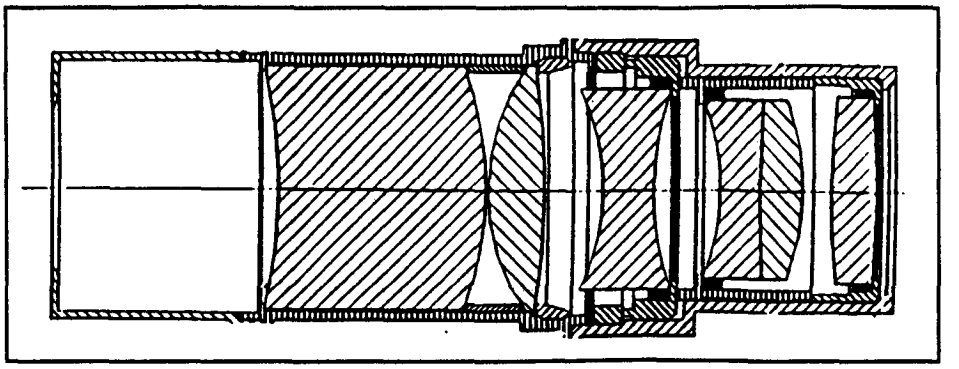

Figure 3.4.4-4 An Existing CAL Corporation Eyepiece Design

eyepiece design investigated by CAL Corporation for the SILEX project.

3.4.4.2 Detector Optics

There are various detectors in an optical ISL system:

- communications receiver
- acquisition detector
- fine pointing detector

The primary consideration for the detector optics is to establish a field of view corresponding to the detector surface image plane. As shown in Figure 3.4.4-5, the image deflection from centre, S, at the detector surface is related to the angular offset of the incoming image, $\theta_{objective}$, the telescope/eyepiece magnification, M (= $f_{objective}/f_{eyepiece}$, and the effective focal length of the detector optics, $f_{detector}$:

$$S = M\tan(\theta_{objective})f_{detector} \quad (22)$$

Typical CCD detectors have dimensions of around 5x5mm (for a 288x288 acquisition detector) to 0.3x0.3 mm (fine pointing detector). Using a telescope magnification of 30, for example, if the acquisition detector must have a field of view of $\pm 4000\ \mu$rad ($\theta_{objective}$ = 4000 μrad) then the focal length required for the detector optics is around 21 mm.

The aperture, d, of the detector optics must be sufficient to collect the entire incoming beamwidth at the desired maximum field of view angle, $\theta_{objective}$. This depends upon the distance from the eyepiece, L, as follows:

$$d = p + 2LM\tan(\theta_{objective}) - 2(f_{objective} + f_{eyepiece}) \quad (23)$$
$$\tan(\theta_{objective})$$

where:

p = pupil diameter from the eyepiece (see section 3.4.4.1).

Like the eyepiece, the detector optics must also be aplanatic (assuming the CCD surface is planar), and if more than one wavelength is to be detected then they must also be achromatic.

3.4.4.3 Laser Optics

The design of the optics for a semiconductor laser is complicated by the fact that the laser output comes from a narrow interface line in the lasing crystal as shown in Figure 3.4.4-6. The optics must collect the light from this line and collimate it into a circular beam with the Gaussian beamwidth selected to maximize the output of the telescope as discussed in section 3.4.2.3.

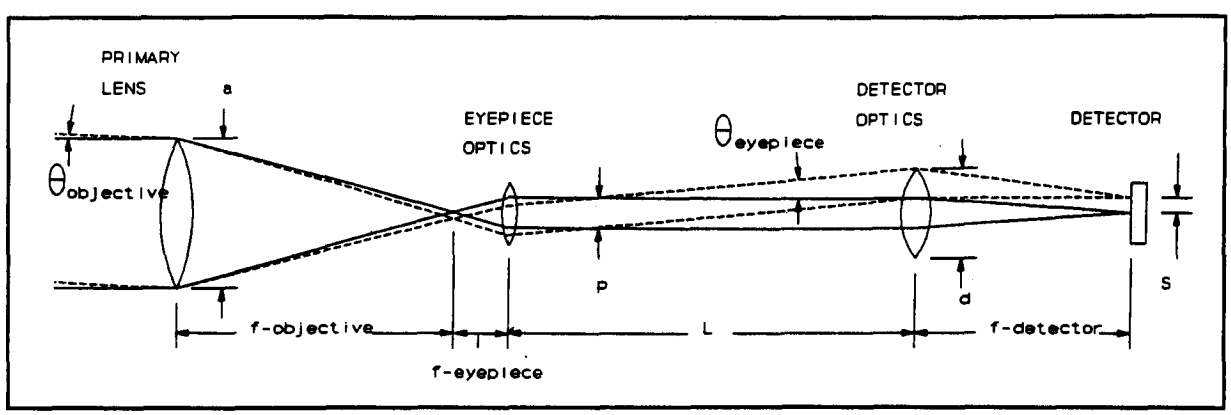

Figure 3.4.4-5 The Detector Image Plane

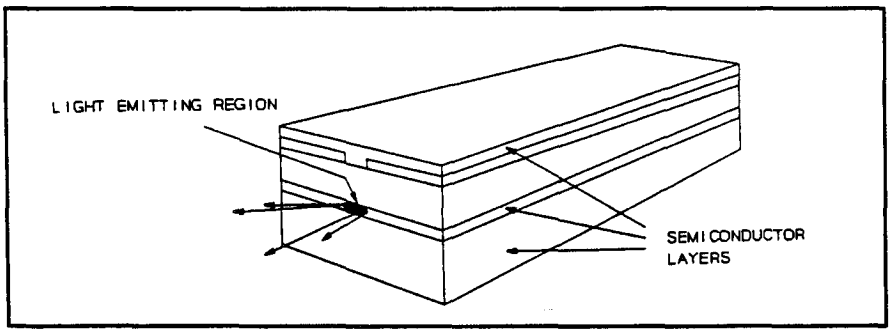

Figure 3.4.4-6 Output Face of a Typical Semiconductor Diode Laser

The divergence angle of the light leaving the laser is generally 20-30 degrees for semi-conductor lasers, and the corresponding astigmatic distance (ie: the length of the focal line) is 1-10 μm long.

To perform the function of circularizing and collimating the beam the optics must be designed to correct this astigmatism as shown in Figure 3.4.4-7. There are a variety of hardware methods of achieving this. A simple approach, shown in the preceding figure, is to place a cylindrical lens after the collimating optics. Figure 3.4.4-8 shows such an example of a commerically available astigmatism correction lens designed specifically for use with laser diodes.

Making the laser optics achromatic is not necessary since the laser will be producing a beam with a narrow spectral bandpass, typically around 2 nm wide.

3.4.4.4 Beam Splitters/Combiners

Beam splitters and combiners are needed in an Optical ISL system to:

- divide the incoming signal onto several detectors (eg: redundant communications detectors, redundant fine tracking detectors, etc.),
- combine the outputs of several sources into the optical path (eg: redundant or ganged communications lasers, beacon lasers, etc.),

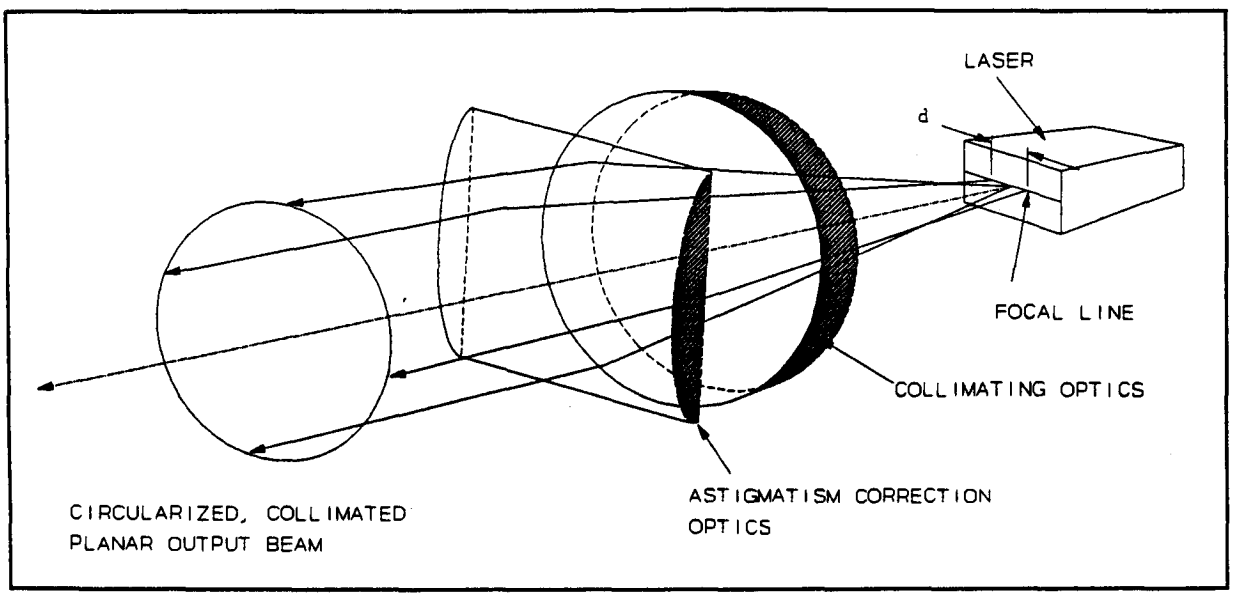

Figure 3.4.4-7 Circularizing and Collimating the Laser Beam

ASTIGMATISM CORRECTION OPTICS

Diode Lasers tend to exhibit considerable beam astigmatism. In the simpler, gain-guided devices, this can be tens of microns, whereas in the case of index guided lasers, the astigmatism is typically less than 5 microns.

Astigmatism often needs to be corrected if a small spot size or ultra-precise collimation are required. Two cylindrical lenses are offered for this purpose. The 4.1 meter focal length lens is designed to correct the 5 microns of astigmatism typical of index guided near-infrared lasers, and the 1.5 meter focal length lens is designed to correct the 45 microns of astigmatism found in gain-guided visible laser diodes. Laboratory tests show that by slight rotation about the optical axis these lenses can be adjusted to correct astigmatism in the 2-5micron and 40-45 micron ranges without introducing additional aberrations.

An astigmatic correction lens, if required, should be placed after the collimator lens.

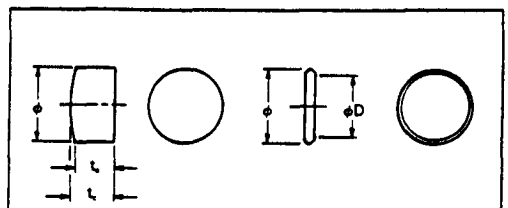

06 LCC 005 06 LCC 007

Melles Griot also offers a range of collimated diode laser heads. All of these emit a collimated beam of light which is also astigmatically corrected with excellent wavefront quality. Beam circularization optics and integral thermoelectric temperature control are offered as options (see Chapter 20, Diode Lasers, Optics and Accessories).

SPECIFICATIONS:
ASTIGMATISM CORRECTION CYLINDER LENSES

Diameter: 10 ± 0.05mm

Glass Type: BK7

Design Wavelength: 670–830nm

Wedge: 0.1mm

Coating:
Single Layer MgF_2 at 670nm (06 LCC 005)
Single Layer MgF_2 at 780nm (06 LCC 007)

Astigmatism Correction Lenses

ϕ (mm)	ϕD (clear aperture) (mm)	t_c (mm)	t_c (mm)	Focal Length (mm)	Diode Astigmatism Correction (microns)	PRODUCT NUMBER
10.0	9.0	5.1	5.0	1450 ± 50	40-45	06 LCC 005
10.0	8.0	2.0	2.0	4175 ± 100	2-5	06 LCC 007

Figure 3.4.4-8 A Commerically Available Astigmatism Correction Lens for Laser Diodes

- isolate the high power outgoing beam from entering the receiver optics.

Two types of beam splitter/combiner techniques can be employed:

a) dichroic splitters/combiners split or combine two beams of different wavelength,

b) polarizing splitters/combiners split or combine a single wavlength by separating orthogonal axes of the light.

Dichroic devices use specific combinations of optical interference filter coatings to selectively pass a desired wavelength while reflecting other wavelengths. The coatings can be put on open surfaces, but are often sandwiched between two flat plates to protect them and to help control coating thickness variations. Figure 3.4.4-9, taken from Reference 68, shows an exam-

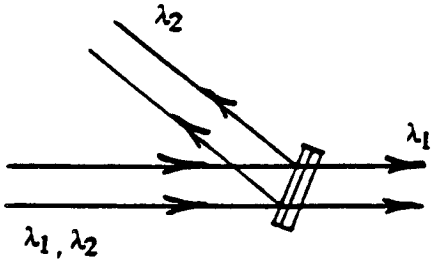

Dichroic combination/separation of two beams.

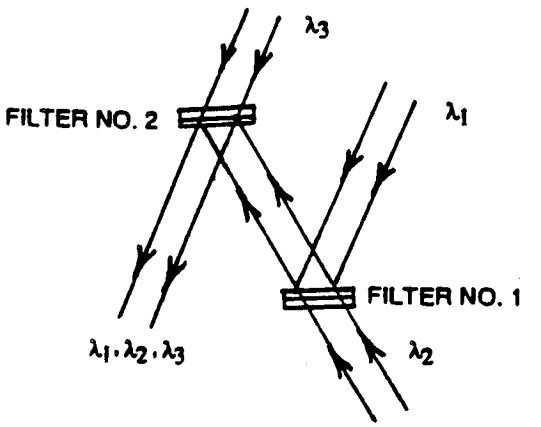

Dichroic combination/separation of three beams.

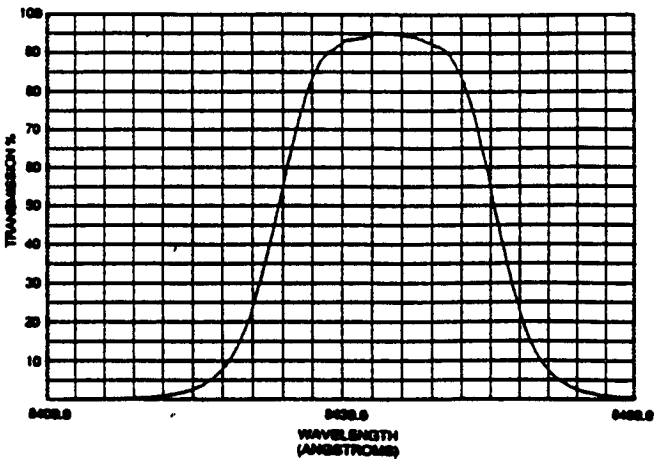

Spectral trace of one combining/separating filter.

Figure 3.4.4-9 Examples of Dichroic Beamsplitters/Combiners (see Reference 4)

ple of a beamsplitter and its bandpass for the transmitted light. Multiple filters can be used to separate or combine several wavelengths as is also shown.

The limitations of this type of splitter/combiner are:

- its transmissivity is usually limited to around 95% for each filter. Such devices must therefore be used sparingly in the system.
- to keep the transmissivity high, the minimum useful bandpass is around 2.5 to 3.0 nm. This limits the number of beams which can be separated or combined within a given spectral range.

Polarizing beamsplitters/combiners can be used to provide the signal separation between two beams, or communications channels, which have very similar wavelengths. If the wavelengths are too close together, for example, then a dichroic filter technique may not adequately separate them. The disadvantage of using polarizing devices is that a maximum of 50% of a cirularly polarized total beam power is generally available in either polarization.

A number of methods are available for fabricating such polarizing beamsplitters, but the most common is to employ polarization by reflection at the Brewster angle as shown in Figure 3.4.4-10. Light incident on a surface at the Brewster angle reflects around 15% of the light in the s-plane while the other 85% is transmitted. 100% of the p-plane is transmitted. By combining many layers of such surfaces together, more of the s-plane can be successively reflected until the s and p components of the light are almost completely separated. To achieve multiple layers, dielectric coatings can be laid onto a face. In a cube beamsplitter these are protected by being placed on the sloped, internal face between the two prism halves. An application for these types of beamsplitters in the SILEX program is described in Reference 69 in which transmissivities of 0.97 to 0.99 or better were achieved.

3.4.4.5 Steering Mirrors

Fine pointing steering mirrors are almost essential to any long-range Optical ISL system because they provide the capability to track the incoming beam with high accuracy (1-2 μrad) and high response rate (up to 1 kHz or more) over a range sufficient to cover the fine pointing range (200-300 μrad). These ranges and accuracies refer to values in front of the telescope.

As shown in Figure 3.4.4-11(a) and (b), the steering mirror compensates for angular movement of the incoming beam, $\theta_{eyepiece}$, by tilting an amount θ_{mirror}. The beam reflecting off the steering mirror is thereby kept parallel to the optical network axis so that it continues to be focused on the centre of the detector.

A few points must be considered when using such a steering mirror:

1) The steering mirror should not be used in any uncollimated beam path (eg: before the eye-

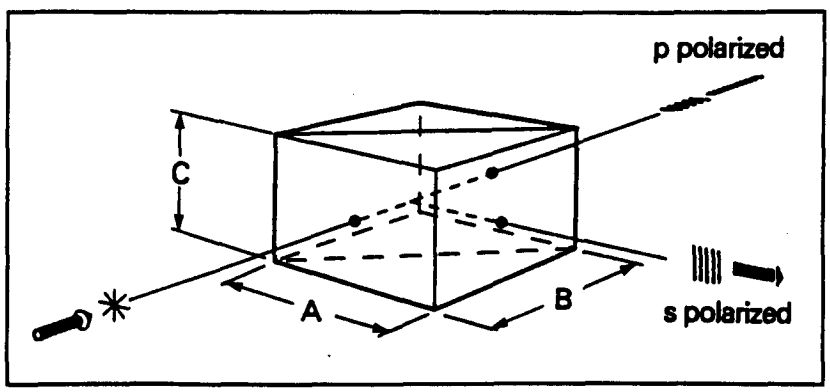

Figure 3.4.4-10 A Polarizing Cube Beamsplitter Employing Multilayer Dielectric Coatings

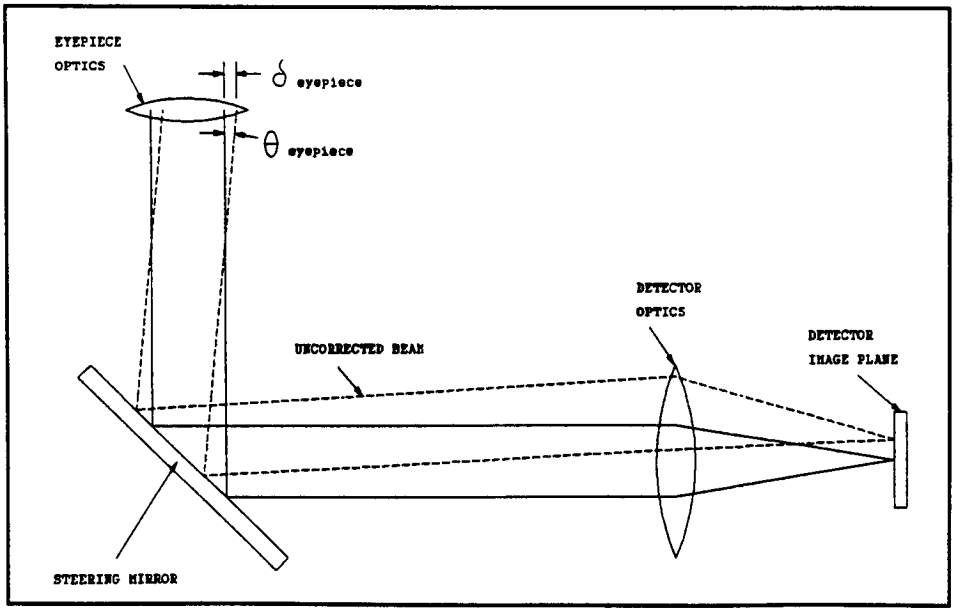

Figure 3.4.4-11(a) Uncorrected Beam Deflection with a Steering Mirror

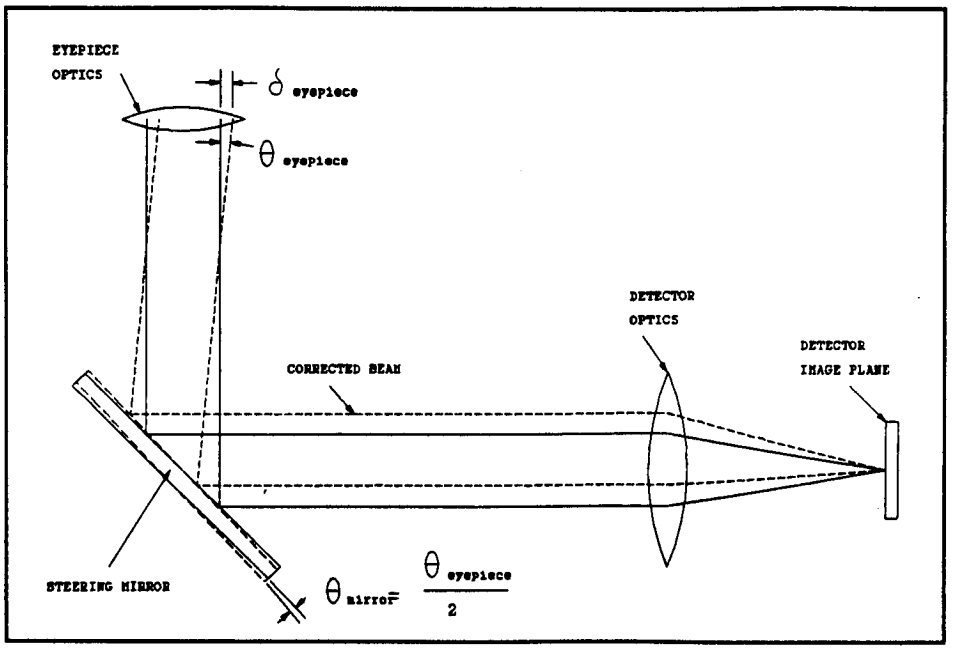

Figure 3.4.4-11(b) Correcting the Beam Deflection Using a Steering Mirror

piece) because the path length changes with the degree of angular correction required. If the mirror were placed before the eyepiece, for example, a small change in the path length could greatly de-focus the outgoing beam, reducing the beam width and intensity. The mirror itself may also exhibit some degree of translational movement of the mirror face which would cause a similar effect.

2) Since the mirror must provide a high response rate, it will be capable of exciting the structure on which it is mounted. Such a coupling may then excite the optical network, deteriorating the system performance. The steering mirror should therefore be mounted in a manner which decouples these dynamics from the optical structures.

3) Surface distortions of the mirror must stay within acceptable limits during operation. This may be a particularly stringent requirement at higher response frequencies.

3.4.4.6 Spectral Isolators to Isolate the Transmit and Receive Beams

As indicated in the previous sections, it is important to isolate the high power transmit beams from the receive beam since the receiver detectors may be capable of detecting both spectral bands. The performance of the communications link depends upon a dark background at the detector, and the sensitivity of the detector is such that it could completely lose the received signal if even a small percentage of the transmit beam enters it.

The SILEX project has developed a spectral isolator unit to perform this isolation while also providing the capability to intentionally feed a small portion of the transmit beam into the communication and fine tracking detectors as a means of calibrating them. Figure 3.4.4-12 shows a block diagram of such a unit.

In this example the transmit beam is reflected off filter F1 into the outgoing optical path with less than -60 dB of the signal passing through to the flip-flop mirror. Filter F1 is designed to pass the incoming (receive) signal which has a spectral range offset from the transmit beam of 40 nm. This receive beam is then split into two by the beamsplitter, with one beam going to the receivers and the other to the fine tracking detectors. The portion of the transmit beam which passes through filter F1 is normally reflected off the flip-flop mirror into a light trap, but during calibration the flip-flip mirror is moved out of this path so that the beam reflects off the corner cube reflector back onto F1. F1 then reflects this calibration beam back into the communications and fine tracking optics which use it for calibration.

The entire unit has a mass of less than 1 kg.

3.4.5 Other Optics Hardware Design Issues

3.4.5.1 Stray Light

Stray light in the optical system must be controlled to prevent it from illuminating the various detectors since most of them cannot independently distinguish between stray light and the receive signal. Stray light levels as little as 100 picoWatts incident on the communications detector, for example, can increase the bit error rate by an order of magnitude. The most significant sources of stray light are:

- celestial sources (the sun, moon, stars, etc...) which produce light incident on the sidewalls of the telescope tube or elsewhere in the optical system,
- the transmit beam or acquisition beam, which may have partial reflection off internal filters and other optical elements.

To a large extent, the second of the above sources is dealt with by a spectral isolator, described in section 3.4.4.6. To handle the first source, the following techniques can be considered:

A) Thermal Window

The use of a thermal window, described in section 3.4.5.3, reduces the level of solar and celestial radiation entering the optics by around 95%

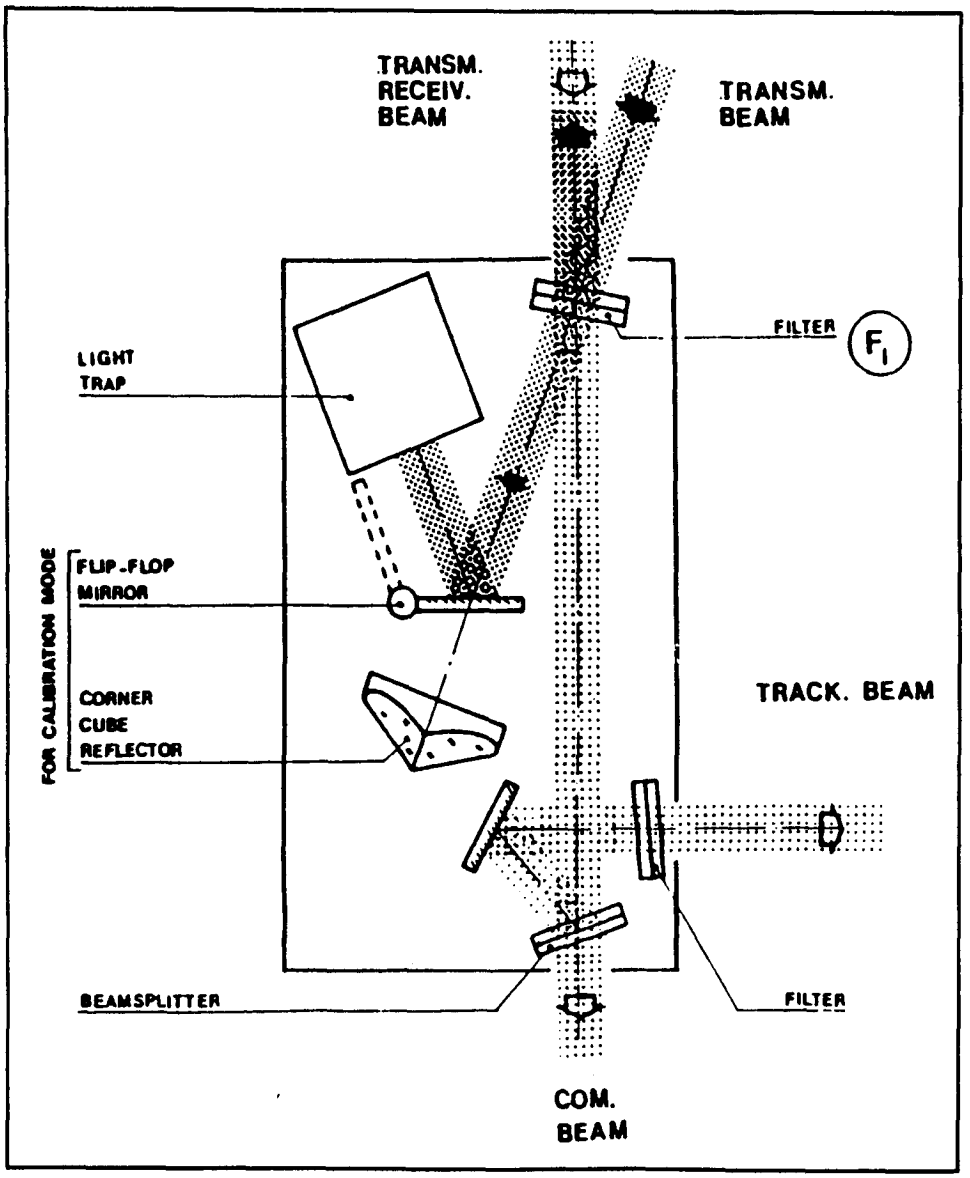

Figure 3.4.4-12 An Example of a SILEX Spectral Isolator Unit

while reducing the level of the narrow band receive signal by only 3-5%. This provides an immediate improvement in the ratio of signal to stray light.

B) Coudé Telescope

The Coudé telescope configuration provides a natural limitation to light paths entering the eyepiece due to the long, enclosed focal path leaving the secondary mirror. Because most of this path is enclosed and out of the primary optics tube, this design reduces the range of possible paths for external light to enter the optical path. The CAL Corporation Coudé design study, discussed in section 3.4.3.4, concluded that the Coudé design, combined with the thermal window, provides sufficient stray light control to handle direct sunlight to within 2 degrees of the optical axis.

C) Baffles in the Telescope

Baffling the telescope tube can be used to cause most light entering the telescope off-axis to be incident on a surface which does not provide forward reflection into the optical path. Figure 3.4.5-1 shows an example of such a technique applied to a telescope design.

D) Lyot Stop on the Eyepiece

A Lyot stop on the eyepiece limits the field of view of the system to within the inside of the telescope tube walls. This limits the number of walls or baffle edges which are visible to the internal optics system. Further knife-edge stops can be employed at other optics apertures in the system with the knife-edge facing out.

E) Antireflective Paints on Internal Surfaces

A diffuse black coating such as Chemglaze Z306 should be applied to all interior surfaces of the optics tubes and structure to reduce reflection of light from these surfaces.

F) High Quality Surface Finishes for Optical Elements

Surface microroughness of lenses and mirrors causes diffuse light scattering in the system, and this is of particular concern for those elements in the objective tube which are exposed to a wide field of view. Surface microroughness on the order of 20 Angstroms is typically achieved, although 10 Angstroms can be obtained with extreme care. Coatings on the lenses and mirror can help reduce diffuse reflections.

3.4.5.2 Radiation

For space applications, particularly in geosynchronous orbits, radiation becomes a concern. For the telescope and optics the primary sources are:

- energetic protons

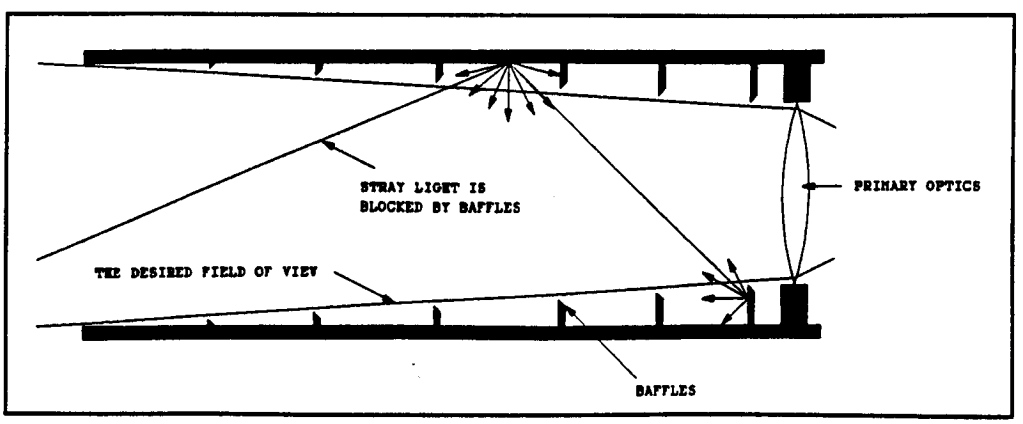

Figure 3.4.5-1 Using Baffles to Reduce Stray Light Entering the Optics

- ultraviolet light (UV)
- atomic oxygen

Depending upon the orbital altitude and the corresponding dosage expected, most glasses experience bulk transmission loss. Although this tends to vary with the type of glass, typical glasses may lose 5-10% transmissivity per year. A simple solution is to use radiation resistant glasses which tend to be affected more at the UV wavelengths than the infrared.

Absorbed doses of energetic protons are also known to cause bulk transmission damage in glass from 10^3 rads Si and greater. There are a number of factors affecting the degree of loss:

- absorbed dose
- wavelength at which the loss is measured
- type of glass and glass melt
- type of radiation
- dose rate
- glass temperature

The dose rate and temperature dependences stem primarily from the fact that thermal recovery occurs at a fairly constant, temperature dependent rate. Most testing is performed at much higher dose rates than those encountered in space in order to reach the desired total dose in a reasonable length of time. These tests are therefore worse than would occur at a lower dose rate for a longer length of time.

To protect the optics from energetic protons radiation resistant glasses can be used in place of the standard glass types. Table 3.4.5-1 lists some equivalents.

Pure fused silica such as Suprasil-W should be used for any front aperture lens or thermal window since this is extremely resistant to particle radiation effects. Silica is known to exhibit transmissivity losses when exposed to high doses of UV however, so a UV reflective coating is required on its exterior surface.

Table 3.4.5-1 Schott Radiation Resistant Equivalent Glasses

Standard Non-Rad Resistant Glass	Suggest Rad Resistant Equivalent Glass
SF6	SF6 G5
SK2	SK4 G13
SF55	SF4 G6
BaSF2	SF5 G10
LaF2	LaF13 G5
	LaF21 G7

Refractive index changes do not occur in fused silica, but may occur in glasses. This effect is on the order of 10^{-5} to 10^{-4} change in refractive index. While 10^{-5} change in index would not present a serious problem, a 10^{-4} change would. Although expensive, testing of the glasses can be performed to find those with the least change.

The optical coatings should also be chosen for radiation resistance. The following coatings are known to have good resistance to particle and UV radiation:

- magnesium fluoride (MgF_2)
- silicon dioxide (SiO_2)
- thorium fluoride (ThF_4)
- zinc sulfide (ZnS)
- zirconium oxide (ZrO_2)

Magnesium fluoride is also highly resistant to atomic oxygen effects, and should be considered for any front aperture lens or thermal window on the telescope.

3.4.5.3 Thermal Effects

Thermal effects on the optics show up principally in the following ways:

- distortion of optical elements (mirrors, lenses, etc...) affecting their individual optical characteristics,
- changes to spacing and alignment of the optical elements due to distortions in the support structure,

- stresses on optical elements due to differential expansion with their support structures,
- changes to refractive indices of lenses.

To reduce these effects some of the following methods can be used:

1) Thermal gradients within the system can be reduced by insulating the telescope and optics with MLI (multi-layer insulation). Metal-based mirror substrates also provide high thermal conductivity, providing uniform mirror temperatures.

2) To reduce structural deflections composite materials such as PEEK (poly ether ether ketone) reinforced with carbon fibres can be laid-up with almost zero thermal expansion along the optical axis. Such composites also have extremely high strength/mass ratios. Where optical elements are mounted the materials for the structure should be chosen, where possible, with a coefficient of thermal expansion matching that of the optical element.

3) The mirrors should be mounted near their centres, not by their edges as shown in Figure 3.4.5-2. This avoids stressing the mirrors due to differential expansion with the telescope housing.

Even employing these measures, CAL Corporation's previous studies of telescopes for Optical ISL applications have shown that, given a satellite mounting surface temperature of -20 to +50 deg C, a telescope protected only with MLI could have a corrector plate temperature varying between -115 and -65 deg C (non sun-facing and sun-facing) and an objective mirror temperature varying between -77 and +263 deg C. Such a wide swing of temperatures can cause system distortions sufficient to significantly reduce the telescope performance.

To reduce the temperature swing between sun-facing and non sun-facing, CAL Corporation has independently investigated a concept for a thermal control window to be mounted in front of the telescope aperture as shown in Figure 3.4.5-3. This thermal window reflects around 95% of the solar spectrum by sandwiching a number of specially design optical coatings between two plates. Figure 3.4.5-4 shows the solar spectrum and a possible spectral bandpass for such a window. Using this, the temperature range of the corrector plate above can be reduced to -174 to -147 deg C and the range for the primary mirror reduced to -98 to +49 deg C.

3.4.6 Two Telescope Concepts

To support the system level analysis in this study, two candidate telscope concepts suitable for a LEO-GEO intersatellite link were prepared. Two sizes were established for the telescope, 200 mm, and 136 mm aperture diameters, where the larger diameter is intended for higher (100 Mbps) bit rates, and the smaller diamter for lower (1 Mbps) bit rates. These concepts were prepared only to establish an overview of the requirements of the system and are subject to further optimization and a more thorough concept analysis in later phases.

A Coudé configuration with Maksutov-Cassegrain optics was chosen for the larger, 200 mm aperture requirement. This is shown in Figures 3.4.6-1 and 3.4.6-2. This combination was chosen for the following reasons:

- The Maksutov-Cassegrain optics design has been previously examined in detail by CAL Corp. and shown to meet the requirements of the SILEX program. Because of the heavy Maksutov corrector plate however, it would be recommended that a standard Cassegrain approach be further investigated against the final system field of view required.
- The spherical mirror and corrector plate of the Maksutov-Cassegrain design are less expensive to manufacture than comparably sized aspherics. A high surface finish can be fabricated and measured also, typically to much better than $\lambda/30$.
- The enclosed nature of the Maksutov-Cassegrain helps seal the optics and allows a

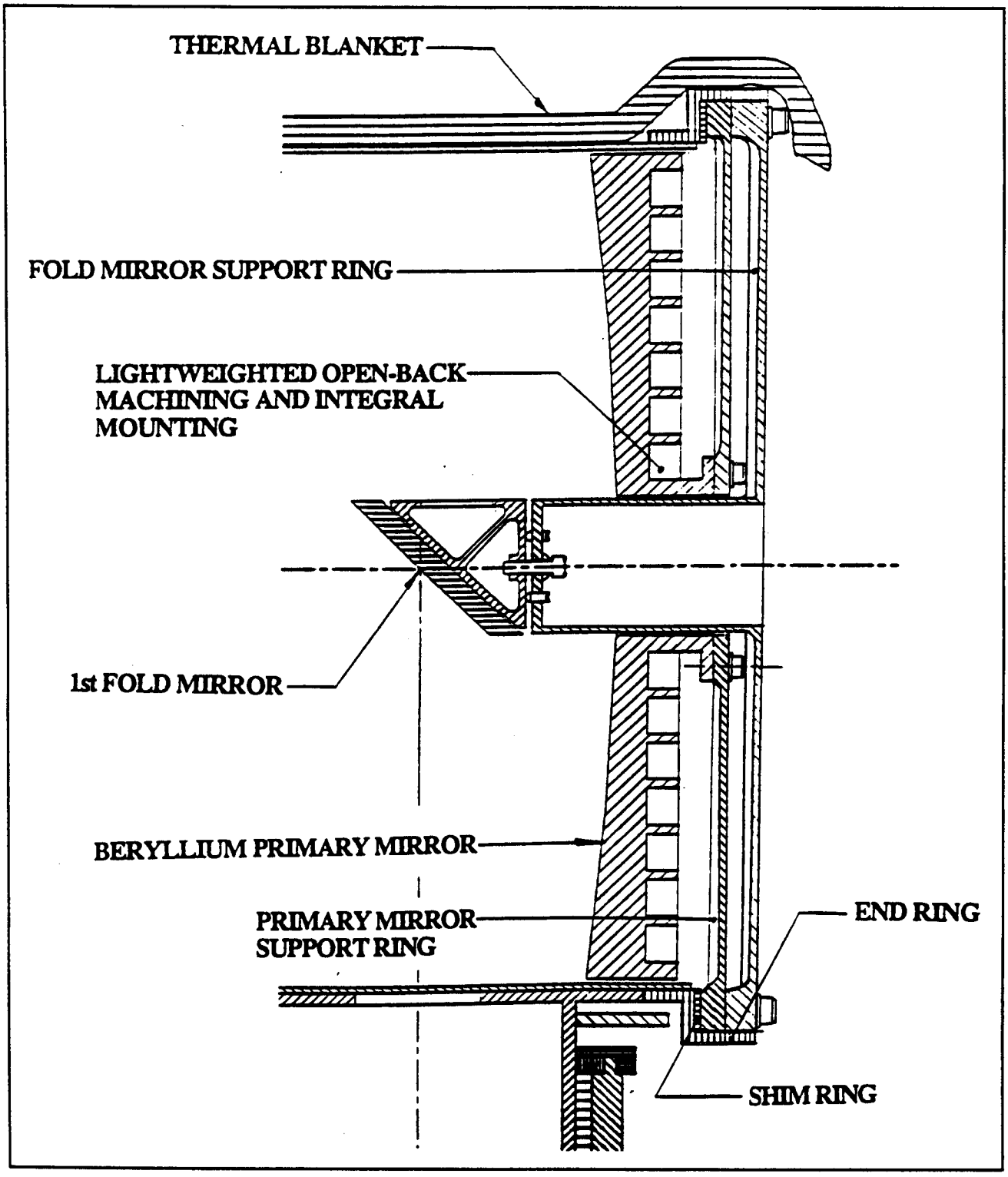

Figure 3.4.5-2 A Primary Mirror Mounting Concept to Reduce Mirror Distortions

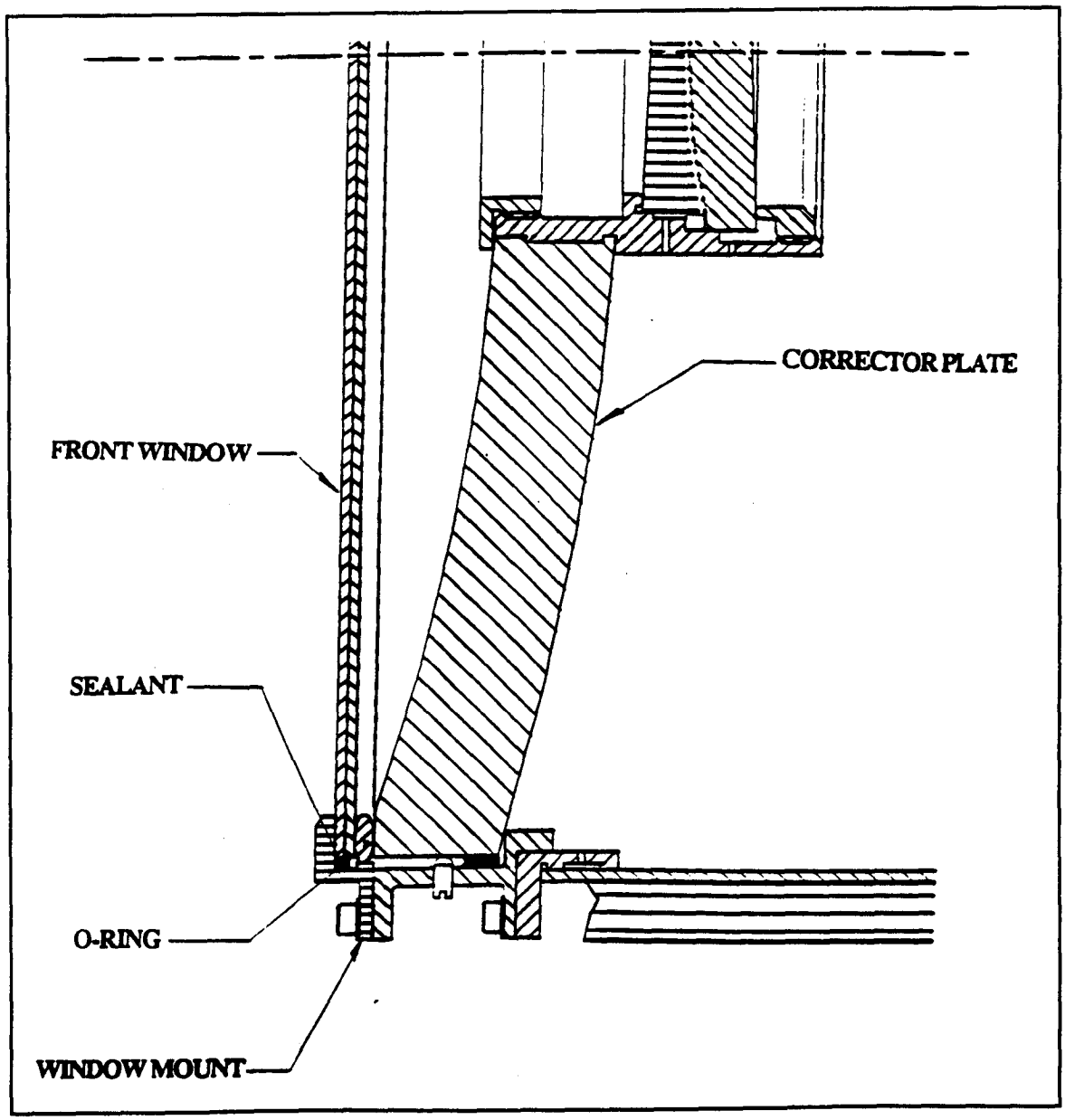

Figure 3.4.5-3 A Previously Developed Thermal Window Concept

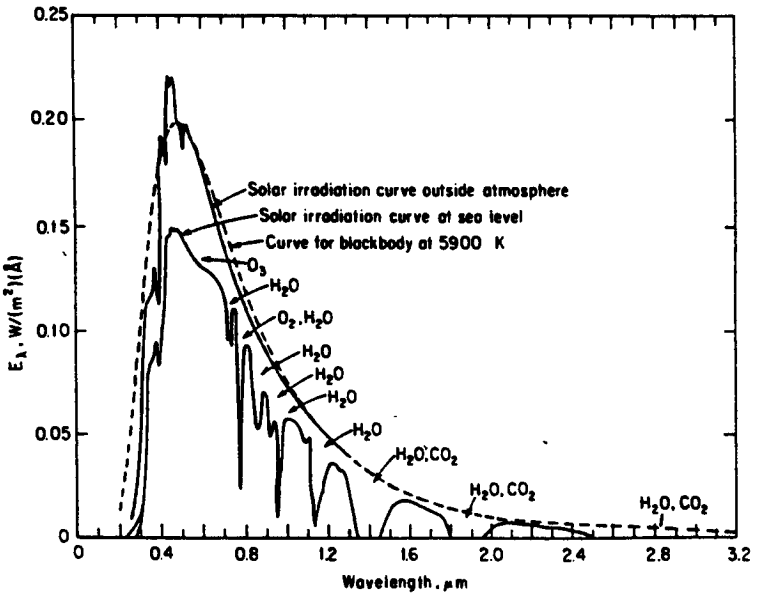

Spectral distribution curves related to the sun; shaded areas indicate absorption at sea level due to the atmospheric constituents shown. [*Valley* (1965).]

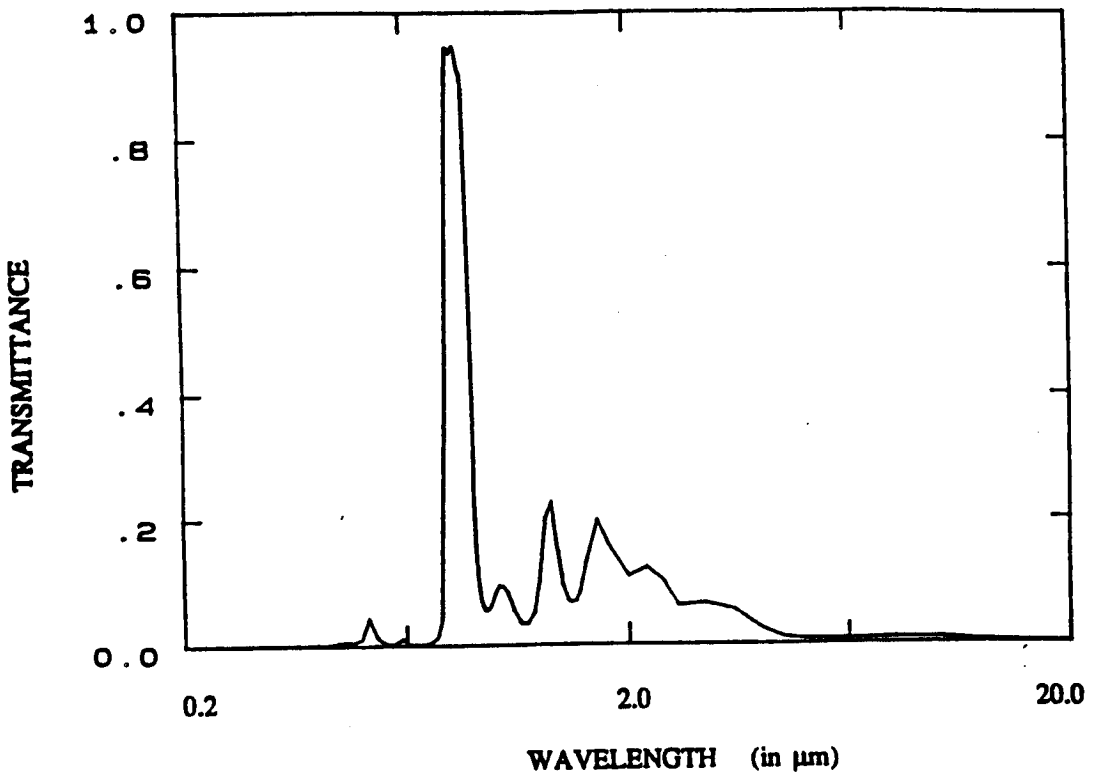

Figure 3.4.5-4 The Solar Spectrum and a Possible Spectral Bandpass for the Thermal Window

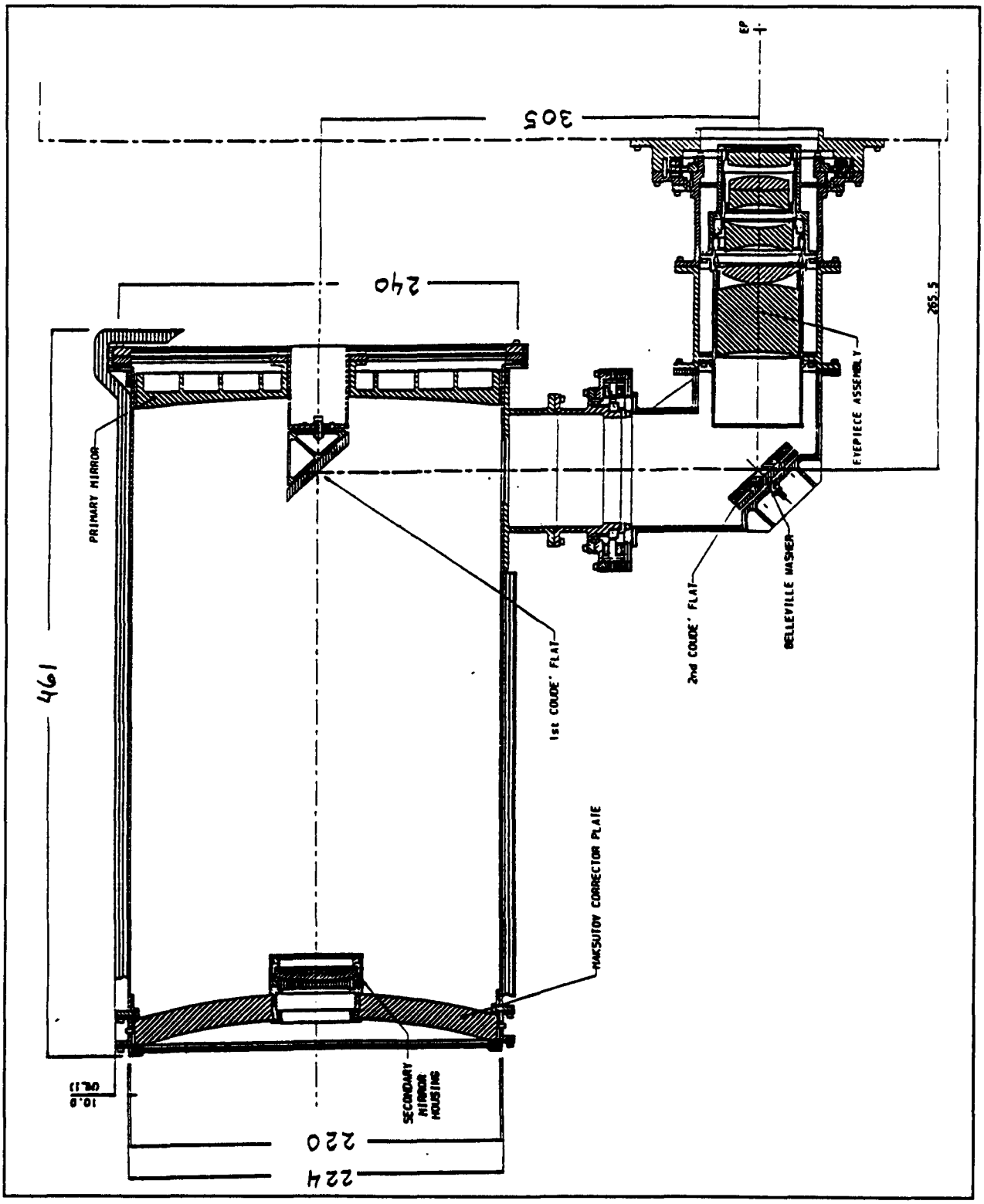

Figure 3.4.6-1 200 mm Aperture Coud) Telescope Concept

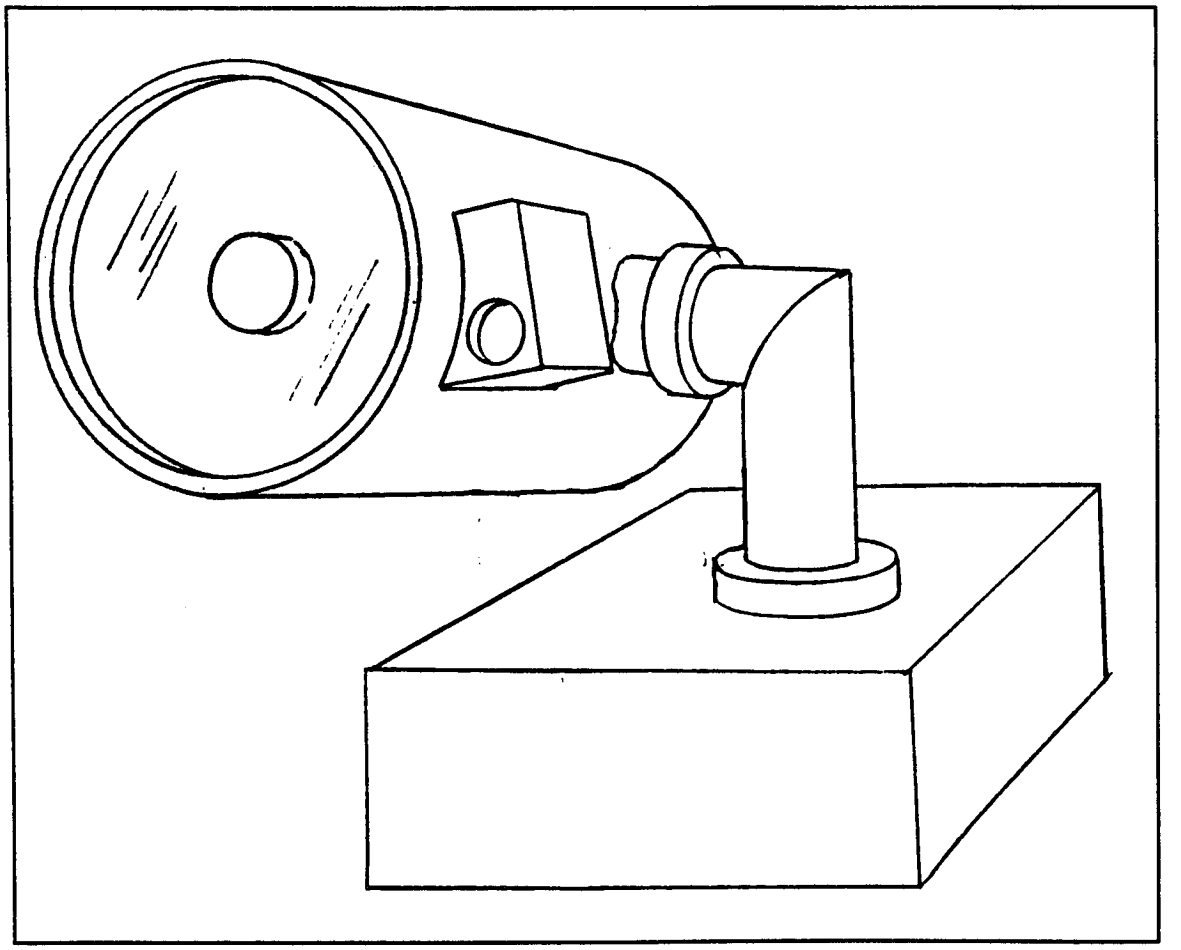

Figure 3.4.6-2 A Possible Layout of a 200 mm Coudé OISL Telescope

thermal control window and MLI to be employed to control thermal effects.

- The Coudé configuration saves about 20 kg off the comparable fully gimballed design, such as that used by SILEX. The 200 mm aperture is still large enough that the periscope approach is not mass efficient.
- The Coudé configuration also allows the optical network to be hard-mounted within the spacecraft decks, reducing thermal and mechanical interfacing problems.
- The Coudé configuration provides a great deal of natural stray-light reduction.

Some of the key optical specifications for the telescope and eyepiece would typically be as follows:

objective mirror diameter:	210 mm
diameter of secondary mirror:	50 mm
clear field of view:	$\pm 8700\,\mu$rad
surface errors:	$< \lambda/30$ RMS
effective focal length of primary/secondary:	1000 mm
focal length of eyepiece:	33 mm
magnification:	30:1
effective pupil diameter:	8.3 mm
aperture (diameter) of eyepiece:	> 28 mm

A preliminary mass estimate for this telescope is 12.0 kg as broken out in Table 3.4.6-1.

The second, 136 mm, telescope concept was based upon a periscope configuration with standard Cassegrain optics. In this case the smaller 136 mm

Table 3.4.6-1 Mass of 200 mm Coudé Telescope Concept

Maksutov Corrector Plate:	1.60 kg
Objective Mirror + Bracket:	0.75
Secondary Mirror + Structure:	0.45
Thermal Window + Housing:	0.60
Telescope Tube (PEEK) + MLI:	1.00
1st Coudé Flat + Structure:	0.20
2nd Coudé Flat + Structure:	0.80
Coudé Tube Sections:	2.10
2 Motors + Bearings:	3.50
Eyepiece Optics + Structure:	1.00
TOTAL:	12.0 kg

aperture is small enough to make the periscope approach mass effective. Furthermore, the smaller optics elements make aspherics reasonably cost effective and can be fabricated to good (λ/30) finishes.

Some of the key optical specifications for the 136 mm telescope and eyepiece would typically be as follows:

objective mirror diameter:	145 mm
diameter of secondary mirror:	36 mm
clear field of view:	$\pm$8700 μrad
surface errors:	< λ/30 RMS
effective focal length of primary/secondary:	500 mm
focal length of eyepiece:	16.7 mm
magnification:	30:1
effective pupil diameter:	4.2 mm
aperture (diameter) of eyepiece:	> 15 mm

This concept, shown in Figures 3.4.6-3 and 3.4.6-4, has an estimated mass of 8.0 kg, broken out as shown in Table 3.4.6-2.

The beacon transmitter, in each concept, has been left as a separate unit mounted to the side of the telescope to avoid complicating the communications optical path. This is possible since the beacon will likely have a much larger beamwidth requirement than the communications beam and therefore does not require a large aperture telescope. The mass of the beascon has not been included here.

Table 3.4.6-1 Mass of 136 mm Periscope Telescope Concept

Objective Mirror + Bracket:	0.25 kg
Secondary Mirror + Structure:	0.20
Thermal Window + Housing:	0.20
Telescope Tube (PEEK) + MLI:	0.50
Azimuth Flat + Structure:	0.60
Elevation Flat + Structure:	0.50
2 Motors + Bearings:	5.00
Eyepiece Optics + Structure:	0.75
TOTAL:	8.0 kg

3.5 Technology drivers

The main technology drivers can be identified as follows:

1) Detector sensitivity
2) Laser power
3) Telescope diameter
4) Acquisition and tracking
5) Heterodyne frequency tracking
6) Wavefront alignment
7) External modulators

The relative impact of these drivers is somewhat for different wavelengths as defined by the laser type.

3.5.1 Detector Sensitivity

All of the lasers being studied are in a wavelength region where the system is dominated by shot noise (the noise caused by the statistical variation of the arrival rate of the signal photons) rather than thermal noise. The receiver sensitivity is therefore evaluated in terms of the number of photons per bit required to receive the signal stream with the specified bit error rate.

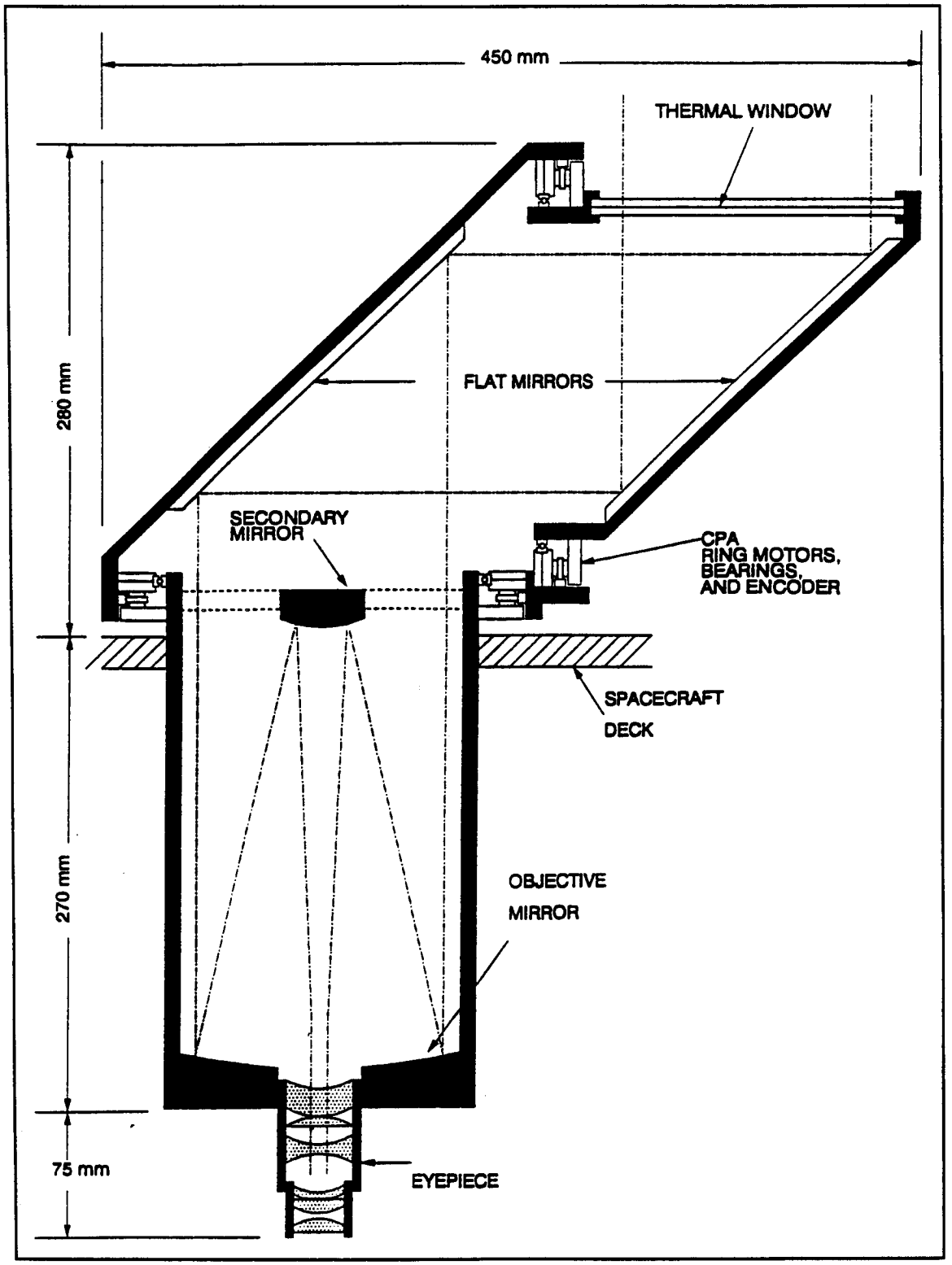

Figure 3.4.6-3 136 mm Aperture Periscope Telescope Concept

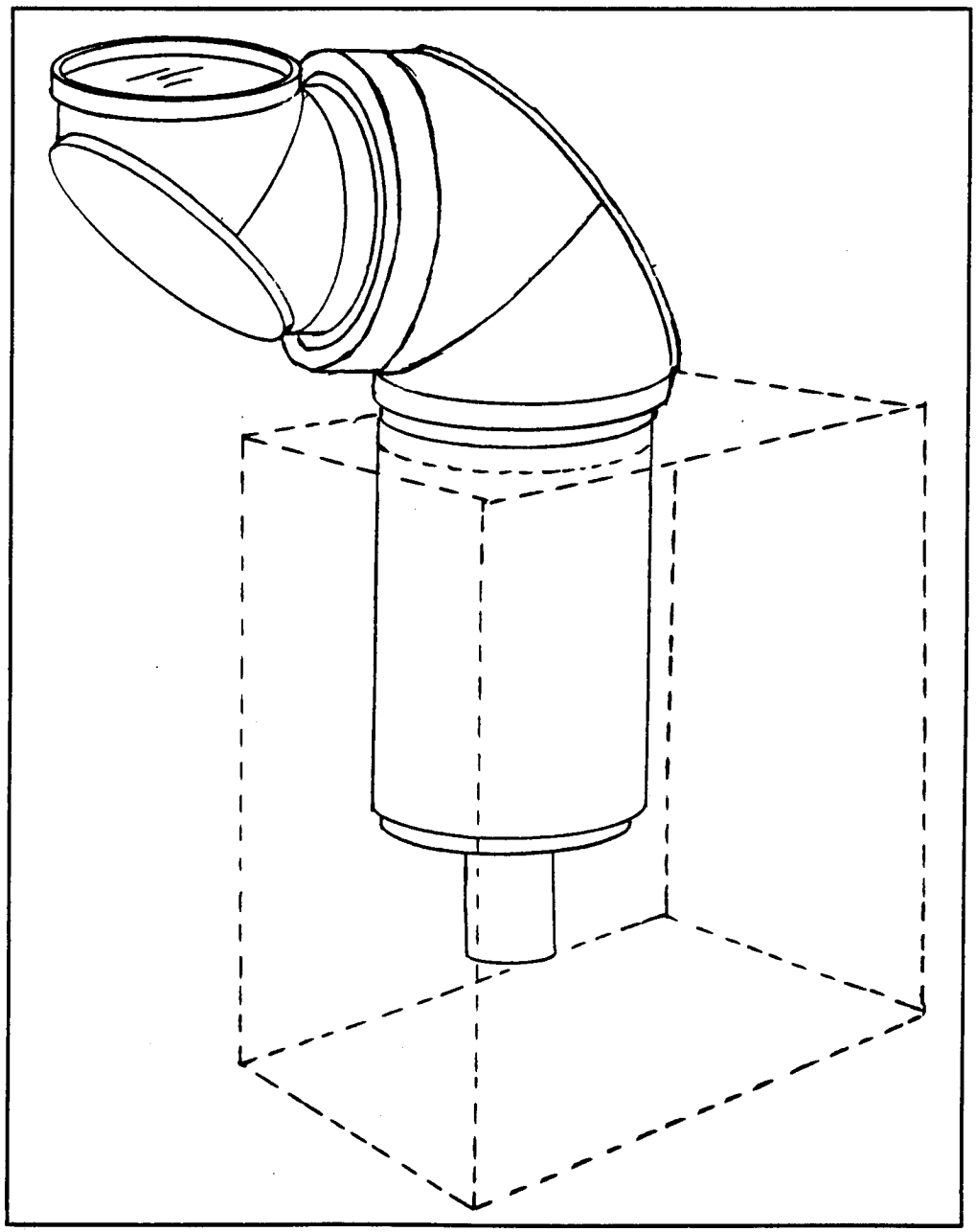

Figure 3.4.6-4 A Possible Layout of a 136 mm Periscope OISL Telescope

The theoretical number of photons per bit varies between 10 and 40 depending upon the type of modulation used, but in practice the theoretical numbers are greatly exceeded. The departure from theoretical depends upon the bit rate, the wavelength and upon whether the detection process is heterodyne or direct detection.

The present state of detector technology is such that only gradual improvement can be expected. Such improvement would mainly occur at the longer wavelength where the quantum efficiency falls off. Further refinements of fabrication techniques or introduction of new material processing techniques might result in improved performance by improving the quantum efficiency.

3.5.2 Laser Power

The required laser power is proportional to bit rate and increases with increasing range. The available power is greater for some laser types than for others. The CO_2 laser at 10.6m can generate up to 10 watts of power, and this power is concentrated in a very narrow line width which is ideal for heterodyne systems. It is not so ideal for ASK modulation since the laser operates CW and power during the zero bits is discarded, instead PSK or FSK modulation is preferred.

The solid state laser diodes operating in the region between 0.8 and 1.55 μm can generate up to about 100mW at a single frequency and in a single spatial mode. The single spatial mode is required to provide a well defined laser beam in the far field and the single frequency is required for efficient heterodyne detection. The line width is not as narrow as for the CO_2 laser but it is narrow enough for satisfactory heterodyne detection of the higher bit rates.

The Nd:Yag laser at a wavelength of 1.06 μm can generate about 1.0 watts of optical power. This is also at a single frequency and in a single spatial mode required for optimum performance in an ISL link.

Higher transmitter powers can be obtained by using multiple laser transmitters all operating at slightly different wavelengths. The laser beams are then combined at the transmit terminal and separated at the receive end by means of wavelength sensitive filters.

System performance can be improved by increased power in a single mode and by higher DC to optical power conversion efficiency. The system would also benefit by reduction in mass or more tolerance to temperature variations. Some improvement in all these areas can be expected as the technology improves.

3.5.3 Telescope Diameter

The telescope diameter defines the telescope gain. The gain is proportional to $(\Delta D/\lambda)^2$ so that the shorter wavelengths have the highest gain. However, higher gain implies a narrower beamwidth with increased difficulty in tracking and pointing the telescope. At the higher bit rates a higher power is needed at the detector, which is mainly provided by a larger telescope diameter. However, a significant fraction of the terminal mass is contained in the telescope and gimbals required to direct and support it. A trade-off is required to determine the optimum between laser power and telescope gain. Telescope design is a fairly mature technology but some further mass reduction might be expected.

3.5.4 Acquisition and Tracking

A significant problem associated with the very narrow beam transmitting and receiving telescopes is the initial acquisition of the cooperating station and subsequent tracking of the beam. This problem is compounded by the fact that both terminals are located on unstable platforms with attitude uncertainities up to ± 0.5 degrees or about 18000 μradians wheresa the basic beam width may be as little as 10 μradians. There are of the order of 3 million beams in the two dimensional uncertainty field of voew. The acquisition approach is to use a much larger acquisition beacon on the transmit side and a CCD detector field on the receive side. These two techniques make acquisition possible even for the shorter wavelengths.

After acquisition is accomplished the received signal must be tracked. This cannot be done with the coarse pointing mechanism. Instead a fine pointing mechanism is required which responds rapidly enough to follow vibrations and distortions on the host satellite.

A number of acquisition procedures have been proposed on different programsand these procedures will be demonstrated in space in the next few years. Further iterations of the acquisition and tracking system can be expected at both the system and unit level before the optimum system emerges.

3.5.5 Heterodyne Frequency Tracking

For a heterodyne system it is essential that the frequency of the local oscillator laser is controlled so that the difference between the received laser frequency and LO frequency is kept constant and equal to the required intermediate frequency. This requires accurate frequency control for both the transmitter and local oscillator so that acquisition can occur. In addition, a phase lock loop is required on the receive side pulling the local oscillator frequency to compensate for doppler frequency shifts and drifts in the received signal frequency.

The control and stabilization of the laser frequencies is one of the items that make heterodyne systems more complex than the direct detection system.

Acquisition of the frequency by means of the phase lock loop, for a heterodyne system, is a critical step in the acquisition sequence which must be successfully accomplished before acquisition can be considered complete.

3.5.6 Wavefront Alignment

For a heterodyne system, the local oscillator signal profile must be matched to the received signal profile at the surface of the detector in both phase and amplitude. This requires that the two phase fronts match and that the two signal peaks are not displaced and that they arrive from the same direction.

With careful adjustment degradations as low as 1 to 3 dB have been achieved. Detailed analysis and eventual testing is required to ensure that this degradation is not exceeded over temperature or life.

3.5.7 External Modulators

Nd:Yag and CO^2 lasers are CW lasers which are generally modulated using an external modulator. This is in contrast to laser diodes which can be modulated by proper control of the drive voltage. External modulators are fabricated using an electro-optical material to provide the required modulation characteristics. The modulators have significant insertion loss requiring the addition of thermal control for proper operation.

Further development of modulator units is required to maximize the modulation efficiency and minimize the insertion loss in order to maximize the system performance. Present day external modulator loss is one of the degradations which are associated with heterodyne systems and not with direct detection systems using laser diodes. These degradations are preventing the heteroydne systems from achieving its full potential capability and competing effectively with direct detect systems.

This Page Intentionally Left Blank

SECTION 4

LINK BUDGET ANALYSIS

4.0 LINK BUDGET ANALYSIS

4.1 Generic Link Budgets

4.1.1 Terminal Configuration

The link budget model is based on a two way link with a transmitter and a receiver at both terminals. The same telescope is used in both directions and the telescope is assumed identical at both terminals. Because of these assumptions, some elements of the optical circuit appear in the path at the transmit terminal and then again at the receive terminal. A schematic of the optical system for a direct detection system is given in Figure 4.1-1 and for a heterodyne system in Figure 4.1-2. They are essentially the same except for the addition of a local oscillator laser and the L.O. coupler.

4.1.2 Link Budget Model

A typical link budget is shown in Table 4.1-1. This shows all the line items that contribute to the link performance. The line items are explained in Section 4.1.3.

The sample budget in Table 4.1-1 is a 1 Gbps Geo-Geo link using a AlGaAs. The first column is for FSK modulation and heterodyne detection. The section column in the same except that direct detection is used. Both systems use the identical modulator, however, there are some degradations that apply to the heterodyne system which are not present for the direct detection system. These are principally the L.O. alignment losses and the necessity of converting to circular polarization at the transmit terminal and back to linear at the receive terminal so that the polarization can be aligned with the L.O. polarization.

4.1.3 Line Item Descriptions for Laser Link Budget

The link budget shown in Table 1 is divided into seven blocks consisting of:

a) Transmit Telescope
b) Transmitter/Modulator
c) Transmit Optical Path
d) Space Loss
e) Receive Telescope
f) Receive Optical Path
g) Receiver/Detector

The entries for each line item are in dB unless otherwise noted. The entries for each block are added and the resulting sum presented opposite the blocks title.

A system margin of not less than 3.0 dB is retained to take care of possible errors in estimating the performance of the various elements in the overall link.

The various contributors to each of the seven block is discussed in detail in the following paragraphs. The model is based on the assumption of a two way link where the telescope at each end is used for both transmit and receive. This results in elements of the optical path appearing twice, once at the transmit and once at the receive end.

4.1.3.1 Transmit Telescope

There are seven contributors to the telescope performance. In addition, the noise equivalent angle (NEA) which is the one σ pointing error is listed for information.

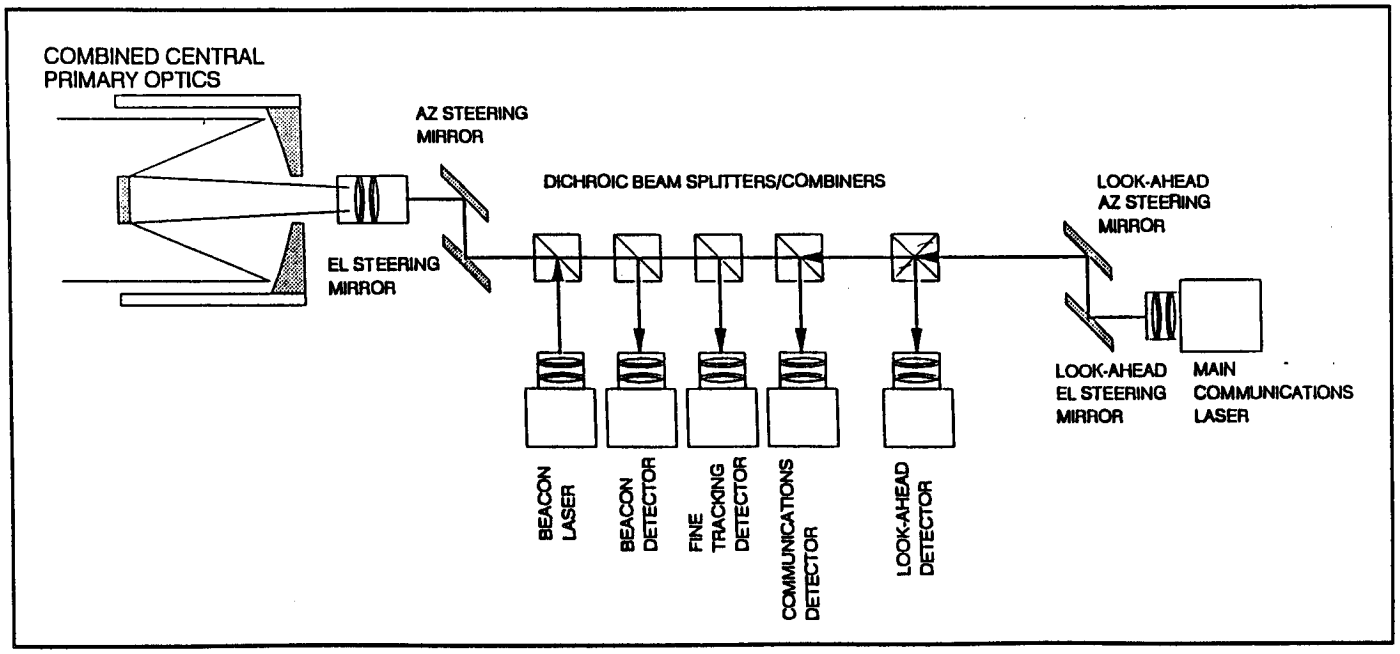

Figure 4.1-2 Optical Network for Combined Primary Optics (Direct/Detection)

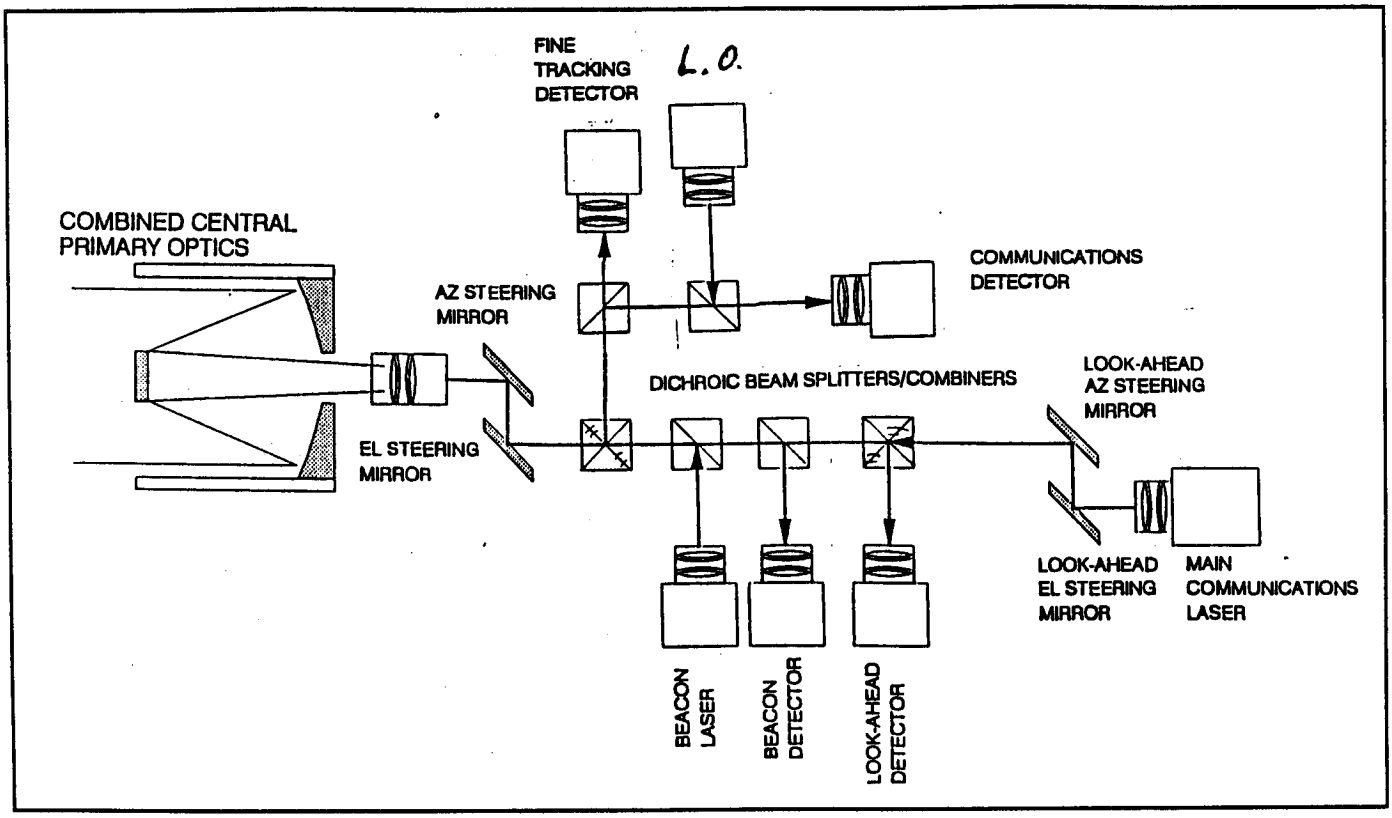

Figure 4.1-1 Optical Network for Combined Primary Optics (Heterodyne)

Table 4.1-1 Simple Link Budet Showing all Loss Elements

	Heterodyne		Direct detection	
Laser Type	AlGaAs		AlGaAs	
Wavelength (nm)	850		850	
Bit Rate (Mbps)	1000		1000	
Modulator type	Bias		Bias	
Modulator type	FSK		ASK	
Detection type	Heterodyne		Direct	
Path Length (km)	73000		73000	
TRANSMIT TELESCOPE GAIN (dB)		116.9		116.9
Aperture Diameter (cm)	30.0		30.0	
Aperture Gain	120.9		120.9	
Aperture Eff./blockage	1.8		1.8	
Support Member Blockage	0.0		0.0	
Surface Errors	0.5		0.5	
Defocusing	0.2		0.2	
Transmission Loss	0.8		0.8	
Pointing Loss	0.7		0.7	
N.E.A. (micro rad.)	0.3		0.3	
TRANSMITTER POWER (dBW)		-7.8		-7.1
Average Laser Power (dBW	-7.5		-7.1	
(Watts)	0.18		0.19	
Modulator Efficiency	0.0		0.0	
Modulator Transmission	0.0		0.0	
Polarizer Loss	0.3		0.0	
TRANSMIT OPTICS PATH LOSS (dB)		-0.7		-0.7
Fine Pointing Mirrors	0.1		0.1	
Beacon Laser Coupler	0.1		0.1	
Beacon Detector Coupler	0.1		0.1	
Fine Track. Det. Coupler	0.1		0.1	
Comms. Det. Coupler	0.1		0.1	
Look-ahead Coupler	0.1		0.1	
Look-ahead Mirrors	0.1		0.1	
SPACE LOSS (dB)		-300.7		-300.7
RECEIVE TELESCOPE GAIN (dB)		119.3		119.3
Aperture Diameter (cm)	30.0		30.0	
Aperture Gain	120.9		120.9	
Aperture Eff./blockage	0.3		0.3	
Suppor Member Blockage	0.0		0.0	
Surface Errors	0.5		0.5	
Transmission Loss	0.8		0.8	
RECEIVE OPTICS PATH LOSS (dB)		-2.8		-0.5
Fine Pointing Mirrors	0.1		0.1	
Beacon Laser Coupler	0.1		0.1	
Beacon Detector Coupler	0.1		0.1	
Fine Track. Det. Coupler	0.14		0.14	
Comms. Det. Coupler	0.1		0.1	
Polarizer loss	0.3		0.0	
L. O. coupler loss	0.2		0.0	
Wavefront mismatch	0.3		0.0	
Alignment mismatch	1.5		0.0	
RECEIVER SENSITIVITY (dBW)		-78.8		-75.8
Photon Energy (J)	2.34E-19		2.34E-19	
Av. Ph./Bit at BER=10^-6	55.0		110.0	
Rcv. Sens. (dBW)	-78.9		-75.9	
Extinction ratio assumed	0.05		0.05	
Laser Linewidth	0.1		0.0	
Background Illumination	0.0		0.07	
SYSTEM MARGIN		3.0		3.0

ical diffraction limited gain of the telescope under the assumptions that the light intensity is uniform across the aperture, and that there is no blockage or imperfections in the optics. This is the maximum gain (compared to an isotropic radiator) that can be achieved from the aperture. The remaining entries subtract from this gain.

2) Aperture Efficiency/Blockage

This is the theoretically determined degradation to the aperture gain due to non-uniform intensity across the aperture and the loss due to the blockage of the small central secondary mirror of the telescope optics. The calculation is based on an Airy distribution fir the aperture, which is an approximation to the actual illumination provided by the laser.

3) Support Member Blockage

This is the blockage caused by the support for the central secondary mirror. It has been decided that the mirror would be supported by the transparent telescope window so the loss from this item is zero. However, it has been retained as a line item.

4) Surface Errors

The diffraction limited aperture gain (Item 1) is based on the assumption of a plane wavefront at the telescope aperture. This entry is an estimate of the loss of gain resulting from random imperfections to the reflector, lenses and window surfaces.

5) Defocussing

Maximum theoretical gain requires perfect alignment of the telescope and the laser source so that the laser appears as a point source located at the focal point of the telescope. Departures from this condition will result in a spherically curved wavefront with subsequent loss in gain.

6) Transmission Loss

The telescope consists f reflecting surfaces, lenses and windows, all of which have transmission loss, which must be accounted for.

7) Pointing Loss

There is a loss of gain due to imperfect pointing of transmit telescope so that the target may be part way down on the beam contour. This mispointing has two principle sources:

a) Transmitter pointing information is obtained by tracking the signal received from the cooperating target. Imperfect pointing results from noise in the tracking system and disturbances introduced by the platform.

b) The transmit beam is pointed at the place where the target will be located when the transmit signal arrives. The mechanism that achieved this look-ahead pointing is an additional source of pointing error.

8) Noise Equivalent Angle (NEA)

This is the standard deviation of the pointing error that must be achieved to provide the link performance tabulated.

4.1.3.2 Transmitter/Modulator

This block consists of four items which include the laser itself, the modulator and the polarizer, if required.

1) Laser Transmitter Power

This is the optical power generated by the laser. The average laser power is used to correspond to the average number of photons per bit used for the receiver. This power output has to be achieved over the temperature range experienced by the laser.

2) Modulator Transmission

This is the loss of power due to the presence of the modulator even when the signal remains

unmodulated. For the case of the laser diodes, where the signal is modulated by driving the laser, this entry is zero.

3) Modulator Efficiency

This is the efficiency of the modulation process. Some losses associated with the modulation process are included int he photon per bit value used for the detector. For ASK, the principle degradation is due to the depth of modulation represented by the extinction ratio. For FSK and PSK the degradation due to the transmission time between states is included in the photon per bit value.

The line item of modulator efficiency includes only the loss 3 dB) due to zero bit blockage when ASK modulation is generated by an external modulator.

4) Polarizer Loss

For an intersatellite link the orientation of the two satellites is not fixed but rather is continually changing. Thus, if the detector is polarization sensitive, such as in a Heterodyne system, then the transmit terminal must convert linear polarization to circular polarization and the receive station must convert back to linear polarization.

4.1.3.3 Transmit Optics Path

Between the transmitter and the telescope there are a number of elements which perform a variety of functions:

1) Fine Pointing Mirrors

The whole telescope is pointed by a course pointing mechanism which may have a range up to 360 deg. in azimuth and 0-0 deg. in elevation. To achieve pointing accuracies required to satisfy the pointing loss budget, a fine pointing mechanism is needed which redirects the optical path without moving the telescope. The fine pointing mechanism consists of two mirrors moved in orthogonal directions with the only loss being the reflectivity of the two mirrors.

2) Beacon Laser Coupler

For initial acquisition, a high power laser generating a wider beam width is used at both ends of the link. The beacon is coupled into the main optical path by means of a wavelength sensitive mirror placed at an angle of 45°. The entry is the loss imparted to the transmit laser beam.

3) Beacon Detector Coupler

During acquisition, both terminals transmit a wider beacon beam and both terminals operate a beacon detector, which is coupled into the main optical path by means of a wavelength sensitive mirror. The entry in this line item is the loss imparted to the transmit laser beam.

4) Fine Track Detector Coupler

For accurate tracking of the narrow beamwidth communication signal, a sensitive detector is required. This taps off a fraction of the received wavelength but is quite transparent to the transmit wavelength. This detector is part of a feed back loop, which controls the position of the fine pointing mirrors.

5) Comms Detector Coupler

This is a wavelength sensitive mirror set at 45°, which is reflective to the receive wavelength but is quite transparent to the transmit wavelength.

6) Look Ahead Detector Coupler

Because the satellites are in motion, the transmit beam must be pointed ahead to the place where the cooperating terminal will be when the signal arrives. The magnitude and direction of the look ahead angle is calculated from a knowledge of the motions of the two satellites and the orientation of the transmitting terminal. To ensure that the look ahead angle is achieved, a look ahead detector issued, which is part of the feed back loop controlling the position of the look ahead mirrors. The coupler taps off a small fraction of the transmit signal so loss tot he transmit beam is the magnitude of the coupling plus the transmission loss.

7) Look Ahead Mirrors

These mirrors, operating in two orthogonal directions, generate the look ahead angle, introduce a loss due to the reflectivity of the two mirrors.

4.1.3.4 Space Loss

This is the space loss given by the equation $(\lambda /4\pi R)^2$ and gives the correct receive power in combination with the transmit and receive telescope gains. The parameter R is the maximum range between the two satellites at which communications is required and λ is the laser wavelength expressed in the same units as R. Since the forward and return links will operate at slightly different wavelengths, the space loss in the two directions will be slightly different.

4.1.3.5 Receive Telescope

The receive telescope is similar to the transmit telescope with some significant exceptions.

Two categories of degradation are omitted on the receive side.

The one, "pointing losses", is omitted because the detector, while small, is larger than the diffraction limited spot of the telescope, and can tolerate a mis-pointing error of the magnitude expected from the tracking system.

The other, "defocussing", is omitted because the detector is large enough to tolerate a spot size, which is somewhat larger than the diffraction limit.

1) Aperture Gain

The aperture gain is given by the same formula as for the transmit telescope.

2) Aperture Efficiency/Blockage

This is different from the transmit case because the signal impinging on the receive telescope is uniform illumination and the detector has no angular sensitivity. for the receive case therefore, this term includes only the blockage of the central secondary mirror.

3) Support Member Blockage

This term is zero for the same reason as for the transmit case.

4) Surface Errors

Surface errors have the same impact on receive as on transmit effectively taking energy from the main beam and scattering it the sidelobe regions.

5) Transmission Loss

This is the same as for the transmission and will have the same magnitude.

4.1.3.6 Receive Optics Path

The receive optics path is similar to the transmit optics path with some significant differences:

1) Fine Pointing Mirrors

These are the same mirrors, except at other end of the link, and have the same loss as the transmit mirrors.

2) Beacon Laser Coupler

The beacon laser coupler has the same impact on the system as the beacon laser at the transmit terminal.

3) Beacon Detector Coupler

This has the same loss as the one at the transmit terminal

4) Fine Track Detector Coupler

This coupler diverts a fraction of the communications signal to be used by the fine tracking system. The coupling factor is chosen to provide enough energy to the tracking system so that the required NEA can be achieved. An insertion loss of 0.1 dB is added to the coupling factor.

5) Communications Detector Coupler

This coupler is used to separate the transmit path from the receive path. It has only a nominal insertion loss in both paths.

6) Polarizer Loss

As explained for the transmitter, the two terminals of the intersatellite link do not have a fixed orientation and will experience polarization rotation of the linear polarization. For systems which are polarization sensitive (Heterodyne systems) the polarization must be converted from linear to circular at the transmit end and converted back to linear at the receive end.

7) Local Oscillator Coupler

For a Heterodyne (or Homodyne) system an additional coupler is needed to combine the local oscillator signal and the incoming communications signal. This will have an insertion loss of the Receive path dependent upon the coupling factor selected.

8) Wavefront Mismatch

This is the mismatch between the signal wavefront and the L.O. wavefront and consists of such errors as difference in wavefront curvatures. The loss exists only for Heterodyne systems.

9) Alignment Mismatch

This is the mismatch between the alignment of the signal beam and the L.O. beam. It includes such things as the beam axis misalignment. The loss exists only for Heterodyne systems.

4.1.3.7 Receiver

The receiver noise level is determined by short noise (statistical variation of photon arrival rate) rather than thermal noise. For this reason, the basic receiver sensitivity is given by the average number of photons required to detect a bit with a given probability of error.

1) Photon Energy

This is the energy in Joules of one photon given by the equation $E = hc/\lambda$, where h is planck's constant $h = 6.626 \times 10^{-34}$ J-sec and λ is the laser wavelength in the same units as C, the velocity of light.

2) Average Photons/Bit at BER = 10^{-6}

This is the minimum number of photons required to detect a bit with an error rate of less than 10^{-6}. For on/off keying, the average is between the "on" bit and the "off" bit as well as the long term average of all the bits. The number of quoted is experimentally determined by a number of experimenters in a number of laboratories using the best technology available. It includes the effects of an imperfect detector such as excess noise and dark current, and imperfect modulator effects such as the extinction ratio for ASK.

3) Receiver Sensitivity

This is the product of the number of photons/bit, the number of bits per second, and the energy per photon. It converts the receiver sensitivity from photons/bit to watts.

4) Laser Line Width

The Heterodyne system is quite sensitive to the line width of the laser and local oscillator sources, and the performance is degraded depending upon the ratio of line width to it rate and upon the type of modulation used.

5) Background Illumination

The receive telescope also collects photons from the background surrounding the signal source. This background increases the shot noise and makes the signal more difficult to detect.

6) Extinction Ratio Assumed

The average photons/bit for ASK is influenced by the extinction ratio of the laser modulator.

This extinction ratio is listed for information only.

4.1.4 Performance Degradation

4.1.4.1 Degradation of Direct Detection Systems by Background Illumination

Timo and Jacobson [44] have analyzed the impact of background noise on the performance of direct detectors and compared this with the heterodyne/homodyne configuration. They show that the ideal direct detector gives a bit error rate of 10^{-9} with only ten photons per information bit compared to 18 to 40 for homodyne and heterodyne configurations. However, when the background noise currents are considered and direct detection performance degrades rapidly whereas, due to the reduced bandwidth, the homodyne/heterodyne system is able to discriminate against these noise currents and largely maintain performance. The noise currents are of two types, those due to background lights such as scattered sunlight, and that due to leakage currents in the detector. The former is controlled by means of a narrow band filter in the receive path which is just wide enough to pass the received signal. The filter width must be such that it passes the laser wavelength after taking account of manufacturing tolerances on both the transmitter and filter as well as aging effects and temperature drifts. Current filters are some ten nanometres wide and this may be about as narrow as practical to fabricate.

The other source of background noise, that of leakage current in the detector, can be reduced by controlling the fabrication process. Avalanche photo detectors are being fabricated with an excess noise current close to the theoretical minimum with the result that, in an environment without a background of scattered light, the performance of the direct detection receiver is coming close to that for the heterodyne receiver.

The impact of background light has been calculated by Provencher and Spence [45] for typical intersatellite links for the ACTS Laser Communications Experiment. The calculation was carried out for BPPM and 1) No background radiation, 2) for sunlight earth in the field of view, 3) Sunlight sky in the view. All cases are for direct detection receiver.

Figure 4.1-3 shows the case for no background noise but only detector noise currents. The X-axis is the received signal photons per bit required to achieve the bit error rate shown on the Y-Axis. The number of photons are rather high mainly because a photo detector with poor performance parameters was assumed. However, of interest is the degradation caused by the background light shown in Figure 4.1-4. The sunlight earth in Figure 4.1-4 shows only modest additional degradation.

The additional degradation due to background light would be worse if the performance characteristics of an up to date photon detector had been used. The calculation procedure of Provencher and Spence [45] has been used to estimate the degradation due to background illumination of 50 pico watts 50×10^{-12} watts incident on the detector. This is approximately the level expected for a telescope looking at the sunlight earth and using a fairly narrow optical filter of 10 to 20 μm bandwidth. The outcome of this calculation is shown in Figure 4.1-5. For low bit rates, a PIN diode detector with high impedance load resistor was assumed followed by a baseband amplifier. For high bit rates, this was changed to an APD with a much lower impedance load resistor.

Figure 4.1-5 shows the degradation in dB as a function of bit rate. At very high bit rates, the number of background photons per bit is very small and the main noise source is the shot noise due to the random arrival of the incident photons.

As the bit rate decreases, the number of background photons per bit increases, and the degradation due to the background increases. There is an additional degradation due to the detector dark current and which also increases as the bit rate decreases. AT very low bit rates the noise is dominated by these two noise sources (dark current and background illumination) and the degradation due to background illumination is set by the relative magnitudes of the two sources. This results in an S shaped curve as seen in Figure 4.1-5.

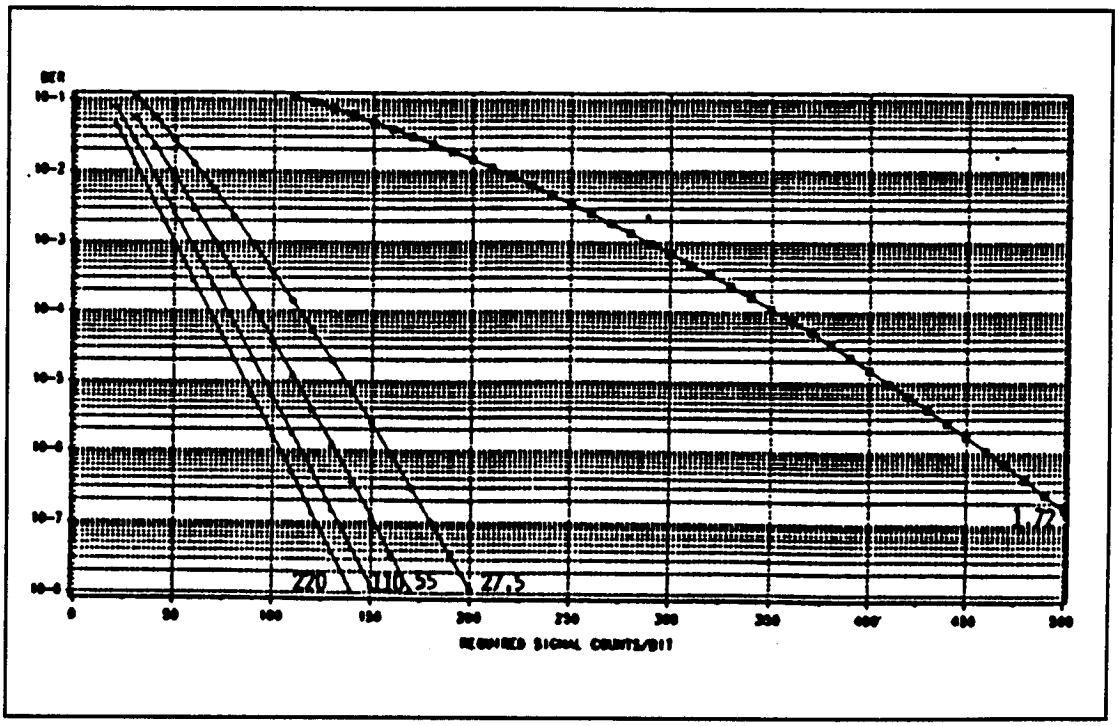

Figure 4.1-3 BPPM BER vs Required Signal Counts

BIT Data Rates: 1.72, 27.5, 55, 110 and 220 Mbps (No background radiation sources in ACTS or Aircraft recv. fov).

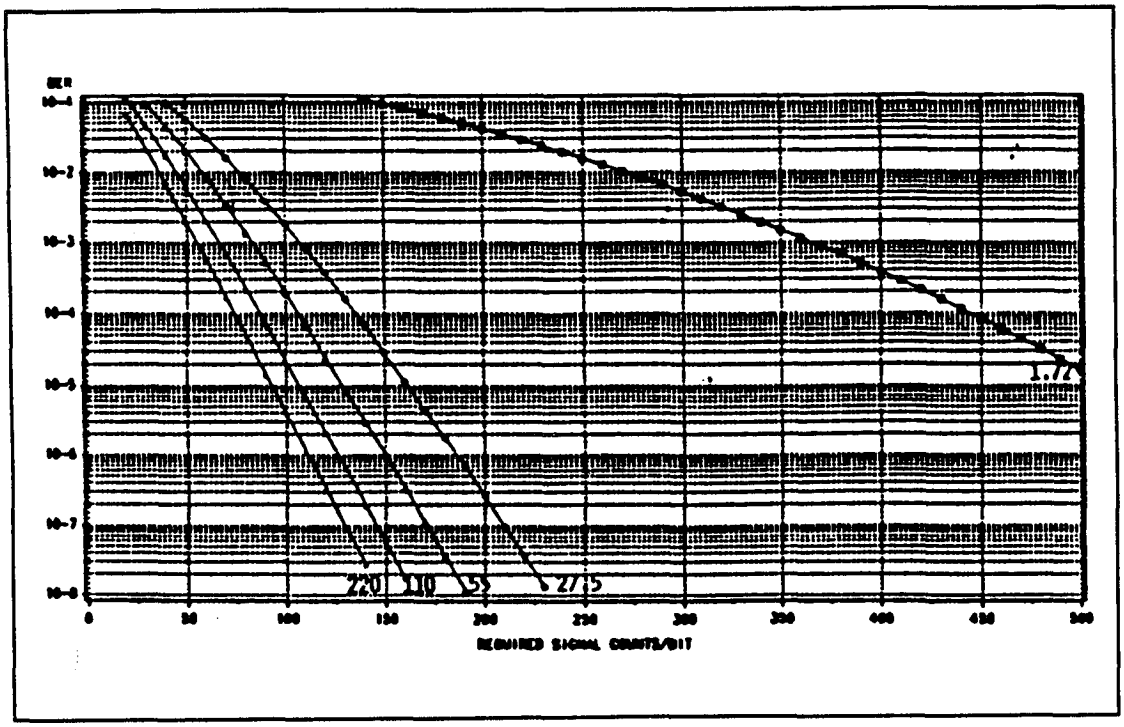

Figure 4.1-4 ACTS BPPM BER vs Required Signal Counts

BIT Data Rates: 1.72, 27.5, 55, 110 and 220 Mbps (sunlit earth in acts rec.fov).

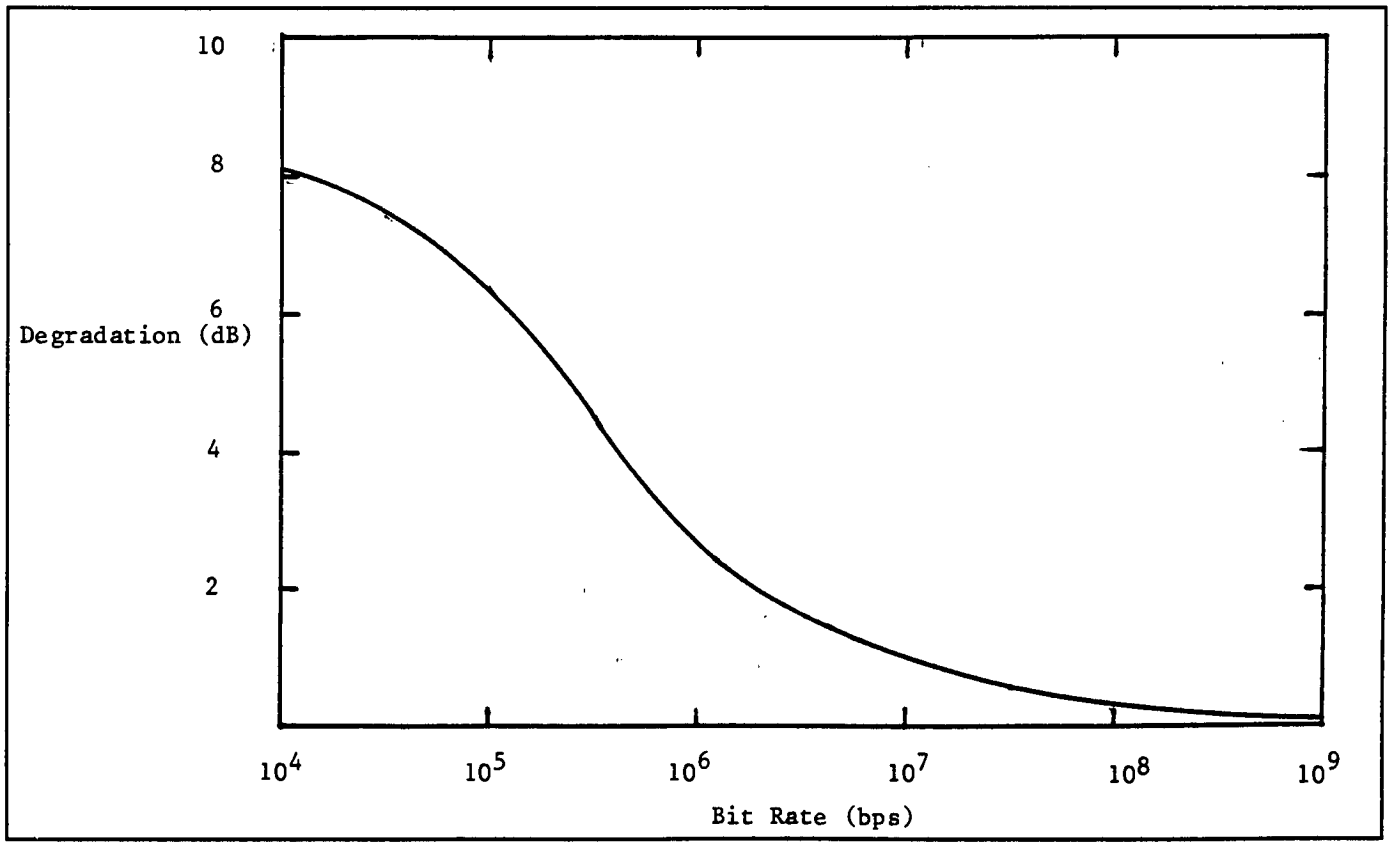

Figure 4.1-5 Link Degradation due to Background Light from the Sunlight Earth

A Heterodyne/Homodyne system largely eliminates these degradations because of the ability to perform much narrower filtering at the IF and baseband frequencies.

An interesting characteristic is that the low bit rates require more photons per bit than the higher bit rates. This is because in the longer bit periods of the lower bit rates more background photons are received and therefore the number of signal photons must also be larger. This is evident in Figure 4.1-3 with only detector leakage currents. This is in contrast to measurements which show that more photons per bit are required at the higher bit rates. The discrepancy is due to the fact that Provencher and Spence [45] have neglected the noise contribution of the detector capacitance. This noise component increases as the square of the bit rate and therefore dominates at the higher bit rates. As seen in Figure 3.2.2-13 the number of photons per bit to achieve a BER of 10^{-6} is fairly constant below about 200 mbps and then increases rapidly as the bit rate increases to 1 Gbps and beyond. In the region below 100 Mbps the increasing contribution due to the detector capacitance would balance the decreasing effect of the detector leakage currents. Above about 100 Mbps the effect of the leakage currents is negligible whereas the capacitance effect continues to increase.

4.1.4.2 Degradation of Heterodyne/ Homodyne Systems Due to Laser Line Widths

The line width of the laser source impacts the choice of modulation and demodulation schemes. If a direct detection receiver is used the line width of the source has little impact on the performance of the overall system. However, for heterodyne and homodyne systems the impact is significant making narrow width sources mandatory for these systems.

Barry and Lee [43] have analyzed the impact of the line width on the performance of heterodyne systems. They describe two degradations to the receiver performance caused by non zero line width. First there is a reduction in receiver sensitivity so that the received power must be increased to maintain the same bit error rate. However, a floor develops in the BER curve so that very low bit error rates cannot be achieved no matter how much power is incident on the receiver. This is illustrated in Figure 4.1-6.

In detail, the impact of line width on performance depends upon the type of modulation used. Figure 4.1-7 shows the position of the floor applicable to FSK as a function the line width to bit rate ratio, with h (frequency difference between ONE and a ZERO divided by the bit rate) as a parameter. For large h the floor can be maintained at low bit error rates even with wide line widths. It is seen that the line width must be low in order to keep the line width to bit rate ratio low and maintain good BER performance. The higher bit rated requires a higher transmitter power to communicate over a given range but the narrow line width lasers have lower power capability . thus there is a complex trade-off between all the interrelated parameters.

With ASK homodyne receiver, Figure 4.1-8 shows that the floor depends for integration time r equal to the bit period T, on the line width to bit rate ratio. Even with a ratio of 0.1 a significant degradation in performance occurs and with a ratio of 0.25 the limiting BER is about 10^{-7} even for very large receive powers. The performance of the ASK homodyne receiver can be improved by selecting the optimum integration time $\tau_{opt} < T$. As shown in Figure 4.1-9, the floor has disappeared leaving a manageable degradation effect.

Because of the impact on demodulator performance of heterodyne systems, a great deal of emphasis is being placed on reducing the line width of laser generators. The first step is to design a single mode laser. This entails making the laser lase in only one mode by suppressing secondary modes. This reduces the power of the laser so the second step is to increase the power in the single mode. The other requirement is to reduce the line width of the single mode.

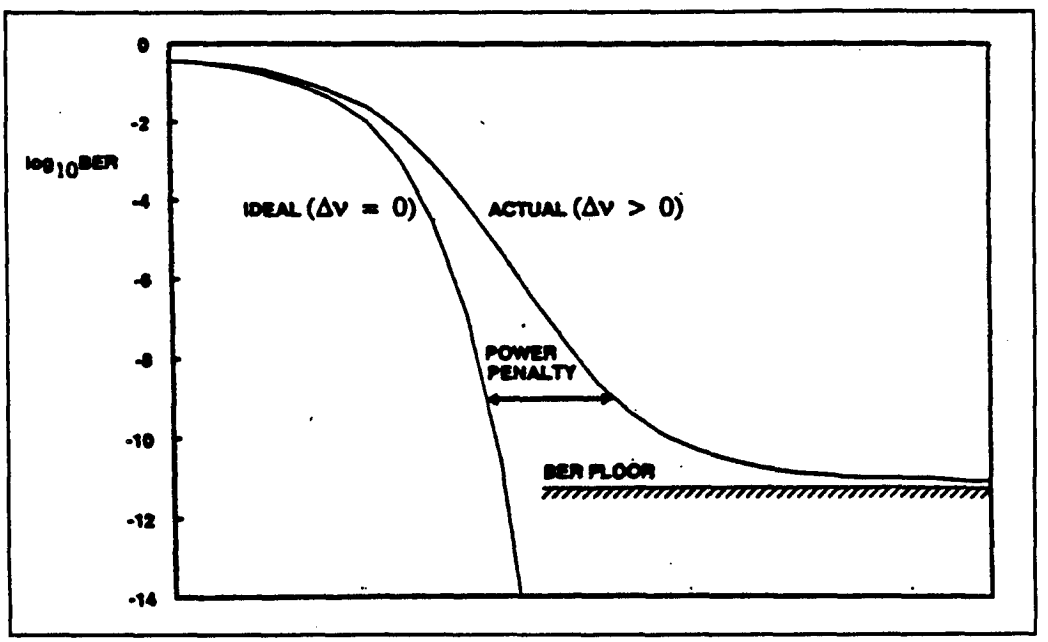

Figure 4.1-6 Phase Noise has Two Effects on a BER Curve, a Power Penalty, Which Causes a Shift to the Right, and a BER Floor, Which is a Lower Limit on the Probability of a BIT Error.

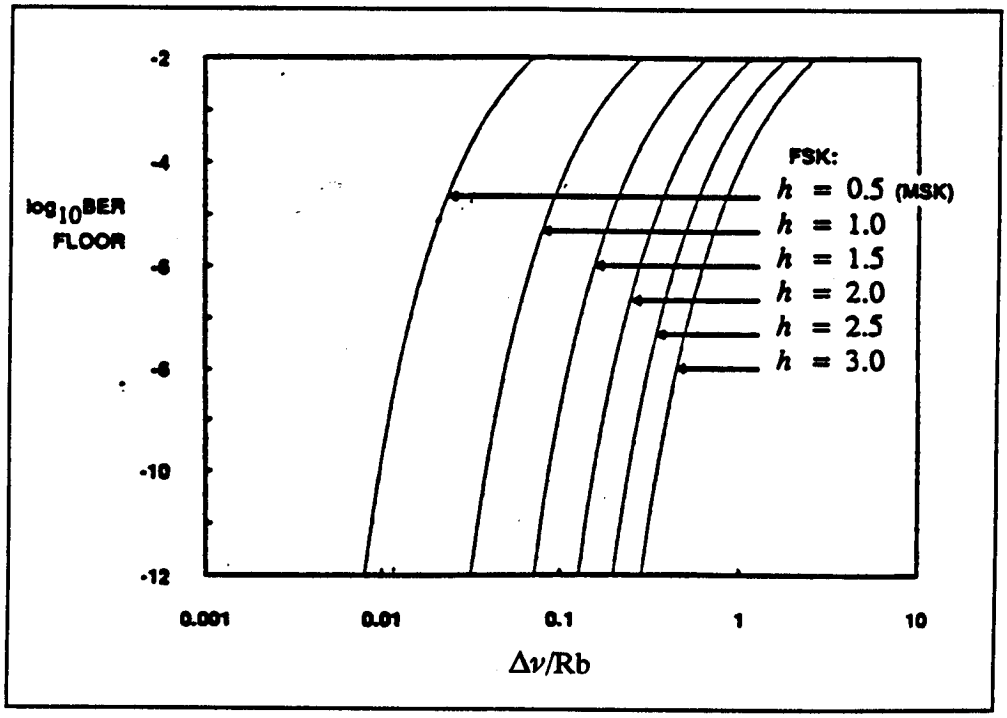

Figure 4.1-7 BER Floor for Heterodyne FSK Discriminator Reception due to Phase Noise

Plotted versus Δν/Rb Where Δν is the sum of the transmitter and LO laser linewidths and Rb is the bit rate. The parameter is h, the deviation ratio, which is the frequency difference between a one and zero divided by the bit rate.

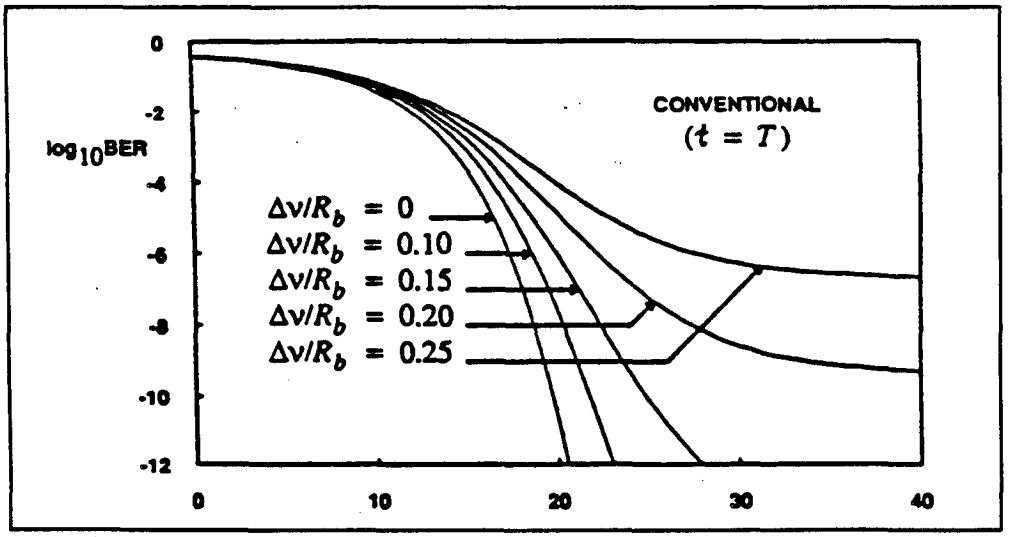

Figure 4.1-8 BER Curves for a Conventional Heterodyne ASK Homodyne Receiver.

The parameter is Δν/Rb where Δν is the IF linewidth and Rb is the bit rate. The curve labeled Δν/Rb = 0.25 exhibits a large BER floor and never achieves BER = 10^{-9}, even for infinite M (number of photons per bit).

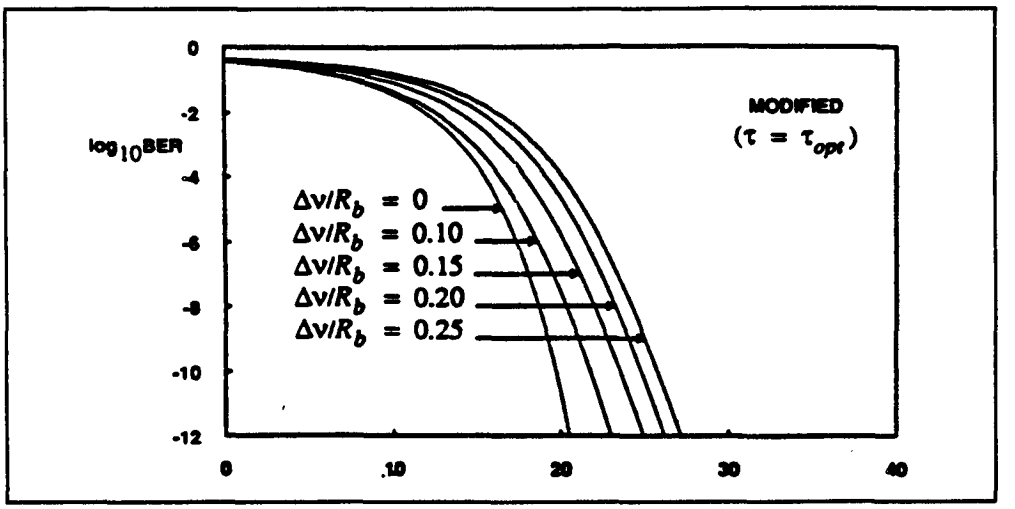

Figure 4.1-9 BER Curves for a Modified Heterodyne ASK Homodyne Receiver with $t = t_{opt}$

The Δν/Rb parameters are identical to those in Figure 4.1-8.

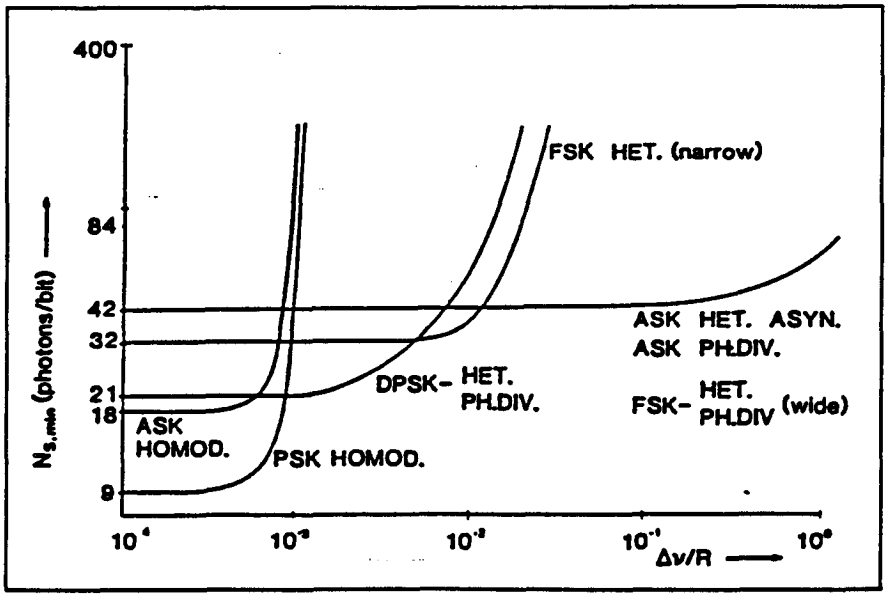

Figure 4.1-10 Sensitivity Limits

Expressed in minimum required signal photons/bit (Ns,min), as a function of beat linewidth Δv normalized to data rate R, for various binary modulation formats and coherent receiver concepts. (Sufficiently high local oscillator power is assumed

Leeb [64] presents a tutorial on coherent optical receivers. In particular, he presents the effect of laser linewidth (as a fraction of the bit rate) on the photons/bit required to achieve a bit error rate of 10^{-9} for a number of modulation and detection combinations. His graph is reproduces as Figure 4.1-10. There are five different curves to represent seven different systems. Each curve starts at very low line width, at the theoretical minimum number of photons per bit. This value remains constant until the line width approaches a threshold value above which the required number of photons per bit increases rapidly. The maximum value of line width/bit rate at which degradation is still negligible, has been taken from this graph and inserted in Table 4.1-2 which presents the maximum line width as a function of bit rate and system configuration.

4.2 Performance Analysis

4.2.1 Heterodyne/Direct Detection Comparison

Detailed link budgets have been generated for comparison of Heterodyne and direct detection systems. These have been carried out for a Geo-Geo link with a separation of 120 degrees for all four laser wavelengths and for 1Gbps, 100 Mbps and 1 Mbps. These link budgets are reproduced in Appendix B.

The performance comparison is largely determined by the difference in detector sensitivity illustrated in Figure 3.2.2-13. This shows that the detector sensitivity is fairly constant below about 100 Mbps but degrades rapidly at higher bit rates. The sensitivity of direct detection detectors is poorer than heterodyne detectors and degrades more rapidly at higher bit rates.

Table 4.1-2 Maximum Line Width for Negligible Detection of Coherent System Performance (evaluated at threshold of curve) as a Function of System Configuration and Bit Rate

	Limit (photons/bit)	$\Delta\upsilon$/R (threshold)	1 Gbps	100mbps	1 mbps	19.2 Kbps
ASK Hetero.	42	10^{-1}	100 MHz	10 MHz	100 kHz	1.9 kHz
FSK Hetero. (Wide)	42	10^{-1}	100 MHz	10 MHz	100 kHz	1.9 kHz
FSK Hetero (Narrow)	32	$5x10^{-3}$	5 MHz	0.5 MHz	5 kHz	96 Hz
DPSK Hetero.	21	10^{-3}	1 MHz	100 kHz	1 kHz	1.9 Hz
PSK Homodyne	9	$3x10^{-4}$	300 kHz	30 kHz	300 Hz	5.8 Hz
ASK Homodyne	18	$3x10^{-4}$	300 kHz	30 kHz	300 Hz	5.8 Hz

Below 100 Mbps heterodyne systems have a few dB advantage except, as shown in Figure 3.2.2-13 for AlGaAs lasers operating in the vicinity of 0.85 μm. A direct detector at this wavelength is only slightly less sensitive than a heterodyne detector and the heterodyne system has additional losses, due mainly to matching the local oscillator and received signal phase fronts and the use of a circular polarizer at both transmit and receive terminals. These losses are listed in Table 4.1-1. There is an additional loss due to the use of an external modulator at the transmitter.

The results of the link budget analysis are summarized in Table 4.2-1. A 3-4 dB advantage for the heterodyne over the direct detection configuration is shown for the CO_2 and InGaAsP lasers based on the difference in transmitter power. A smaller advantage is shown for the Nd:Yag laser, and for the A1GaAs laser, the direct detection system shows improved performance compared to the heterodyne system.

Figure 4.2-1 shows that direct detection receivers in the 850 nm region have achieved sensitivities close to that of heterodyne receivers. Additional losses inherent in the heterodyne system make the direct detection system comparable in performance at least below about 100 mbps. Above 100 mbps the direct detection sensitivity degrades more rapidly than for heterodyne making the use of heterodyne system preferred at bit rates above 1 Gbps.

Table 4.2-1 Heterodyne Advantage over Direct Detection (dB)

GEO-GEO	CO_2	InGaAsP	Nd:Yag	AlGaAs
1 Gbps	3.5	4.7	2.9	0.2
100 Mbps	3.6	4.2	0	-2.3
1 Mbps	4.5	5.2	1.0	-1.3

4.2.2 Comparison of Laser Types

Detailed link budgets comparing the four lasers at different bit rates and different path lengths are provided in Appendix C. For comparison purposes, four of these budgets are summarized in Table 4.2-2. These are the four lasers in the Geo to Leo path with 19.2 Kbps in the forward direction and 100 Mbps in the return direction. The 100 Mbps link is the limiting requirement determining the aperture diameter. In the forward direction any laser can be used, so AlGaAs is assumed in all cases except for the second column where the InGaAsP laser is used for both directions.

The largest aperture is required by the InGaAsP so the A1GaAs laser is the preferred diode laser.

Similarly the aperture for the $C0_2$ laser is larger than for the Nd:Yag laser and this combined with the complexity and shorter life of the CO_2 laser means that the Nd:Yag is the preferred option of the two high power lasers. In addition, the CO_2 laser has never been considered for a direct detection system (only a heterodyne system) so reliable receive performance figures for direct detection as a function of bit rate are not avail-

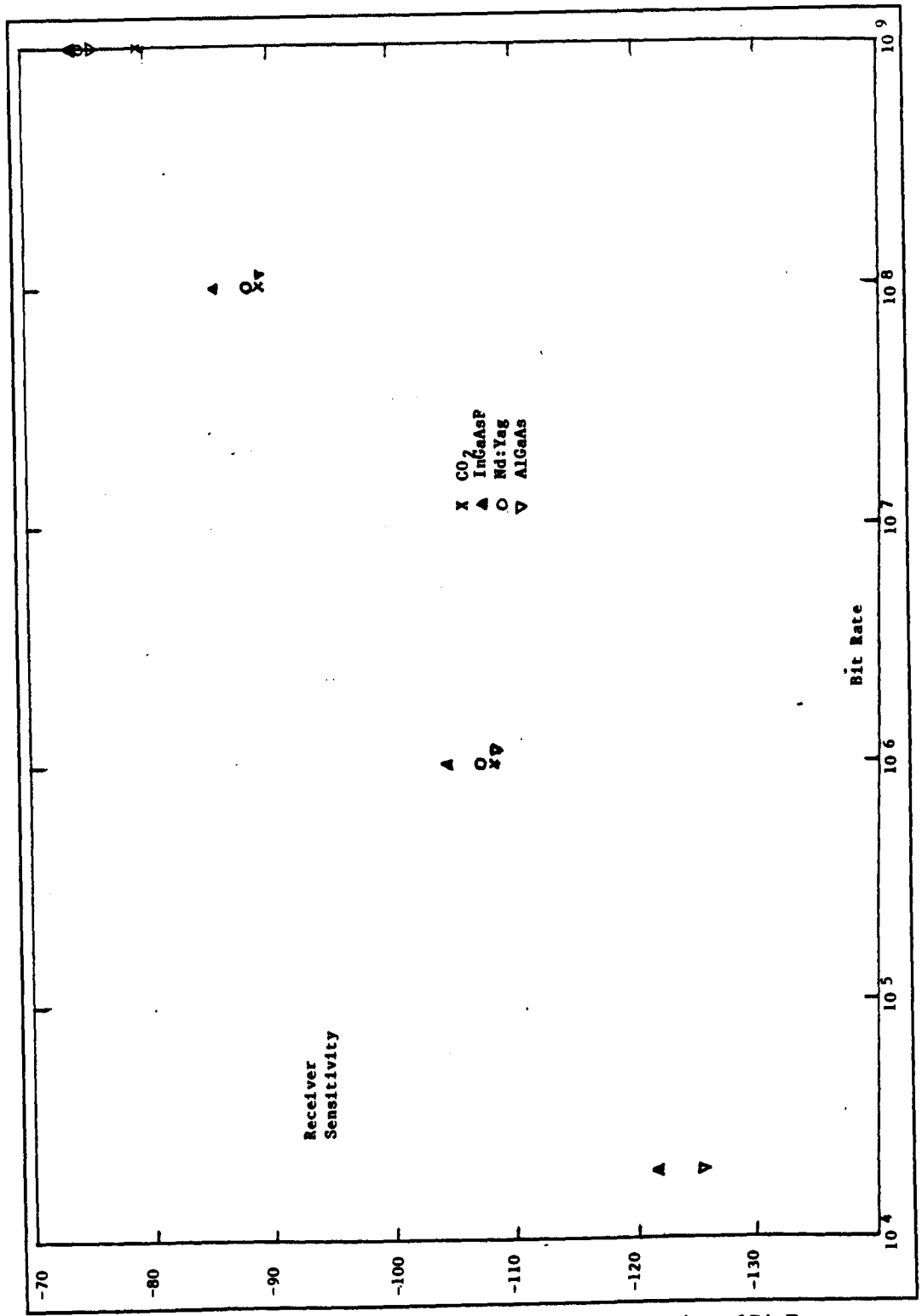

Figure 4.2-1 Receiver Sensitivity for the Four Lasers as a Function of Bit Rates (Direct detection used in all cases.)

Table 4.2-2 GEO to LEO Direct Detection Comparison (19.2 Kbps/100 Mbps)

Return laser (100 mbps)	CO_2	InGaAsP	Nd:Yag	AlGaAs
Aperture Diameter (CM)	15	22	8	13.6
Laser Power (W)	9	0.1	0.85	0.08
Modulation	FSK	ASK	FSK	ASK
Detection	Direct	Direct	Direct	Direct
Forward laser (19.2 Kbps)	AlGaAs	InGaAsP	AlGaAs	AlGaAs
Laser power (MW)	0.6	0.7	5	0.1

able and have been estimated. This leaves Nd:Yag and AlGaAs lasers as potential candidates.

The comparison is made in a different way in Figure 4.2-1. The receiver sensitivity is plotted in dBw for different bit rates and for the four laser types. The poorest sensitivity is that of InGaAsP which differs from the others by 2-4 dB. The CO_2 laser appears good but this is based on unreliable data as explained in the previous paragraph. This comparison also suggests that the Nd:Yag and the AlGaAs diode laser are the preferred options. The Nd:Yag laser with approximately one watt of optical power would be preferred for the higher bit rates while the AlGaAs would be preferred for systems where the bit rate can be supported.

In conclusion, direct detection using AlGaAs is the preferred system below about 100 mbps because of the simplicity of the system and because the sensitivity is comparable to a heterodyne system at these bit rates. Above about 1 Gbps a heterodyne system is preferred with the Nd:Yag laser the preferred option. The choice of Nd:Yag is based partly on performance and partly on improved reliability with a potentially longer life. In the region between 100 mbps and 1 Gbps the choice is less clear and will require more detailed trade-off studies for each case. However, the use of a number of AlGaAs lasers with direct detection receivers with combined bit rate up to 1 Gbps is a potential contender. The lasers operate at different wavelengths and are combined using wavelength multiplexing onto a single beam.

SECTION 5

ACQUISITION AND TRACKING

5.0 ACQUISITION AND TRACKING

5.1 Optical Inter-Satellite Link Control

High data rate communications using optical wavelengths requires very narrow beamwidths, on the order of 10 microradians, to achieve the required power concentration at the receiver. To achieve persistent alignment of the transmitted beam on the receiver, precise and cooperative beam pointing by the transmitter and tracking by the receiver are required. The problem of achieving this alignment has three component functions:

Acquisition - Each Satellite finds its partner;

Tracking - Continuously follow the partner satellite with the receiving telescope;

Pointing - Continuously illuminate the partner satellite with the transmit beam;

and is, therefore, often called the PAT (Pointing, Acquisition, and Tracking) problem.

During the acquisition phase the transmitter and receiver terminals achieve mutual pointing and tracking by first finding one another within a wide field of view, and then sequentially narrowing the angular field of pointing uncertainty. Once each terminal has located the other to high precision, communication can begin while alignment of the beam is maintained by the pointing function and alignment of the receive optics is maintained by the tracking function.

In the subsequent sections each of the above link control functions will be examined.

5.2 Acquisition

5.2.1 Introduction

Acquisition of the partner satellite position typically begins as an open loop technique requiring knowledge of the orbital and attitude ephemeris of both satellites. The basic objective of acquisition is to reduce the uncertainty of the transmitting partner's position from some initial value to the final angular resolution needed by the receiving system to sustain the communications link.

Figure 5.2-1 shows the parameters used to characterize the link during acquisition. In this context the objective of acquisition is to reduce Ω_u, the initial uncertainty solid angle, to Ω_r, the final resolution solid angle.

Two General Approaches can be used:

One Way

Data flow is only one way (simplex). A wide beam is used at the transmitter to illuminate the entire uncertainty region of the partner. The beam serves both as a beacon and for communication This technique requires very precise knowledge of the partner position, and can consume a large amount of transmitted optical power.

Two Way

Data can flow both ways (duplex). When acquisition is complete, a low power, narrow beam is used at both satellites for communication and to aid in tracking.

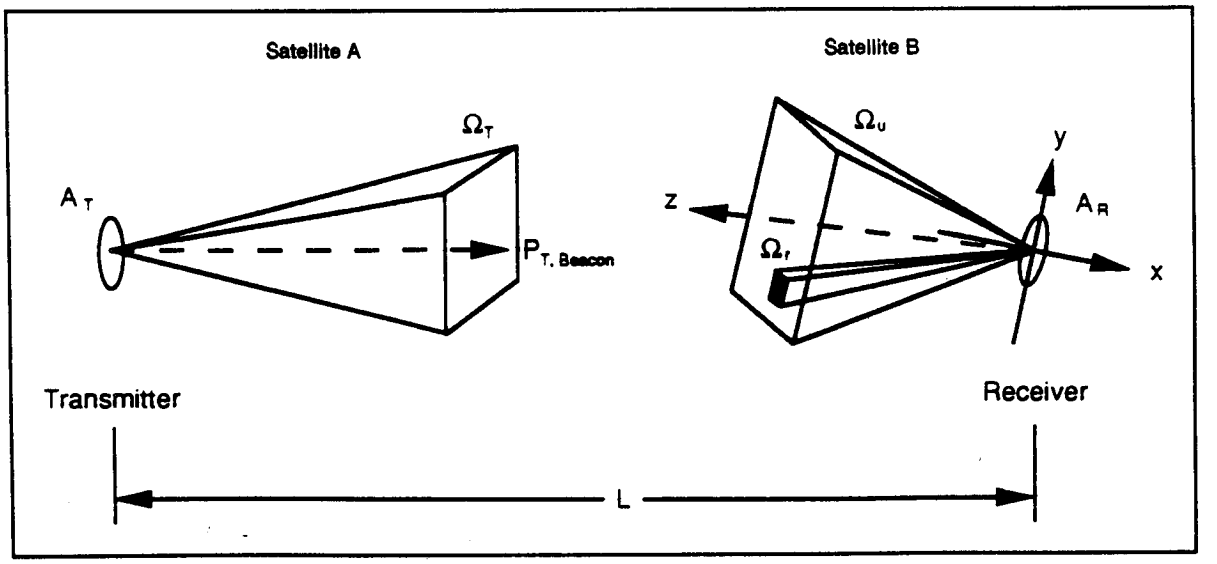

Figure 5.2-1 Acquisition-Phase Parameters

Within the scope of this study we are interested in satellites engaged in duplex communication. Therefore, two-way acquisition must be used.

5.2.2 Two-Way Acquisition

A beacon is used to illuminate the target satellite to give it a signal on which to align its receiving optics. There are two basic ways to direct the beacon onto the target:

Static Wide Beacon

A single wide beam illuminates the entire region of uncertainty in the partner position (typically $\pm 0.2°$). A high power beacon is required.

Scanning Beacon

A narrow beacon scans the region of uncertainty in the partner's position. Scanning stops when the partner senses the beacon and returns its own beacon in the determined direction. This is the approach used by SILEX. A more complex beacon pointing and scanning system is needed for this approach.

In both cases the link acquisition sequence follows these steps:

(1) When the beacon of satellite A falls within the uncertainty field of view, Ω_u, of the partner satellite B, satellite B can acquire the beacon.

(2) During this acquisition, satellite B reduces the uncertainty of the position of satellite A to the resolution field of view, Ω_r. Satellite B can now track satellite A to high precision.

(3) In order for satellite A to do the same, satellite B now sends a beacon back to satellite A with a beam width solid angle of no less than Ω_r. Since this beacon is narrower than that of satellite A it can be of lower power.

(4) When satellite A detects the beacon of satellite B, the uncertainty of satellite B's position will be reduced to the resolution field of view.

(5) Satellite A can now turn off its beacon laser and turn on its communication laser using the narrower Ω_r field of view.

(6) On sensing the communication laser, satellite B can likewise shut down its beacon and begin to use its own communication laser.

(7) Link acquisition is now complete and mutual link lock is maintained by the tracking and pointing systems.

A slight variation to the above is possible on noting that satellite B's beacon requires a beam divergence similar to that of its communication laser. Satellite B's beacon function could therefore be performed by its communication laser. SILEX uses this approach.

5.2.3 Beacon Characteristics

There are a number of characteristics which specify the beacon and its usage. Principal among these are the beam width, the optical power, the laser lifetime, and the beam deflection properties. Other characteristics such as the optical wavelength, and whether the beacon is pulsed or continuous typically follow from those. The system design could also call for a modulated beacon to provide a signature and other information to the partner.

The beam width is driven by the power required by the acquisition detector, the power available from the beacon laser, and the maximum desired acquisition time. The magnitude of the optical power is determined by the link equation, which cast in terms of beacon power is:

$$P_{BT} = K\frac{P_{BR}^{*}\theta_B^2 L^2}{A_R} \qquad [5.2.3\text{-}1]$$

where

P_{BT}	=	Transmitted beacon power by laser
P_{BR}^{*}	=	Received beacon power required at detector
θ_B	=	Beam width
L	=	Length of the optical link
K	=	Constant representing all other terms in the link equation
A_R	=	Receive Telescope Aperture Area

The largest practical beamwidth is one which covers the entire uncertainty cone. In that case $\theta_B=\theta_u$. The smallest beamwidth would be that of the communications beam, θ_c, in which case the communications laser would also serve as the beacon.

Clearly, because of the θ_B^2 term, the power required to illuminate the entire uncertainty cone, which can be up to 0.5 degrees wide, can be very high. It is impractical to use a defocused communication laser for this purpose since the communication laser is optimized for sustained narrow beam operation. Therefore, if the entire uncertainty cone is to be illuminated a special high power beacon laser is required.

If the communications laser were to be used as a beacon, then it must be scanned over the uncertainty cone. The maximum expected time to perform such a scan will be discussed in the acquisition performance section, but essentially this time is proportional to the ratio of the uncertainty cone solid angle to the beacon solid angle, or $(\theta_u/\theta_B)^2$. Since uncertainty cones are typically about 5000 μrad across and communications beams are about 10 μrad across, the acquisition times experienced with this approach can be prohibitive.

A compromise approach would be to use a high power beacon of a diameter that is a substantial fraction of the uncertainty cone, and then scan the cone during acquisition. That is the approach used by SILEX where a 700 μrad beacon integrating the output of 19 laser diodes scans a 7000 μrad uncertainty cone. In order to boost the power available from the source, it may be possible to pulse the beacon. This kind of approach, using a Nd:YAG laser, was employed in the Air Force Space Communications Flight Test [102]. However, one must be careful to integrate the power over exposure period taking into account pulse duration since modern semiconductor acquisition detectors are sensitive to the energy received over an integrated time interval, not the instantaneous received power. Where ground based systems are concerned there is, of course, much more latitude in the choice of laser sources in order to achieve high output power. An example is the Argon laser beacon used by ETS-VI [103].

The required beacon lifetime is a serious consideration driving the selection of the beacon laser technology and output power. Typically the higher the laser power the shorter its lifetime. The minimum required beacon life can be estimated quite simply:

Min. Lifetime = (Mean Acq. Time) × (No. of Acq. Cycles during the Mission Life) [5.2.3-2]

In a GEO to LEO link the minimum acquisition rate is driven by the eclipse of the LEO orbit by the Earth. For example, a 90 minute LEO orbit being eclipsed every orbit would result in an acquisition cycle every 90 minutes. This would total to 29,000 acquisition cycles during a typical 5 year mission life. At the 2 minute maximum acquisition time reported by SILEX this would result in a approximate required beacon life of 1000 hours.

In the GEO to GEO case there is no eclipse of the link. The acquisition rate here is driven by the noise in the pointing and tracking systems. The principal drivers influencing the rate are then the link burst error probability, P_E^*, and the bandwidth of the pointing and tracking systems. For example, if $P_E^*=10^{-6}$ and the bandwidth is 1 kHz, it will be shown later that approximately 40,000 acquisition cycles occur over a 5 year lifetime. Therefore for a SILEX type system a 1333 hour beacon lifetime would be needed. This figure can be readily improved since the acquisition rate is directly proportional to P_E^* and the system bandwidth.

The characteristics of the beacon deflection system become a consideration when the beacon beam width is less than the uncertainty cone, and the beacon must be scanned. The maximum deflection angle in azimuth and elevation required for the scan, assuming a circular cone and beam, is the difference between the cone width and beacon width, $(\theta_u - \theta_B)$. The angular resolution, or step size, required to produce an overlapping scan is less than or equal to the beacon width. Therefore the deflection resolution of the scanning-mirror system must be

$$\leq M_B\theta_B \qquad [5.2.3\text{-}3]$$

with a deflection range of

$$M_B(\theta_u - \theta_B) \qquad [5.2.3\text{-}4]$$

Where M_B is the beacon optical system equivalent magnification up to the deflection mirror.

If the same optical system, such as the telescope optical assembly, is used for both the beacon and the tracking/pointing systems then $M_B = M_{Track}$. This will result in a great difference in the tolerances required of the tracking system and those required of the beacon deflection system. For example in SILEX the beacon deflection range is approximately 6300 μrad, but the tracking system has a 34 μrad field of view. Likewise the beacon divergence is as large as 700 μrad, but the tracking system precision is 0.1 μrad. Therefore, the requirements on the beacon deflection mechanism can be radically different from those imposed on the tracking and pointing system. Consequently it can be very difficult to integrate both functions into the same deflection assembly, and separate assemblies may be a better solution. SILEX chose to integrate the assemblies and did so by effectively stacking two deflection assemblies, a coarse and a fine, on top of one another.

5.2.4 Acquisition Detectors

The acquisition phase always involves searching for the partner beacon within a wide field of view (FOV). In SILEX, for instance, this FOV is 1050 μrad (0.06°) for the GEO satellite and 8500 μrad (0.49°) for the LEO satellite [104]. The ETS-VI experiment has an 8000 μrad (0.468°) acquisition FOV [103, 105]. A U.S. Air Force/McDonnell-Douglas experiment [102] had a 17,453 μrad (1°) FOV for the GEO satellite and 3491 μrad (0.2°) FOV for the ground station.

A number of detector designs can be used to monitor this large field of view for the beacon signal. The kind preferred at present is the CCD detector array. Both SILEX and ETS-VI use a CCD array, that of SILEX being an array of 288×288 pixels with 23 μm pixel size. The Hughes study [106] proposed use of a Silicon PIN Quad detector for the GEO acquisition sensor, and a Silicon array for the LEO sensor. Interestingly the older (1978) Air Force/McDonnell-Douglas experiment uses an Avalanche Photo-Diode (APD) quad-de-

tector formed by arranging four APDs about a pyramid mirror as part of a two stage acquisition method incorporating a Wide-Field detector (WFD) and a Narrow-Field detector (NFD) both of similar design.

The CCD array has the advantage of providing very precise information about the location of the beacon within the field of view. Furthermore, if the pixel size and number are selected appropriately, the field of view monitored by a single CCD pixel, or small group of pixels, can correspond to the angular resolution of the tracking detector. In this case, acquisition is a simple three step process of detecting the beacon, aligning it to the tracking detector axis, and then handing control over to the fine tracking detector. The principal drawback to the CCD is that it has many pixels that must be read serially and then processed by an acquisition algorithm. This can be a time consuming process when compared to the simple processing required of a four element quadrant detector, and could therefore miss a fast moving beacon. However, through judicious system design the beacon scan rate can be adjusted to match the CCD-acquisition processing capability. Also, the speed of modern electronics to process the CCD information is increasing. CAL Corp., for example, has a versatile space-qualified CCD acquisition and processing product suitable for this application.

5.2.5 Performance of the Acquisition System

The Principal measure of acquisition performance is the acquisition time:

$$T_a \geq T + T_p + T_s \qquad [5.2.5\text{-}1]$$

where

- T_a = Acquisition Time
- T = exposure time of the detector used
- T_p = processing time to read the detector and decide on an action
- T_s = time for the beacon to scan into the field of view

A typical value of T_a is 20 seconds.

Another performance measure is the acquisition probability. This is the probability of achieving a successful acquisition in one attempt. It tends to increase with the received signal energy and decrease with the number of detector elements (however, increasing the number of detector elements improves the precision of the determination of the partner position during each acquisition cycle).

The performance of acquisition systems generally depends on the received signal energy, E_r, the average energy in the set of background sources, E_{bj}, and on the number of detector resolution cells, N. Ideally, the received optical signal energy will focus onto a single cell if the resolution angle is much greater than the telescope diffraction-limited field of view, $\Omega_r > \theta_f^2$ (The minimum telescope resolution angle). The optical energy into a telescope resolution cell of an N cell array can then be expressed as:

Signal: $$E_r \approx \frac{P_t A_r T}{\Omega_{ut} L^2} \qquad [5.2.5\text{-}2]$$

- Pt = signal power uniformly distributed over Ω_{ut}
- A_r = receive telescope aperture area
- L = total path length
- T = exposure time

Background: $$E_{bj} \approx P_{bj} T \qquad [5.2.5\text{-}3]$$

- P_{bj} = background power into cell j

For small Ω_r:

$$P_{bj} \approx A_r \cos\theta_j \int_{\lambda}^{\lambda+\Delta\lambda} \left(L_e(\lambda)\Omega_{rj} + \sum_{i=1}^{I_f} H_{ei}(\lambda)\right) d\lambda \qquad [5.2.5\text{-}4]$$

Where:

- $L_e(\lambda)$ = spectral radiance of the continuous background radiation into Ω_{rj}.
- $H_{ei}(\lambda)$ = spectral radiance of a point source i (e.g., stars) into Ω_{rj}.

I_j = Total number of point sources included in the jth cell resolution angle, Ω_{rj}.
λ = wavelength of light
θ_j = angle between cell j and the centre of the lens plane.

T now becomes a design parameter that is chosen sufficiently long that $(E_r + E_{bj})$ will exceed the signal detection threshold of a resolution cell.

The detector cell diameter needed to cover the resolution angle Ω_r is approximately $f_r\sqrt{\Omega_r}$. Where f_r is the receiver optical system equivalent focal length. The total number of array cells needed to cover the uncertainty region is $N=\Omega_u/\Omega_r$. Therefore an array of detector elements can be used to collect power simultaneously from each non-overlapping resolution solid angle within the uncertainty region; or, alternatively a lesser number of detector cells can be scanned sequentially over the uncertainty region. In the latter case, if M cells participate in the scan then the new scanning acquisition time becomes:

$$T_{as} \leq \frac{N}{M}(T + T_p) + T_s \qquad [5.2.5\text{-}5]$$

The inequality, $\leq$, is intended to indicate the dependence of T_{as} on the scanning algorithm employed. If the algorithm can terminate any time during a scan on the condition that the M-cell array detects a beacon signal then the total time is less than the above left hand side. Optimizing T_{as} would require knowledge of the statistics of the likely position of the beacon signal within the field of view. Intuitively the most likely position would be at the centre of the field of view, in which case a spiral scan pattern beginning from the centre may be the optimal choice. Lopez and Yong [6] have analyzed a number of square and spiral search patterns and estimated the resulting acquisition times.

Another possible acquisition strategy involves a series of zooming steps where the receiving optics is zoomed onto the acquired beacon. Initially the entire uncertainty region is observed and a coarse acquisition decision made of the beacon position. With each zooming step the optics narrow the field of view about the previous step's position determination. At the final step the resolution field of view, Ω_r, is achieved. At each zoom step less background energy enters the detector while the signal energy remains constant. The signal to noise ratio, therefore, increases with each step and with it the acquisition probability increases. The total acquisition probability for an S step search now becomes:

$$P_a = \prod_{i=1}^{s} Pa_i \qquad [5.2.5\text{-}6]$$

where Pa_i is the acquisition probability of the i^{th} acquisition step.

With zooming, the acquisition time increases because there are now S zoom steps:

$$T_{az} >+ T_{pf} + \sum_{i=1}^{s}(T_i + T_{zi}) \qquad [5.2.5\text{-}7]$$

where:

T_{pf} = processing time for the final decision step
T_{zi} = time to perform zooming step i
T_i = exposure time for the i^{th} step

If the target is drifting across the receiver's field of view the acquisition times in all of the above techniques must be chosen small enough to prevent drift of the target out of the field of view before a positive acquisition decision is made and ISL control is handed over to the tracking system.

5.2.6 Example Techniques

5.2.6.1 Silex

The SILEX system is intended to operate between a LEO terminal on the SPOT4 satellite and a GEO terminal on the ESA ARTEMIS satellite. The SILEX acquisition method progresses through a series of four phases illustrated in Figure 5.2-2.

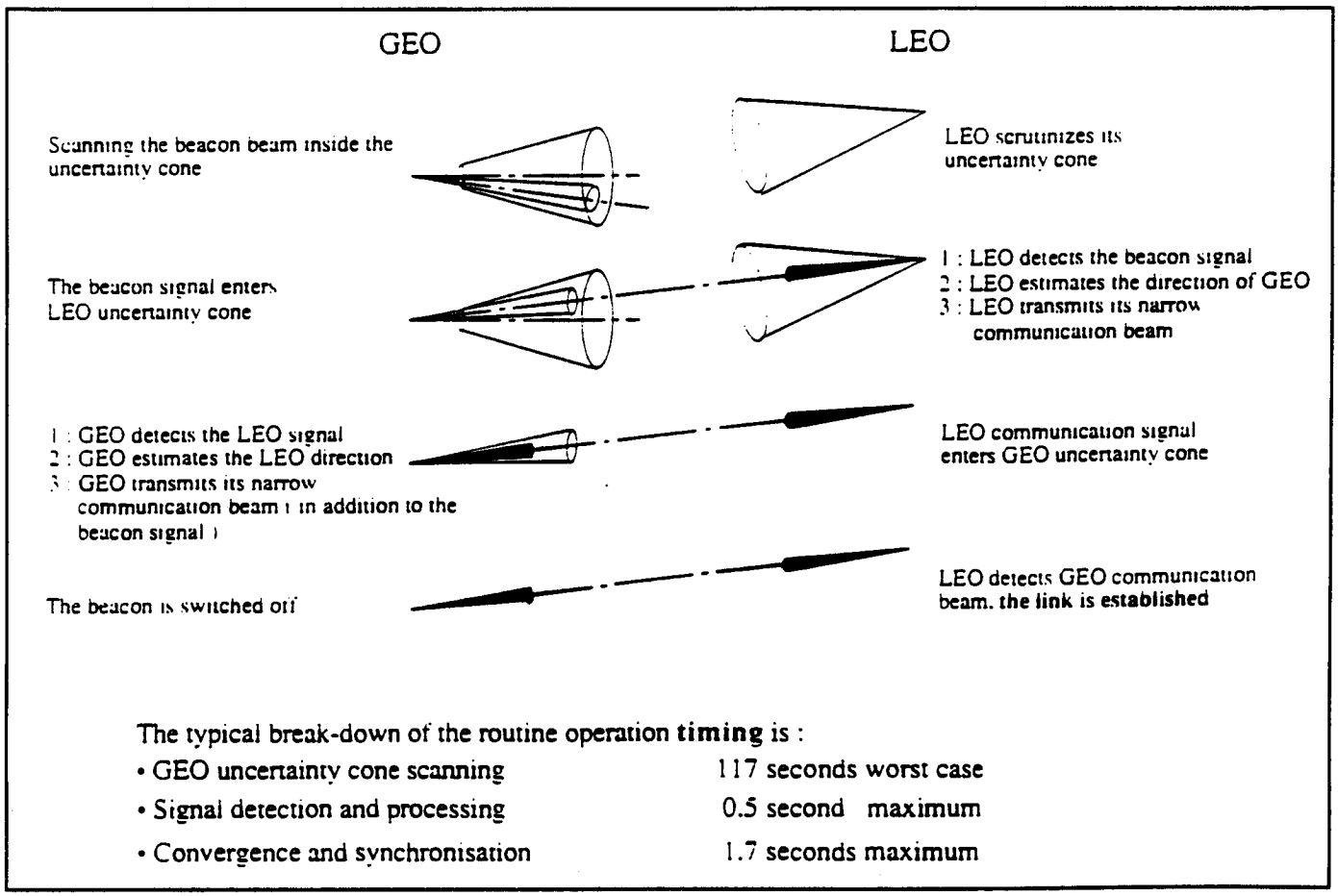

Figure 5.2-2 SILEX Acquisition Strategy

Phase 1

The GEO terminal transmits a 700 μrad wide acquisition beacon signal and scans it across its 1050 μrad uncertainty cone.

The LEO terminal monitors its 8500 μrad uncertainty cone with its wide field, 288'288 pixel CCD acquisition detector.

Phase 2

When the LEO terminal is hit by the beacon, it aligns its line of sight with the incoming signal source. This is done by noting the beacon position on the CCD wide field detector and then aligning the beacon signal onto a 240 μrad field of view, 14×14 pixel CCD fine tracking detector. The signal is then "rallyed" to the centre of this detector where the system then starts tracking the beacon, within a 34 μrad field of view, using the central four pixels as a quadrant detector. The LEO then transmits an 8 μrad communication beam towards the GEO terminal taking into account the required point-ahead offset angle.

Phase 3

When the GEO terminal detects the LEO signal, it stops scanning its beacon beam, and starts tracking the incoming beam using a similar 14×14 pixel CCD fine tracking detector. It then turns off its wide-beam beacon and also transmits a narrow, 8

μrad, communication beam with an adequate point-ahead.

Phase 4

The narrow, higher power density communication beam reaches the LEO satellite. The higher power available at the LEO terminal permits it to improve its tracking and pointing performance up to a specified 0.1 μrad accuracy. This likewise increases the average optical power received at GEO allowing it also to improve tracking and pointing performance.

Acquisition is now complete and communication may be initiated.

The total time taken for this sequence is expected to be less than 120 seconds.

5.2.6.2 ETS-VI

The Japanese Engineering Test Satellite-VI (ETS-VI) experiment consists of a laser communication link between the ETS-VI satellite in GEO orbit and a ground station in Japan [105]. A great deal of laser power is therefore available at the ground station, which makes this part of the link less characteristic of a true ISL.

The acquisition sequence followed is:

(1) The ground station directs a 100 μrad wide 0.51 micron argon laser beam at the expected ETS-VI satellite position.

(2) At the satellite, the course pointing assembly scans a $\pm$1.5 degree region of uncertainty in ground station position with an 8000 μrad field of view acquisition CCD until it detects the beacon. The CCD is able to locate the beacon to a precision of 32 μrad.

(3) The satellite then turns on a laser diode and directs a 60 μrad beacon beam back at the ground station.

(4) The ground station detects the satellite beacon and narrows its beacon width to 20 μrad to increase the power density at the satellite, and then tracks the satellite to 1 μrad accuracy.

(5) The satellite aligns the beacon signal on a quadrant fine tracking detector with a 400 μrad field of view and 2 μrad pointing accuracy.

(6) The satellite now narrows its beacon beam to a final 30 μradian width.

(7) On confirmation of stable tracking, the link is considered established and the beacon lasers are now used for communications.

5.2.6.3 Air Force Space Communications Flight Test

McDonell-Douglas Astronautics Company and the U.S. Air Force investigated the design of a laser communications system between a GEO satellite and a ground station [102]. This confers a similar power advantage to the ground station laser as that of ETS-VI.

The acquisition sequence followed is:

(1) The ground station raster scans a 300 μrad laser beacon over the $\pm 0.1^{\circ}$ satellite uncertainty region. The beacon is a pulsed Nd:YAG laser modulated with a 10.5 kbit/sec signal for beacon identification and low data rate information uplink.

(2) The satellite observes a $\pm 0.15^{\circ}$ uncertainty region with its wide field detector (WFD). When the WFD senses the beacon, the signal is aligned on a Narrow Field Detector with a 500 μrad field of view and $\pm$50 μrad tracking precision.

(3) The satellite sends a 100 μrad wide beacon down to the ground station.

(4) The ground terminal detects the satellite beacon and centres the signal on the acquisition and

tracking detector and corrects pointing errors such that the transmitter is centred in the scan pattern. When the satellite's beacon is confirmed to be correctly centred, the ground station will stop scanning its beacon.

(5) The ground terminal continues to monitor the satellite beacon until the precision of its position is confirmed to be within ± 15 μrad. The Ground station then narrows the beacon beamwidth to 15 μrad.

(6) The increased beacon power density enables the satellite to enter tracking mode by passing beacon tracking to a Fine Tracking quadrant detector which can track the ground station to ± 0.6 μrad precision. The satellite now narrows its beam width to 5 μrad.

(7) The increased satellite beam power density enables the ground receiver to enter tracking mode with ± 5 μrad precision.

(8) Mutual communication between the two satellites can now begin.

Simulation indicated that the mean acquisition time should be 2.9 seconds, with a maximum of 9 seconds.

5.2.6.4 Ball Aerospace ISL Testbed

Ball Aerospace assembled a laboratory testbed to investigate laser acquisition and tracking system design issues [108]. This testbed is included here because they proposed an interesting "composite" scan acquisition technique. This technique proceeds as follows:

(1) The receiver assembly in the lab is illuminated by a static beacon laser.

(2) To locate the beacon a motorized coarse steering mirror at the receiver performs a spiral search, beginning at the centre of the uncertainty cone, in a series of discrete steps.

(3) At each coarse step position a pair of fine steering mirrors performs a raster scan search for the beacon signal.

(4) When the beacon is detected on a coarse "lateral effect cell" and on the fine tracking quadrant detector all scanning stops.

(5) Control now switches to a closed loop tracking mode.

The technique is interesting because it is the only one in which the fine tracking detector participates in the acquisition process. The transition from acquisition to tracking mode can therefore be done very quickly thereby alleviating concerns about drift of the partner out of the tracking field of view during acquisition.

5.2.7 Recommendations

All of the acquisition methods discussed have merit. The deciding factors in choosing a particular approach are the performance in terms of acquisition time and probability, and the overall complexity of the design which will impact cost and reliability. The SILEX approach is very elegant in that it makes efficient use of a beacon and communication laser, and has the tracking CCD participate in the final stages of acquisition. This effectively operates like the Ball Aerospace technique without the need to scan the acquisition detector over the acquisition field of view. However, the Ball approach devotes only tracking hardware to the acquisition function thereby simplifying the design.

Consequently, the optimal approach, from the standpoint of minimizing hardware complexity, is to equip the two satellites with different acquisition hardware. Like SILEX, only one satellite needs a beacon. Let this be satellite A. The beacon can be locked to the telescope and thereby pointed using the telescope coarse pointing assembly. The other satellite, satellite B, does not need a beacon since when it detects the beacon it can determine the partner location to high precision and use the communication laser as the return beam. Instead of a beacon, satellite A needs acquisition detectors to locate the partner to the required precision. Here again, a modified SILEX ap-

proach appears the most attractive. A wide field CCD acquisition detector can be locked to the telescope assembly having light directed onto it with a mirror. This mirror will, however, contain a hole in its centre of a diameter corresponding to the fine tracking detector field of view. The tracking detector is also a CCD. When the beacon signal falls on the acquisition detector the telescope assembly is steered so as to align the signal with the system optical boresight. When the signal enters the fine tracking field of view it penetrates the hole in the acquisition mirror falling on the fine tracking CCD. The fine tracking subsystem then proceeds to align the optical system to sufficient precision to allow the communication laser to be pointed accurately back to satellite A. Therefore, the acquisition strategy for satellite B consists of statically monitoring its cone of uncertainty until illuminated by the beacon, and then returning the communication laser signal when the beacon is detected.

The acquisition function of satellite A consists of scanning its uncertainty cone with the beacon laser. Satellite A, however, does not need a dedicated acquisition detector. Instead a Ball-like strategy can be employed where the fine tracking detector participates in the acquisition process. Essentially, the fine tracking detector monitors the region of the sky illuminated by the beacon for signs of the returning communication signal. Since the beacon is locked to the telescope, the tracking detector is inherently aligned with the outgoing beacon. The fine tracking detector however, has a narrow field of view compared to the size of the uncertainty cone so the angular beacon/detector scan rate must be adjusted so that the return signal does not miss the detector. For instance, over GEO to LEO distances the round-trip propagation time, and hence the minimum time a response can be expected from the partner, is about 250 msec. The detector must therefore dwell on each region of the sky for at least this amount of time to be assured of seeing the return signal. The response time of the tracking detector to the communication laser signal is necessarily very fast, on the order of milli seconds. When the satellite B signal is detected then satellite A switches its communication laser on and the beacon off.

The benefit of this approach is simplicity. Satellite A has a beacon but no dedicated acquisition detector. Satellite B has a dedicated acquisition detector but no beacon. Each terminal is therefore lighter and more reliable than if they were identical. The drawback is that the acquisition time may be longer than would be the case if satellite A also had an acquisition detector. For instance with a 1° initial uncertainty cone and a 400 μrad tracking detector field of view (recommended in section 5.4) the minimum acquisition time would be almost 8 minutes. However, if the initial uncertainty cone could be reduced to 0.25°, which is reasonable, then the minimum acquisition time would be only 30 seconds.

5.3 Tracking

5.3.1 Introduction

Once the acquisition subsystem has located the partner satellite it is the purpose of the tracking subsystem to maintain alignment of the receiver optical axis with the propagation direction of the incoming signal beam. Tracking this incoming beam to high precision is necessary in order to minimize the receiver's field of view and thereby maximize the signal to background optical power ratio, and also to permit accurate pointing of a narrow transmit beam back to the partner.

Figure 5.3-1 shows the elements of the tracking function. The tracking function shares most of the optical path with the communication function. Indeed, most proposed implementations direct a fraction of the communication beam to the tracking detector. The exceptions [109] use a beacon at a wavelength different from the communication beam for tracking. In this case a dichroic beam splitter redirects only the beacon energy to the tracking detector.

The first component of the subsystem is the receive telescope of diameter D_R which is mechanically steered by the Coarse Tracking Assembly (CTA). The telescope directs the received light into the Fine Tracking Assembly (FTA) which includes the Fine Tracking Mechanism (FTM) and the Fine Tracking Detector (FTD). The signals from the FTD drive the control

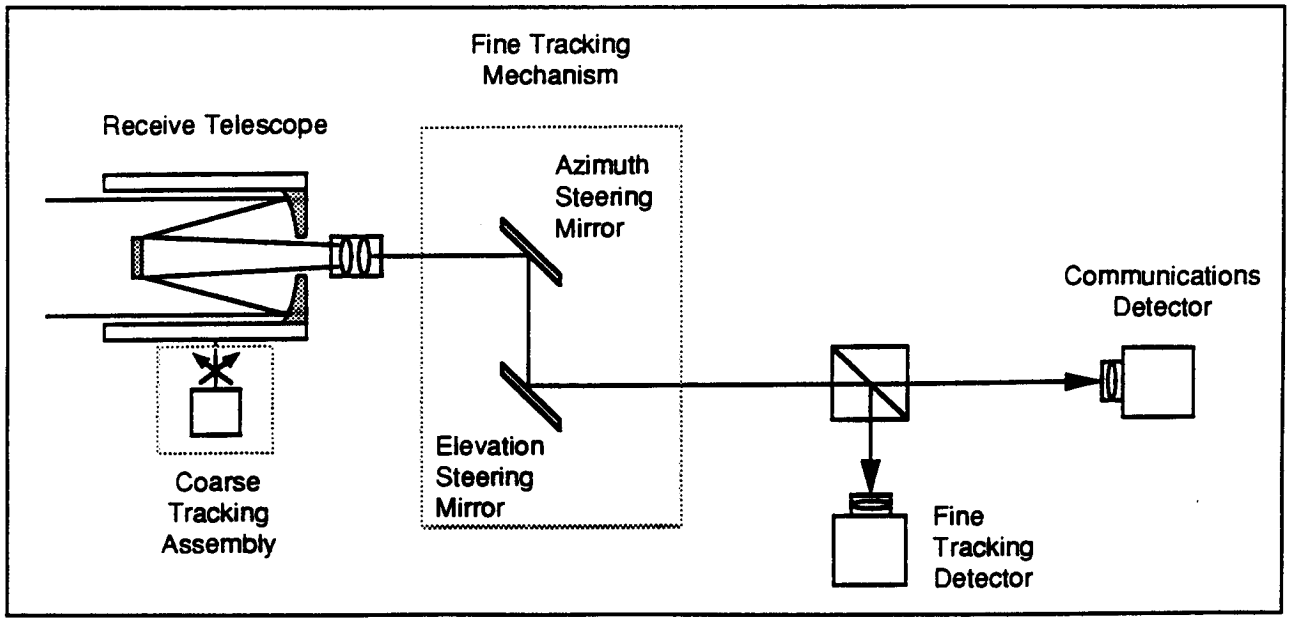

Figure 5.3-1 Tracking Function Elements

electronics to adjust the CTA and FTM in order to maintain the received signal centred on the FTD which is also aligned with the communications detector. In this way stable alignment by the tracking subsystem translates into stable, uninterrupted reception of communication data. Loss of track-lock by the tracking function results in total loss of received communication which is perceived by the communication function initially as a burst error [110], and then as a sustained communications dropout. Once lock is lost by the tracking function the acquisition function must be reactivated in order to reacquire the partner satellite.

5.3.2 The Tracking Assemblies

In many of the published ISL systems there is an overlap of the optical path between the tracking function and the pointing function. In that case the various assemblies required to track the incoming beam are referred to as pointing assemblies. This is because they point the receiver and transmitter optics at the partner satellite. However, the approach taken here is to present a general analysis of the system requirements. The tracking and pointing functions have, therefore, been separated and will be treated in isolation. They may be united later after overlaps in their functional requirements are identified.

5.3.2.1 Coarse Tracking Assembly

The principal responsibility of the CTA is movement of the receive telescope to keep the optical system axis aligned to the partner satellite's signal over the full range of motion available to the telescope, and to the precision needed to keep the signal within the dynamic range of the Fine Tracking Assembly. The CTA also compensates for large amplitude, low frequency platform motions. The CTA typically consists of a 2- or 3-axis gimballed telescope or flat mirror (the ETS-VI approach), a relay optics assembly, gimbal angle sensing devices, and gimbal servo drive motors.

The range of motion of the CTA is determined by the range of travel of the partner satellite in the local coordinates. This range is the smallest for the GEO to GEO case where the two satellites are essentially fixed with respect to one another. For the GEO to LEO case, the GEO satellite only needs a small range of motion, but the LEO satellite may need to track over almost an entire sphere. The most demanding case is

for the GEO to Tundra/Molnya link where both satellites track over a large range.

The orbit parameters are discussed in Section 2 with detailed graphs given over a 24 hour period for a number of examples in Appendix A. An examination of the curves in the Appendix show that for some cases the telescope must be pointed over a wide angular range. A problem in telescope placement arises when the required elevation range includes large negative values and large positive values. In this case, the satellite body will inevitably get in the way, and so at least two telescopes are required.

The angular rates for both terminals have been calculated and are presented in Appendix A. These rates are very small except in the case when the cooperating terminal passes close to the azimuth axis (keyhole). In this case the azimuth angle must change by the order of 180 degress in a short time, with the allowed time decreasing the closer the path gets to the azimuth axis. The rate can be kept small by mounting the telescope do that the keyhole points away from the region occupied by the other terminal.

Assuming that the key hole can be avoided the required tracking rates will be very slow and hence not very demanding of the tracking assembly. Perhaps more demanding are the local librational and platform vibration motions of the satellite. The high frequency, low amplitude motions will be compensated by the FTM. The CTA must compensate the remaining high amplitude low frequency motions. Most satellites are not expected to librate unless disturbed, but some residual motion non-the-less remains which can not be eliminated by the attitude control system. This residual motion would generally be of the same order as the above relative-motion rates, and, therefore, be readily compensated. However, should the optical ISL be required to track during rapid satellite attitude manoeuvers then the CTA tracking rates must be specified accordingly. As an example, the Hughes study [106] specified CTA gimbal requirements of 200 μrad (0.011°) per second angular rate, and up to 1 μrad per second^2 angular acceleration.

The angular resolution required of CTA motions will be determined largely by the tracking range of the FTM. Essentially, when the FTM tracks the signal to the limits of its mechanism then the CTA must move the telescope assembly one step in the appropriate direction. This step size must be less than the FTM track range in order for the FTA to maintain an uninterrupted lock on the signal. This resolution step size is determined by:

$$\textit{CTA Resolution} \leq \frac{\textit{Angular Range of FTA Tracking Optics}}{\textit{Magnification of Optical System up to the Tracking Optics}}$$

[5.3.2.1-1]

In actuality, the CTA resolution is considerably better than required by the above relationship. In ETS-VI the CTA accuracy is 32 μrad, but the external, before magnification, fine tracking range is $\pm$454 μrad. In SILEX the CPA accuracy is 174 μrad, and the external fine tracking range is $\pm$800 μrad for the LEO satellite and $\pm$457 μrad for the GEO satellite (the two telescopes use different magnifications), an even wider range is specified for the acquisition scan.

5.3.2.2 Fine Tracking Assembly

5.3.2.2.1 Fine Tracking Mechanism

The principal function of the FTM is to keep the received optical signal aligned onto the communications detector. Since the detector is typically in the order of 100 microns across with a lens about 15 mm wide and with the FTM usually located many centimetres away from the detector, very precise alignment is required. In order to maintain this alignment the FTM must track the receive beam over an angular range at least as large as the angular precision of the CPA. It must also maintain the alignment while the CPA is in motion. Furthermore the FTM also functions to compensate for high frequency (up to 1 kHz) platform disturbances.

As seen in Figure 5.3-1, the FTM resides in the afocal part of the optical network between the telescope optics and the detectors for tracking and communica-

tions. The preferred method of deflecting the optical beam is with moveable mirrors. Two mirrors can be used to individually control the azimuth and elevation deflections, or a single two-axis mirror can be used for both deflections.

The FTM range of motion is linked to the CTA precision according to the previous CTA resolution formula. The exact range is determined through trade-off of a number of considerations. Generally, the larger the FTM motion amplitude, the poorer its precision. and frequency response. However, a large FTM range means a relaxed CTA resolution requirement. Therefore, this is a trade-off between a more expensive CTA or a more expensive FTM. Reliability is another factor. Because the CTA is a moving, motorized assembly, but the FTM is usually solid state, the CTA is considered less reliable. It is, therefore, desirable to move the CTA as infrequently as possible. Another reason to minimize CTA motions is that the CTA moves a massive telescope which can impart disturbances into the host platform.

Basically, it is desirable move the FTM over a wide angular range to high precision. The trade-off of the previous considerations will determine the selection of specific FTM and CTA characteristics. The angular range selected will impact the design of the telescope optical assembly. The field of view of the telescope during tracking magnification must match or exceed the FTM range according to the relation:

$$FOV_{Track} \geq \frac{FTM\ Range}{Magnification} \qquad [5.3.2.2\text{-}1]$$

in order for the partner signal to be detectable over the full range. Another consideration driven by the range is the size and placement of the FTM from the telescope assembly exit pupil. This determines the size of the FTM mirror according to:

$$FTM\ Width \geq \frac{Exit\ Pupil\ Diameter + Angular\ Range \times Distance\ Pupil}{\sin(mean\ inclination)} \qquad [5.3.2.2\text{-}2]$$

Figure 5.3-2 illustrates these parameters. Since, from a frequency response consideration, it is desirable to minimize the FTM size, it is therefore also desirable to locate the FTM as close to the exit pupil as possible.

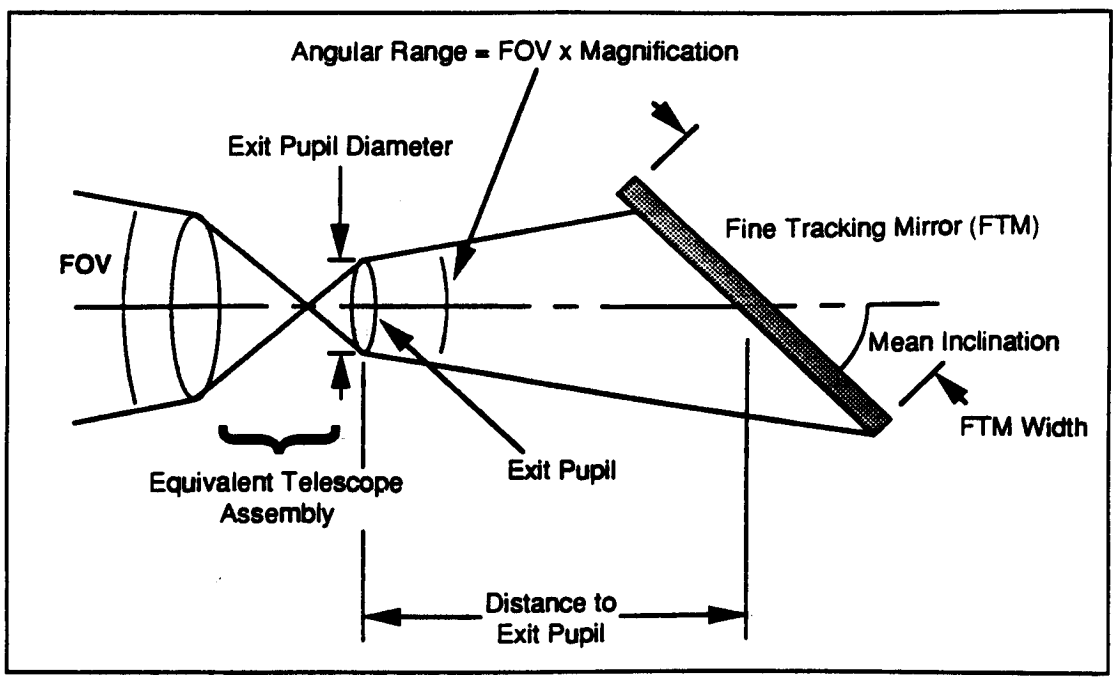

Figure 5.3-2 FTM Size Calculation

The precision of the FTM from tracking considerations alone is determined by the size of the communication detector assembly. However, the final ISL system design may call for the FTM to also perform the pointing of the transmit beam which has additional requirements. The influence of the communications detector can be seen in Figure 5.3-3. The communications detector of diameter d_c has associated optics of equivalent focal length f_c. To insure that the signal stays focused on the detector, the angular range of the optical signal in the afocal path cannot exceed

$$2\,arctan\left(\frac{d_c}{2f_c}\right) \approx \frac{d_c}{f_c}. \qquad [5.3.2.2\text{-}3]$$

This figure is necessarily the upper bound of the FTM precision. For illustration, typical values are a 100 micron detector with 1 cm optics, which results in a 10 mrad precision.

When the FTM is also used to point the transmit beam, the precision must be such that the emerging beam will continuously illuminate the target. This requires an angular alignment smaller than the beam width. The minimum beam width is determined by the diameter of the main objective. Including the effect of magnification by the telescope assembly, the precision required to point a diffraction limited beam is:

$$< 2.44\left(\frac{\lambda}{D_T}\right) \times Magnification \qquad [5.3.2.2\text{-}4]$$

For a 10 μrad beam with 25× magnification and pointed to 10% of the beamwidth, the required resolution is 25 μrad. Clearly the pointing requirements are critical to the system design.

The final FTM design consideration is the frequency response. The determining criteria here is the bandwidth of the platform disturbances to be countered by the FTM. Ideally the FTM bandwidth should match that of the disturbances expected, but realistically there is a limit to what is achievable. That limit is in the range of 1 to 2 kHz for piezoelectric controllers. This value is determined by a number of considerations. One is the FTM mass, hence the desire to keep this mass low by making the FTM as small as possible. The other is the ability of the FTM transducers to measure the FTM position at these high frequencies and feed accurate information back to the controller. In this case both accurate phase and amplitude information is critical for stable FTM control. As an example of what is to be expected of a typical satellite platform, Figure 5.3-4 shows the disturbance spectrum for OLYMPUS [112]. The spectrum was measured using microaccelerometers onboard the spacecraft. It is seen that the spectral density ($\mu rad^2/Hz$) is of noticeable amplitude sufficient to require compensation up to 300 Hz.

Two types of actuators are typically used to meet the FTM functional requirements: piezo-electric and inductive moving coil. Piezo-electric actuators are popular for ground-based precision mirror positioning

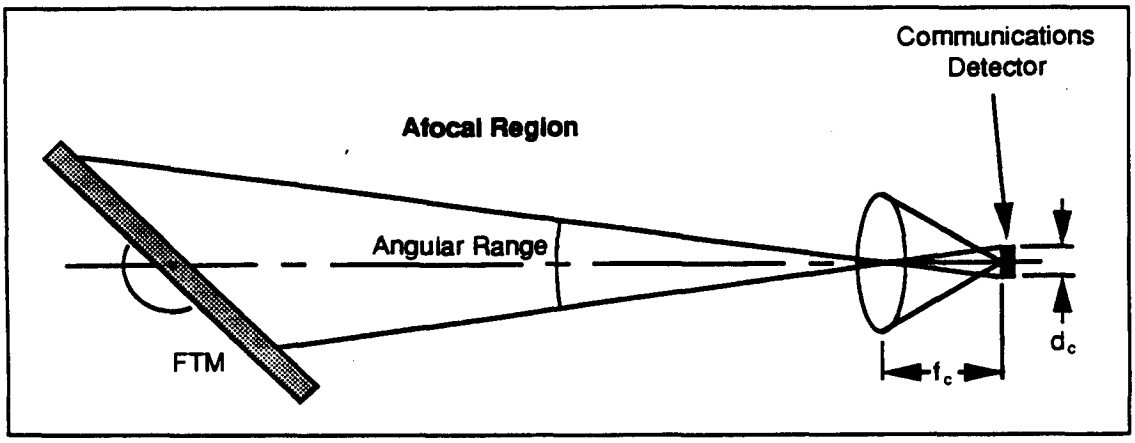

Figure 5.3-3 FTM Angular Range Calculation

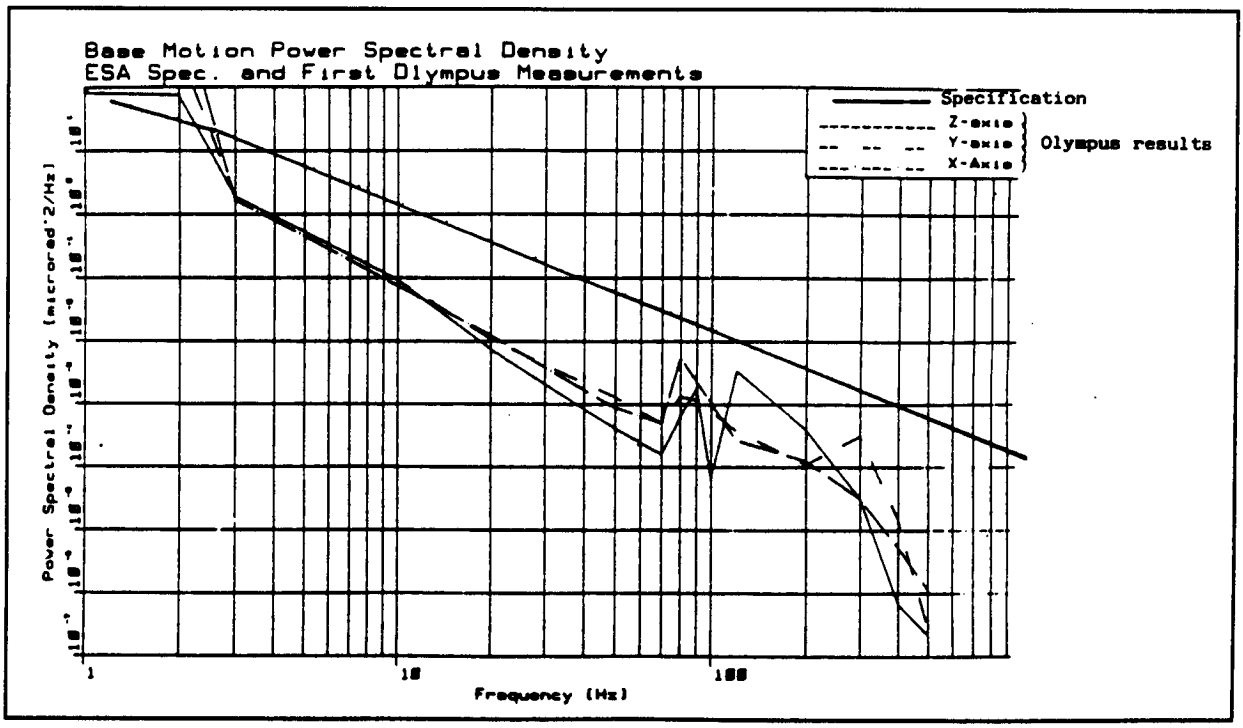

Figure 5.3-4 Spectrum of Olympus Induced Microvibrations

systems [113]. They are also receiving increasing consideration for space ISL systems [114, 115]. Among proposed systems, ETS-VI is planning to incorporate piezo-electric mirror actuators in its point-ahead assembly [116]. Piezo-electrics have the advantages of being simple, accurate, and fast. However the dynamic range is comparatively small. In order to meet the ± 160 mrad FTM range to 20 μrad accuracy of Silex, and the ± 6.8 mrad FTM range to 30 μrad accuracy of ETS-VI both systems chose to use moving coil electrodynamic actuators. In the case of SILEX, a single two-axis mirror is employed for the wide acquisition scan, fine tracking, and beam pointing. Consequently this assembly was named the Compound Fine Pointing Assembly (CFPA). Positioning control is accomplished with four axial moving coil actuators [117] coupled to inductive linear position sensors. ETS-VI separates the azimuth and elevation control functions by using two single-axis gimbal mirrors. Each is controlled by a moving coil actuator with a position sensor [103]. Ball Aerospace also designed a moving coil actuated FSM to steer a beryllium mirror for ISL applications [118]. This design was chosen as an illustrative solution by the COMSAT report [109]. In this case $\pm 2^{\circ}$ range with 80 nrad tracking accuracy and 1.2 kHz response was achieved.

5.3.2.2.2 Fine Tracking Detectors

Historically the preferred choice for the fine tracking detector is the four quadrant detector (4QD). This detector consists of a cluster of four individual detectors arranged in a 2×2 square with each measuring the optical signal intensity falling upon it. Associated signal processing electronics is used to determine the location of the centre of a light spot falling within the quadrant. This type of detector has the advantages of being simple and accurate. Also, the method of determining the spot position is well understood, as will be discussed in the next section.

Generally the detectors consist of a single monolithic semiconductor such as the Silicon photo-diode used by ETS-VI [103]. However, older systems such as the Air Force Space Communication Flight Test [102] used four Avalanche Photo-Diodes arranged about a pyramid mirror to produce the same functional effect.

An interesting variation in quadrant detector design is seen in SILEX where four pixels within a 14×14 square CCD array form the quadrant [119, 120, 121]. The actual CCD used consists of a 16×16 array where the outer pixel border is used only for calibration. Each pixel cell in this detector is manufactured to the very small size of 23 microns (the signal spot size is 11.5 microns) and has a 17 μrad field of view. This size is smaller than is typical for 4QDs (in contrast the ETS-VI tracking sensor has a 1 mm diameter [116]), and offers the advantage of a high precision position determination with a shorter equivalent focal length for the receiver optics. Unlike most 4QDs, this detector has no dead zone between the pixels. A dead zone introduces error in the spot position estimate. A drawback, cited in the past, against using a CCD for this application was that a CCD must be read and processed serially. This is an inherently slower operation than the immediate parallel processing possible with a 4QD. However, the CCD chosen for SILEX is capable of being read at 20 kHz (i.e. 20k images/second). This rate is ample for maintaining control over the 1 kHz tracking bandwidth required. In fact, the sensor is read at an 8 kHz rate during fine tracking.

An additional benefit of using a sensor with more than four pixels is that the remaining pixels can participate in the acquisition sequence. In SILEX, the entire 14×14 tracking sensor area is used during acquisition to position the signal spot near the tracking field of view. The signal is then "rallyed" to the central four pixels used for tracking. The improved resolution of the tracking CCD over the acquisition CCD implies that acquisition can proceed swiftly while the signal is still on the tracking CCD. An example is when track is lost because the signal has drifted over to the pixels near the four used during tracking.

5.3.3 Tracking Accuracy

The error in tracking the receive beam position is significant because it affects the integrity of both the received communication beam and the pointing of the transmit beam. Improper tracking alignment will lead to communication dropouts or burst errors. The error in receive beam tracking influences transmit beam pointing because the receive beam position information is used as the reference to point the transmit beam. Errors in the pointing control system are negligible in comparison to the influence of the tracking errors [122]. Noise in the received signal, the detector, and the associated signal processing circuitry result in an uncertainty in the position of the signal location. This Uncertainty is frequently expressed as an angle called the "noise equivalent angle", NEA. The NEA is defined as the angular error that produces a position error signal equal to the rms noise of the detector. In other words it is the uncertainty in the partner position due to noise in the system. It is, therefore, also expressed as the standard deviation in the partner's angular position estimate, σ_{NEA}. The subsequent analysis will focus on deriving a σ_{NEA} expression suitable for ISL.

The four quadrant detector is used not only for satellite ISL but also for optical range finders and object tracking. Consequently 4QD tracking accuracy has received much attention in the published literature. Gagliardi and Sheikh [123] examined the problem of tracking a laser beam and included the tracking control loop contribution. They also determined the influence of background noise and atmospheric scattering on the signal position estimate. Tyler and Fried [124] examined 4QD performance when used to track an incoherently illuminated object of general shape and distance in the presence of noise. The limit of a distant circular object represents the ISL case. The results give the expected variance in the signal position. Kazovsky [125] examined the application of 4QD to laser range finders and trackers where the target object tracked is illuminated by a laser source. The immediate signal processing circuitry influence was considered. He was able to determine the systematic error introduced by the circuity and the signal dependant error due to noise in the received signal.

Figure 5.3-5 shows the geometry of a quadrant detector. X_1 through X_4 represent the QD pixels with the origin of the coordinate system at the central junction. The spot position estimate is determined from the error signals formed from the difference of the individual pixel signals. From this position the signal tracking misalignment, or "error angle" can be determined.

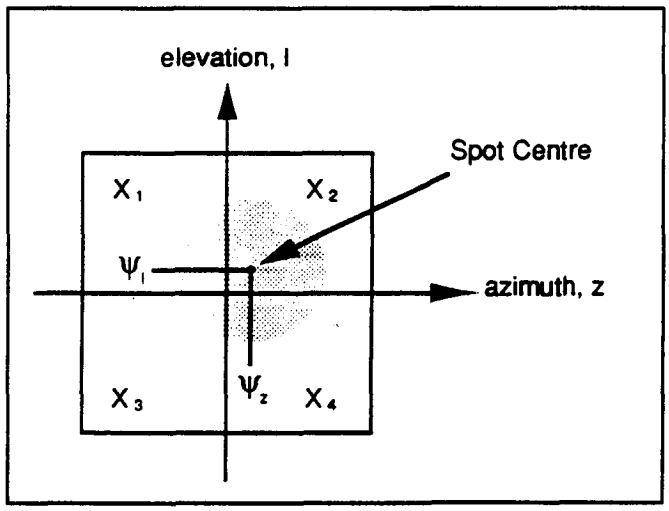

Figure 5.3-5 Quadrant Detector Geometry

The azimuth and elevation error signals are:

$$e_z = (X_2 + X_4) - (X_1 + X_3) \qquad [5.3.3\text{-}1a]$$

$$e_l = (X_1 + X_2) - (X_3 + X_4) \qquad [5.3.3\text{-}1b]$$

The "spot" coordinates are $(\psi_z f_t, \psi_l f_t)$, where

ψ = error angle
f_t = tracking system focal length.

The noise equivalent angle is the standard deviation of ψ. For a uniformly illuminated circular object of diameter b at a distance R the standard deviation of the angular measurement error was determined by Tyler and Fried to be:

$$\sigma_\psi = \frac{\pi[(3/16)^2 + (n/8)^2]^{1/2}(\lambda/D_R)}{\sqrt{SNR}} \qquad [5.3.3\text{-}2]$$

where,

$$n = \frac{(b/R)}{(\lambda/D_R)}$$

= the angular dia. of the target normalized to the resolution of the optics.

SNR = signal to detector-noise power ratio
= SNR_V^2, the square of the voltage ratio.

In the satellite ISL case n 1, therefore,

$$\sigma_\psi \approx \left(\frac{3\pi}{16}\right)\left(\frac{\lambda}{D_R}\right)\frac{1}{\sqrt{SNR}} \qquad [5.3.3\text{-}3]$$

With the exception of the SILEX detector, most 4QDs have a narrow dead zone between the pixels which generates no signal. Young, Germann, and Nelson [118] considered the dead zone contribution to the NEA and formulated a correction factor to account for its influence. The correction factor is a function of the dead zone width, dz, and the characteristic diameter of the light spot, d:

$$\sigma_\psi' = \sigma_\psi F\left(\frac{dz}{d}\right) . \qquad [5.3.3\text{-}4]$$

The correction function, $F(x)$, depends an the spot intensity profile. Two forms of $F(x)$ are offered. For a uniform intensity profile:

$$F(x) = \left(\sqrt{1 - x^2} - x\right)^{-1} . \qquad [5.3.3\text{-}5a]$$

For a Gaussian profile (where $d = 1/e^2$ diameter), which is similar to an Airy profile:

$$F(x) = e^{2x^2}\left(\int_{2x}^{\infty} e^{-t/2}dt\right)^{-1} . \qquad [5.3.3\text{-}5b]$$

Associated with the 4QD is the post processing electronics and the FTM control loop. Gagliardi and Sheikh considered the bandwidth of these, as well as background and circuit noise sources to produce the following expression for the effective tracking SNR of a point source beam:

$$SNR_t = \frac{n_s^2}{B_L(n_s + 4n_b + n_{oc})} \qquad [5.3.3\text{-}6]$$

where:

n_s = average source photoelectron count collected over the entire detector
$= \frac{\eta \lambda P_s}{h_p c}$,
n_b = average background noise photoelectron count per quadrant
$= \frac{\eta \lambda P_b}{h_p c}$,
n_{oc} = white thermal circuit noise electron count,
B_L = tracking loop noise bandwidth,
η = quantum efficiency of the detector,
h_p = Planck's constant,
P_s = received signal power,
P_b = Background Optical Power in $\Delta\lambda$ spectral passband
$= L_e(\lambda)\left(\frac{A_d}{f_t^2}\right) A_r \Delta\lambda$
for $A_d << f_t^2$, and for uniformly distributed background radiation,
A_d = Quadrant detector area,
D_R = receive telescope diameter.

The standard deviation of the tracking error can now be expressed as:

$$\sigma_\psi = \frac{\theta_{dl}}{\sqrt{\gamma}} \qquad [5.3.3\text{-}7]$$

θ_{dl} = diffraction limited field of view = $2.44\lambda/D_r$,

$$\gamma = \frac{n_s}{B_L}\left(\frac{16}{3\pi}\right)^2\left(\frac{n_s}{n_s + n_b + N_{oc}}\right) . \qquad [5.3.3\text{-}8]$$

Typical NEA values that have been reported are 0.25 to 0.35 μrad for the COMSAT study [109] and 0.07 μrad for SILEX [119].

Tracking to less than the telescope's diffraction limited resolution is possible when $\gamma > 1$. This capability is demonstrated in the SILEX design where the signal spot size is 11.5 microns, representative of the telescope's resolution, but the tracking detector surface accuracy is specified as 0.1 micron. Breadboard tests have shown the actual performance to be better than this specification [119].

The traxing error expressions just given consider the detector, signal, and tracking loop noise effects. A completely general expression must consider platform jitter effects. According to Chen, Jeganathan and Lesh [126] the sensor and platform mean square errors are additive:

$$\sigma_\psi^2 = \sigma_S^2 + \sigma_P^2 . \qquad [5.3.3\text{-}9]$$

With $H(\omega)$ representing the tracking loop closed-loop transfer function against angular frequency ω, P_S the signal power, $S_N(\omega)$ the additive signal, detector, and electronics noise power spectral density, and $S_P(\omega)$ the platform jitter power spectrum, the mean square tracking error becomes:

$$\sigma_\psi^2 = \frac{1}{P_S}\frac{1}{2\pi}\int |H(\omega)|^2 S_N(\omega)\, d\omega + \frac{1}{2\pi}\int |1 - H(\omega)|^2 S_P(\omega)\, d\omega . \qquad [5.3.3\text{-}10]$$

Held and Barry [122] investigated the σ_S^2 term and defined the noise equivalent angle to be $S_N(\omega)/P_S$. In a digital tracking controller S_N must be filtered to half the controller sampling frequency. An analog controller naturally filters S_N to the bandwidth of $H(\omega)$. Consequently the effect of S_N increases with increasing tracking loop bandwidth and decreasing signal to noise ratio. The platform jitter, S_P, however, is sensed by the tracking detector and compensated for by the tracking loop. The larger the loop bandwidth, the higher the frequency disturbance it can compensate. As a result, the influence of S_P decreases with increasing loop bandwidth. If a high optical signal to noise ratio can be maintained the σ_S tracking noise contribution can be made negligibly small. Consequently, the tracking loop bandwidth should be designed with as high a control bandwidth as possible to subdue platform effects.

In Held and Barry's study three closed loop ISL controllers were devised to provide typical tracking error results. These controllers consisted of Gyro, Mass, and Complementary stabilized systems. At a wavelength of 0.9 microns, a track loop damping ratio of 0.725, and a

receiver aperture diameter of 20 cm the RMS tracking error due to sensor effects alone were found to be:

σ_S = 0.007 μrad for the Gyro and Mass Stabilized Systems,
σ_S = 0.170 μrad for the Complementary filter System.

When additional platform disturbances, modelled as coulomb friction torque acting at the gimbal bearings, were considered the total RMS tracking error increased to:

σ_ψ = 0.038 μrad for the Gyro stabilized system,
σ_ψ = 11.64 μrad for the Mass Stabilized system,
σ_ψ = 0.036 μrad for the Complementary filter System.

The inferior performance of the mass-stabilized system was claimed to be due to not rejecting low frequency disturbances due to flexure pivot coupling between the coarse gimbal and platform, and because the friction disturbance power resides predominantly at low frequencies.

5.3.4 Recommendations

The coarse tracking assembly and telescope gimbals are effectively one and the same. Though not discussed here, they are typically implemented with direct-drive DC brushless motors. The trend in fine pointing has been to magnetic voice-coil actuated mirrors. Piezo-electric actuation is also receiving consideration. Where wide angular range is needed the voice coil approach is the best because it can provide that range to high precision. For tracking detectors, historically the four quadrant detector using APD or PIN diodes has been preferred, but the new CCD approach used by SILEX has the advantages of high precision without a dead-zone. Also, it may speed re-acquisition during small misalignments; and can be used to participate in the acquisition phase as noted in the previous section.

5.4 Pointing

5.4.1 Introduction

In a two-way optical ISL system, once the acquisition sequence is complete and the partner's beam is being tracked to maximum precision, a local communication beam is transmitted back to the partner. The problem of aiming and controlling this beam is known as pointing.

The pointing problem is in many ways functionally similar to the tracking problem. A narrow beamwidth is required for energy-efficient communication, so a telescope of diameter D_T is needed to produce the desired beamwidth. The telescope must be steered using a course pointing assembly (CPA). Since the beam is narrower than the position tolerance of the CPA, a fine pointing mechanism (FPM) is needed in the optical path between the laser optics and the telescope optical assembly. Finally, to control the pointing direction relative to the receive beam a pointing beam detector is required. These elements of the pointing system are illustrated in Figure 5.4-1. All of these components and assemblies have a counterpart in the tracking system. Furthermore, since the transmit beam is directed in almost the same direction as the receive beam, the physical layout of the optical path is similar. Consequently most proposed ISL designs functionally overlap the pointing and tracking equipment using one telescope, CPA, and FPA for both functions. Exceptions, such as the Hughes proposal [106, 122], arise largely because of differing receive and transmit telescope requirements.

The physical requirements underlying the design of the CPA and FPM are effectively the same as those of the tracking CTA and CTM. Since these were discussed at length in the tracking section, including special considerations for pointing, they will not be discussed further here. The emphasis, instead, will be on those considerations unique to pointing and on the aspects of pointing that influence communication integrity.

One special characteristic of pointing is the need to point the transmit beam in a slightly different direction

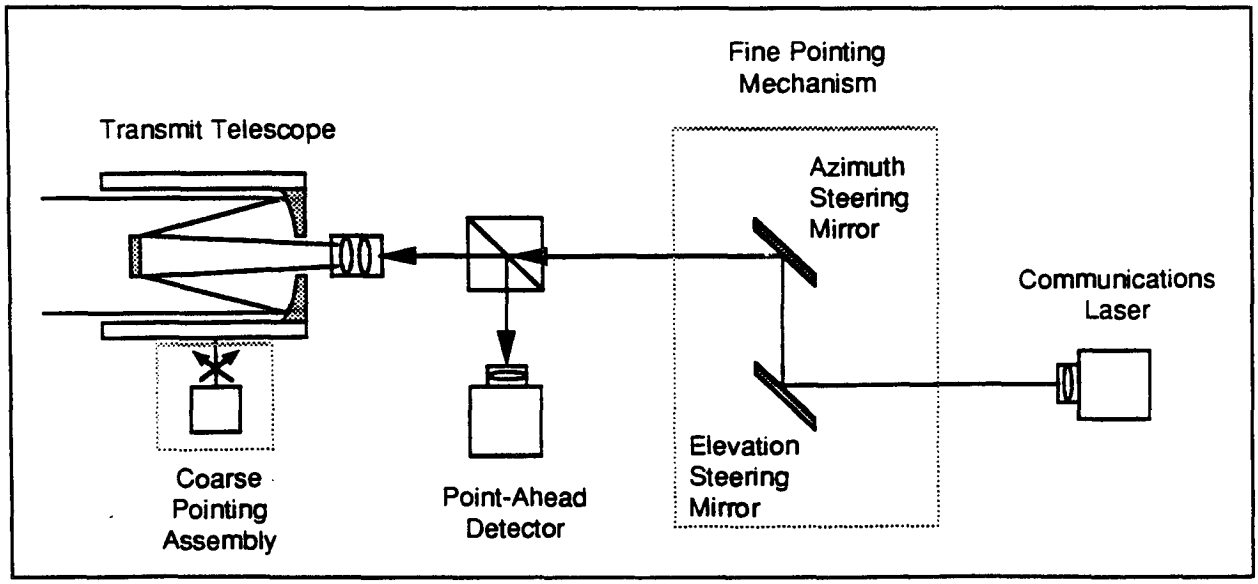

Figure 5.4-1 Pointing Function Elements

as the receive beam. This is a consequence of the finite speed of light, the narrow beam width, and the relative motion of the two satellites. The management of this "point ahead" will be the first topic of discussion, illustrated with examples of proposed design solutions.

A challenging aspect of the pointing problem is the achievement of high pointing accuracy. Similar concerns exist in tracking, but the solutions are more apparent. Tracking precision can be relaxed by expanding the tracking field of view and increasing the receive telescope diameter. Accurate pointing, however, requires accurate knowledge of the partner's position, and the ability to accurately point the beam in that direction. Hence the many noise sources in the ISL system, including those contributing to the noise equivalent angle, influence the performance and design of the pointing system. How these noise sources combine to cause communication interruptions will be examined. Finally, if the noise results in a sustained mispoint, tracking lock will be lost with reactivation of the acquisition function. The frequency of reacquisition will be investigated.

5.4.2 Point-Ahead

A unique aspect of optical ISL communication over RF ISL is that if you aim your transmit beam directly at where you currently see your partner, then your partner will not be in that region of space when the beam signal arrives. To illustrate, a 10 μrad beam spreads to 400 metres diameter over a 40,000 km link. If the two satellites have a 10 km/sec relative velocity, then during the signal round-trip travel time, the partner satellite will have moved 2,666 metres. Clearly the signal missed the satellite.

An obvious solution is to broaden the beamwidth. This is certainly a simple solution, but the increased transmit laser power needed to maintain an adequate wavefront power density may not be acceptable. Consequently the preferred solution is to keep the beam narrow, but to point the beam to where the partner is expected to be during beam arrival. This requires pointing the transmit beam ahead of the receive beam in the direction of relative travel.

Figure 5.4-2 illustrates how the point-ahead angle, θ_P, is calculated. To calculate θ_P at satellite A, satellite A is considered stationary with respect to satellite B. Satellite B is travelling in its orbit at a relative velocity,

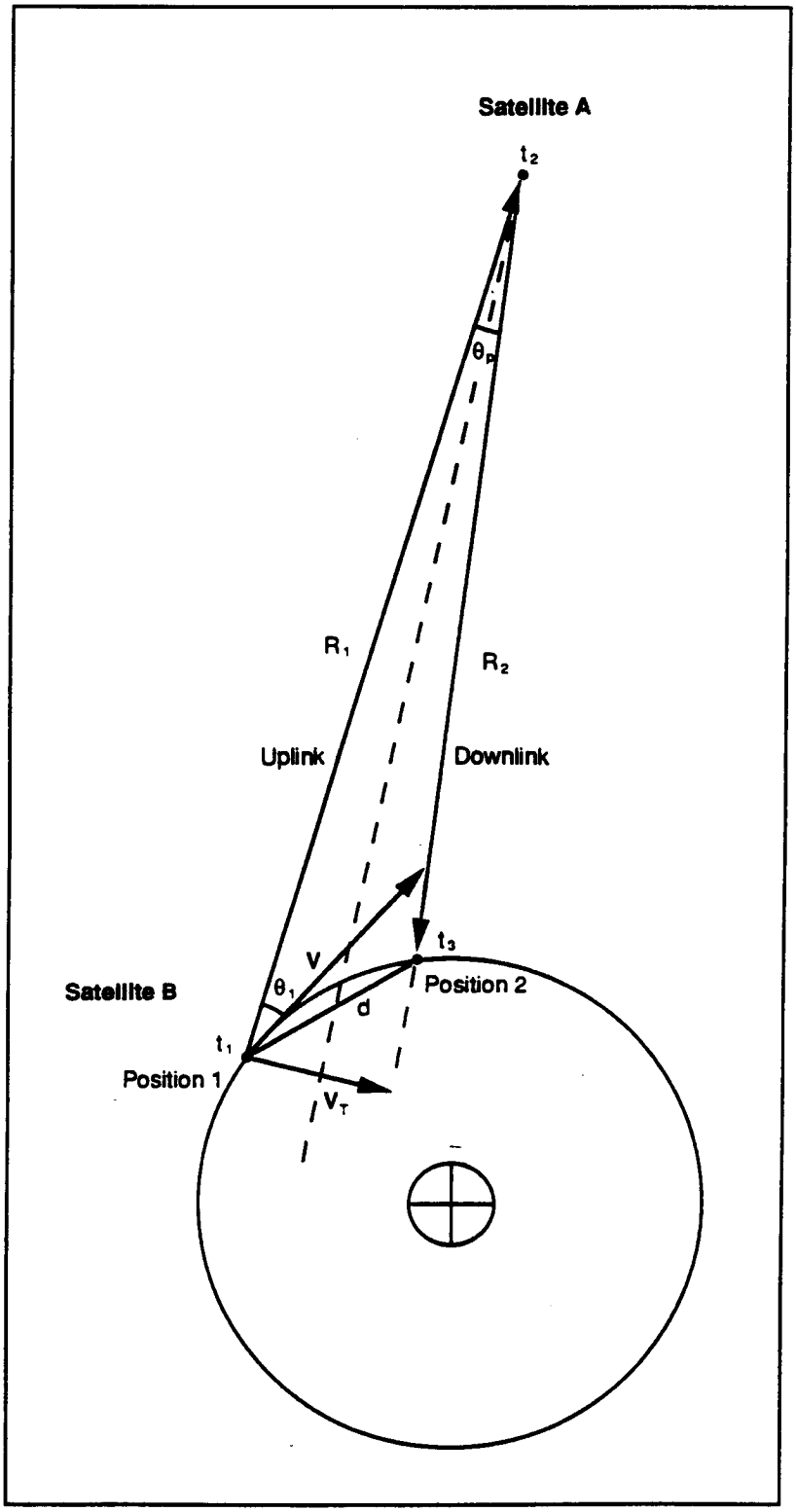

Figure 5.4-2 Point-Ahead Angle Calculation

V. At time t_1 satellite B transmits its signal from position 1 to satellite A which receives it at time t_2. Immediately satellite A transmits its signal targeted to intercept satellite B at position 2, which the signal does at time t_3. The time taken for this process $(t_3 - t_1)$ is the total distance travelled by the signals divided by the speed of light:

$$(t_3 - t_1) = \frac{(R_1 + R_2)}{c} \cdot \qquad [5.4.2\text{-}1]$$

The relative distance travelled by satellite B in this interval is d, the exact value of which depends on both satellites' orbital ephemerides. The ephemerides information is also needed to exactly evaluate R_1 and R_2. With this information in hand evaluation of θ_P is simple geometry:

$$\theta_P = arccos\left(\frac{R_1^2 + R_2^2 - d_2}{2R_1R_2}\right) \cdot \qquad [5.4.2\text{-}2]$$

However, this is unnecessarily complicated. As seen in the earlier example, the beam diameter covers approximately 15% of the distance, d, travelled by satellite B. Also, in the same example, d represents only about 6% of the circumference of a typical 300 km LEO orbit. Therefore a number of approximations can legitimately be made to estimate the point-ahead angle to sufficient precision.

First, assume $R_1 \approx R_2 = R$. The difference does not contribute significantly to the total transit time. Next, assume during $(t_3 - t_1)$, satellite B travels in a straight line at velocity V, rather than in a circular orbit. The speed normal to $R \equiv R_1$, is then:

$$V_N = | V | \sin(\theta_1) \cdot \qquad [5.4.2\text{-}3]$$

The point-ahead angle can now be estimated as:

$$\theta_P \approx \frac{V_N(t_3 - t_1)}{R} \approx \frac{V_N(2R/c)}{R} = \frac{2V_N}{c} \cdot \qquad [5.4.2\text{-}4]$$

The immediate values of V and θ_1 at t_1 still need be determined from knowledge of each satellite's orbital ephemerides. This information is stored locally in each satellite and updated periodically from a ground-based control centre.

The typical range of point-ahead angles is from 0 to 70 μradians. For a GEO to Radarsat link the maximum point-ahead angles are about 50 μrad in both the east-west and north-south direction (See appendix A). For GEO to GEO links the maximum point-ahead angle is about 20 μrad. In GEO to GEO links this angle remains approximately constant. However, for GEO to LEO, and GEO to inclined orbit links this angle can vary greatly with time. The point-ahead angle is controlled open-loop using the stored orbital ephemerides. Therefore, it is essential that the ephemerides be kept accurate to a fraction of a beamwidth, i.e. on the order of 10 metres, and that clocks on both satellites are kept synchronized to within a millisecond.

5.4.3 The Point-Ahead Assembly

The purpose of the point-ahead assembly is to maintain the point-ahead angle at the current desired magnitude and direction. To do so requires a means to measure the angle between the receive and transmit beams, and a method to control the angle. Since the magnitude of the point-ahead angle is small, less than 70 μrad, and must be controlled to microradian accuracy, the candidate mechanisms for its control are similar to those of the fine tracking assembly; such as measuring the angle with a quadrant detector, and using piezo-electric actuated mirrors for its adjustment. However the bandwidth requirements for point-ahead are considerably relaxed over fine tracking. For instance the COMSAT report estimates 1 Hz response is sufficient. Another difference between control of point-ahead and the fine tracking problem is that fine tracking is essentially a boresight alignment problem dedicated to keeping the light spot at the centre of the 4QD. The common solution is to dedicate a fast, static control procedure to this task. Point-ahead, in contrast, is not a static control problem. The transmit light spot must be kept at an regulated offset from the centre of the detector. The required offset also changes slowly with time. Consequently a programmable control algorithm

must be used with a variable offset that is updated periodically.

Because of the above considerations the preferred point-ahead solution is to use a separate narrow-range beam deflection assembly for point-ahead control, and then share the remainder of the optical path with the receive beam as illustrated in Figure 5.4-3. The reuse of the receive components certainly saves weight and improves system reliability.

Many different design approaches are possible to solve the pointing problem. To illustrate the possibilities, several proposed systems will be examined.

5.4.4 Example Techniques

5.4.4.1 SILEX

The optical path followed by the SILEX receive and transmit beams is illustrated in Figure 5.4-4 [104]. The paths overlap completely after the point-ahead assembly (PAA). The emerging beamwidth is 8 μrad. The probability that the beam will mispoint by more than 1.7 μrad is less than 10^{-6}. The PAA consists of a two-axis actuated mirror of ±65 mrad range and 100 Hz bandwidth. There is no indication of an optical point-ahead sensor being used. The point-ahead angle is controlled open loop using knowledge of the satellite orbits and the attitude of the host spacecraft. Computation of the angle is performed autonomously by each terminal from ephemeris data loaded and updated daily from the ground.

5.4.4.2 ETS-VI

The ETS-VI point-ahead implementation [116] works by modulating the transmit and receive beams before combining them in point-ahead sensor:

$$f_d = 8\ \text{kHz}, f_u = 315\ \text{Hz}$$

Figures 5.4-5 through 5.4-7 illustrate the method.

The beams are combined on a single quadrant detector which is used to determine the azimuth (Azd) and elevation (Eld) of each beam using the technique discussed earlier in "tracking". A bandpass filter (BPF) separates the receive and transmit signals.

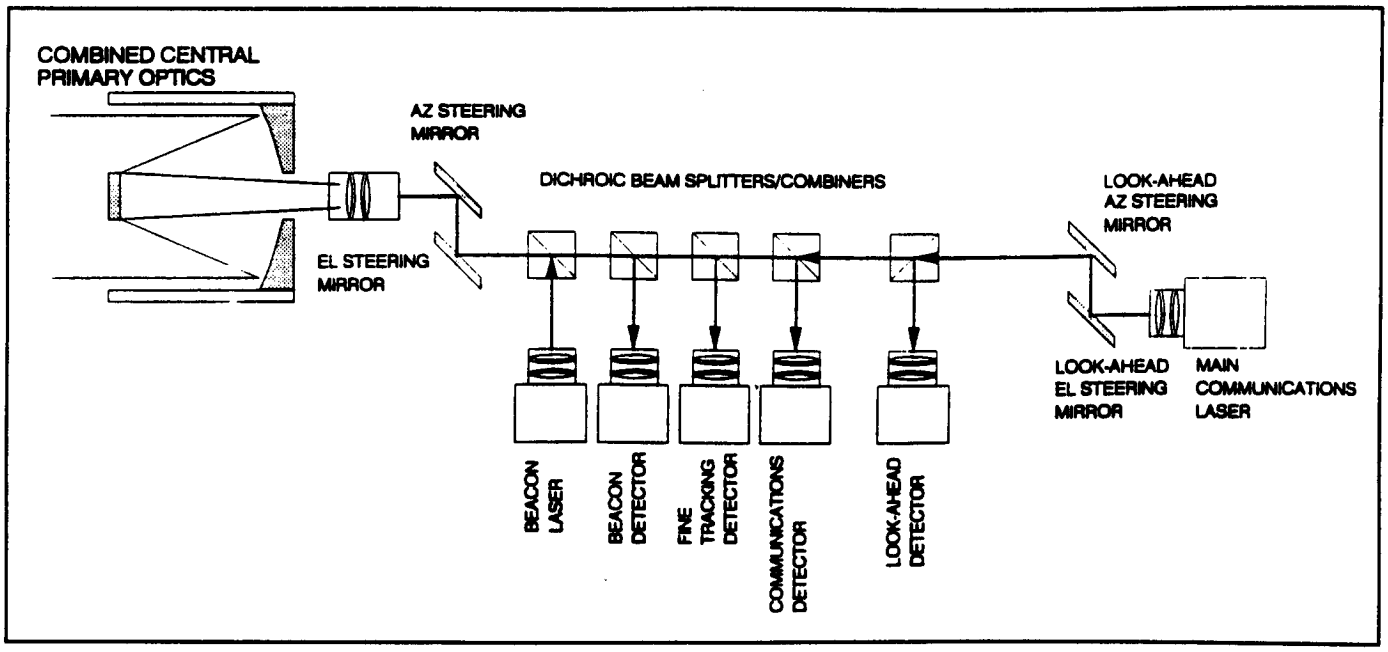

Figure 5.4-3 Optical Network for Combined Pointing/Tracking

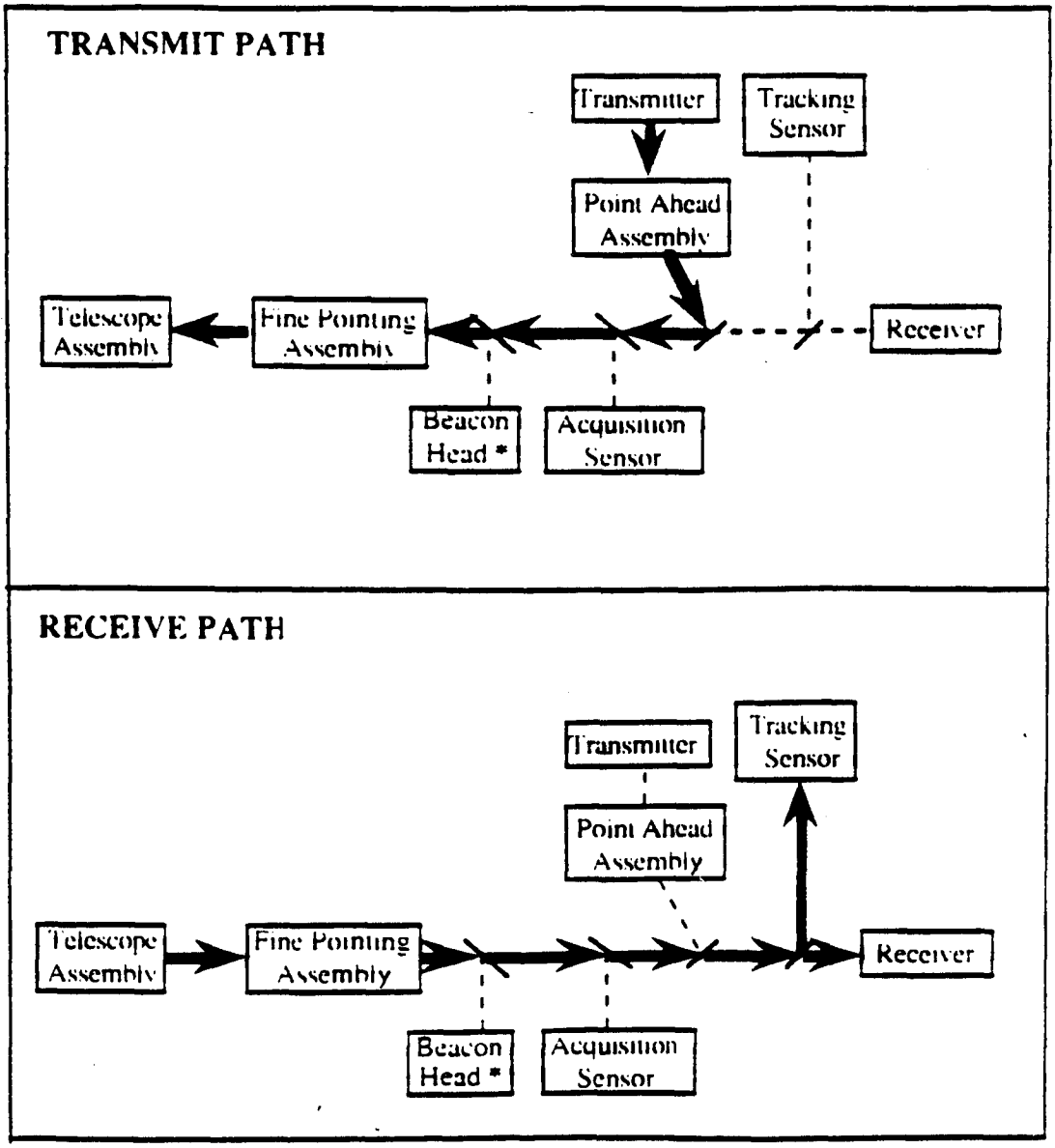

Figure 5.4-4 SILEX Receive/Transmit Optical Paths

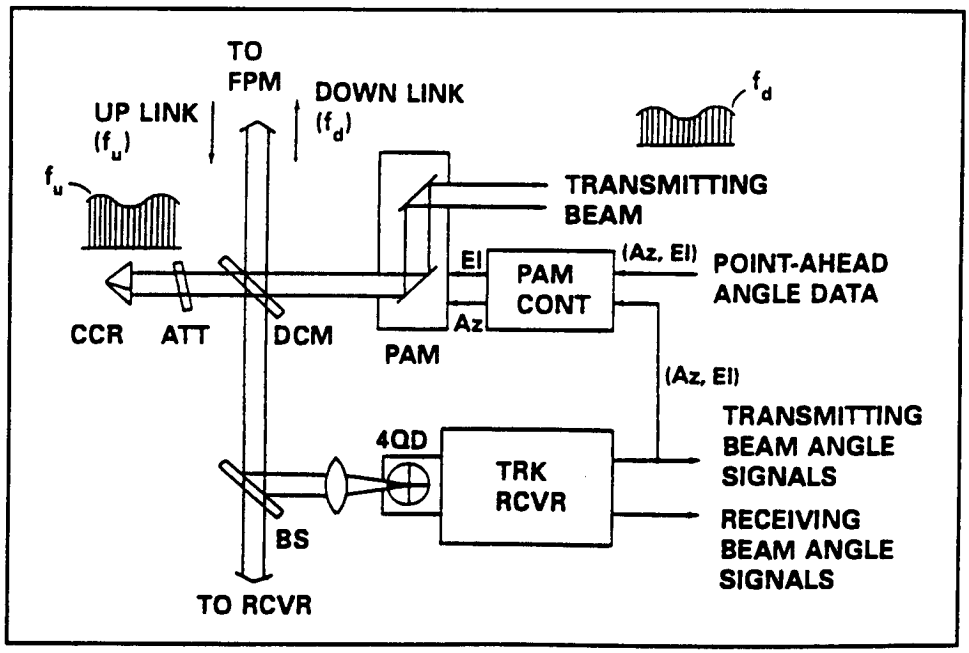

Figure 5.4-5 ETS-VI Point-Ahead with Offset Feedback

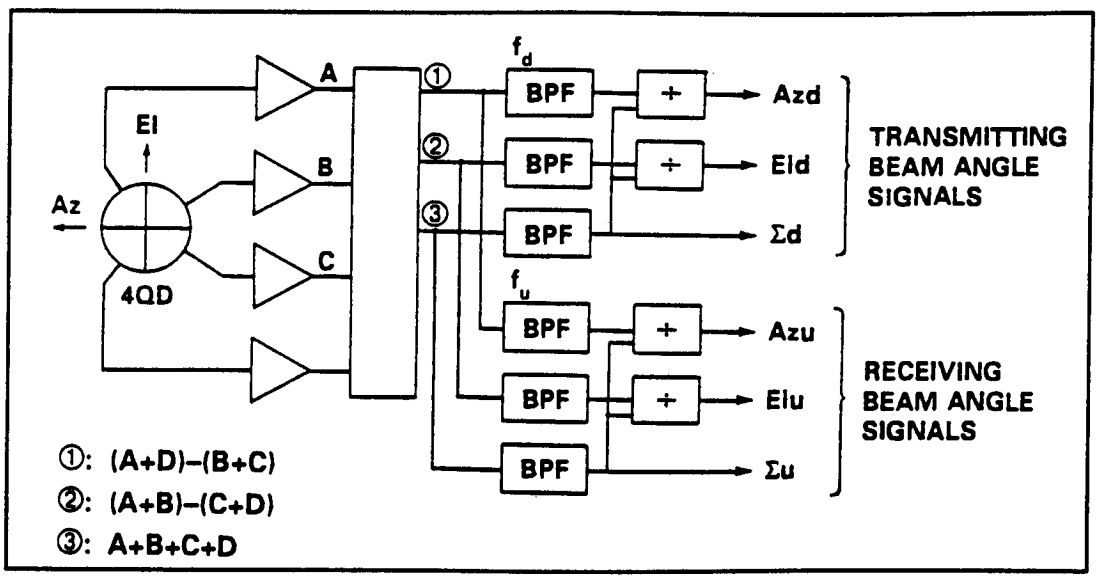

Figure 5.4-6 Functional Block Diagram of ETS-VI Tracking Receiver

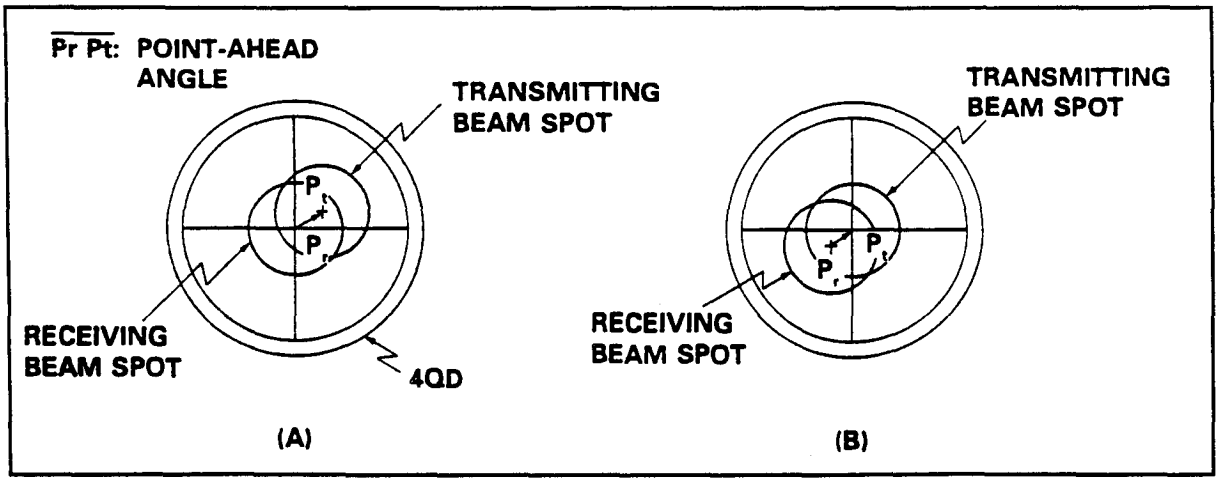

Figure 5.4-7 ETS-VI Point-Ahead Angle on 4QD Sensor

The approach taken is to centre either the receive or transmit beam on the detector and then measure the angle of the other beam relative to it. This increases the likelihood of both beams remaining on the detector at all times.

The other design parameters of the ETS-VI system are:

beamwidth	= 30 μrad
Pointing accuracy	= 2 μrad
Point-ahead deflection	= ±33 μrad
Pointing Stability	< 1 μrad

5.4.4.3 COMSAT

COMSAT investigated the application of optical ISL for interconnecting INTELSAT communications satellites separated by up to 60° [109]. They proposed a typical optical network where the optical path is shared by the transmit and receive beams, with the exception of the point-ahead mechanism (PAM), as illustrated in Figure 5.4-8. They separated the point-ahead function from the fine tracking function because the point-ahead requirements were much less demanding than those of tracking. In this application (GEO to GEO) the point-ahead angle is fairly constant, the range of motion needed was 100 μrad with 0.5% accuracy, and control bandwidth was only 1 Hz. This stands in contrast to the fine steering mechanism which had ±2° of travel with 80 nrad tracking accuracy within the optical path and 1.2 kHz bandwidth.

The interesting aspect of the COMSAT design is the way the point-ahead angle is dynamically optimized. This is done in cooperation with the partner satellite. Initially adjustment of the point-ahead angle relies on ephemeris data uploaded from the ground. This data includes the relative spatial coordinates and trajectory of the two satellites, their tangential velocities and their separation distance, From this the initial point-ahead angle and direction is calculated on board each satellite.

Once fine track has been achieved, but before high speed communication begins, the point-ahead angle is optimized to remove any errors in the ephemeris data. This is accomplished by slowly spiralling the transmit beam causing the partner to receive a time-varying intensity pattern. The receiver relays back to the transmit terminal when maximum power is observed. The transmit terminal then locks onto the position in its spiral pattern which maximizes the received power and thereby optimizes the point-ahead angle. This process is repeated by the other terminal transmitter. Depending on the frequency of changes in the tangential velocity and orbital spacing, the point-ahead angle is updated by periodically repeating this optimization process.

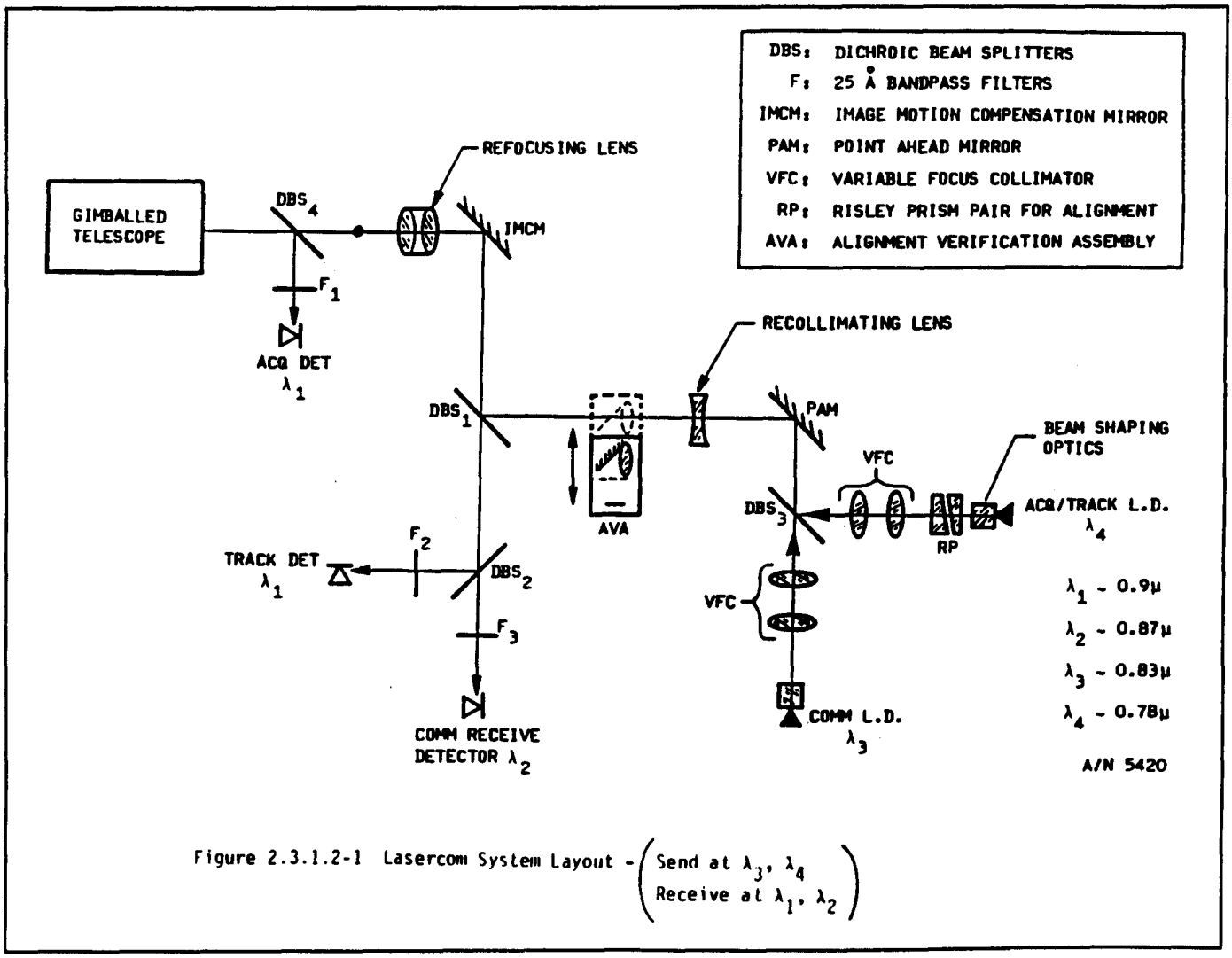

Figure 2.3.1.2-1 Lasercom System Layout - (Send at λ_3, λ_4 / Receive at λ_1, λ_2)

Figure 5.4-8 COMSAT Optical Path

5.4.5 Noise-Induced Pointing Errors

Pointing a transmit beam is a delicate process requiring great precision in both the tracking and pointing assemblies. The problem is that the transmit beam is best kept narrow to maximize the power density at the receiver, but a narrow beam can tolerate only an even narrower mispoint. When the mispoint exceeds the beamwidth communication reception stops, with an attendant loss of data. If such a severe mispoint persists beyond the tracking system response period, then track-lock is considered lost and the link must be reacquired. In tracking it is possible to expand the receiver field of view to relax the tracking accuracy constraint. The analogous operation in pointing is to expand the transmit beam. Since this requires increasing transmit laser power, it is desirable to keep the beam narrow. As we have seen, tracking and pointing mechanisms of the required precision are readily available. The remaining issue of concern, then, is noise in the system which introduces a random mispoint angle and serves to corrupt the communications integrity of the ISL system.

This random mispoint has already been accounted for in the link equation. In section 3.4.2, equation 2 it is

represented by θ, the angle of receiver from central transmit axis. The representation, however, is general. In this section the optimum value of θ will be derived, and it will be shown that this value introduces a -4dB loss into the equation. The influence of noise-induced mispoint on the communication error rate will also be examined.

Figure 5.4-9 shows the basic parameters under consideration. The mispoint angle, , is a random variable, the distribution of which is needed for this analysis to proceed. It is assumed that the pointing error distribution contains two contributions:

(1) a static error on each axis (E_x, E_y) which contributes a radial angle $E = E_x^2 + E_y^2$.

(2) a dynamic error on each axis due to tracking sensor, electronic, and platform noise effects. These effects are characterized by stationary Gaussian noise resulting in a Gaussian mispoint distribution with standard deviation % in the x-y Cartesian coordinates. This θ is the same as the θ_ψ considered at length in the previous tracking section.

In Polar coordinates the dynamic error results in a Rayleigh probability density distribution of ε with standard deviation θ [127, sec 2.14][128]:

$$P_E(\varepsilon) = \frac{\varepsilon}{\sigma^2} \exp\left[-\frac{1}{2}\left(\frac{\varepsilon}{\sigma}\right)^2\right] \qquad [5.4.5\text{-}1]$$

Incorporation of the static error term results in a Rician distribution [129]:

$$P_E(\varepsilon, E) = \frac{\varepsilon}{\sigma^2} \exp\left(-\frac{\sigma^2 + E^2}{2\sigma^2}\right) I_0\left(\frac{\varepsilon E}{\sigma^2}\right) \qquad [5.4.5\text{-}2]$$

Where I_0 is the modified Bessel function of zero order.

A mispoint results when the mispoint angle, ε, exceeds some angle ε^* where the received power drops below the detectable level. The communication system sees this as a burst error because even if the mispoint only lasts a microsecond at 1 Gbps a thousand consecutive bits would be lost. If the mispoint persists longer than the tracking system response time then the system will loose its lock on the receive beam and reacquire the link causing a sustained communication dropout.

The probability of mispoint is:

$$P_E(\varepsilon > \varepsilon^*) \equiv P_E{}^* = \int_{\varepsilon^*}^{\infty} P_E(\varepsilon, E)\, d\varepsilon \qquad [5.4.5\text{-}3]$$

Integration of $P(\varepsilon, E)$ does not yield an analytical solution. So, instead, a simplified approach is used considering only the Rayleigh distribution of the dynamic error centred on $(\varepsilon - E)$. Therefore,

$$\varepsilon^* = \int_{(\varepsilon^* - E)}^{\infty} P_E(\varepsilon)\, d\varepsilon = \exp\left[-\frac{1}{2}\left(\frac{\varepsilon^* - E)}{\sigma}\right)^2\right] \cdot [5.4.5\text{-}4]$$

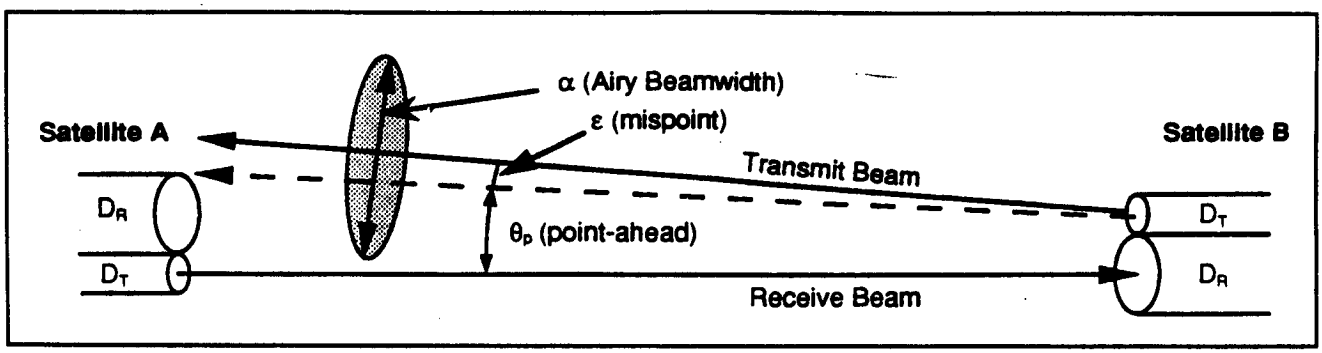

Figure 5.4-9 Mispoint Angle Parameters

This is the Burst Error Probability, or rate. The burst error rate is generally specified at the outset. It is ε^*, the maximum tolerable mispoint angle, that is the unknown. Solving for ε^*:

$$\varepsilon^* = \sigma\sqrt{-2\ln(P_E^*)} + E \qquad [5.4.5\text{-}5]$$

This approximation has been determined to be very slightly pessimistic [129]. In the analysis that follows it is assumed that the static mispoint contribution, E, is negligible. The pointing error distribution is then purely Rayleigh. Interestingly, this assumption has been experimentally verified in the SILEX test bed. The SILEX system pointing error distribution obtained is reproduced in Figure 5.4-10 [104]. This result compares very favourably with the normalized Rayleigh distribution of Figure 5.4-11.

The objective now is to select an optimum beam width, α_o, that will maximize the power available at ε^* while minimizing the power outside $\varepsilon > \varepsilon^*$, where it is not detected, and within $\varepsilon < \varepsilon^*$ where the power level is within specification anyway. Therefore, ε^* represents the angle used in the link equation to account for mispoint losses.

It is up to angle ε^* that the tracking and communication systems must operate. Designing them to operate only up to some lesser angle is a contradiction, since then a burst error would occur before ε^*. To design the system to operate beyond ε^* is an overdesign better accommodated by adding a gain margin at ε^*.

Recasting the link equation to highlight only the terms relevant to this analysis, and lumping all the constants into K:

$$Power\ Received = \frac{K}{\alpha^2}\left[\frac{2J_1(7.664\varepsilon/\alpha)}{7.664\,\varepsilon/\alpha}\right]^2 Power\ Transmitted \qquad [5.4.5\text{-}6]$$

Where:

J_1 = the Bessel function of the first kind,

α = the full Airy beamwidth to the first dark ring

$= \dfrac{2.44\lambda}{D_T}$,

λ = wavelength of transmit beam;

and the term in square brackets, is the normalized Airy function, $A(\varepsilon^*, \alpha)$.

The power received has a peak value within the Airy diameter found by:

$$\frac{d\,(Power\ Received)}{d\alpha} = 0\ , \qquad [5.4.5\text{-}7]$$

with the solution [110, 111]:

$$\frac{\alpha}{\varepsilon^*} = 4.16\ . \qquad [5.4.5\text{-}8]$$

This result, overlapped with the beam Airy pattern is plotted in Figure 5.4-12. Therefore the optimum beamwidth is:

$$\alpha_o = 4.16\,\varepsilon^*\ . \qquad [5.4.5\text{-}9]$$

The optimum mispoint power loss is found by substituting α_o into $A(\varepsilon_x, \alpha)$, with the result:

$$A(\varepsilon^*, \alpha_o) = 0.40 = -4\ \text{dB}. \qquad [5.4.5\text{-}10]$$

The optimum Airy beam diameter can now be determined from the burst error rate specification:

$$\alpha_o = 4.16\varepsilon^* = 5.88\sigma\sqrt{-\ln(P_E^*)}\ . \qquad [5.4.5\text{-}11]$$

The mispoint probability distribution can also be used to determine other attributes of the communication link such as the expected bit error rate, <BER>:

$$<BER> = \int_0^\infty BER(\varepsilon)\,P_E(\varepsilon)\,d\varepsilon \qquad [5.4.5\text{-}12]$$

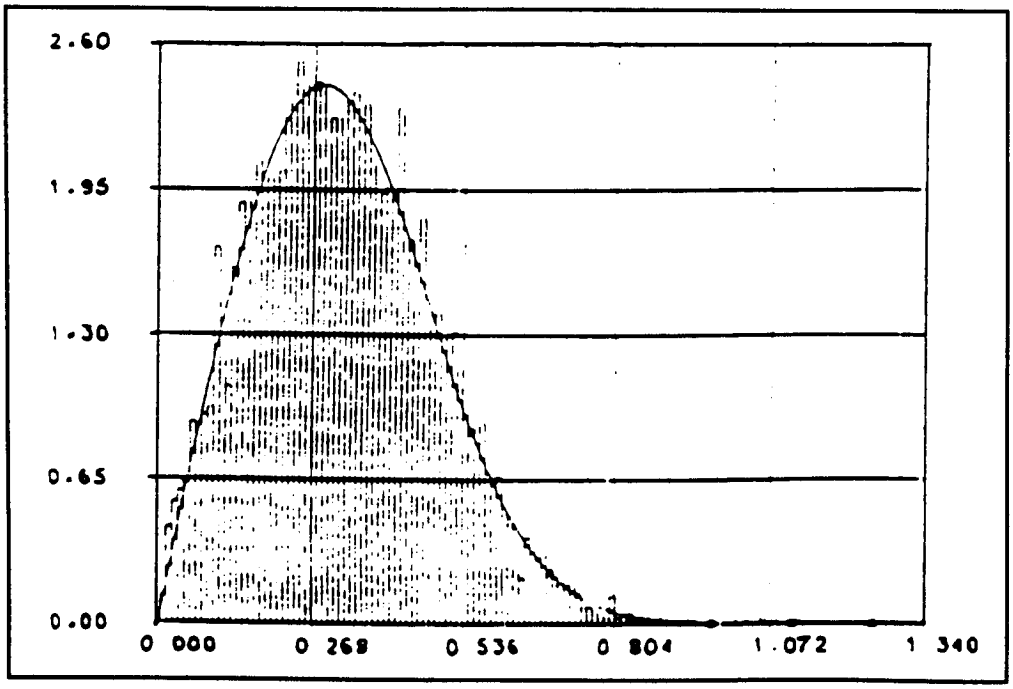

Figure 5.4-10 SILEX Pointing Error Distribution

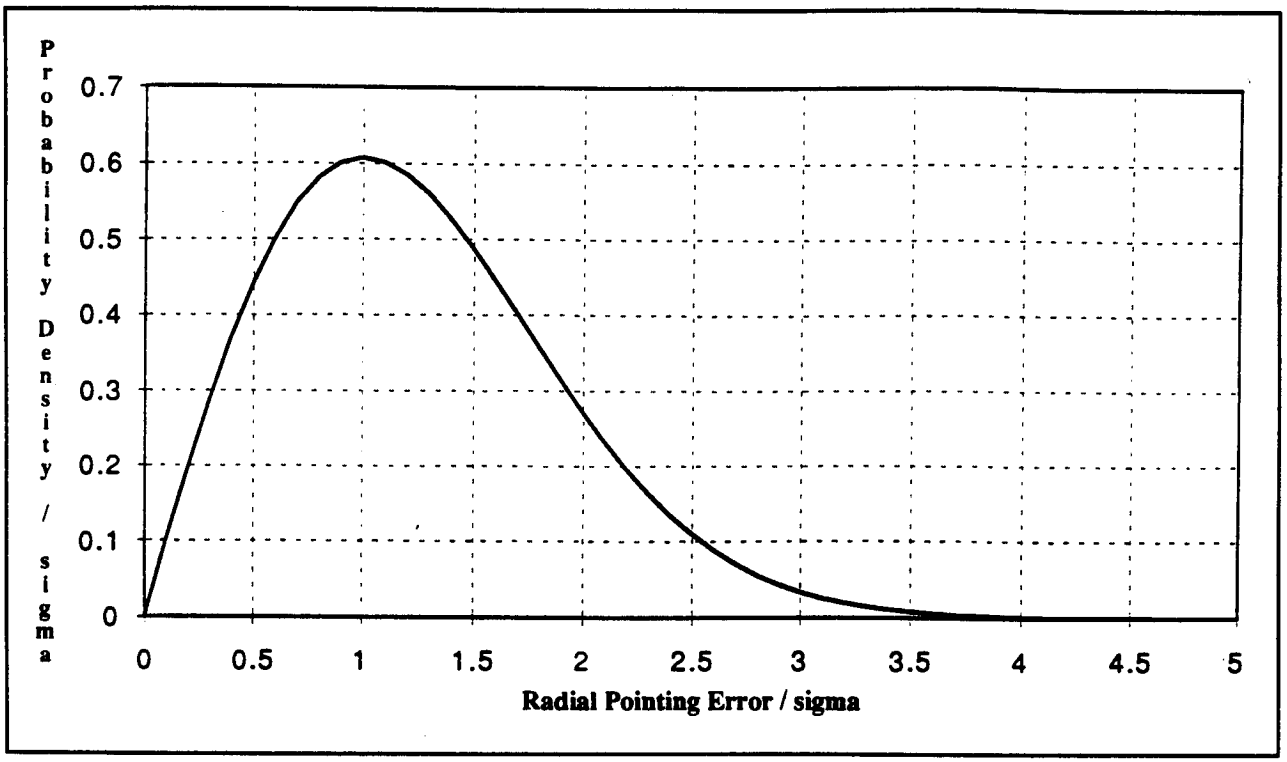

Figure 5.4-11 Normalized Rayleigh Distribution

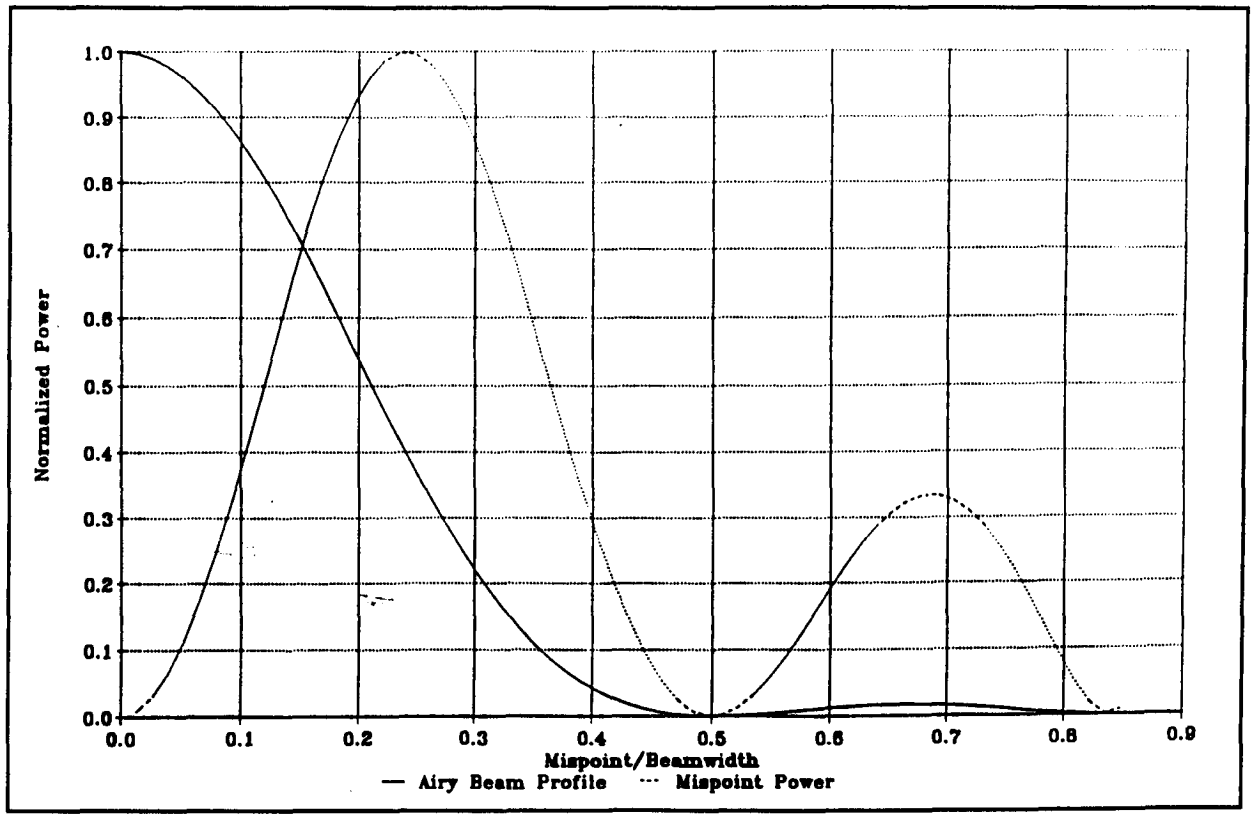

Figure 5.4-12 Received Power Profile/Airy Profile

Since BER(ε) can be a complex analytical expression, or may only be represented by a graph of empirical data, <BER> may need to be evaluated numerically. In this case Peters and Sasaki [130] claim the integration can be simplified since it is sufficient to integrate only to 5σ.

Another parameter of interest is the mean mispoint angle. This is found quite simply as:

$$<\varepsilon> = \int_0^\infty \varepsilon P_E(\varepsilon)\, d\varepsilon = \sigma\sqrt{\frac{\pi}{2}} \ . \qquad [5.4.5\text{-}13]$$

This can prove useful for approximating mean link behaviour such as the bit error rate.

If the receive telescope diameter is fixed and free to differ in size from the transmit telescope diameter, and the partner mispoint is assumed independent of the local mispoint then the optimal Airy diameter from the above analysis can be used to determine the optimal transmit telescope diameter. This is simply:

$$D_T = \frac{2.44\lambda}{\alpha_o} = \frac{\lambda}{2.41\sigma\sqrt{-\ln(P_E^*)}} \ . \qquad [5.4.5\text{-}14]$$

This result is plotted in Figure 5.4-13 for representative values of P_E^*. The implication from these plots is that a smaller telescope is better, since a large telescope leads to a narrow beam and greater probability of mispoint. This assumes that the transmit laser power can be scaled for the indicated beamwidth. An analysis like this was used by Hughes in their design [106] to select a tracking telescope diameter smaller than the receive telescope diameter. Alternatively Figure 5.4-13 can be used to determine the required accuracy once the diameter and burst error probability are established or to determine the resulting burst error probability once the diameter and the tracking accuracy are established.

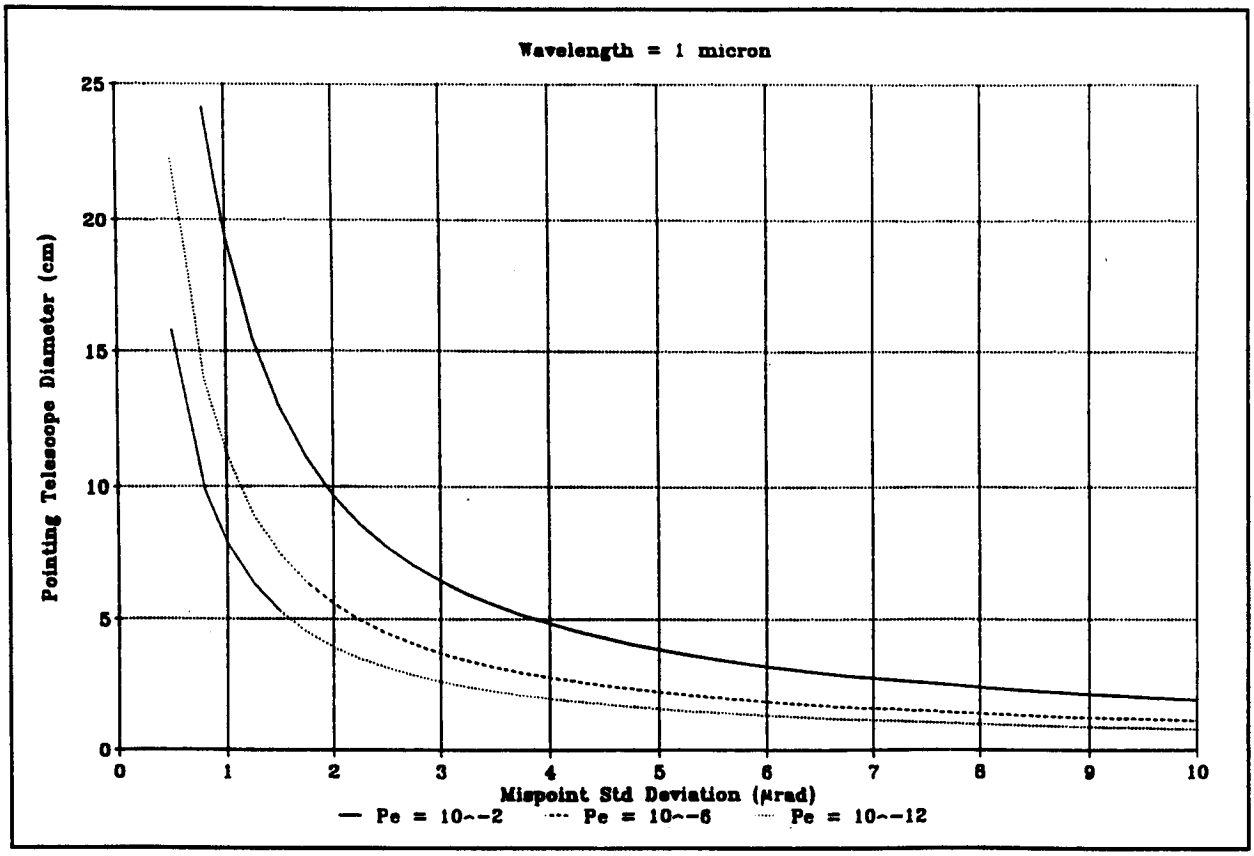

Figure 5.4-13 Optimum Pointing Telescope Diameter

The assumptions underlying the derivation of the optimal transmit telescope diameter are not entirely realistic. The two satellites are a mutually interacting system where each partner's mispoint is dependant on the local mispoint. This is because the partner's signal to noise ratio drops with increased mispoint. That causes an increase in the partner's noise equivalent angle, which contributes to α, which in turn will cause the partner to mispoint. This will cause a similar increase in the local noise equivalent angle and increased local mispoint. This cyclic process can destabilize the link.

5.4.6 Interactive-Mispoint Algorithm

Determination of link stability requires a numerical approach which simulates the mutually interactive influence of mispoint on each of the two satellites. Hxhe algorithm used to model this process must cycle back and forth between the satellites reevaluating the mispoint distribution on each cycle. If the link lock is stable then the average mispoint angle converges to a finite value, otherwise it diverges.

The assumptions used are:

(i) There is no initial mispoint. $\varepsilon = 0$.

(ii) The signal to noise ratio, SNR, is purely a function of received signal power and varies only with the mispoint:

$$SNR(\varepsilon) = A(\varepsilon) SNR_0,$$

where:

$$A(\varepsilon) = Airy\ function = \left[\frac{2J_1\left(\frac{\pi D_T}{\lambda} \sin\varepsilon\right)}{\frac{\pi D_T}{\lambda} \sin\varepsilon} \right]^2,$$

$$SNR_0 = SNR(0).$$

(iii) The mispoint standard deviation, σ_ε, is only a function of the local signal to noise ratio. All other parameters are considered fixed.

(iv) The mispoint angle is Rayleigh distributed.

$$P(\varepsilon) = \frac{\varepsilon}{\sigma_\varepsilon^2} \exp\left[-\frac{1}{2}\left(\frac{\varepsilon}{\sigma_\varepsilon}\right)^2\right] .$$

The algorithm begins at satellite A and proceeds through the following steps:

(1) Satellite A: initially pointing is perfect with $\varepsilon_A = 0$, and $\sigma_{\varepsilon,A} = 0$.

(2) Satellite B: since satellite A doesn't mispoint, $SNR_B = SNR_{B,0}$.

This SNR causes the satellite to mispoint with an initial standard deviation of

$$\sigma_{\varepsilon,B}{}^0 = \sigma_\varepsilon(SNR_{B,0}) ,$$

and with a mispoint distribution of

$$P_B(\varepsilon) = \frac{\varepsilon}{(\sigma_{\varepsilon,B}{}^0)^2} \exp\left[-\frac{1}{2}\left(\frac{\varepsilon}{\sigma_{\varepsilon,B}{}^0}\right)^2\right] .$$

(3) Satellite A: because of the mispoint distribution of satellite B, satellite A now experiences a lower SNR which leads to a larger $\sigma_{\varepsilon,A}$. The mean mispoint standard deviation now produced by A is

$$<\sigma_{\varepsilon,A}> = \int_0^\infty \sigma_{\varepsilon,A}(SNR_A(\varepsilon))\, P_B(\varepsilon)\, d\varepsilon .$$

Recall that from [130] the integration upper bound can be terminated at $5\sigma_{\varepsilon,B}$.

The mispoint distribution of satellite A is now:

$$P_A(\varepsilon) = \frac{\varepsilon}{<\sigma_{\varepsilon,A}>^2} \exp\left[-\frac{1}{2}\left(\frac{\varepsilon}{<\sigma_{\varepsilon,A}>}\right)^2\right] .$$

(4) Satellite B: because of the mispoint distribution of satellite A, satellite B now experiences a lower SNR which leads to a larger $\sigma_{\varepsilon,B}$. The mean mispoint standard deviation now produced by B is

$$<\sigma_{\varepsilon,B}> = \int_0^\infty \sigma_{\varepsilon,B}(SNR_B(\varepsilon))\, P_A(\varepsilon)\, d\varepsilon .$$

The mispoint distribution of satellite B is now:

$$P_B(\varepsilon) = \frac{\varepsilon}{<\sigma_{\varepsilon,B}>^2} \exp\left[-\frac{1}{2}\left(\frac{\varepsilon}{<\sigma_{\varepsilon,B}>}\right)^2\right] .$$

(5) The algorithm now loops back to step 3.

The algorithm terminates when $<\sigma_\varepsilon>$ converges to a finite value. This convergence indicates that the link lock is stable. If stable link lock is not possible then $<\sigma_\varepsilon>$ will diverge.

If all constant parameters at both satellite terminals are equal, including the telescope diameters, then the algorithm simplifies to the following recursive series:

$$<\sigma_\varepsilon>^n = \int_0^\infty \sigma_\varepsilon(SNR(\varepsilon))\, P^{n-1}(\varepsilon)\, d\varepsilon , \qquad [5.4.6\text{-}1]$$

$$P^n(\varepsilon) = \frac{\varepsilon}{(<\sigma_\varepsilon>^n)^2} \exp\left[-\frac{1}{2}\left(\frac{\varepsilon}{<\sigma_\varepsilon>^n}\right)^2\right] , \qquad [5.4.6\text{-}2]$$

$$<\sigma_\varepsilon>^0 = \sigma_\varepsilon(SNR(0)) , \qquad [5.4.6\text{-}3]$$

where $<\sigma_\varepsilon>^\infty < \pi/2$ indicates stable link lock.

This algorithm would use the previous parameter optimization procedure to establish the starting conditions. The initial given is the burst error probability, $P_E{}^*$, selected to achieve an acceptable burst error and link reacquisition rate. Then select a σ using equation [5.4.5-11] to achieve an acceptable α_o. The τ found will define the initial acceptable SNR. This will also determine ε^* which is used to define the receive laser power.

After the algorithm has stabilized, use $<\sigma>$ and the previous ε^* (still the maximum allowable mispoint) to evaluate $P_E{}^*$. If the value is now too high something must be done to increase the SNR in order to decrease σ before restarting the algorithm. Clearly this represents a second level of iteration. A comprehensive analysis would generate a plot of initial SNR values against final $P_E{}^*$ for a range of telescope diameters allowing quick selection of an appropriate design.

A study of ISL behaviour using this kind of algorithm was performed by Peters and Sasaki [131] using an expression for σ including only noise equivalent angle effects. They used the approach to determine the final bit error rate (BER) for a stable link according to the theory they developed [130]. Their results show that link stability is strongly determined by the initial noise equivalent angle, which in turn is determined by the initial tracking signal to noise ratio. However, once the link is stable then performance improves without bound as the signal to noise ratio is increased by increasing the receive/transmit telescope diameter. Figure 5.4-14 shows some of their results. This result was confirmed by this author while experimenting with the above algorithm.

Clearly it is important to perform this type of analysis on any preliminary ISL design to confirm its operational viability.

5.4.7 Link Reacquisition Probability

Due to the random nature of the mispoint angle it is inevitable that the transmit beam will mispoint long enough to force the partner to reacquire the link. The proportion of time spent in mispoint was determined as $P_E{}^*$. However, reacquisition represents a much more prolonged communication interruption. It can also require use of a beacon which impacts the available lifetime of the device. Clearly it is important to understand the expected frequency of link acquisition.

This frequency is difficult to formulate since it is dependant on the specific tracking loop behaviour and the noise power spectrum. However, an estimate can be derived assuming white noise and a uniform low-pass tracking loop response.

The link is reacquired when the mispoint angle $\varepsilon > \varepsilon^*$ for a period $\tau > \tau^*$. τ^* is the minimum time needed for the tracking system to sense the mispoint. Therefore, given a joint probability distribution of ε and $\tau, f(\varepsilon, \tau)$, the probability of reacquisition is:

$$P(\varepsilon^*, \tau^*) = \int_{\tau^*}^{\infty}\int_{\varepsilon^*}^{\infty} f(\varepsilon,\tau)\, d\varepsilon d\tau \ . \qquad [5.4.7\text{-}1]$$

Restated,

$$P(\varepsilon^*,\tau^*) = \lim_{T\to\infty} \frac{T^*}{T} \ , \qquad [5.4.7\text{-}2]$$

where T^* is the total time spent in the severe mispoint region $\varepsilon > \varepsilon^*$ and $\tau > \tau^*$ during the period T. Representing the number of times spent in severe mispoint during period T by $n(T)$:

$$\begin{aligned} P(\varepsilon^*,\tau^*) &= \lim_{T\to\infty} \frac{n(T)\,\overline{\tau^*}}{T} \\ &= \frac{\overline{\tau^* n(T)}}{T} \ , \end{aligned} \qquad [5.4.7\text{-}3]$$

where $\overline{\tau^*}$ is the mean period for $\tau > \tau^*$ thereafter, overstrike always refers to the mean) and $\overline{n\,(T)}$ is the ensemble-mean number of acquisition cycles in period T. Therefore:

$$\overline{n(T)} = P(\varepsilon^*,\tau^*)\frac{T}{\overline{\tau^*}} \qquad [5.4.7\text{-}4]$$

The mean period in which to expect a single acquisition cycle is now:

$$T_1 = \frac{\overline{\tau^*}}{P}(\varepsilon^*,\tau^*) \ , \ \ \overline{n(T_1)} = 1 \ . \qquad [5.4.7\text{-}5]$$

Assuming the occurrence of severe mispoint is equally probable at any time within T_1, and $T_1 >> \tau^*$, then the mean period between each acquisition cycle is T_1.

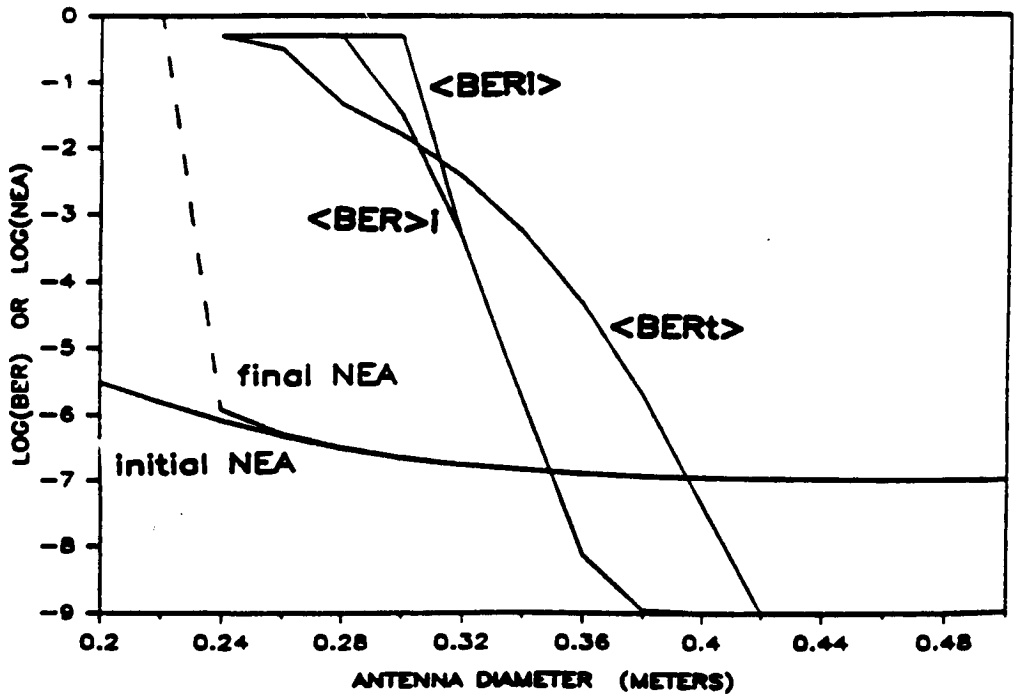

Tracking and communications sub-system performance for various antenna diameters. For diameters less than 0.24 meters, the iteration diverged. The NEA is in radians. No minimium in the BER is observed

Figure 5.4-14 Tracking and Communications Sub-System Performance vs Telescope Diameter

Since, by definition, there is only one occurrence of $\varepsilon > \varepsilon^*$ and $\tau > \tau^*$ during T_1, and since $\bar{\tau}^* << T_1$, this model is an excellent candidate for Poisson statistics where the probability of n acquisition cycles within a time interval T, $P(n, T)$, is:

$$P(n, T) = \frac{(T/T_1)^n \exp(-T/T_1)}{n!} \quad . \qquad [5.4.7\text{-}6]$$

Solving for T_1 requires determination of $\bar{\tau}^*$. This is found by:

$$\bar{\tau}^* = \int_{\tau^*}^{\infty}\int_{\varepsilon^*}^{\infty} \tau f^*(\varepsilon,\tau)\, d\varepsilon\, d\tau \quad . \qquad [5.4.7\text{-}7]$$

where $f^*(\varepsilon, \tau)$ is the probability density of ε and τ within the region $\varepsilon > \varepsilon^*$ and $\tau > \tau^*$. Therefore:

$$\int_{\tau^*}^{\infty}\int_{\varepsilon^*}^{\infty} \tau f^*(\varepsilon,\tau)\, d\varepsilon\, d\tau = 1 \quad . \qquad [5.4.7\text{-}8]$$

The problem now is that we know ε is Rayleigh distributed, but we know nothing about τ.

To proceed some assumptions need to be made. First, assume that ε and τ are statistically independent. Therefore:

$$f^*(\varepsilon,\tau) = p^*(\varepsilon) q^*(\tau) \quad , \qquad [5.4.7\text{-}9]$$

where

$$p^*(\varepsilon) = \frac{P(\varepsilon)}{P_E^*}, \; restricted\; \varepsilon > \varepsilon^* \quad . \qquad [5.4.7\text{-}10]$$

Ordinarily, a definition of $q^*(\tau)$ is needed to evaluate

$$\bar{\tau}^* = \int_{\tau^*}^{\infty} \tau\, q^*(\tau)\, d\tau \quad . \qquad [5.4.7\text{-}11]$$

However, since a number of simplified assumptions need be made in the derivation of $q^*(\tau)$ anyway, there is an easier way.

Begin by defining $q(\tau)$ as the probability distribution of mispoint durations for $\tau > 0$. Realistically, ε is a function of time, characterised by a given spectrum. Since ε is the result of noise in the signal and sensor, assume it to be a band-limited white Rayleigh process. Therefore all frequencies of ε are equally likely. The response of the combined tracking and pointing systems will effectively bandlimit the spectrum of ε to B_T. The implication is that the frequency probability density function is uniformly distributed over the band 0 to B_T. However, this assumes that the occurrence of individual frequencies is mutually exclusive, which is not generally true. Many frequencies can coexist simultaneously. For instance, a mispoint of duration τ can result from the addition of a group of waveforms with a variety of frequencies of differing amplitude. However, derivation of a distribution for τ resulting from an ensemble of non mutually-exclusive events is quite daunting, so to proceed with the analysis it will be assumed that one frequency dominates the generation of τ, and that this frequency is uniformly distributed:

$$\begin{aligned} P(f_\varepsilon) &\approx \frac{1}{B_T} \qquad f_\varepsilon \le B_T \\ &= 0 \qquad f_\varepsilon > B_T \end{aligned} \qquad [5.4.7\text{-}12]$$

From this $q(\tau)$ can readily be found by making another simplifying assumption that the duration of a mispoint of a given frequency is half the period of that frequency since every cycle contains at least two symmetrical but opposing half cycles. Therefore:

$$Prob(f_2 \ge f_\varepsilon \ge f_1) = \int_{f_1}^{f_2} \frac{df}{B_T} = P_{f_1 f_2} \quad , \qquad [5.4.7\text{-}13]$$

but

$$f = \frac{1}{2\tau}$$

$$\therefore P_{f_1 f_2} = -\int_{\tau_1}^{\tau_2} \frac{d\tau}{2B_T \tau^2} = -P_{\tau_2 \tau_1} \quad , \qquad [5.4.7\text{-}14]$$

where $\tau_1 > \tau_2$.

Therefore:

$$q(\tau) = \frac{1}{2B_T\tau^2} \quad \tau \geq \frac{1}{2B_T}$$
$$= 0 \quad \tau < \frac{1}{2B_T} . \qquad [5.4.7\text{-}15]$$

An acquisition cycle is triggered when τ exceeds some value τ^*, a period greater than the shortest period allowed by the response of the system:

$$\tau \geq \tau^* = \frac{K_a}{2B_t} \quad K_a > 1 . \qquad [5.4.7\text{-}16]$$

The distribution of ε in this region is given by $q^*(\tau)$ which is simply,

$$q^*(\tau) = \frac{K_a}{2B_T\tau^2} . \qquad [5.4.7\text{-}17]$$

$\overline{\tau^*}$ can be found from $q^*(\tau)$, but is more easily derived by noting that $\overline{\tau^*}$ is half the period of the mean frequency in the region $f \leq BT/K_a$. Since the region is uniformly distributed, this is just the median frequency. Therefore

$$\overline{\tau^*} = \frac{K_a}{B_T} . \qquad [5.4.7\text{-}18]$$

The probability of severe mispoint can now be calculated:

$$P(\varepsilon^*, \tau^*) = \int_{\varepsilon^*}^{\infty}\int_{\tau^*}^{\infty} p(\varepsilon)\, q(\tau)\, d\tau\, d\varepsilon$$
$$= P_E^* \int_{\tau^*}^{\infty} q(\tau)\, d\tau \qquad [5.4.7\text{-}19]$$
$$= P_E^* \int_{\frac{K_a}{2B_T}}^{\infty} \frac{d\tau}{2B_T\tau^2}$$
$$= \frac{P_E^*}{K_a}$$

We can now estimate the mean period between acquisition cycles to be:

$$\overline{T_1} = \frac{\overline{\tau^*}}{P(\varepsilon^*, \tau^*)} = \frac{K_a}{B_T}\left(\frac{K_a}{P_E^*}\right) = \frac{K_a^2}{B_T P_E^*} \qquad [5.4.7\text{-}20]$$

Therefore, the expected number of acquisition cycles during a mission of duration T_m is:

$$\overline{n_a} = \frac{T_m}{\overline{T_1}} = \frac{T_m B_T P_E^*}{K_a^2} \qquad [5.4.7\text{-}21]$$

As an illustrative example, assume a 5 year mission with the following characteristics:

P_E^* = 10^{-6},
B_T = 1 kHz,
K_a = 2,
T_m = 5 years = 1.58×10^8 sec.

The result is 4000 seconds, or 1.11 hours, between reacquisitions, with 39,000 acquisition cycles in total during the mission.

5.4.8 Recommendations

Two concerns dominate the pointing problem: maintenance of a point-ahead angle; and tolerance of noise. Over the GEO to LEO and GEO to GEO distances considered here it is imperative to use a narrow communication beam requiring point-ahead. The established means of maintaining this point-ahead angle employs a separate assembly of mirrors and detectors. However, with modern high speed detectors and control electronics it should be possible to overlap point-ahead control with the tracking function by tracking to an angular offset, the angle determined with locally stored orbital ephemeris. This approach would simplify the ISL system design considerably.

Noise has its greatest influence within the ISL system on pointing, so it is imperative that all noise sources be identified and quantified. The basic rule is to maximize received signal strength and broaden the tracking controller bandwidth as much as possible. Once the noise behaviour is identified and a range of telescope diameters selected a stable ISL design can be developed using the interactive-link algorithm presented.

The ISL network proposed overlaps the pointing and tracking functions without using a point-ahead mechanism or detector (Figure 5.4-15). Instead, the point-ahead function is performed by the fine tracking assembly and controller.

The system is calibrated to cause the transmit beam to align with the optical network boresight. CCD-type Quadrant detectors are used for receive beam fine-tracking. In order to avoid the use of a separate point-ahead assembly, the receive signal is offset from the quadrant detector centre by an amount equivalent to the point-ahead angle. The point-ahead offset is controlled open-loop from orbital ephemeris data periodically uploaded from ground.

This approach is made possible through the appropriate design of the network optics, and through the use of a programmable controller. In the case of the optical network, a 25× magnification telescope/eyepiece assembly, and a 350 mm path between the telescope eyepiece and a 15 mm communication detector lens. Combined, this design provides a 300 μrad communication field of view. This is more than adequate to accommodate the $\pm 50\,\mu$rad maximum offset required for point-ahead. The programmable controller is needed to dynamically adjust the offset of the receive beam from the tracking detector centre, and also to provide the fast response for compensating fine tracking disturbances. This approach differs from the other published methods which use a controller with a static control law to maintain a zero offset throughout the tracking phase. CAL feels this type of control can be accomplished with a space-qualified microprocessor-based CCD acquisition and processing system already developed by CAL.

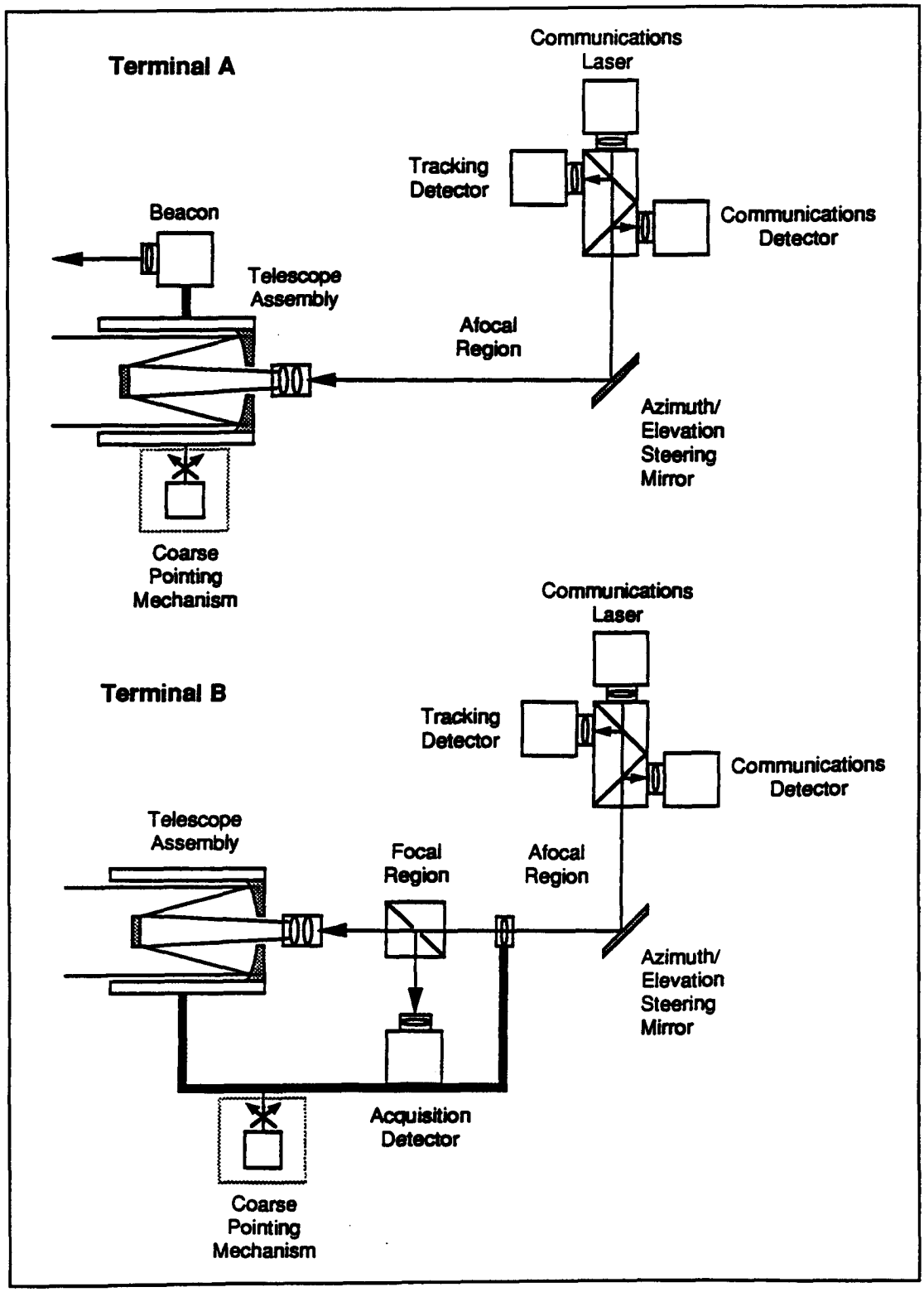

Figure 5.4-15 Proposed ISL Optical Network

This Page Intentionally Left Blank

SECTION 6

TERMINAL DESIGN

6.0 TERMINAL DESIGN

6.1 Design Procedure

The optical intersatellite link is characterized by very narrow beam widths which minimize the transmitter power requirements by increasing the acquisition and tracking requirements. This places great importance on the design of the acquisition and tracking systems. The step by step design procedure presented below has been generally followed in the present design exercise except tht step 5 and 6 have not been attempted.

1. On the basis of range, bit rate, bit error rate, laser wavelength and power, evaluate the link and determine the minumum telescope diameter to support the communications traffic assuming equal diameter for transmit and receive. From the minimum diameter the maximum λ/D is calculated.

2. The maximum mispoint angle ε_{max} is optimally placed at 4 dB down on the beam contour which is at 0.24 times the full beam width to the first null or $0.58\,\lambda/D$.

3. From the tracking specification for loss of lock probability (P_E) or burst probability and the maximum mispoint angle determined above, determine the maximum noise equialent angle (NEA) from

$$NEA = \frac{\varepsilon_{max}}{\sqrt{-2ln\,(P_E)}} = \frac{0.58\,\lambda/D}{\sqrt{-2ln\,(P_E)}}$$

4. The minimum SNR is then obtained from

$$\sqrt{SNR} = \frac{1}{NEA}\frac{3\pi}{16}\left(\frac{\lambda}{D}\right)$$

   From the SNR and the tracking loop bandwidth, determine the signal power required for tracking.

5. Evaluate the bit error rate over the beam width and determine the average bit error rate by integrating over a Rayliegh distributed pointing error out to 5 x NEA. Compare the average bit error rate to the bit error rate versus pointing angle to determine the pointing loss value for communications.

6. Carry out an analysis of link stability and on the basis of this, and taking into account the tracking power requirements and the communications pointing loss; reoptimize the link parameters.

7. The optics optimized above, and the required sensor power, determine the acquisition beacon power and the acquisition strategy.

6.2 Requirements

6.2.1 Baseline - 100 Mbps Direct Detection

The baseline system is required to provide communications between a geostationary satellite (GEO) and a low earth orbit satellite (LEO). The bit rate in the forward direction, from GEO to LEO is 19.2 kbps which is sufficient to provide command capability of the LEO satellite. The bit rate in the return direction is 100 mbps which is required to handle the high data rates generated on the LEO satellite. This requires a 100 mbps transmitter on the LEO satellite with a co-operating 100 mbps receiver on the GEO satellite. In the forward direction the GEO transmitter and the LEO receiver both operate at 19.2 kbps. Apart from this difference the two terminals are very similar in design.

A mini specification for the GEO/LEO link is given in Table 6.2-1 which is based on the link budget of table

6.2-2. A conceptual diagram of the optical system is shown in Figure 6.2-1 for the LEO terminal and in Figure 6.2-2 for the GEO terminal. An AlGaAs laser diode with approximately 80 mw is sufficient to transmit 100 mbps with a telescope of 13.6 cm diameter. The modulation in the return direction is QPPM to maximize performance for the high bit rate. In the forward direction simple ASK gives adequate performance.

The telescope diameter is derived from the telescope gain requirements based on the link budgets to meet the range and bit rate objectives. The other telescope parameters are design parameters with the values listed to indicate the design chosen.

The course pointing mechanism (CPM) consists of the motor driven gimbals to point the telescope in the direction of the target satellite. These have to cover a range determined by the orbit parameters. In this case, the geostationary satellite has to point the telescope only in the direction of the earth equal to ± 15 degrees in both pitch and roll. On the other hand, the LEO satellite must cover the entire hemisphere with some additional range to minimize the probability of hitting the end of the range in the middle of the pass. The precision of the course pointing mechanism must be small enough so that the telescope can be moved without going beyond the range of the fine pointing mechanism.

The slew rate of the CPM is large to minimize the elapsed time in the event that the azimuth stop is reached or, in the case of acquisition, to reach the indicated pointing direction.

The optical encoder determines the pointing angle of the telescope with a resolution such that any motion of the course pointing mechanism is easily determined.

The fine pointing mechanism is used to point the beam to an accuracy which is small compared to the beam width and with a response time capable of following the spectrum of disturbances expected.

Acquisition is achieved by means of a broadened beam using a high power beacon laser on the transmit side and a wide angle CCD detector on the receive side. The time allocated for acquisition is 120 seconds and the probability of achieving contact in that time is 95%.

After contact is established the probability that contact is lost due to noise in the tracking system should be less than 0.04% per hour which translates to an availability of better than 0.998.

Two laser transmitters and two detectors are provided in a 2 for 1 redundancy configuration. The two lasers are wavelength multiplexed as are the two detectors in such a way that one detector works with one transmitter and if either the laser or detector fails the other is not useable.

Two fine track detectors are also provided in a 2 for 1 redundancy configuration. The two detectors are connected with a 3 dB power split so that each of the track detectors will work with either of the laser transmitters.

6.2.2 Option 1 - 1 Gbps Link with Wavelength Multiplexing

There are two options described for increasing the bit rate capability of the return link to one giga bit per second (1 Gbps). The one, described in this section, uses a series of wavelength multiplexed AlGaAs lasers to achieve the total throughput of 1 Gbps. A conceptual diagram is given in Figure 6.2-3 for the LEO terminal and in Figure 6.2-4 for the GEO terminal. The bit rate of each channel (laser) has been raised, compared to the baseline, to 250 mbps so that only four operating lasers are required to provide the required 1 Gbps. A total of 6 wavelength multiplexed lasers are provided for redundancy purposes.

On the receive side of the return link, the same direct detection QPPM receivers are used as for the baseline, with the bit rate per channel increased to 250 mbps to match the transmit bit rate. A total of six receivers are used for redundancy purposes. The six receivers are wavelength multiplexed in the same manner as the lasers in such a way that there is a one to one correspondence between the lasers and receivers. Each receiver works with only one laser so that if either the laser or the receiver fails then the complete channel is

Table 6.2-1 Optical ISL Requirements (Baseline)

TERMINAL		GEO	LEO
Bit Rate	forward (kbps) return (Mbps)	19.2 100	19.2 100
Bit Error Rate		10^{-6}	10^{-6}
Laser		AlGaAs	AlGaAs
Wavelength (m)		0.8 - 0.9	0.8 - 0.9
Wavelength stability		TBD	TBD
Laser power (mw)		1	80
Detection		direct	direct
Modulation	forward return	ASK QPPM	ASK QPPM
Telescope	type diameter (mm) magnification	Reflective 136 30	Reflective 136 30
Course pointing mechanism (CPM)	coverage (deg) orientation precision (μRad) slew rate (deg/sec)	± 15 pitch ± 15 Roll TBD ± 100 20	± 200 Azimuth -10 to +100 elevation TBD ± 100 20
Encoder	type resolution (μRad)	optical ± 15	optical ± 15
Tracking	mirror range (μR) detector type detector range (μRad) maximum point ahead angle (μrad) tracking accuracy (NEA μRad) response frequency (Hz)	± 200 CCD ± 200 ± 50 ± 0.5 1200	± 200 CCD ± 200 ± 50 ± 0.5 1200
Mass		TBD	TBD
Power		TBD	TBD
Temperature Range (°C)		15 - 25	15 - 25
Temperature Gradient		TBD	TBD
Acquisition	beacon transmitter beacon power (w) beacon wavelength (μm) wavelength stability (deg) cone of uncertainty (deg) acquisition time (sec)	separate telescope ≤ 3.8 0.8 - 0.9 TBD ± 0.15 120	separate telescope ≤ 3.8 0.8 - 0.9 TBD ± 0.5 120
Detector range (Rad) detector type probability (%)		± 9000 CCD 95	± 9000 CCD 95
Probability of losing lock (%/hour)		0.04	0.04
Availability		.95	.95

Table 6.2-2 Baseline Link Budget for 100 Mbps Direct Detection System

	Forward		Return	
Laser Type	AlGaAs		AlGaAs	
Wavelength (nm)	850		850	
Bit Rate (Mbps)	0.0192		100	
Modulator type	Bias		Bias	
Modulation type	ASK		ASK	
Detection type	Direct		Direct	
Path Length (km)	47000		47000	
TRANSMIT TELESCOPE GAIN (dB)		110.1		110.3
Aperture Diameter (cm)	13.6		13.6	
Aperture Gain	114.0		114.0	
Aperture Eff./blockage	1.8		1.8	
Support Member Blockage	0.0		0.0	
Surface Errors	0.5		0.5	
Defocusing	0.2		0.2	
Transmission Loss	0.8		0.8	
Pointing Loss	0.6		0.4	
N.E.A. (micro rad.)	0.62		0.5	
TRANSMITTER POWER (dBW)		-34.1		-10.9
Average Laser Power(dBW)	-34.1		-10.9	
(Watts)	0.000389		0.081	
Modulator Efficiency	0.0		0.0	
Modulator Transmission	0.0		0.0	
Polarizer Loss	0.0		0.0	
TRANSMIT OPTICS PATH LOSS (dB)		-0.7		-0.7
Fine Pointing Mirrors	0.1		0.1	
Beacon Laser Coupler	0.1		0.1	
Beacon Detector Coupler	0.1		0.1	
Fine Track. Det. Coupler	0.1		0.1	
Comms. Det. Coupler	0.1		0.1	
Look-ahead Coupler	0.1		0.1	
Look-ahead Mirrors	0.1		0.1	
SPACE LOSS (dB)		-296.8		-296.8
RECEIVE TELESCOPE GAIN (dB)		112.4		112.4
Aperture Diameter (cm)	13.6		13.6	
Aperture Gain	114.0		114.0	
Aperture Eff./blockage	0.3		0.3	
Support Member Blockage	0.0		0.0	
Surface Errors	0.5		0.5	
Transmission Loss	0.8		0.8	
RECEIVE OPTICS PATH LOSS (dB)		-7.4		-0.5
Fine Pointing Mirrors	0.1		0.1	
Beacon Laser Coupler	0.1		0.1	
Beacon Detector Coupler	0.1		0.1	
Fine Track. Det. Coupler	6.97		0.14	
Comms. Det. Coupler	0.1		0.1	
Polarizer loss	0.0		0.0	
L. O. coupler loss	0.0		0.0	
Wavefront mismatch	0.0		0.0	
Alignment mismatch	0.0		0.0	
RECEIVER SENSITIVITY (dBW)		-119.4		-89.3
Photon Energy (J)	2.34E-19		2.34E-19	
Av. Ph./Bit at BER=10^-6	45.0		45.0	
Rcv. Sens. (dBW)	-126.9		-89.8	
Extinction ratio assumed	0.05		0.05	
Laser Linewidth	0.0		0.0	
Background Noise	7.5		0.5	
SYSTEM MARGIN		3.0		3.0

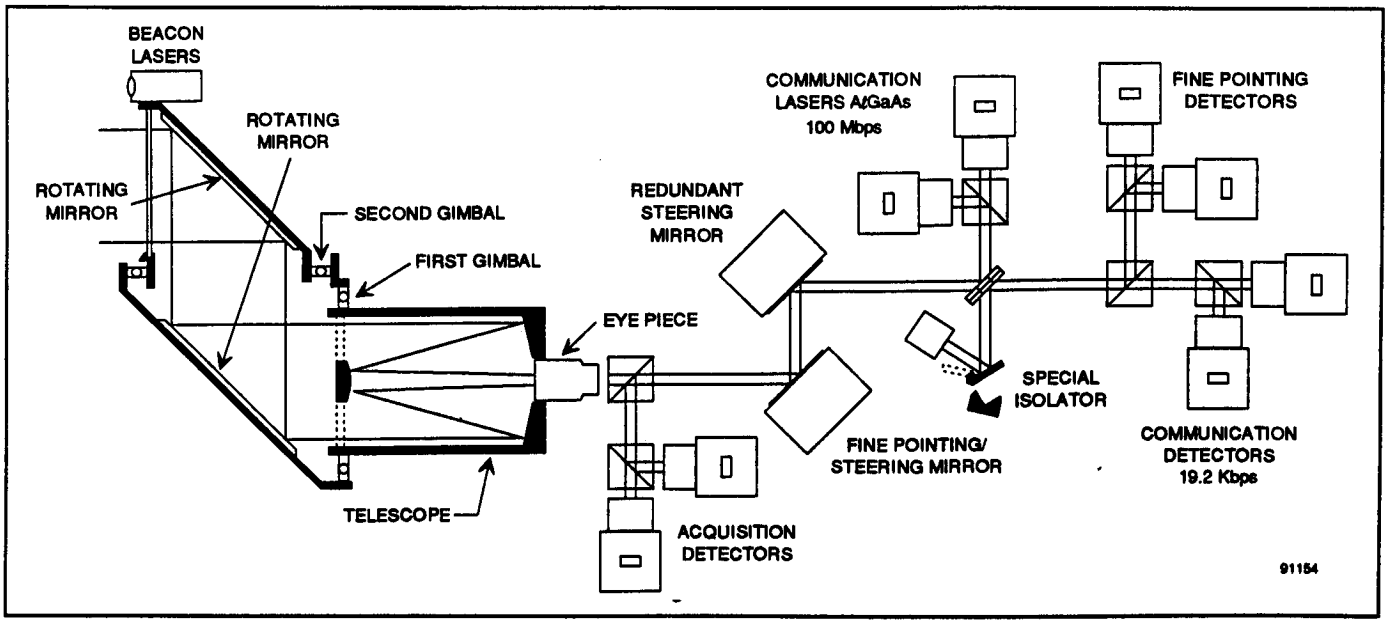

Figure 6.2-1 Conceptual Diagram of the Baseline LEO Terminal Operating at 100 Mbps

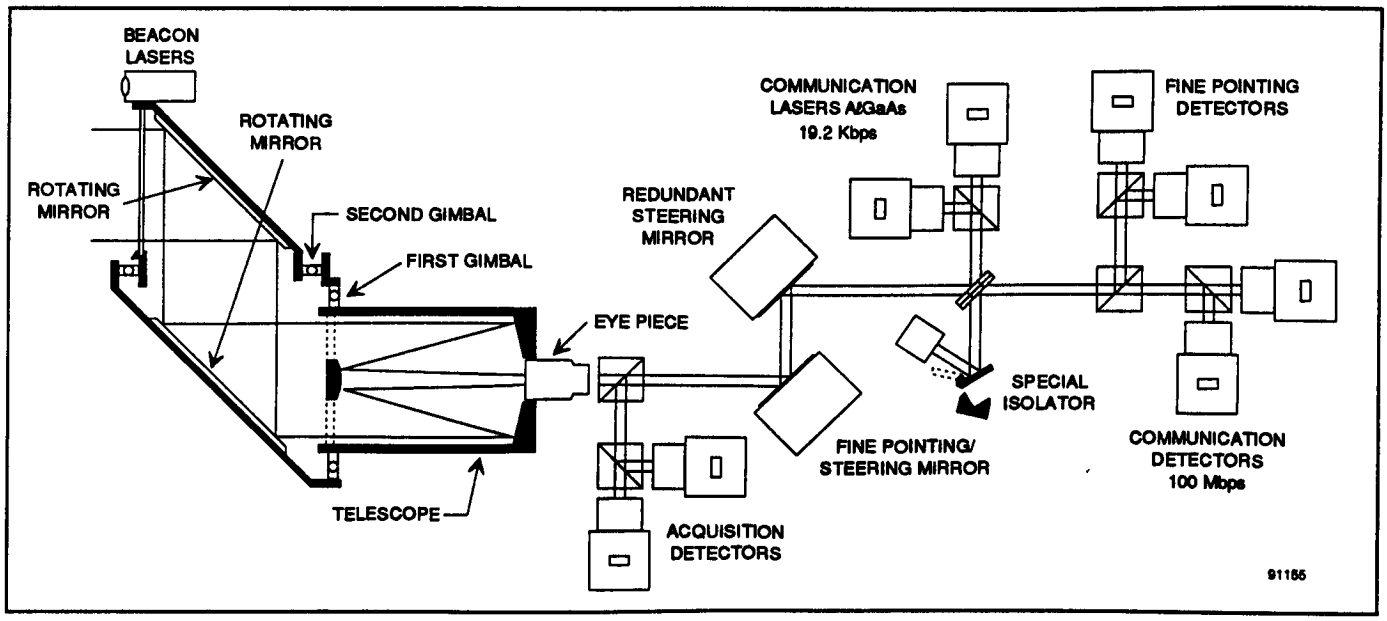

Figure 6.2-2 Conceptual Diagram of the Baseline GEO Terminal Operating at 100 Mbps

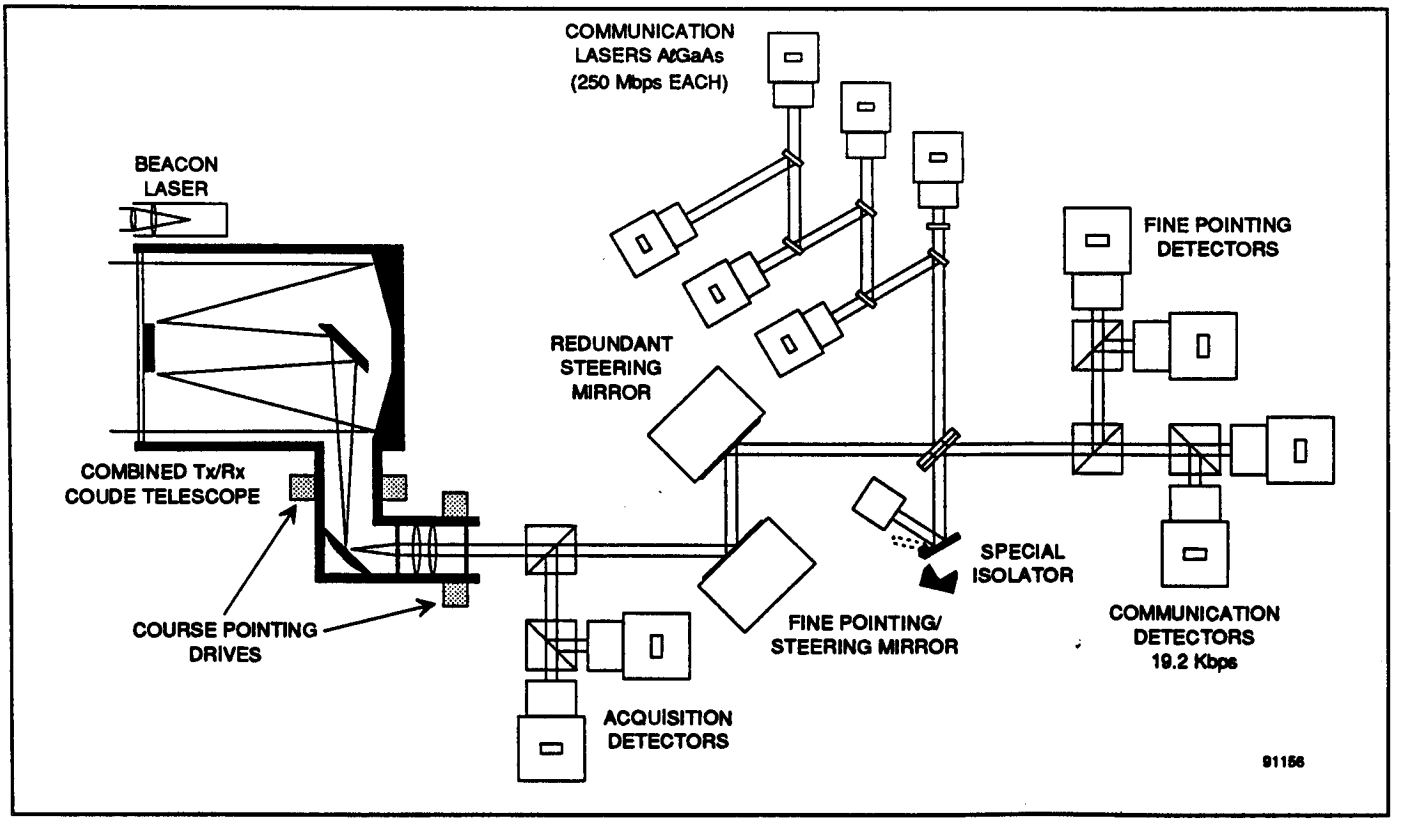

Figure 6.2-3 Conceptual Diagram of the Option 1 LEO Terminal Operating at 1 Gbps

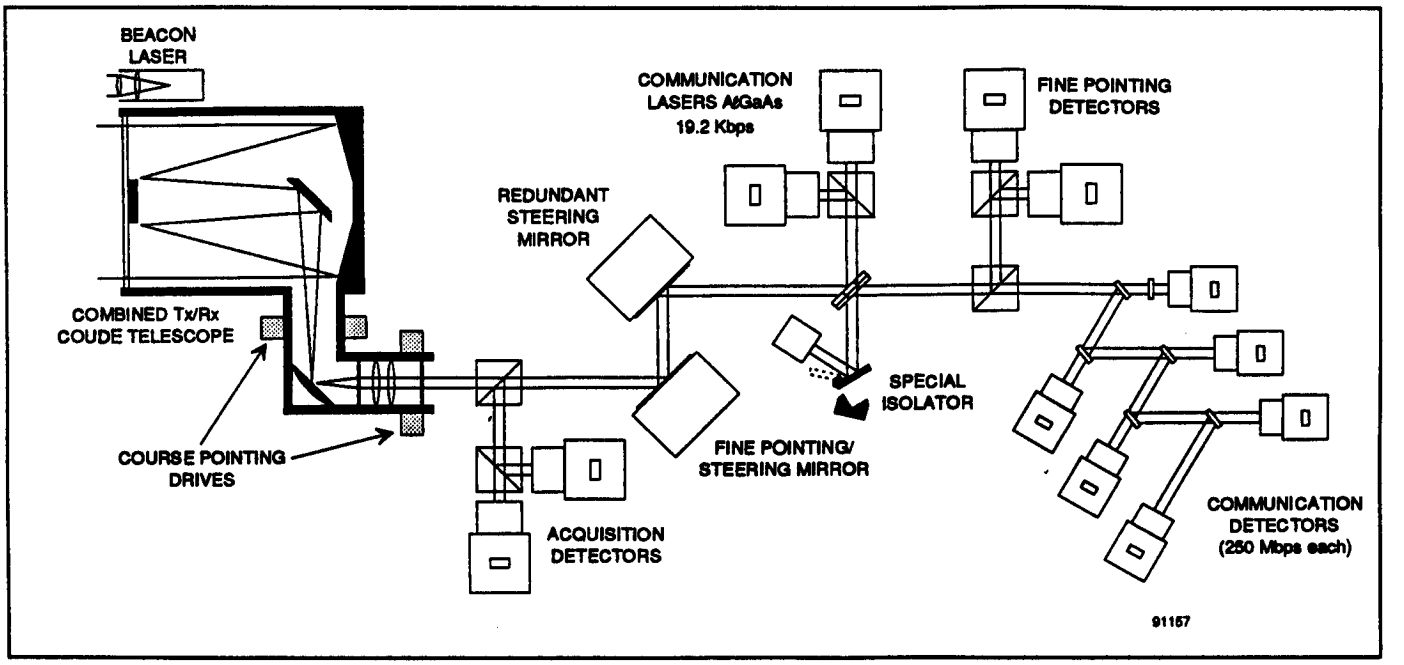

Figure 6.2-4 Conceptual Diagram of the Option 1 GEO Terminal Operating at 1 Gbps

Table 6.2-3 Option 1 Optical ISL Requirements (where different from baseline)

		GEO Terminal	LEO Terminal
Transmitter	type	AlGaAs	AlGaAs
	number	single laser	four wavelength multiplexed lasers
	laser wavelength (μm)	0.8 - 0.9	0.8 - 0.9
	wavelength stability	TBD	TBD
	laser power (each) (mW)	1	80
	bit rate per channel	19.2 kbps	250 Mbps
	redundancy	2 for 1	6 for 4
	telescope diameter (mm)	180	180
Receiver	type	APD direct detection	APD direct detection
	number	four wavelength multiplexed detectors	single detector
	redundancy	6 for 4	2 for 1

lost. Option 1 parameters that differ from the baseline are given in Table 6.2-3. These requirements are based on the link budget of Table 6.2-4.

In the forward direction, the bit rate at 19.2 kbps is unchanged from the baseline and the same configuration is used.

Two fine track detectors are provided in a 2 for 1 redundancy configuration. The two detectors are connected with a 3 dB power split so that each of the track detectors will work with all six of the lasers.

6.2.3 Option 2 - 1 Gbps with Heterodyne Detection System

The second option increases the bit rate in the return direction by using a single 1 Gbps Nd:Yag laser and a heterodyne receiving system. In the forward direction the bit rate remains at 19.2 kbps and the same AlGaAs laser with direct detection receiver is used as for the baseline. Option 2 parameters that differ from the baseline are given in Table 6.2-5 which is based on the link budget of Table 6.2-6. A conceptual diagram is shown in Figure 6.2-5 for the LEO terminal and in Figure 6.2-6 for the GEO terminal.

The redundancy requirement is 2 for 1 for both the lasers and receivers, the lasers operate at different wavelengths and are combined into a single optical path by wavelength multiplexers. This means that each receiver operates only with one laser and if either the laser or the receiver fails then the other is not useable.

As with the other options, the fine pointing detectors are connected with a 3 dB power splitter so that each work with either transmitter.

Table 6.2-5 Option 2 Optical ISL Requirements (where different from baseline)

		LEO Terminal	GEO Terminal
Transmitter	type	Nd:Yag	AlGaAs
	laser power (mW)	800	1
	wavelength (μm)	0.96 - 1.06	0.8 - 0.9
	wavelength stability	TBD	TBD
	modulation	PSK	ASK
	number	One	one
	redundance	2 for 1	2 for 1
	bit rate per channel	1 Gbps	19.2 kbps
	telescope diameter (mm)	215	215
Receiver	type	Direct detection	Heterodyne
	redundancy	2 for 1	2 for 1

Table 6.2-4 Option 1 Link Budget for 1 Gbps Wavelength Multiplexed Direct Detection System

	Forward		Return	
Laser Type	AlGaAs		AlGaAs	
Wavelength (nm)	850		850	
Bit Rate (Mbps)	0.0192		250	
Modulator type	Bias		Bias	
Modulation type	ASK		ASK	
Detection type	Direct		Direct	
Path Length (km)	47000		47000	
TRANSMIT TELESCOPE GAIN (dB)		112.4		112.4
Aperture Diameter (cm)	18.0		18.0	
Aperture Gain	116.5		116.5	
Aperture Eff./blockage	1.8		1.8	
Support Member Blockage	0.0		0.0	
Surface Errors	0.5		0.5	
Defocusing	0.2		0.2	
Transmission Loss	0.8		0.8	
Pointing Loss	0.7		0.7	
N.E.A. (micro rad.)	0.5		0.5	
TRANSMITTER POWER (dBW)		-38.4		-11.1
Average Laser Power(dBW)	-38.4		-11.1	
(Watts)	0.000145		0.078	
Modulator Efficiency	0.0		0.0	
Modulator Transmission	0.0		0.0	
Polarizer Loss	0.0		0.0	
TRANSMIT OPTICS PATH LOSS (dB)		-0.7		-0.7
Fine Pointing Mirrors	0.1		0.1	
Beacon Laser Coupler	0.1		0.1	
Beacon Detector Coupler	0.1		0.1	
Fine Track. Det. Coupler	0.1		0.1	
Comms. Det. Coupler	0.1		0.1	
Look-ahead Coupler	0.1		0.1	
Look-ahead Mirrors	0.1		0.1	
SPACE LOSS (dB)		-296.8		-296.8
RECEIVE TELESCOPE GAIN (dB)		114.9		114.9
Aperture Diameter (cm)	18.0		18.0	
Aperture Gain	116.5		116.5	
Aperture Eff./blockage	0.3		0.3	
Support Member Blockage	0.0		0.0	
Surface Errors	0.5		0.5	
Transmission Loss	0.8		0.8	
RECEIVE OPTICS PATH LOSS (dB)		-7.4		-0.5
Fine Pointing Mirrors	0.1		0.1	
Beacon Laser Coupler	0.1		0.1	
Beacon Detector Coupler	0.1		0.1	
Fine Track. Det. Coupler	6.97		0.14	
Comms. Det. Coupler	0.1		0.1	
Polarizer loss	0.0		0.0	
L. O. coupler loss	0.0		0.0	
Wavefront mismatch	0.0		0.0	
Alignment mismatch	0.0		0.0	
RECEIVER SENSITIVITY (dBW)		-119.0		-84.8
Photon Energy (J)	2.34E-19		2.34E-19	
Av. Ph./Bit at BER=10^-6	50.0		50.0	
Rcv. Sens. (dBW)	-126.5		-85.3	
Extinction ratio assumed	0.05		0.05	
Laser Linewidth	0.0		0.0	
Background Noise	7.5		0.5	
SYSTEM MARGIN		3.0		3.0

Table 6.2-6 Option 2 Link Budget for 1 Gbps Heterodyne Detection System

	Forward		Return	
Laser Type	AlGaAs		Nd:Yag	
Wavelength (nm)	850		1060	
Bit Rate (Mbps)	0.0192		1000	
Modulator type	Bias		External	
Modulation type	ASK		PSK	
Detection type	Direct		Hetrodyne	
Path Length (km)	47000		47000	
TRANSMIT TELESCOPE GAIN (dB)		114.4		112.5
Aperture Diameter (cm)	21.5		21.5	
Aperture Gain	118.0		116.1	
Aperture Eff./blockage	1.8		1.8	
Support Member Blockage	0.0		0.0	
Surface Errors	0.5		0.5	
Defocusing	0.2		0.2	
Transmission Loss	0.8		0.8	
Pointing Loss	0.3		0.3	
N.E.A. (micro rad.)	0.35		0.35	
TRANSMITTER POWER (dBW)		-45.0		-3.5
Average Laser Power(dBW)	-45.0		-0.6	
(Watts)	0.00003		0.87	
Modulator Efficiency	0.0		2.5	
Modulator Transmission	0.0		0.1	
Polarizer Loss	0.0		0.3	
TRANSMIT OPTICS PATH LOSS (dB)		-0.7		-0.7
Fine Pointing Mirrors	0.1		0.1	
Beacon Laser Coupler	0.1		0.1	
Beacon Detector Coupler	0.1		0.1	
Fine Track Det. Coupler	0.1		0.1	
Comms. Det. Coupler	0.1		0.1	
Look-ahead Coupler	0.1		0.1	
Look-ahead Mirrors	0.1		0.1	
SPACE LOSS (dB)		-296.8		-294.9
RECEIVE TELESCOPE GAIN (dB)		116.4		114.5
Aperture Diameter (cm)	21.5		21.5	
Aperture Gain	118.0		116.1	
Aperture Eff./blockage	0.3		0.3	
Suppor Member Blockage	0.0		0.0	
Surface Errors	0.5		0.5	
Transmission Loss	0.8		0.8	
RECEIVE OPTICS PATH LOSS (dB)		-0.5		-2.7
Fine Pointing Mirrors	0.1		0.1	
Beacon Laser Coupler	0.1		0.1	
Beacon Detector Coupler	0.1		0.1	
Fine Track Det. Coupler	0.14		0.14	
Comms. Det. Coupler	0.1		0.1	
Polarizer loss	0.0		0.3	
L. O. Coupler loss	0.0		0.3	
Wavefront Mismatch	0.0		0.3	
Alignment mismatch	0.0		1.3	
RECEIVER SENSITIVITY (dBW)		-119.0		-77.9
Photon Energy (J)	2.34E-19		1.87E-19	
Av. Ph./Bit at BER=10^-6	50.0		85.0	
Rcv. Sens. (dBW)	-126.5		-78.0	
Extinction ratio assumed	0.05		0.05	
Laser Linewidth	0.0		0.1	
Background Illumination	7.5		0.00	
SYSTEM MARGIN		6.7		3.0

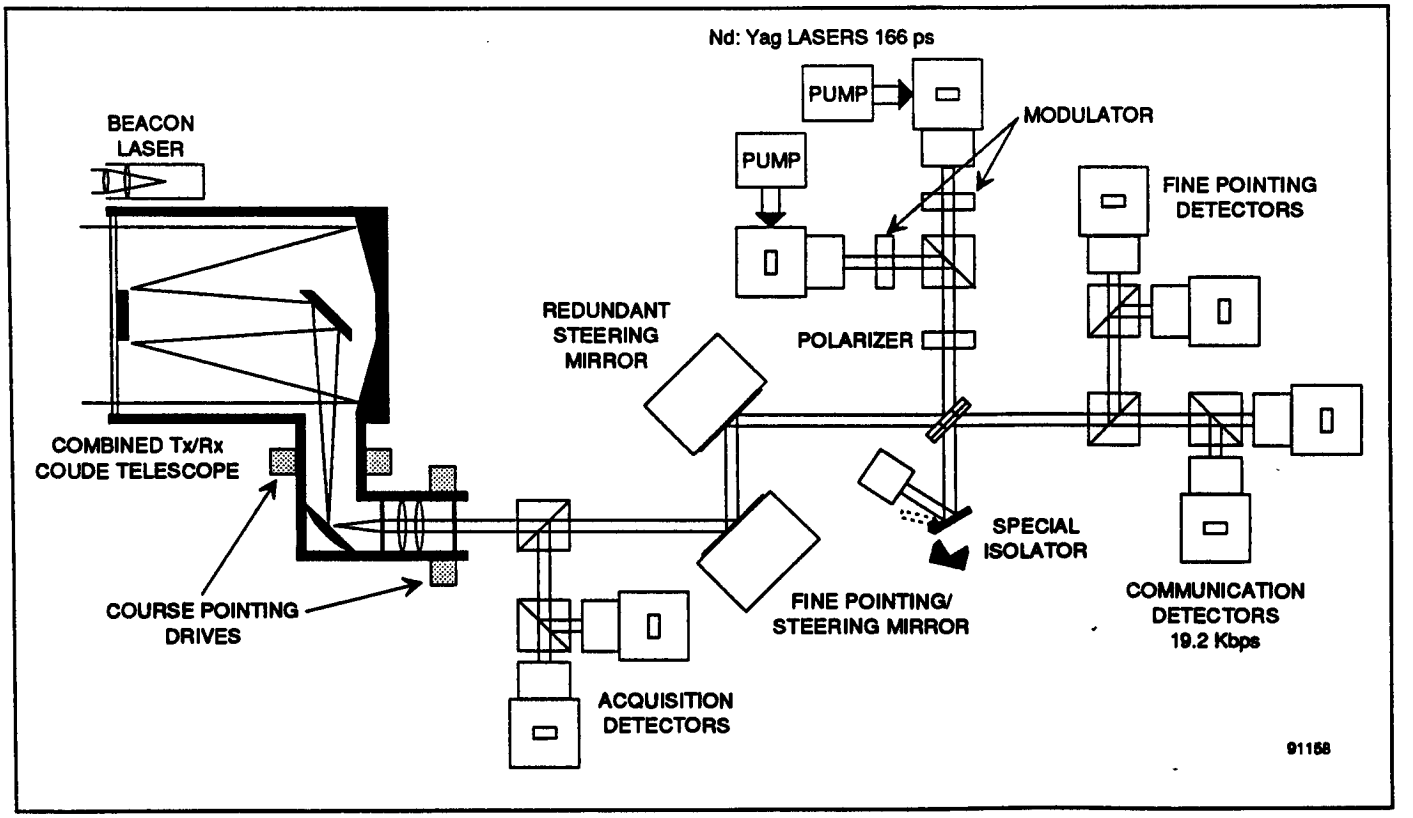

Figure 6.2-5 Conceptual Diagram of the Option 2 LEO Terminal Operating at 1 Gbps

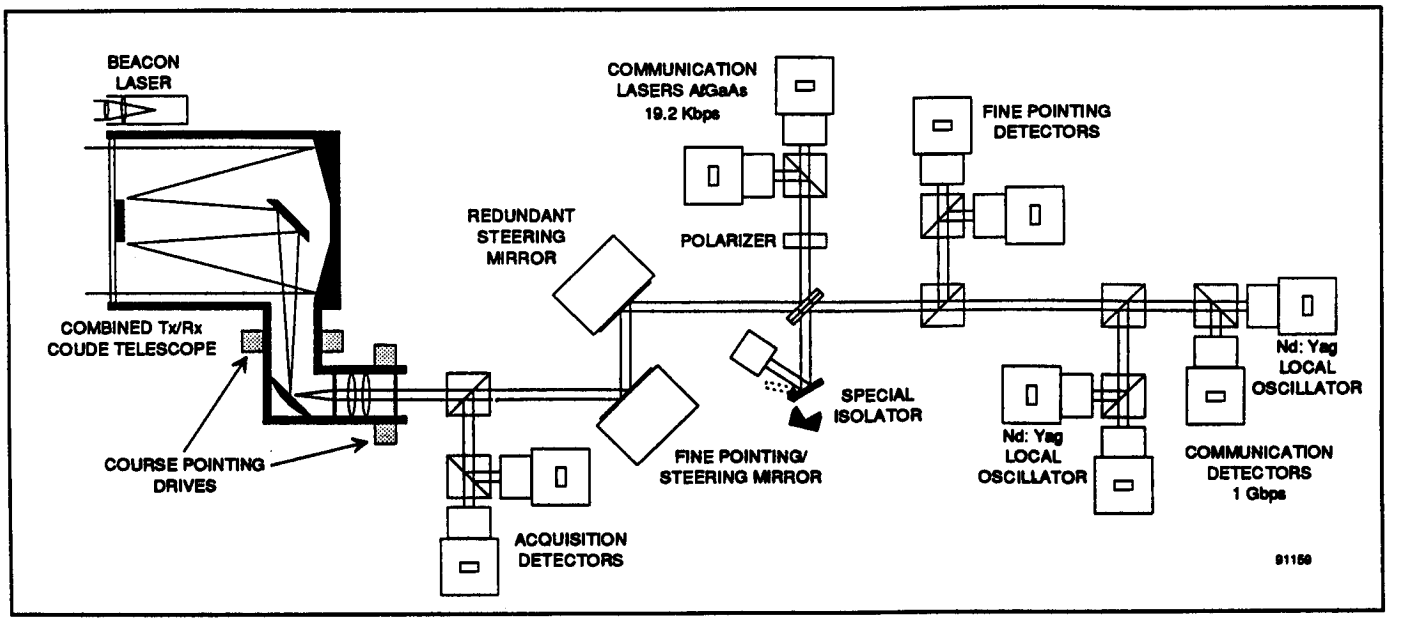

Figure 6.2-6 Conceptual Diagram of the Option 2 GEO Terminal Operating at 1 Gbps

6.3 Optical Path Layout

6.3.1 Design of the Beacon Transmitter

The beacon transmitter is a multiple laser diode assembly with a minimum power output of 3.8W. This power is spread over a wider beam width than the communications laser beam width which is dependent on the ability to detect the presence of the beacon signal at the acquisition detector. The beacon transmitter does not make use of the main telescope since it has a broad beam. The acquisition detector does use the main telescope in order to maximize the sensitivity of the receive system. The beacon transmitter is scanned over the cone of uncertainty and when contact is made it is unlikely to be at the peak of the beam. A 3 dB pointing loss is included for this factor. In addition 3 dB loss is included for the power division to drive the main and redundant acquisition detectors. The beacon beam width is of the order of 700 μRad which is less than the cone of uncertainty for the GEO spacecraft and much less than that for the LEO satellite. Typical beacon laser telescopes are refractive designs with about a 2-3 cm diameter.

An alternative approach is to enlarge the beacon laser beam width until the beam width equals the cone of uncertainty. This cone is equal to $\pm$ 8700 μRad for Radarsat and $\pm$ 2600 μRad for the geostationary satellite. When this is done it is still possible to close the loop by increasing the dwell time or integrating the signal over many bit periods. To cover the larger cone of uncertainty of $\pm$ 8700 μRad the bit period must be increased by more than two orders of magnitude. Unfortunately the number of background noise photons also increases by two orders of magnitude with the result that the reduced signal level is immersed in background noise photons and much larger integration times would be required to detect the signal source. Much more detailed analysis would be needed to determine the integration time required to ensure acquisition.

The scanning beacon approach is recommended.

6.3.2 Communication and Acquisition Detector Optical Path Design

In order to design the optical path, the requirements specified in Table 6.3-1 must first be identified. An F/4 collection telescope has been assumed. The selection of the F/# is a tradeoff between size and performance. As the telescope speed is improved the telescope length diminishes but the manufacturing tolerances become more stringent. On the US LITE program an F/1.7 Dall Kirkam design with a 20 cm aperture was employed. The high speed was dictated by volume constraints but super invar metering rods and careful thermal control were required to maintain the sensitivity [94].

The telescope could be either reflective or refractive depending upon the aperture size, the operating wavelength, the weight and stability requirements. For this analysis a Cassegrain telescope will be employed since it the most commonly employed design for OISL applications [95]. Also, a certain amount of athermalization is obtained with this design provided temperature gradients are minimized. Another advantage of the Cassegrain is that an intermediate image is formed, before the eyepiece, allowing a field stop (Lyot stop) to be positioned to limit the stray radiation from off axis sources such as the sun.

Table 6.3-1 Baseline OISL System Requirements

Telescope Type	Cassegrain
Diameter (a)	13.6 cm
F/# (F_{obj} / a)	4
Magnification	30
Acquistion FOV LEO	8700 μrad ($\pm$.5 degrees)
Acquistion FOV GEO	2600 μrad ($\pm$0.15 degrees)
CPA Precision	200 μrad peak to peak
Fine Pointing FOV	400 μrad peak to peak
Look Ahead Angle	100 μrad peak to peak
Communication Detector FOV	100 -150 μrad peak to peak

Following the collection telescope an eyepiece is employed to collimate the optical beam while magnifying the telescope field of view.

The Magnification is given by:

$$M = \frac{Tan\,(\theta_{eyepiece})}{Tan\,(\theta_{eyepiece})} = \frac{F_{obj}}{F_{eye}}$$

For this analysis a magnification of 30 was selected. This selection requires a tradeoff between the system FOV and the allowed optical element size. If the magnification is too low then the large collimated beam diameter will lead to large detector lens diameters. Alternatively, as will be illustrated in the next section, a large magnification and acquisition FOV can lead to a excessively large acquisition detector lens diameter.

$$P = \frac{a}{M}$$

Figure 6.3-1 illustrates the interaction of the basic optical parameters. For the baseline OISL design the derived parameters are:

pupil diameter equals 4.5 mm
the objective lens focal length equals 544 mm
the eyepiece focal length equals 18.1 mm
the eyepiece aperture equals 14.3 mm

6.3.2.1 Design of the Optical Path for the Acquisition Detector

The acquistion detector is placed as close as possible to the optical telescope eyepiece so as to minimize the beam diameter. Figure 6.3-2 illustrates optical layout for the acquistion detector receiver. The beacon laser radiation is captured by the primary telescope and collimated by the eyepiece. Once the beam emerges from the eyepiece it strikes the beam splitter and is directed into the acquistion detector lens. The optical beam splitter may be a dichroic element if the beacon laser operates at a wavelength different from the communication laser, otherwise the beam splitter will only be a partial reflector. Given an acquisition field of view of ± 8700 μradians, the aperture diameter of the acquistion detector lens is given by:

$$d = p + 2LMTan\theta - 2(F_{obj} + F_{eye})\,Tan\theta$$

where:

p	mm	is the eyepiece pupil diameter
F_{obj}	mm	is the telescope focal length

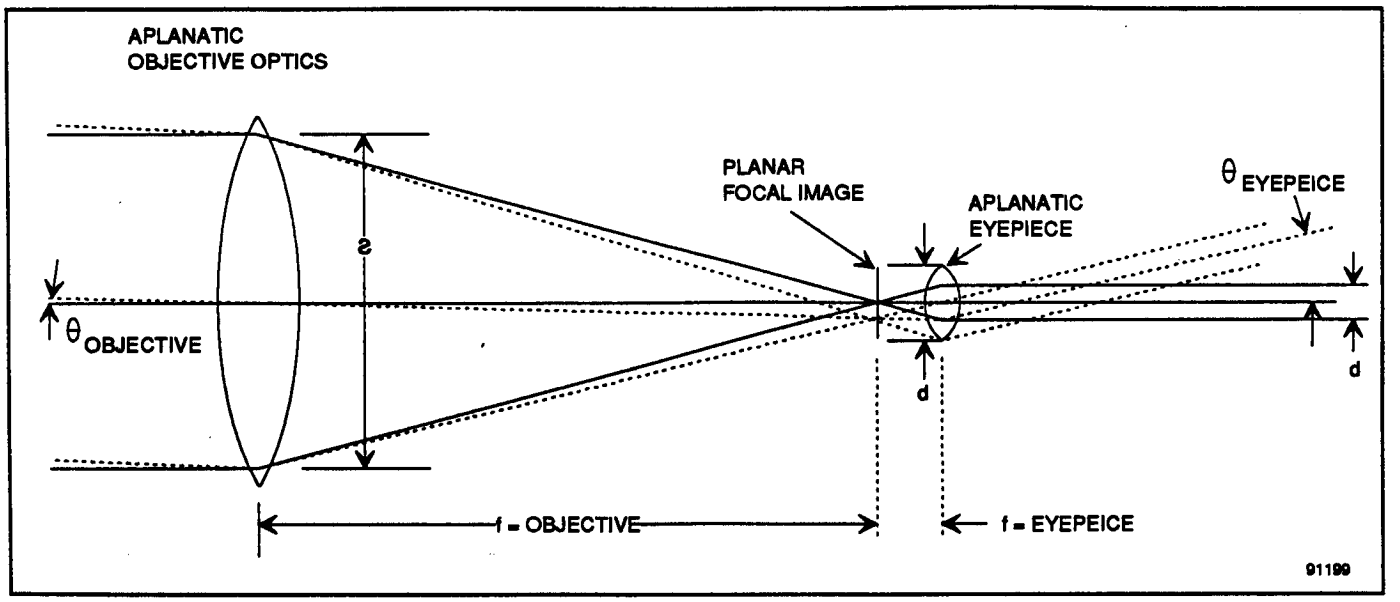

Figure 6.3-1 OISL Telescope Optical Schematic

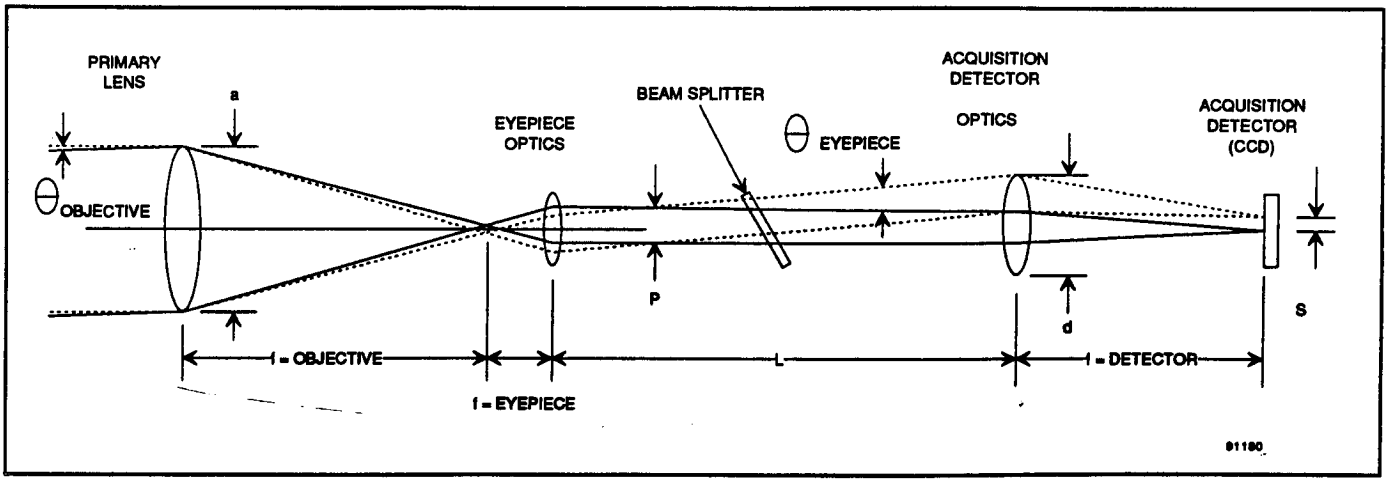

Figure 6.3-2 The Acquistion Detector Optical Layout

F_{eye}	mm	is the eyepiece focal length
L	mm	is the separation between the acquistion detector lens and the eyepiece
M	-	is the magnification of the eyepiece
θ	rad	is the acquistion half angle field of view

A close examination of this equation reveals that for the OISL application, the second term dominates. Table 6.3-2 illustrates the predicted beam diameter as a function of eyepiece/acquisition lens separation. Note that once the optical beam leaves the telescope eyepiece, the beam diverges requiring an increasing larger collection optics clear aperture. If the FOV is large enough then a runaway condition can be reached in which the packaging of the redundant optics becomes a very difficult problem. Figure 6.3-3 illustrates the relative size increase which can occur between the beamsplitter and the detector collection lens.

Table 6.3-2 Acquisition Detector Lens Diameters

Eyepiece/Acquistion Detector Separation (L) mm	Acquistion Detector Lens Diameter (d) mm
50	21
75	34
100	47
125	60
150	73

To avoid this runaway condition, a design modification was implemented, based upon a wide angle lens for a SLR Camera in which a deflection mirror is accommodated between the lens and the image plane [85]. As illustrated in Figure 6.3-7, the acquisition detector beam splitter can be placed directly behind the eyepiece on the underside of the optical bench. By employing a negative front lens group and a rear positive lens group (reversed telephoto lens) the back focal length can be lengthened (beyond the effective lens focal length), allowing a beam splitter to be accommodated before the detector array. The disadvantage with this design is that the placement of the beamsplitter after the correction elements, within the converging beam, will be very sensitive to misalignment especially since the detector is effectively viewing a ± 15 degree FOV (For an acquistion FOV of $\pm .5$ degrees or 8700 μradians).

Charge coupled detectors are commonly employed as acquistion detectors. The course pointing assembly is adjusted until the beacon laser spot size is aligned in the center of the array.

The acquisition detector size is determined by the desired detector lens F/# and the system FOV. As illustrated in Figure 6.3-4, assuming a CCD array size of 10 mm square the detector lens focal length shall be 36

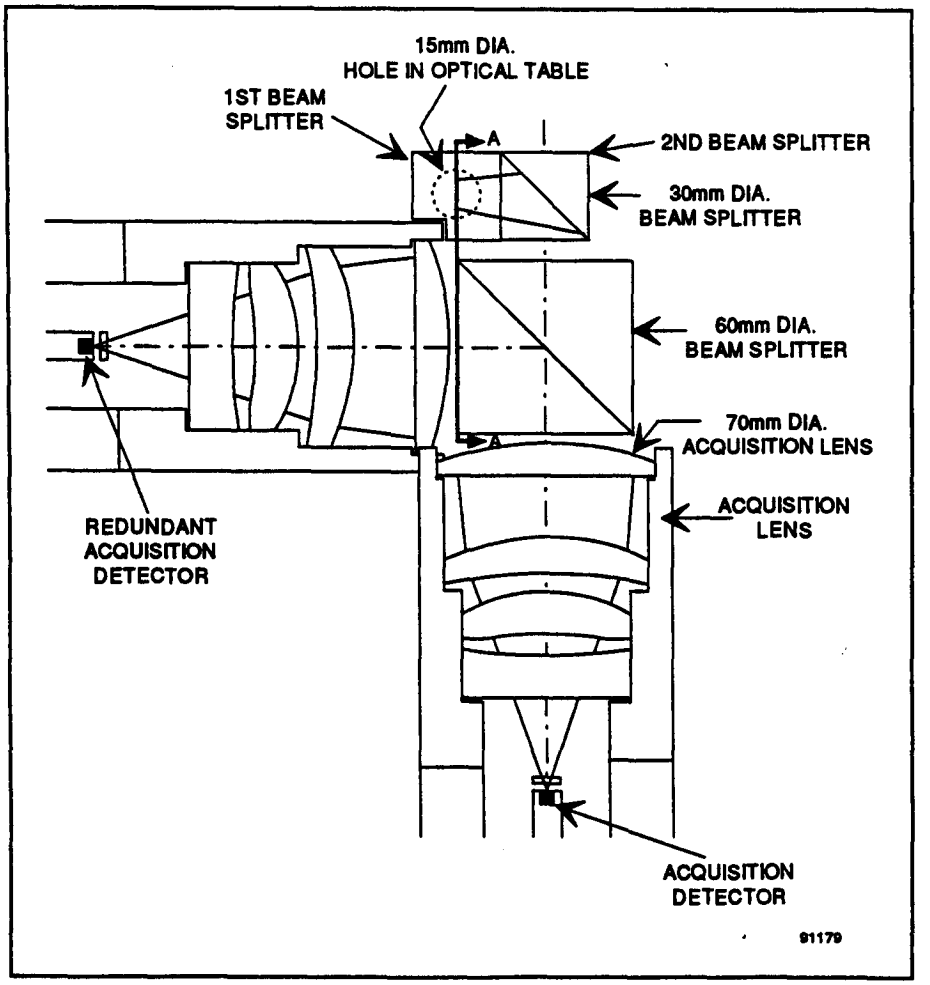

Figure 6.3-3 The Acquistion Detector Beam Diameters

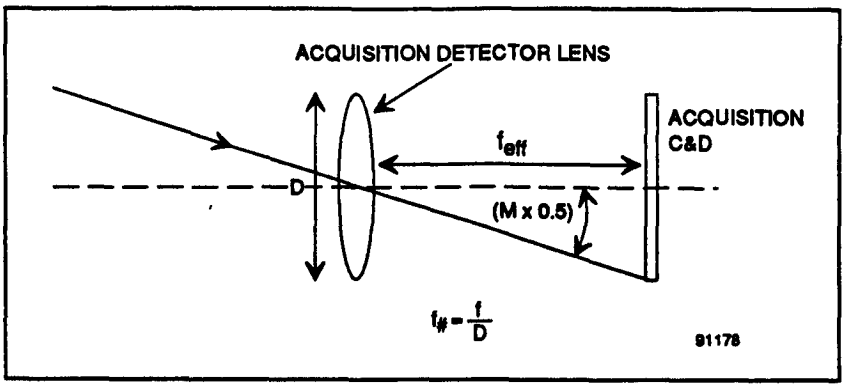

Figure 6.3-4 The Acquistion CCD Detector Size Requirements

the lens F/# will be 1.8. With a course pointing precision of 200 μradians peak to peak the maximum pixel size to ensure acquistion is 76 μm square. This yields a CCD array format of only 131 pixels square. However, manufacturability considerations will reduce the desired pixel size to about 20 - 40 μm increasing the pixel count to better than 256 x 256.

Therefore during course pointing the stabilization algorithms will drive the beacon laser spot to the center of the CCD array; where the center of the array is defined by an area of about 4 pixels square. Since the beacon laser spot will be close to diffraction limited (3.5 μm diameter) the actual signal will only appear on a single pixel within this central area. The software algorithms will have to be adapted to ensure that the stabilized condition is recognized. Should it be necessary to reduce this number to a single pixel, the CCD could be moved closer to the detector lens however, this would require a faster lens leading to manufacturability problems.

Clearly further detailed tradeoffs are required before the optimum acquistion detector design is established.

6.3.2.2 Communications Optical Path Design

The communication optical path is designed using the same mathematical relationship established in the previous section. However, the required aperture diameter is significantly reduced since the communication detector FOV is only $\pm$ 75 μradians.

Table 6.3-3 illustrates the required aperture diameter as a function of eyepiece/detector lens separation. However, the first section of the optical path also includes the fine pointing mirrors therefore, the fine pointing FOV must be accounted for in the design. Since the aperture size for the communication and fine pointing detectors are not significantly different a 15 mm diameter is sufficient for the baseline. In this way some design margin will exist to allow for fabrication and assembly tolerances. Figure 6.3-8 illustrates the optical design for the baseline system in which a 15 mm beam diameter was employed. A comprehensive optical tolerancing budget must be formulated using an optical software design program before the final aperture diameter is established. For the Option 1 and Option 2 requirements, the larger telescope diameter leads to a 20 - 25 mm aperture diameter for the communications and fine pointing optical path.

Table 6.3-3 Communication and Fine Pointing Detector Lens Diameters

Eyepiece/Detector Lens Separation (L) mm	Communication Lens Diameter (mm)	Fine Pointing Lens Diameter (mm)
150	5.1	5.8
175	5.2	6.1
200	5.3	6.3
225	5.4	6.7
250	5.5	6.9
275	5.6	7.2
300	5.8	7.4
325	5.9	7.7

The communication detector design also includes a spectral isolator. The spectral isolator shown is based upon the SILEX design. The portion of the transmit beam which passes through the beam splitter is reflected off of the flip-flop mirror into the light trap. The light trap contains a highly absorbent "optical black" coating which absorbs the radiation, ensuring that no scattered laser radiation reaches the communication detectors. However, for inflight calibration purposes, the flip-flop mirror is moved out of the path so that the beam is retroreflected into the communications and fine tracking detector optics.

6.3.3 Optomechanical Design Considerations

To ensure that the required optical performance is obtained once the OISL system is deployed in space a comprehensive opto-mechanical tolerancing budget must be established. Within the budget, optical manufacturing, assembly and environmental factors must be accounted. Optical design programs such as CodeV are designed to generate manufacturing and assembly

tolerances based upon various figures of merit such as wavefront error. The difficulty arises when the effect of the operating environment is included. Figure 6.3-5 illustrates a typical formulation of a wavefront error budget for a space based optical instrument [134].

The impact of thermal gradients can be modelled using optical design programs but careful thermal engineering is required to ensure that the actual gradients do not exceed the design limits. Most optical instruments which are deployed in space utilize passive athermalization techniques such as opposing index of refraction coefficients and low thermal expansion materials such as Invar and carbon fiber composites. Also passive coolers, heaters and temperature sensors could be employed to control the optical bench temperature within 5 degrees or better. On larger Satellites a centralized cooling system may be available to draw away excess heat.

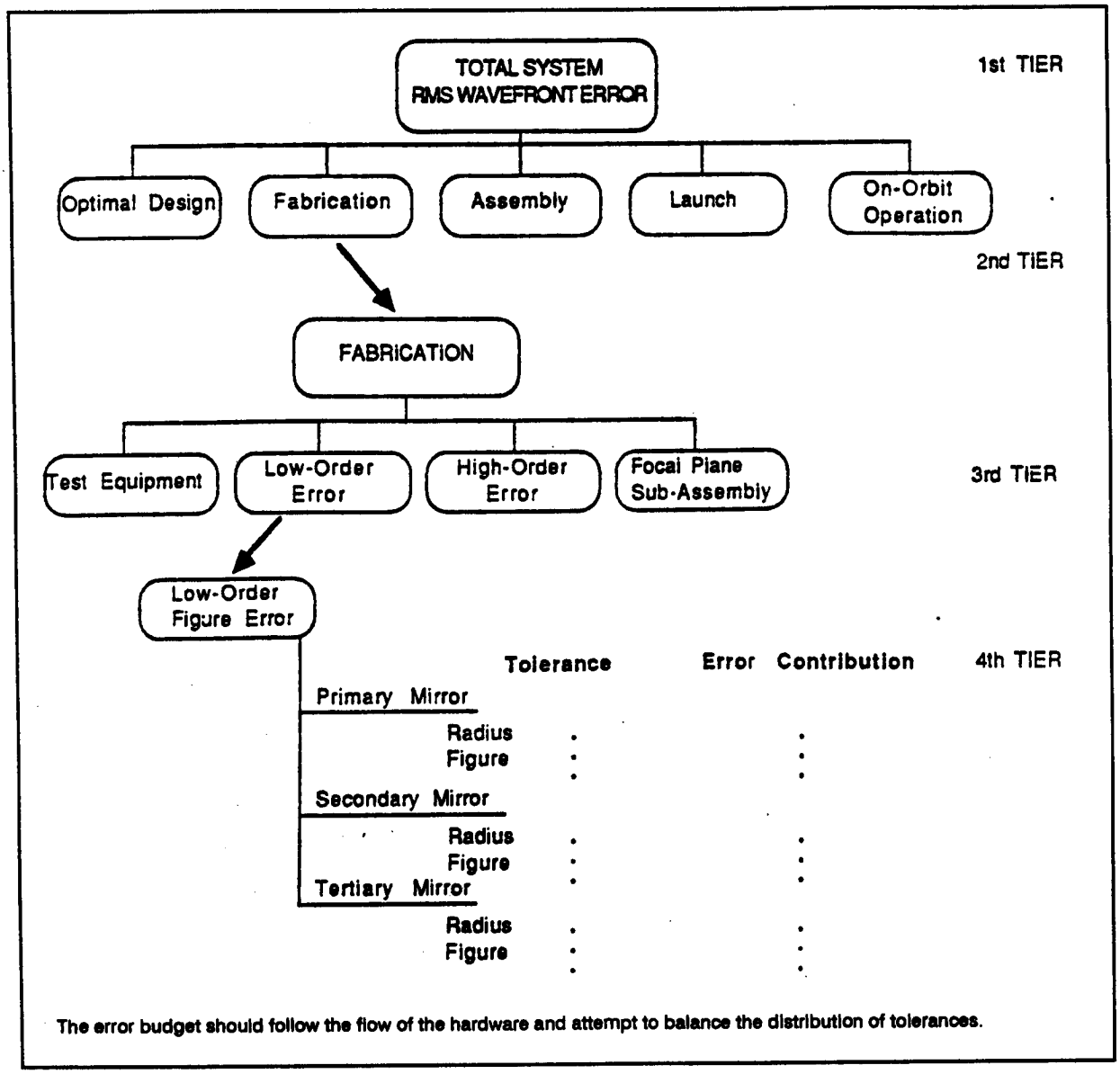

Figure 6.3-5 A Typical Wavefront Error Budget for a Space Based Optical Instrument

Stable mounting techniques for all optical elements is essential to survive the vibration and shock environment subjected to the equipment during launch. Since no post launch optical alignment is desired mechanical finite structural element modelling is essential. However, the range of travel for the fine pointing, course pointing mirrors along with the optical apertures can be slightly oversized to allow for some active focus compensation capability.

6.3.4 Optical Path Layout

6.3.4.1 Baseline

As stated earlier the selected telescope for the baseline configuration is a periscope design with a fixed telescope and moveable mirrors which directs the beam over a hemisphere or greater. A sketch of the telescope is given in Figure 6.3-6. The telescope is a casegrain configuration with a central secondary mirror and the eye piece mounted in the middle of the primary mirror. For the geostationary terminal the axis of the telescope (axis of the first gimbal) is oriented parallel to the earths axis of rotation. See Section 6.7 for a discussion of mounting orientation. Mounting of the terminal on the LEO satellite is less clear so the interface between the telescope and the optical bench is based on the concept for the geostationary terminal and would not necessarily be applicable to the LEO terminal.

The optical bench is mounted on a honey comb panel and the telescope is mounted on the same panel. This is accomplished by means of three or more legs which provide a space between the telescope and the panel, see Figure 6.3-7. This space is needed so that the acquisition detector can be as close to the eye piece as possible as this minimizes the size of the acquisition detector. The wavelength of the beacon detector, received by the acquisition detection is reflected by the reflective mirror cube. Redundancy for the acquisition detector is provided by two CCD's mounted on two sides of a smaller cube. This cube is not wavelength sensitive but divides the power equally between the two detectors.

All other wavelengths pass through a hole to the front of the panel and then are bent through 90° so that the optical path is parallel to the panel. The optical path layout for the baseline system is shown in Figure 6.3-8. The layout includes two 2-axis fine pointing mirrors in a 2 for 1 redundancy configuration. There are two AlGaAs lasers either of which provides the full traffic capability of 100 mbps on the LEO terminal or 19.2 kbps on the geostationary terminal. These are tuned to slightly different wavelengths and combined with a reflecting filter cube. The transmit signal is combined with the receive signal also by means of a reflecting filter which passes the receive signal and reflects the transmit signals. Any leakage of the transmit signals through this filter is trapped in the light trap. Alternatively the leakage transmit signal can be reflected back for detection by the communications receivers.

A small fraction of the receive signal is tapped-off for use by the fine pointing detectors. This is accomplished by means of a wavelength insensitive reflecting surface. There are two fine pointing detectors in a 2 for 1 redundancy arrangement. The power is divided equally between them by a wavelength insensitive reflecting surface.

The fine pointing detectors are CCD detectors with a total range of 200 μRad. This range is required because the received signal spot will be positioned off axis by the amount of the point ahead angle (equal to 50 μRad in any direction) so that the transmit beam is always directed along the axis of the telescope. In this way separate point ahead mirrors are not required since the dual task of point ahead and five pointing is accomplished by a single set of fine pointing mirrors.

There are two communications detectors in a 2 for 1 redundancy arrangement. These are coupled into the optical path by means of a reflective filter. In this way one detector receives signal from only one laser while the other receives signal from the other laser. Thus if one of the lasers fails then the associated detector can no longer be used. The received signal does not generally fall in the centre of the detector but is received off centre by the amount of the look ahead angle. The detector diameter is about 100 μm which is sufficient to accommodate a deviation of $\pm$ 50 μRad provided

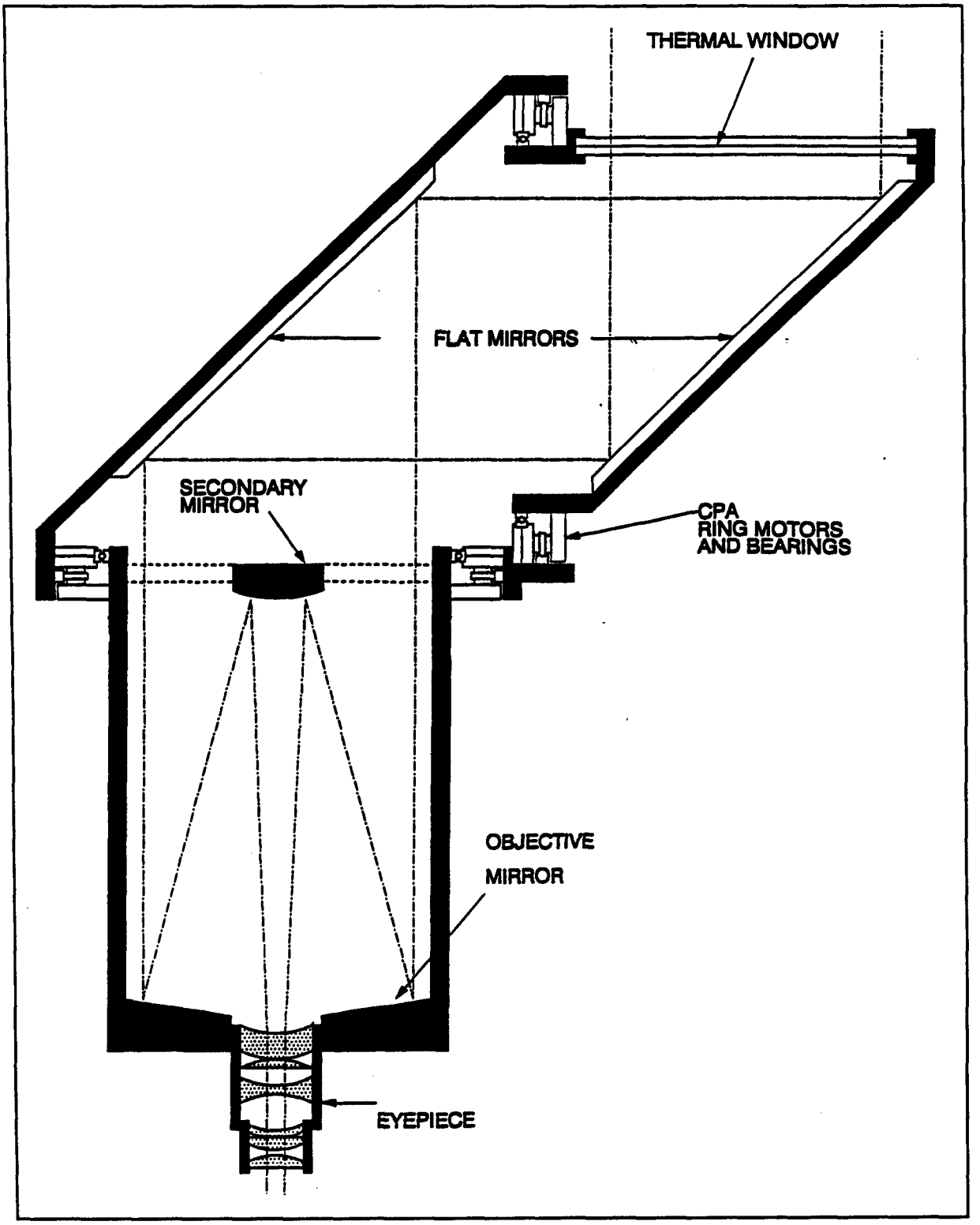

Figure 6.3-6 Telescope Concept for the Baseline OISL

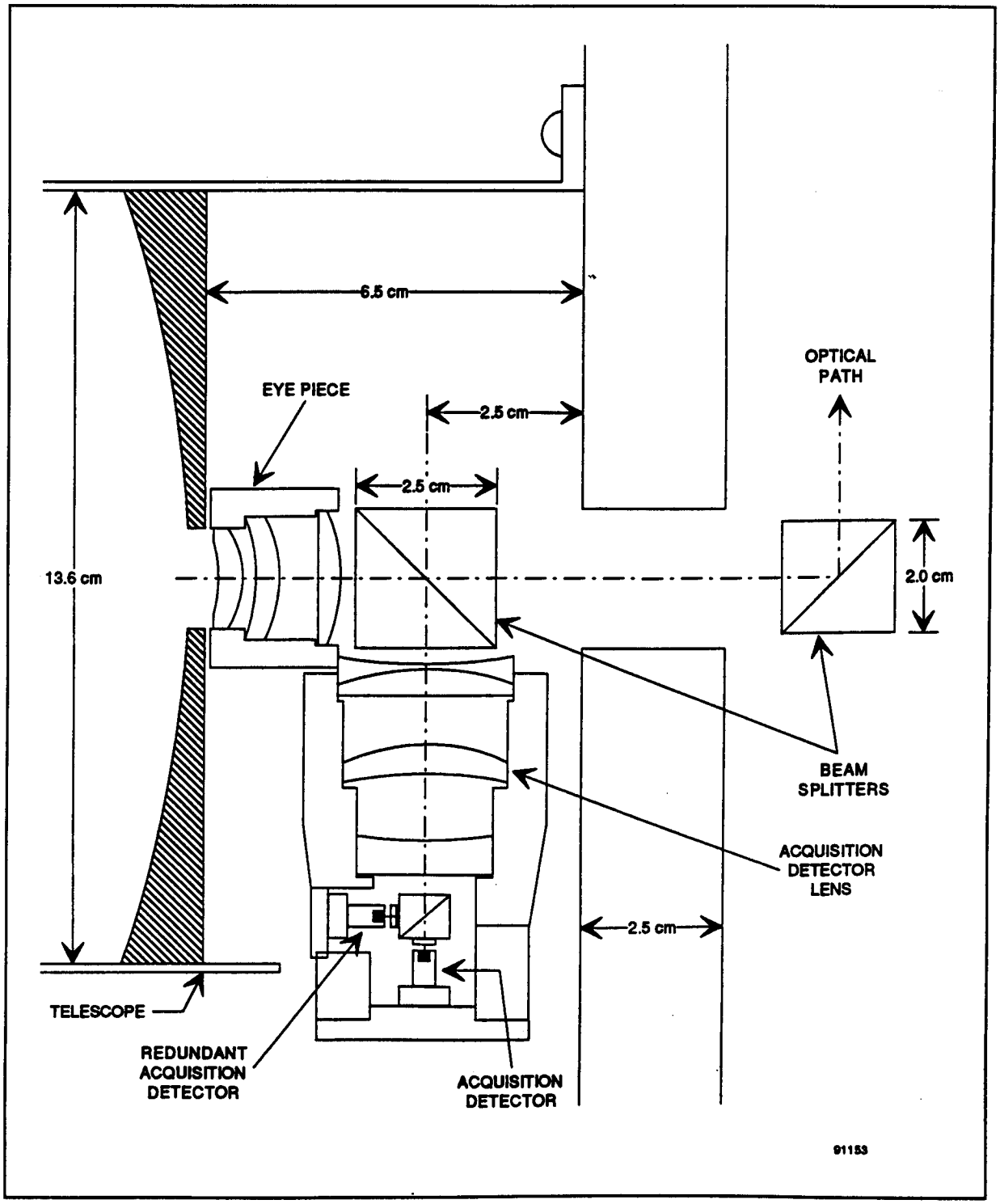

Figure 6.3-7 Acquisition Detector Mounted Immediately Behind Eye Piece

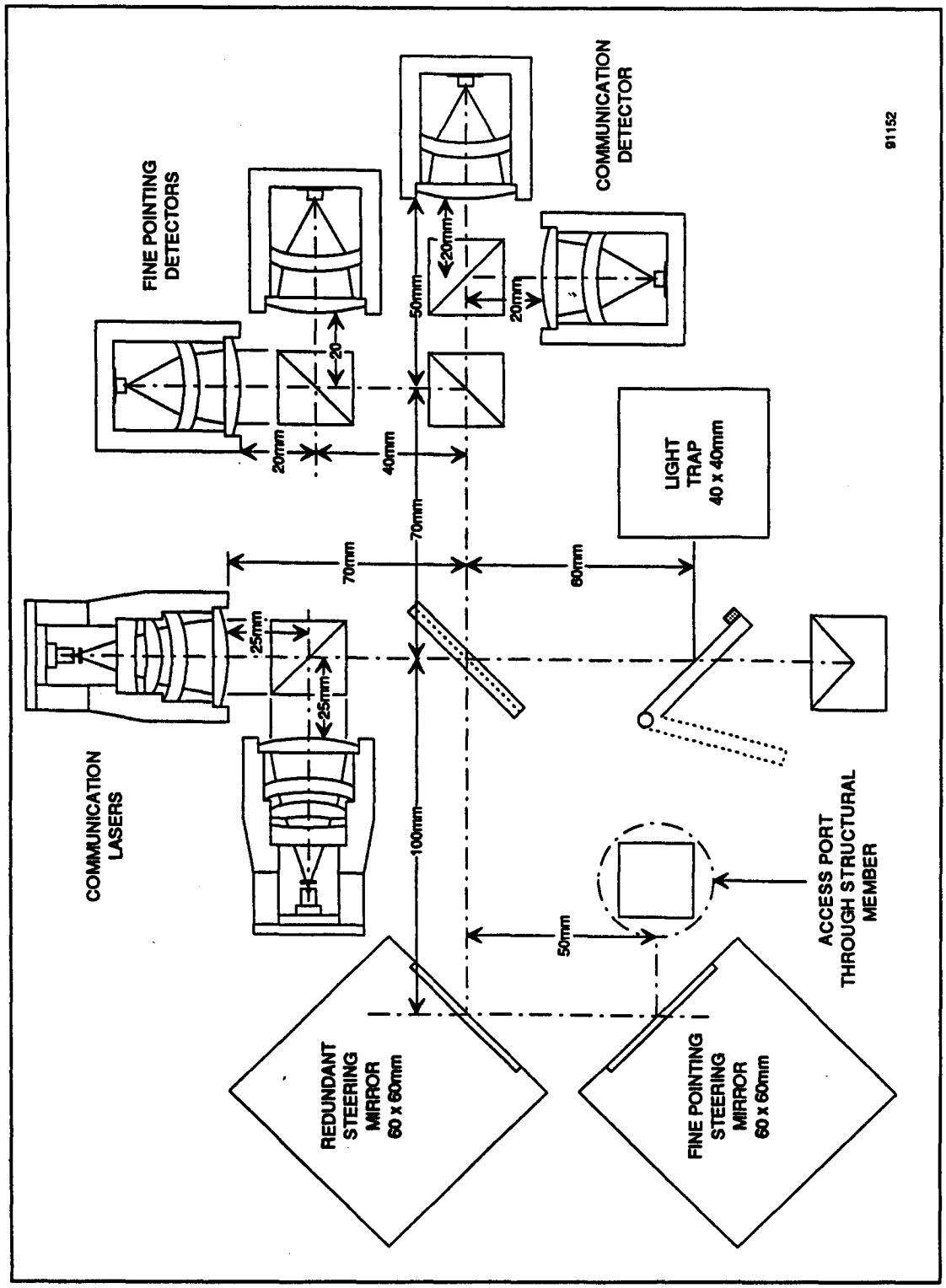

Figure 6.3-8 Preliminary Optical Path Layout for 100 Mbps Baseline System

the focal length of the detector optics is kept short. The receiver bit rate is 100 mbps on the geostationary satellite and 19.2 kbps on the LEO satellite.

The layout shown in Figure 6.3-8 is mounted on a panel of only about 260 mm by 350 mm (or 10 1/4" by 14"). This dimension can be reduced to about 250 x 250 mm by folding the optical path and mounting the fine pointing detectors and the communications detectors on the back of the panel along with the acquisition detectors. This has the additional advantage that all detectors are mounted on the back of the panel away from the laser which is mounted on the front. This arrangement minimizes the risk of stray laser light reaching the detectors and degrading the performance. It does not reduce the level of laser light which might find its way down the optical path into one or other of the detectors.

6.3.4.2 Option 1 - 1 Gbps Link with Wavelength Multiplexing

The GEO terminal for the option 1 system is shown in Figure 6.3-9 and the LEO terminal in Figure 6.3-10. The layout is the same as the baseline except that the telescope has increased in size to 180 mm diameter which is in the range where the coudé configuration is optimum. The mounting to the optical bench is unchanged from the baseline however, with the acquisition detector mounted adjacent to the eye piece behind the structural member and with the communications signal passing through a hole in the structure and then bent through 90° to be in the plane of the structure.

The transmitter on the GEO terminal and the receiver on the LEO terminal are unchanged from the baseline since they still operate at 19.2 Kbps. The transmitter onthe LEO terminal and the receiver on the LEO terminal are upgraded to 1 Gbps which is accomplished by having four channels of 250 mbps each and each operating at different wavelengths so that they can be combined by wavelength selective mirrors. As seen in Figure 6.3-10, there are 6 lasers in a 6 for 4 redundancy configuration.

The GEO terminal, shown in Figure 6.3-9 has six multiplexed receivers each capable of receiving 250 Mbps of data so four are required to support the 1 Gbps rate. Each receiver operates at a different wavelength which is mateched to the transmit wavelength on a one to one basis. Thus if either a laser or a detector fail then both the laser and detector become inoperative.

6.3.4.2 Option 2 - 1Gbps Link with Heterodyne Receiver

The GEO terminal for the option 2 system is shown in Figure 6.3-11 and the LEO terminal in Figure 6.3-12. The layout is basically the same as the baseline and option 1 except that the 1 Gbps bit rate is achieved by a single 1 watt Nd:Yag laser on the LEO terminal combined with a heterodyne receiver at the GEO terminal. The Nd:Yag laser is pumped by a laser diode and stabilized by means of a photodiode which detects the scattered light from the Nd:Yag laser. The 1 watt power level is currently achieved by combining the outputs from three such lasers. However recent technology innovations suggest that a single diode pumped Nd:Yag laser will meet the 1 Watt requirement by 1993. Modulation of the Nd:Yag laser which is required on the LEO terminal, is provided by an external modulator. Such modulators are currently under development and actual performance capabilities are projected.

An optical polarizer is provided at both the transmit and receive terminal. This converts linear polarization of the transmitter to circular polarization for propagation through space. The circularly polarized signal is received without any sensitivity to orientation of the spacecraft and then converted back to linear with a polarization aligned with that of the local oscillator signal.

The Nd:Yag local oscillator laser at the receive terminal is a low power unit and can be easily achieved by the single unit shown. The local oscillator laser is, however, complicated by the necessity to match the wavefront of the local oscillator signal to that of the incoming signal power. This requires a set of optics between the Nd:Yag laser and the L.O. coupler (labeled the wavefront forming optics).

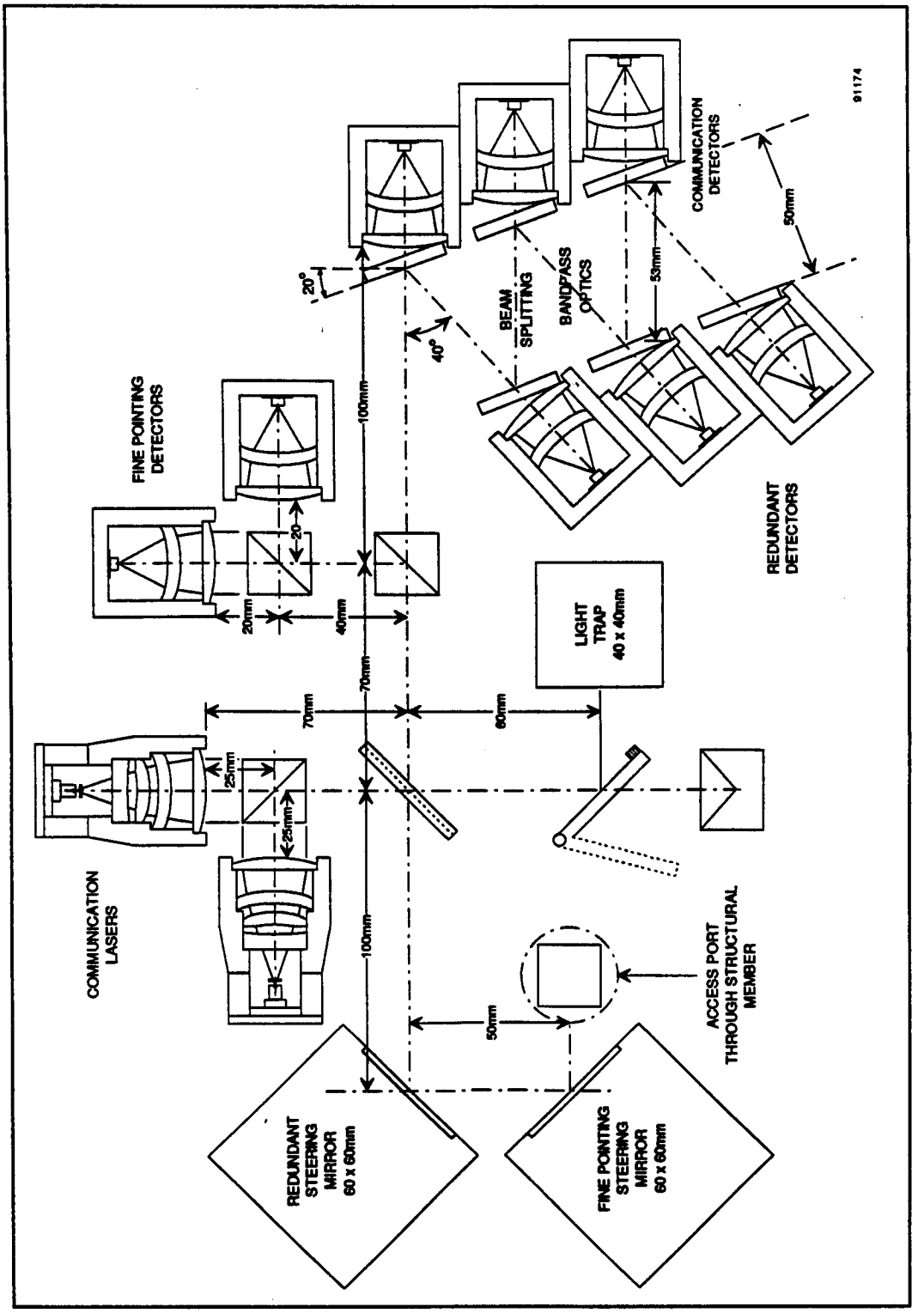

Figure 6.3-9 Preliminary Optical Path Layout for the Wavelength Multiplexed 1 Gbps System - GEO Terminal

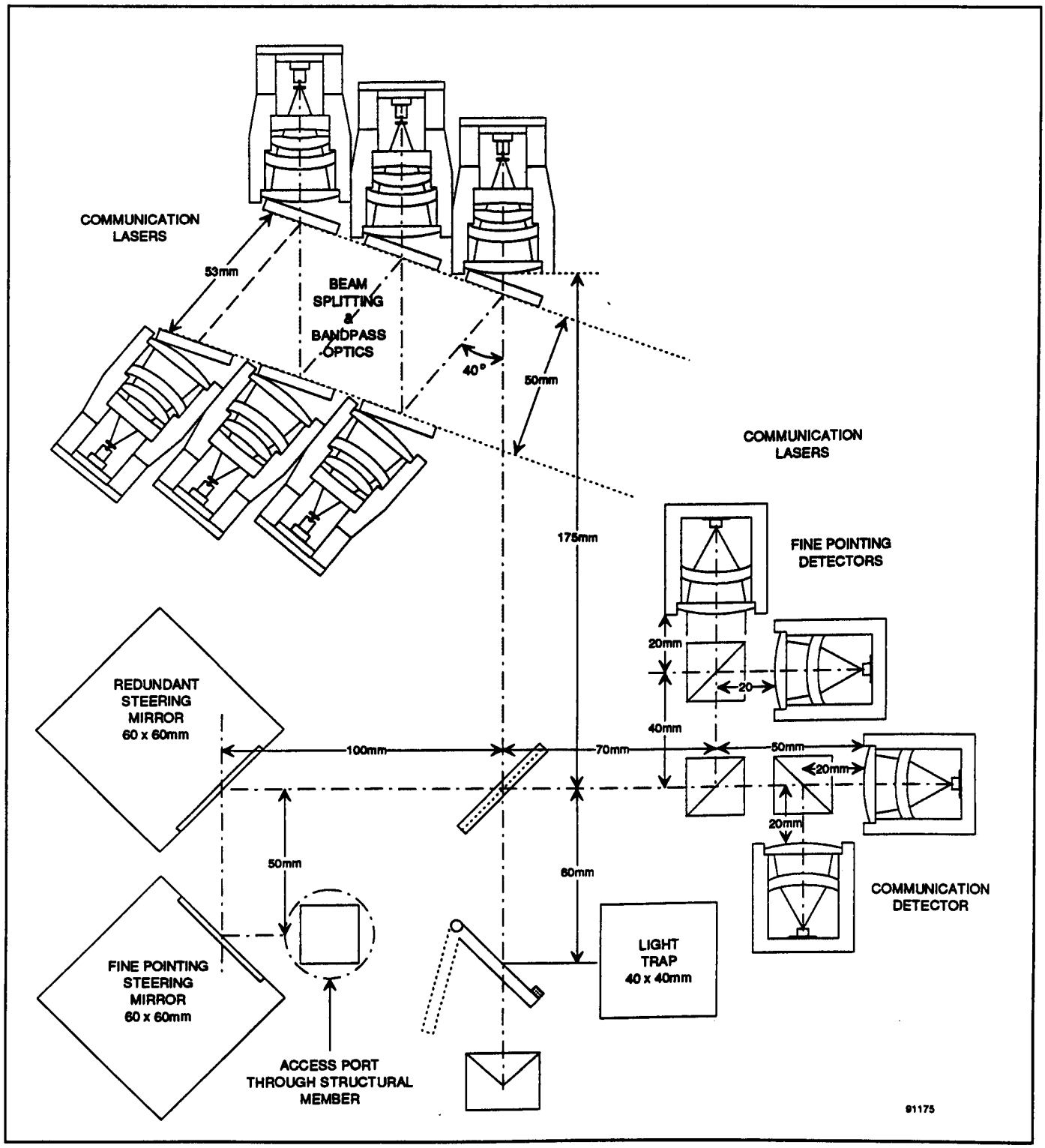

Figure 6.3-10 Preliminary Optical Path Layout for the Wavelength Multiplexed 1 Gbps System - LEO Terminal

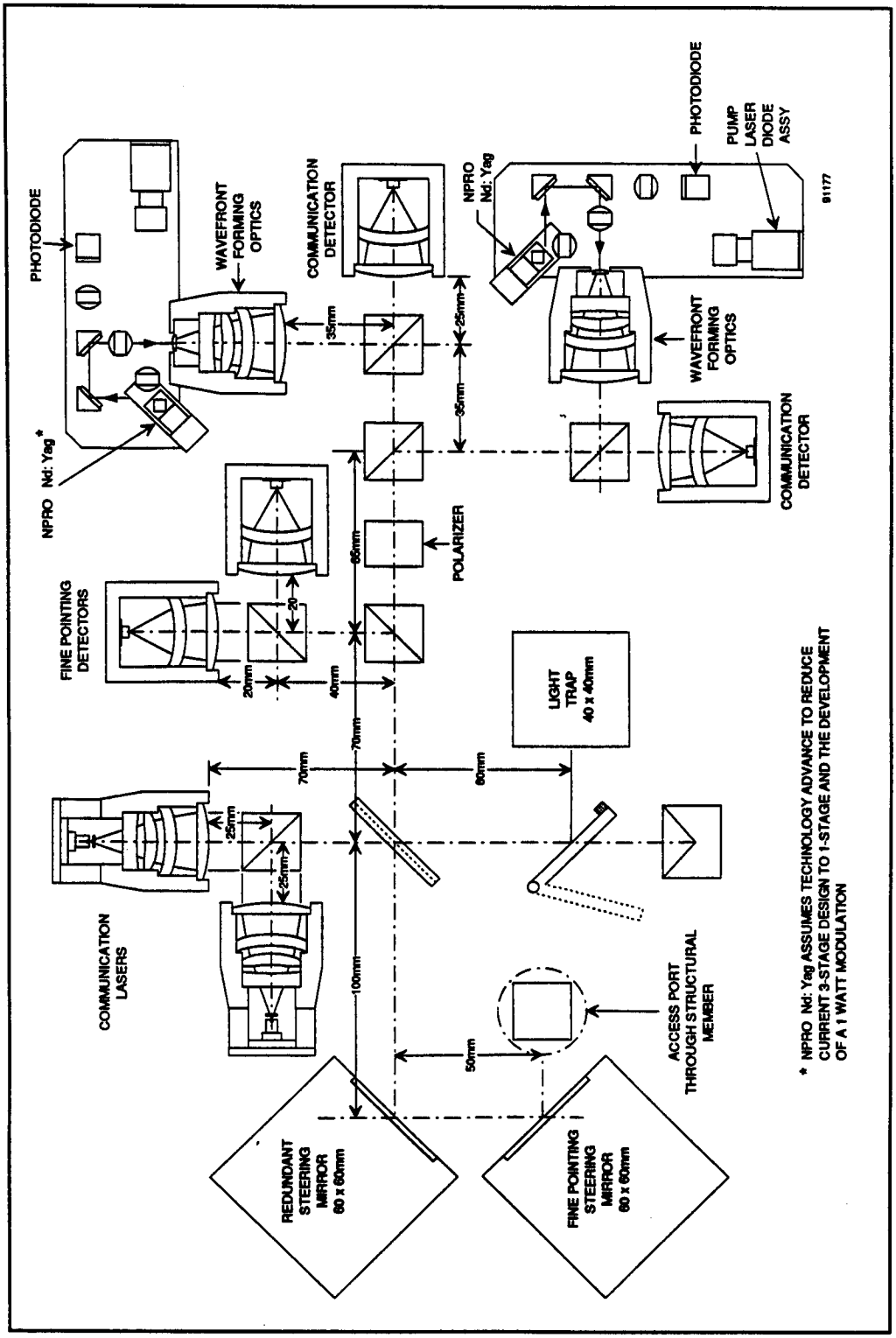

Figure 6.3-11 Preliminary Optical Path Layout for the Heterodyne 1 Gbps System - GEO Terminal

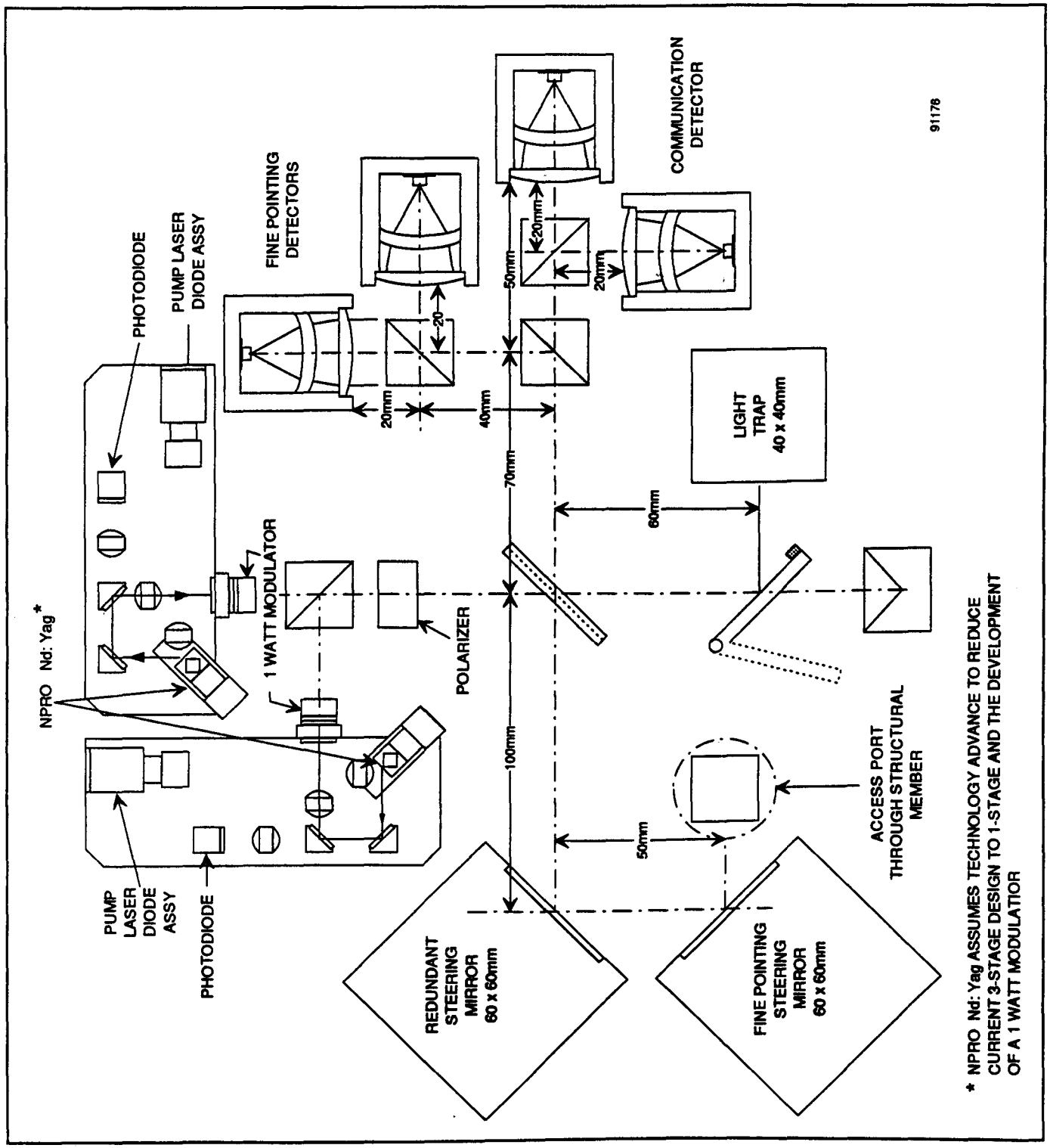

Figure 6.3-12 Preliminary Optical Path Layout for the Heterodyne 1 Gbps System - LEO Terminal

6.4 Electrical Design

The opto-mechanical subsystem of the OISL has been discussed in detail in sections 6.1 to 6.3 of this report. The electrical subsystem, illustrated in Figure 6.4-1, is of equal importance, however, it will not be discussed in as great detail since many of the elements of the electrical design are common to most satellite communications payloads.

The OISL electrical system can be divided into the following subsystems:

1. The receiver subsystem consisting of the communication detectors, the preamplifier and the demodulation electronics.

2. The transmitter subsystem consisting of the laser source and the modulation electronics.

3. The pointing, acquisition and tracking electronics required to control and drive the fine pointing mirrors and coarse pointing assembly and control the fine pointing and tracking acquisition detectors.

4. The thermal control electronics consisting of the heaters and temperature sensors required to monitor and control the temperature of the optical bench. The subsystem could also include thermoelectric coolers if active cooling of the lasers and laser modulators is required.

5. A digital computer subsystem is required to control the electronic subsystems and to perform health and safety monitoring for the system.

6. A power supply subsystem is required to drive all of the subsystems specified above. Further discussion of the power consumption can be found in Section 6.6.

6.4.1 The Receiver Electronics Design

6.4.1.1 The Baseline and Option 1 Design

For the baseline design, as well as the design of option 1, the detector and detector electronics will be similar with some optimization for the different data rates (100 versus 250 Mbit/s). The detector shall consist of an Avalanche Photodiode (APD) and an optimized hybrid preamplifier configured in a transimpedance operating mode. This analog front end will provide a voltage output, stabilized to a set level by an internal AGC function, to the demodulator circuit. A typical direct detection receiver schematic is illustrated in Figure 3.2.2-1.

For a slower GEO/LEO link a simple photodiode with a separate baseband amplifier is adequate although the APD could be employed to retain design similarity between the GEO and LEO OISL payloads.

The demodulator design for the GEO/LEO link employs the simple ASK format due to the low data rates. For the high speed LEO/GEO link the more complex QPPM format is employed.

On the LEO platform the demodulated signals consist of spacecraft command signals or OISL terminal command signals. In either case the data stream is directed to the command subsystem which then executes the instructions.

On the GEO satellite the majority of the demodulated information is data which is routed via a conventional microwave link to a ground station on earth.

6.4.1.2 Design Option Two

The GEO to LEO link employs a diode laser and direct detection detector as discussed in section 6.4.1.1. However, for the LEO to GEO link a single Nd:Yag laser system operating at 1 Gbps is employed in a heterodyne configuration. This requires additional circuitry to enable the local oscillator laser frequency to track the frequency of the incoming signal.

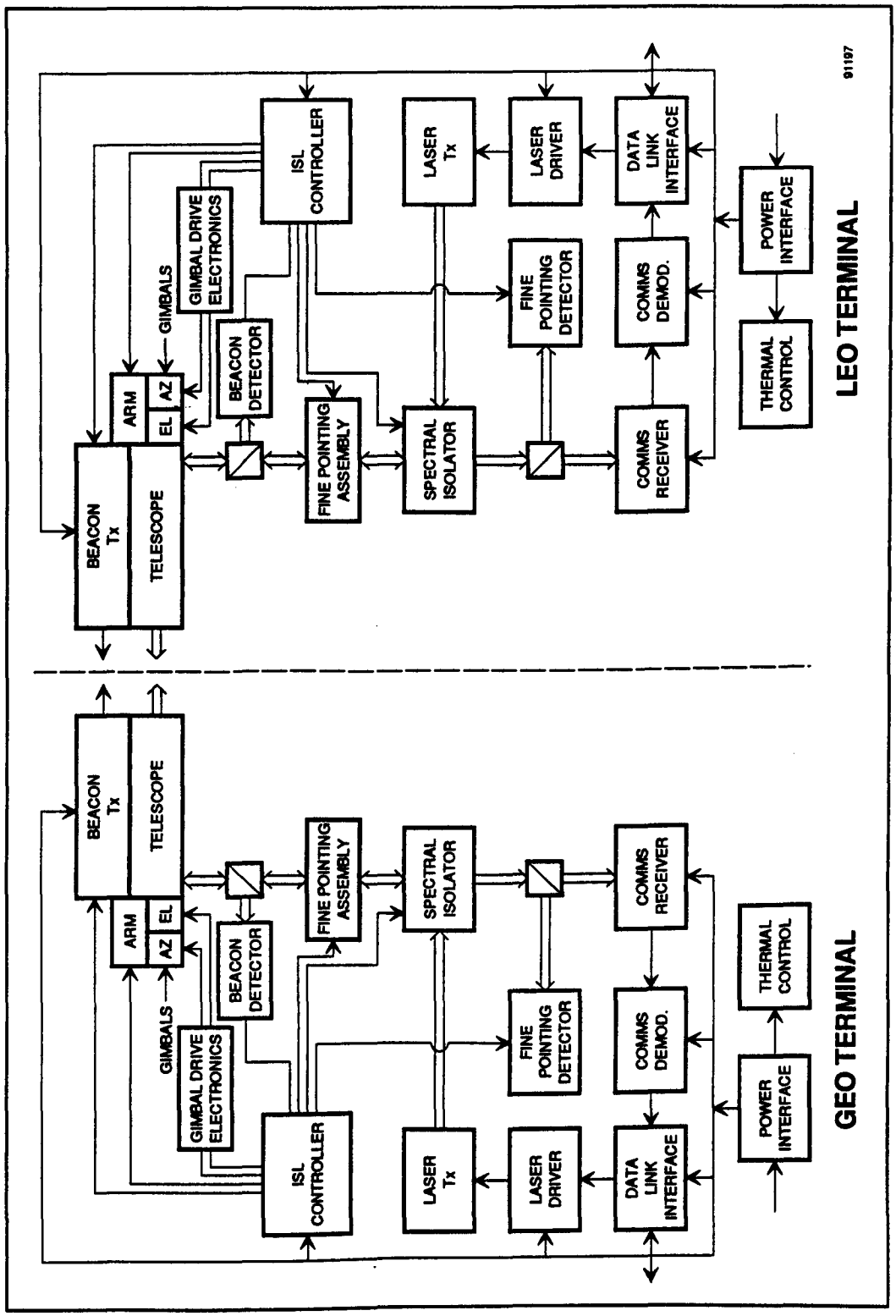

Figure 6.4-1 Optical ISL Electrical Block Diagram

For this heterodyne detection scheme a Nd:Yag local oscillator signal is mixed with the incoming communication signal on the detector element. When a Nd:Yag system is employed sufficient power is available to permit a PIN Fet to be employed.

6.4.2 The Transmitter Electronics Design

6.4.2.1 The Baseline Design and Option 1

The 80 mwatt laser power required for both the baseline and option 1 LEO to GEO link can be provided by a single laser diode source such as the Quantum well CW laser illustrated in Figure 3.1.2-2. To drive this laser source a hybrid drive circuit will be employed based upon silicon bipolar technology. Figure 3.1.4-4 illustrates a typical circuit design.

To ensure Transmitter high performance the modulator drive current line and the diode current monitor must be impedance matched to the low diode laser impedance (2 ohms). If impedance matching cannot be achieved then provision must be made in the drive circuit to ensure that the power reflected by the laser can be absorbed.

6.4.2.2 Design Option 2

For design option 2 a 0.8 watt Nd:Yag laser system has been baselined, unfortunately if state of the art components were employed today, three diode pumped

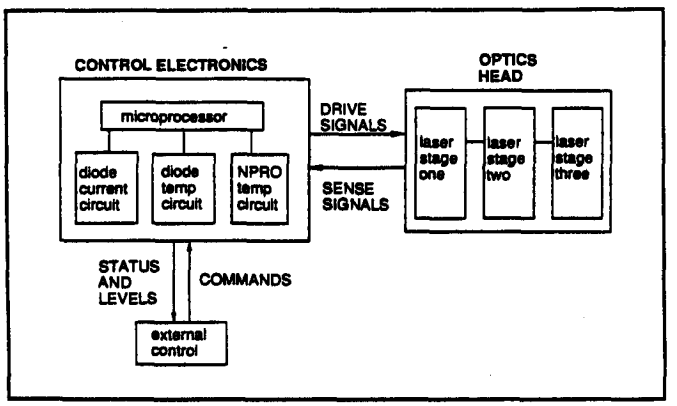

Figure 6.4-2 Block Diagram Showing Laser Control Electronics

systems would have to be employed in order to achieve the desired output power Furthermore, a high power Nd:Yag laser modultor has not yet been developed although several different vendors are currently under contract to deliver prototype units for evaluation. Figure 6.4-2 illustrates the electronic control functions required for a diode pumped Nd:Yag laser system. Note that this diagram contains three separate laser heads since it represents current technology.

For the heterodyne configuration described in Section 6.3.4, it is assumed that a single 1 watt Nd:Yag laser and a 1 watt modulator will become available in a few years.

6.4.3 Pointing, Acquisition and Tracking (PAT) Electronics Design

The pointing, acquisition and tracking electronics support separate functions but they employ common mirrors and detectors to meet their requirements. All of the control software will reside in the computer located within the OISL controller.

The coarse pointing electronics control the coarse pointing mirrors or the Coude mounts employed for design option 1 and option 2. The control electronics guide the coarse pointing assembly to an established location during acquisition or will support the tracking function when large movements are required. The electronics monitors the angular position of the mirrors, adjusting the pointing mechanism in accordance with signals receiver from the acquisition or fine pointing CCD.

The acquisition CCD is an integral part of the PAT subsystem. The CCD readout structure can be configured for a serial readout or with an x-y addressable readout depending upon the PAT algorithm employed. The acquisition CCD signal output is directed to the search pattern generator and the feedback control electronics.

The control electronics for the fine pointing mirrors links the mirrors to the fine point detectors via a feedback loop and the point ahead angle. These mirrors are adjusted to maintain track. While the acquisition

detectors are used only for the beacon laser the fine pointing detector has a dual role after contact is established with the communication laser and the beacon laser is turned off. See section 6.5 for further details on the acquisition procedure.

6.4.4 The Thermal Control System Electronics Design

The laser diode wavefront mode structure is critical for maintaining diffraction limited performance, however, it is also very sensitive to thermal induced optical cavity changes. To reduce the sensitivity researchers have employed a three mirror structure [133]. Alternatively, active thermal control using a thermoelectric cooler and a thermistor can be employed.

Similarly the operating environment of the entire optical instrument must be controlled to ensure that thermal induced wavefront errors do not exceed specified levels. Active temperature control of the optical bench can be implemented in a variety of ways depending upon the size of the platform.

For small payloads a series of resistive heaters and temperature sensors are often employed in a feedback configuration to stabilization the optical bench temperature to better than ± 5 degrees. The use of cold patch radiators or thermal louvres are also important for the removal of excess energy [132]. For large satellite centralized liquid cooling systems are also available to remove excess energy.

In general the thermal control will be provided by the ISL controller in which a required optical bench temperature and operating tolerance are stored. The heaters and cooling system will be employed to maintain the optics within the operating window. If the optics exceed the allowed operating range then a flag will be raised and the ground station informed of the problem via the GEO OISL link.

6.4.5 Control, Status and Data Processing Electronics Design

Many of the control, status and data processing functions have already been discussed in the previous sections. As indicated, the central computer control will reside in the OISL controller. All data integrity and digital processing will be directed by this electronics assembly as well as control of the PAT assembly. Built in test functions such as power monitoring of the laser source and in-flight calibration employing the spectral isolator flip mirror will also be controlled on a periodic or as required basis from this assembly.

6.5 Acquisition Procedure

An optimum acquisition procedure is outlined in section 5.2.7. This is based on a GEO terminal which has a beacon laser but no acquisition detector and a LEO terminal which has an acquisition detector but no beacon laser. In this way the mass and cost of the ISL terminals are reduced though at the penalty of increased acquisition time.

The configuration presented here retains a redundant beacon laser and a redundant acquisition detector at both terminals. The extra hardware could be dropped at a later date when a better estimate of acquisition time and equipment reliability is obtained. With two way acquisition capability the search rate can be increased and the acquisition time reduced, and in addition the optimum procedure can be used for acquisition in the event of failure of either both beacon lasers or both acquisition detectors at either terminal.

6.5.1 Primary Mode of Acquisition

Acquisition begins when initiated by the central controller station. The central controller will calculate the pointing directions for both the LEO and GEO terminal and indicate the time at which acquisition should begin. The GEO and LEO terminals slew to the designated direction so that the cooperating terminals are within the respective cones of uncertainty. Figure 6.5-1 shows the relative sizes of the cones of uncertainty for

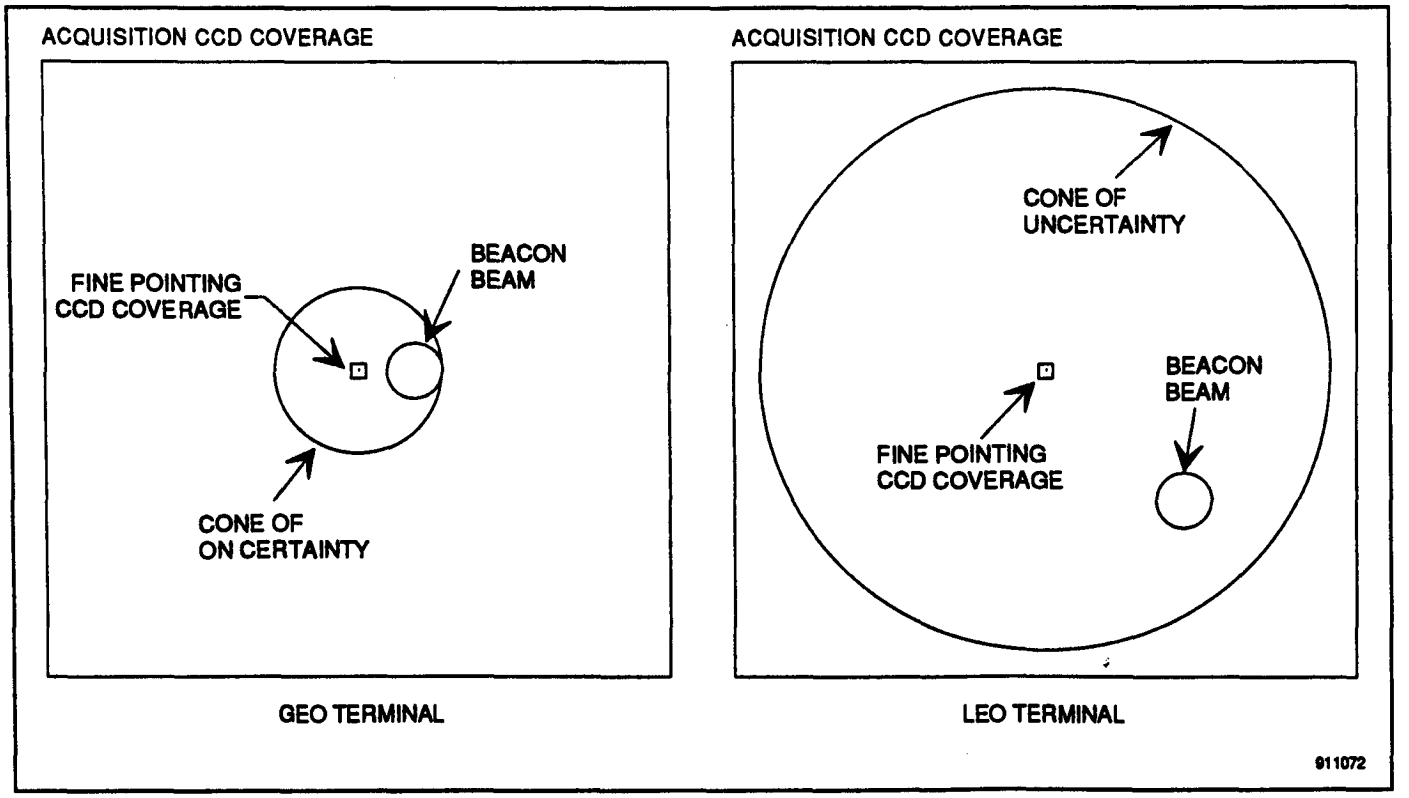

Figure 6.5-1 Relative Angular Dimensions of Cones of Uncertainty, Laser Beam Width and Detector Fields of View

the LEO and GEO terminals as well as other angular dimensions except that the smarter items are about twice relative size. The acquisition CCD's are turned on at both the LEO and GEO terminals and at the designed time the beacon transmitter on the GEO terminal is turned on and stepped over its cone of uncertainty. The step size is determined by the size of the beacon beam width and the dwell time is sufficient to provide the minimum detectable signal at the receive terminal. This allows time for the LEO terminal to respond during the dwell time. The GEO beacon is selected because the GEO terminal has a smaller cone of uncertainty and a raster scan can be accomplished in less time than a similar scan on the LEO terminal.

When the GEO beacon illuminates the LEO terminal, the signal is received on the LEO acquisition CCD which then directs the LEO telescope to point in the indicated direction. There are two standards for judging if the telescope is directed in the correct direction. The one, if it is within the range of the fine pointing CCD currently specified at 400 μRad ($\pm$ 200 μRad) and the second if it is within the beam width of the communications laser which is of the order of 8 μRad ($\pm$ 4 μRad). The first can be achieved by the course pointing mechanism which has a precision of 200 μRad ($\pm$ 100 μRad). The second can only be achieved by activating the fine pointing mirrors on the LEO terminal. The fine pointing mirrors are driven by the tracking detectors which nominally detect the GEO communications laser. However, the GOE communications laser is not yet directed at the LEO terminal so the LEO tracking detectors are activated by the beacon laser radiation. This is achieved first by placing a transparent region in the center of the acquisition detector deflection mirror. This allows the beacon signal to reach the communications detector and the tracking detectors. However, at the communications wavelength, the tracking detector receives only a few percent of the signal power, so the track detector coupler

is a filter which reflects the beacon wavelength and passes the communications signal.

This ensures that there is sufficient power reaching the track detectors to ensure detection of the beacon laser. The fine pointing mirrors are then driven to point the LEO terminal communications laser accurately at the GEO terminal.

At this point the LEO terminal turns on its beacon transmitter. The GEO terminal receives this signal on its acquisition CCD and directs its antenna towards the received signal using the course pointing mechanism with a precision of 200 μRad. This is sufficient to ensure that the Leo signal can be received on the fine pointing CCD which is activated by the LEO beacon to drive the fine pointing mirrors to accuratly point the telescope. At this time the communications lasers are turned on and when these signals are received on the fine pointing CCD it takes over control of the fine pointing mechanism.

The point ahead angle is determined and included in the positioning of the fine pointing mirrors when these are activated by the beacon laser as well as by the communications laser.

At this point acquisition is complete. The beacon lasers and the acquisition detectors are turned off and the communications receivers and other equipment are turned on. The two terminals execute a hand shake to indicate that acquisition has been successful and transmission of data begins.

6.5.2 Alternate Acquisition Mode

This essentially is the optimum procedure described in Section 5.2.7. The difference from that described in the previous section is that the step size for the beacon laser on the GEO terminal is reduced sot that the cone of uncertainty is covered by the GEO track detector rather than the beacon laser. When it is done the LEO terminal can respond using its communications laser rather than its beacon laser and the acquisition detector on the GEO terminal would be unused. The alternate procedure is thus suitable in the event of complete failure of either of these units. For the present system, specified in section 6.2.1, the field of view of the track detector is $\pm$ 200 μRad. This is stepped by the course pointing mechanism which has a precision of $\pm$ 100 μRad so that the step size is not greater than 200 μRad to ensure complete coverage of the uncertainty cone by the track detector. For an uncertainty cone of $\pm$ 0.15 degrees or $\pm$ 2600 μRad the number of steps exceeds 600. Assuming a dwell time of 0.25 sec the time to completely search the cone of uncertainty exceeds 2.5 minutes.

The alternate acquisition procedure could also be used in the reverse direction using the LEO beacon laser and the GEO acquisition detector. However, because of the increased size of the LEO cone of uncertainty, the acquisition time would be about 10 times as long which is completely unacceptable.

6.6 Weight and Power Budgets

6.6.1 Baseline

The weight and power budgets for the baseline system are presented in Tables 6.6-1 and 6.6-2 respectively. Table 6.6-1 shows a mass budget including margin) of less than 30 kg. The power budget for the LEO terminal in Table 6.6-2 has two cases, the operational phase and the acquisition phase. During acquisition all units associated with acquisition are active simultaneously whereas during the operational phase all units associated only with acquisition are turned off. These are principally the beacon laser and acquisition detectors but in addition the power requirements of the course pointing mechanism are considerably reduced. The power budget during operation is close to 50 watts and during acquisition close to 80 watts including a margin of 10%. The power budget for the GEO terminal is slightly less during operation due to the lower communications laser power. However, this difference is expected to be considerably less than the one watt budgeted for this laser on the LEO terminal.

Table 6.6-1 Mass Budget for the Baseline Configuration (GEO and LEO)

Unit/Module	Unit Mass	Number	Total
Telescope & CPA	8.00	1	8.00
Beacon Laser	0.50	2	1.00
Beacon Detector	0.20	2	0.40
ACQ Coupler	0.07	1	0.07
Fine Pointing Ass.	0.15	2	0.30
Spectral Isolator	0.80	1	0.80
AlGaAs Laser	0.25	2	0.50
Laser Driver	0.08	2	0.16
Fine Point Detector	0.15	2	0.30
Track Coupler	0.07	1	0.07
Receive Module	0.30	2	0.60
Comms. Demodulator	0.20	2	0.40
Data Link Interface	0.50	2	1.00
Thermal Interface	2.00	1	2.00
Power Interface	0.50	2	1.00
Structure	6.00	1	6.00
ISL Controller	2.00	2	4.00
Sum			26.60
Margin			2.66
Total			29.26

Table 6.6-2 Power Budget for Baseline Configuration (LEO)

Unit/Module	RF Power	Eff. %	Operat. Power	ACQ. Power
Attitude Sensor			1	10
Beacon Laser	3.8	15		25.3
ACQ. Detector				2
Fine Point Mirror			6	6
AlGaAs Laser	0.08	10	0.8	0.8
Laser Driver		80	0.2	0.2
Track Detector			2	2
Receive Module			0.6	
Demodulator			0.3	
Data Interface			6	
Thermal Interface			10	10
Power Interface		85	4.6	3.7
ISL Controller			10	10
Sum (W)			41.5	70
Margin (W)			4.15	7
Total (W)			45.65	77

6.6.2 Option 1: 1 Gbps with Wavelength Multiplexed Sources

The mass budget for this option is given in Table 6.6-3 and the power budget in Table 6.6-4. The mass is similar to the baseline except that the GEO terminal has 6 receivers and demodulators and the LEO terminal has 6 lasers and laser drivers.

The power budget is changed in a similar manner for the operational power, however, for the LEO terminal acquisition can be completed using only one of the multiplexed AlGaAs lasers slightly reducing the acquisition power for this case.

6.6.3 Option 2: 1 Gbps with Heterodyne Detection

The mass and power budget for this option are given in Tables 6.6-5 and 6.6-6 respectively. For this option there are additional items included in both the mass and power budget mainly associated with the local oscillator and the need to match wavefronts of the communications signal and the local oscillator.

The tables show that the GEO terminal use AlGaAs lasers for transmit since the bit rate is only 19.2 Kbps and a Nd:Yag L.O. laser to receive the 1 Gbps from the LEO terminal. Similarly the LEO terminal uses a Nd:Yag laser to transmit the 1 Gbps data stream but has only a simple direct detection receiver for the 19.2 Kbps signal. To complete acquisition the LEO terminal must use is Nd:Yag laser resulting in an acquisition power of about 100W even though the operating power level is much lower.

Table 6.6-3 Mass Budget for the Option 1 Terminal with Wavelength Multiplexed Sources

Unit/Module	Unit Mass	GEO Terminal;		LEO Terminal	
		Number	Total	Number	Total
Telescope & CPA	12.00	1	12.00	1	12.00
Beacon Laser	0.50	2	1.00	2	1.00
Beacon Detector	0.20	2	0.40	2	0.40
ACQ Coupler	0.07	1	0.07	1	0.07
Fine Pointing Ass.	0.15	2	0.30	2	0.30
Spectral Isolator	0.80	1	0.80	1	0.80
AlGaAs Laser	0.25	2	0.50	6	1.50
Laser Driver	0.08	2	0.16	6	0.48
Fine Point Detector	0.15	2	0.30	2	0.30
Track Coupler	0.07	1	0.07	1	0.07
Receive Module	0.30	6	1.80	2	0.60
Comms. Demodulator	0.20	6	1.20	2	0.40
Data Link Interface	0.50	2	1.00	2	1.00
Thermal Interface	2.00	1	2.00	1	2.00
Power Interface	0.50	2	1.00	2	1.00
Structure	6.00	1	6.00	1	6.00
ISL Controller	2.00	2	4.00	2	4.00
SUM			32.60		31.92
MARGIN			3.26		3.192
TOTAL			35.86		35.112

Table 6.6-4 Power Budget for the Option 1 Terminal with Wavelength Mutliplexed Sources

Unit/Module	RF Power	Eff. %	GEO Terminal		LEO Terminal	
			ACQ. Power	Operat. Power	ACQ. Power	Operat. Power
Attitude Sensor			10	1	10	1
Beacon Laser	3.8	15	25.3		25.3	
ACQ. Detector			2		2	
Fine Point Mirror			6	6	6	6
AlGaAs Laser	0.08	10	0.8	0.8	0.8	3.2
Laser Driver		80	0.2	0.2	0.2	0.8
Track Detector			2	2	2	2
Receive Module				2.4		0.6
Demodulator				1.2		0.3
Data Interface				6		6
Thermal Interface			10	10	10	10
Power Interface		85	3.7	5	3.7	5.1
ISL Controller			10	10	10	10
Sum (W)			70	44.6	70	45
Margin (W)			7	4.46	7	4.5
Total (W)			77	49.06	77	49.5

Table 6.6-5 Mass Budget for the Option 2 Terminal with Heterodyne Detection

Unit/Module	Unit Mass	GEO Terminal		LEO Terminal	
		Number	Total	Number	Total
Telescope & CPA	13.00	1	13.00	1	13.00
Beacon Laser	0.50	2	1.00	2	1.00
Beacon Detector	0.20	2	0.40	2	0.40
ACQ Coupler	0.07	1	0.07	1	0.07
Fine Pointing Ass.	0.15	2	0.30	2	0.30
Spectral Isolator	0.80	1	0.80	1	0.80
AlGaAs Laser	0.25	2	0.50	0	0.00
Nd:Yag Laser	1.60	0	0.00	2	3.20
Laser Driver	0.08	2	0.16	2	0.16
Fine Point Detector	0.15	2	0.30	2	0.30
Track Coupler	0.07	1	0.07	1	0.07
Polarizer	0.10	1	0.10	1	0.10
Nd:Yag L.O. Laser	1.00	2	2.00	0	0.00
Laser Driver	0.08	2	0.16	0	0.00
L.O. Coupler	0.07	2	0.14	0	0.00
Receive Module	0.30	2	0.60	2	0.60
Comms. Demodulator	0.70	2	1.40	2	1.40
Data Link Interface	0.50	2	1.00	2	1.00
Thermal Interface	2.00	1	2.00	1	2.00
Power Interface	0.50	2	1.00	2	1.00
Structure	6.00	1	6.00	1	6.00
ISL Controller	2.00	2	4.00	2	4.00
Sum			35.00		35.40
Margin			3.5		3.54
Total			38.5		38.94

Table 6.6-6 Power Budget for the Option 2 Terminal with Heterodyne Detection

Unit/Module	RF Power	Eff. %	GEO Terminal		LEO Terminal	
			ACQ. Power	Operat. Power	ACQ. Power	Operat. Power
Attitude Sensor			10	1	10	1
Beacon Laser	3.8	15	25.3		25.3	
ACQ. Detector			2		2	
Fine Point Mirror			6	6	6	6
AlGaAs Laser	0.08	10	0.8	0.8		
Nd:Yag Laser	0.87	5			17.4	17.4
Laser Driver		80	0.2	0.2	4.4	4.4
Track Detector			2	2	2	2
Nd:Yag L.O. Laser	0.08	5		1.6		
Laser Driver		80		0.4		
Receive Module				0.6		0.6
Demodulator				0.3		0.3
Data Interface				6		6
Thermal Interface			10	10	10	10
Power Interface		85	3.7	4.9	7.4	8.2
ISL Controller			10	10	10	10
Sum (W)			70	43.8	94.5	65.9
Margin (W)			7	4.38	9.45	6.59
Total (W)			77	48.18	103.95	72.49

6.7 Spacecraft Interfaces

6.7.1 ISL Gimbal Orientation

To have an intersatellite link it is necessary to have a terminal on the satellite at both ends of the link. For the GEO-LEO link one terminal is on a geostationary satellite while the other is on a low earth orbit satellite. The LEO satellite can have different heights above the earths surface. Radarsat has been chosen as a model partly because it could make use of an intersatellite link and partly because it has a near polar orbit with a keyhole problem associated with the gimbal orientation which does not appear on an orbit with low inclination angle.

Tracking systems experience the key hole effect when the line of sight to the other spacecraft passes through the azimuth axis. At this point the system must rotate 180 degrees in azimuth before tracking can continue. The communications link will be broken for a time which depends upon the slew rate around the aximuth, the antenna beam width and the angular rate of target motion. The size of the key hole also depends upon these factors. It is possible to reduce the key hole size and the outage duration by maximizing the slew rate and the beam diameter however, the best approach is to point the azimuth axis away from those direction in which the line of sight can occur.

For the GEO satellite the line of sight to a LEO satellite is limited to about ± 10 degrees from the Nadir. The key hole can be completely avoided by putting the aximuth axis normal to the nadir line, such as parallel to the earths axis of rotation. That is, normal to the satellite orbit.

For a LEO satellite with low inclination angles the aximuth axis can be oriented in the same manner (i.e. normal to the orbit plane) in order to completely avoid

the key hole. However, for a near polar orbit the key hole cannot be avoided completely as the normal to the polar orbit intersects the geostationary orbit on every orbit. The key hole is encountered whenever the geostationary satellite is located at the intersection at the time the intersection occurs. The size of the key hole is much reduced compared to an aximuth axis along the zenith line, because the angular rates are much reduced. However, the time duration of the outage is largely controlled by the slew rate and is only reduced if the slew rate is increased.

6.7.2 Geostationary Terminal

The selected orientation for the azimuth axis (first gimbal) is parallel to the earths rotation axis, i.e. north/south. Most communications satellites have an extension of the north and south panel beyond the earth facing panel in the direction of the earth. The first choice for mounting location is on the inside of this extension with the telescope projecting inward from the panel. It is also possible to project outward from the panel but in that case it must be kept clear of the solar panels.

Figure 6.7-1 shows conceptually how the OISL would be mounted on a geostationary satellite.

6.7.3 Radarsat Terminal

Figure 6.7-2 shows radarsat fully deployed and oriented in its flight position. The spacecraft travels in the direction of the long dimension of the antenna array and tipped at an angle to the vertical so that the antenna does not radiate vertically downward but at an angle to the Nadir line. The best position for the OISL terminal is the upper edge which has the best view of the upper hemisphere. However, this surface is the launch interface and is occupied by the launch adapter. It will be difficult to find space to stow the telescope for launch.

Figure 6.7-3 shows Radarsat in the stowed configuration. It is possible to find space to stow the telescope on the side of the spacecraft between the stowed solar panel and the antenna module. However from this location only half of the upper hemisphere is visible and it would be necessary to install a second terminal on the opposite side to obtain full coverage of the upper hemisphere.

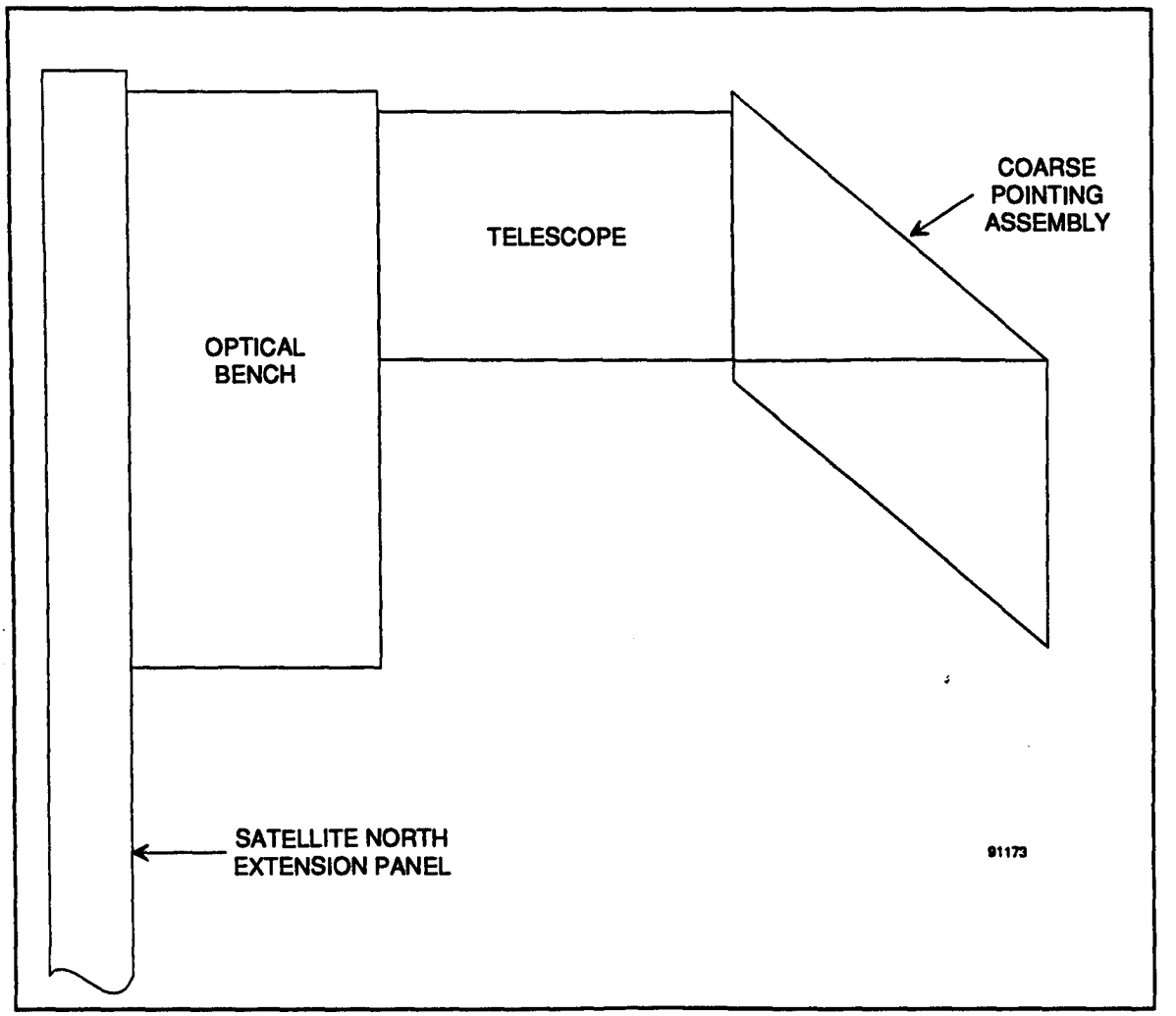

Figure 6.7-1 The Optical Intersatellite Link Mounted on a Typical Geostationary Satellite

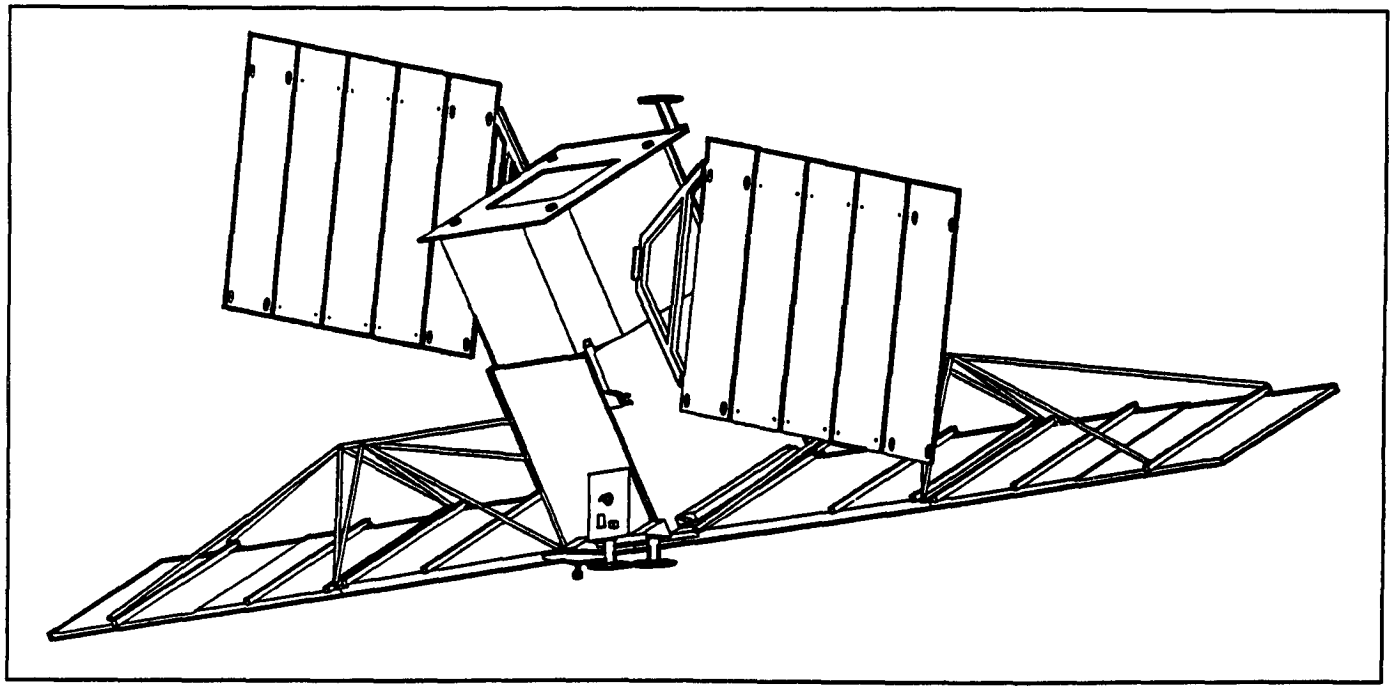

Figure 6.7-2 Radarsat Shown Fully Deployed

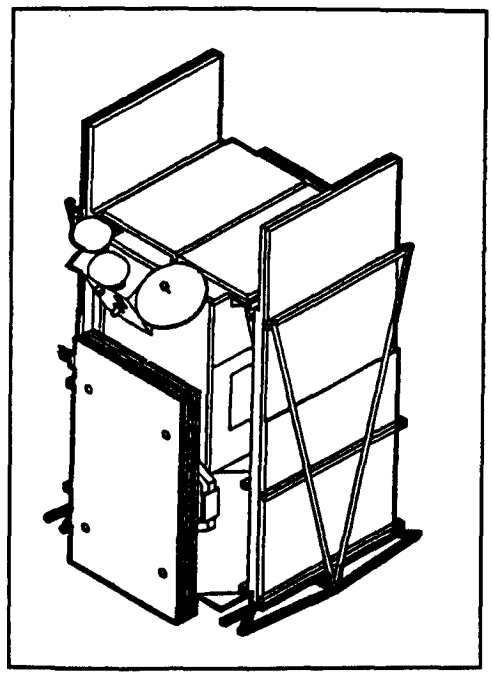

Figure 6.7-3 Radarsat in the Stowed Configuration

This Page Intentionally Left Blank

SECTION 7

CANADIAN INDUSTRY CAPABILITIES

7.0 CANADIAN INDUSTRY CAPABILITIES

7.1 Introduction

The above review of basic technologies and the system analysis and design exercise that followed have provided the study team with a good general overview of the technology and an impression, admittedly somewhat subjective, of the ability of Canadian industry to develop an optical ISL.

In this section we address more rigorously the capability of Canadian industry to participate in the development of this technology and make some suggestions as to where in industry the capability lies. We conclude that, although little existing hardware (or software) exists in Canada that is directly applicable to OISL development (EG&G's direct detection system being a notable exception), the broad range of expertise required does exist. Furthermore, the Canadian space industry leaders have sufficient experience in the development of space-qualified systems at the level of complexity and risk represented by an OISL program to be able to tackle this complex task.

7.2 Canadian Industry Capability Review - Methodology

Section 3.5 identified the critical technologies required for development of an OISL. In summary they are as follows:

- Detector sensitivity
- Laser output power
- Telescope design
- Pointing, acquisition and tracking

In addition, for heterodyne systems:

- Frequency tracking
- Wavefront alignment
- External modulators

The methodology used to identify Canadian industry capabilities in these critical areas is depicted in Figure 7-1.

The steps were as follows:

Step 1

The reference publication "High Technology Opportunities", published by Investment Canada was used as the source list of Canadian companies, augmented in some cases by working knowledge of industry capabilities already existing in the study team.

This document was created to facilitate and expand cooperation between Canadian and foreign firms in the laser-based opto-electronic industry. It contains profiles of Canadian firms and research institutes with relevant capability, and was last updated in 1989.

As a cross check, an additional source list was used. This was "Guide to Canadian Aerospace Related Industries", published by the USAF Systems Command Liaison Office Ottawa in August 1990. This document lists 10 companies under "electro-optics" (including CAL, Spar and EG&G) and 19 under lasers (including MPB Technologies).

The output of this review was a list of Canadian companies having some level of relevant capabilities.

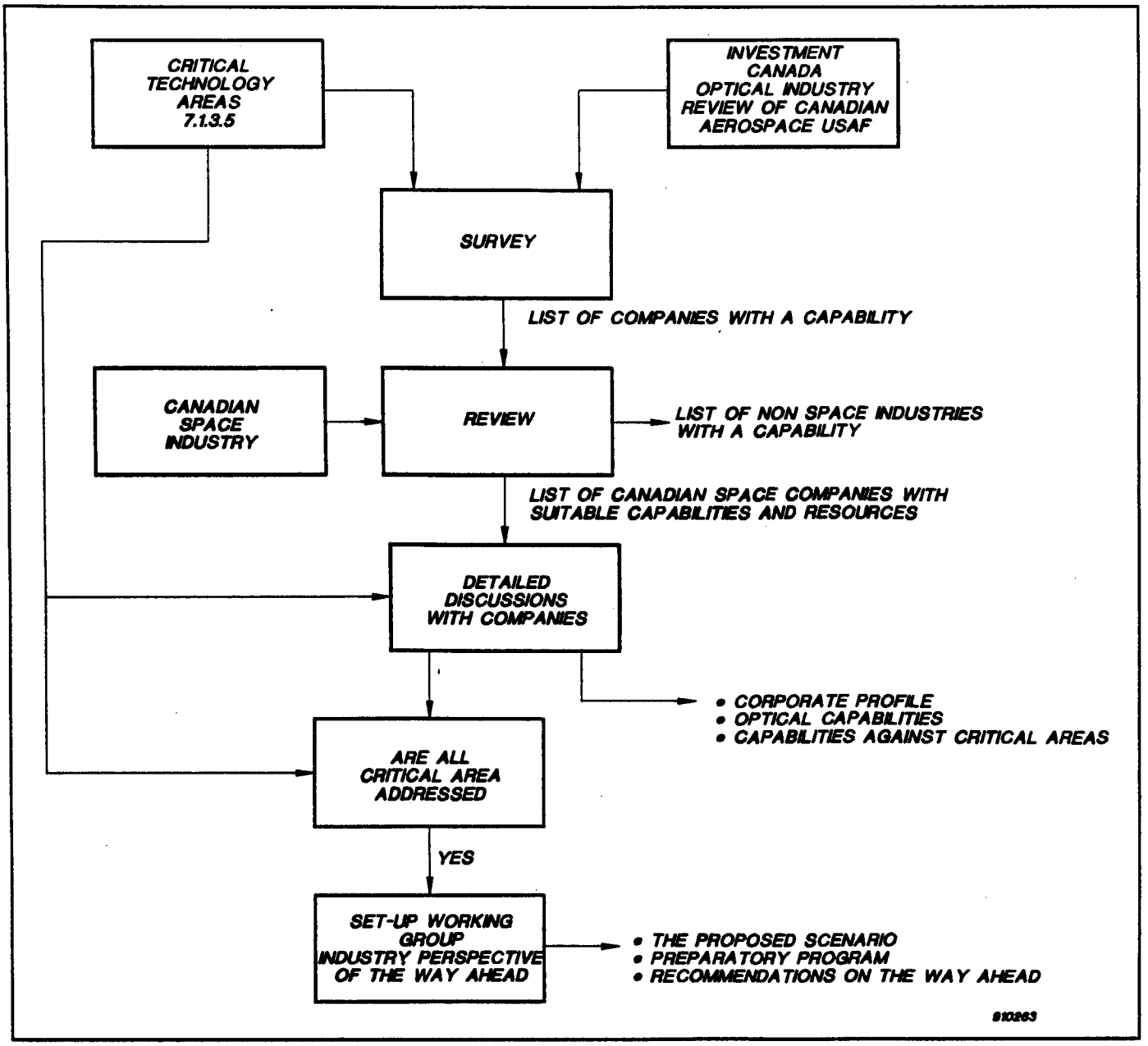

Figure 7-1 Identification of Canadian Industry Capabilities Methodology

Step 2

The list was refined to produce a pair of short lists in which at least one company was identified as having a capability against each of the main technology areas (critical or not).

The companies were segregated into those with space experience and those without and is indicated in Table 7-1.

Step 3

To streamline the process, it was decided to concentrate first on companies with space experience and only to turn to other companies to fill any gaps identified in the overall capability.

Detailed discussions regarding capabilities and plans were held with the space companies identified in Table 7-1. Each company was asked to provide:

a. A Profile of Corporate Capabilities (a sample questionnaire is provided as Figure 7-2 and the results are provided as Appendix D.)

b. A Matrix to indicate present and near-future capabilities provided as Table 7-2.

In addition, the system designs/options described in Section 6 were discussed and company capabilities in the applicable technology areas identified. A summary of the results is provided in Table 7-3. From the table it can be seen that the Canadian space industry has a technology base in all areas; there are no obvious gaps in capability.

Table 7-1 Canadian Industry with Potential OISL Capability

Space Industry Companies	Non-Space Industry Companies	
	Company	Speciality
CAL Corp	APS	Optics
EG&G	Dalsa Inc	Sensors, CCDS
MPB	Hughes Leitz	Optics
SED	Inc	Optics, Lasers
Spar	Interoptics	Optics
	Laser Institute	Laser

The review, and the discussions that preceded established that, whilst the Canadian technology base is sound, there is very little direct experience at optical ISL development. To date Canadian industries involvement in inter-satellite link technology has largely been at RF-using existing technology (S, Ku-Band links for space station (Spar)) or new frequencies (60 GHz) technology development for DND (Spar/ComDev).

It should, at this point, be acknowledged that the industry review is not exhaustive. Having established that a technology base exists within at least a subset of Canadian industry (most of the major space companies were contacted) no attempt was made to identify any competing capability. In the case of specific ISL products, we relied on the collective knowledge of the team to identify these (there are very few) and are confident no significant Canadian product has been overlooked.

Step 4

The above review suggests that Canadian industry has the technology base from which to develop a complete optical ISL capability. What is lacking is a heritage of space-qualifiable products and experimentation from which to proceed. This lack of heritage is likely to make Canadian industry involvement in existing or near-term OISL programs unlikely (beyond the existing SILEX involvement).

On the other hand, our studies of emerging technologies both for telecommunications and remote sensing suggest that optical ISL technology is a key feature of many future systems designs. Furthermore, Canadian industry, as a strong competitor in these areas, cannot afford to be shut out of such a key technology.

One clear strategy to adopt in these circumstances is to push forward with a national program which draws on the existing industry strengths and establishes an OISL credibility and heritage through development and demonstration of the key technologies. Such a pro-

PROFILE OF CORPORATE CAPABILITIES

Key Personnel: Include names of the top two executives within the company. Please identify one executive as the key contact person.

Nature of Business: Please identify your company's mission/markets.

Major Achievements: Please elaborate on scientific/technical breakthroughs, successful commercialized/marketed products, and other events that you feel are significant to your company's development.

Company Profile: Please provide the following information:

- The year your company was established;
- Total number of employees;
- Identify how many are in Sales & Marketing and R&D functions;
- Annual Revenues by Product/Service for most current fiscal year (exact data or growth percentage figures are accepted);
- R&D Expenditures - as a % of overall revenues;
- Stock listing - is your company publicly traded or privately held; and
- Total number of Customers.

Company Background: A brief description of the company including historical development and general direction.

Business Description: Current Products: Identify and briefly describe each of your products and their applications.
Future Product Directions: Identify and describe current methods of product distributions both direct and indirect (i.e. Direct Sales, Distributors, Manufacturer Agents).

Principal Clients: Firms with which that you repeatly conduct business.

Collaborative Agreements: Identify current collaborative business arrangements (i.e. business partners, agreements with Universities, etc ...).

Partnering Interests: Identify and describe the type of business opportunities your company is seeking (i.e. investment, distribution of your product/service, representing other groups in Canada/ the Unites States, commercial collaboration (e.g. OEMs), and joint research).

Figure 7-2 Profile of Corporate Capabilities Questionnaire

Table 7-2 Present and Near-Future Capabilities Matrix

Canada's Corporate Capabilities			CAL Corp., Ottawa	EG&G Canada Ltd.	EOSD/ATSG	SED Systems Inc.	MPB Technologies
Areas	Electronics		X	X	X	X	X
	Lasers			X			X
	Optics		X	X	X	X	X
Technology	Control	Electronics	X		X	X	X
		Software	X		X	X	X
		Power	X		X	X	
	Imaging	Recognition					X
		Holographic			X		
		Optics	X		X	X	X
		Digital	X		X	X	
		Spectroscopy			X	X	X
		Displays			X		X
		Reproductions					X
	Light & Energy Sources	UV					X
		Visible					
		IR		X		X	X
	Materials & Substrates		X				X
	Mechanical		X		X	X	X
	Sensors		X	X		X	X
Markets	Aerospace (Civil)		X		X	X	X
	Automotive						
	Communications		X	X		X	X
	Defense (Air & Space)		X	X	X	X	X
	Defense (Land/Sea)			X	X	X	X
	Construction						
	Educational Training						X
	Energy/Power						X
	Environment					X	X
	Industrial/Control			X			X
	Industrial/Inspection						
	Industrial/Processing						X
	Information Technology						X
	Instrument/Lab.			X			X
	Medical						
	Natural Resources						

gram could go all the way to flight test and demonstration of a representative link or seek international collaboration for the full-scale development stage. In either case a domestic Preparatory Program will be an essential ingredient.

Accordingly, the study team invited MPB Technologies and SED to join them for the purposes of outlining a structured program leading to full OISL capability in Canada. This program is described in the next section.

Table 7-3 Company Capabilities for System Design/Options Applicable Technology Areas

Technology		Capability
Program Management		Spar, CAL, SED
System Engineering		Spar, CAL, SED
I&T		Spar, CAL, SED
Optics	Telescope	CAL, Spar
	Optical Bench	Spar, SED, MPB, CAL
Lasers	Beacon Laser Assembly	EG&G, MPB
	Comms Laser Assembly	EG&G, MPB
	Laser Drivers	EG&G, MPB
Receivers	Acquisition Detectors	EG&G (DALSA) SED
	Track Detectors	EG&G (DALSA) SED
	Receiver Module	EG&G, SED, MPB
Mechanisms	Coarse Pointing Assembly	Spar
	Attitude Sensors	Spar
	Beacon Mirror Steering	SED, Spar, MPB
	Fine Pointing Mirrors	SED, Spar, MPB
	Point Ahead Mirrors	SED, Spar, MPB
Electronics	Drivers	SED, MPB, Spar
	Modulator/Demodulator	EG&G, SED, MPB, Spar
	Data Link Interface	EG&G, Spar MPB
	System Controller	SED, Spar, MPB
Other	Thermal Control	SED, Spar
	Power Supplies/Conditioning	SED, Spar
	Structure	SED, Spar

SECTION 8

AN OUTLINE OISL TECHNOLOGY DEVELOPMENT PROGRAM

8.0 AN OUTLINE OISL TECHNOLOGY DEVELOPMENT PROGRAM

8.1 Introduction

A key output of the present study has been the identification of a baseline Canadian industry capability. However, this needs to be put in context against existing OISL programs and worldwide competition before a proper picture emerges of Canadian industries present competitive position, from which a viable national OISL program can be structured.

This section briefly reviews the current status of the plans of Europe, Japan and USA for optical intersatellite links. From this the need for a domestic program is identified. A scenario for establishing a multi-national optical relay program is described as one possible option and program elements are identified including a domestic Preparatory Program to develop key technologies and a National Test Bed on which to demonstrate them. An indication of schedule and cost is given.

The section concludes with a recommendation that CSA fund an activity to further develop the ideas presented.

8.2 Offshore OISL Capabilities and Programs

In the US, Japan and Europe, a common theme among the space agencies has been to orient their R&D towards data relay satellite programs. These programs are an indispensable factor in operating their space infrastructure.

In Europe, the Data Relay Satellite (DRS) program is expected to be confirmed this year. It will provide communications between Columbus, Hermes, Polar Platform and the ground. In addition, and closely associated with DRS, ESA plans an experimental Artemis (GEO) program. Through Artemis and France's SPOT-IV (LEO) program it is intended to demonstrate essential technologies for relay satellites including optical links employing the SILEX and SOUT terminals.

In Japan the Engineering Test Satellite-6 (ETS-6) program will be used to assess new technologies including optical intersatellite communications and on-board switching and to test data relays. ETS-6 will be used in conjunction with the ADEOS scientific satellite to test optical cross-links, however the baseline communication experiment will be between ETS-6 and an optical ground station. The ETS-6 program will allow development of the experimental tracking and data relay satellite program (E-TDRS). An inter-satellite optical communications experiment is then planned between it and the Japanese Experimental Module attached to Space Station.

In the US, the emphasis has been on the application of S and Ku-Bands for STS, TDRSS and Space Station. In fact, Canadian industry (Spar) has made significant inroads into this market and has been selected to supply all the communications cross-link antennas for Space Station. NASA now plans to fly their Laser Communications Transceiver (LCT) originally slated for the Advanced Communications Technology Satellite on Space Station. The primary mode of operation will be communication with the ground, however, the capability to allow communication with a GEO satellite will be incorporated. NASA plans to procure the Advanced TDRSS comprising some nine (9) satellites as a follow-on to TDRSS. The system would be operational 1997 - 2012. ATDRSS would employ the use of Ka-Band to meet increased data rate requirements. It could also

provide a platform for an optical link with Space Station using the LCT.

Figure 8-1 shows the schedule for the programs identified above. It is clear that considerable work is ongoing in all Agencies. The optical inter-satellite work is proceeding almost in parallel. NASA and NASDA plan to take a two-step approach. The first to test communication from space to ground and then between two payloads in space. ESA plans to go directly to a space to space test (even though space to ground tests are also planned) between SILEX and SOUT in LEO and Artemis in GEO. It should be cautioned that DRS is slipping and that without it the agencies lack a suitable GEO end to their links.

It is understood that an International Working Group on Intersatellite Optical Communications comprising representatives from NASA, ESA, NASDA and CSA has been formed. Further it's task is to initially exchange rationale on the design approaches taken by each agency, particularly regarding tracking and acquisition, and later to examine the possibility of interoperability and cooperative or collaborative endeavours.

8.3 The Need for a National Program and a Possible Scenario

8.3.1 The Need

Although not discussed, the financial dimensions of the European, Japanese and US programs and their impact in terms of technology development will be fundamental for the national industries concerned.

While the developments are aimed at supporting each countries space infrastructure, we can expect national industries to fully exploit the capabilities developed in the commercial market. The market is clearly developing for crosslinks with the trend towards distributed world wide communications system architectures employing many interconnected satellites in various orbits. One of the best published commercial systems is the Iridium system proposed by Motorola. The essential features of the system include 77 active satellites in

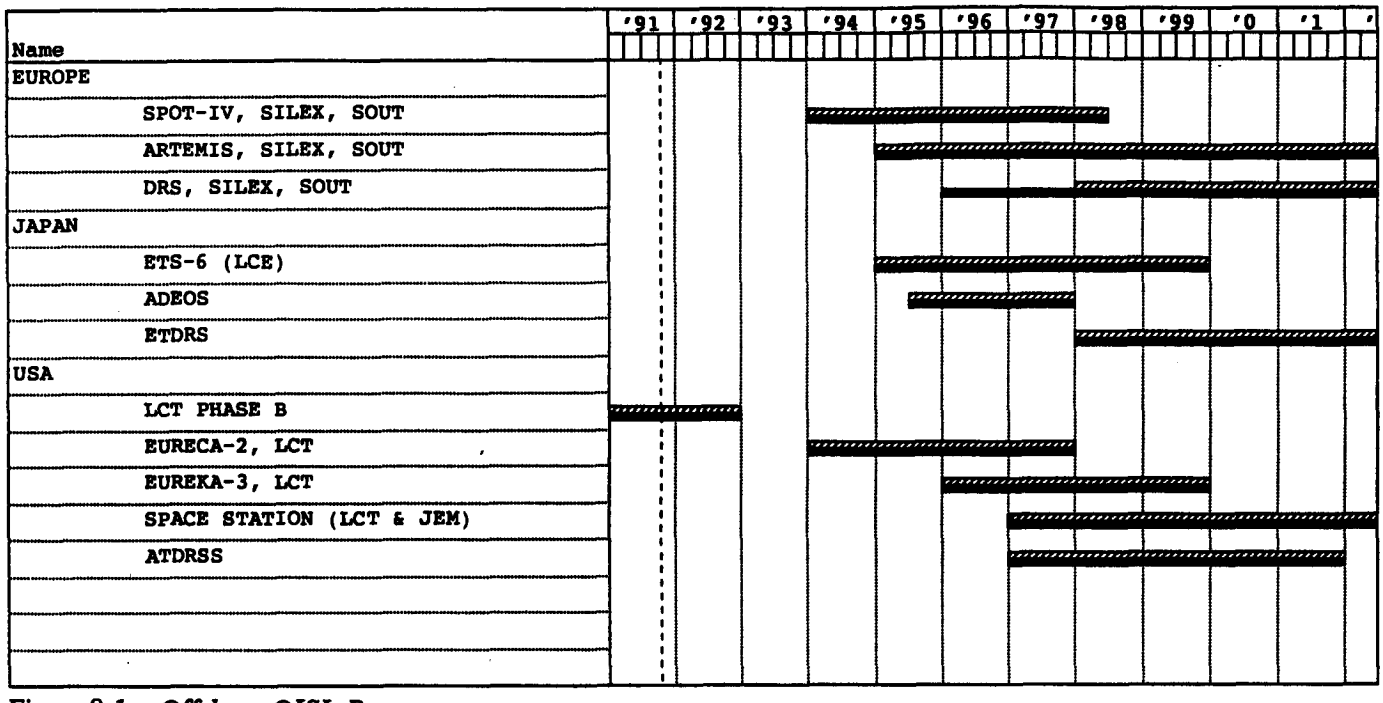

Figure 8-1 Offshore OISL Programs

LEO, evenly spread on seven orbital planes each of them connected to it's neighbours by six intersatellite links supported by 462 active ISL terminals. The proposed ISL's would be at Ka-Band, however, conceptually they could be optical. The U.S. Department of Defence's BRILLIANT PEBBLES and BRILLIANT EYES programs are considering OISL's. The system architectures for these programs are similar to Iridium but each will have some 200-400 active satellites.

A major concern is that if Canada does not embark on a significant development program,then we will have abandoned the market to the industry of other nations.

Referring back to the schedule, Figure 8-1, it is clear that although some experiments will fly earlier, the majority of these OISL development thrusts come to fruition in the 1996-1998 time frame. In some cases development has been slowed by funding constraints, in others development started based on the technology of a few years ago has proved difficult to complete quickly. Whatever the reasons, it is clear that Canadian industry, working from a sound foundation of relevant technology, can compete against this schedule.

8.3.2 A Possible Scenario

The following is not intended to be a plan in itself, but it is intended to suggest that there is merit in considering development of a plan. Thus, the purpose here is to describe a scenario and the possible elements of a plan. There will eventually be a need to clearly establish in detail the content, cost and schedule of all possible elements of any scenario. Further, it is suggested that the eventual plan become an integral part of the Long Term Space Plan currently being considered by CSA.

a. Objective

To undertake a domestic optical intersatellite link development program. The program should target cooperative work with international partners in the first instance, but should also address stand-alone work with international partners.

b. Approach

There are two possible approaches for the Canadian program; to develop either the GEO or LEO end of the link. The early stages of the program are likely to involve the same technology and sub-system development, but the aim will be to enter cooperative flight test (and to the degree possible, cooperative development) with a partner country who will provide the other end of the link.

The existence of the necessary geostationary data relay satellites, equipped with optical ISL's in the timescales shown in Figure 8-1 is by no means certain. If they are not developed in time, OISL's deployed in LEO orbit will face severe restrictions in their test and evaluation programs. A dedicated OISL relay, implemented on a GEO smallsat orbited over North America would enable a range of cooperative experiments to be undertaken (subject to interoperability considerations), and would also be suitable for stand-alone space-to-ground work.

Alternatively, the OISL could be implemented on a LEO satellite, possibly a future Radarsat or polar orbiting communications smallsat. Again, realistic service demonstration would only be possible through interoperation with a suitable GEO relay such as ATDRSS or ARTEMIS/DRS. Without such interoperability more limited LEO-to-ground testing could be done, though in these circumstances the stand-alone GEO is probably the more attractive alternative.

In order to put a suitable cooperative program in place, it will be necessary to take an aggressive approach in the "International Optical Communications Working Group" and ESA and to move ahead quickly on a Preparatory Program to explore the key technologies.

c. Strategic Linkages

Strategic Linkages with the ESA, NASDA and NASA programs as well as domestic programs should be fostered in order to maximize the benefits to the domestic program. As a direct

consequence of the CSA's participation in the International Optical Working Group, a multinational program could be proposed. Similarly CSA could sponsor a mini-satellite program in ESA. In any event, it will be necessary to standardize system interfaces, acquisition and tracking, and communications methods and protocols as well as make maximum use of existing programs and technology.

In this regard, a Canadian role in ESA's SOUT program should be encouraged; CAL Corp. and Spar are at the time of writing investigating a role in developing the telescope and coarse pointing subsystem.

Domestically, a linkage with any smallsat bus development would be most desirable.

d. Team Canada

All of Canada's major space activities have been undertaken in cooperation with other countries. This has been achieved through close collaboration between Government and the Space industry. Key has been the development and enhancement of technology and skills necessary to maintain a solid Canadian industry infrastructure.

In recent years, the international space industry has gone through a period of mergers and acquisitions that have changed the competitive balance and created a global market.

Canada's ability to continue to achieve success will be dependant upon a high degree of cooperation and interaction of government officials and space industry and between the individual members of space industry. Spar has gained a commitment from all the companies identified in Table 7-1 to work together towards the success of the scenario proposed here.

8.4 Program Elements, Schedule and Cost Estimates

8.4.1 The Proposed Scenario

Key to the program is the early identification of cooperative development opportunities (and the resolution of the GEO/LEO question) and successful interoperability. For this reason it is recommended that a systematic operational research approach be adopted based on an iterative process of the optimization of the design based upon the analysis of requirements, leading to the generation of a simulation model. In this way interoperability and system control would be assured. This Phase 0 activity would provide a basis for:

- Agency to Agency discussions
- Industry to industry discussions, and
- Program alternative identification and selection

This activity would then lead into a Phase A, System Design and Specification activity

The Phase A would comprise:

- System design and specification and cost estimates, and
- Risk identification

Phase A would be followed by a normal Phase B

- Sub-system specification
- Proof-of-concept demonstration of critical hardware
- Proposal for Phase C/D, full scale development and launch

A program overview responsive to the cooperative project window of opportunity described above is provided as Figure 8-2.

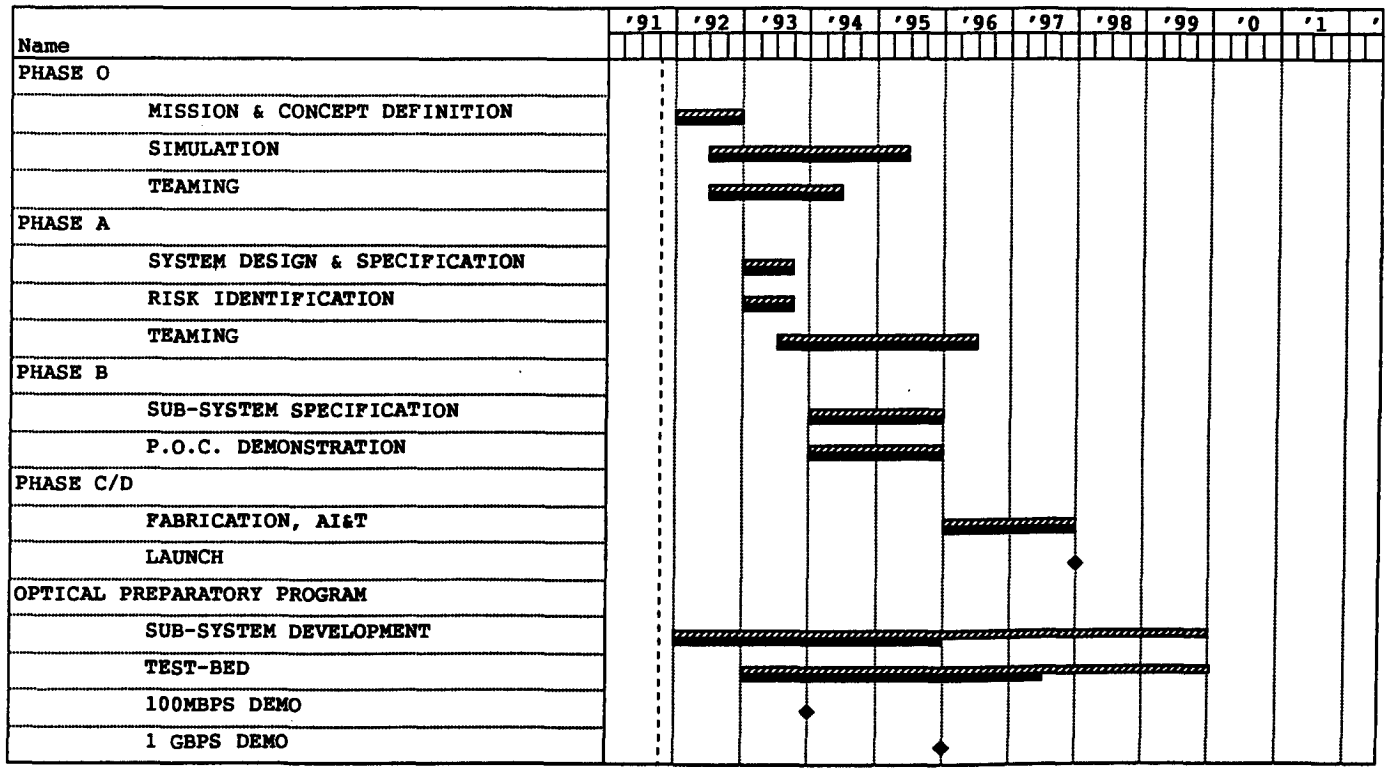

Figure 8-2 OISL Program Overview

ROM costs for each phase would be as follows:

Phase	ROM
O	$750K
A, B	$5M - $10M

8.4.2 Optical Link Preparatory Program

The objectives of the proposed scenario are ambitious and Canadian industry, though it possesses a strong foundation in the relevant technologies, cannot point to a heritage of OISL components, sub-systems or systems. This can be remedied by initiating an Optical Link Preparatory Program (OLPP) to focus development of Canadian OISL technology and provide a means of demonstrating it prior to flight of a link.

The OLPP will be focused around the development and maintenance of a national Optical Link Test Bed which will be used to demonstrate and evaluate the necessary OISL technology as well as to explore concepts for complete systems.

Within industry, key components and sub-systems will be developed and integrated into the test-bed to provide first a 100 Mbps demonstration link, with the eventual aim of demonstrating a 1 Gbps link.

The test bed will provide a phased approach to increasing Canadian industries OISL capability. In the first stage the demonstration of 100 Mbps capability will represent meaningful progress (100 Mpbs is a useable bandwidth for a number of remote sensing and telecommunications applications) and will permit industry to develop and integrate all the key sub-systems required. It will also permit industry to tackle the challenges of overall system integration and test and to explore options for acquisition, tracking and stabilization.

As discussed in Section 6 above, the extension of capability to 1 Gbps requires a change in the approach to

transmitter and receiver design. Options such as wavelength multiplexing or heterodyne detection using an alternative laser wavelength will be explored on the test bed.

With such a phased approach we believe that Canadian industry can demonstrate a basic capability early, and so lever a worthwhile position in a cooperative program to develop a flight OISL.

8.4.2.1 Component and Subsystem Development

It is clear from the above discussion that the key technologies required to demonstrate OISL system capability on the test-bed can be identified now.

Table 8-1 lists elements of the OLPP that the study team believes need to be addressed. The priority assigned is a reflection of the phased approach to development; high priority elements are required for demonstration of the 100 Mbps capability and need to be addressed as early as possible. Lower priority elements can be tackled later as they contribute to increased performance downstream.

For completeness a capsule description of each development line item is included as Appendix D.

8.4.2.2 The Test Bed

The components and sub-systems developed will be evaluated and demonstrated in a test-bed designed to explore all the systems and integration aspects of the OISL.

The test bed would be located at a suitable CSA facility (possibly David Florida Laboratories) and would be a national facility with the following basic uses.

- demonstration and proof-of-concept of complete OISL systems
- standard test/evaluation facility for individual components and sub-system development
- test rig for development and evaluation of system design issues such as acquisition and track algorithms.
- capability demonstrator for CSA and Canadian industry
- reference system for trouble shooting flight systems

Clearly the test-bed, if it is to be an evolving expression of current Canadian OISL technology, cannot simultaneously address all the above uses. Its use, and particularly the control of its configuration would have to be carefully integrated into the OISL flight program as it develops. Issues such as ownership (CSA) vs management (CSA or an industry prime) would have to be addressed as part of the detailed planning of the program.

8.4.2.3 Schedule and Test

A nominal schedule for the OLPP is shown on Figure 8-2 against the cooperative program. Key milestones are demonstration of 100 Mbps and 1Gbps capabilities and the OLPP, starting as much as 2 years ahead of the Phase B will provide proof-of-concept demonstrations required.

It should be emphasized that the test-bed is intended as a continuing program, or at least within the span of current OISL development out to the end of the decade.

The OLPP is not intended to be a high cost program. Within the program, high costs associated with space qualification, packaging and QA will be avoided, whilst providing proof-of-concept level equipment and building experience and credibility. It is anticipated that costs in the start-up years will not exceed $2M/year. If the program were started in FY 1992/93 the OLPP will provide basic technology development to a cooperative OISL flight program at a total cost of approximately $10M.

Table 8-1 *Proposed Canadian Optical ISL Hardware Developments*

Subsystem	Unit	Lambda	Data Rate	Priority	Risk	Cost
Acquisition and Tracking	Fine Pointing/Point-Ahead Mirror/Assy.	N/A	--	Medium	Medium	Medium
Acquisition and Tracking	FPM/PAM CCD-Acq. Drive Control Electronics	N/A	--	High	Medium	Medium
Acquisition and Tracking	Receivers - CCD Version - Pos. Sens. APD.	780-900 780-900	--	Low Low	Low Medium	Medium Medium
Beacon	Laser source	780-900	N/A	Medium	Low	Medium
Beacon Telescope	Beacon Tel. Assy.	As required	--	Medium	Low	Medium
Comms	Modulators	NA	1,300,100 Mb/s	Medium	Medium	Low (1)
	Laser drivers - normal - heterodyne	820/1032/1064 820/1032/1064	300 Mb/s 1 Gb/s	Low Medium	Low Low	Low Medium
	Laser sources - normal - heterodyne	820/1032/1064 820/1032/1064	300 Mb/s 1 Gb/s	High High	Low Medium	Medium Medium
	Receivers - normal - heterodyne - Opt. Preamp. Rx	820/1032/1064 1032/1064 820/1032/1064	300 Mb/s 1 Gb/s	Medium High High	Low Medium Medium	Low High High
	Demodulators - normal - heterodyne	N/A N/A	300 Mb/s 1 Gb/s	Low Medium	Low Medium	Low (1) Low (1)
Optical Bench	Multiplexer/Demultiplexer	As required	--	Medium	Low	Low
	Spectral Isolator	As required	--	Low	Low	Low
	DichroicFilters	As required	--	Low	Low	Low
Optical Bench Unit	2 Axis Stabilized Fine Pointing Mirror	820-1064	2 Mbls 1 Gb/s	Medium	Medium	High
	Compant bench design using innovative techniques	820-1064	2 Mbls 1 Gb/s	Low	Medium High	Medium
Telescope	Objective	As required	--	High	Low	Medium
	Eyepiece	As required		High	Low	Medium
	Thermal Control Window	As required		Medium	Medium	Medium
	Coarse Pointing Assembly	N/A		High	Low	Medium
Telescope & Drivers	Telescope - composite lightweight structure - hybrid refractive/diffractive	820-1064 820-1064	10 Mb/s - 1 Gb/s	Medium Low	Medium Low	Medium[2] Medium
	CPA - Parallel mirrors - Coude	820-1064 820-1064	2-10 Mbls 10-1 Gbls	Low Low	Low Low	Low Low

Notes: (1) If implemented as ASIC's, both Development and qualification cost would be high.

There is also the question of the National Laser Comms. Test Bed. It is assumed that the prototypes and engineering model examples discussed here are integrated into the Test Bed for systems evaluation. CAL has interests in this level of work as expressed at previous meeting with both Spar and CRC.

SPAR

8.4.2.5 Conclusions and Recommendations

This study has provided a review of basic OISL technology and outlined a concept for a 100 Mbps OISL, with growth capability to support 1 Gbps.

The process has served to highlight the key technologies that must be mastered in order to successfully develop the OISL. The industry study team has reviewed the capabilities of Canadian industry, with emphasis on those companies with existing space expertise, and has concluded that Canada does prosses sufficient capability in the relevant technologies to consider the development of a complete optical ISL. The review did confirm, however, that Canadian industry has generally developed little that is specifically applicable to an OISL and cannot therefore demonstrate a heritage in this area.

Our ongoing involvement in manned space, satellite communication and remote sensing has convinced us that these space systems will make increasing use of inter-satellite communications links in the future-many of which are likely to be optical. This view is clearly shared by the rest of the space community as OISL development figures in a number of programs, in NASA, ESA and NASDA in particular.

The scope and schedule of such programs does not indicate that the technology gap is wide and impossible to close, but it does suggest that Canada should begin work in this area without delay, to avoid being left behind.

Two parallel thrusts are recommended. The team believes that the most effective route to fielding an OISL is via an international cooperative program where Canada would provide one end of an optical link and join with an international partner (or partners) to demonstrate interoperability and end-to-end communications. A possible example is to provide a first generation geosynchronous optical data relay satellite.

In parallel, and to provide the OISL technology credibility and focus on which to base the flight program, the team recommends that an Optical Link Preparatory Program be initiated immediately. Such a program would provide an ongoing development, evaluation and demonstration base through the use of a ground test-bed on which both component development and system concepts could be tested.

We believe that the OLPP should begin as soon as possible, so as to provide early experience in Canada in the key technologies whilst the details of an international cooperative OISL program are being finalized.

Appendix B to the report lists a number of key areas where useful development could be carried out now, but further work is required to better detail the OLPP program, its cost, schedule and the details of the work.

It is therefore recommended that the Spar team be contracted to fully define the OLPP and its links to potential international programs with a view to beginning work in FY92/93.

SECTION 9

LIST OF REFERENCES

9.0 LIST OF REFERENCES

[1] M. Ross, "The History of Space Laser Communications", SPIE Vol. 885, pp. 2-9 (1988)

[2] P. Huber, W. Reiland, V. Klein and A. Popescu, "Full Scale Laboratory Breadboard Model (LBM) of a Free Space Laser Transceiver package", PIE Vol. 1218, pp. 467-477 (1990)

[3] E. Bonek and H. Lutz, "CO_2 Laser Communication Technology for Intersatellite Data Links", ESA J. Vol 5 pp 83-98 (1981).

[4] D.J. Wilson, G.D.J. Constant, R. Foord and J.M. Vaughan, Infrared Physics Vol. 31, No. 1 pp 109-115 (1991)

[5] V.W.S. Chan, J. of Lightwave Tech Lt-5, No. 4 pp. 663-637 (1987).

[6] R.G. Marshalek and G.A. Koepf, Opt. Eng. vol 27, No. 8 pp. 663-676 (1988)

[7] U.E. Hochuli and P.R. Haldeman, "Life Problems of dc and rf-excited low power cw CO_2 Waveguide Lasers", Rev. Sci Instrum. Vol 57, No. 9 p. 2238-2241 (1986).

[8] P.C. Condor, R.M. Jenkins and J.R. Redding "Recent Advances in CO_2 Laser Technology" SPIE Vol. 806, pp. 27-33 (1987).

[9] L.A. Newman and R.A. Hart, "Recent R&D Advanced in Sealed-off CO_2 Lasers", Laser Focus/Electro Optics, Vol. 23, No. 6 pp. 80-96 (1987).

[10] D. He and D.R. Hall, IEEE J. quan Electon. QE-14 pp 377 (1978)

[11] G.A. Griffiths, SPIE Vol. 227, p. 6-11 (1980)

[12] D.He and D.R. Hall, IEEE J. Quan. Electon QE-14, p. 377 (1978).

[13] C.A. Worrell, "Infrared Optical Constants for CO_2 Laser Waveguide Materials", J. of Mat Sci Vol. 21 p. 781-787 (1986).

[14] I.E. Ross, "CO_2 Waveguide Lasers", SPIE Vol. 1042 p. 55-62 (1989).

[15] P. Vidaud, D.He and D.R. Hall, "High Efficiency RF Excited CO_2 Laser", Optics Comm. Vol. 56, No. 3 pp. 185-190 (1985)

[16] W.L. Wolfe & G.J. Zissis "The Infrared Handbook", Chapter 15 (1985).

[17] C.K. Chan. E. Tward and W.W. Burt, Adv. in Cryo. Eng. Vol 35 p. 1239 - 1256 91990).

[18] G. Davy "Review of the Oxford Cryocooler", Adv. in Cryo. Eng. Vol. 35, p. 1423-1430 (1990)

[19] J.H. McElroy et al, "CO2 Laser Communications Systems for Near Earth Space Applications", Proc. of IEEE, Vol. 65 No. 2 pp 221-257 (1977)

[20] R.G. Marshalek, "Comparison of Optical Technologies for Intersatellite Link Payloads, Part I", COMSAT Review, Vol. 18 No. 2 pp. 191-214 (1988).

[21] D.K. Paul, "Comparison of Optical Technologies for Intersatellite Link Payloads, Part II", COMSAT Review, Vol. 18 No. 2 pp. 215-238 (1988).

[22] Specification for a PV HgCdTe detector, from Societe Anonyme de Telecommunications, Paris.

[23] W.K. Pratt, "Laser Communication System", John Wiley & Sons (1969)

[24] B.L. Patel et al, "Coherent Optical Intersatellite Links, SPIE Vol. 19\191 p. 615-626 (1989).

[25] S. Marcus and G.M. Carter, "Electro Optically Q Switched CO_2 Waveguide Laser, Appl. Optics, Vol 18 No. 16 pp. 2824-2826 (1979).

[26] D. Letalick et al, "CO_2 Waveguide Laser with Programmable Pulse Profile", Opt. Eng. Vol 28 pp 172-179 (1989).

[27] R.C. Harvey, CO_2 Lasers for Military Applications", SPIE Vol. 1042 pp. 42-54 (1989).

[28] Tilton et al "Recent RF Excited CO_2 Waveguide Laser Development at Hughes Aircraft Industrial Electronics Group" paper presented at Lasers 90, SanDiego Nov. (1990)

[29] D.E. Bowker Ed, "Earth Science requirements for the Inforamtion Sciences Exp. System", NASA CP-3072, July (1990)

[30] C.J. Wenzler et al, "Design of a CO_2 Laser Power Control System for a Spacelab Microgravity Experiment", NASA-TM-103112, August (1990).

[31] N. McAvey, "10.6 Micron Communications System", NASA-TM x-524-65-461 (1965).

[32] Private Communication, L. Newman, United Technology Optical Systems Feb. (1991).

[33] P. Pace and J. Cruickshank, "Long Term Operation of a Sealed Waveguide CO_2 Laser", Rev. Sci. Instr. Vol. 52, No. 10 pp. 1493-1496 (1981).

[34] P. Leakman and K.D. Leakman, "Sealed Off RF Excited CO_2 Lasers and Method of Manufacture Such Lasers", US Patent 4,393,506 (1980)

[35] S.J. Pang et al, "Thermal Desorption Measurements for Aluminum Alloy 6003 and stainless Steel 304", J. Vac Sci Tech. Vol. A5 No. 4 pp. 2576 1987).

[36] U.E. Hochuli and P.R. Haldemann, "Efficient 30 Watt 140 MHz RF Amplifier for CW CO_2 Waveguide Laser Excitation", Rev. Sci Instr. Vol 59, No. 11 pp. 2380-2383 (1988).

[37] W. Reiland et al, "Optical Intersatellite Communication Links: State of CO_2 Laser Technology", SPIE Vol. 616, pp. 69-76 (1986).

[38] N.W. Harris et al, "Wideband Long Pulse Operation of an Efficient Electro-optic Modulator at 10.6 microns "Opt Letters Vol. 15, No. 20, pp. 1156-1158 (1990)

[39] T. Petch "Electro Optic GigaHertz CO_2 Laser Modulator", SPIE Vol. 1131, p. 168-175 (1989).

[40] B.M. Oliver, "Thermal and Quantum Noise" Proc. IEEE Vol. 53, pp. 436-454 May (1965).

[41] W. Reiland, W. English and M. Endemann, SPIE Vol. 616, pp. 56-76 (1986).

[42] A.L. Scholtz et al., "Realization of a 10 micron Homodyne Receiver", J. of Lightwave Tech. Vol. LT-5, No. 4 pp. 625-632 (1987).

[43] J.R. Bary and E.A. Lee "Performance of Coherent Optical Receivers", Proc. of the IEEE Vol. 78, No. 8, August 1990, page 1369.

[44] U. Timor and G. Jacobsen "A Comparison of Sensitivity Degradations for Optical Homodyne Versus Direct Detection of On-Off Keyed Signals", J. of Lightwave Technology LT6 (11) pp. 1782-1788 (1988).

[45] C. provencher and R. Spence "A Laser Communication Experiment Utilizing the ACTS Satellite and An Airborne Laser Transceiver". SPIE Vol. 885 Free Space Laser Communications Technologies (1988) p. 143

[46] L.G. Kzovsky "Impact of Phase Noise on Optical Heterodyne Communications Systems" J. Optical Communications, Vol. 7, No. 2 pp. 66-78, 1986.

[47] R.E. Peile "Error correction for optical space communications" SPIE volume 756 Optical Technologies for Space Communications Systems (1987) page 86.

[48] M. Wittig, "The Importance of Pointing-Acquisition and Tracking for Optical Communication Payloads", pp. 30-36, SPIE Vol. 1131, Optical Space Communication, Paris, 1989.

[49] P.J. Crepin et al., "Silex Beacon Equipment", pp. 258-263, SPIE Vol. 1218, Free Space Laser Communication Technologies II, Los Angeles, 1990.

[50] B.D. Seery, "The Goddard Optical Communications Program", pp. 13-26, SPIE Vol. 1218, op. cit..

[51] N.W. Carlson et al., "CW operating characteristics of grating-surface-emitting master oscillator power amplifier laser arrays", paper CWF13, pp. 250-251, CLEO '91, Baltimore Maryland.

[52] Papers CFD4 to CFD6 and CW14 to CW16 on strained layer long wavelength lasers, pp. 252-253 and 498-499, CLEO '91, op. cit.

[53] C.G. Dupuy et al., "Talbot filtering for modal discrimination: modelling and fabrication", paper CW17, pp. 254-255, CLEO '91 op. cit.

[54] V.W. S. Chan, "Intersatellite Optical Heterodyne Communication Systems", pp. 204-215, SPIE Vol. 1131, op. cit.,

[55] R.K. Zimmerman Jr., "Hybrid current driver designed for a space-borne laser transmitter", pp. 17-25, SPIE Vol. 1044, Optomechanical Design of Laser Transmitters and Receivers, Los Angeles, 1989.

[56] B.D. Seery et al., "NASA direct detection laser diode driver", pp. 102-110, SPIE Vol. 1044, op. cit..

[57] David Sarnoff Research Center, 1986, Private Communication.

[58] R.P. Mathur et al., "Analysis of SILEX tracking sensor performance", pp. 129-141, SPIE Vol. 1218, op. cit.

[59] R.C. Short et al., "Performance of a demonstration system for simultaneous laser beacon tracking and low data rate optical communications with multiple platforms, SPIE Vol. 1417, Free-Space Laser Communication Technologies III, Los Angeles, 1991.

[60] E. Corpaccioli et al., "An acquisition sensor for optical communications in space", SPIE vol. 1131, op. cit.

[61] Ch. Noldeke, "Transmission schemes for optical telecommunications in Space" SPIE Vol. 1131, op. cit.

[62] X. Sun et al., "World timing recovery in direct detection optical PPM communications systems with avalanche photodiodes using aphase lock loop" pp. 666-673, IEEE Trans. on Comm, 38, 5, 1990.

[63] O.K. Tonguz, "Impact of spontaneous emission noise on the sensitivity of direct-detection lightwave receivers using optical amplifiers," pp. 1343-1344 IEEE Electronics Letters 26, 17, 1990.

[64] W.R. Leeb, "Heterodyne and homodyne detection in optical space communications", pp. 216-227, SPIE Vol. 1131, op. cit.

[65] Vanhove, Laurent, & Perbos, "System Analysis of Optical Interorbit Communications", SPIE Proceedings Vol 810, 1987.

[66] Klien & Degnan, "Optical Antenna Gain", Applied Optics Vol 13 No. 9, September 1974.

[67] Cornwell, D.M., "Far Field and Phase Front Characterization of a High-Power Semiconductor Laser for Free Space Optical Communications", SPIE Proceedings, 1991.

[68] Cotton, J.M., "Narrow Band Optical Interference Filters", SPIE Proceedings, 1991.

[69] Vukobratovich, D., "Ultra-Lightweight Optics for Laser Communications", SPIE Proceedings, Vol 1218, 1990.

[70] Vukobratovich, D., "Lightweight Laser Communications Mirror Made with Metal Foam Cores", Optical Sciences Center, University of Arozona, Tucson, Arizona, 1990.

[71] M. Ross, "The History of Space Laser Communications", SPIE Vol. 885, p. 2 (1985).

[72] Chapter 5, Optical Configuration and System Design in Laser Satellite Communication, M. Katzman Editor, (1987).

[73] S. Manhart and R. Birkl, "Straylight and Backscattered Light, SPIE Vol. 1131, pp. 45-53 (1989)

[74] M.A. Grant et al., "A lightweight User Terminal for an Optical Data Relay Satellite, SPIE Vol. 1218 p. 51-61 (1990)

[75] E.A. Swanson and R.S. Bondurant, "Using Fiber Optics to Simplify Free Space Lasercomm Systems, SPIE vol. 1218 pp. 70-82 (1990).

[76] R.S. bondurant et al, "An Optomechanical Subsystem for Space Based Coherent Optical Communication", SPIE Vol. 996 pp. 92-100 (1988).

[77] W.L. Casey et al., "Laser Communication System Design", SPIE Vol. 996 pp. 28-35 (1988).

[78] M. Shikatani et al., "Optical Intersatellite LInk Experiment between the Earth Station and ETS-VI", SPIE Vol. 1218 p. 2-12 (1990).

[79] H. Levenstein, "Wide Field of View Optics Applied to Multi-user Optical Communication, SPIE Vol. 1044 pp. 173-178 (1989)

[80] P. Henneberg and H. Schubert, "A New Telescope Concept for Space Communication", SPIE Vol. 1218 pp. 153-159 (1990).

[81] M. Detaille and P. Houmault, "Telescope Considered as a Very High Gain Antenna", SPIE Vol. 1218 pp. 160-168 (1990).

[82] E.T. nelsen et al, "Wide field of view PtSi Infrared focal plane array", SPIE Vol. 1308 p. 36-44 (1990).

[83] E.r. Fossum, "III-V CCD's" Proc. of the IEEE charge coupled wokship, June 1991.

[84] S.H. Castles "Current Developments in NASA cryogenic cooler technology", Advances in Cryogenic Eng. Vol. 35 (1989).

[85] M. Laikin, "Lens Design" p. 79 Marcel Dekker Inc. N.Y. (1991).

[86] "Orbiting Blue Lasers for Submarine Data Links", Lasers and Optronics Vol. 6, No. 6 pp 25-25 (1987).

[87] "High Power Diode Pumped Nd:Yag Lasers for Free-space Communication, R. Wallace et al, SPIE Vol. 1417, (1991).

[88] A.L. Scoltz et al, "Receiver Concepts for Data Transmission at 10 microns, "Rpoc ESA Workship on Space Laser Applications and Technology, ESA SP-202, May (1984).

[89] K.E. Wilson et al, "Gopex: A Deep-space Optical Communications Demonstration with the Galileo Spacecraft", SPIE Vol. 1417 (1991).

[90] B.D. Seery, "The Goddard Optical Communications Program", SPIE Vol. 1218, pp. 13-26 (1990).

[91] "Diode Pumped Solid State versus Semiconductor Lasers for Free Space Communications", SPIE Vol. 1218 (1990).

[92] J. Gazdewich, A. Waksbert, C.Dreze, "The Development of Heterodyne based optical intersatellite communications", MPB Technologies Inc. for Department of Communications DSS Contract No. 1ST84-00177, 1986.

[93] D. Atkinson, C. Dreze, A. Waskberg, "Technology development for wideband Intersatellite laser communication systems", MPB Technologies Inc. for Department of Communications DSS Contract No. 36001-7-3591/01-ST 1990.

[94] Bondurant et al, "An Opto-mechanical subsystem for Space Based Coherent Optical Communications", SPIE Vol. 996, pp. 92-100 (1988).

[95] Chapter 5, Optical Configuration and System Design in Laser Satellite Communication; M. Katzman, Editor (1987).

[96] A.L. Scholtz, A.K. Phillip & W.R. Leeb "Receiver Concepts for Data transmission Space Applications and Technology ESA SP-202 may (1984).

[97] D.L. Spears "Wide-Band CO_2 Laser photomixers" SPIE Vol. 227 p. 105-116 (1980).

[98] J.F. Shanley et al "Performance Characteristics of HgCdTe. Heterodyne Receiver" SPIE Vol. 1181 (1989).

[99] M. Sirieix: H. Hotheimer "Conceptual Design and Applications of HgCdTe Infrared Photodiodes for Heterodyne Systems" Proc. of the international conf. on Heterodyne Systems and Tech. March (1980).

[100] J.R. Teague, "1.06 m wideband laser modulator - Fabrication and life testing", McDonnell-Douglas Astronautics Co. for Goddard space flight center, contract NASA-CR-144783 (1975).

[101] Gatenby, P.V., Boereboom, P.A., Grant, M.A., "Design of a Periscopic Coarse Pointing Assembly for Optical Multiple Access", SPIE Proceedings, Vol 1522, June 1991.

[102] M. Ross, P. Freedman, J. Abernathy, G. Matassov, J. Wolf, and J.D. Barry, "Space Optical Communications with the Nd:YAG laser", Proc. IEEE Vol. 66, No. 3, March 1978, pp. 319-344.

[103] K. Komatu, S. Kanda, K. Hirako, and T. Ohashi, "Laser beam acquisition and tracking system for ETS-VI laser communication equipment (LCE)", SPIE Vol. 1218 - Free-Space Laser Communication Technologies II, 1990, pp. 96-107.

[104] SILEX - "The Space Optical Communications", Matra, 1990

[105] M. Shikatani, S. Yoshikado, Y. Arimoto, Y. Suzuki, Y. Takahashi, and T. Aruga, "Optical intersatellite link experiment between the earth station and ETS-VI", SPIE Vol. 1218 - Free-Space Laser Communication Technologies II, 1990, pp. 2-12.

[106] Hughes Aircraft Company, "A study to define the impact of laser communication systems on their host spacecraft", final report, a study under contract NAS 5-27139, prepared for NASA Goddard Space Flight Centre, April 1984.

[107] J.M. Lopez and K. Yong, "Acquisition, tracking, and fine pointing control of space-based laser communication systems", SPIE Vol. 295 - Control and Communication Technology in Laser Systems, 1981, pp. 100-114.

[108] E.L. Coffelt and T.H. Ebben, "Optical transceiver platform for laser communication experiments", SPIE Vol. 616 - Optical Technologies for Communication Satellite Applications, 1986, pp. 22-28.

[109] COMSAT Laboratories, "The study of optical intersatellite links", final report, submitted to INTELSAT under contract INTEL-384, August 1985.

[110] J.D. Barry and G.S. Mecherle, "Beam pointing error as a significant design parameter for satellite-borne, free-space optical communication systems", Optical Engineering Vol. 24 No. 6, Nov/Dec 1985, pp. 1049-1054.

[111] J.D. Barry and G.S. Mecherle, "Communication channel burst errors induced by Gaussian distributed mispointing", SPIE Vol. 616 - Optical Technologies for Communication Satellite Applications, 1986, pp. 137-140.

[112] G. Oppenhuser and M. Wittig, The European SILEX project: concept, performances, status and planning, SPIE Vol. 1218 - Free-Space Laser Communication Technologies II, 1990, pp. 27-37.

[113] Physik Instrumente, "Products for Micropositioning", catalog CAT 109-12/90.15, Physik Instrumente (PI) GmbH & Co. Siemensstrasse 13-15, W-7517 Waldbronn, Germany.

[114] H. Hibon and J.M. Betermier, "Breadboarding of a high bandwidth acquisition and fine tracking system for satellite optical communications" SPIE Vol. 1131 - Optical Space Communication, 1989, pp. 116-127

[115] K. Shiratama, T. Hamuro, Y. Ohgushi, and M. Shimizu, "Fine pointing mechanism using multilayered piezo-electric actuator for optical ISL system", SPIE Vol. 1218 - Free-Space Laser Communication Technologies II, 1990, pp. 117-128.

[116] M. Shimizu, K. Shiratama, and Y. Ohgushi, "Point-ahead mechanism for ETS-VI optical ISL experiment", SPIE Vol. 1218 - Free-Space Laser Communication Technologies II, 1990, pp. 646-657.

[117] R.H. Kern and U. Kugel, "Pointing, acquisition and tracking (PA) subsystems and components for optical space communication systems", SPIE Vol. 1131 - Optical Space Communication, 1989, pp. 97-107.

[118] P.W. Young, L.M. Germann, and R. Nelson, "Pointing, acquisition, and tracking subsystem for space-based laser communications", SPIE Vol. 616 - Optical Technologies for Communication Satellite Applications, 1986, pp. 118-128.

[119] R.P. Mathur, C.I. Beard, and D.J. Purll, "Analysis of Silex tracking sensor performance", SPIE Vol. 1218 - Free-Space Laser Communication Technologies II, 1990, pp. 129-141.

[120] P. Dautriche and G. Boucharlat, "THX 31160 a new area array CCD sensor for laser tracking applications", SPIE Vol. 1131 - Optical Space Communication, 1989, pp. 83-87.

[121] R.J. Mathur and D.J. Purl, "Tracking sensor developments for optical intersatellite links", SPIE Vol. 1131 - Optical Space Communication, 1989, pp. 88-96.

[122] K.J. Held and J.D. Barry, "Precision optical pointing and tracking from spacecraft with vibrational noise", SPIE Vol. 616 - Optical Technologies for Communication Satellite Applications, 1986, pp. 160-173.

[123] R.M. Gagliardi and M. Sheikh, "Pointing error statistics in optical beam tracking", IEEE Trans. on Aerospace and Elec. Systems Vol. AES-16 No. 5, Sept. 1980, pp. 674-682.

[124] G.A. Tyler and D.L. Fried, "Image-position error associated with a quadrant detector", J. Opt. Soc. Am. Vol. 72 No. 6, June 1982, pp. 804-808.

[125] L.G. Kazovsky, "Theory of tracking accuracy of laser systems", Optical Engineering Vol. 22 No. 3, May/June 1983, pp. 339-347.

[126] C.C. Chen, M. Jenanathan, and J.R. Lesh, "Spatial acquisition and tracking for deep-space optical communication packages", SPIE Vol. 1417 - Free-Space Laser Communication Technologies III, 1991, pp. 240-250.

[127] H. Taub and D.L. Shilling, "Principles of Communication Systems", McGraw-Hill Book Company, 1971.

[128] G.A. Koepf, R. Peters, and R.G. Marshalek, "Analysis of burst error occurrence on optical intersatellite link (ISL) design", SPIE Vol. 616 - Optical Technologies for Communication Satellite Applications, 1986, pp. 129-136.

[129] J.L. Vanhove, B. Laurent, and J.L Perbos, "System analysis of optical interorbit communications", SPIE Vol. 810 - Optical Systems for Space Applications, 1987, pp. 164-171.

[130] R.A. Peters and M. Sasaki, "Effect of coding on the BER of an optical ISL", SPIE Vol. 756 -Optical Technologies for Space Communication Systems, 1987, pp. 70-77.

[131] R.A. Peters and M. Sasaki, "An iterative approach to calculating the performance of two coupled optical intersatellite link tracking subsystems", SPIE Vol. 756 - Optical Technologies for Space Communication Systems, 1987, pp. 78-85.

[132] J. Berger et al opt. Let. 13, 1988

[133] D. Mengers, L. Fanto, and N. Ackermann, "Predicting two words the performance of solar illuminated thermal louvers for the GOES I,J.K. Instruments", Proc. of the 22nd Thermophysics conference, June 1987.

[134] J.W. Figoski, "Design and Tolerance Specification of a wide field, three mirror, un- obscured, high resolution sensor", SPIE Vol. 1049, pp. 157-165 (1989).

[135] T. Petsch, Private Communications, Schrack Aerospace.

[136] C. Drèze, D. Atkinson, A. Waksberg, "Study of a 1 Gbps 0.84 μm heterodyne system for ISL applications", SPIE Vol. 1218 on "Free-Spase Laser Communication Technologies II", Los Angwles, Jan 1991, pp. 83-94.

This Page Intentionally Left Blank

DOCUMENT CONTROL DATA

(Security classification of title, body of abstract and indexing annotation must be entered when the overall document is classified)

1. ORIGINATOR (the name and address of the organization preparing the document. Organizations for whom the document was prepared, e.g. Establishment sponsoring a contractor's report, or tasking agency, are entered in section 8.)

Spar Aerospace Limited
Satellite & Communications Systems Division
21025 Trans Canada Hwy, Ste-Anne-de-Bellevue, Quebec

2. SECURITY CLASSIFICATION (overall security classification of the document. including special warning terms if applicable)

Unclassified

3. TITLE (the complete document title as indicated on the title page. Its classification should be indicated by the appropriate abbreviation (S,C or U) in parentheses after the title.)

Optical Intersatellite Link System Study

4. AUTHORS (Last name, first name, middle initial)

BUTTNER, Gary J.
KING, Donald T.
LUNSHER, Wolfram H.H.J.
MacGREGOR, Andrew D.
MOODY, Harry J.
SINCLAIR, Lawrence

5. DATE OF PUBLICATION (month and year of publication of document)

November 1991

6a. NO. OF PAGES (total containing information. Include Annexes, Appendices, etc.)

438

6b. NO. OF REFS (total cited in document)

136

7. DESCRIPTIVE NOTES (the category of the document, e.g. technical report, technical note or memorandum. If appropriate, enter the type of report, e.g. interim, progress, summary, annual or final. Give the inclusive dates when a specific reporting period is covered.)

TECHNICAL REPORT (FINAL CONTRACT REPORT)

8. SPONSORING ACTIVITY (the name of the department project office or laboratory sponsoring the research and development. Include the address.)

Communications Research Centre
3701 Carling Avenue
Materiel Management " "
P.O. Box 11490, Station H, Ottawa, Ontario K2H 8S2

9a. PROJECT OR GRANT NO. (if appropriate, the applicable research and development project or grant number under which the document was written. Please specify whether project or grant)

PROJECT No. 041LL-A4

9b. CONTRACT NO. (if appropriate, the applicable number under which the document was written)

027ST-36001-0-3600/A

10a. ORIGINATOR'S DOCUMENT NUMBER (the official document number by which the document is identified by the originating activity. This number must be unique to this document.)

Spar project 3670-F

10b. OTHER DOCUMENT NOS. (Any other numbers which may be assigned this document either by the originator or by the sponsor)

None

11. DOCUMENT AVAILABILITY (any limitations on further dissemination of the document, other than those imposed by security classification)

(X) Unlimited distribution
( ) Distribution limited to defence departments and defence contractors; further distribution only as approved
( ) Distribution limited to defence departments and Canadian defence contractors; further distribution only as approved
( ) Distribution limited to government departments and agencies; further distribution only as approved
( ) Distribution limited to defence departments; further distribution only as approved
( ) Other (please specify):

12. DOCUMENT ANNOUNCEMENT (any limitation to the bibliographic announcement of this document. This will normally correspond to the Document Availabilty (11). However, where further distribution (beyond the audience specified in 11) is possible, a wider announcement audience may be selected.)

Full unlimited announcement

13. ABSTRACT (a brief and factual summary of the document. It may also appear elsewhere in the body of the document itself. It is highly desirable that the abstract of classified documents be unclassified. Each paragraph of the abstract shall begin with an indication of the security classification of the information in the paragraph (unless the document itself is unclassified) represented as (S), (C), or (U). It is not necessary to include here abstracts in both offical languages unless the text is bilingual).

This is a study of laser intersatellite and interorbit links including geostationary to geostationary links, geostationary to low earth orbit links and geostationary to the highly inclined elliptical orbits of Molniya and Tundra types. The study covered solid state, semiconductor diode and gaseous lasers with wavelengths ranging from 0.6 μm and bit rates up to 1 Gbps.

The first part of the study was devoted to a review of technology capability in the areas of detector sensitivity, laser power, telescope performance and acquisition and tracking procedures. Calculations or orbital parameters were also undertaken

This was followed by a conceptual design of a baseline 100 Mbps GEO to LEO link, plus two high bit rate options.

Baseline: A 100 Mbps link using an AlGaAs laser and direct detection receiver
Option 1: A 1 Gbps link using 4 wavelength multiplexed AlGaAs lasers with 4 direct detection receivers.
Option 2: A 1 Gbps link using a single 1W Nd:Yag laser and a heterodyne receiver.

The final part of the report reviews Canadian industrial capability in optical technology and outlines an approach to achieving an operational laser intersatellite link.

14. KEYWORDS, DESCRIPTORS or IDENTIFIERS (technically meaningful terms or short phrases that characterize a document and could be helpful in cataloguing the document. They should be selected so that no security classification is required. Identifiers, such as equipment model designation, trade name, military project code name, geographic location may also be included. If possible keywords should be selected from a published thesaurus. e.g. Thesaurus of Engineering and Scientific Terms (TEST) and that thesaurus-identified. If it is not possible to select indexing terms which are Unclassified, the classification of each should be indicated as with the title.)

Optical Intersatellite Links
Lasers
Laser Direct Detection Receivers
Laser heterodyne receivers
CCD Acquisition
Point ahead angle